

# Design and development of new therapeutics against infectious diseases using computational and experimental approaches

**Edited by**

Parth Sarthi Sen Gupta, Yogendra Kumar Mishra  
and Simone Brogi

**Published in**

Frontiers in Cellular and Infection Microbiology



## FRONTIERS EBOOK COPYRIGHT STATEMENT

The copyright in the text of individual articles in this ebook is the property of their respective authors or their respective institutions or funders. The copyright in graphics and images within each article may be subject to copyright of other parties. In both cases this is subject to a license granted to Frontiers.

The compilation of articles constituting this ebook is the property of Frontiers.

Each article within this ebook, and the ebook itself, are published under the most recent version of the Creative Commons CC-BY licence. The version current at the date of publication of this ebook is CC-BY 4.0. If the CC-BY licence is updated, the licence granted by Frontiers is automatically updated to the new version.

When exercising any right under the CC-BY licence, Frontiers must be attributed as the original publisher of the article or ebook, as applicable.

Authors have the responsibility of ensuring that any graphics or other materials which are the property of others may be included in the CC-BY licence, but this should be checked before relying on the CC-BY licence to reproduce those materials. Any copyright notices relating to those materials must be complied with.

Copyright and source acknowledgement notices may not be removed and must be displayed in any copy, derivative work or partial copy which includes the elements in question.

All copyright, and all rights therein, are protected by national and international copyright laws. The above represents a summary only. For further information please read Frontiers' Conditions for Website Use and Copyright Statement, and the applicable CC-BY licence.

ISSN 1664-8714  
ISBN 978-2-8325-5175-2  
DOI 10.3389/978-2-8325-5175-2

## About Frontiers

Frontiers is more than just an open access publisher of scholarly articles: it is a pioneering approach to the world of academia, radically improving the way scholarly research is managed. The grand vision of Frontiers is a world where all people have an equal opportunity to seek, share and generate knowledge. Frontiers provides immediate and permanent online open access to all its publications, but this alone is not enough to realize our grand goals.

## Frontiers journal series

The Frontiers journal series is a multi-tier and interdisciplinary set of open-access, online journals, promising a paradigm shift from the current review, selection and dissemination processes in academic publishing. All Frontiers journals are driven by researchers for researchers; therefore, they constitute a service to the scholarly community. At the same time, the *Frontiers journal series* operates on a revolutionary invention, the tiered publishing system, initially addressing specific communities of scholars, and gradually climbing up to broader public understanding, thus serving the interests of the lay society, too.

## Dedication to quality

Each Frontiers article is a landmark of the highest quality, thanks to genuinely collaborative interactions between authors and review editors, who include some of the world's best academicians. Research must be certified by peers before entering a stream of knowledge that may eventually reach the public - and shape society; therefore, Frontiers only applies the most rigorous and unbiased reviews. Frontiers revolutionizes research publishing by freely delivering the most outstanding research, evaluated with no bias from both the academic and social point of view. By applying the most advanced information technologies, Frontiers is catapulting scholarly publishing into a new generation.

## What are Frontiers Research Topics?

Frontiers Research Topics are very popular trademarks of the *Frontiers journals series*: they are collections of at least ten articles, all centered on a particular subject. With their unique mix of varied contributions from Original Research to Review Articles, Frontiers Research Topics unify the most influential researchers, the latest key findings and historical advances in a hot research area.

Find out more on how to host your own Frontiers Research Topic or contribute to one as an author by contacting the Frontiers editorial office: [frontiersin.org/about/contact](https://frontiersin.org/about/contact)



# Design and development of new therapeutics against infectious diseases using computational and experimental approaches

## Topic editors

Parth Sarthi Sen Gupta — D Y Patil International University, India

Yogendra Kumar Mishra — University of Southern Denmark, Denmark

Simone Brogi — University of Pisa, Italy

## Citation

Sen Gupta, P. S., Mishra, Y. K., Brogi, S., eds. (2024). *Design and development of new therapeutics against infectious diseases using computational and experimental approaches*. Lausanne: Frontiers Media SA. doi: 10.3389/978-2-8325-5175-2

## Table of contents

- 05 **Editorial: Design and Development of new Therapeutics Against Infectious Diseases Using Computational and Experimental Approaches**  
Simone Brogi, Parth Sarthi Sen Gupta and Yogendra Kumar Mishra
- 08 **Exploring the mechanism of action of Xuanfei Baidu granule (XFBD) in the treatment of COVID-19 based on molecular docking and molecular dynamics**  
Li Xiong, Junfeng Cao, Xingyu Yang, Shengyan Chen, Mei Wu, Chaochao Wang, Hengxiang Xu, Yijun Chen, Ruijiao Zhang, Xiaosong Hu, Tian Chen, Jing Tang, Qin Deng, Dong Li, Zheng Yang, Guibao Xiao and Xiao Zhang
- 29 **Vaccines against candidiasis: Status, challenges and emerging opportunity**  
Satya Ranjan Sahu, Swagata Bose, Manish Singh, Premalata Kumari, Abinash Dutta, Bhabasha Gyanadeep Utkalaja, Shraddheya Kumar Patel and Narottam Acharya
- 42 **Meta-analysis of active tuberculosis gene expression ascertains host directed drug targets**  
Nirmaladevi Ponnusamy and Mohanapriya Arumugam
- 55 **In silico high-throughput screening system for AKT1 activators with therapeutic applications in sepsis acute lung injury**  
Ziyi Wang, Xuesong Wang, Zhe Guo, Haiyan Liao, Yan Chai, Ziwen Wang and Zhong Wang
- 69 **Integration of molecular modelling and *in vitro* studies to inhibit LexA proteolysis**  
Zachariah P. Schuurs, John P. McDonald, Laura V. Croft, Derek J. Richard, Roger Woodgate and Neha S. Gandhi
- 86 **Computer-aided genomic data analysis of drug-resistant *Neisseria gonorrhoeae* for the Identification of alternative therapeutic targets**  
Aqsa Qasim, Samavia Jaan, Tehreem Ul Wara, Muhammad Shehroz, Umar Nishan, Sulaiman Shams, Mohibullah Shah and Suvash Chandra Ojha
- 101 **Emerging evidence on Monkeypox: resurgence, global burden, molecular insights, genomics and possible management**  
Ruchi Sharma, Kow-Tong Chen and Rohit Sharma
- 122 **Elucidation of novel compounds and epitope-based peptide vaccine design against C30 endopeptidase regions of SARS-CoV-2 using immunoinformatics approaches**  
Saigha Marriam, Muhammad Sher Afghan, Mazhar Nadeem, Muhammad Sajid, Muhammad Ahsan, Abdul Basit, Muhammad Wajid, Sabeen Sabri, Muhammad Sajid, Imran Zafar, Summya Rashid, Sheikh Arslan Sehgal, Dalal Hussien M. Alkhalifah, Wael N. Hozzein, Kow-Tong Chen and Rohit Sharma

- 140 ***Lactobacillus acidophilus* NCFM and *Lactiplantibacillus plantarum* Lp-115 inhibit *Helicobacter pylori* colonization and gastric inflammation in a murine model**  
Siqi Shen, FeiFei Ren, Haiming Qin, Ihtisham Bukhari, Jing Yang, Dafang Gao, Arthur C. Ouwehand, Markus J. Lehtinen, Pengyuan Zheng and Yang Mi
- 152 **Eco-friendly synthesized nanoparticles as antimicrobial agents: an updated review**  
Shilpa Borehalli Mayegowda, Arpita Roy, Manjula N. G., Soumya Pandit, Saad Alghamdi, Mazen Almeahmadi, Mamdouh Allahyani, Nasser S. Awwad and Rohit Sharma
- 165 **A new candidate epitope-based vaccine against PspA PhtD of *Streptococcus pneumoniae*: a computational experimental approach**  
Mona Shafaghi, Zohreh Bahadori, Seyed Mahmoud Barzi, Elnaz Afshari, Hamid Madanchi, Seyed Fazlollah Mousavi and Ali Akbar Shabani
- 189 ***Corynebacterium bovis* infection after autologous fat grafting in breast augmentation: a case report**  
Xin You, Yao Yao, JianHua Gao and YunJun Liao



## OPEN ACCESS

EDITED AND REVIEWED BY  
Nahed Ismail,  
University of Illinois Chicago, United States

## \*CORRESPONDENCE

Simone Brogi  
✉ simone.brogi@unipi.it  
Parth Sarthi Sen Gupta  
✉ parth.biotech@gmail.com  
Yogendra Kumar Mishra  
✉ mishra@mci.sdu.dk

RECEIVED 23 June 2024

ACCEPTED 28 June 2024

PUBLISHED 05 July 2024

## CITATION

Brogi S, Sen Gupta PS and Mishra YK (2024)  
Editorial: Design and development of new  
therapeutics against infectious diseases using  
computational and experimental approaches.  
*Front. Cell. Infect. Microbiol.* 14:1453729.  
doi: 10.3389/fcimb.2024.1453729

## COPYRIGHT

© 2024 Brogi, Sen Gupta and Mishra. This is an  
open-access article distributed under the terms  
of the [Creative Commons Attribution License](#)  
(CC BY). The use, distribution or reproduction  
in other forums is permitted, provided the  
original author(s) and the copyright owner(s)  
are credited and that the original publication  
in this journal is cited, in accordance with  
accepted academic practice. No use,  
distribution or reproduction is permitted  
which does not comply with these terms.

# Editorial: Design and development of new therapeutics against infectious diseases using computational and experimental approaches

Simone Brogi<sup>1\*</sup>, Parth Sarthi Sen Gupta<sup>2\*</sup>  
and Yogendra Kumar Mishra<sup>3\*</sup>

<sup>1</sup>Department of Pharmacy, University of Pisa, Pisa, Italy, <sup>2</sup>School of Biosciences and Bioengineering, D. Y. Patil International University (DYPIU), Pune, Maharashtra, India, <sup>3</sup>Smart Materials, NanoSYD, Mads Clausen Institute, University of Southern Denmark, Sønderborg, Denmark

## KEYWORDS

infectious diseases, viruses, pathogens, bacteria, novel therapeutics

## Editorial of the Research Topic

Design and development of new therapeutics against infectious diseases using computational and experimental approaches

Because of growing concerns about future outbreaks caused by pathogens, we launched a Research Topic in 2022, namely “Design and Development of new Therapeutics Against Infectious Diseases Using Computational and Experimental Approaches” hosted by the journal *Frontiers in Cellular and Infection Microbiology*. In this scenario, the most important consideration should be the enrichment of current armamentariums in terms of antivirals (or broad-spectrum antivirals) and novel antibiotic agents considering that future pandemic conditions should interest emerging and re-emerging viruses with pandemic potential as well as increasing resistance to current antibacterial agents from emerging resistance-bacteria strains around the world, with particular interest in nosocomial infections and potentially untreatable disorders. Based on the World Health Organization (WHO), these events are expected to be future outbreaks that could damage public health (WHO-report-1, 2024; WHO-report-2, 2024). Due to this urgency, the integration of computational and experimental approaches can accelerate the development of novel strategies, thereby allowing the establishment of novel countermeasures against infectious diseases, thereby limiting disease progression and the possibility of increasing the number of potential events that could allow the expansion of these important threats. Accordingly, the combination of the mentioned approaches can significantly reduce, for example, the time required to identify promising compounds against infectious diseases, optimize their use, and possibly translate these compounds into clinical settings. On the other hand, there are different types of therapeutic agents that could be employed in the treatment of several infectious diseases, nevertheless, the potential resistance to many antibiotic agents and the insurgence of mutated viruses that can escape from vaccines;



therefore, in these current cases, there is also a major need for the development of novel therapeutics to effectively treat infectious diseases. Moreover, relevance is assumed by the identification of novel delivery systems that improve the targeting of crucial pathogenic factors and the host immune response. Accordingly, with this aim, we introduce this Research Topic that attracted scientists in the field, and we were able to consider several submissions with a final number of published articles of 12. Among the articles of the Research Topic, 9 of them were Original Research articles, including 1 Case Report and 3 were Review articles, including 1 Mini-Review. These articles provided novel insights into the mechanisms of different infectious diseases and potential therapeutic approaches that could be useful for the development of novel antibacterial and antiviral agents.

Starting from research articles in the antiviral field, Xiong et al. applied a computational protocol based on network pharmacology, molecular docking, and molecular dynamics (MD) to explore the constituents of *Xuanfei Baidu* granule (XFBD) as anti-COVID-19 agents. Interestingly, the findings demonstrated that XFBD contains two significant active chemical components: I-SPD and chypodol. These components limit NLRP3 activation, which in turn reduces inflammatory response and apoptosis. By blocking the activation and chemotaxis of inflammatory cells via CSF2, I-SPD and vestitol can stop the progression of an inflammatory storm (Xiong et al.). Marriam et al. used different *in silico* procedures to identify a novel epitope-based peptide vaccine against the C30 endopeptidase regions of SARS-CoV-2. Furthermore, the proposed target was used in a virtual screening procedure to identify small molecules from the ZINC database that could interfere with endopeptidase function (Marriam et al.). Regarding the antiviral topic, a review by Sharma et al. was published under the Research Topic. In particular, they analyzed emerging evidence related to the Monkeypox infection. Among them, the global burden, resurgence, and possible management were reviewed in the mentioned paper (Sharma et al.).

Regarding the development of potential antimicrobial agents, some research articles were published under the Research Topic. Qasim et al. focused their work on the relevant topic of resistance pathogens. They conducted computer-aided genomic data analysis and bioinformatics techniques to identify potential new drug and vaccine targets against *Neisseria gonorrhoeae* infection. Interestingly, using a reverse vaccinology technique, two outer membrane proteins (AKP15153.1, AKP15828.1) were identified as potential vaccine candidates. Accordingly, a chimeric vaccine construct was generated using the top lead B- and T-cell overlapping epitopes. The molecular docking and MD simulation analyses indicated that the top-ranked vaccine candidate (V7) exhibited stable molecular interactions with human immune cell receptors (Qasim et al.). Schuurs et al. investigated covalent warheads and  $\beta$ -turn mimetic to identify LexA inhibitors coupling computational and experimental data. Two computational protocols, one for screening the  $\beta$ -turn mimetic and the other for considering a library of compounds containing covalent warheads that may target catalytic residue S119 to effectively inhibit the proteolytic function of LexA. Over 100 top-ranked molecules were tested using a RecA-mediated cleavage experiment to determine whether the compounds could prevent LexA

cleavage in *E. coli*. Notably, a previously undiscovered covalent scaffold prevents RecA-mediated LexA cleavage was identified (Schuurs et al.). Shafaghi et al. conducted a study combining *in silico* and *in vitro* approaches to identify a novel candidate epitope-based vaccine targeting PspA PhtD of *Streptococcus pneumoniae*. Using immunoinformatics techniques, a fusion construct was created (PAD), by combining the immunodominant sections of PhtD (PD) with the immunodominant areas of PspA (PA) from families 1 and 2. This experiment aimed to evaluate the immunogenicity of the PAD fusion protein and assess its ability to protect against *S. pneumoniae* infection, both alone and in combination with PA and PD. Using computational techniques, the physicochemical properties, antigenicity, allergenicity, toxicity, and three-dimensional structure of the constructions were assessed. Molecular docking with the HLA receptor and immunological simulation were also performed. After immunizing mice, blood levels of antibodies and cytokines were measured, and the ability of antibodies to operate *in vitro* was assessed, as well as the survival rates of mice and the drop in bacterial loads in their blood and spleen. According to these findings, the fusion protein may be employed as a pneumococcal vaccine that is not dependent on serotype or as a useful ally protein in conjunction with a conjugate polysaccharide vaccine (Shafaghi et al.). Shen et al. described *in vitro* and *in vivo* experiments to determine the function of different *Lactobacillus* strains and their combinations in preventing *Helicobacter pylori* colonization and stomach mucosa irritation. Of all probiotics, *L. acidophilus* NCFM and *L. plantarum*, Lp-115 exerted a noteworthy effect on *H. pylori* elimination, reducing its adhesion and inhibiting the inflammatory response caused by *H. pylori* infection. The results of the present study provide significant value for the management of *H. pylori* infection, indicating the possibility of further clinical interventions with the two probiotic strains or their combination (Shen et al.). Wang et al. developed an *in silico* screening platform to identify possible chemicals able to activate AKT1 for the potential treatment of sepsis acute lung injury (SALI). Starting from the 3D structure of AKT1 (PDB ID 1UNR) and AKT activator molecules, the authors screened the ChemDiv database. Results showed that one of the top-ranked compounds (compound 7460-0250) selectively enhanced AKT1 phosphorylation and downregulated LPS-induced apoptosis in human umbilical vein endothelial cells (HUVECs) by activating the AKT-mTOR pathway. It was found that upregulated mTOR directly interacts with Bax to decrease apoptosis. *In vivo* studies have confirmed that the substance may lower SALI by activating the AKT-mTOR signaling pathway, reducing lung damage, and increasing the survival rate in mice with sepsis caused by cecum ligation and puncture (Wang et al.). An interesting meta-analysis of transcriptome from healthy and infected individuals, conducted by Ponnusamy and Arumugam, identified new potential therapeutic targets for drug repurposing studies by examining host directed drug-target interaction networks and protein interaction networks (human and *Mycobacterium tuberculosis*). Comparative research between healthy and tuberculosis cohorts provided insights into differentially expressed genes (DEGs) and made it possible to track these DEGs during vaccination or medication therapy. Furthermore, potential genes to target multidrug-resistant *M. tuberculosis* were identified. Among them, some kinases active in tuberculosis infection and ribosomal proteins, as well as proteins that enhance host-immune responses, were

suggested as promising targets to be exploited for developing innovative anti-tubercular drug candidates (Ponnusamy and Arumugam). Again, a case report presented by You et al. described a patient with *Corynebacterium bovis* infection after fat breast augmentation. It is still unknown what caused the infection. The patient denied having been in an animal or tainted cow product, and she had no prior history of breast damage. Accordingly, this case report highlights the possible dangers of using fat-derived products that have been cryopreserved, including the risk of infection and adipocyte necrosis. The findings also emphasize the importance of comprehensive preoperative assessment and postoperative monitoring for the early detection and management of problems. Finally, high-throughput sequencing technology can be a useful diagnostic and therapeutic guide for diseases that do not respond to culture (You et al.). Finally, two review articles on the development of antimicrobial agents were published under the Research Topic. In the first article, Sahu et al. discussed the numerous coordinated efforts that have been made to date to create anti-*Candida* vaccines, along with a pan-fungal vaccine alternative. The authors have provided an updated context regarding vaccines undergoing clinical trials, obstacles, and potential future developments (Sahu et al.). Mayegowda et al. discussed nanoparticles (NPs) that can be employed for a variety of biological entities, including plants, bacteria, fungi, actinomycetes, viruses, and algae, each of which has a unique set of capabilities. Many pharmaceutical applications, including tissue engineering, pathogen or protein detection, antimicrobial agents, anticancer mediators, drug delivery vehicles, functional food formulations, and pathogen identification, can benefit from the use of NPs. These applications can also aid translational research into medical fields. In this review, the potential of eco-friendly synthesis to develop NPs as antimicrobial agents is described in detail (Mayegowda et al.).

In conclusion, we would like to express our gratitude to the Frontiers editorial staff for their generous ongoing support, as well as to all of the authors and co-authors for their significant contributions to this Research Topic and the reviewers for their invaluable effort in assessing the submitted manuscripts. We are also grateful to the guest editors. When all these efforts were combined, the Research Topic was successful. In addition to being a useful source of knowledge and inspiration for researchers and students, we anticipate that this topic will promote drug design and discovery for the treatment of infectious diseases. You can gain free access to the Research Topic

by clicking on this link <https://www.frontiersin.org/research-topics/37720/design-and-development-of-new-therapeutics-against-infectious-diseases-using-computational-and-experimental-approaches/magazine>.

## Author contributions

SB: Conceptualization, Data curation, Formal analysis, Writing – original draft, Writing – review & editing. PS: Conceptualization, Data curation, Formal analysis, Writing – original draft, Writing – review & editing. YM: Conceptualization, Data curation, Formal analysis, Writing – original draft, Writing – review & editing.

## Acknowledgments

The authors wish to thank all the contributors of the Research Topic, reviewers and the Editorial Office of Frontiers in Cellular and Infection Microbiology for the helpful advice during the management of the submitted manuscripts.

## Conflict of interest

The authors declare that the research was conducted in the absence of any commercial or financial relationships that could be construed as a potential conflict of interest.

The author(s) declared that they were an editorial board member of Frontiers, at the time of submission. This had no impact on the peer review process and the final decision.

## Publisher's note

All claims expressed in this article are solely those of the authors and do not necessarily represent those of their affiliated organizations, or those of the publisher, the editors and the reviewers. Any product that may be evaluated in this article, or claim that may be made by its manufacturer, is not guaranteed or endorsed by the publisher.

## References

WHO-report-1. (2024). Available online at: <https://www.who.int/news-room/fact-sheets/detail/antimicrobial-resistance> (Accessed 18 June 2024).

WHO-report-2. (2024). Available online at: <https://www.who.int/news/item/21-11-2022-who-to-identify-pathogens-that-could-cause-future-outbreaks-and-pandemics> (Accessed 18 June 2024).



## OPEN ACCESS

## EDITED BY

Parth Sarthi Sen Gupta,  
Indian Institute of Science Education  
and Research Berhampur (IISER), India

## REVIEWED BY

Xu Jia,  
Chengde Medical College, China  
Suprabhat Mukherjee,  
Kazi Nazrul University, India

## \*CORRESPONDENCE

Xiao Zhang  
954073462@qq.com  
Guibao Xiao  
1250374226@qq.com  
Zheng Yang  
yzixjj@163.com

<sup>†</sup>These authors have contributed  
equally to this work and share  
first authorship

## SPECIALTY SECTION

This article was submitted to  
Clinical Microbiology,  
a section of the journal  
Frontiers in Cellular and  
Infection Microbiology

RECEIVED 09 June 2022

ACCEPTED 14 July 2022

PUBLISHED 10 August 2022

## CITATION

Xiong L, Cao J, Yang X, Chen S, Wu M,  
Wang C, Xu H, Chen Y, Zhang R, Hu X,  
Chen T, Tang J, Deng Q, Li D, Yang Z,  
Xiao G and Zhang X (2022) Exploring  
the mechanism of action of Xuanfei  
Baidu granule (XFBD) in the treatment  
of COVID-19 based on molecular  
docking and molecular dynamics.  
*Front. Cell. Infect. Microbiol.* 12:965273.  
doi: 10.3389/fcimb.2022.965273

## COPYRIGHT

© 2022 Xiong, Cao, Yang, Chen, Wu,  
Wang, Xu, Chen, Zhang, Hu, Chen,  
Tang, Deng, Li, Yang, Xiao and Zhang.  
This is an open-access article  
distributed under the terms of the  
Creative Commons Attribution License  
(CC BY). The use, distribution or  
reproduction in other forums is  
permitted, provided the original  
author(s) and the copyright owner(s)  
are credited and that the original  
publication in this journal is cited, in  
accordance with accepted academic  
practice. No use, distribution or  
reproduction is permitted which does  
not comply with these terms.

# Exploring the mechanism of action of Xuanfei Baidu granule (XFBD) in the treatment of COVID-19 based on molecular docking and molecular dynamics

Li Xiong<sup>1†</sup>, Junfeng Cao<sup>1†</sup>, Xingyu Yang<sup>1</sup>, Shengyan Chen<sup>1</sup>,  
Mei Wu<sup>1</sup>, Chaochao Wang<sup>1</sup>, Hengxiang Xu<sup>1</sup>, Yijun Chen<sup>1</sup>,  
Ruijiao Zhang<sup>2</sup>, Xiaosong Hu<sup>2</sup>, Tian Chen<sup>2</sup>, Jing Tang<sup>3</sup>,  
Qin Deng<sup>3</sup>, Dong Li<sup>1</sup>, Zheng Yang<sup>2\*</sup>, Guibao Xiao<sup>3\*</sup>  
and Xiao Zhang<sup>2\*</sup>

<sup>1</sup>Clinical Medicine, Chengdu Medical College, Chengdu, China, <sup>2</sup>Chengdu Medical College of Basic Medical Sciences, Chengdu, China, <sup>3</sup>Department of Infectious Diseases, First People's Hospital of Ziyang, Ziyang, China

**Purpose:** The Corona Virus Disease 2019 (COVID-19) pandemic has become a challenge of world. The latest research has proved that *Xuanfei Baidu granule* (XFBD) significantly improved patient's clinical symptoms, the compound drug improves immunity by increasing the number of white blood cells and lymphocytes, and exerts anti-inflammatory effects. However, the analysis of the effective monomer components of XFBD and its mechanism of action in the treatment of COVID-19 is currently lacking. Therefore, this study used computer simulation to study the effective monomer components of XFBD and its therapeutic mechanism.

**Methods:** We screened out the key active ingredients in XFBD through TCMSP database. Besides GeneCards database was used to search disease gene targets and screen intersection gene targets. The intersection gene targets were analyzed by GO and KEGG. The disease-core gene target-drug network was analyzed and molecular docking was used for verification. Molecular dynamics simulation verification was carried out to combine the active ingredient and the target with a stable combination. The supercomputer platform was used to measure and analyze the number of hydrogen bonds, the binding free energy, the stability of protein target at the residue level, the solvent accessible surface area, and the radius of gyration.

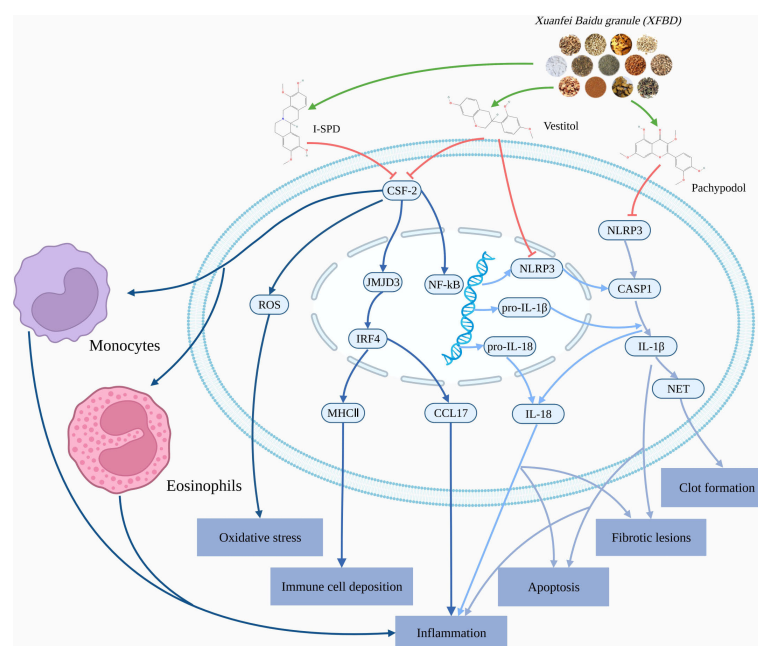
**Results:** XFBD had 1308 gene targets, COVID-19 had 4600 gene targets, the intersection gene targets were 548. GO and KEGG analysis showed that XFBD played a vital role by the signaling pathways of immune response and inflammation. Molecular docking showed that I-SPD, Pachypodol and

Vestitol in XFBD played a role in treating COVID-19 by acting on NLRP3, CSF2, and relieve the clinical symptoms of SARS-CoV-2 infection. Molecular dynamics was used to prove the binding stability of active ingredients and protein targets, CSF2/I-SPD combination has the strongest binding energy.

**Conclusion:** For the first time, it was found that the important active chemical components in XFBD, such as I-SPD, Pachypodol and Vestitol, reduce inflammatory response and apoptosis by inhibiting the activation of NLRP3, and reduce the production of inflammatory factors and chemotaxis of inflammatory cells by inhibiting the activation of CSF2. Therefore, XFBD can effectively alleviate the clinical symptoms of COVID-19 through NLRP3 and CSF2.

#### KEYWORDS

COVID-19, Xuanfei Baidu granule, bioinformatics analysis, molecular docking, molecular dynamics



#### GRAPHICAL ABSTRACT

The mechanisms analysis of Xuanfei Baidu Granules (XFBD) in the treatment of COVID-19.

## Introduction

Coronavirus disease 2019 (COVID-19) is a highly infectious disease caused by severe acute respiratory syndrome coronavirus 2 (SARS-CoV-2) (Lai et al., 2020). Since the outbreak of COVID-19, it has been characterized by strong infectivity, long treatment time after infection, and high mortality of patients with severe illness (Fogarty H, et al., 2020; Rowan NJ, et al., 2020; Goldman DT, et al., 2021). The latest clinical

research findings that the main physiological and pathological feature of severe COVID-19 is “cytokine storm”, also known as inflammatory storm (Ouédraogo et al., 2020). It is an immune response produced by a positive feedback loop between cytokines and immune cells, and it is also the state which the body’s immune system has evolved from “self-protection” to “over-protection” (Bellanti and Settignano, 2020). Therefore, the outbreak of inflammation is an important pathological factor leading to the aggravation and even death of patients with



respiratory damage caused by COVID-19 (Liu et al., 2021), however, there is no clear antiviral therapy for COVID-19 in the clinic (Panyod et al., 2020). The latest clinical trials show that traditional Chinese medicine has a significant effect on viral pneumonia. Clinical studies have shown that XFBD combined with conventional drugs can significantly improve clinical symptoms such as fever, cough, fatigue, loss of appetite, etc. XFBD treatment can increase the number of white blood cells and lymphocytes to improve immunity, while significantly reducing C-reactive protein and erythrocyte sedimentation rate to play an anti-inflammatory effect (Xiong et al., 2020; Zhao et al., 2021a). Meta-analysis demonstrated that XFBD alleviated clinical symptoms in most patients with mild or moderate COVID-19, and reduced the transition of mild patients to severe disease (Runfeng et al., 2020; Wang et al., 2022). At present, the symptomatic treatment of COVID-19 with integrated traditional Chinese and Western medicine has been clinically applied in China, and good therapeutic effects have been achieved.

Currently, the National Health Commission of China recommends the traditional Chinese medicine compound *Xuanfei Baidu Granule* (XFBD) for the clinical treatment of COVID-19 (Xie, 2020).

*Xuanfei Baidu granule* (XFBD) consists of 13 Chinese materia herbs: bitter almond, atractylodes, artemisia annua, patchouli, polygonum cuspidatum, verbena, reed root, ephedra, coix seed, exocarpium, licorice, semen lepidii, and gypsum (Zhao et al., 2021a). XFBD is a traditional Chinese medicine compound for the treatment of anti-epidemic, which is designed for the pathological characteristics of wet toxin (Xie, 2020). XFBD has the effects of inhibiting viral infections, promoting the absorption of lung inflammation, and reducing inflammatory factors.

A large number of clinical studies have shown that *Xuanfei Baidu granule* (XFBD) can effectively relieve the clinical symptoms of COVID-19 patients (Li et al., 2021a). The latest clinical study found that XFBD combined with conventional drugs significantly improved the clinical symptoms of COVID-19 patients, increased the number of white blood cells and lymphocytes, and decreased C-reactive protein and erythrocyte sedimentation rate. This result suggested that XFBD had a potential immunomodulatory role in the treatment of COVID-19 (Xiong et al., 2020).

However, there is currently a lack of more in-depth and systematic research on *Xuanfei Baidu granule* (XFBD) in the treatment of COVID-19. And XFBD is a traditional Chinese medicine compound, its complex components also hinder the related research in the treatment of COVID-19. Molecular dynamics can comprehensively and systematically simulate the interaction and binding stability between small molecule monomers and protein targets with the help of powerful computing power.

Molecular dynamics (MD) is an interdisciplinary subject based on the knowledge of physics, chemistry, life science, materials and other disciplines. It uses large computer clusters (or even supercomputers) as the carrier, it aims to obtain data such as microstructure, physical and chemical properties, and performance characterization parameters of materials by calculation (Santos et al., 2019). It is a supplement and in-depth excavation of the traditional materials discipline mainly based on experiments. Through the data obtained by calculation, the mechanism behind the experiment is researched and analyzed at multiple levels from the microscopic, mesoscopic and macroscopic scales. So that it is not only limited to “qualitative”, but can rise to the theoretical height of “quantitative” (Anuar et al., 2021). It analyzes the behavioral law of molecular motion by solving the potential function of intermolecular interaction and the equation of motion, simulates the dynamic evolution process of the system, and provides microscopic quantities (such as: the coordinates and velocity of molecules, etc.) and macroscopic observable quantities (such as: the relationship between the temperature, pressure, heat capacity of the system, etc.) (Sivakumar et al., 2020), so as to study the equilibrium properties and mechanical properties of the composite system, it is an effective research method to study the properties of drugs and protein stability. Firstly, molecular dynamics solves the equation of motion for a many body system composed of atomic nuclei and electrons. Secondly, molecular dynamics can not only directly simulate the macroscopic evolution characteristics of matter, but also obtain calculation results that are consistent with or similar to the experimental results. Finally, molecular dynamics can give the microscopic evolution process of the system from the atomic level, and intuitively show the mechanism and law of the experimental phenomenon. Therefore, molecular dynamics can provide a clear picture of the microstructure, particle motion and their relationship with macroscopic properties. Molecular dynamics can also make our research more efficient, more economical, and more predictable.

This study used bioinformatics to screen out potential effective monomers from *Xuanfei Baidu granule* (XFBD). The core intersection targets of XFBD and COVID-19 were screened by GeneCards database. PPI, GO and KEGG were used to analyze the potential associations between gene targets to explore the mechanisms of action and potential pathways. Molecular system movement was used to their simulate the result of calculating interrelationships from the cellular level to the chemical group level. Molecular docking was used to determine the affinity of monomeric compounds and protein targets, molecular dynamics was used to simulate the stability of bound complexes. The research on the mechanism of XFBD in the treatment of COVID-19 will promote its clinical application, lay a solid foundation for related research and promote further research.

## Material and methods

### Identification and screening of active compounds

Traditional Chinese Medicine Systems Pharmacology Database (TCMSP, <http://tcmspw.com/>) was used to screen and analyse all compounds of the thirteen Chinese medicinal herbs in *Xuanfei Baidu granule* (XFBD) (Daina et al., 2019). Compounds of XFBD are screened according to two key parameters, namely oral bioavailability (OB) and drug similarity (DL), in the assessment categories of absorption, distribution, metabolism and excretion. OB was defined as the degree to which active ingredients are used by the body (Ru et al., 2014). OB largely determines the effect of the compound on the disease, DL is used to screen and refine candidate compounds early in drug development. In this study, the active compounds in XFBD were selected according to the criterion of  $OB \geq 30\%$  and  $DL \geq 0.18$  (Xu et al., 2012).

### The intersection of disease and drug gene targets

We used the GeneCards (<https://genecards.weizmann.ac.il/v3/>), “COVID-19” and “SAR-Cov-2” were used to be the key words to obtain the disease gene targets, and COVID-19-related genes were screened from genecard with relevance score  $\geq 5$  as the threshold, relevance score is a comprehensive evaluation of the association between genes and research diseases. We also imported the 13 Chinese materia herbs of *Xuanfei Baidu granule* (XFBD) into genecards to obtain drug gene targets. The drug gene targets and the disease gene targets were combined through the venny website to obtain intersection gene targets.

### Xuanfei Baidu granule treatment of COVID-19 interaction protein targets (Protein-Protein Interaction) network building

The STRING database was used to analyze the protein-protein interaction (PPI) of *Xuanfei Baidu granule* (XFBD) in the treatment of COVID-19. STRING database covers the majority of known human protein-protein interaction information (Szklarczyk et al., 2019). In order to further clarify the interaction between potential protein targets, all potential therapeutic protein targets of XFBD on COVID-19 were imported into Cytoscape 3.7.1 to analyze (Shannon et al., 2003), we defined the protein type as “Homo sapiens”, and obtained relevant information on protein interactions by STRING database. Finally, the network topology parameters

were analyzed by Cytoscape 3.7.1, and the hub protein targets were screened out according to the criterion that the node degree value and the betweenness center value were greater than the average value.

### The gene target enrichment analysis

The interaction gene targets were used in DAVID database for gene ontology (GO) functional annotation and Kyoto Encyclopedia of Genes and Genomes (KEGG) enrichment analysis. We obtained the molecular function (MF), cellular component (CC) and related biological process (BP) of the gene targets through GO enrichment. The disease-related targets obtained from screening were input into the DAVID database by entering the list of target gene names and selecting the species as “homo sapiens” (Huang Da et al., 2009). In this study, KEGG pathway enrichment analysis was performed on the relevant signaling pathways involved in the target, and gene target screening was performed under the condition of  $p < 0.05$ . The main biological processes and signaling pathways of *Xuanfei Baidu Granules* (XFBD) on COVID-19 were analyzed. This study visualized the results of GO enrichment and KEGG enrichment by the Omicshare Tools platform (Cao et al., 2022).

### Network diagram of “Disease-core target gene-drug”

Cytoscape 3. 7. 1 network map software was used to construct a disease-core target gene-drug network and conduct topological analysis. The core gene targets can be screened based on the node degree value greater than two times the median (Cao et al., 2022).

### Component target molecular docking and validation of the docking protocol

Molecular docking was used to study the molecular affinity of *Xuanfei Baidu granule* (XFBD) small-molecule potent antiviral compounds with COVID-19 protein targets. The protein crystal structure used for docking was downloaded from the PDB database, and the 3D structure of the small molecule was downloaded from the PUBCHEM database, and energy minimization was performed under the MMFF94 force field. In this study, AutoDock Vina 1.1.2 software was used for molecular docking work. Before docking, PyMol 2.5 was used to process all receptor proteins, including removal of water molecules, salt ions and small molecules (Kim et al., 2016). Then set up the docking box, use the PyMol plugin center of mass.py to define the center of the docking box based on the

position of the crystal ligand, and set the box side length to 22.5 angstroms. In addition, ADFRsuite 1.0 was used to convert all processed small molecules and receptor proteins into the PDBQT format necessary for docking with AutoDock Vina 1.1.2. When docking, the exhaustiveness of the global search is set to 32, and the rest of the parameters remain the default settings. The output highest scoring docked conformation was considered to be the binding conformation for subsequent molecular dynamics simulations (Kim et al., 2016). The study used the original crystal ligand of the protein target as a positive reference, and we analyzed and compared the binding posture of the original crystal ligand and protein, the chemical bond length and the chemical bond angle by re-docking the original crystal ligand and protein. Finally, the consistency of the binding mode can indicate the correctness of the molecular docking protocol (Cao et al., 2022).

## Molecule dynamics

The highest scoring conformations determined by molecular docking analysis were further validated by running 50ns molecular dynamics simulations. Molecular dynamics (MD) simulation is a comprehensive set of molecular simulation methods combining physics, mathematics and chemistry. This method mainly relies on Newtonian mechanics to simulate the motion of molecular systems, we calculate macroscopic properties such as thermodynamic quantities of a system by taking samples from an ensemble of different states of a molecular system.

In this study, all-atom molecular dynamics simulations were performed based on the small molecule and protein complexes obtained from the molecular docking results as the initial structure, and the simulations were performed using AMBER 18 software (Maier et al., 2015). The charge of the small molecule was calculated in advance by the antechamber module and the Hartree-Fock (HF) SCF/6-31G\* of the gaussian 09 software before the simulation. Afterwards, small molecules and proteins were described using the GAFF2 small molecule force field and the ff14SB protein force field, respectively. Each system used the LEaP module to add hydrogen atoms to the system, added a truncated octahedral TIP3P solvent box at a distance of 10 Å, and added Na<sup>+</sup>/Cl<sup>-</sup> to the system to balance the system charge (Harrach and Drossel, 2014). Finally, the simulated topology and parameter files were exported.

Ligands were parameterized using a generic amber force field (GAFF) using a combination of AmberTools18 and ACPYPE 51 protocols (Wang et al., 2006). After the initial addition of hydrogen atoms to each system, the system uses the steepest descent algorithm for vacuum minimization. Solvent was then added and the system ions were equilibrated using counter ions (Na<sup>+</sup>/Cl<sup>-</sup>). The proteins were all energy minimized using the steepest descent method and the conjugate gradient

method. This was followed by an NVT and NPT ensemble (1000 ps, dt of 2 fs) and an MD run (100 ns, dt of 2 fs) at 298 K temperature and 1 bar pressure using the skip integrator algorithm. The coordinates and energy of the system are saved every 10 ps. Finally, 50ns production simulations were carried out for each system under periodic boundary conditions. For all simulations, the van der Waals force (vdw) cutoff and short-range electrostatic interactions were set to 10 Å. The Particle-Mesh-Ewald (PME) method is used to evaluate long-range electrostatic interactions. Molecular dynamics simulation trajectories include protein-ligand complex root mean square deviation (RMSD), root mean square fluctuation (RMSF), radius of gyration and solvent accessible surface area (SASA).

## MMGBSA binding free energy calculation

The binding free energy was investigated using the MM-PBSA method, and the conformational stability was studied in detail. The binding free energies between proteins and ligands for all systems were calculated by the MM/GBSA method (Hou et al., 2011). The molecule dynamics trajectory of 50 ns was used for calculation, and the specific formula is as follows:

$$\begin{aligned}\Delta G_{\text{bind}} &= \Delta G_{\text{complex}} - (\Delta G_{\text{receptor}} + \Delta G_{\text{ligand}}) \\ &= \Delta E_{\text{internal}} + \Delta E_{\text{VDW}} + \Delta E_{\text{elec}} + \Delta G_{\text{GB}} + \Delta G_{\text{SA}}\end{aligned}$$

In the formula,  $E_{\text{internal}}$  represents internal energy,  $E_{\text{VDW}}$  represents van der Waals interaction and  $E_{\text{elec}}$  represents electrostatic interaction. The internal energy includes bond energy ( $E_{\text{bond}}$ ), angular energy ( $E_{\text{angle}}$ ) and torsional energy ( $E_{\text{torsion}}$ ); GGB and GGA are collectively referred to as solvation free energy, where GGB is the polar solvation free energy and GGA is the non-polar solvation free energy. For this paper, the GB model developed by Nguyen was used for calculation ( $\text{igb} = 2$ ). The non-polar solvation free energy (GSA) was calculated based on the product of surface tension ( $\gamma$ ) and solvent accessible surface area (SA),  $\text{GSA} = 0.0072 \times \text{SASA}_{15}$ . The entropy change is ignored in this study due to high computational resource consumption and low precision (Cao et al., 2022).

## Results

### Identification of potentially active compounds in *Xuanfei Baidu granule*

In total, 178 potential compounds in *Xuanfei Baidu granule* (XFBD) were retrieved from the TCMSP database with the criteria of  $\text{DL} \geq 0.18$  and  $\text{OB} \geq 30\%$ , by further improving the OB score ( $\text{OB} \geq 74\%$ ), five core active compounds in XFBD were screened out, shown in Table 1.

**TABLE 1** The core active compounds in *Xuanfei Baidu Granules* (XFBD) Binding free energies and energy components.

MOL_ID	Molecule Name	OB	MW	Alogp	Caco2	BBB	DL
MOL013287	Physovenine	106.219	262.34	2.08	0.50	0.20	0.18
MOL012922	I-SPD	87.34	327.41	3.09	0.75	0.20	0.54
MOL007207	Machiline	79.64	285.37	2.82	0.78	0.08	0.23
MOL005890	pachypodol	75.06	356.40	2.99	0.83	0.11	0.39
MOL000500	Vestitol	74.65	272.32	3.14	0.85	0.29	0.20

OB, oral bioavailability.  
MW, molecular weight.  
BBB, blood brain barrier.  
DL, drug similarity.

### Obtained common gene targets by intersection

We obtained 1308 *Xuanfei Baidu granule* (XFBD) gene targets and 4600 COVID-19 gene targets. A total of 548 intersection gene targets were processed by Venny, shown in Figure 1.

### Core intersection target screening and PPI network diagram

We obtained intersection genes targets of relevance score through GeneCards, relevance score $\geq 5$  which were considered as a core intersection gene target, through STRING database analysis of 33 mapping of the core intersection gene targets of COVID-19 and XFBD, the study constructed the PPI network interaction map of the target protein of XFBD in the treatment of COVID-19, shown in Figure 2A. 11 core genes (such as CSF2, IFNG, NLRP3, etc.) were obtained by setting the interaction score (confidence degree $>0.95$ ), and the study used the 11 core gene targets to reconstruct the core PPI network, shown in Figure 2B.

### GO and KEGG enrichment analysis

The 33 intersection gene targets were imported into the DAVID database for enrichment analysis. Under the condition of  $p<0.05$ , the GO enrichment analysis yielded a total of 277 GO entries, including 239 BP entries, 23 CC entries, and 15 MF entries. According to the number of targets contained, the top 10 BP, CC and MF compressions were screened. The results showed that in biological processes, biological processes were highly correlated with inflammation and viral replication, mainly involving the cytokine-mediated signaling pathway, inflammatory response, and immune response. Among cell components, extracellular space, extracellular region and cell surface account for a relatively large amount. In molecular functions, cytokine activity, protein binding and receptor

binding are relatively high, shown in Figures 3A–F. KEGG pathway analysis yielded 72 pathways with  $p<0.05$ . According to the number of targets contained, the first 15 pathways were screened. The results showed that the enriched pathways involved multiple pathways related to inflammation and immune response, mainly coronavirus disease COVID-19, influenza A, cytokine-cytokine receptor interaction and other signaling pathways, shown in Figures 3G, H.

### Disease-core gene target-drug network

The disease-core gene target-drug network was constructed to show the main signal pathway and biological process of *Xuanfei Baidu granule* (XFBD) in the treatment of COVID-19, shown in Figure 4.

### Molecular docking

The 11 core intersection gene targets were selected for molecular docking. The stability of receptor-ligand binding depends on the binding energy. The lower the binding energy of the complex, the more stable the receptor-ligand binding conformation. The results show that the binding of CSF2/I-SPD complex is mainly maintained by hydrogen bonding and hydrophobic interaction. For example, I-SPD can form hydrogen bonding with GLN-43 on CSF2 protein, and also with TYR-71, LEU-42, ILE-104, PRO-105 forms a hydrophobic interaction, shown in Figure 5A. The binding of CSF2/Vestitol complex is mainly through hydrophobic interaction, for example, the small molecule Vestitol and PRO-76, LEU-42, TYR-71, ILE-104, PRO-105 on the protein form hydrophobic interaction, shown in Figure 5B. In the NLRP3/I-SPD binding complex, the small molecule I-SPD forms hydrogen bonds with GLN-468, SER-470, ALA-72, and also with VAL-197, GLU-473, LEU-472, TYR-476, PHE -419 forms a hydrophobic interaction. In addition, we also observed that I-SPD and ARG-422 form cationic pi conjugation, shown in Figure 5C. The binding of NLRP3/Pachypodol suggested that the small molecule





FIGURE 1

Intersection targets-active ingredient networks. Targets of the intersection of *Xuanfei Baidu granule* (XFB) and COVID-19.

Pachypodol forms hydrogen bonds with VAL-197, GLU-200 and GLU-213, and also forms hydrophobic interactions with LEU-199 and PRO-196 on the protein, shown in Figure 5D, molecular docking result scores are shown in Figure 6.

## Molecular dynamics results

The root mean square partiality of molecular dynamics simulation is used to reflect the movement process of the complex. The larger the RMSD value of the complex, the more severe the fluctuation and the more intense the movement. On the contrary, the movement is stable. The RMSD of the four systems gradually converged in the first 5 ns of the simulation, and kept stable fluctuations in the subsequent simulations. It is suggested that the motion of the four complexes is stabilized

after the combination of the kinetics. In comparison, CSF2/Vestitol (red line) has the lowest RMSD, followed by NLRP3/I-SPD, then CSF2/I-SPD, and finally NLRP3\_Pachypodol, indicating that the stability of these complexes is CSF2/I-SPD, CSF2/Vestitol, NLRP3/I-SPD, NLRP3/Pachypodol. However, it is worth emphasizing that the RMSD results of all complexes suggest that small molecules can bind to proteins and maintain a relatively stable state. The results are shown in Figure 7.

## Combined free energy calculation results

Based on the trajectory of the molecular dynamics simulation, we calculated the binding energy using the MMGBSA method, which can more accurately reflect the binding mode of small molecules and target proteins. The

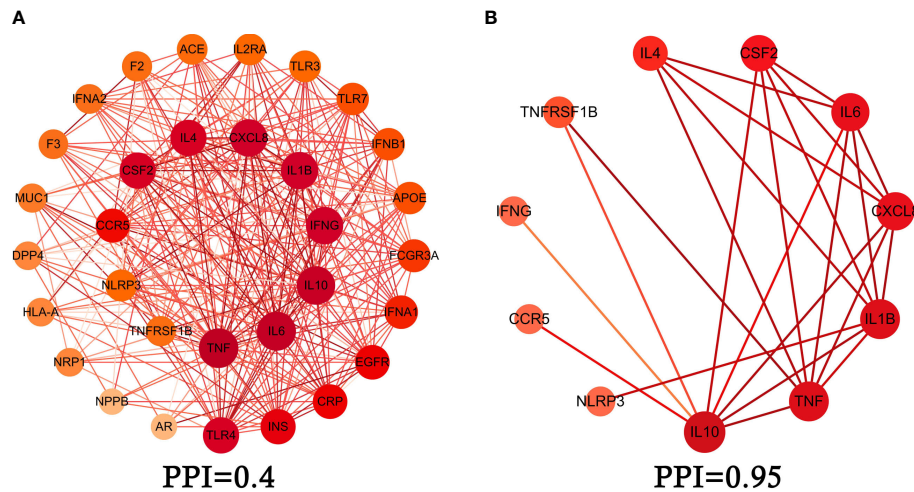


FIGURE 2  
Protein-protein interaction (PPI) network. (A) PPI network of protein target, (B) PPI network of core protein target (confidence>0.95).

binding energies of CSF2/I-SPD, CSF2/Vestitol, NLRP3/I-SPD, and NLRP3\_Pachypodol complexes were  $-20.89 \pm 1.32$  kcal/mol,  $27.57 \pm 2.78$  kcal/mol,  $-30.52 \pm 1.17$  kcal/mol, and  $-21.65 \pm 3.36$  kcal/mol. The negative values indicate that both molecules have binding affinity for the target protein, and lower value indicate stronger binding. Obviously, our calculations show that these molecules and the corresponding proteins have a certain binding affinity and are very strong. Among them, NLRP3/I-SPD and CSF2/Vestitol have higher binding energies. For the binding energy of the NLRP3/I-SPD complex, the energy decomposition shows that the van der Waals energy is the main contribution energy. For the binding energy of the CSF2/Vestitol complex, the energy decomposition shows that the electrostatic energy is the main contribution energy. The experimental results are shown in Table 2.

## Hydrogen bond analysis

Hydrogen bonds are one of the strongest non-covalent binding interactions. The more the number, the better the binding. The results suggest that the number of hydrogen bonds between small molecules and NLRP3 is significantly more than the number of hydrogen bonds with CSF2. Combining the above binding modes, we can see that the number of hydrogen bonds is small. The interaction of molecules and NLRP3 may be dominated by hydrogen bonding, especially the NLRP3/I-SPD complex with the strongest binding energy. The interaction of small molecules with CSF2 may not mainly occur through hydrogen bonding, but through hydrophobic interaction. The results are shown in Figure 8.

## The stability of the target protein at the residue level

To explore the local fluctuations of macromolecular proteins at the residue level, the vibrations of each residue after compound binding were explored as root mean square fluctuations (RMSF). RMSF can reflect the flexibility of proteins during molecular dynamics simulations. Usually, after the drug binds to the protein, the flexibility of the protein decreases, thereby achieving the effect of stabilizing the protein and exerting the effect of enzymatic activity. The RMSF of the CSF2 and NLRP3 proteins after binding different small molecules is generally low, indicating that the protein as a whole has good rigidity, shown in Figure 9. It is worth noting that for CSF2, the decrease in RMSF after the binding of Vestitol small molecule indicates a significant decrease in protein rigidity; however, for NLRP3, the effect of I-SPD and Pachypodol on protein RMSF was not different.

## Analysis of the radius of gyration

The radius of gyration (Rg) reflects the compactness of the embodiment and can reflect the degree of binding of the system. For the CSF2 protein, the Rg after combining two small molecules acts at 13.7 angstroms; for the NLRP3 protein, the compactness after combining the small molecules is about 23.8 angstroms. The overall values are low, implying that the system is denser and more closely combined. It is worth mentioning that the CSF2 protein is smaller, and the Rg of CSF2 is smaller than that of NLRP3, the results are shown in Figure 10.

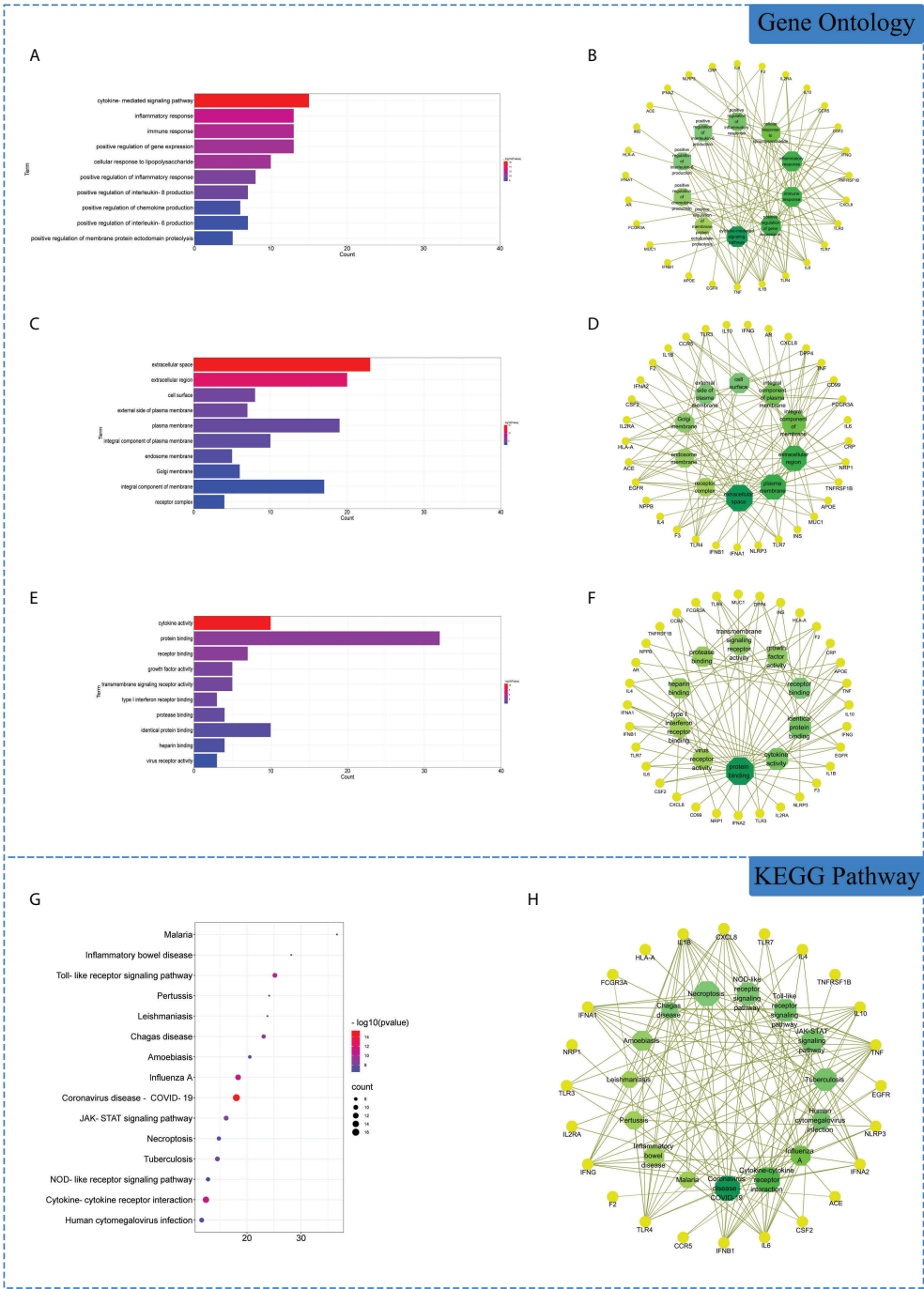


**FIGURE 3** Gene Ontology (GO) and Kyoto Encyclopedia of Genes and Genomes (KEGG) analysis of related genes. **(A)** The top 10 terms in biological processes (BP) were greatly enriched. **(B)** The subnetwork displayed the first 10 BP terms and related genes. **(C)** The top 10 terms in cellular components (CC) were greatly enriched. **(D)** The subnetwork displayed the first 10 CC terms and related genes. **(E)** The top 10 terms in molecular function (MF) were greatly enriched. **(F)** The subnetwork displayed the first 10 MF terms and related genes. **(G)** The first 15 KEGG pathways were showed. **(H)** the subnetworks displayed the first 15 KEGG pathways and related.

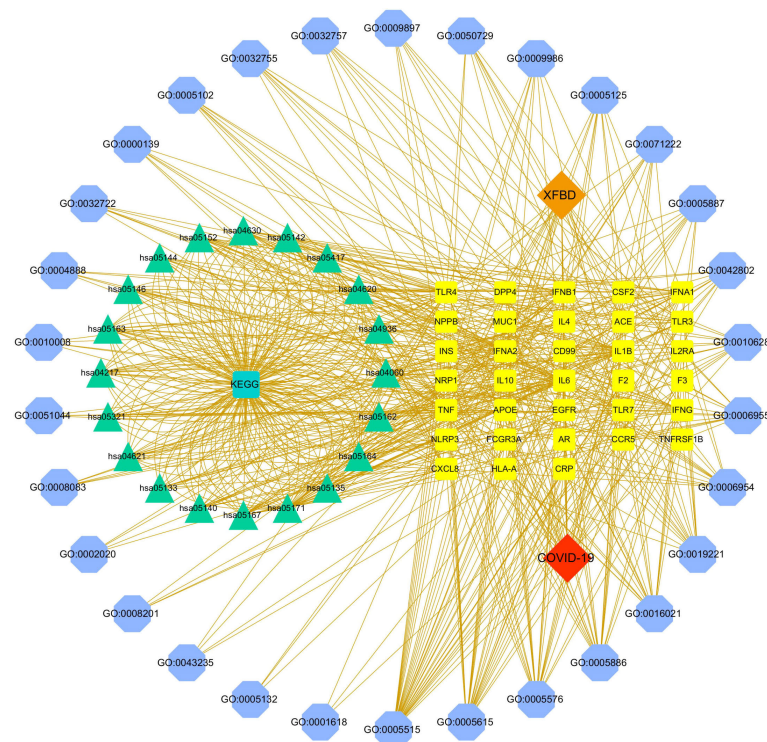


FIGURE 4

Disease-core gene target-drug network. Square nodes represent gene targets, triangular nodes represent signaling pathways (KEGG), and octagonal nodes represent gene ontology (GO) of related genes.

## Analysis of solvent accessible surface area

Solvent accessible surface area is calculated as the interface surrounded by solvent. This solvent behaves differently under different conditions and is therefore a useful parameter for studying protein conformational dynamics in a solvent environment. The contact area between the four complexes and water is similar, and the small molecule has little effect on the effect of protein and water, the results are shown in Figure 11.

## Discussion

This study explored the pharmacological mechanism of *Xuanfei Baidu granule* (XFB) in the treatment of COVID-19 by molecular docking and molecular dynamics simulation based on molecular system movement. For the first time, it was found that the important active chemical components I-SPD and Pachypodol in XFB could reduce the inflammatory response and apoptosis by inhibiting the activation of NLRP3, and reduce the production of inflammatory response. And I-

SPD and Vestitol could inhibit the activation and chemotaxis of inflammatory cells through CSF2, prevent the generation of inflammatory storm. Therefore, Vestitol, Pachypodol and I-SPD in XFB could effectively treat COVID-19 through NLRP3 and CSF2 and reduce the clinical symptoms of patients.

## Bioinformatics analysis of XFB

Pachypodol, I-SPD and Vestitol in XFB play a role in treating COVID-19 by acting on NLRP3, CSF2, and relieve the clinical symptoms of SAR-Cov-2 infection.

Pachypodol and I-SPD reduce inflammation and apoptosis by inhibiting the activation of NLRP3, thereby exerting protective effects on the respiratory and nervous systems of patients. Analysis of protein interaction network PPI suggested that NLRP3 was closely related to viral infections and inflammatory responses targets, GO analysis results suggest that NLRP3 is mainly located in extracellular space, KEGG pathway analysis found that NLRP played a role in coronavirus disease COVID-19, influenza A and other pathways. The analysis results suggest that the SARS-CoV 3a



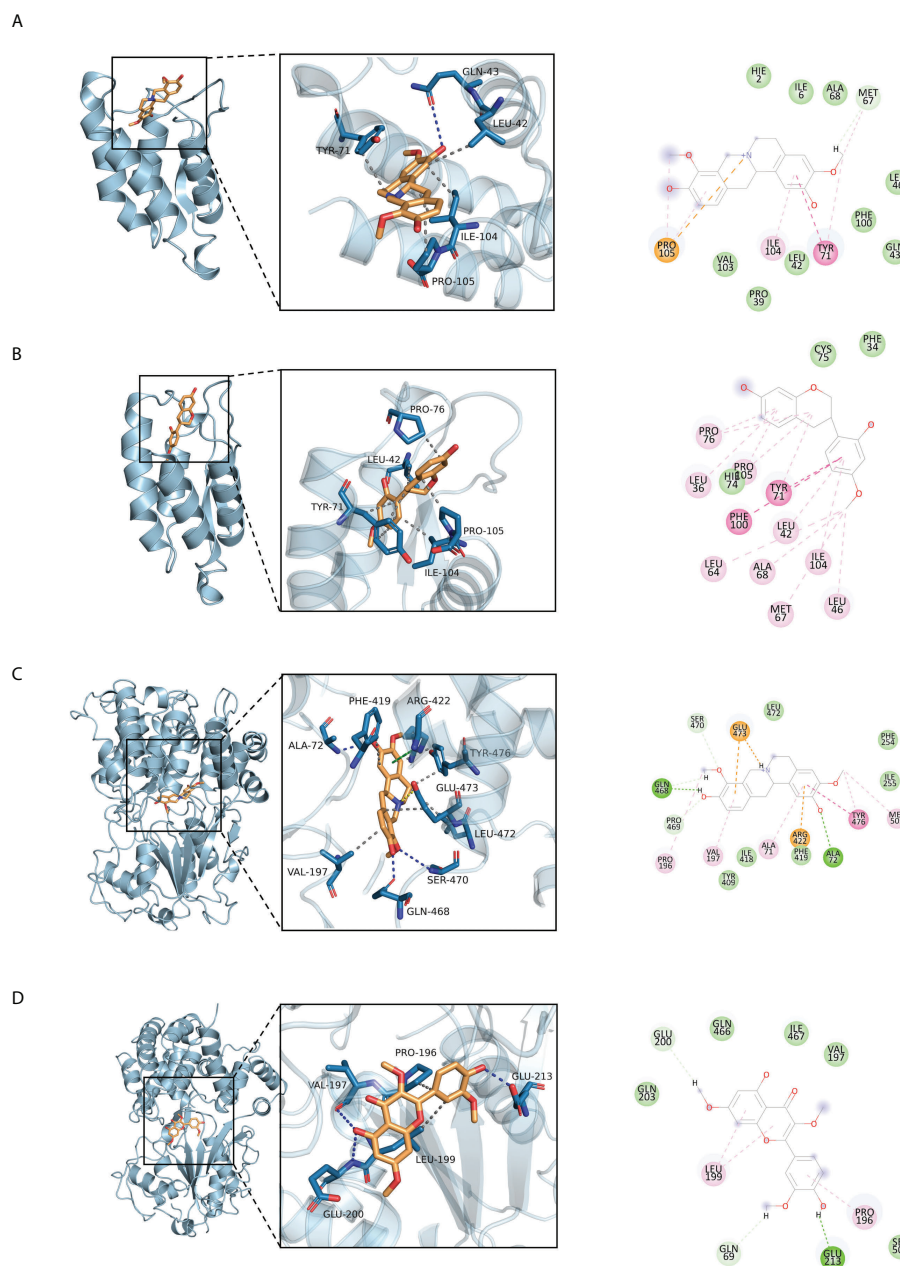


FIGURE 5

Molecular docking of active ingredients and core targets. (A) CSF2/I-SPD, (B) CSF2/Vestitol, (C) NLRP3/I-SPD, (D) NLRP3/Pachypodol.

protein, as a transmembrane pore-forming viral protein, can activate the NLRP3 inflammasome by forming ion channels in macrophages. At the same time, NLRP3 is found to play a role in pathways such as influenza A, and the inflammasome NLRPS can induce the production of the inflammatory cytokine IL-10 in host cells, resulting in an inflammatory cytokine storm.

Inflammatory cytokine storms can cause acute respiratory distress syndrome (ARDS) and acute lung injury (ALI).

Vestitol and I-SPD mainly act on CSF2 to suppress cytokine storm and infiltration of immune cells. CSF2 was closely related to inflammatory targets in PPI. GO analysis results suggest that CSF2 is mainly located in extracellular region. KEGG pathway

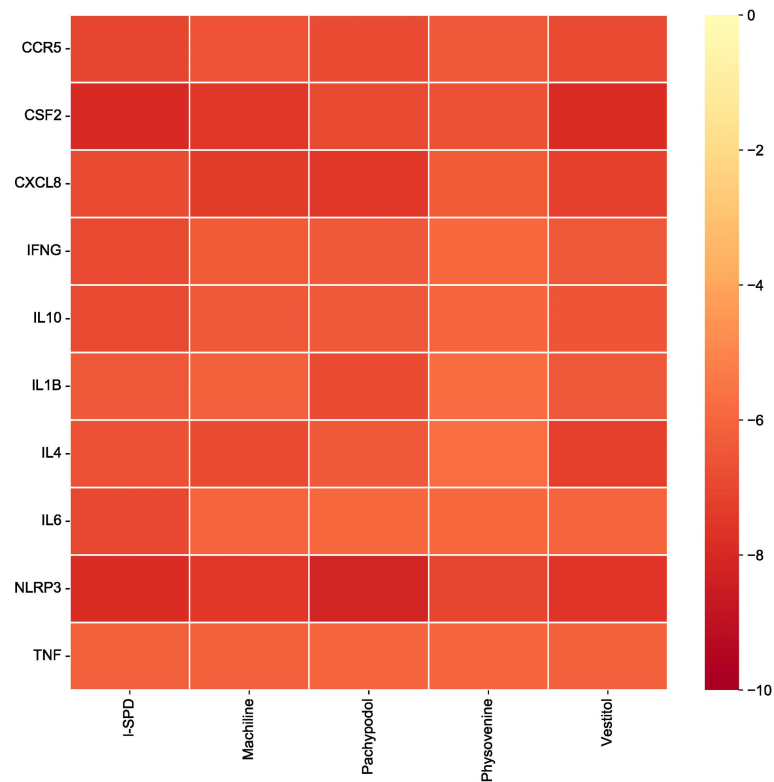


FIGURE 6  
Screening docking results between ligands and receptors.

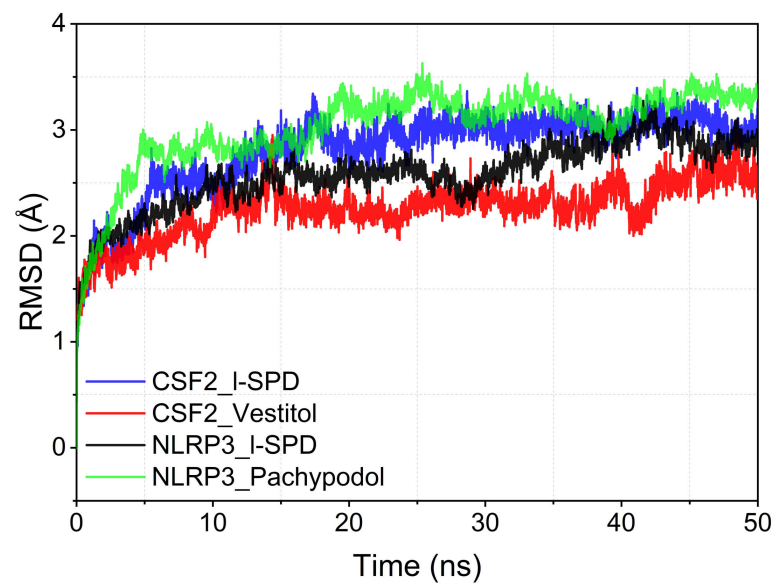


FIGURE 7  
Complex root mean square deviation (RMSD) difference over time. ns, nanosecond.

TABLE 2 Binding free energies and energy components predicted by MM/GBSA (kcal/mol).

System name	CSF2/I-SPD	CSF2/Vestitol	NLRP3/I-SPD	NLRP3/Pachypodol
$\Delta E_{vdw}$	$-31.85 \pm 0.83$	$-35.21 \pm 1.70$	$-39.13 \pm 4.72$	$-26.90 \pm 1.87$
$\Delta E_{elec}$	$-74.07 \pm 6.98$	$1.43 \pm 2.49$	$-77.18 \pm 10.66$	$-15.70 \pm 5.59$
$\Delta G_{GB}$	$88.70 \pm 7.47$	$10.83 \pm 2.40$	$90.77 \pm 6.69$	$24.61 \pm 4.35$
$\Delta G_{SA}$	$-3.67 \pm 0.11$	$-4.63 \pm 0.15$	$-4.97 \pm 0.18$	$-3.65 \pm 0.23$
$\Delta G_{bind}$	$-20.89 \pm 1.32$	$27.57 \pm 2.78$	$-30.52 \pm 1.17$	$-21.65 \pm 3.36$

$\Delta E_{vdw}$ : van der Waals energy.  
 $\Delta E_{elec}$ : electrostatic energy.  
 $\Delta G_{GB}$ : electrostatic contribution to solvation.  
 $\Delta G_{SA}$ : non-polar contribution to solvation.  
 $\Delta G_{bind}$ : binding free energy.

analysis found that CSF2 played a role in cytokine-cytokine receptor interaction and other pathways. CSF2 can be seen as an attractive mediator. CSF2 is produced as a pro-inflammatory cytokine by many cells, including macrophages, T cells, endothelial cells, and epithelial cells. CSF2 can control the production and differentiation of granulocytes and macrophages, and CSF2 has the effect of promoting tissue inflammation

However, the current bioinformatic analysis results can only predict potential relationships between drugs and gene targets and proteins. Therefore, the use of molecular docking and

molecular dynamics in this study can verify the potential relationship of XFBD in the treatment of COVID-19.

### Analysis of molecular docking and molecular dynamics

There is a strong affinity between active ingredient of medicine (such as Pachypodol, I-SPD and Vestitol) and the protein targets (such as NLRP3 and CSF2) through molecular docking tests. Molecular dynamics suggest that they can

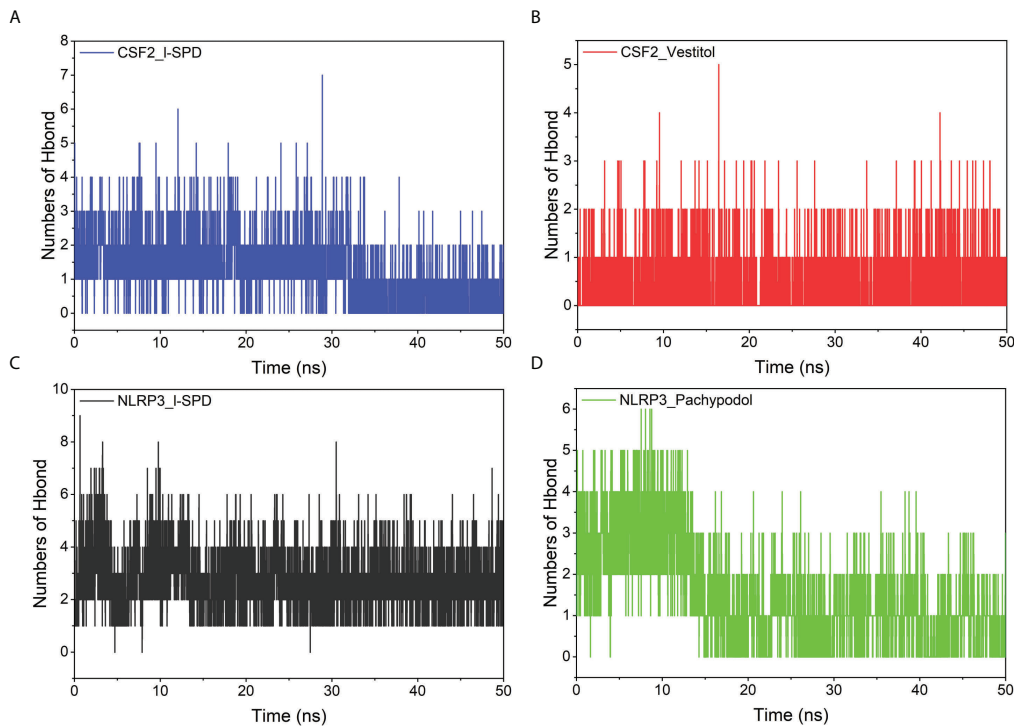


FIGURE 8  
Changes in the number of hydrogen bonds between small molecule ligands and protein receptors in complex system simulations (A) CSF2/I-SPD, (B) CSF2/Vestitol, (C) NLRP3/I-SPD, (D) NLRP3/Pachypodol.

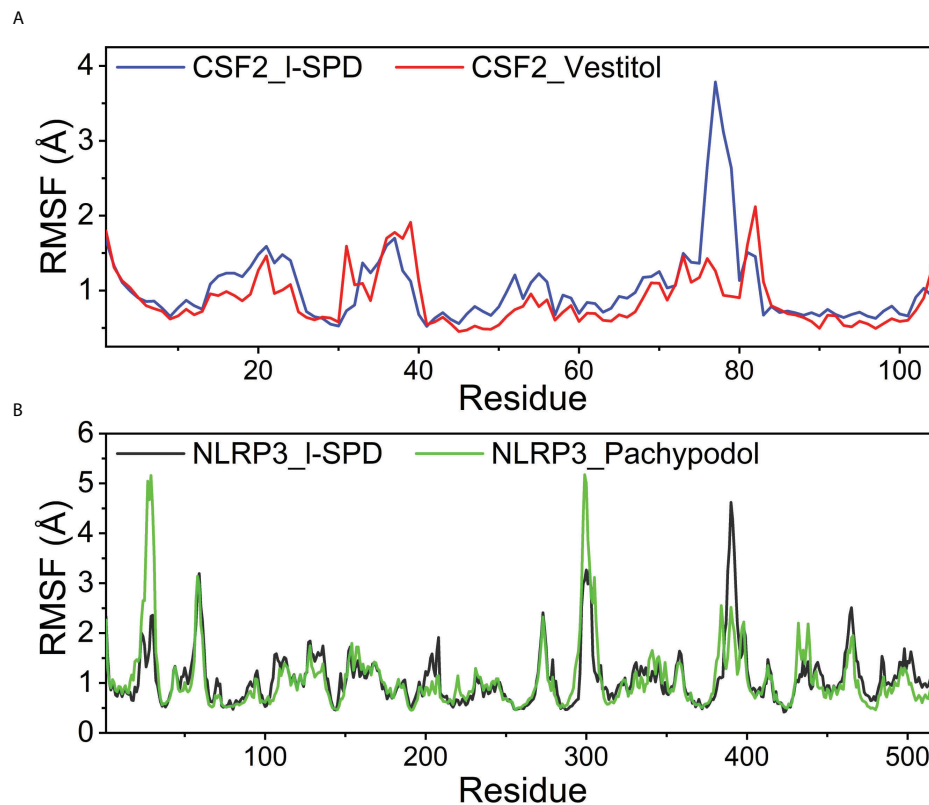


FIGURE 9  
Changes in the stability of protein targets at the residue level (A) CSF2/I-SPD and CSF2/Vestitol. (B) NLRP3/I-SPD and NLRP3/Pachypodol.

maintain a very stable binding state, and then play a pharmacological role in the treatment of COVID-19.

I-SPD could stably act on NLRP3 and CSF2, especially NLRP3/I-SPD showed strong stability. Molecular docking showed that the binding energies of small molecules to NLRP3 and CSF2 reached -7.9 and -8.0. Based on the trajectory of the molecular dynamics simulation, we calculated the binding energy using the MMGBSA method, which could more accurately reflect the binding mode of small molecules and target proteins. The binding free energy results showed NLRP3/I-SPD and CSF2/I-SPD were  $-39.13 \pm 4.72$  kcal/mol and  $-31.85 \pm 0.83$  kcal/mol, for the binding energy of the NLRP3/I-SPD complex, the energy decomposition showed that the van der Waals energy was the main contributing energy. In the molecular dynamics simulation, the RMSDs of NLRP3/I-SPD and CSF2/I-SPD both converged gradually in the first 5 ns of the simulation and preserved stable fluctuations in subsequent simulations, implying that the kinetics of the four complexes are stabilized after binding, and CSF2/I-SPD binding was more stable than NLRP3/I-SPD. NLRP3/I-SPD binding results suggested that small molecule I-SPD forms hydrogen bonds with GLN-468, SER-470, ALA-72, and also formed with VAL-197, GLU-473, LEU-472, TYR-476, PHE-419 Hydrophobic interaction.

The binding of Pachypodol to NLRP3 is relatively stable, molecular docking showed that the binding energies of small molecules to NLRP3 reached -8.2. The binding free energy results show NLRP3/Pachypodol was  $-26.90 \pm 1.87$  kcal/mol. The number of hydrogen bonds of NLRP3/Pachypodol is relatively stable. The high fluctuation of residues in NLRP3/Pachypodol may be due to the influence of its own multiple peptide chains. NLRP3/Pachypodol binding results suggested that small molecule Pachypodol formed hydrogen bonds with VAL-197, GLU-200, GLU-213, and also formed with LEU-199 and PRO-196 Hydrophobic interaction.

Vestitol combined with CSF2 can form stable complex, but there were some abnormal fluctuations, which may be due to the influence of the number and angle of binding bonds. molecular docking showed that the binding energies of small molecules to CSF2 reached -7.9. The binding free energy results showed CSF2/Vestitol was  $-35.21 \pm 1.70$  kcal/mol, for the binding energy of the CSF2/Vestitol complex, the energy decomposition showed that electrostatic energy was the main contributing energy. We found that RMSF decreased after CSF2 bound to the small molecule Vestitol, suggesting that protein rigidity was significantly decreased. CSF2/Vestitol binding

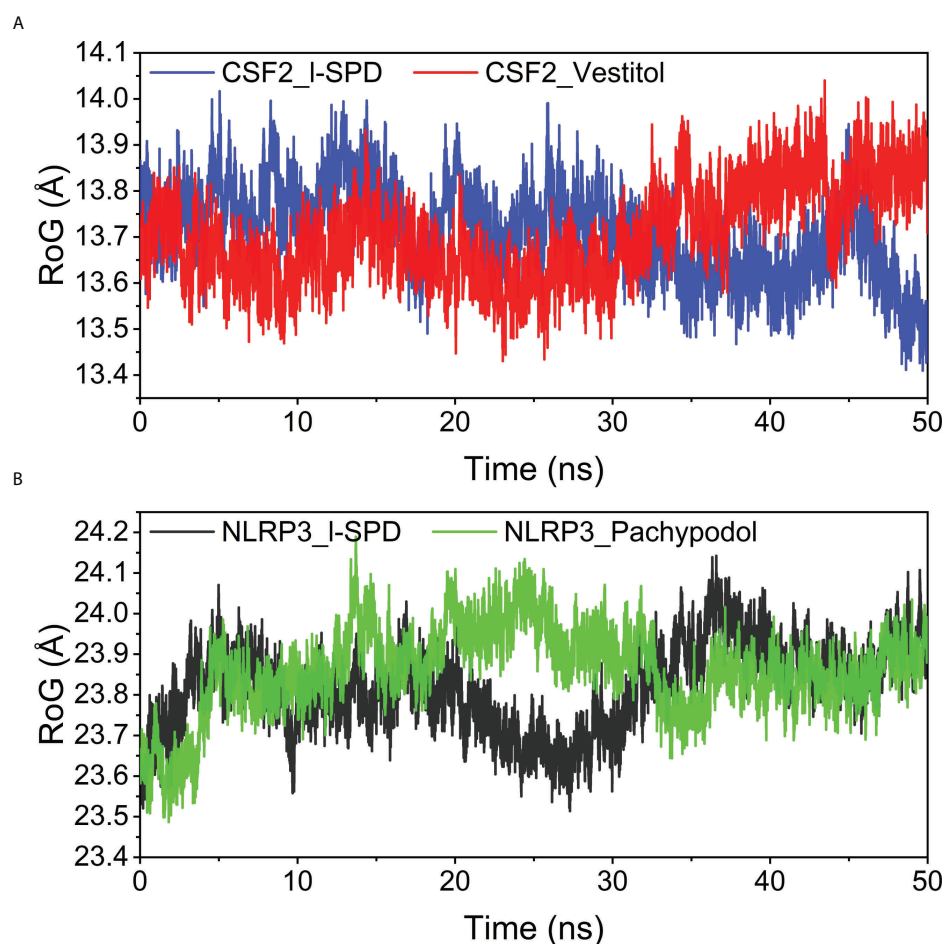


FIGURE 10

Analysis of protein folding state and overall conformation (A) CSF2/I-SPD and CSF2/Vestitol. (B) NLRP3/I-SPD and NLRP3/Pachypodol. ns, nanosecond.

results suggested that PRO-76, LEU-42, TYR-71, ILE-104, PRO-105 on small molecules and proteins form hydrophobic interactions.

We presented the microscopic evolution process of the complex system from the level of small molecules and protein residues through molecular docking and molecular dynamics. Computer simulations visualized the binding states of NLRP3/I-SPD, CSF2/I-SPD, NLRP3/Pachypodol and CSF2/Vestitol. The simulation results showed that the combination of the four complexes can remain relatively stable in the kinetic simulation, thus providing theoretical support for the role of small molecule drugs.

There are certain differences between Xuanfei Baidu granule (XFBD) and traditional single small molecule drugs in the treatment of COVID-19 (Choudhury et al., 2021; Yan et al., 2021). Because Xuanfei Baidu granule (XFBD) as a traditional Chinese medicine compound contains thousands of active small molecules, XFBD can treat diseases through

multiple small molecular components acting on multiple disease-related target proteins, while reducing the adverse drug reactions. Therefore, molecular docking and molecular dynamics can be used to more deeply and objectively study the mechanism of action of small molecules in XFBD that coordinate and interact with each other to treat COVID-19. Some studies have used network pharmacology methods to enrich the targets and pathways of traditional Chinese medicines (such as: Lung Cleansing and Detoxifying Decoction (LCDD)) and explore their therapeutic effects on COVID-19 (Xu et al., 2021). This study not only analyzed and drew on relevant network pharmacology research results, but also used the supercomputer platform to simulate the relationship between small molecule drugs and protein targets through molecular dynamics. For example, molecular dynamics can show the movement stable between small molecule drugs and protein targets. The root mean square deviation partiality (RMSD) of molecular

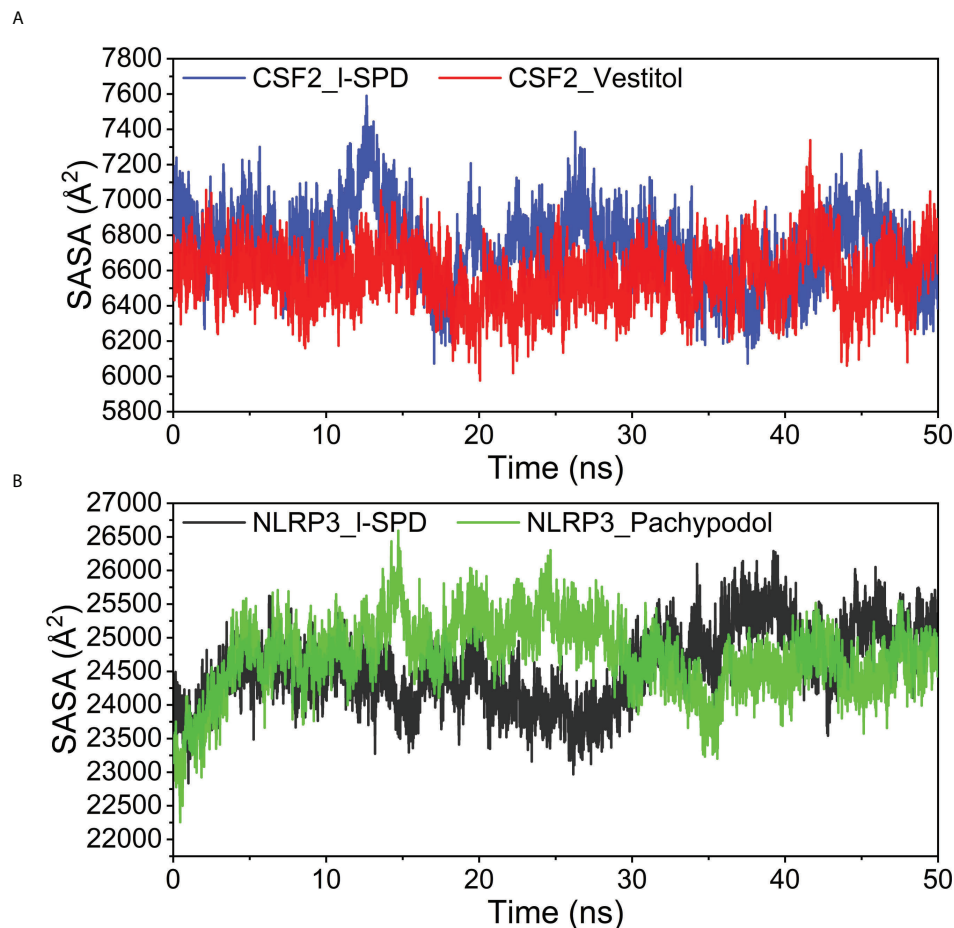


FIGURE 11 Analysis of Solvent Accessible Surface Area (SASA) (A) CSF2/I-SPD and CSF2/Vestitol. (B) NLRP3/I-SPD and NLRP3/Pachypodol. ns, nanosecond.

dynamics simulation can reflect the movement process of the complex.

Therefore, the results of this study could further explain the mechanism of action and related signaling pathways of XFBD in the treatment of COVID-19.

## Pachypodol and I-SPD can reduce inflammation and apoptosis through NLRP3

As an essential component of the innate immune system, the NLRP3 inflammasome is important for antiviral host defense, and its abnormal activation can lead to pathological tissue damage during infection.

The NLRP3 inflammasome is a high molecular weight protein complex composed of the upstream sensor protein NLRP3 and the downstream effector protein caspase-1 (Lamkanfi and Dixit, 2012). When caspase-1 is activated, it

promotes the activation of cytokines IL-1 $\beta$  and IL-18 (Mangan et al., 2018), which eventually leads to cell rupture and apoptosis (Liu et al., 2016; Orning et al., 2019; Liu et al., 2020). During COVID-19, the NLRP3 inflammasome is overactivated (Ratajczak et al., 2021), leading to the production of IL-1 $\beta$ /18 and promoting cytokine storm (Lin et al., 2019). Viruses are stimulators of cytokine release syndrome development (Tisoncik et al., 2012). Cytokine storm usually causes patients to express clinical symptoms such as fever, hypotension, and hypoxemia (Shimabukuro-Vornhagen et al., 2018). Elevated levels of IL-1 $\beta$  produced by the NLRP3 inflammasome further activate neutrophils, resulting in increased levels of the neutrophil extracellular traps (NETs) production. High levels of NETs lead to increased clot formation associated with COVID-19 and damage to endothelial and alveolar cells (Zhao et al., 2021b). Activation of NLRP3 requires at least two steps: initiation and activation (Xue et al., 2019). The first step of initiation is activation of the nuclear factor kappa B (NF- $\kappa$ B) signaling pathway (Gritsenko et al., 2020). NF- $\kappa$ B can enhance



the transcription of pro-IL-1 $\beta$ , pro-IL-18 and NLRP3 (Afonina et al., 2017). Moreover, the oligomerization of NLRP3 and the assembly of NLRP3 and pro-caspase-1 into the NLRP3 inflammasome (Strowig et al., 2012), which is mainly composed of adenosine triphosphate (ATP) (Karmakar et al., 2016), oxidized mitochondrial DNA (ox-mtDNA) (Jia et al., 2020), and mitochondrial reactive oxygen species (mtROS) (Zhong et al., 2016) participated in the completion. SARS-CoV-2 can cross the BBB into the central nervous system, directly infect brain tissue, and affect human neural progenitor cells and brain organoids (Zhang et al., 2020).

I-SPD and Pachypodol have the ability to penetrate the blood-brain barrier and inhibit NLRP3-mediated inflammatory responses in the central nervous system. SARS-CoV-2 invades brain tissue in two ways: the hematogenous pathway and the neuronal retrograde pathway. BBB permeability is increased in patients with neurodegenerative diseases, promoting SARS-CoV-2 neuroinvasion (Zubair et al., 2020). NLRP3 is activated by SARS-CoV-2 in the central nervous system, and high levels of peripheral cytokines (such as IL-1 $\beta$  and IL-6) can directly pass through the BBB or reduce BBB integrity (Mohammadi et al., 2020), inducing peripheral leukocytes and monocytes penetration, impairs immune homeostasis in the brain (Heneka et al., 2013; Yan et al., 2020). At the same time, NLRP3 promotes the aggregation of peptides into pathogenic fibrils and the production of inflammatory cytokines, promotes mitochondrial dysfunction and apoptosis (Freeman and Swartz, 2020), and evolves into neurological lesions.

Therefore, we believe that I-SPD and Pachypodol can reduce the inflammatory response and apoptosis caused by the new coronavirus by acting on NLRP3, thereby exerting a protective effect on the respiratory and nervous systems of patients.

## Vestitol and I-SPD prevent the generation of inflammatory storm and the infiltration of immune cells by inhibiting the overexpression of CSF2

Colony-stimulating factor 2 (CSF2), also known as granulocyte-macrophage colony-stimulating factor (GM-CSF) (Damiani et al., 2020). CSF2 is produced and secreted by many different types of cells, mainly monocytes, macrophages and eosinophils (Hamilton and Anderson, 2004), and normally regulates inflammatory responses and immune activation (Shi et al., 2006).

CSF2 can induce the survival and activation of macrophages and neutrophils, promote the maturation of alveolar macrophages, and play the functions of phagocytosis and killing of viruses (Mehta et al., 2015). The transcription factor PU.1 potentiates the promoting effect of CSF2 on the maturation of alveolar macrophages (Berclaz et al., 2007). Elevated levels of

CSF2 in alveolar macrophages stimulate the production of reactive oxygen species (ROS). CSF2 affects the activation and proliferation of immune cells (Hamilton, 2008), and plays an important role in maintaining immune homeostasis in lung tissue (Rösler and Herold, 2016).

CSF2 regulates the Th1 immune response by inducing the production of dendritic cells (Wang et al., 2000; Miller et al., 2002). Interestingly, CSF2 can exert protective effects in humans. CSF2 can regulate the metabolism of vascular collagen (Ponomarev et al., 2007; Li et al., 2015; Shiomi and Usui, 2015), promote the proliferation and migration of vascular endothelial cells, thereby contributing to the process of angiogenesis (Tisato et al., 2013), and induce keratinocyte proliferation and migration, which in turn stimulates wound healing (Szabowski et al., 2000; Barrientos et al., 2008). CSF2 has been shown to protect the lung by restoring barrier function and stimulating epithelial cell proliferation (Huang et al., 2011), and the alveolar epithelium exerts a protective effect against oxidative stress-induced mitochondrial damage (Sturrock et al., 2012). However, when SARS-CoV-2 infected lung tissue, CSF2 was one of the most up-regulated genes in the cells. A cohort study demonstrated a positive correlation between CSF2 and disease severity in COVID-19 patients (Zhao et al., 2021c). High levels of CSF2 are found in the blood of severe COVID-19 patients (Wu and Yang, 2020), so CSF2 is a proxy for excessive inflammation in severe COVID-19 patients (Kluge et al., 2020). When CSF2 is overexpressed in the body, activated monocytes induce T cell death, resulting in lymphopenia, pathological hyperinflammatory immune response, pulmonary fibrosis and severe immune cell infiltration (Xing et al., 1996).

The crucial downstream signaling of CSF2R has been shown to involve JAK2/STAT5 (Lehtonen et al., 2002), ERK (Hansen et al., 2008; Achuthan et al., 2018), NF- $\kappa$ B and the phosphoinositide 3-kinase-AKT pathway (Perugini et al., 2010; Van De Laar et al., 2012). CSF2 is regulated by JAK2, and when activated by phosphorylation, regulates the proper differentiation and maturation of macrophages (Notarangelo and Pessach, 2008), and participates in various intracellular signaling pathways such as STAT5 and MAPK (Hansen et al., 2008). Janus kinase (JAK) activates tyrosine kinase, which then phosphorylates STAT3. Phosphorylated STAT3 activates NF- $\kappa$ B and upregulates the expression of inflammatory cytokines, thereby enhancing inflammation, cell damage and fibrosis (Cao et al., 2022). Macrophages repolarize through the CSF2/CSF2R axis to acquire the M1 phenotype (Ao et al., 2017). Mouse experiments confirmed that CSF2-IRF4 signaling can upregulate MHC class II expression (Van Der Borght et al., 2018). CSF2 enhances the antigen-presenting capacity of macrophages by increasing the expression of MHC-II (Ushach and Zlotnik, 2016). CSF2 upregulates IRF4 expression by enhancing JMJD3 demethylase activity (Yashiro et al., 2018), and activated IRF4 can upregulate CCL17 expression in

monocytes/macrophages, mediating the production of inflammation (Achuthan et al., 2016). CSF2 produces airway inflammation by activating airway eosinophils after segmental allergen challenge (Liu et al., 2002). CSF2 induces infiltration and activation of eosinophils in the Th2 network (Nakagome and Nagata, 2011), producing and releasing specific granule proteins *in vitro* (Nagata et al., 1998), ultimately leading to airway pathology. The use of anti-CSF2 receptor monoclonal antibodies to target patients with severe pulmonary disease in COVID-19 can significantly improve clinical symptoms (De Luca et al., 2020; Temesgen et al., 2020).

Therefore, we believe that I-SPD and Vestitol inhibit the overexpression of CSF2 and prevent the generation of inflammatory storm and infiltration of immune cells, preventing mild and common COVID-19 patients from turning into severe ones.

## The mechanisms analysis of Xuanfei Baidu in the treatment of COVID-19

The summary of the mechanisms analysis of *Xuanfei Baidu granule* (XFBD) in the treatment of COVID-19 is shown in Graphical Abstract.

## Conclusion

This study revealed the pharmacological mechanism of *Xuanfei Baidu Granule* (XFBD) in the treatment of COVID-19 through molecular docking and molecular dynamics simulation. The results showed that the important active chemical components I-SPD and Pachypodol in *Xuanfei Baidu Granules* (XFBD) can reduce the inflammatory response and apoptosis by inhibiting the activation of NLRP3, and reduce the production of inflammatory response. I-SPD and Vestitol can inhibit the activation and chemotaxis of inflammatory cells through CSF2, preventing the generation of inflammatory storm.

Therefore, Vestitol, Pachypodol and I-SPD in *Xuanfei Baidu Granules* (XFBD) can effectively alleviate the clinical symptoms of COVID-19 patients through NLRP3 and CSF2.

Current molecular docking and molecular dynamics analyses are difficult to quantify. Since the research based on molecular dynamics is still in the stage of simulation analysis, the body function is a continuous and dynamic process. The process of disease occurrence, drug development and efficacy are also dynamic. This study will verify the pharmacological mechanism of *Xuanfei Baidu Granules* (XFBD) in the treatment of COVID-19, as well as the target and related signaling pathways of active ingredients through cell experiments in the future.

## Data availability statement

The datasets presented in this study can be found in online repositories. The names of the repository/repositories and accession number(s) can be found in the article/Supplementary Material.

## Author contributions

LX, JC, XZ, GX, ZY contributed to the conception of the study; JC, XY, SC, MW, CW, HX, YC, DL contributed significantly to analysis and manuscript preparation; JC, HX, YC, RZ, XH, TC, JT, QD performed the data analyses and wrote the manuscript; XZ, GX, JC, ZY helped perform the analysis with constructive discussions. All authors contributed to the article and approved the submitted version.

## Funding

This study was supported by “Sichuan College Students’ innovation and entrepreneurship training program (S20 2113705049)”.

## Conflict of interest

The authors declare that the research was conducted in the absence of any commercial or financial relationships that could be construed as a potential conflict of interest.

## Publisher’s note

All claims expressed in this article are solely those of the authors and do not necessarily represent those of their affiliated organizations, or those of the publisher, the editors and the reviewers. Any product that may be evaluated in this article, or claim that may be made by its manufacturer, is not guaranteed or endorsed by the publisher.

## Supplementary material

The Supplementary Material for this article can be found online at: <https://www.frontiersin.org/articles/10.3389/fcimb.2022.965273/full#supplementary-material>

## References

- Achuthan, A., Aslam, A. S. M., Nguyen, Q., Lam, P. Y., Fleetwood, A. J., Frye, A. T., et al. (2018). Glucocorticoids promote apoptosis of proinflammatory monocytes by inhibiting ERK activity. *Cell Death Dis.* 9 (3), 267. doi: 10.1038/s41419-018-0332-4
- Achuthan, A., Cook, A. D., Lee, M. C., Saleh, R., Khiew, H. W., Chang, M. W., et al. (2016). Granulocyte macrophage colony-stimulating factor induces CCL17 production via IRF4 to mediate inflammation. *J. Clin. Invest.* 126 (9), 3453–3466. doi: 10.1172/JCI87828
- Afonina, I. S., Zhong, Z., Karin, M., and Beyaert, R. (2017). Limiting inflammation—the negative regulation of NF- $\kappa$ B and the NLRP3 inflammasome. *Nat. Immunol.* 18 (8), 861–869. doi: 10.1038/ni.3772
- Anuar, N., Wahab, R. A., Huyop, F., Amran, S. I., Hamid, A. A. A., Halim, K. B. A., et al. (2021). Molecular docking and molecular dynamics simulations of a mutant acinetobacter haemolyticus alkaline-stable lipase against tributyrin. *J. Biomol. Struct. Dyn.* 39 (6), 2079–2091. doi: 10.1080/07391102.2020.1743364
- Ao, J. Y., Zhu, X. D., Chai, Z. T., Cai, H., Zhang, Y. Y., Zhang, K. Z., et al. (2017). Colony-stimulating factor 1 receptor blockade inhibits tumor growth by altering the polarization of tumor-associated macrophages in hepatocellular carcinoma. *Mol. Cancer Ther.* 16 (8), 1544–1554. doi: 10.1158/1535-7163.MCT-16-0866
- Barrientos, S., Stojadinovic, O., Golinko, M. S., Brem, H., and Tomic-Canic, M. (2008). Growth factors and cytokines in wound healing. *Wound Repair Regen.* 16 (5), 585–601. doi: 10.1111/j.1524-475X.2008.00410.x
- Bellant, J. A., and Settupane, R. A. (2020). The allergist/immunologist, the janus gatekeeper of inflammation, COVID-19 and beyond. *Allergy Asthma Proc.* 41 (6), 395–396. doi: 10.2500/aap.2020.41.200084
- Berclaz, P. Y., Carey, B., Fillipi, M. D., Wernke-Dollies, K., Geraci, N., Cush, S., et al. (2007). GM-CSF regulates a PU.1-dependent transcriptional program determining the pulmonary response to LPS. *Am. J. Respir. Cell Mol. Biol.* 36 (1), 114–121. doi: 10.1165/rncmb.2006-0174OC
- Cao, J., Li, L., Xiong, L., Wang, C., Chen, Y., and Zhang, X. (2022). Research on the mechanism of berberine in the treatment of COVID-19 pneumonia pulmonary fibrosis using network pharmacology and molecular docking. *Phytomed. Plus.* 2 (2), 100252. doi: 10.1016/j.phyplu.2022.100252
- Choudhury, A., Das, N. C., Patra, R., Bhattacharya, M., Ghosh, P., Patra, B. C., et al. (2021). Exploring the binding efficacy of ivermectin against the key proteins of SARS-CoV-2 pathogenesis: An in silico approach. *Future Virol* 16 (4). doi: 10.2217/fvl-2020-0342
- Daina, A., Michielin, O., and Zoete, V. (2019). SwissTargetPrediction: Updated data and new features for efficient prediction of protein targets of small molecules. *Nucleic Acids Res.* 47 (W1), W357–w364. doi: 10.1093/nar/gkz382
- Damiani, G., McCormick, T. S., Leal, L. O., and Ghannoum, M. A. (2020). Recombinant human granulocyte macrophage-colony stimulating factor expressed in yeast (sargramostim): A potential ally to combat serious infections. *Clin. Immunol.* 210, 108292. doi: 10.1016/j.clim.2019.108292
- De Luca, G., Cavalli, G., Campochiaro, C., Della-Torre, E., Angelillo, P., Tomelleri, A., et al. (2020). GM-CSF blockade with mavrilimumab in severe COVID-19 pneumonia and systemic hyperinflammation: A single-centre, prospective cohort study. *Lancet Rheumatol.* 2 (8), e465–e473. doi: 10.1016/S2665-9913(20)30170-3
- Fogarty, H., Townsend, L., Ni Cheallaigh, C., Bergin, C., Martin-Loeches, I., Browne, P., et al. (2020). COVID19 coagulopathy in Caucasian patients. *Br J Haematol.* 189 (6), 1044–49. doi: 10.1111/bjh.16749
- Freeman, T. L., and Swartz, T. H. (2020). Targeting the NLRP3 inflammasome in severe COVID-19. *Front. Immunol.* 11, 1518. doi: 10.3389/fimmu.2020.01518
- Goldman, D. T., Sharma, H., Finkelstein, M., Carlon, T., Marinelli, B., Doshi, A. H., et al. (2021). The Role of Telemedicine in the Maintenance of IR Outpatient Evaluation and Management Volume During the COVID-19 Global Pandemic. *J Vasc Interv Radiol* 32 (3), 479–81. doi: 10.1016/j.jvir.2020.12.009
- Gritsenko, A., Yu, S., Martin-Sanchez, F., Diaz-Del-Olmo, I., Nichols, E. M., Davis, D. M., et al. (2020). Priming is dispensable for NLRP3 inflammasome activation in human monocytes *In vitro*. *Front. Immunol.* 11, 565924. doi: 10.3389/fimmu.2020.565924
- Hamilton, J. A. (2008). Colony-stimulating factors in inflammation and autoimmunity. *Nat. Rev. Immunol.* 8 (7), 533–544. doi: 10.1038/nri2356
- Hamilton, J. A., and Anderson, G. P. (2004). GM-CSF biology. *Growth Fact.* 22 (4), 225–231. doi: 10.1080/08977190412331279881
- Hansen, G., Hercus, T. R., McClure, B. J., Stomski, F. C., Dottore, M., Powell, J., et al. (2008). The structure of the GM-CSF receptor complex reveals a distinct mode of cytokine receptor activation. *Cell* 134 (3), 496–507. doi: 10.1016/j.cell.2008.05.053
- Harrach, M. F., and Drossel, B. (2014). Structure and dynamics of TIP3P, TIP4P, and TIP5P water near smooth and atomistic walls of different hydroaffinity. *J. Chem. Phys.* 140 (17), 174501. doi: 10.1063/1.4872239
- Heneka, M. T., Kummer, M. P., Stutz, A., Delekate, A., Schwartz, S., Vieira-Saecker, A., et al. (2013). NLRP3 is activated in alzheimer's disease and contributes to pathology in APP/PS1 mice. *Nature* 493 (7434), 674–678. doi: 10.1038/nature11729
- Hou, T., Wang, J., Li, Y., and Wang, W. (2011). Assessing the performance of the MM/PBSA and MM/GBSA methods. 1. the accuracy of binding free energy calculations based on molecular dynamics simulations. *J. Chem. Inf. Model.* 51 (1), 69–82. doi: 10.1021/ci100275a
- Huang, F. F., Barnes, P. F., Feng, Y., Donis, R., Chronos, Z. C., Idell, S., et al. (2011). GM-CSF in the lung protects against lethal influenza infection. *Am. J. Respir. Crit. Care Med.* 184 (2), 259–268. doi: 10.1164/rccm.201012-2036OC
- Huang Da, W., Sherman, B. T., and Lempicki, R. A. (2009). Systematic and integrative analysis of large gene lists using DAVID bioinformatics resources. *Nat. Protoc.* 4 (1), 44–57. doi: 10.1038/nprot.2008.211
- Jia, X., Qiu, T., Yao, X., Jiang, L., Wang, N., Wei, S., et al. (2020). Arsenic induces hepatic insulin resistance via mtROS-NLRP3 inflammasome pathway. *J. Haz. Mat.* 399, 123034. doi: 10.1016/j.jhazmat.2020.123034
- Karmakar, M., Katsnelson, M. A., Dubyak, G. R., and Pearlman, E. (2016). Neutrophil P2X7 receptors mediate NLRP3 inflammasome-dependent IL-1 $\beta$  secretion in response to ATP. *Nat. Commun.* 7, 10555. doi: 10.1038/ncomms10555
- Kim, S., Thiessen, P. A., Bolton, E. E., Chen, J., Fu, G., Gindulyte, A., et al. (2016). PubChem substance and compound databases. *Nucleic Acids Res.* 44 (D1), D1202–D1213. doi: 10.1093/nar/gkv951
- Kluge, S., Janssens, U., Welte, T., Weber-Carstens, S., Marx, G., and Karagiannis, C. (2020). German Recommendations for critically ill patients with COVID-19. *Med. Klin. Intensivmed. Notfallmed.* 115 (Suppl 3), 111–114. doi: 10.1007/s00063-020-00689-w
- Lai, C. C., Shih, T. P., Ko, W. C., Tang, H. J., and Hsueh, P. R. (2020). Severe acute respiratory syndrome coronavirus 2 (SARS-CoV-2) and coronavirus disease-2019 (COVID-19): The epidemic and the challenges. *Int. J. Antimicrob. Agents* 55 (3), 105924. doi: 10.1016/j.ijantimicag.2020.105924
- Lamkanfi, M., and Dixit, V. M. (2012). Inflammasomes and their roles in health and disease. *Annu. Rev. Cell Dev. Biol.* 28, 137–161. doi: 10.1146/annurev-cellbio-101011-155745
- Lehtonen, A., Matikainen, S., Miettinen, M., and Julkunen, I. (2002). Granulocyte-macrophage colony-stimulating factor (GM-CSF)-induced STAT5 activation and target-gene expression during human monocyte/macrophage differentiation. *J. Leukoc. Biol.* 71 (3), 511–519. doi: 10.1189/jlb.71.3.511
- Li, F., Li, Y., Zhang, J., Li, S., Mao, A., Zhao, C., et al. (2021a). The therapeutic efficacy of xuanfei baidu formula combined with conventional drug in the treatment of coronavirus disease 2019: A protocol for systematic review and meta-analysis. *Med. (Baltimore)*. 100 (3), e24129. doi: 10.1097/MD.00000000000024129
- Lin, L., Xu, L., Lv, W., Han, L., Xiang, Y., Fu, L., et al. (2019). An NLRP3 inflammasome-triggered cytokine storm contributes to streptococcal toxic shock-like syndrome (TSLS). *PLoS Pathog.* 15 (6), e1007795. doi: 10.1371/journal.ppat.1007795
- Li, R., Rezk, A., Miyazaki, Y., Hilgenberg, E., Touil, H., Shen, P., et al. (2015). Proinflammatory GM-CSF-producing b cells in multiple sclerosis and b cell depletion therapy. *Sci. Transl. Med.* 7 (310), 310ra166. doi: 10.1126/scitranslmed.aab4176
- Liu, B. M., Martins, T. B., Peterson, L. K., and Hill, H. R. (2021). Clinical significance of measuring serum cytokine levels as inflammatory biomarkers in adult and pediatric COVID-19 cases: A review. *Cytokine* 142, 155478. doi: 10.1016/j.cyt.2021.155478
- Liu, L. Y., Sedgwick, J. B., Bates, M. E., Vrtis, R. F., Gern, J. E., Kita, H., et al. (2002). Decreased expression of membrane IL-5 receptor alpha on human eosinophils: I. loss of membrane IL-5 receptor alpha on airway eosinophils and increased soluble IL-5 receptor alpha in the airway after allergen challenge. *J. Immunol.* 169 (11), 6452–6458. doi: 10.4049/jimmunol.169.11.6452
- Liu, Z., Wang, C., Yang, J., Chen, Y., Zhou, B., Abbott, D. W., et al. (2020). Caspase-1 engages full-length gasdermin d through two distinct interfaces that mediate caspase recruitment and substrate cleavage. *Immunity* 53 (1), 106–114.e105. doi: 10.1016/j.immuni.2020.06.007
- Liu, X., Zhang, Z., Ruan, J., Pan, Y., Magupalli, V. G., Wu, H., et al. (2016). Inflammasome-activated gasdermin d causes pyroptosis by forming membrane pores. *Nature* 535 (7610), 153–158. doi: 10.1038/nature18629



- Maier, J. A., Martinez, C., Kasavajhala, K., Wickstrom, L., Hauser, K. E., and Simmerling, C. (2015). ff14SB: Improving the accuracy of protein side chain and backbone parameters from ff99SB. *J. Chem. Theory Comput.* 11 (8), 3696–3713. doi: 10.1021/acs.jctc.5b00255
- Mangan, M. S. J., Olhava, E. J., Roush, W. R., Seidel, H. M., Glick, G. D., and Latz, E. (2018). Targeting the NLRP3 inflammasome in inflammatory diseases. *Nat. Rev. Drug Discovery* 17 (8), 588–606. doi: 10.1038/nrd.2018.97
- Mehta, H. M., Malandra, M., and Corey, S. J. (2015). G-CSF and GM-CSF in neutropenia. *J. Immunol.* 195 (4), 1341–1349. doi: 10.4049/jimmunol.1500861
- Miller, G., Pillarisetty, V. G., Shah, A. B., Lahrs, S., Xing, Z., and Dematteo, R. P. (2002). Endogenous granulocyte-macrophage colony-stimulating factor overexpression *in vivo* results in the long-term recruitment of a distinct dendritic cell population with enhanced immunostimulatory function. *J. Immunol.* 169 (6), 2875–2885. doi: 10.4049/jimmunol.169.6.2875
- Mohammadi, S., Moosaie, F., and Aarabi, M. H. (2020). Understanding the immunologic characteristics of neurologic manifestations of SARS-CoV-2 and potential immunological mechanisms. *Mol. Neurobiol.* 57 (12), 5263–5275. doi: 10.1007/s12035-020-02094-y
- Nagata, M., Sedgwick, J. B., Kita, H., and Busse, W. W. (1998). Granulocyte macrophage colony-stimulating factor augments ICAM-1 and VCAM-1 activation of eosinophil function. *Am. J. Respir. Cell Mol. Biol.* 19 (1), 158–166. doi: 10.1165/ajrcmb.19.1.3001
- Nakagome, K., and Nagata, M. (2011). Pathogenesis of airway inflammation in bronchial asthma. *Auris. Nasus. Larynx.* 38 (5), 555–563. doi: 10.1016/j.janl.2011.01.011
- Notarangelo, L. D., and Pessach, I. (2008). Out of breath: GM-CSF/alpha mutations disrupt surfactant homeostasis. *J. Exp. Med.* 205 (12), 2693–2697. doi: 10.1084/jem.20082378
- Orning, P., Lien, E., and Fitzgerald, K. A. (2019). Gasdermins and their role in immunity and inflammation. *J. Exp. Med.* 216 (11), 2453–2465. doi: 10.1084/jem.20190545
- Ouédrago, D. D., Tiendrébéogo, W. J. S., Kaboré, F., and Ntsiba, H. (2020). COVID-19, chronic inflammatory rheumatic disease and anti-rheumatic treatments. *Clin. Rheumatol.* 39 (7), 2069–2075. doi: 10.1007/s10067-020-05189-y
- Panyod, S., Ho, C. T., and Sheen, L. Y. (2020). Dietary therapy and herbal medicine for COVID-19 prevention: A review and perspective. *J. Tradit. Complement. Med.* 10 (4), 420–427. doi: 10.1016/j.jtcme.2020.05.004
- Perugini, M., Brown, A. L., Salerno, D. G., Booker, G. W., Stojkoski, C., Hercus, T. R., et al. (2010). Alternative modes of GM-CSF receptor activation revealed using activated mutants of the common beta-subunit. *Blood* 115 (16), 3346–3353. doi: 10.1182/blood-2009-08-235846
- Ponomarev, E. D., Shriver, L. P., Maresz, K., Pedras-Vasconcelos, J., Verthelyi, D., and Dittel, B. N. (2007). GM-CSF production by autoreactive T cells is required for the activation of microglial cells and the onset of experimental autoimmune encephalomyelitis. *J. Immunol.* 178 (1), 39–48. doi: 10.4049/jimmunol.178.1.39
- Ratajczak, M. Z., Bujko, K., Ciechanowicz, A., Sietatycka, K., Cymer, M., Marlicz, W., et al. (2021). SARS-CoV-2 entry receptor ACE2 is expressed on very small CD45(-) precursors of hematopoietic and endothelial cells and in response to virus spike protein activates the Nlrp3 inflammasome. *Stem Cell Rev. Rep.* 17 (1), 266–277. doi: 10.1007/s12015-020-10010-z
- Rowan, N. J., and Laffey, J. G. (2020). Challenges and solutions for addressing critical shortage of supply chain for personal and protective equipment (PPE) arising from Coronavirus disease (COVID19) pandemic - Case study from the Republic of Ireland. *Sci Total Environ.* 725, 138532. doi: 10.1016/j.scitotenv.2020.138532
- Rösler, B., and Herold, S. (2016). Lung epithelial GM-CSF improves host defense function and epithelial repair in influenza virus pneumonia-a new therapeutic strategy? *Mol. Cell Pediatr.* 3 (1), 29. doi: 10.1186/s40348-016-0055-5
- Ru, J., Li, P., Wang, J., Zhou, W., Li, B., Huang, C., et al. (2014). TCMSAP: A database of systems pharmacology for drug discovery from herbal medicines. *J. Cheminform.* 6, 13. doi: 10.1186/1758-2946-6-13
- Runfeng, L., Yunlong, H., Jicheng, H., Weiqi, P., Qin Hai, M., Yongxia, S., et al. (2020). Lianhuaqingwen exerts anti-viral and anti-inflammatory activity against novel coronavirus (SARS-CoV-2). *Pharmacol. Res.* 156, 104761. doi: 10.1016/j.phrs.2020.104761
- Santos, L. H. S., Ferreira, R. S., and Caffarena, E. R. (2019). Integrating molecular docking and molecular dynamics simulations. *Methods Mol. Biol.* 2053, 13–34. doi: 10.1007/978-1-4939-9752-7\_2
- Shannon, P., Markiel, A., Ozier, O., Baliga, N. S., Wang, J. T., Ramage, D., et al. (2003). Cytoscape: A software environment for integrated models of biomolecular interaction networks. *Genome Res.* 13 (11), 2498–2504. doi: 10.1101/gr.1239303
- Shi, Y., Liu, C. H., Roberts, A. I., Das, J., Xu, G., Ren, G., et al. (2006). Granulocyte-macrophage colony-stimulating factor (GM-CSF) and T-cell responses: what we do and don't know. *Cell Res.* 16 (2), 126–133. doi: 10.1038/sj.cr.7310017
- Shimabukuro-Vornhagen, A., Gödel, P., Subklewe, M., Stemmler, H. J., Schlößer, H. A., Schlaak, M., et al. (2018). Cytokine release syndrome. *J. Immunother. Cancer* 6 (1), 56. doi: 10.1186/s40425-018-0343-9
- Shiomi, A., and Usui, T. (2015). Pivotal roles of GM-CSF in autoimmunity and inflammation. *Mediators Inflammation* 2015, 568543. doi: 10.1155/2015/568543
- Sivakumar, K. C., Haixiao, J., Naman, C. B., and Sajeevan, T. P. (2020). Prospects of multitarget drug designing strategies by linking molecular docking and molecular dynamics to explore the protein-ligand recognition process. *Drug Dev. Res.* 81 (6), 685–699. doi: 10.1002/ddr.21673
- Strowig, T., Henao-Mejia, J., Elinav, E., and Flavell, R. (2012). Inflammasomes in health and disease. *Nature* 481 (7381), 278–286. doi: 10.1038/nature10759
- Sturrock, A., Seedahmed, E., Mir-Kasimov, M., Boltax, J., Mcmanus, M. L., and Paine, R. (2012). GM-CSF provides autocrine protection for murine alveolar epithelial cells from oxidant-induced mitochondrial injury. *Am. J. Physiol. Lung Cell Mol. Physiol.* 302 (3), L343–L351. doi: 10.1152/ajplung.00276.2011
- Szabowski, A., Maas-Szabowski, N., Andrecht, S., Kolbus, A., Schorpp-Kistner, M., Fusenig, N. E., et al. (2000). C-jun and JunB antagonistically control cytokine-regulated mesenchymal-epidermal interaction in skin. *Cell* 103 (5), 745–755. doi: 10.1016/S0092-8674(00)00178-1
- Szkarczyk, D., Gable, A. L., Lyon, D., Junge, A., Wyder, S., Huerta-Cepas, J., et al. (2019). STRING v11: Protein-protein association networks with increased coverage, supporting functional discovery in genome-wide experimental datasets. *Nucleic Acids Res.* 47 (D1), D607–d613. doi: 10.1093/nar/gky1131
- Temesgen, Z., Assi, M., Shweta, F. N. U., Vergidis, P., Rizza, S. A., Bauer, P. R., et al. (2020). GM-CSF neutralization with lenzilumab in severe COVID-19 pneumonia: A case-cohort study. *Mayo. Clin. Proc.* 95 (11), 2382–2394. doi: 10.1016/j.mayocp.2020.08.038
- Tisato, V., Secchiero, P., Rimondi, E., Giancesini, S., Menegatti, E., Casciano, F., et al. (2013). GM-CSF exhibits anti-inflammatory activity on endothelial cells derived from chronic venous disease patients. *Mediators Inflammation* 2013, 561689. doi: 10.1155/2013/561689
- Tisoncik, J. R., Korth, M. J., Simmons, C. P., Farrar, J., Martin, T. R., and Katze, M. G. (2012). Into the eye of the cytokine storm. *Microbiol. Mol. Biol. Rev.* 76 (1), 16–32. doi: 10.1128/MMBR.05015-11
- Ushach, I., and Zlotnik, A. (2016). Biological role of granulocyte macrophage colony-stimulating factor (GM-CSF) and macrophage colony-stimulating factor (M-CSF) on cells of the myeloid lineage. *J. Leukoc. Biol.* 100 (3), 481–489. doi: 10.1189/jlb.3RU0316-144R
- Van De Laar, L., Coffey, P. J., and Woltman, A. M. (2012). Regulation of dendritic cell development by GM-CSF: Molecular control and implications for immune homeostasis and therapy. *Blood* 119 (15), 3383–3393. doi: 10.1182/blood-2011-11-370130
- Van Der Borght, K., Scott, C. L., Martens, L., Sichien, D., Van Isterdael, G., Nindl, V., et al. (2018). Myocarditis elicits dendritic cell and monocyte infiltration in the heart and self-antigen presentation by conventional type 2 dendritic cells. *Front. Immunol.* 9, 2714. doi: 10.3389/fimmu.2018.02714
- Wang, Y., Greenhalgh, T., and Wardle, J. (2022). Chinese Herbal medicine ("3 medicines and 3 formulations") for COVID-19: Rapid systematic review and meta-analysis. *J. Eval. Clin. Pract.* 28 (1), 13–32. doi: 10.1111/jep.13614
- Wang, J., Snider, D. P., Hewlett, B. R., Lukacs, N. W., Gaudie, J., Liang, H., et al. (2000). Transgenic expression of granulocyte-macrophage colony-stimulating factor induces the differentiation and activation of a novel dendritic cell population in the lung. *Blood* 95 (7), 2337–2345. doi: 10.1182/blood.V95.7.2337
- Wang, J., Wang, W., Kollman, P. A., and Case, D. A. (2006). Automatic atom type and bond type perception in molecular mechanical calculations. *J. Mol. Graphics Model.* 25 (2), 247–260. doi: 10.1016/j.jmgm.2005.12.005
- Wu, D., and Yang, X. O. (2020). TH17 responses in cytokine storm of COVID-19: An emerging target of JAK2 inhibitor fedratinib. *J. Microbiol. Immunol. Infect.* 53 (3), 368–370. doi: 10.1016/j.jmii.2020.03.005
- Xie, L. X. (2020). Interpretation of the 7th edition of the "diagnosis and treatment guidelines of coronavirus disease 2019 in china": Progress and challenges. *Chronic. Dis. Transl. Med.* 6 (2), 75–78. doi: 10.1016/j.cdtm.2020.04.001
- Xing, Z., Ohkawara, Y., Jordana, M., Graham, F., and Gaudie, J. (1996). Transfer of granulocyte-macrophage colony-stimulating factor gene to rat lung induces eosinophilia, monocytosis, and fibrotic reactions. *J. Clin. Invest.* 97 (4), 1102–1110. doi: 10.1172/JCI118503
- Xiong, W. Z., Wang, G., Du, J., and Ai, W. (2020). Efficacy of herbal medicine (Xuanfei baidu decoction) combined with conventional drug in treating COVID-19: A pilot randomized clinical trial. *Integr. Med. Res.* 9 (3), 100489. doi: 10.1016/j.imr.2020.100489
- Xue, Y., Enosi Tuipulotu, D., Tan, W. H., Kay, C., and Man, S. M. (2019). Emerging activators and regulators of inflammasomes and pyroptosis. *Trends Immunol.* 40 (11), 1035–1052. doi: 10.1016/j.it.2019.09.005
- Xu, F., Hou, T., Shen, A., Jin, H., Xiao, Y., Yu, W., et al. (2021). Mechanism deconvolution of Qing fei pai Du decoction for treatment of coronavirus disease

2019 (COVID-19) by label-free integrative pharmacology assays. *J. Ethnopharmacol.* 280, 114488. doi: 10.1016/j.jep.2021.114488

Xu, X., Zhang, W., Huang, C., Li, Y., Yu, H., Wang, Y., et al. (2012). A novel chemometric method for the prediction of human oral bioavailability. *Int. J. Mol. Sci.* 13 (6), 6964–6982. doi: 10.3390/ijms13066964

Yan, Y. Q., Fang, Y., Zheng, R., Pu, J. L., and Zhang, B. R. (2020). NLRP3 inflammasomes in parkinson's disease and their regulation by parkin. *Neuroscience* 446, 323–334. doi: 10.1016/j.neuroscience.2020.08.004

Yan, H., Lu, J., Wang, J., Chen, L., Wang, Y., Li, L., et al. (2021). Prevention of cyclophosphamide-induced immunosuppression in mice with traditional Chinese medicine xuanfei baidu decoction. *Front. Pharmacol.* 12, 730567. doi: 10.3389/fphar.2021.730567

Yashiro, T., Yamaguchi, M., Watanuki, Y., Kasakura, K., and Nishiyama, C. (2018). The transcription factors PU.1 and IRF4 determine dendritic cell-specific expression of RALDH2. *J. Immunol.* 201 (12), 3677–3682. doi: 10.4049/jimmunol.1800492

Zhang, B. Z., Chu, H., Han, S., Shuai, H., Deng, J., Hu, Y. F., et al. (2020). SARS-CoV-2 infects human neural progenitor cells and brain organoids. *Cell Res.* 30 (10), 928–931. doi: 10.1038/s41422-020-0390-x

Zhao, N., Di, B., and Xu, L. L. (2021b). The NLRP3 inflammasome and COVID-19: Activation, pathogenesis and therapeutic strategies. *Cytokine Growth Fact. Rev.* 61, 2–15. doi: 10.1016/j.cytogfr.2021.06.002

Zhao, J., Guo, D., Fan, M., and Liu, Y. (2021a). Efficacy and safety of xuanfei baidu granules for treating COVID-19: A protocol for systematic review and meta-analysis. *Med. (Baltimore)*. 100 (20), e25653. doi: 10.1097/MD.00000000000025653

Zhao, Y., Kilian, C., Turner, J. E., Bosurgi, L., Roedl, K., Bartsch, P., et al. (2021c). Clonal expansion and activation of tissue-resident memory-like Th17 cells expressing GM-CSF in the lungs of severe COVID-19 patients. *Sci. Immunol.* 6 (56). doi: 10.1126/sciimmunol.abf6692

Zhong, Z., Umemura, A., Sanchez-Lopez, E., Liang, S., Shalpour, S., Wong, J., et al. (2016). NF- $\kappa$ B restricts inflammasome activation via elimination of damaged mitochondria. *Cell* 164 (5), 896–910. doi: 10.1016/j.cell.2015.12.057

Zubair, A. S., Mcalpine, L. S., Gardin, T., Farhadian, S., Kuruvilla, D. E., and Spudich, S. (2020). Neuropathogenesis and neurologic manifestations of the coronaviruses in the age of coronavirus disease 2019: A review. *JAMA Neurol.* 77 (8), 1018–1027. doi: 10.1001/jamaneurol.2020.2065



## OPEN ACCESS

EDITED BY  
Simone Brogi,  
University of Pisa, Italy

REVIEWED BY  
Hector M. Mora-Montes,  
Universidad de Guanajuato, Mexico  
Hong Xin,  
Louisiana State University,  
United States  
Dwi Murtiastutik,  
Airlangga University, Indonesia

\*CORRESPONDENCE  
Narottam Acharya  
narottam\_acharya@ils.res.in;  
narottam74@gmail.com

<sup>†</sup>These authors have contributed  
equally to this work

SPECIALTY SECTION  
This article was submitted to  
Clinical Microbiology,  
a section of the journal  
Frontiers in Cellular and  
Infection Microbiology

RECEIVED 25 July 2022  
ACCEPTED 02 August 2022  
PUBLISHED 18 August 2022

CITATION  
Sahu SR, Bose S, Singh M, Kumari P,  
Dutta A, Utkalaja BG, Patel SK and  
Acharya N (2022) Vaccines against  
candidiasis: Status, challenges and  
emerging opportunity.  
*Front. Cell. Infect. Microbiol.*  
12:1002406.  
doi: 10.3389/fcimb.2022.1002406

COPYRIGHT  
© 2022 Sahu, Bose, Singh, Kumari,  
Dutta, Utkalaja, Patel and Acharya. This  
is an open-access article distributed  
under the terms of the [Creative  
Commons Attribution License \(CC BY\)](#).  
The use, distribution or reproduction  
in other forums is permitted, provided  
the original author(s) and the  
copyright owner(s) are credited and  
that the original publication in this  
journal is cited, in accordance with  
accepted academic practice. No use,  
distribution or reproduction is  
permitted which does not comply with  
these terms.

# Vaccines against candidiasis: Status, challenges and emerging opportunity

Satya Ranjan Sahu<sup>1,2†</sup>, Swagata Bose<sup>1,3†</sup>, Manish Singh<sup>1†</sup>,  
Premlata Kumari<sup>1,2</sup>, Abinash Dutta<sup>1</sup>,  
Bhabasha Gyanadeep Utkalaja<sup>1,2</sup>,  
Shraddheya Kumar Patel<sup>1,2</sup> and Narottam Acharya<sup>1\*</sup>

<sup>1</sup>Laboratory of Genomic Instability and Diseases, Department of Infectious Disease Biology,  
Institute of Life Sciences, Bhubaneswar, India, <sup>2</sup>Regional center of Biotechnology, Faridabad, India,  
<sup>3</sup>School of Biotechnology, Kalinga Institute of Industrial Technology, Bhubaneswar, India

Candidiasis is a mycosis caused by opportunistic *Candida* species. The occurrence of fungal infections has considerably increased in the last few years primarily due to an increase in the number of immune-suppressed individuals. Alarming bloodstream infections due to *Candida* sp. are associated with a higher rate of morbidity and mortality, and are emerged as major healthcare concerns worldwide. Currently, chemotherapy is the sole available option for combating fungal diseases. Moreover, the emergence of resistance to these limited available anti-fungal drugs has further accentuated the concern and highlighted the need for early detection of fungal infections, identification of novel antifungal drug targets, and development of effective therapeutics and prophylactics. Thus, there is an increasing interest in developing safe and potent immune-based therapeutics to tackle fungal diseases. In this context, vaccine design and its development have a priority. Nonetheless, despite significant advances in immune and vaccine biology over time, a viable commercialized vaccine remains awaited against fungal infections. In this minireview, we enumerate various concerted efforts made till date towards the development of anti-*Candida* vaccines, an option with pan-fungal vaccine, vaccines in the clinical trial, challenges, and future opportunities.

## KEYWORDS

Mycosis, *Candida*, drug resistance, immunity, whole cell vaccine, pan-fungal vaccine, antibody

**Abbreviations:** CDC, Centers for Disease Control and Prevention; DOX, doxycycline; NK, natural killer; DC, dendritic cells; HKY, heat killed yeast; GXM, glucuronoxylomannan; HSA, human serum albumin; GUTIs, genitourinary tract infections; TT, tetanus toxoid; CFA, complete Freund's adjuvant; Als, Agglutinin-like sequence; NP, nanoparticle.



## Introduction

In addition to viruses and bacteria, fungi are the other organisms, that are either equally or more dangerous to human health. Out of about 4 million diverse fungal species, ~300 species have been identified as human pathogens to cause diseases (Hawksworth and Lucking, 2017). Candidiasis, aspergillosis, mucormycosis, and cryptococcosis are standout fungal infections. Despite the currently available diagnosis and treatment, approximately 1.5 million infectants succumb per year accounting for fungal infections worldwide, and the fatality rate is very similar to that caused by *Mycobacterium tuberculosis* (Mtb) or human immunodeficiency virus (HIV) and is more than the deaths due to malaria or breast or prostate cancer (Brown et al., 2012). Among these fatalities, *Candida* species alone are primarily accountable for the bulk of fungal infections. Fungal infections caused by *Candida* species range from superficial mucosal candidiasis such as vulvovaginal candidiasis (VVC) and oropharyngeal candidiasis to life threatening bloodstream infections such as candidemia. Systemic candidiasis is frequently reported as a consequence of intestinal dysbiosis, impaired host immunity, and high-risk associated medical therapy like immunosuppressive therapy, central venous catheters, or surgical interventions (Butler et al., 2009; Garcia-Vidal et al., 2013; Manohar et al., 2018; Peroumal et al., 2019). Candidiasis represents the 4th and 6th most common healthcare-associated bloodstream infections in the United States and Europe, respectively (Marchetti et al., 2004; Kim and Sudbery, 2011). CDC estimates ~10 per 100,000 people of candidemia incidences and nearly 25,000 such cases nationwide each year. Candidemia is estimated to affect nearly half a million patients per year worldwide (Tso et al., 2018). Since candidemia is usually diagnosed using blood cultures, about 50% of invasive *Candida* infections are undetected as the infections hit the essential internal organs like the heart, kidney, bones, etc. (Berenguer et al., 1993). Therefore, the existing epidemiology and incidence of invasive candidiasis date is most likely imprecise and underestimated, and it could be nearly 2-3 folds higher than that reported. The lack of a rapid diagnosis using a reliable and accurate methodology is yet another concern to *Candida* management. The late and poor diagnosis of invasive candidiasis has only contributed to the rise in multi-organ failures by septicemia-associated fatality. *Candida albicans* is by far the major cause of infections among all *Candida* species, trailed by *Candida glabrata*, *Candida parapsilosis*, *Candida tropicalis*, and *Candida krusei*. Moreover, the recent emergence of drug resistant *Candida auris* has challenged the existing healthcare system (Allert et al., 2022).

Much of the available information and strategy for overcoming bacterial and viral infections have also been deployed for curbing the fungal invasion. As of today, chemotherapy is the sole available option for overcoming

fungal diseases. Polyenes, echinocandins, and azoles are the three major classes of antifungals currently being prescribed (Ford et al., 2015; Lee et al., 2021). These antifungals exhibit a narrow spectrum of activity to work only against certain fungal species and cytotoxicity, and often cause side effects. Azoles are the widely prescribed drugs that target ergosterol biosynthesis pathways. They inhibit the accumulation of ergosterol in the fungal cell membrane and fluidity. Although not many reports are available to suggest immediate side effects of the use of azoles, liver toxicity, and hormone-related adverse effects have been associated with the prolonged use of azoles (Benitez and Carver, 2019). Amphotericin B of the polyene group also acts on ergosterol to alter fungal cell membrane permeability, but it is nephrotoxic and expensive. Unlike azoles and amphotericin B, the echinocandin class of drugs inhibits 1,3- $\beta$  glucan synthase by noncompetitive inhibition and reduces  $\beta$ -glucan deposition on the fungal cell wall. Caspofungin was the first intravenously administered antifungal in this group. The caspofungin users suffer from fever, headache, allergic reactions, and local inflammation of the veins (Kounis, 2013). Despite the advances accomplished so far, overcoming and eliminating the fungal infection has remained a domain of concern for healthcare professionals, globally. In addition to these limited options of anti-fungal drugs, continuous rise in the number of cases, the emergence of drug resistance isolates, infections by varieties of fungal strains, increase in immuno-compromised hosts, etc. further advocate for the urgency to develop better diagnostics, novel antifungal drugs, immunotherapeutics, and fungal vaccines.

In this review, we have emphasized the fight against *Candida* infections, more importantly, the current status of developing a successful vaccine. Vaccines against invasive pathogens represent a major step forward in combating illnesses, and developing an effective and successful anti-*Candida* vaccine is an apparent way to prevent candidemia. In recent years, based on the studies of host-fungal interaction, several groups have reported the immunogenicity and efficacy of different kinds of potential vaccine candidates against *Candida* in animal models (Ibrahim et al., 2006; Spellberg et al., 2006; Spellberg et al., 2006). Even few potential vaccines have been found to be effective and safe in initial clinical trials (Schmidt et al., 2012; De Bernardis et al., 2012). Through this review, we enumerate the multiple concerted initiatives made to date in the formulation of several categories of *Candida* vaccines, an option with pan-fungal vaccine, vaccines in a clinical trial, and challenges in developing a successful anti- candidiasis vaccine ahead with us.

## Candida vaccines

Vaccines play a critical role in preventing deaths, hospitalization, and the spreading of diseases caused by

infectious agents. As a protective and preventive strategy, various vaccination programs have been placed in several countries and achieved remarkable success in reducing morbidity and mortality associated with various infections. Vaccinations prevent 6 million fatalities per year all across the world (Andre et al., 2008). Even after prolonged efforts, currently, there is no commercialized anti-*Candida* vaccine that has been approved for human use (Santos and Levitz, 2014). However, several anti-*Candida* experimental vaccines have been identified during the last few decades, and two of them have been undertaken for clinical trials (Tso et al., 2018). Since the fatality rate due to fungal infections by the drug resistant strains and the number of immunocompromised individuals are on the rise, the development of an effective fungal vaccine and its successful implementation will be a great help to mankind. An updated summary of available potential *Candida* vaccine candidates has been given below (Figure 1 and Table 1).

## Live-attenuated whole cell vaccines

Live attenuated vaccine is nothing but the whole pathogen that has just been “weakened” (attenuated) such that it elicits enough protective immune response but does not cause disease in healthy people. It causes a very mild infection that ensures a

long-lasting protective immune memory. The concept of live attenuated vaccines came from the Vaccinia virus, which causes cowpox in cattle but cross-protects smallpox in humans (Riedel, 2005). Live-attenuated vaccine strategy is commonly and effectively used in combating viral diseases such as influenza, polio, mumps, rubella, measles, varicella, and rotavirus (Saccante and Woods, 2010; Leibovitch and Jacobson, 2016). Such approaches have been taken to develop a vaccine against SARS-COV2 also, and it appears to be the lifesaver against COVID19 (Sapkal et al., 2021). On the same line, several studies reported the ability of various avirulent or low-virulent strains of *C. albicans* to protect against candidiasis. *C. albicans* strain PCA-2 is a caspofungin resistant mutant of its isogenic 3153A strain. Mice immunized with PCA-2 elicit an innate immune response by increasing the number of peripheral blood polymorphonuclear cells (PMNs) with high candidacidal activity. Consequently, an adoptive transfer of macrophage cells from PCA-2 administered mice conferred substantial protection against subsequent infection (Bistoni et al., 1986). Fernandez-Arenas, E. et al., in their study used low virulent *C. albicans* strains CM1613 (a Mitogen Activated Protein Kinase MKC1 deletant), CNC13 (a MAP-kinase HOG1 deletant), and a morphologically defective mutant 92' as whole cell vaccines in murine models (Fernandez-Arenas et al., 2004). Among these strains, only CNC13 strain immunized mice got partially protected (~60–70%) when they were re-challenged with a

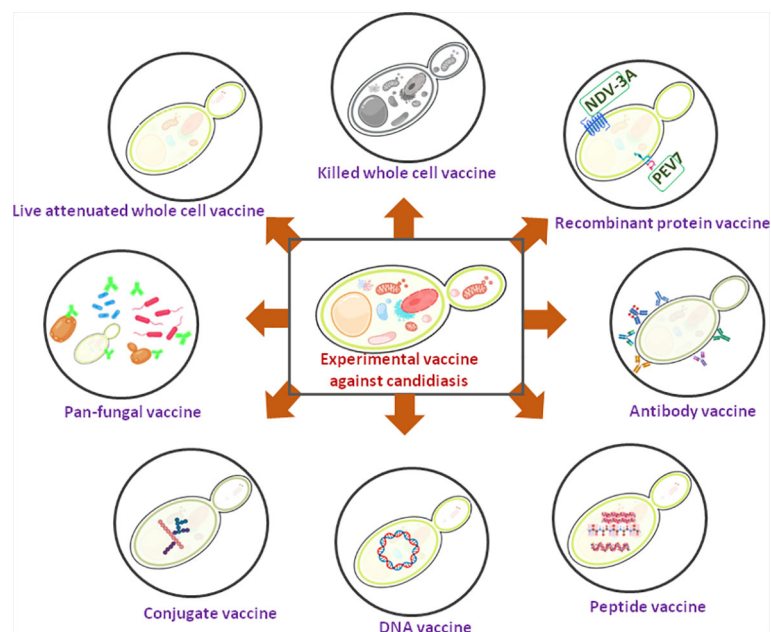


FIGURE 1

A schematic diagram showing experimental *Candida* vaccines. Two recombinant protein vaccines are under clinical trial (showing green).

TABLE 1 Summary of experimental anti-*Candida* vaccine candidates.

Vaccine category	Description	Clinical trial stage	Cross-protection (non- <i>C. albicans</i> organisms)	Reference
LA	Hyphal-defective <i>C. albicans</i> strain PCA-2		<i>S. aureus</i>	Bistoni et al. (1986)
LA	MAP kinase-defective <i>hog1Δ C. albicans</i> strain CNC13			Fernández-Arenas et al. (2004)
LA	Cell wall-defective <i>ecm33Δ C. albicans</i> strain RML2U			Martínez-López et al. (2008)
LA	Filamentation-repressible <i>C. albicans</i> strain tet-NRG1			Saville et al. (2009)
LA	Yeast-locked <i>C. albicans</i> strain <i>cph1Δ/efg1Δ</i>			Yang et al. (2009)
KV	heat-killed <i>S. cerevisiae</i> yeast (HKY)		<i>A. fumigatus</i> , <i>C. grubii</i> , and <i>C. posadasii</i>	(Liu et al. 2012), Liu et al. (2011a), Capilla et al. (2009)
Conjugate	laminarin-CRM conjugation			Torosantucci et al. (2005)
Conjugate	β-glucan coupled with a MF59			Pietrella et al. (2010)
Conjugate	Lam-CRM197, a laminarin conjugated with diphtheria toxoid (CRM197)			Cassone et al. (2010)
Conjugate	Lam-CRM197 coupled with MF59			Wang et al. (2015)
Recombinant	recombinant N-terminus of Als1 (rAls1p-N)			Ibrahim et al. (2006)
Recombinant	recombinant N-terminus of Als3 (rAls3p-N)		<i>S. aureus</i>	Spellberg et al. (2006)
Recombinant	Recombinant N-terminus of Als3p plus alum adjuvant (NDV-3)	Phase I b/2a clinical trial		Schmidt et al. (2012)
Recombinant	recombinant Sap2p			De Bernardis et al. (2012)
Recombinant	PEV7, a truncated Sap2p embedded into the bilipid layer of an influenza virosomes	Phase I clinical trial		De Bernardis et al. (2012)
Recombinant	47-kDa fragment of <i>C. albicans</i> Hsp90's from its carboxyl end (Mycograb)			Matthews et al. (1987), Matthews et al. (1989)
Recombinant	recombinant form of N-terminus of Hyr1 (rHyr1p-N)		<i>C. glabrata</i> , <i>C. krusei</i> , <i>C. parapsilosis</i> and <i>C. tropicalis</i>	Luo et al. (2011)
Recombinant	recombinant enolase (Eno1p)			Shibasaki et al. (2014)
Peptide	Fba (derived from <i>C. albicans</i> cell surface fructose bisphosphatealdolase [Fab]) or peptide Met6 (derived from <i>C. albicans</i> β-1,2-mannotriose [β-(Man)3] protein)			Xin and Cutler (2006), Xin et al. (2008), Han et al. (1998), Xin et al. (2006)
Peptide	Dendritic cells (DCs) stimulated by either Fba peptide (YGKDVKDLFDYAQE) or Met6 peptide (PRIGGQRELKKITE)			Xin et al. (2016)
Peptide	Fba peptide (14-mer) conjugated with each one of five peptide mimotopes from Met6 (PS2, PS31, PS28, PS55, and PS76)			Xin (2019)
extracellular vesicles	fungal extracellular vesicles (EV)			Edwards et al. (2018)
Cell wall extract	β-mercaptoethanol-extracted <i>C. albicans</i> Cell wall proteins			Chaffin et al. (1998), Martínez et al. (1998)

LA, live attenuated; KV, Killed vaccine.

lethal dose of wild-type infection. This study further demonstrated that both the cellular and humoral responses were induced upon CNC13 immunization that elicited effective protection. This study also showed a clear difference in the antibody pattern in the sera of non-vaccinated and vaccinated animals with the CNC13 mutant. The cell wall acts as an interface between the host and fungal pathogens and its composition plays an important role in eliciting the host immune response. Ecm33, a glycosylphosphatidylinositol-anchored protein, is involved in the biogenesis and fungal cell wall integrity. The *C. albicans* strain RML2U (*ecm33Δ* Δ) is defective in its interaction with endothelial and epithelial cells

because of its cell wall structure modification and was shown to protect vaccinated BALB/c mice (Martínez-López et al., 2008). Nrg1 is a transcription factor that negatively regulates morphological transition in *C. albicans*. SSY50-B is a genetically modified *C. albicans* strain where the expression of *NRG1* is governed by a tetracycline-regulatable promoter. The absence or supplementation of doxycycline (DOX) to the growth media regulates the expression of *NRG1*, thereby, the morphology and virulence get manipulated. B cell deficient mice immunized with tet-NRG1mutat strain remained protected upon subsequent infection similar to wild type mice strain, while the same was not witnessed with T cell deficient

mice. However, survival was only evidenced when tet-NRG1 mutant was enforced to grow in yeast form (Saville et al., 2009). Similarly, the double-deletion mutant *cph1ΔΔ/efg1ΔΔ* *C. albicans* is avirulent as it is locked in the yeast form (Lo et al., 1997). Although the *cph1ΔΔ/efg1ΔΔ* mutant cells proliferate in infected mice, its immunization only partially protects mice from systemic infections upon the lethal dose of virulent challenge. Even its booster dose did not improve the degree of protection (Yang et al., 2009). The *gpi7* *C. albicans* mutant is yet another avirulent strain and its immunization protected mice against pan-fungal invasive candidiasis (Shen et al., 2020). In this strain, the  $\beta$ -glucan layer of the cell wall is exposed that facilitating Dectin-1 receptor dependent nuclear translocation of RelB in macrophages, the release of Interleukin 18, and the production of protective antibodies. The study also found that IgG antibodies present in the patients recovering from invasive candidiasis and *gpi7* mutant-immunized mice are very similar. BCG (Bacillus Calmette-Guérin) is an antibacterial live attenuated vaccine that induces non-specific cross-protection against a wide range of infections (Mangtani et al., 2014). Immunization with BCG induces a protective innate immune response against pathogens like *C. albicans* and *Staphylococcus aureus* in addition to *Mycobacterium tuberculosis*, and this study provided a concept of “trained immunity”. Trained immunity provides an enhanced protective response to a secondary infection caused either by the same or different pathogens, mostly mediated by the innate immune system (Netea et al., 2011). Monocytes/macrophages and natural killer (NK) cells play critical roles in contributing to trained immunity, and such immunity is independent of T and B cell responses (Kleinnijenhuis et al., 2014). It was found that BCG vaccination induces epigenetic modifications by altering the methylation status of histones in the regulatory elements of associated genes in circulating monocytes that facilitate increased production of proinflammatory cytokines leading to a “trained” state (van 't Wout et al., 1992; Kleinnijenhuis et al., 2012). Despite these advances, most of the avirulent strains failed to reach a clinical trial stage. Possible reasons include (i) due to weakened immune systems, currently, it is not advocated to use in immunocompromised individuals, (ii) stability of the attenuation of the genetically modified or mutant strains is questionable as it was found in the case of viruses that the virulence is not suppressed permanently and they regained virulence in immune-deficient individual and caused infection (Lancaster and Pfeiffer, 2011), although similar reports do not exist yet to support in the case of attenuated fungal strains, (iii) though the vaccine candidates govern substantial and marked protection in animal models, some of them failed to show similar response in human volunteers at a clinical trial, and (iv) live attenuated vaccines share a common flaw with biologics in that they are difficult to keep stable during the manufacturing, transporting, and preservation phases (van 't Wout et al., 1992).

## Killed whole cell vaccines

In comparison to the live attenuated vaccines, killed vaccines are stable and non-pathogenic as they cannot revert. The ease and low cost of its preparation along with substantial safety make it a choice against the *Candida* vaccine. Intranasal vaccination with heat-killed *C. albicans* plus a heat-labile genetically engineered toxin from *Escherichia coli* as an adjuvant R192G provided a substantial degree of protection in animal models (Cardenas-Freytag et al., 1999). However, the same combination used for mucosal vaccination did not ensure full protection against experimental vaginal candidiasis (Cardenas-Freytag et al., 2002). Besides, this vaccine candidate has not been tested in immune-compromised animal models. The subcutaneous immunization with heat-killed *S. cerevisiae* yeast (HKY) also provided cross-protection to *C. albicans*, *A. fumigatus*, and *Coccidioides posadasii* infections (Capilla et al., 2009; Liu et al., 2011a; Liu et al., 2011b; Stevens et al., 2011). However, homologous proteins to components of HKY responsible for such cross-protection are yet to be demonstrated. Interestingly, the total cellular proteins extracted by  $\beta$ -mercaptoethanol treatment and their subsequent subcutaneous immunization to mice increased survivability (75%) with a decreased fungal burden than in the control groups (Thomas et al., 2006). A combined vaccine formulation of MV140 and V132 has been tested to prevent both bacterial as well as fungal genitourinary tract infections (GUTIs) (Martin-Cruz et al., 2020). The heat-inactivated polyvalent bacterial vaccine MV140 prevents RUTIs by eliciting Th1/Th17 and IL-10 immune responses, while the V132 is a heat-inactivated vaccine candidate developed against RVVCs. The report suggested that the vaccine combination activates human dendritic cells (DCs) to polarize potent IFN- $\gamma$  and IL-17A double positive T cells and FOXP3<sup>+</sup> regulatory T<sub>reg</sub> cells. In addition, MV140/V132 promotes epigenetic reprogramming in human DCs to induce trained immunity. Even after these positive results in basic research, these candidates have not progressed to clinical trials.

## Conjugate vaccines

A conjugate vaccination combines a weak antigen with a robust antigen as a carrier, causing the immune system to respond more strongly to the weaker antigen. Conjugating proteins to polysaccharides facilitates easy recognition of the abundant fungal cell wall glycan components by the immune system, and thereby antibodies recognize the pathogen quickly. The first conjugate vaccine was developed against *Cryptococcus neoformans* where the capsular polysaccharide, glucuronoxylomannan (GXM) of the fungus was covalently linked to tetanus toxoid (TT). Vaccination of the conjugates with an adjuvant monophosphoryl lipid A (MPL) protected 70% of intravenously challenged mice (Devi, 1996). Similarly, a universal, pan-fungal vaccine was made by conjugating laminarin, a  $\beta$ -glucan polysaccharide isolated from



brown algae, with inactivated diphtheria toxin (CRM). Subcutaneous immunization of mice with this conjugate along with complete Freund's adjuvant (CFA) protected against invasive candidiasis and aspergillosis by 70% and 80%, respectively. A similar conjugation with cholera toxin was equally efficient in curing vaginal candidiasis in Wistar rats (Torosantucci et al., 2005; Pietrella et al., 2010). However, the underlying mechanism by which these conjugates provide protective immune responses is still unknown. Vaccination of Lam-CRM197, a laminarin conjugated with diphtheria toxoid, with MF59 adjuvant significantly reduced the mortality of infected mice (Wang et al., 2015). In another report,  $\beta$ -1,2-mannotriose was conjugated to a peptide fragment from fructose bisphosphate aldolase (Fba) of *C. albicans* and tetanus toxin (TT). Almost all of the mice immunized with  $\beta$ -(Man)3-Fba-TT survived the infection (Xin et al., 2012). Passive transfer studies indicated that antibodies but not the cell-mediated immune responses were responsible for the protection of invasive candidiasis by such vaccinations. In a recent report, KLH-conjugates were generated by covalently linking  $\beta$ -1,2-mannan, N-terminal peptide epitopes of *C. albicans* cell wall phosphomannan complex, and Als1p (rAls1p-N) protein with keyhole limpet hemocyanin (KLH) and human serum albumin (HSA) through homobifunctional disuccinimidyl glutarate (Liao et al., 2019). The study found that the resultant glycopeptides with or without any external adjuvant produced high levels of IgG antibodies in immunized mice, and the obtained antisera cross-reacted with the cell surface of a number of fungi. Although these results advocate the potential use of these conjugates as antifungal vaccines, none of these candidates have been taken to clinical trials.

## Recombinant protein vaccines

Since the live attenuated or killed whole cell vaccines are enriched with antigens and heterogeneous in compositions, they may encode many unwanted immunological responses including allergenic and/or reactogenic responses in addition to the desirable ones. Such concerns prompted the researchers to introduce recombinant protein or subunit vaccines as potential vaccine candidates (Petrovsky and Aguilar, 2004). Advancements in genetic engineering, host-pathogen interaction, and cellular immunology have helped vaccinologists to formulate efficient recombinant protein or subunit vaccines. The basic principle involves the transfer and expression of the desired gene encoding an immunogenic antigen related to the virulence and pathogenicity of the fungus to elicit a robust immune response. Here, protein antigens are usually mixed with a suitable adjuvant or a protein carrier, most commonly bacterial toxoids, to develop a robust immune response and stable immunization (Cassone, 2008; Santos and Levitz, 2014). In contrast, live attenuated or killed *Candida* vaccines, recombinant vaccines were usually considered safer as they are free of any infectious agents,

stable in the host, and easy to immunize. Several studies were carried out on recombinant vaccines and only the prominent ones have been discussed here. Agglutinin-like sequence (Als) proteins are the cell membrane proteins of *C. albicans* involved in the fungal adherence to host endothelium cells, which ultimately leads to the cause of invasive candidiasis (Hoyer and Cota, 2016). Als1 and Als3 proteins in combination with or without adjuvants have been proposed as vaccine candidates against invasive candidiasis. Subcutaneous immunization of the recombinant N-terminus of Als1 (rAls1p-N) resulted in a survival rate of 50–57 percent subsequent to the lethal challenge of *C. albicans* (Ibrahim et al., 2006). This vaccine was quite effective in both immunocompetent and immunosuppressed mice against both Oropharyngeal candidiasis and *Candida* vaginitis (Spellberg et al., 2005). In the murine model of oropharyngeal and vaginal candidiasis, vaccination with the rAls3-N elicited a robust antibody generation, was more effective and had a higher survival rate than rAls1-N (Spellberg et al., 2006). Notably, it also ensures a safeguard against *S. aureus* infection, implying the carrying of evolutionarily conserved epitopes, shared across such distantly related species (Lin et al., 2009). Furthermore, *Candida* Als3 is structurally similar to a *S. aureus* clumping factor (Spellberg et al., 2008). In a phase I clinical trial, NDV-3A, a rAls3-N vaccine formulated with Alhydrogel adjuvant, increased the antibody titers in revaccinated people at two different doses, including the level of cytokines and IgG and IgA1 titers (Schmidt et al., 2012). Currently, NDV-3A is ongoing in a phase two of clinical trials to assess the vaccine's immuno-therapeutic efficacy in women with RVVC (Edwards et al., 2018). NDV-3A has also been tested against *C. auris*, and *in vitro* studies revealed that anti-Als3 antibodies developed in the vaccinated mice cross-reacted with this fungus, block biofilm development, and recuperate macrophage-mediated fungal clearance (Singh et al., 2019). Thus, NDV-3A appears to be an extremely promising vaccine candidate for use against *C. albicans* and *C. auris*. Another prominent example in this listing is secretory aspartyl proteases (SAP). SAP is a group of ten secretory proteins of *C. albicans* and they play important roles in fungal cells adhesion, epithelial as well as endothelial invasion, and metabolism (Naglik et al., 2003). Among all, Sap2 is the most abundantly expressed SAP. Intravaginal or intranasal immunization of rats with recombinant Sap2, either with or without cholera toxin as an adjuvant, resulted in *Candida* vaginal infection clearance (De Bernardis et al., 2002). PEV7, a truncated Sap2 protein (77–400 amino acid length) embedded into the bilipid layer of influenza virosomes was also developed by the same research group and has been found to provide efficient protection against vaginal candidiasis (De Bernardis et al., 2012). Intramuscular immunization of PEV7 in mice and rats generate a robust serum antibody response and anti-Sap2 IgG and IgA was also detected in the vaginal fluid of animals. PEV7 has also been advanced to human trials for RVVC



treatment. Another study found that recombinant Sap2 protein from *C. parapsilosis* is highly immunogenic and demonstrated that immunization of mice with CpSap2 showed enhanced protection compared to vaccination with Sap2 protein from *C. albicans*, and *C. tropicalis* (Shukla and Rohatgi, 2020). Heat shock protein 90 (HSP-90) is a ubiquitous stress-induced chaperone that plays a critical role in balancing and overcoming the stressful environment within the host cell. It is found in the cell wall of *C. albicans* and is vitally important for yeast survival and viability. The carboxyl terminal 47-kDa fragment of Hsp90 is highly immunogenic, and antibodies against it are associated with a better prognosis, whereas low levels are linked to mortality (Matthews et al., 1987; Matthews and Burnie, 1989; Burnie and Matthews, 2003). Pre-clinical assessment of the efficacy of Mycograb (NeuTec Pharma plc), a human genetically recombinant antibody against heat shock protein 90 (rP-HSP90C) has been carried out recently (Matthews et al., 2003). Mycograb in combination with Amphotericin B provided complete protection for *C. albicans*, *C. krusei*, and *C. glabrata* infections. Another study evaluated the efficacy of chitosan hydrogel (CH-HG) as an adjuvant in recombinant HSP90C protein vaccine (Li et al., 2021). In comparison to free rP-HSP90C, CH-HG-loaded rP-HSP90C produced stable rP-HSP90C-specific IgG, enhanced Th1, Th2, Th17 responses, and a stronger CTL response. Consequently, CH-HG-rP-HSP90C vaccination enhanced protection to pathogenic challenge and increased the survival rate of infected mice. Hyphal-regulated cell wall protein1 (Hyr1) is a GPI-anchored mannose protein present on the fungal cell during hyphal formation. Subcutaneous immunization of a recombinant form of N-terminus of Hyr1 (rHyr1-N) with either CFA or aluminum hydroxide to both immunocompetent and neutropenic mice showed substantial protection to *C. albicans*, *C. glabrata*, *C. krusei*, *C. parapsilosis*, and *C. tropicalis* infection (Cassone et al., 2010; Luo et al., 2011). This study claimed that the protection is governed by an enhanced antibody titer raised against rHyr1p-N. Consequently, passive immunization with anti-Hyr1p IgG extended the survival of *C. albicans* infected mice. They also suggested the contribution of T- and B-cells in the mechanism of rHyr1p-N governed protection against pathogenesis (Luo et al., 2011).

## Peptide vaccine

Like whole cell vaccines, recombinant proteins also possess several antigenic epitopes, which can result in both the induction of a protective immune response along with adverse and unfavourable ones. Therefore, the concept of peptide vaccines carrying highly desired and specific epitopes was explored (Sesardic, 1993). Peptide vaccines are being considered for preventing and giving protection through active and passive

immunization (Xin et al., 2012; Cassone and Casadevall, 2012). Besides, epitope based vaccines are cost effective, less time-consuming, highly efficacious, and safe for use in humans (Backert and Kohlbacher, 2015). Several synthetic vaccine candidates have already been attempted as a therapeutic or prophylactic agent against many diseases like influenza, hepatitis B virus (HBV), hepatitis C virus, HIV, tuberculosis, pneumonia, histoplasmosis, coccidioidomycosis, sporotrichosis, blastomycosis, paracoccidioidomycosis, candidiasis, aspergillosis, cryptococcosis, and other mycoses as well. Active immunization with dendritic cells (DCs) stimulated by either Fba peptide of sequence YGKDVKDLFDYAQE or Met6 peptide of sequence PRIGGQRELKKITE showed protection in both cyclophosphamide-induced neutropenia and healthy mice (Xin, 2016). Further, the protective efficacy of a synthetic Fba peptide (14-mer) conjugated with each one of five peptide mimotopes from Met6 (PS2, PS31, PS28, PS55, and PS76) was also evaluated (Xin et al., 2019). Although all of the five mimotopes elicited specific antibody responses, only three of them protected against invasive candidiasis in mice. Using computational tools, Tarang et al., screened the *Candida* proteome (6030 proteins) and shortlisted specific epitopes belonging to HLA class I, HLA class II, and B-cell. To enhance the vaccine efficacy, a multivalent recombinant protein against *C. albicans* (mvPC) was designed by joining the selected 18-most promising epitopes by molecular linkers. With the addition of a synthetic adjuvant (RS09), it was predicted that with enhanced immunogenicity, mvPC will be a potent vaccine candidate (Tarang et al., 2020). The efficacy of this candidate vaccine against candidiasis is yet to be demonstrated in animal or clinical setups. Several reports suggest that both pathogenic and non-pathogenic bacteria, archaea, and eukaryotic cells secrete extracellular or membrane vesicles (EVs) as a mode for cell-free intercellular communication (Bose et al., 2020). EVs carry a range of cargo compounds that play a role in cellular competition, fitness, survival, invasion, bypassing of the host immune system, establishment, and infection. Especially, fungal species from ascomycetes and basidiomycetes produce EVs that possess a wide range of biologically active molecules that showed a significant degree of virulence (Rodrigues et al., 2011; Freitas et al., 2019; Vargas et al., 2020; Rizzo et al., 2020). For example, when RAW 264.7 macrophages were stimulated with EVs secreted out of *C. albicans* cells produced nitric oxide (NO), IL-12, IL-10, and TGF- $\beta$ . The bone marrow-derived macrophages (BMDM) upon stimulation by *C. albicans* EVs produced NO, IL-12, tumor necrosis factor alpha (TNF- $\alpha$ ), and IL-10, whereas the bone marrow-derived dendritic cells (BMDC) produced IL-12, TNF- $\alpha$ , and TGF- $\beta$  (Vargas et al., 2020). Despite the promising implications of EVs in vaccine development, like a whole cell vaccine, the structure, and composition of EVs are very complex, thus they may show a wide range of immunological responses, and thereby efficacy of such vaccines remain a concern.

## DNA vaccines

In DNA vaccines, a recombinant plasmid construct containing the cDNA of the desired antigen is transfected into the host's APCs (mainly DCs) to elicit immunity. In addition to the antigen, the gene encoding the co-stimulatory molecules or cytokines can be inserted into the plasmids as well. For example, a plasmid carrying non-methylated CpGs is sensed by TLR9 (found on DCs), which further induces adaptive immunity. A single study compared the efficacy of two vaccine formulations (recombinant hsp90-CA protein and hsp90-CA-encoding DNA vaccine) to induce protective responses against both systemic and vaginal candidiasis in BALB/c mice. While the intradermal immunization of a DNA vaccine resulted in a 64% prolonged survival duration of mice compared to a PBS control, the intranasal vaccination failed to provide any protection. The intradermal recombinant hsp90-CA protein priming, followed by a booster dose *via* intranasal or intradermal induced a significant increase of hsp90-CA-specific IgG and IgA antibodies in comparison with the control group (Raska et al., 2008).

## Antibody mediated vaccine

Studies to develop an antibody-based diagnosis of various fungal infections are on the rise, and some of the outcomes also look promising. The mAb JF5 for the detection of invasive pulmonary aspergillosis and mAb (CAGTA) for deep-seated *C. albicans* infection are a few of those examples (Thornton, 2008; Martinez-Jimenez et al., 2014). Recently, Rudkin et al. generated seventeen recombinant human anti-*Candida* monoclonal antibodies (mAbs) from single B cells potentially used for diagnosis and therapeutics against pan-fungal infections. They amplified and cloned the human antibody encoding variable domain (V) targeting *C. albicans* epitopes from the cDNA of B cells isolated from recovered patients with mucosal candidiasis. The purified mAbs were found to cross-react with most pathogenic *Candida* species and exhibit strong fungal killing activity *in vitro*, and protect against a lethal challenge in a murine model (Rudkin et al., 2018).

## Pan-fungal vaccine providing cross protection to other pathogens

Infection with a single strain of pathogen occasionally confers protection on a host by preventing infection with a closely relevant strain of that pathogen. In the case of candidiasis, cross protection has also been reported. On a similar line, protection against other fungal or bacterial pathogens by experimental *Candida* vaccines was also found. For example, the subcutaneous immunization with heat-killed *S.*

*cerevisiae* yeasts (HKY) ensured protection against a range of fungal species, including *A. fumigatus*, *C. albicans*, and *C. posadasii* (Capilla et al., 2009; Liu et al., 2011b). The recombinant Als-3 protein of *C. albicans* also protects against *S. aureus* infection (Lin et al., 2009). It suggests that these distantly related species share common epitopes. Not surprisingly, CaAls3 protein shares structural similarities to a clumping factor found in *S. aureus* (Spellberg et al., 2008). This strategy may be harnessed to generate “convergent immunity” that will protect from diseases caused by pathogens from various kingdoms. Immunization of mice with calnexin in glucan particles showed resistance to a wide range of infections caused by *A. fumigatus*, *Blastomyces dermatitidis*, *Fonsecaea pedrosoi*, *Histoplasma capsulatum*, and *Pseudogymnoascus destructans*, mediated by evoking calnexin-specific CD4<sup>+</sup> T cells. In 2015, researchers used genetically modified CD4<sup>+</sup> T cells to identify an amino acid sequence from the chaperone calnexin protein that showed minimal divergence amongst all Ascomycetes (Wuthrich et al., 2015). Furthermore, a 13-mer peptide (LVVKNPAAHHAIS) derived from the conserved region of calnexin induced a robust immunological response to reduce the severity of *B. dermatitidis* infection (Wuthrich et al., 2015). F-box protein Fbp1 is a *Cryptococcus* virulence factor involved in regulating host-fungus interactions (Wang et al., 2019). The study demonstrated that immunized mice with heat-killed *fbp1Δ* cross-protected fungal pathogens such as *C. neoformans*, *Cryptococcus gattii*, and *A. fumigatus* by eliciting superior protective Th1 host immunity, albeit less protective against *C. albicans*.

## Nanoparticles as an alternative vaccine

Nanotechnology has already been employed as an alternative to increasing the bio-distribution, treatment effectiveness, and lowering side effects of certain antifungal drugs (Voltan et al., 2016). Antigens can also be delivered by using nanoparticles (NPs). Han and Cutler used liposomes derived from phosphatidylcholine and cholesterol to carry mannan adhesin fraction extracted from *C. albicans* as a potent NPs based *C. albicans* vaccine (Han and Cutler, 1995). Vaccination protected both immuno-competent and -suppressed mice against *C. albicans* and *C. tropicalis*. A specific monoclonal antibody MAb B6.1 was isolated from the immunized mice and was found to protect against widespread infection including RVCC (Han et al., 1998). Another study evaluated *C. albicans* ribosomes trapped in the liposomes of dimyristoyl phosphatidylcholine (DMPC) and dimyristoyl phosphatidyl glycerol (DMPG) as a potential vaccine and found that upon immunization about 60% animals survived with invasive candidiasis (Eckstein et al., 1997). NPs of recombinant HSP90 protein and nickel chelating liposomes associated with norAbuMDP pyrogen adjuvant were injected intradermal to

BALB/c mice and a comparable Th1 and Th2 response as in Freund's complete adjuvant vaccine was observed (Masek et al., 2011). Similarly, Knotigová et al. evaluated rHSP90 in nickel chelating liposomes associated with two pyrogen-free adjuvants (norAbuMDP and norAbuGMDPs) as a potential NP-based vaccine in ICR mice and rabbits (Knotigová et al., 2015). Recently monoolein based liposomes for delivery of *C. albicans* cell wall proteins Cht3p and Xog1p were explored (Carneiro et al., 2015). In another study, ADS1 and ADS2 formulations were evaluated which differed only in lipid concentrations for cell wall protein loading, found that ADS1 but not ADS2 protected against fungal infection in mice (Carneiro et al., 2016).

## Vaccines in various stages of clinical trials

Although several candidate vaccines have been identified, and they appear to be efficient and safe in animal models, only two candidates have reached clinical trials Phase I in humans. The first vaccine uses alum as an adjuvant and the N-terminus of a recombinant Als3 protein of *C. albicans* as antigen (Nova Digm, US). NDV-3A is the first vaccine to demonstrate preclinical efficacy in protecting from diseases caused by both fungal and bacterial pathogens (novadigm.net). According to a phase I clinical trial, the NDV vaccine was found to be nontoxic and effectively produced antibody and T-cell immune responses in healthy individuals (Schmidt et al., 2012). Seventy three adult volunteers were immunized with two doses of NDV-3A. After the 1<sup>st</sup> dose of immunization, all the individuals produced anti-Als3p IgG antibodies in comparison to placebo as a control. After the second dose, a robust IgA1 antibody titer with effective IgG response, and IL-17 and IFN- $\gamma$  T cells cytokines production were observed in all the subjects. The phase 2 randomized, double-blind, placebo-controlled clinical trial has also been recently completed, and the report suggested that one-dose of NDV-3A vaccine was also safe and effective in patients with recurrent vulvovaginal candidiasis (RVVC). The vaccine reduced the frequency of vulvovaginal candidiasis for up to 12 months in women under 40 years old (Edwards et al., 2018). However, NDV-3A vaccination in a population of military trainees did not impede the nasal or oral acquisition of *S. aureus* (Millar et al., 2021). Another vaccine being conducted in the clinical trial (Phase I) was on the Sap2 protein of *C. albicans* in virosomal formulation against RVVC (PEV7, Pevion Biotech AG, Switzerland) (Sandini et al., 2011; De Bernardis et al., 2012). PEV7 was safe and effective, and the vaccinated individuals produced specific and functional B cell memory (www.pevion.com). We expect that these clinical studies will be further extended to larger cohorts including immunosuppressed individuals or at least to individuals receiving corticosteroids and antibiotics in the future.

## Challenges in developing a successful anti-candidiasis vaccine and future perspective

Among the estimated ~4 million fungal species on the planet Earth, about 300 species are pathogenic and cause diseases in humans (Stop neglecting fungi, 2017; Hawksworth and Lucking, 2017). While most fungal infections are found in immune-deficient individuals, some fungi cause diseases even in healthy adults. In addition to these diversified fungal pathogens, the site of fungal infections also varies widely, from the scalp of the head to the nails of the toes. Although these infections are superficial and not life threatening, occasionally the current regime of treatment using fungal drugs becomes ineffective. Moreover, systemic fungal infections are very serious as they target most of the internal organs through the circulatory system in animals and humans. Additionally, some fungi do not have terrestrial life rather they survive as commensals in humans and animals and might regulate host physiology. Most of the studies so far considered *C. albicans* only as a pathogenic yeast causing both primary and secondary infections, however being a commensal, it may maintain a mutualistic relationship with the host that has not been explored yet. Our recent study suggests a mutualism between *C. albicans* and mice, and *C. albicans* modulating gut microbiota, metabolism, and immunity for the benefit of the host (Peroumal et al., 2022). In that context, using anti-fungal drugs will only cause dysbiosis similar to antibiotics and will enhance the severity of fungal and other secondary infections. At the same time, this long association of fungi and the host also suggests that both humans and *C. albicans* have evolved to recognize and develop some kinds of escape mechanisms to protect each other. The fact that the immunocompetent host is rarely affected by *Candida* infections again implements that humans have developed immunotolerance towards the commensal fungal pathogens. In contrast, to escape the host immune defense systems, *C. albicans* adapts and evades by altering its shape, size, and genetic makeup. Morphological and genome plasticity is frequently found in clinical isolates of *C. albicans*. Probably, the immune memory of the host fails to recognize this newly evolved pathogen in immune compromised situations. Secondly, immune compromised patients may not respond to vaccines. Therefore, conceptually, it becomes difficult and challenging to develop drugs and immunotherapeutics against *Candida* species. While designing a suitable drug or a vaccine, it is important to take into account that it should not target the commensal state of *C. albicans* or other such fungi as it may be deleterious to the host development, and those should be equally effective in immune suppressed individuals. One way to overcome this issue is to validate drug and vaccine candidates at the preclinical stage itself by using humanized and immunodeficient mice models such as SCID or Nude rather than using inbred animals. Further, they need to be revalidated using higher animals. It is most likely that the antigenic-peptide based vaccines may not differentiate between

commensal and pathogenic states of *Candida*, in that context, a whole cell vaccine specifically designed against the pathogenic form has the advantage. Among the *Candida* species, *C. albicans* is the frequently clinically isolated pathogen. However, reports suggest that *C. parapsilosis* is frequently found in children, whereas *C. glabrata* is more prevalent among older aged adults. Thus, the candidate vaccines should also target *C. albicans* as well as non-*albicans* species. Since birth, *C. albicans* and non-*albicans* species evolve with humans. Ironically, although their life cycle operates in humans, we are not immune to fungal infections. They are highly likely to adopt to various niches in the human gut and other sites to evade the host's defense system. In fact, genetic, phenotypic, and morphological plasticity is commonly found in *C. albicans* and other non-*albicans* species. Therefore, fungal infections today have become one of the most challenging diseases to manage in humans. In addition to the vaccine, the adjuvant also plays an important role in the additional activation of T- or B-cells, thereby enhancing the immune response. The antigenicity of the immunogen is also greatly enhanced by the presence of a suitable adjuvant. Freund's adjuvant and alum adjuvant are commonly used in animals and humans, respectively. In the future, in order to achieve better efficacy without side effects, new adjuvants or modified adjuvants should be tested. Since fungal infections those are invasive and occur in immuno-compromised individuals, it will be challenging to have a vaccine that is equally effective in healthy and weaker individuals. Normally, the vaccine elicits either weak or no immune response in immune deficient individuals, in such a scenario, passive immunotherapy could be the other option. Passive immunotherapy, also known as adoptive immunotherapy, requires direct administration of immune system components, such as monoclonal antibodies, activated macrophages, etc. As discussed earlier, monoclonal antibody C7 (MAb C7) and Mycograb are some of the examples used in animals, however, their use, safety, and effectiveness for human use are yet to be determined.

Early diagnosis, identification of novel antifungals with high safety and low side effects, prophylactics, and immune-therapeutics are the need of the hour to combat fungal infections. Undoubtedly, we need a safe and effective fungal vaccine (s), however, challenges are immense both conceptually as well as on technical fronts to develop a successful vaccine against Candidiasis and other mycoses. So, the design of an effective vaccine should be such that (i) it should be highly immunogenic, (ii) it should protect against a wide range of fungal pathogens, (iii) it will not only target the market appealing superficial but also it should protect from bloodstream infections, and (iv) more importantly, it will be equally effective in individuals with compromised immunity. Thus, an approach to developing a pan-fungal vaccine should be ideal. In our laboratory, we have generated an array of DNA polymerase subunit knockouts of *C. albicans*, and some of them exhibit reduced or constitutive filamentation. A few of those strains show altered cell wall architectures and slow growth phenotypes (Acharya et al., 2016; Peroumal et al., 2019). Their ability to develop systemic candidiasis and protection against pathogenic

challenges is being explored to develop a whole-cell vaccine. Such knockouts may be generated for non-*albicans* species as well as to develop multivalent vaccine strains. Although there is a long way to go to develop a successful *Candida* vaccine, the future looks promising, and with the efforts of several immunologists working in the field, it will be feasible to have a multivalent vaccine similar to as against viruses and bacteria.

## Conclusion

Despite those fungal diseases are equally critical and fatal as viral and bacterial diseases, the nonavailability of broad-spectrum antifungals, early diagnostics, and approved vaccines clearly indicate the need for rigorous and coordinated efforts from researchers, public health authorities, and funding agencies. Global estimates suggest about a billion people getting affected by fungal infections and over 1.5 million infected people get killed by fungal diseases every year. Fungal diseases are still not taken seriously by health care providers probably as the fungal infections occur mostly as secondary to a primary disease such as AIDS, cancer, organ transplantation, etc. Therefore, a delay in treatment results in serious illness, organ dysfunction, and death. In the last two pandemic years, we have witnessed a rise in fungal infections due to SARS-CoV2 infections, and many of those infected patients succumbed to various mold infections. Since vaccination has been the major preventive measure for several infectious diseases, a safe and effective multivalent vaccine that targets the *Candida* species is a strong medical need of the hour to avoid deaths. More importantly, the vaccine should target both systemic candidiasis and mucosal infections. As the whole cell vaccines against viruses and bacteria are widely accepted, a similar approach may be undertaken to identify stable and more antigenic live attenuated strains of *C. albicans* that may protect a wide range of fungal infections. Considering the importance of trained immunity, such vaccines may also provide cross protection against bacterial infections.

## Author contributions

NA conceptualized and designed the manuscript, SS, SB, MS, PK, AD, BU, and SKP prepared an initial draft of the manuscript. NA wrote the final draft. NA obtained the funding. All authors contributed to the article and approved the submitted version.

## Acknowledgments

We thank our other laboratory colleagues for their inputs and helpful discussions. Financial support to NA's laboratory by Institutional core grant, DBT (BT/PR15470/MED/29/997/2015



and BT/PR32817/MED/29/1495/2020), and SERB (EMR-2016-000640) are greatly acknowledged.

## Conflict of interest

The authors declare that the research was conducted in the absence of any commercial or financial relationships that could be construed as a potential conflict of interest.

## References

- Acharya, N., Manohar, K., Nayak, S., Chatterjee, A., and Dalei, A. (2016). DNA Polymerase: A putative drug target against candidiasis. *Front. Life Sci.*, 12–22.
- Allert, S., Schulz, D., Kammer, P., Grossmann, P., Wolf, T., Schauble, S., et al. (2022). From environmental adaptation to host survival: Attributes that mediate pathogenicity of *Candida auris*. *Virulence* 13, 191–214. doi: 10.1080/21505594.2022.2026037
- Andre, F. E., Booy, R., Bock, H. L., Clemens, J., Datta, S. K., John, T. J., et al. (2008). Vaccination greatly reduces disease, disability, death and inequity worldwide. *Bull. World Health Organ* 86, 140–146. doi: 10.2471/BLT.07.040089
- Backert, L., and Kohlbacher, O. (2015). Immunoinformatics and epitope prediction in the age of genomic medicine. *Genome Med.* 7, 119. doi: 10.1186/s13073-015-0245-0
- Benitez, L. L., and Carver, P. L. (2019). Adverse effects associated with long-term administration of azole antifungal agents. *Drugs* 79, 833–853. doi: 10.1007/s40265-019-01127-8
- Berenguer, J., Buck, M., Witebsky, F., Stock, F., Pizzo, P. A., and Walsh, T. J. (1993). Lysis-centrifugation blood cultures in the detection of tissue-proven invasive candidiasis: disseminated versus single-organ infection. *Diagn. Microbiol. Infect. Dis.* 17, 103–109. doi: 10.1016/0732-8893(93)90020-8
- Bistoni, F., Vecchiarelli, A., Cenci, E., Puccetti, P., Marconi, P., and Cassone, A. (1986). Evidence for macrophage-mediated protection against lethal *Candida albicans* infection. *Infection Immun.* 51, 668–674. doi: 10.1128/iai.51.2.668-674.1986
- Bose, S., Aggarwal, S., Singh, D. V., and Acharya, N. (2020). Extracellular vesicles: An emerging platform in gram-positive bacteria. *Microbial Cell* 7, 312–322. doi: 10.15698/mic2020.12.737
- Brown, G. D., Denning, D. W., Gow, N. A., Levitz, S. M., Netea, M. G., and White, T. C. (2012). Hidden killers: human fungal infections. *Sci. Transl. Med.* 4, 165rv113. doi: 10.1126/scitranslmed.3004404
- Burnie, J., and Matthews, R. (2003). The role of antibodies against hsp90 in the treatment of fungal infections. *Drug News Perspect.* 16, 205–210. doi: 10.1358/dnp.2003.16.4.829331
- Butler, G., Rasmussen, M. D., Lin, M. F., Santos, M. A., Sakthikumar, S., Munro, C. A., et al. (2009). Evolution of pathogenicity and sexual reproduction in eight *Candida* genomes. *Nature* 459, 657–662. doi: 10.1038/nature08064
- Capilla, J., Clemons, K. V., Liu, M., Levine, H. B., and Stevens, D. A. (2009). *Saccharomyces cerevisiae* as a vaccine against coccidioidomycosis. *Vaccine* 27, 3662–3668. doi: 10.1016/j.vaccine.2009.03.030
- Cardenas-Freytag, L., Cheng, E., Mayeux, P., Domer, J. E., and Clements, J. D. (1999). Effectiveness of a vaccine composed of heat-killed *Candida albicans* and a novel mucosal adjuvant, LT(R192G), against systemic candidiasis. *Infection Immun.* 67, 826–833. doi: 10.1128/IAI.67.2.826-833.1999
- Cardenas-Freytag, L., Steele, C., Wormley, F. L. Jr., Cheng, E., Clements, J. D., and Fidel, P. L. Jr. (2002). Partial protection against experimental vaginal candidiasis after mucosal vaccination with heat-killed *Candida albicans* and the mucosal adjuvant LT(R192G). *Med. mycology* 40, 291–299. doi: 10.1080/mmy.40.3.291.299
- Carneiro, C., Correia, A., Collins, T., Vilanova, M., Pais, C., Gomes, A. C., et al. (2015). DODAB: monoolin liposomes containing *Candida albicans* cell wall surface proteins: a novel adjuvant and delivery system. *Eur. J. Pharm. Biopharm* 89, 190–200. doi: 10.1016/j.ejpb.2014.11.028
- Carneiro, C., Correia, A., Lima, T., Vilanova, M., Pais, C., Gomes, A. C., et al. (2016). Protective effect of antigen delivery using monoolin-based liposomes in experimental hematogenously disseminated candidiasis. *Acta biomaterialia* 39, 133–145. doi: 10.1016/j.actbio.2016.05.001
- Cassone, A. (2008). Fungal vaccines: real progress from real challenges. *Lancet Infect. Dis.* 8, 114–124. doi: 10.1016/S1473-3099(08)70016-1
- Chaffin, W. L., Lopez-Ribot, J. L., Casanova, M., Gozalbo, D., and Martinez, J. P. (1998). Cell wall and secreted proteins of *Candida albicans*: identification, function, and expression. *Microbiology and molecular biology reviews* 62(1), 130–80. doi: 10.1128/MMBR.62.1.130-180
- Cassone, A., Bromuro, C., Chiani, P., and Torosantucci, A. (2010). Hyr1 protein and beta-glucan conjugates as anti-candida vaccines. *J. Infect. Dis.* 202, 1930. doi: 10.1086/657417
- Cassone, A., and Casadevall, A. (2012). Recent progress in vaccines against fungal diseases. *Curr. Opin. Microbiol.* 15, 427–433. doi: 10.1016/j.mib.2012.04.004
- De Bernardis, F., Amacker, M., Arancia, S., Sandini, S., Gremion, C., Zurbriggen, R., et al. (2012). A virosomal vaccine against candidal vaginitis: immunogenicity, efficacy and safety profile in animal models. *Vaccine* 30, 4490–4498. doi: 10.1016/j.vaccine.2012.04.069
- De Bernardis, F., Boccanera, M., Adriani, D., Girolamo, A., and Cassone, A. (2002). Intravaginal and intranasal immunizations are equally effective in inducing vaginal antibodies and conferring protection against vaginal candidiasis. *Infection Immun.* 70, 2725–2729. doi: 10.1128/IAI.70.5.2725-2729.2002
- Devi, S. J. (1996). Preclinical efficacy of a glucuronoxylomannan-tetanus toxoid conjugate vaccine of *Cryptococcus neoformans* in a murine model. *Vaccine* 14, 841–844. doi: 10.1016/0264-410X(95)00256-Z
- Dziadek, S., Bundle, D. R., and Cutler, J. E. (2008). Synthetic glycopeptide vaccines combining b-mannan and peptide epitopes induce protection against candidiasis. *Proceedings of the National Academy of Sciences* 105 (36), 13526–13531. doi: 10.1073/pnas.0803195105
- Eckstein, M., Barenholz, Y., Bar, L. K., and Segal, E. (1997). Liposomes containing *Candida albicans* ribosomes as a prophylactic vaccine against disseminated candidiasis in mice. *Vaccine* 15, 220–224. doi: 10.1016/S0264-410X(96)00137-5
- Edwards, J. E. Jr., Schwartz, M. M., Schmidt, C. S., Sobel, J. D., Nyirjesy, P., Schodel, F., et al. (2018). A fungal immunotherapeutic vaccine (NDV-3A) for treatment of recurrent vulvovaginal candidiasis—a phase 2 randomized, double-blind, placebo-controlled trial. *Clin. Infect. Dis. an Off. Publ. Infect. Dis. Soc. America* 66, 1928–1936. doi: 10.1093/cid/ciy185
- Fernandez-Arenas, E., Molero, G., Nombela, C., Diez-Orejas, R., and Gil, C. (2004). Contribution of the antibodies response induced by a low virulent *Candida albicans* strain in protection against systemic candidiasis. *Proteomics* 4, 1204–1215. doi: 10.1002/pmic.200300678
- Ford, C. B., Funt, J. M., Abbey, D., Issi, L., Guiducci, C., Martinez, D. A., et al. (2015). The evolution of drug resistance in clinical isolates of *Candida albicans*. *eLife* 4, e00662. doi: 10.7554/eLife.00662
- Freitas, M. S., Bonato, V. L. D., Pessoni, A. M., Rodrigues, M. L., Casadevall, A., and Almeida, F. (2019). Fungal extracellular vesicles as potential targets for immune interventions. *mSphere* 4. doi: 10.1128/mSphere.00747-19
- Garcia-Vidal, C., Viasus, D., and Carratala, J. (2013). Pathogenesis of invasive fungal infections. *Curr. Opin. Infect. Dis.* 26, 270–276. doi: 10.1097/QCO.0b013e32835fb920
- Han, Y., and Cutler, J. E. (1995). Antibody response that protects against disseminated candidiasis. *Infection Immun.* 63, 2714–2719. doi: 10.1128/iai.63.7.2714-2719.1995
- Han, Y., Morrison, R. P., and Cutler, J. E. (1998). A vaccine and monoclonal antibodies that enhance mouse resistance to *Candida albicans* vaginal infection. *Infection Immun.* 66(12), 5771–5776. doi: 10.1128/IAI.66.12.5771-5776.1998

## Publisher's note

All claims expressed in this article are solely those of the authors and do not necessarily represent those of their affiliated organizations, or those of the publisher, the editors and the reviewers. Any product that may be evaluated in this article, or claim that may be made by its manufacturer, is not guaranteed or endorsed by the publisher.



- Hawthornth, D. L., and Lucking, R. (2017). Fungal diversity revisited: 2.2 to 3.8 million species. *Microbiol. Spectr.* 5(4), 5–4. doi: 10.1128/microbiolspec.FUNK-0052-2016
- Hoyer, L. L., and Cota, E. (2016). *Candida albicans* agglutinin-like sequence (Als) family vignettes: A review of als protein structure and function. *Front. Microbiol.* 7, 280. doi: 10.3389/fmicb.2016.00280
- Ibrahim, A. S., Spellberg, B. J., Avanesian, V., Fu, Y., and Edwards, J. E. Jr. (2006). The anti-candida vaccine based on the recombinant n-terminal domain of Als1p is broadly active against disseminated candidiasis. *Infection Immun.* 74, 3039–3041. doi: 10.1128/IAI.74.5.3039-3041.2006
- Jermey, A. (2017). Stop neglecting fungi. *Nat. Microbiol.* 2, 17120. doi: 10.1038/nmicrobiol.2017.120
- Kim, J., and Sudbery, P. (2011). *Candida albicans*, a major human fungal pathogen. *J. Microbiol.* 49, 171–177. doi: 10.1007/s12275-011-1064-7
- Kleinnijenhuis, J., Quintin, J., Preijers, F., Joosten, L. A., Iffrim, D. C., Saeed, S., et al. (2012). Bacille calmette-guerin induces NOD2-dependent nonspecific protection from reinfection via epigenetic reprogramming of monocytes. *Proc. Natl. Acad. Sci. United States America* 109, 17537–17542. doi: 10.1073/pnas.1202870109
- Kleinnijenhuis, J., Quintin, J., Preijers, F., Joosten, L. A., Jacobs, C., Xavier, R. J., et al. (2014). BCG-Induced trained immunity in NK cells: Role for non-specific protection to infection. *Clin. Immunol.* 155, 213–219. doi: 10.1016/j.clim.2014.10.005
- Knotigova, P. T., Zyka, D., Masek, J., Kovalova, A., Krupka, M., Bartheldyova, E., et al. (2015). Molecular adjuvants based on nonpyrogenic lipophilic derivatives of norAbuMDP/GMDP formulated in nanoliposomes: stimulation of innate and adaptive immunity. *Pharm. Res.* 32, 1186–1199. doi: 10.1007/s11095-014-1516-y
- Kounis, N. G. (2013). Caspofungin-induced fatal complete heart block: Another manifestation of kounis syndrome. *J. Pharmacol. Pharmacother.* 4, 161–162. doi: 10.1177/0976500X20130201
- Lancaster, K. Z., and Pfeiffer, J. K. (2011). Mechanisms controlling virulence thresholds of mixed viral populations. *J. Virol.* 85, 9778–9788. doi: 10.1128/JVI.00355-11
- Lee, Y., Puumala, E., Robbins, N., and Cowen, L. E. (2021). Antifungal drug resistance: Molecular mechanisms in *Candida albicans* and beyond. *Chem. Rev.* 121, 3390–3411. doi: 10.1021/acs.chemrev.0c00199
- Leibovitch, E. C., and Jacobson, S. (2016). Vaccinations for neuroinfectious disease: A global health priority. *Neurotherapeutics* 13, 562–570. doi: 10.1007/s13311-016-0453-3
- Liao, J., Pan, B., Liao, G., Zhao, Q., Gao, Y., Chai, X., et al. (2019). Synthesis and immunological studies of beta-1,2-mannan-peptide conjugates as antifungal vaccines. *Eur. J. Med. Chem.* 173, 250–260. doi: 10.1016/j.ejmech.2019.04.001
- Lin, L., Ibrahim, A. S., Xu, X., Farber, J. M., Avanesian, V., Baquir, B., et al. (2009). Th1-Th17 cells mediate protective adaptive immunity against *Staphylococcus aureus* and *Candida albicans* infection in mice. *PLoS Pathog.* 5, e1000703. doi: 10.1371/journal.ppat.1000703
- Liu, M., Capilla, J., Johansen, M. E., Alvarado, D., Martinez, M., Chen, V., et al. (2011a). *Saccharomyces* as a vaccine against systemic aspergillosis: 'the friend of man' a friend again? *J. Med. Microbiol.* 60, 1423–1432. doi: 10.1099/jmm.0.033290-0
- Liu, M., Clemons, K. V., Bigos, M., Medovarska, I., Brummer, E., and Stevens, D. A. (2011b). Immune responses induced by heat killed *Saccharomyces cerevisiae*: a vaccine against fungal infection. *Vaccine* 29, 1745–1753. doi: 10.1016/j.vaccine.2010.12.119
- Liu, M., Clemons, K. V., Johansen, M. E., Martinez, M., Chen, V., Stevens, D. A., et al. (2012). *Saccharomyces* as a vaccine against systemic candidiasis. *Immunol. Invest.* 41, 847–855. doi: 10.3109/08820139.2012.692418
- Li, X., Yang, Y., Yang, F., Wang, F., Li, H., Tian, H., et al. (2021). Chitosan hydrogel loaded with recombinant protein containing epitope c from HSP90 of *Candida albicans* induces protective immune responses against systemic candidiasis. *Int. J. Biol. Macromolecules* 173, 327–340. doi: 10.1016/j.jbiomac.2021.01.105
- Lo, H. J., Kohler, J. R., DiDomenico, B., Loebenberg, D., Cacciapuoti, A., and Fink, G. R. (1997). Nonfilamentous *C. albicans* mutants are avirulent. *Cell* 90, 939–949. doi: 10.1016/S0092-8674(00)80358-X
- Luo, G., Ibrahim, A. S., French, S. W., Edwards, J. E. Jr., and Fu, Y. (2011). Active and passive immunization with rHyr1p-n protects mice against hematogenously disseminated candidiasis. *PLoS One* 6, e25909. doi: 10.1371/journal.pone.0025909
- Mangtani, P., Abubakar, I., Ariti, C., Beynon, R., Pimpin, L., Fine, P. E., et al. (2014). Protection by BCG vaccine against tuberculosis: a systematic review of randomized controlled trials. *Clin. Infect. Dis. an Off. Publ. Infect. Dis. Soc. America* 58, 470–480. doi: 10.1093/cid/cit790
- Manohar, K., Peroumal, D., and Acharya, N. (2018). TLS Dependent and independent functions of DNA polymerase eta (Poleta/Rad30) from pathogenic yeast *Candida albicans*. *Mol. Microbiol.* 110, 707–727. doi: 10.1111/mmi.14004
- Marchetti, O., Bille, J., Fluckiger, U., Eggimann, P., Ruef, C., Garbino, J., et al. (2004). Epidemiology of candidemia in Swiss tertiary care hospitals: secular trends, 1991–2000. *Clin. Infect. Dis. an Off. Publ. Infect. Dis. Soc. America* 38, 311–320. doi: 10.1086/380637
- Martin-Cruz, L., Sevilla-Ortega, C., Benito-Villalvilla, C., Diez-Rivero, C. M., Sanchez-Ramon, S., Subiza, J. L., et al. (2020). A combination of polybacterial MV140 and *Candida albicans* V132 as a potential novel trained immunity-based vaccine for genitourinary tract infections. *Front. Immunol.* 11, 612269. doi: 10.3389/fimmu.2020.612269
- Martinez, J. P., Gil, M. L., López-Ribot, J. L., and Chaffin, W. L. (1998). Serologic response to cell wall mannoproteins and proteins of *Candida albicans*. *Clinical microbiology reviews* 11(1), 121–41. doi: 10.1128/CMR.11.1.121
- Martinez-Jimenez, M. C., Munoz, P., Guinea, J., Valerio, M., Alonso, R., Escribano, P., et al. (2014). Potential role of *Candida albicans* germ tube antibody in the diagnosis of deep-seated candidemia. *Med. mycology* 52, 270–275. doi: 10.1093/mmy/myt025
- Martinez-Lopez, R., Nombela, C., Diez-Orejas, R., Monteoliva, L., and Gil, C. (2008). Immunoproteomic analysis of the protective response obtained from vaccination with *Candida albicans* ecm33 cell wall mutant in mice. *Proteomics* 8, 2651–2664. doi: 10.1002/pmic.200701056
- Masek, J., Bartheldyova, E., Turanek-Knotigova, P., Skrabalova, M., Korvasova, Z., Plockova, J., et al. (2011). Metallochelating liposomes with associated lipophilised norAbuMDP as biocompatible platform for construction of vaccines with recombinant h-tagged antigens: preparation, structural study and immune response towards rHsp90. *J. Control Release* 151, 193–201. doi: 10.1016/j.jconrel.2011.01.016
- Matthews, R., and Burnie, J. (1989). Cloning of a DNA sequence encoding a major fragment of the 47 kilodalton stress protein homologue of *Candida albicans*. *FEMS Microbiol. Lett.* 51, 25–30. doi: 10.1111/j.1574-6968.1989.tb03413.x
- Matthews, R. C., Burnie, J. P., and Tabachali, S. (1987). Isolation of immunodominant antigens from sera of patients with systemic candidiasis and characterization of serological response to *Candida albicans*. *J. Clin. Microbiol.* 25, 230–237. doi: 10.1128/jcm.25.2.230-237.1987
- Matthews, R. C., Rigg, G., Hodgetts, S., Carter, T., Chapman, C., Gregory, C., et al. (2003). Preclinical assessment of the efficacy of mycograb, a human recombinant antibody against fungal HSP90. *Antimicrobial Agents chemotherapy* 47, 2208–2216. doi: 10.1128/AAC.47.7.2208-2216.2003
- Millar, E. V., Bennett, J. W., Barin, B., Carey, P. M., Law, N. N., English, C. E., et al. (2021). Safety, immunogenicity, and efficacy of NDV-3A against *Staphylococcus aureus* colonization: A phase 2 vaccine trial among US army infantry trainees. *Vaccine* 39, 3179–3188. doi: 10.1016/j.vaccine.2021.04.031
- Naglik, J. R., Challacombe, S. J., and Hube, B. (2003). *Candida albicans* secreted aspartyl proteinases in virulence and pathogenesis. *Microbiol. Mol. Biol. Rev.* 67(3), 400–28. doi: 10.1128/MMBR.67.3.400-428.2003
- Netea, M. G., Quintin, J., and van der Meer, J. W. (2011). Trained immunity: a memory for innate host defense. *Cell Host Microbe* 9, 355–361. doi: 10.1016/j.chom.2011.04.006
- Peroumal, D., Manohar, K., Patel, S. K., Kumari, P., Sahu, S. R., and Acharya, N. (2019). Virulence and pathogenicity of a *Candida albicans* mutant with reduced filamentation. *Cell. Microbiol.* 21, e13103. doi: 10.1111/cmi.13103
- Peroumal, D., Sahu, S. R., Kumari, P., Utkalaja, B., and Acharya, N. (2022). Commensal fungi *Candida albicans* modulates dietary high-fat induced alterations in metabolism, immunity, and gut microbiota. *bioRxiv*. doi: 10.1101/2022.03.23.485455
- Petrovsky, N., and Aguilar, J. C. (2004). Vaccine adjuvants: current state and future trends. *Immunol. Cell Biol.* 82, 488–496. doi: 10.1111/j.0818-9641.2004.01272.x
- Pietrella, D., Rachini, A., Torosantucci, A., Chiani, P., Brown, A. J., Bistoni, F., et al. (2010). A beta-glucan-conjugate vaccine and anti-beta-glucan antibodies are effective against murine vaginal candidiasis as assessed by a novel *in vivo* imaging technique. *Vaccine* 28, 1717–1725. doi: 10.1016/j.vaccine.2009.12.021
- Raska, M., Belakova, J., Horynova, M., Krupka, M., Novotny, J., Sebestova, M., et al. (2008). Systemic and mucosal immunization with *Candida albicans* hsp90 elicits hsp90-specific humoral response in vaginal mucosa which is further enhanced during experimental vaginal candidiasis. *Med. mycology* 46, 411–420. doi: 10.1080/13693780701883508
- Riedel, S. (2005). Edward Jenner And the history of smallpox and vaccination. *Proc. (Bayl Univ Med. Cent)* 18, 21–25. doi: 10.1080/08998280.2005.11928028
- Rizzo, J., Rodrigues, M. L., and Janbon, G. (2020). Extracellular vesicles in fungi: Past, present, and future perspectives. *Front. Cell Infect. Microbiol.* 10, 346. doi: 10.3389/fcimb.2020.00346
- Rodrigues, M. L., Nosanchuk, J. D., Schrank, A., Vainstein, M. H., Casadevall, A., and Nimrichter, L. (2011). Vesicular transport systems in fungi. *Future Microbiol.* 6, 1371–1381. doi: 10.2217/fmb.11.112

- Rudkin, F. M., Raziunaite, I., Workman, H., Essono, S., Belmonte, R., MacCallum, D. M., et al. (2018). Single human b cell-derived monoclonal anti-candida antibodies enhance phagocytosis and protect against disseminated candidiasis. *Nat. Commun.* 9, 5288. doi: 10.1038/s41467-018-07738-1
- Saccante, M., and Woods, G. L. (2010). Clinical and laboratory update on blastomycosis. *Clin. Microbiol. Rev.* 23, 367–381. doi: 10.1128/CMR.00056-09
- Sandini, S., La Valle, R., Deaglio, S., Malavasi, F., Cassone, A., and De Bernardis, F. (2011). A highly immunogenic recombinant and truncated protein of the secreted aspartic proteases family (rSap2t) of candida albicans as a mucosal anticandidal vaccine. *FEMS Immunol. Med. Microbiol.* 62, 215–224. doi: 10.1111/j.1574-695X.2011.00802.x
- Santos, E., and Levitz, S. M. (2014). Fungal vaccines and immunotherapeutics. *Cold Spring Harbor Perspect. Med.* 4, a019711. doi: 10.1101/cshperspect.a019711
- Sapkal, G. N., Yadav, P. D., Ella, R., Deshpande, G. R., Sahay, R. R., Gupta, N., et al. (2021). Inactivated COVID-19 vaccine BBV152/COVAXIN effectively neutralizes recently emerged B.1.1.7 variant of SARS-CoV-2. *J. Travel Med.* 28 (4). doi: 10.1093/jtm/taab051
- Saville, S. P., Lazzell, A. L., Chaturvedi, A. K., Monteagudo, C., and Lopez-Ribot, J. L. (2009). Efficacy of a genetically engineered candida albicans tet-NRG1 strain as an experimental live attenuated vaccine against hematogenously disseminated candidiasis. *Clin. Vaccine Immunol. CVI* 16, 430–432. doi: 10.1128/CI.00480-08
- Schmidt, C. S., White, C. J., Ibrahim, A. S., Filler, S. G., Fu, Y., Yeaman, M. R., et al. (2012). NDV-3, a recombinant alum-adjuvanted vaccine for candida and staphylococcus aureus, is safe and immunogenic in healthy adults. *Vaccine* 30, 7594–7600. doi: 10.1016/j.vaccine.2012.10.038
- Sesardic, D. (1993). Synthetic peptide vaccines. *J. Med. Microbiol.* 39, 241–242. doi: 10.1099/00222615-39-4-241
- Shen, H., Yu, Y., Chen, S. M., Sun, J. J., Fang, W., Guo, S. Y., et al. (2020). Dectin-1 facilitates IL-18 production for the generation of protective antibodies against candida albicans. *Front. Microbiol.* 11, 1648. doi: 10.3389/fmicb.2020.01648
- Shukla, M., and Rohatgi, S. (2020). Vaccination with secreted aspartyl proteinase 2 protein from candida parapsilosis can enhance survival of mice during c. tropicalis-mediated systemic candidiasis. *Infection Immun.* 88(10), e00312–20. doi: 10.1128/IAI.00312-2
- Shibasaki, S., Karasaki, M., Tafuku, S., Aoki, W., Sewaki, T., Ueda, M., et al. (2014). Oral immunization against candidiasis using Lactobacillus casei displaying enolase 1 from Candida albicans. *Scientia Pharmaceutica* 82(3), 697–708. doi: 10.3797/scipharma.1404-07
- Singh, S., Uppuluri, P., Mamouei, Z., Alqarihi, A., Elhassan, H., French, S., et al. (2019). The NDV-3A vaccine protects mice from multidrug resistant candida auris infection. *PLoS Pathog.* 15, e1007460. doi: 10.1371/journal.ppat.1007460
- Spellberg, B. J., Filler, S. G., and Edwards, J. E. Jr. (2006). Current treatment strategies for disseminated candidiasis. *Clin. Infect. Dis. an Off. Publ. Infect. Dis. Soc. America* 42, 244–251. doi: 10.1086/499057
- Spellberg, B. J., Ibrahim, A. S., Avanesian, V., Fu, Y., Myers, C., Phan, Q. T., et al. (2006). Efficacy of the anti-candida rAls3p-n or rAls1p-n vaccines against disseminated and mucosal candidiasis. *J. Infect. Dis.* 194, 256–260. doi: 10.1086/504691
- Spellberg, B. J., Ibrahim, A. S., Avenissian, V., Filler, S. G., Myers, C. L., Fu, Y., et al. (2005). The anti-candida albicans vaccine composed of the recombinant n terminus of Als1p reduces fungal burden and improves survival in both immunocompetent and immunocompromised mice. *Infection Immun.* 73, 6191–6193. doi: 10.1128/IAI.73.9.6191-6193.2005
- Spellberg, B., Ibrahim, A. S., Yeaman, M. R., Lin, L., Fu, Y., Avanesian, V., et al. (2008). The antifungal vaccine derived from the recombinant n terminus of Als3p protects mice against the bacterium staphylococcus aureus. *Infection Immun.* 76, 4574–4580. doi: 10.1128/IAI.00700-08
- Stevens, D. A., Clemons, K. V., and Liu, M. (2011). Developing a vaccine against aspergillosis. *Med. mycology* 49 Suppl 1, S170–S176. doi: 10.3109/13693786.2010.497775
- Tarang, S., Kesharwani, V., LaTendresse, B., Lindgren, L., Rocha-Sanchez, S. M., and Weston, M. D. (2020). In silico design of a multivalent vaccine against candida albicans. *Sci. Rep.* 10, 1066. doi: 10.1038/s41598-020-57906-x
- Thomas, D. P., Viudes, A., Monteagudo, C., Lazzell, A. L., Saville, S. P., and Lopez-Ribot, J. L. (2006). A proteomic-based approach for the identification of candida albicans protein components present in a subunit vaccine that protects against disseminated candidiasis. *Proteomics* 6, 6033–6041. doi: 10.1002/pmic.200600321
- Thornton, C. R. (2008). Development of an immunochromatographic lateral-flow device for rapid serodiagnosis of invasive aspergillosis. *Clin. Vaccine Immunol. CVI* 15, 1095–1105. doi: 10.1128/CI.00068-08
- Torosantucci, A., Bromuro, C., Chiani, P., De Bernardis, F., Berti, F., Galli, C., et al. (2005). A novel glyco-conjugate vaccine against fungal pathogens. *J. Exp. Med.* 202, 597–606. doi: 10.1084/jem.20050749
- Tso, G. H. W., Reales-Calderon, J. A., and Pavelka, N. (2018). The elusive anti-candida vaccine: Lessons from the past and opportunities for the future. *Front. Immunol.* 9, 897. doi: 10.3389/fimmu.2018.00897
- van 't Wout, J. W., Poell, R., and van Furth, R. (1992). The role of BCG/PPD-activated macrophages in resistance against systemic candidiasis in mice. *Scandinavian J. Immunol.* 36, 713–719. doi: 10.1111/j.1365-3083.1992.tb03132.x
- Vargas, G., Honorato, L., Guimaraes, A. J., Rodrigues, M. L., Reis, F. C. G., Vale, A. M., et al. (2020). Protective effect of fungal extracellular vesicles against murine candidiasis. *Cell. Microbiol.* 22, e13238. doi: 10.1111/cmi.13238
- Volant, A. R., Quindos, G., Alarcon, K. P., Fusco-Almeida, A. M., Mendes-Giannini, M. J., and Chorilli, M. (2016). Fungal diseases: could nanostructured drug delivery systems be a novel paradigm for therapy? *Int. J. Nanomedicine* 11, 3715–3730. doi: 10.2147/IJN.S93105
- Wang, X. J., Sui, X., Yan, L., Wang, Y., Cao, Y. B., and Jiang, Y. Y. (2015). Vaccines in the treatment of invasive candidiasis. *Virulence* 6 (6), 309–315. doi: 10.4161/215055594.2014.983015
- Wang, Y., Wang, K., Masso-Silva, J. A., Rivera, A., and Xue, C. (2019). A heat-killed cryptococcus mutant strain induces host protection against multiple invasive mycoses in a murine vaccine model. *mBio* 10. doi: 10.1128/mBio.02145-19
- Wuthrich, M., Wang, H., Li, M., Lerksthirat, T., Hardison, S. E., Brown, G. D., et al. (2015). Fonsecaea pedrosoi-induced Th17-cell differentiation in mice is fostered by dectin-2 and suppressed by mincle recognition. *Eur. J. Immunol.* 45, 2542–2552. doi: 10.1002/eji.201545591
- Xin, H. (2016). Active immunizations with peptide-DC vaccines and passive transfer with antibodies protect neutropenic mice against disseminated candidiasis. *Vaccine* 34 (2), 245–251. doi: 10.1016/j.vaccine.2015.11.035
- Xin, H., and Cutler, J. E. (2006). Hybridoma passage in vitro may result in reduced ability of antimannan antibody to protect against disseminated candidiasis. *Infection and immunity* 74 (7), 4310–21. doi: 10.1128/IAI.00234-06
- Xin, H., Dziadek, S., Bundle, D. R., and Cutler, J. E. (2008). Synthetic glycopeptide vaccines combining  $\beta$ -mannan and peptide epitopes induce protection against candidiasis. *P. Nat. Acad. of Sci.* 105(36), 13526–13531. doi: 10.1073/pnas.0803195105
- Xin, H., Cartmell, J., Bailey, J. J., Dziadek, S., Bundle, D. R., and Cutler, J. E. (2012). Self-adjuvanted glycopeptide conjugate vaccine against disseminated candidiasis. *PLoS One* 7, e35106. doi: 10.1371/journal.pone.0035106
- Xin, H., Glee, P., Adams, A., Mohiuddin, F., and Eberle, K. (2019). Design of a mimotope-peptide based double epitope vaccine against disseminated candidiasis. *Vaccine* 37, 2430–2438. doi: 10.1016/j.vaccine.2019.03.061
- Yang, Y. L., Wang, C. W., Chen, C. T., Wang, M. H., Hsiao, C. F., and Lo, H. J. (2009). Non-lethal candida albicans cph1/cph1 efg1/efg1 mutant partially protects mice from systemic infections by lethal wild-type cells. *Mycol Res.* 113, 388–390. doi: 10.1016/j.mycres.2008.11.016



## OPEN ACCESS

## EDITED BY

Parth Sarthi Sen Gupta,  
Indian Institute of Science Education  
and Research Berhampur (IISER), India

## REVIEWED BY

Michal Letek,  
Universidad de León, Spain  
Ved Prakash Dwivedi,  
International Centre for Genetic  
Engineering and Biotechnology  
(India), India

## \*CORRESPONDENCE

Mohanapriya Arumugam  
mohanapriya@vit.ac.in

## SPECIALTY SECTION

This article was submitted to  
Clinical Microbiology,  
a section of the journal  
Frontiers in Cellular and  
Infection Microbiology

RECEIVED 03 August 2022

ACCEPTED 21 September 2022

PUBLISHED 05 October 2022

## CITATION

Ponnusamy N and Arumugam M  
(2022) Meta-analysis of active  
tuberculosis gene expression  
ascertains host directed  
drug targets.  
*Front. Cell. Infect. Microbiol.*  
12:1010771.  
doi: 10.3389/fcimb.2022.1010771

## COPYRIGHT

© 2022 Ponnusamy and Arumugam.  
This is an open-access article  
distributed under the terms of the  
Creative Commons Attribution License  
(CC BY). The use, distribution or  
reproduction in other forums is  
permitted, provided the original  
author(s) and the copyright owner(s)  
are credited and that the original  
publication in this journal is cited, in  
accordance with accepted academic  
practice. No use, distribution or  
reproduction is permitted which does  
not comply with these terms.

# Meta-analysis of active tuberculosis gene expression ascertains host directed drug targets

Nirmaladevi Ponnusamy and Mohanapriya Arumugam

Department of Biotechnology, School of Biosciences and Technology, Vellore Institute of Technology, Vellore, Tamil Nadu, India

Multi-drug resistant tuberculosis still remains a major public health crisis globally. With the emergence of newer active tuberculosis disease, the requirement of prolonged treatment time and adherence to therapy till its completion necessitates the search of newer therapeutics, targeting human host factors. The current work utilized statistical meta-analysis of human gene transcriptomes of active pulmonary tuberculosis disease obtained from six public datasets. The meta-analysis resulted in the identification of 2038 significantly differentially expressed genes (DEGs) in the active tuberculosis disease. The gene ontology (GO) analysis revealed that these genes were major contributors in immune responses. The pathway enrichment analyses identified from various human canonical pathways are related to other infectious diseases. In addition, the comparison of the DEGs with the tuberculosis genome wide association study (GWAS) datasets revealed the presence of few genetic variants in their proximity. The analysis of protein interaction networks (human and *Mycobacterium tuberculosis*) and host directed drug-target interaction network led to new candidate drug targets for drug repurposing studies. The current work sheds light on host genes and pathways enriched in active tuberculosis disease and suggest potential drug repurposing targets for host-directed therapies.

## KEYWORDS

tuberculosis, meta-analysis, gene ontology, pathway enrichment, genetic variants, drug repurposing

## Introduction

Tuberculosis (TB) is an infectious disease which remained throughout human history. *Mycobacterium tuberculosis* (*Mtb*) is the main causative agent of TB. Around 10% of individuals develop TB when exposed to *Mtb* and 5% of the infected individuals develop TB within 1-2 years while the remaining 5% develop the disease at any other time (Frieden

et al., 2003). Active TB has higher burden of TB when compared to latent TB (Lee, 2016). Individuals with compromised immune systems, such as people with HIV, diabetes or people with constant tobacco use are at high risk of falling ill.

TB is the 13<sup>th</sup> leading cause of death globally in 2020. Around 86% of new cases reported around the world in 2020 were contributed majorly by China, Indonesia, the Philippines, Pakistan, Nigeria, Bangladesh and South Africa with India leading the list (WHO, 2021). Over the period of time *Mtb* has adopted newer subversion strategies to successfully evade the host immune system enabling it to reside in the host resulting in latent or active disease manifestation (Behar et al., 2010; Ernst, 2018).

The infection results in a complex dynamics between the host and pathogen triggering various immune signalling cascades and cross-talks between molecular components (Casadevall and Pirofski, 2000). Several contributing factors associated with the disease were identified through genetic and biochemical experimental studies. The recent surge of omics data has further aided in understanding of factors influencing predisposition of the disease and markers associated with the disease severity.

With increased availability of gene expression data, studies based on TB blood transcriptomics offers a robust approach to study the immunology of TB. The comparative studied of healthy and TB cohorts shed light on differentially expressed genes (DEGs) and also allow observations of such DEG upon vaccine/drug treatment. Further the DEG analysis also aids in understanding of regulatory mechanisms contributing to the functional consequences.

In the current study, a statistical meta-analysis was carried out using whole blood expression profiles from infected TB patients to identify key human transcriptomics signatures characteristic of the disease. The study also utilized host genetic disease association and drug-repurposing analyses to further to prioritize the results. In addition, the gene ontology and pathway-based annotations identified genes and pathways significantly altered in the diseased condition.

## Materials and methods

### Dataset selection and processing

The whole-blood microarray gene expression profiles of patients with active pulmonary tuberculosis and healthy cohorts were retrieved from NCBI GEO (Barrett et al., 2013). The datasets were further filtered based on the following conditions: (i) The expression profiles were from human patients affected by tuberculosis undergoing no prior treatment, (ii) Only samples from active tuberculosis patients and control groups were considered, (iii) The datasets should include both healthy controls and patient group, (iv) The patient or the control group should not be infected with any other secondary diseases, (v) The patient and control group should include more than 5 samples each.

The background corrected files were processed using limma package in R (Ritchie et al., 2015). The data were quantile normalized, log transformed and missing values were removed. The probe identifiers were converted to Entrez gene IDs. If multiple probes are mapped to a single gene, then the average expression value of the probes were used for the gene. Post normalization, individual datasets were subjected to Principal Component Analysis (PCA). PCA was carried out to observe a distinct separation between the active and control samples.

### Statistical meta-analysis and validation

Statistical meta-analysis was carried out using NetworkAnalyst (Zhou et al., 2019). NetworkAnalyst interprets gene expression data including meta-analysis, tissue specific PPI networks, gene regulatory networks, gene co-expression networks along with networks for toxicogenomics and pharmacogenomics studies. The pre-processed expression values were used as input for the web tool. Differential expression analysis for each dataset was performed using limma with false discovery rate (FDR) cutoff of 0.05. The batch effects were adjusted using ComBat method. The corrected datasets were merged and statistical meta-analysis was carried out using INMEX. The combined effect size method for meta-analysis was used to generate the results. The random effect model which encloses cross-study heterogeneity was used for meta-analysis. Differentially expressed genes (DEG) were obtained using FDR cutoff of 0.01 in the meta-analysis. The DEGs with absolute combined effect size > 1.5 were chosen for genetic variant analyses and drug interaction analyses.

### Validation of meta-analysis

The strength of the results obtained from meta-analysis was further validated by comparing the genes expressed in latent and control samples from the same datasets. Partial Least Square Discriminant Analysis (PLS-DA) was applied to the DEGs. Significant model was selected by 7-fold cross validation. The model performance was evaluated using the area under the Receiver Operating Characteristic (ROC) curve (AUC). All the above validation process was carried out using mixOmics package in R (Rohart et al., 2017).

### Gene and pathway enrichment

Gene and pathway enrichment analysis was carried out using DAVID web server to identify significantly enriched Gene ontology (GO) biological processes (BPs) and KEGG pathways, which were ranked based on the hypergeometric test with FDR cutoff of 0.05 (Sherman et al., 2022). DAVID web server offers functional annotation and enrichment analyses of gene lists provided by the user.



## Protein-protein interaction network construction

A comprehensive human protein-protein interaction network (hPPI) was constructed. High confidence, experimentally verified interactions extracted from STRING database was used for the construction (Szkłarczyk et al., 2021). The STRING database integrates known and predicted associations between proteins encompassing physical interactions and functional associations. Similarly, the pathogen proteins interacting with host DEG were mined from various literature sources (Rapanoel et al., 2013; Penn et al., 2018; Augenstreich and Briken, 2020; Verma et al., 2022). These data were used to construct human protein – *Mtb* protein interaction network (hmPPI).

The highly interconnected components of the hPPI and hmPPI were identified using the Cytoscape plugin CytoHubba. CytoHubba is a user-friendly interface to explore important nodes in biological networks using various topological metrics. The hub genes of the networks were identified using the topological metrics degree and Maximal Clique Centrality (MCC) (Chin et al., 2014).

## Drug-target interaction

The drug compounds interacting with DEG were retrieved from DrugBank Version 5 (Wishart et al., 2018). DrugBank is a comprehensive database which holds information about drugs, their mechanisms, interactions and targets. Drugs with experimental or clinical evidence for direct interactions with the protein were selected. Drugs with pharmacological actions as the same direction of the DEG and drugs with unknown pharmacological actions were excluded. Only DEGs with a combined effect size greater than 1.5 were considered for the analysis.

## Genetic variant analysis

The genetic differences between tuberculosis-affected and healthy individuals can give a mechanistic insight about the disease and functional implication of the affected gene. The single nucleotide polymorphisms (SNPs) proximal to the DEG were obtained from GRASP database (P-value < 5e-8) (Leslie et al., 2014). GRASP database encloses deeply extracted and annotated database of genome-wide association studies (GWAS) results enclosing more than 6.2 million SNP-phenotype association. Similarly, the regulatory SNP were retrieved from Slidebase database using the enhancer regions of the DEG (Ienasescu et al., 2016). SlideBase offers a new way of selecting genes, promoters, enhancers and microRNAs that are

preferentially expressed/used in a specified set of cells/tissues. The genomic regions in linkage disequilibrium (LD) with the SNP were collected from SNAP (Johnson et al., 2008). The association between a gene and its corresponding SNP was prioritized based on the overlap between the genomic location of the DEG or its enhancer and LD region of a SNP. The query tool SNAP enables the identification of single-nucleotide polymorphisms (SNPs) and annotate nearby SNPs in linkage disequilibrium (proxies) based on HapMap project results.

## Results

The work plan and approaches implemented in the current study is illustrated in Figure 1.

### Identification and validation of DEG from meta-analysis

The database querying and filtering identified around 149 GEO microarray datasets for TB-related host response at the time of study (June 2022). Further, filtering based on the study inclusion criteria, a total of six datasets enclosing control and active TB samples were selected for next set analyses (Table 1).

The results of PCA indicated that the samples were clustered based on the observations of the study. However, after batch correction the samples were clustered based on the disease condition as active TB and control. We also observed a few samples outside the clusters before and after the batch correction procedure (Figure 2).

When the datasets DEG were compared, we identified genes regulated in the same direction. The meta-analysis identified a total of 2038 DEG of which 861 genes were up-regulated and 1177 genes were down-regulated (S. Table 1). Further analysis identified a total of 113 genes (up-regulated – 24 and down-regulated- 89) with absolute combined effect size as a reference for the log<sub>2</sub> fold change (logFC) greater than 1.5 (Table 2). S1PR1 ranks first among the up-regulated genes. S1PR1 expression is associated with lymphocyte recirculation. Similarly, FCGR1B is the top-ranking gene which is down-regulated in the active TB. To assess the results obtained from the meta-analysis, we validated the 113 genes with logFC > 1.5 in three datasets GSE19444 (Illumina), GSE54992 (Affimetrix) and GSE62525 (Phalanx) from different platforms. The PLS-DA models showed good sensitivity (above 85%) and specificity (above 83%) in all three datasets. The control, active and latent TB samples formed three different clusters marking clear differentiation (Figure 3). The ROC plot for the models suggest that the PLS-DA model can distinguish active tuberculosis samples from both latent and control groups with high true positive and low false positive rate (Figure 4). These measures show that DEG can act as biomarkers for the detection of active TB cases.



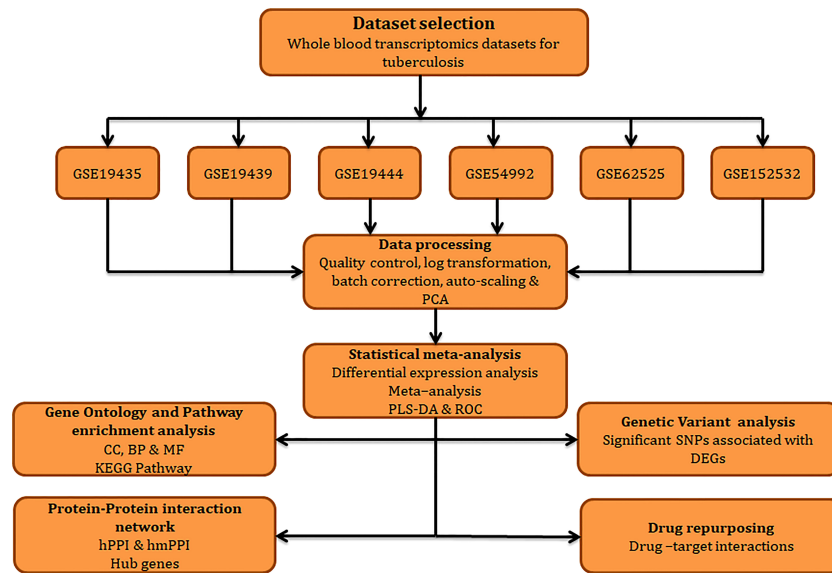


FIGURE 1  
Workflow adopted in this study.

## Identification of significantly enriched gene ontologies

The functional GO was carried out for the up and down regulated DEG identified by the meta-analysis (Table 3). The GO analysis identified that up-regulated DEG significantly involved in cellular components (CCs) were nucleoplasm, nucleus and cytosol. For GO BP analysis, the DEG showed involvement in mRNA splicing, *via* spliceosome, cytoplasmic translation and rRNA processing. Similarly for GO molecular function (MF) analyses, the DEGs were majorly enriched in RNA binding, protein binding and ATP binding. The GO CC analysis of down-regulated DEGs showed involvement in extracellular exosome, cytosol and lysosome. The GO BP analysis identified involvement in defense response to virus, innate immune response and response to virus. The GO MF analysis showed

enriched functions such as protein binding, protease binding and MHC class I protein binding.

## Identification of significantly enriched pathways

The pathway enrichment analysis implemented using DAVID identified various dysregulated pathways mediated by the DEGs (Table 4). The up-regulated DEGs showed enrichment of pathways involved in Spliceosome, Ribosome and Nucleocytoplasmic transport. We also observed pathways overlapping with other infectious diseases such as Herpes simplex virus 1 infection and Coronavirus disease - COVID-19.

The down-regulated DEGs showed involvement in NOD-like receptor signaling pathway, Lysosome and other infectious

TABLE 1 List of GEO datasets used in the meta-analysis.

Dataset	PMID	Platform	Samples*			DEGs
			Active	Latent	Control	
GSE19435	20725040	Illumina	7	0	12	2793
GSE19439	20725040	Illumina	13	17	12	1600
GSE19444	20725040	Illumina	21	21	12	2063
GSE54992	24647646	Affymetrix	9	6	6	4454
GSE62525	26818387	Phalanx	7	7	7	8739
GSE152532	34555657	Illumina	17	69	11	586

\*Only untreated samples were considered for the analysis.

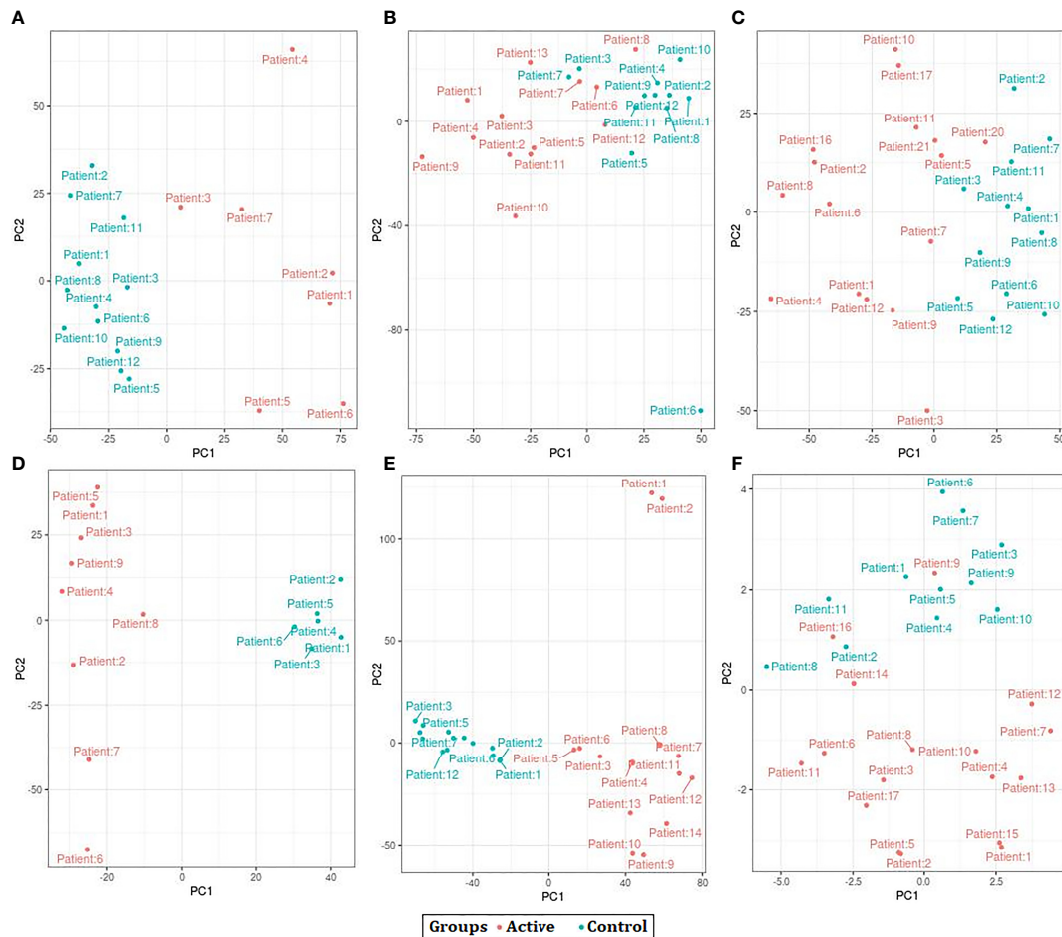


FIGURE 2

Principal Component Analysis (PCA) plots showing the separation control and active samples across all datasets used in the study. (A) GSE19435 (B) GSE19439 (C) GSE19444 (D) GSE54992 (E) GSE62525 (F) GSE152532.

disease pathways such as Influenza A, *Salmonella* infection, Hepatitis C and Epstein-Barr virus infection. We also observed the presence of Tuberculosis pathway in the list. The presence of tuberculosis pathway in our analysis indicated that the genes identified in the meta-analysis demonstrate their significant association with the disease.

## Protein–protein interaction network construction

Identifying the physical interactions between the proteins will provide clues to combat infection. The mapping of 2038 DEGs along with their partners resulted in a network enclosing 325 nodes and 1460 edges (Figure 5). The average number of neighbours in the hPPI was 15. Around 323 genes showed direct

interactions with their partners. The top ten hub genes which showed overlaps in degree and MCC measures are RPL10A, RPS4X, RPS16, RPS23, RPS3, RPS13, RPL7A, RPL4, RPS5 and RPS6. All the identified hub genes were ribosomal proteins involved in RNA binding.

The hmPPI interaction network enclosed 99 nodes and established 66 connections with an average of 1 connection between the neighbours (Figure 6). Due to the availability of limited *Mtb*-host protein-protein interactions we did not observe any hub genes based on the topological metrics.

## Drug – target interaction

The DEGs from the study were queried against DrugBank to mine drugs targeting genes which may be used for repurposing

**TABLE 2** List of top 20 DEGs (absolute combined effect size > 1.5) identified in the meta-analysis.

DEG	Fold change in meta-analysis	FDR P-value in meta-analysis
S1PR1	2.0215	0.000123
ZNF91	1.8479	0
PASK	1.7283	3.29E-06
PIK3IP1	1.7086	7.08E-09
CCR7	1.699	2.22E-06
GRAP	1.6851	1.70E-07
PDCD4	1.6847	0.01366
LAX1	1.68	0.005286
SLC38A1	1.6476	1.59E-06
ABCB1	1.6387	0.001482
FCGR1B	-2.2365	0
VAMP5	-2.2051	6.28E-12
GBP5	-2.0828	0
LY96	-2.0495	3.19E-10
TNFSF13B	-2.0145	3.61E-06
PSMB9	-1.9828	6.79E-13
CASP1	-1.9688	0
IL15	-1.9614	0
RNF135	-1.9367	0.002385
BATF2	-1.9255	0

against TB. A total of 22 drugs targeting 8 DEGs were obtained after the screening process (Table 5). Among them each compound showed association with at least one target gene with few exceptions such as ABCB1 which showed interaction with 14 drugs. Human immunoglobulin G (DB00028) acting on C5 and FCGR1B were also observed. FYN kinase targeted by the Fostamatinib was one among the up-regulated genes.

## Genetic variant analysis

The detection of drug targets which has human genetic support by its involvement in the disease pathology may aid in success of the treatment against the disease by preventing late stage clinical failures. The evidence of involvement in the disease by the 2038 DEGs was retrieved from genome-wide association study (GWAS) datasets. A total of 483 TB-related SNPs were obtained from GRASP database. An overlap between the LD region with a SNP and the DEG location or the enhancer region suggest strong association between the SNP and that particular gene. A total of 33 genes showed association with TB-related SNPs (Table 6).

## Discussion

### Meta-analysis of active tuberculosis samples

The meta-analysis of transcriptomes in this study identified S1PR1 as an up-regulated gene with highest fold change. S1PR1, by the detection of its ligand S1P in the blood and lymph, is crucial for naïve lymphocytes to access the circulatory system. S1P-S1PR1 signaling is crucial for regulating immune cell development and function. S1P-S1PR1 signaling is needed for mature thymocytes to leave the thymus and for T/B cells to leave secondary lymphoid organs and enter the blood or lymph in both homeostatic and pathological situations (Sinha et al., 2009; Zachariah and Cyster, 2010; Allende et al., 2010; Zhang et al., 2012). S1PR1 analog therapy raises IL-6 and lowers IL-10, but it can't stop the mycobacterial infection inside the cell (Arish and Naz, 2022). Consequently, the diminished expression of S1PR1 causes retention of naïve T cells in lymphoid tissues (Skon et al.,

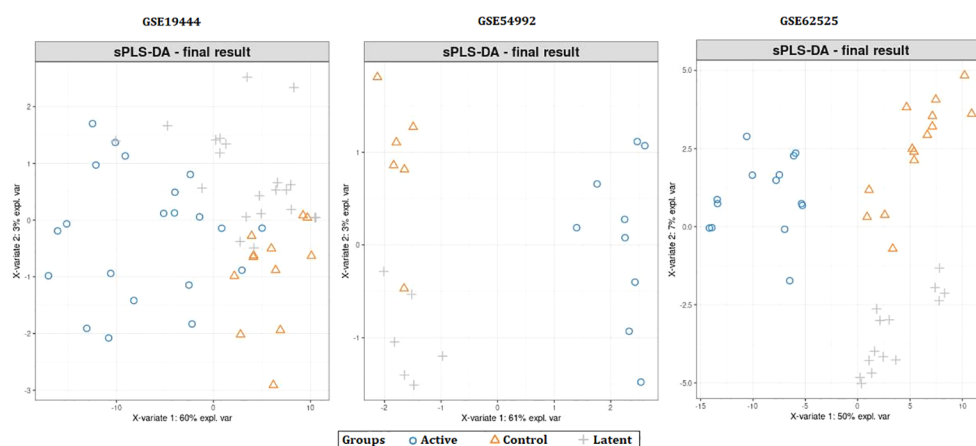


**FIGURE 3**  
Partial least squares-discriminate analysis (PLS-DA) plots showing differentiation between the control and TB samples.

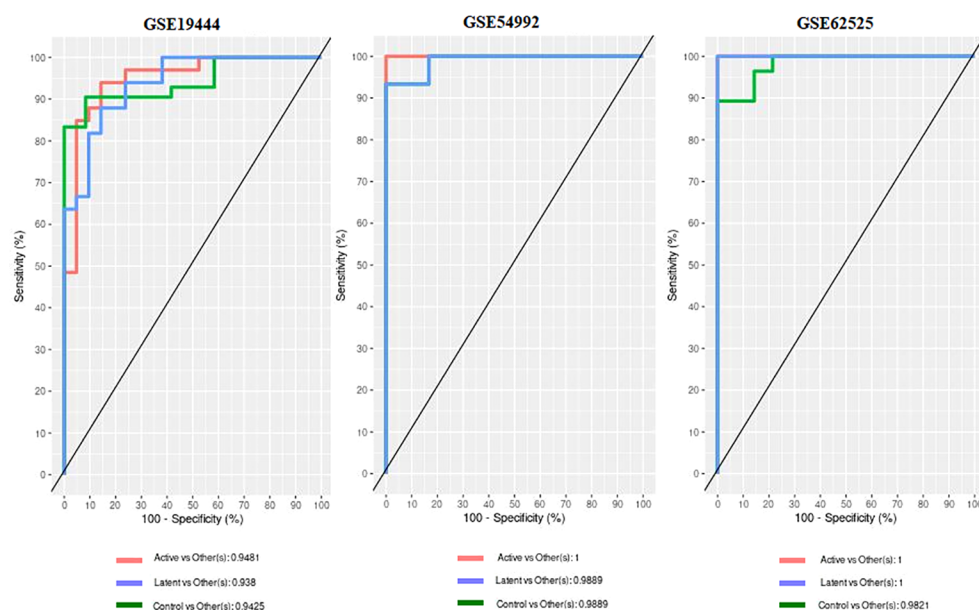


FIGURE 4  
Receiver operating characteristic (ROC) and Area under curve (AUC) from the PLS-DA on the 113 DEGs data.

2013). Similarly, FCGR1B is the top ranking gene with highest fold change and is down-regulated in the active TB condition. The FCGR1B gene is a member of immunoglobulin G, which binds directly with pathogens and neutralizes them. Changes in the Fc gamma receptors affect the response of a host to infection (Song et al., 2017). The FCGR1B gene aids in the host's immune response during a mycobacterial infection. According to Maertzdorf's research, people with TB and LTBI had more DEGs than uninfected individuals (Maertzdorf et al., 2011). In a different study, Satproedprai et al. found that the overexpression of FCGR1B in response to bacterial infection caused a humoral immune response and contributed to the development of lung inflammation (Satproedprai et al., 2015). Our results showed downregulation of FCGR1B, probably as a result of active TB.

The enrichment of spliceosomes and lysosomes in GO, indicates its crucial role in active TB infection. The functions of spliceosomes are also regulated differently in infected macrophages. The lysosomes protect against *Mtb* by controlling how *Mtb* moves through the lysosomes and stopping it from spreading in cells. Pre-mRNA splicing plays a crucial role in regulating gene expression and protein diversity. The Serine/Arginine rich (SR) proteins are the major components contributing to the selective splicing mechanism. The disruption in the RNA splicing mechanism

can lead to crosstalk in the intricate network interactions. The *Mtb* infection alters the patterns of alternate splicing within the macrophages by affecting the expression of SR proteins (Zhang et al., 2018).

The evolution of *Mtb* infection has proven its ability to successfully gain access to host cellular components needed for its survival before the initiation of innate antimicrobial response. The process is accomplished by altering various immune response elements such as interferon (IFN)-induced transmembrane (IFITM) gene family members. The IFITM members receive signals for their activation through type I and II IFN stimulation to preclude the establishment of productive infection. Ranjbar et al. show that IFITM proteins inhibit *Mtb* intracellular growth, indicating that they may contribute to host defense against intracellular bacterial infection (Ranjbar et al., 2015). The IFITMs act on host membrane fluidity at the sites of viral entry by preventing the formation of viral fusion pore. In addition, they increase the trafficking of trapped viruses to the lysosome for its degradation. However, *Mtb* alters this phagocytic mechanism by switching off the acidification of the phagosomes mediated by the IFITM family members. One such example is the vacuolar ATPase, a mediator of endosomal acidification which is excluded from *Mtb*-containing phagosome by *Mtb*'s bacterial tyrosine phosphatase (Ranjbar et al., 2015).

TABLE 3 Top 10 significantly enriched Gene ontologies.

Regulation	Cellular component (cc)	Biological Process (BP)	Molecular Function (MF)
Up	GO:0005654-nucleoplasm	GO:0000398-mRNA splicing, via spliceosome	GO:0003723-RNA binding
	GO:0005634-nucleus	GO:0002181-cytoplasmic translation	GO:0005515-protein binding
	GO:0005829-cytosol	GO:0006364-rRNA processing	GO:0005524-ATP binding
	GO:0005737-cytoplasm	GO:0006357-regulation of transcription from RNA polymerase II promoter	GO:0003724-RNA helicase activity
	GO:0016020-membrane	GO:0006281-DNA repair	GO:0016887-ATPase activity
	GO:0005730-nucleolus	GO:0006412-translation	GO:0003676-nucleic acid binding
	GO:1990904-ribonucleoprotein complex	GO:0006355-regulation of transcription, DNA-templated	GO:0003677-DNA binding
	GO:0022626-cytosolic ribosome	GO:0000122-negative regulation of transcription from RNA polymerase II promoter	GO:0003735-structural constituent of ribosome
	GO:0016607-nuclear speck	GO:0006397-mRNA processing	GO:0004386-helicase activity
	GO:0005840-ribosome	GO:0006338-chromatin remodelling	GO:0003682-chromatin binding
Down	GO:0070062-extracellular exosome	GO:0051607-defense response to virus	GO:0005515-protein binding
	GO:0005829-cytosol	GO:0045087-innate immune response	GO:0042802-identical protein binding
	GO:0005764-lysosome	GO:0009615-response to virus	GO:0003725-double-stranded RNA binding
	GO:0005765-lysosomal membrane	GO:0045071-negative regulation of viral genome replication	GO:0004298-threonine-type endopeptidase activity
	GO:1904813-ficolin-1-rich granule lumen	GO:0032731-positive regulation of interleukin-1 beta production	GO:0001730-2'-5'-oligoadenylate synthetase activity
	GO:0016020-membrane	GO:0006954-inflammatory response	GO:0042803-protein homodimerization activity
	GO:0035580-specific granule lumen	GO:0032755-positive regulation of interleukin-6 production	GO:0002020-protease binding
	GO:0010008-endosome membrane	GO:0050729-positive regulation of inflammatory response	GO:0061133-endopeptidase activator activity
	GO:0005886-plasma membrane	GO:0006915-apoptotic process	GO:0050786-RAGE receptor binding
	GO:0035578-azurophil granule lumen	GO:0032757-positive regulation of interleukin-8 production	GO:0004175-endopeptidase activity

TABLE 4 List of top 10 significantly enriched human pathways in the meta-analysis.

Up regulated pathways	Down regulated pathways
hsa03040:Spliceosome	hsa04621:NOD-like receptor signaling pathway
hsa03010:Ribosome	hsa04142:Lysosome
hsa03013:Nucleocytoplasmic transport	hsa05164:Influenza A
hsa05168:Herpes simplex virus 1 infection	hsa05132:Salmonella infection
hsa04660:T cell receptor signaling pathway	hsa05160:Hepatitis C
hsa03018:RNA degradation	hsa04145:Phagosome
hsa05340:Primary immunodeficiency	hsa05169:Epstein-Barr virus infection
hsa03008:Ribosome biogenesis in eukaryotes	hsa05152:Tuberculosis
hsa05171:Coronavirus disease - COVID-19	hsa05162:Measles
hsa05166:Human T-cell leukemia virus 1 infection	hsa05140:Leishmaniasis

In addition, pathways related to immune mediated cascades such as T cell receptor signaling pathway, Th17 cell differentiation and NF-kappa B signaling pathway were also observed (Urdahl et al., 2011). The order of appearance of T cell receptor signaling pathway down the list indicate that the onset of genes contributing to this pathways are delayed. Nuclear factor-kappa B (NFkB) pathway mediates pro-inflammatory responses which are required by the host to control of many microbial pathogens. The activation of NFkB has proven to increase the viability of intracellular *Mtb* in human macrophages by preventing apoptosis and autophagy (Bai et al., 2013). The lysosomal and pathogenic pathways indicate the dominance of these pathways used by the pathogens to avoid lysosomal targeting. They function by actively manipulating the host vesicular trafficking and reside in a vacuoles altered from the default lysosomal trafficking (Sachdeva and Sundaramurthy, 2020). The overlap of infectious disease pathways signals the usage of similar players for evading the infection and using host counterparts to reproduce.



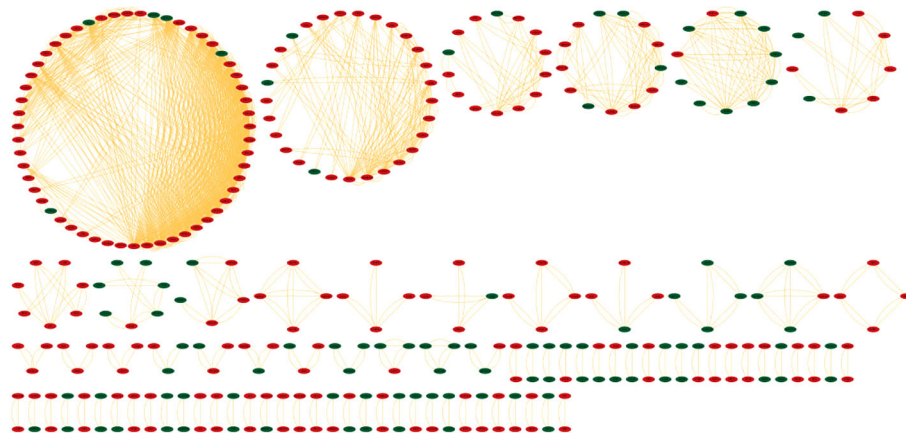


FIGURE 5

Protein-protein interaction network (hPPI) of the 2038 DEGs in the meta-analysis. The up-regulated genes are colored in red and down-regulated genes are colored green. The edges are represented as orange lines.

The PPI networks reveal the involvement of major players contributing to the infection. The hPPI network identified ten hub genes which play crucial role in the infection. All these identified hub genes were ribosomal proteins involved in RNA binding. These RNA-binding proteins play critical roles in co- and post-translational regulation. Due to the distinct differences in ribosome structure between *Mtb* and the host, the ribosome is a multiprotein complex, and the protein-protein interactions of its subunits may be an appealing target for novel antibiotics (Lin et al., 2012). Earlier report based on microarray expression analysis such as Wang et al., also reported up-regulation of 22 unique ribosomal proteins in

tuberculosis infection (Wang et al., 2003). In the current work we identified the involvement of 10 (RPL10A, RPS4X, RPS16, RPS23, RPS3, RPS13, RPL7A, RPL4, RPS5 and RPS6) unique ribosomal proteins in the active disease stage with high degree of connectedness. However, the significance of these genes is unclear and requires future studies. The hmPPI network showed MAT2A of the host protein interacted with ten *Mtb* proteins. MAT2A catalyse the conversion of L-methionine to S-adenosyl-L-methionine in cysteine and methionine metabolism. The *Mtb* protein partners also perform similar function, for example MetK which is a methionine adenosyltransferase (Wang et al., 2003).

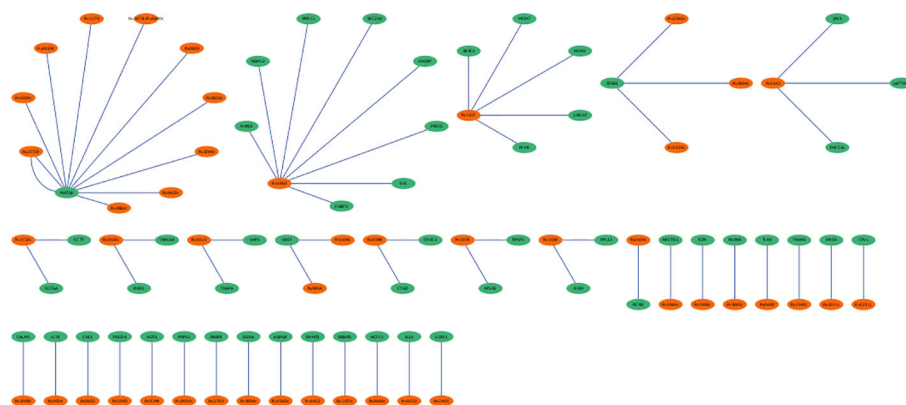


FIGURE 6

*Mtb*-host protein-protein interaction network (hmPPI). The *Mtb* proteins are colored green and human proteins are colored in orange. The edges are represented as blue lines.

TABLE 5 List of drugs in DrugBank targeting DEGs in the meta-analysis.

DEG	Fold change	Drug name	Pharmacological action	Disease treated	Mechanism of action
TSPO	-1.5792	Chlormezanone (DB01178)	Agonist	Muscle spasms	Inhibition of the ascending reticular activating system; Blocking the cortical and limbic – reticular pathways.
		Zopiclone (DB01198)	Agonist	Insomnia	Inhibitory actions of GABA.
FYN	1.5683	Fostamatinib* (DB12010)	Inhibitor	Immune thrombocytopenia	LRRK2 and spleen tyrosine kinase inhibition.
		Dasatinib* (DB01254)	Multitarget	Chronic myeloid leukemia	Src family tyrosine kinase inhibitor.
C5	-1.5903	Human immunoglobulin G (DB00028)	Binder	Immunodeficiency; Autoimmune disorders	Prevent infection by attaching to the surface of invading pathogens and aiding in their disposal before they can infect cells.
		Eculizumab (DB01257)	Antibody	Autoimmune disorders	Inhibition of complement complex C5b-9.
TNFSF13B	-2.0145	Belimumab (DB08879)	Neutralizer	Systemic lupus erythematosus; Active lupus nephritis	Blocks its interaction with B cell receptors - transmembrane activator and calcium-modulator.
ABCB1	1.6387	Medroxyprogesterone acetate	Inhibitor	Secondary amenorrhea; Renal carcinomas	Production of gonadotropin inhibition.
		Fentanyl (DB00813)	Inhibitor	Anesthesia	Inhibition of nerve activity.
		Voacamine (DB04877)	Inhibitor	Multidrug-resistance in tumor cells	It is possibly a substrate for P-glycoprotein (P-gp), an efflux pump responsible for multidrug resistance in tumor cells.
		Tocofersolan (DB11635)	Antagonist	Vitamin E deficiencies	It acts as a free radical chain breaking molecule, halting the peroxidation of polyunsaturated fatty acids and maintaining both the stability and integrity of cell membranes.
		Hycanthone (DB14061)	Inhibitor	Schistosomiasis	
		Concanamycin A (DB14062)	Inhibitor	Fungal infection	Binds to specific cell-surface receptors.
		Dexverapamil* (DB14063)	Inhibitor	Cardiac arrhythmias	Anti-arrhythmia drugs are divided into four main groups: calcium channel blockers; beta-adrenergic blockers; sodium channel blockers; and repolarization prolongers.
		Emopamil* (DB14064)	Inhibitor	Renal injury	
		Lomerizine (DB14065)	Inhibitor	Migraines	Inhibition of calcium influx through cellular membranes.
		Tetrandrine* (DB14066)	Inhibitor	Immunosuppression; Proliferation	Inhibition of calcium influx through cellular membranes.
		Dofequidar (DB14067)	Inhibitor	Neoplasm	Inhibits or prevents the proliferation of NEOPLASM.
		Dexniguldipine (DB14068)	Inhibitor	Hypertension	It exhibited a binding affinity for P-glycoprotein, assuming it could impede P-glycoprotein pumping and modify multidrug resistance.
		Desmethylsertraline (DB14071)	Inhibitor	Depressive disorder	
		Reversin 121 (DB14072)	Inhibitor		
FCGR1B	-2.2365	Human immunoglobulin G*	Antagonist	Immunodeficiency; Autoimmune disorders.	Blocks gamma Fc receptors, preventing the binding and ingestion of phagocytes and suppressing platelet depletion.
MYC	1.5067	Aspirin* (DB00945)	Down regulator	Inflammation; Migraines; Cardiovascular events	Blocks prostaglandin synthesis; With high dose for COX-2 inhibition.

(Continued)

TABLE 5 Continued

DEG	Fold change	Drug name	Pharmacological action	Disease treated	Mechanism of action
		Nadroparin* (DB08813)	Inhibitor	Prophylaxis of thrombotic events	It inhibits coagulation cascade.
S1PR1	2.0215	Fingolimod* (DB08868)	Modulator	Multiple sclerosis	To reduced lymphocyte circulation into the central nervous system.

\*used for tuberculosis via varying mechanism.

The meta-analysis identified the involvement of various kinases in active TB. The drug bank list also narrowed down few drugs acting on kinases. Various classes of tyrosine kinase inhibitors exhibit distinct mechanism of action to inhibit phagocytosis of tubercle bacilli in dose and time-dependent

manner. Early studies have proven that tyrosine kinase inhibitors including Dasatinib, Bosutinib, Imatinib, Nilotinib, Ponatinib, Nintedanib, Fostamatinib and Tirbanibulin reduce the growth of intracellular *Mtb*. The ligation of complement receptors by *Mtb* plays a major role in stimulation of tyrosine phosphorylation (Schlesinger and Desjardin, 2022). Focusing on drugs targeting these proteins can act as a starting point for the development of host mediated drug repurposing studies. The genetic-variant analysis recognized genes contributing to drug resistance such as ABCB1 (Pontual et al., 2017) and susceptibility to latent tuberculosis such as SP110 and OAS1 (Chang et al., 2018; Leisching et al., 2019). Analyzing the genetic variants of the tuberculosis patients before starting any treatment regimens is highly suggested to prevent late stage failures.

TABLE 6 List of DEGs proximal to TB-associated SNPs.

DEG	SNP associated with the gene
ABCB1	rs1128503, rs1045642
ACSS1	rs6138553
ACTA2	rs1800682
BLK	rs2254546
CCR7	rs11659024
CD5	rs10897125
CD6	rs10897125
CIRBP	rs2285899
COX19	rs11761941
CSTA	rs10934559
ENTPD1	rs10882657
FAS	rs1800682
FBXO31	rs10779243
GBP2	rs12121223
GBP5	rs2146340
GMFG	rs10412931
HLA-DPA1	rs3129750
KIF1B	rs11121555
LAP3	rs10939733
MDC1	rs1317834
MICB	rs2532929
OAS1	rs10774671
PBX4	rs1859287
PGD	rs11121555
PSMB10	rs12102971
PSMB8	rs3129750
PSMB9	rs3129750
SCO2	rs12148
SP110	rs3948464
TAP1	rs3129750
TAP2	rs3129750
TIMM10	rs2649662
WDR6	rs1134591

## Conclusion

The current study focuses on meta-analysis and highlights host genes and pathways crucial for tuberculosis disease. The DEGs identified in the current work shed light on promising drug targets for host-directed repurposing therapies. The work also suggests considering the genetic variants associated with the TB-related genes to enhance the success rate of therapies in individuals affected with tuberculosis. Future studies assessing the behavior of the identified DEGs during and after the treatment can ascertain their involvement in the disease pathogenesis and progression.

## Data availability statement

The datasets presented in this study can be found in online repositories. The names of the repository/repositories and accession number(s) can be found in the article/Supplementary Material.

## Author contributions

Collected data, Implemented the analysis and Manuscript writing: NP. Conceived and designed the analysis: MA. All authors contributed to the article and approved the submitted version.

## Funding

This research did not receive any specific grant from funding agencies in the public, commercial, or not-for-profit sectors.

## Acknowledgments

We would like to thank Vellore Institute of Technology (VIT) for providing computational facility.

## Conflict of interest

The authors declare that the research was conducted in the absence of any commercial or financial relationships that could be construed as a potential conflict of interest.

## References

- Allende, M. L., Tuymetova, G., Lee, B. G., Bonifacio, E., Wu, Y. P., and Proia, R. L. (2010). S1P1 receptor directs the release of immature B cells from bone marrow into blood. *J. Exp. Med.* 207 (5), 1113–1124. doi: 10.1084/jem.20092210
- Arish, M., and Naz, F. (2022). Sphingosine-1-phosphate receptors 2 and 3 reprogram resting human macrophages into M1 phenotype following mycobacteria infection. *Curr. Res. Immunol.* 3, 110–117. doi: 10.1016/j.crimmu.2022.05.004
- Augenreich, J., and Briken, V. (2020). Host cell targets of released lipid and secreted protein effectors of mycobacterium tuberculosis. *Front. Cell. Infect. Microbiol.* 10. doi: 10.3389/fcimb.2020.595029
- Bai, X., Feldman, N. E., Chmura, K., Ovrutsky, A. R., Su, W. L., Griffin, L., et al. (2013). Inhibition of nuclear factor-kappa B activation decreases survival of *Mycobacterium tuberculosis* in human macrophages. *PLoS One* 8 (4), e61925. doi: 10.1371/journal.pone.0061925
- Barrett, T., Wilhite, S. E., Ledoux, P., Evangelista, C., Kim, I. F., Tomashevsky, M., et al. (2013). NCBI GEO: archive for functional genomics data sets—update. *Nucleic Acids Res.* 41 (Database issue), D991–D995. doi: 10.1093/nar/gks1193
- Behar, S. M., Divangahi, M., and Remold, H. G. (2010). Evasion of innate immunity by *Mycobacterium tuberculosis*: is death an exit strategy? *Nat. Rev. Microbiol.* 8 (9), 668–674. doi: 10.1038/nrmicro2387
- Casadevall, A., and Pirofski, L. A. (2000). Host-pathogen interactions: Basic concepts of microbial commensalism, colonization, infection, and disease. *Infect. Immun.* 68 (12), 6511–6518. doi: 10.1128/IAI.68.12.6511-6518.2000
- Chang, S. Y., Chen, M. L., Lee, M. R., Liang, Y. C., Lu, T. P., Wang, J. Y., et al. (2018). SP110 polymorphisms are genetic markers for vulnerability to latent and active tuberculosis infection in Taiwan. *Dis. Markers* 2018, 4687380. doi: 10.1155/2018/4687380
- Chin, C. H., Chen, S. H., Wu, H. H., Ho, C. W., Ko, M. T., and Lin, C. Y. (2014). cytoHubba: identifying hub objects and sub-networks from complex interactome. *BMC Syst. Biol.* 8 (4), S11. doi: 10.1186/1752-0509-8-S4-S11
- Ernst, J. D. (2018). Mechanisms of *M. tuberculosis* immune evasion as challenges to TB vaccine design. *Cell Host Microbe* 24 (1), 34–42. doi: 10.1016/j.chom.2018.06.004
- Frieden, T. R., Sterling, T. R., Munsiff, S. S., Watt, C. J., and Dye, C. (2003). Tuberculosis. *Lancet* 362 (9387), 887–899. doi: 10.1016/S0140-6736(03)14333-4
- Ienasescu, H., Li, K., Andersson, R., Vitezic, M., Rennie, S., Chen, Y., et al. (2016). On-the-fly selection of cell-specific enhancers, genes, miRNAs and proteins across the human body using SlideBase. *Database (Oxford)* 2016, baw144. doi: 10.1093/database/baw144
- Johnson, A. D., Handsaker, R. E., Pulit, S. L., Nizzari, M. M., O'Donnell, C. J., and de Bakker, P. I. W. (2008). SNAP: a web-based tool for identification and annotation of proxy SNPs using HapMap. *Bioinformatics* 24 (24), 2938–2939. doi: 10.1093/bioinformatics/btn564
- Lee, S. H. (2016). Tuberculosis infection and latent tuberculosis. *Tuberc. Respir. Dis. (Seoul)* 79 (4), 201–206. doi: 10.4046/trd.2016.79.4.201
- Leisching, G., Cole, V., Ali, A. T., and Baker, B. (2019). OAS1, OAS2 and OAS3 restrict intracellular *M. tuberculosis* replication and enhance cytokine secretion. *Int. J. Infect. Dis.* 80S, S77–S84. doi: 10.1016/j.ijid.2019.02.029
- Leslie, R., O'Donnell, C. J., and Johnson, A. D. (2014). GRASP: analysis of genotype-phenotype results from 1390 genome-wide association studies and corresponding open access database. *Bioinformatics* 30 (12), i185–i194. doi: 10.1093/bioinformatics/btu273
- Lin, Y., Li, Y., Zhu, Y., Zhang, J., Li, Y., Liu, X., et al. (2012). Identification of antituberculosis agents that target ribosomal protein interactions using a yeast two-hybrid system. *Proc. Natl. Acad. Sci. U.S.A.* 109 (43), 17412–17417. doi: 10.1073/pnas.1110271109
- Maertzdorf, J., Repsilber, D., Parida, S. K., Stanley, K., Roberts, T., Black, G., et al. (2011). Human gene expression profiles of susceptibility and resistance in tuberculosis. *Genes Immun.* 12 (1), 15–22. doi: 10.1038/gene.2010.51
- Penn, B. H., Netter, Z., Johnson, J. R., Von Dollen, J., Jang, G. M., Johnson, T., et al. (2018). An *Mtb*-human protein-protein interaction map identifies a switch between host antiviral and antibacterial responses. *Mol. Cell.* 71 (4), 637–648.e5. doi: 10.1016/j.molcel.2018.07.010
- Pontual, Y., Pacheco, V. S. S., Monteiro, S. P., Quintana, M. S. B., Costa, M. J. M., Rolla, V. C., et al. (2017). ABCB1 gene polymorphism associated with clinical factors can predict drug-resistant tuberculosis. *Clin. Sci. (Lond)* 131 (15), 1831–1840. doi: 10.1042/CS20170277
- Ranjbar, S., Haridas, V., Jasenosky, L. D., Falvo, J. V., and Goldfeld, A. E. (2015). A role for IFITM proteins in restriction of *Mycobacterium tuberculosis* infection. *Cell Rep.* 13 (5), 874–883. doi: 10.1016/j.celrep.2015.09.048
- Rapanoel, H. A., Mazandu, G. K., and Mulder, N. J. (2013). Predicting and analyzing interactions between *Mycobacterium tuberculosis* and its human host. *PLoS One* 8 (7), e67472. doi: 10.1371/journal.pone.0067472
- Ritchie, M. E., Phipson, B., Wu, D., Hu, Y., Law, C. W., Shi, W., et al. (2015). Limma powers differential expression analyses for RNA-seq and microarray studies. *Nucleic Acids Res.* 43 (7), e47. doi: 10.1093/nar/gkv007
- Rohart, F., Gautier, B., Singh, A., and Cao, K. A. L. (2017). mixOmics: An R package for 'omics feature selection and multiple data integration. *PLoS Comput. Biol.* 13 (11), e1005752. doi: 10.1371/journal.pcbi.1005752
- Sachdeva, K., and Sundaramurthy, V. (2020). The interplay of host lysosomes and intracellular pathogens. *Front. Cell Infect. Microbiol.* 10, 595502. doi: 10.3389/fcimb.2020.595502
- Satproedprai, N., Wichukchinda, N., Suphankong, S., Inunchot, W., Kuntima, T., Kumpeerasart, S., et al. (2015). Diagnostic value of blood gene expression signatures in active tuberculosis in thais: a pilot study. *Genes Immun.* 16 (4), 253–260. doi: 10.1038/gene.2015.4

## Publisher's note

All claims expressed in this article are solely those of the authors and do not necessarily represent those of their affiliated organizations, or those of the publisher, the editors and the reviewers. Any product that may be evaluated in this article, or claim that may be made by its manufacturer, is not guaranteed or endorsed by the publisher.

## Supplementary material

The Supplementary Material for this article can be found online at: <https://www.frontiersin.org/articles/10.3389/fcimb.2022.1010771/full#supplementary-material>

### SUPPLEMENTARY TABLE 1

List of 2038 DEGs identified by meta-analysis.

- Schlesinger, L. S., and Desjardins, L. E. (2022). *Tuberculosis: The microbe host interface* (London: Taylor & Francis), 292 p.
- Sherman, B. T., Hao, M., Qiu, J., Jiao, X., Baseler, M. W., Lane, H. C., et al. (2022). DAVID: a web server for functional enrichment analysis and functional annotation of gene lists (2021 update). *Nucleic Acids Res.* 50 (W1), W216–W221. doi: 10.1093/nar/gkac194
- Sinha, R. K., Park, C., Hwang, I. Y., Davis, M. D., and Kehrl, J. H. (2009). B lymphocytes exit lymph nodes through cortical lymphatic sinusoids by a mechanism independent of sphingosine-1-phosphate-mediated chemotaxis. *Immunity* 30 (3), 434–446. doi: 10.1016/j.immuni.2008.12.018
- Skon, C. N., Lee, J. Y., Anderson, K. G., Masopust, D., Hogquist, K. A., and Jameson, S. C. (2013). Transcriptional downregulation of S1pr1 is required for establishment of resident memory CD8+ T cells. *Nat. Immunol.* 14 (12), 1285–1293. doi: 10.1038/ni.2745
- Song, F., Qian, Y., Peng, X., Li, X., Xing, P., Ye, D., et al. (2017). The frontline of immune response in peripheral blood. *PLoS One* 12 (8), e0182294. doi: 10.1371/journal.pone.0182294
- Szklarczyk, D., Gable, A. L., Nastou, K. C., Lyon, D., Kirsch, R., Pyysalo, S., et al. (2021). The STRING database in 2021: customizable protein–protein networks, and functional characterization of user-uploaded gene/measurement sets. *Nucleic Acids Res.* 49 (D1), D605–D612. doi: 10.1093/nar/gkab835
- Urdahl, K., Shafiani, S., and Ernst, J. (2011). Initiation and regulation of T-cell responses in tuberculosis. *Mucosal Immunol.* 4 (3), 288–293. doi: 10.1038/mi.2011.10
- Verma, R. N., MdZ, M., GP, S., and Subbarao, N. (2022). Identification of key proteins in host–pathogen interactions between *Mycobacterium tuberculosis* and homo sapiens: A systematic network theoretical approach. *Healthcare Analytics* 2, 100052. doi: 10.1016/j.health.2022.100052
- Wang, J. P., Rought, S. E., Corbeil, J., and Guiney, D. G. (2003). Gene expression profiling detects patterns of human macrophage responses following *Mycobacterium tuberculosis* infection. *FEMS Immunol. Med. Microbiol.* 39 (2), 163–172. doi: 10.1016/S0928-8244(03)00223-2
- WHO (2021). *Tuberculosis*. Available at: <https://www.who.int/news-room/fact-sheets/detail/tuberculosis>.
- Wishart, D. S., Feunang, Y. D., Guo, A. C., Lo, E. J., Marcu, A., Grant, J. R., et al. (2018). DrugBank 5.0: a major update to the DrugBank database for 2018. *Nucleic Acids Res.* 46 (D1), D1074–D1082. doi: 10.1093/nar/gkx1037
- Zachariah, M. A., and Cyster, J. G. (2010). Neural crest-derived pericytes promote egress of mature thymocytes at the corticomedullary junction. *Science* 328 (5982), 1129–1135. doi: 10.1126/science.1188222
- Zhang, W., Niu, C., Fu, R. Y., and Peng, Z. Y. (2018). *Mycobacterium tuberculosis* H37Rv infection regulates alternative splicing in macrophages. *Bioengineered* 9 (1), 203–208. doi: 10.1080/21655979.2017.1387692
- Zhang, L., Orban, M., Lorenz, M., Barocke, V., Braun, D., Urtz, N., et al. (2012). A novel role of sphingosine 1-phosphate receptor S1pr1 in mouse thrombopoiesis. *J. Exp. Med.* 209 (12), 2165–2181. doi: 10.1084/jem.20121090
- Zhou, G., Soufan, O., Ewald, J., Hancock, R. E. W., Basu, N., and Xia, J. (2019). NetworkAnalyst 3.0: a visual analytics platform for comprehensive gene expression profiling and meta-analysis. *Nucleic Acids Res.* 47 (W1), W234–W241. doi: 10.1093/nar/gkz240





## OPEN ACCESS

## EDITED BY

Parth Sarthi Sen Gupta,  
Indian Institute of Science Education  
and Research Berhampur (IISER), India

## REVIEWED BY

Manish Sharma,  
Emory University, United States  
Lin Fengxia,  
Guangzhou University of Chinese  
Medicine, China

## \*CORRESPONDENCE

Zhong Wang  
wz523@mail.tsinghua.edu.cn

## SPECIALTY SECTION

This article was submitted to  
Clinical Microbiology,  
a section of the journal  
Frontiers in Cellular and  
Infection Microbiology

RECEIVED 21 September 2022

ACCEPTED 23 November 2022

PUBLISHED 12 December 2022

## CITATION

Wang Z, Wang X, Guo Z, Liao H,  
Chai Y, Wang Z and Wang Z (2022) In  
silico high-throughput screening  
system for AKT1 activators with  
therapeutic applications in sepsis  
acute lung injury.  
*Front. Cell. Infect. Microbiol.*  
12:1050497.  
doi: 10.3389/fcimb.2022.1050497

## COPYRIGHT

© 2022 Wang, Wang, Guo, Liao, Chai,  
Wang and Wang. This is an open-access  
article distributed under the terms of  
the [Creative Commons Attribution  
License \(CC BY\)](https://creativecommons.org/licenses/by/4.0/). The use, distribution  
or reproduction in other forums is  
permitted, provided the original  
author(s) and the copyright owner(s)  
are credited and that the original  
publication in this journal is cited, in  
accordance with accepted academic  
practice. No use, distribution or  
reproduction is permitted which does  
not comply with these terms.

# In silico high-throughput screening system for AKT1 activators with therapeutic applications in sepsis acute lung injury

Ziyi Wang<sup>1</sup>, Xuesong Wang<sup>1</sup>, Zhe Guo<sup>1,2</sup>, Haiyan Liao<sup>1</sup>,  
Yan Chai<sup>1,3</sup>, Ziwen Wang<sup>1</sup> and Zhong Wang<sup>1\*</sup>

<sup>1</sup>School of Clinical Medicine, Tsinghua University, Beijing, China, <sup>2</sup>Department of Liver Intensive Care Unit, Beijing Tsinghua Changguang Hospital, Beijing, China, <sup>3</sup>Emergency Department, Beijing Friendship Hospital Affiliated Capital Medical University, Beijing, China

**Purpose:** AKT1 is an important target in sepsis acute lung injury (SALI). The current study was aim to construct a high-throughput screening (HTS) system based on the ChemDiv database (<https://www.chemdiv.com/complete-list/>) and use the system to screen for AKT1 activation agents, which may provide clues for the research and development of new drugs to treat SALI.

**Methods:** Based on the existing X-ray structure of AKT1 and known AKT activators, a large-scale virtual HTS was performed on the ChemDiv database of small molecules by the cascade docking method and demonstrated both accuracy and screening efficiency. Molecular docking and molecular dynamics simulations were used to assess the stability and binding characteristics of the identified small-molecule compounds. The protective effect of the new highly selective compound on SALI were verified both *in vitro* and *in vivo* experiments.

**Results:** The small-molecule compound 7460-0250 was screened out as a specific activator of AKT1. Molecular validation experiments confirmed that compound 7460-0250 specifically promoted the phosphorylation of AKT1 and down-regulated the LPS-induced apoptosis of human umbilical vein endothelial cells (HUVECs) by activating the AKT-mTOR pathway. Up-regulated mTOR was detected to directly interact with Bax to reduce apoptosis. *In vivo*, compound 7460-0250 could improved survival rate and alleviated lung injury of sepsis mice induced by cecum ligation and puncture (CLP), parallel with the activation of the AKT-mTOR pathway.

**Conclusion:** Small-molecule compound 7460-0250 was successfully screened and confirmed as a highly selective AKT1 activator, which is a critical target in the development of new therapeutics for SALI.

## KEYWORDS

sepsis, lung injury, HTS - high throughput satellite, apoptosis, AKT1

## Introduction

Sepsis is defined as life-threatening organ dysfunction caused by dysregulated immune response to infection (Singer et al., 2016). Acute lung injury (ALI) is a common and serious complication of sepsis. The incidence of ALI caused by sepsis is 25%-45%, and the mortality is 50%-60% (Kumar, 2020). Changes in vascular function resulting from vascular endothelial cell injury play an important role in the pathogenesis of SALI. In the pathological state, pathogens cause vascular endothelial injury, vascular endothelial inflammation, and vascular leakage, leading to the entry of immune cells and inflammatory factors aggravating SALI (Hussman, 2020; Pan et al., 2020).

The AKT pathway is closely related to cell apoptosis and has been extensively studied in tumors. AKT inhibitors are used to promote the apoptosis of tumor cells to treat cancer (Hua et al., 2021). In recent years, many studies in the field of sepsis have highlighted that activation of the AKT pathway could inhibit the apoptosis of functional cells, reduce the level of inflammation and oxidative stress, and subsequently improve organ function damage in sepsis (Cao et al., 2021; Li et al., 2022). There are 3 isoforms of AKT—AKT1, AKT2, and AKT3—among which AKT1 is most closely connected to apoptosis (Green et al., 2013; Gong et al., 2017; Kim et al., 2020). Previous studies have confirmed that pyrotoxin could improve apoptosis of LPS-induced HUVECs by promoting AKT1 phosphorylation (Wang et al., 2022). Currently, the only activator targeting AKT is SC79, which binds to the pleckstrin homology (PH) domain of AKT at residue 25 (arginine) (Jo et al., 2012). Based on the existing pharmacophore model and X-ray structure of SC79 (PDB ID: 1UNR), HTS of the small molecule ChemDiv database was conducted in the current study and the highly selective AKT1 activator small molecule compound 7460-0250 was obtained. This novel compound was subsequently characterized through molecular docking and molecular dynamics simulation and *in vitro* with LPS-induced HUVECs. Findings from this study provided a new mean for identifying AKT1 activators that have potential clinical applications in the treatment of SALI.

## Materials and methods

### Reagents

Small molecule compound 7460-0250 and MK-2206 were bought from Taosu Bio LTD. (China). Anti-AKT1 (phospho S473) antibody and anti-AKT2 (phospho S474) antibody were bought from Abcam (USA). Anti-Bax antibody and anti-mTOR antibody were from CST (USA). Anti-AKT3 (phospho S472) antibody was from Abnova (China). Annexin V -FITC Apoptosis Kit was purchased from solarbio (China). 10%

fetalbovine serum and crystal violet were from Beyotime (China). Cell counting kit-8 was from Beyotime (China).

### Cell culture

Human Umbilical Vein Endothelial Cells (HUVECs) cultivated by Laboratory of Tsinghua Changgung Hospital were cultured in an Incubator (SANYO, Japan) under standard Conditions (37°C, 5% CO<sub>2</sub>). The experiments were performed after two passages. Cells were cultured in Dulbecco's Modified Eagle Medium (DMEM), high glucose (Gibco, United States) containing.

### Animals

Wild type (WT) male C57BL/6J mice aged 6–8 weeks (Beijing Hufukang Biotechnology Co., LTD, China) were fed under a specific pathogen-free environment in Tsinghua University. The mice were equally divided into 4 groups (n = 7 mice/group): sham, activator group, SALI, and SALI+activator groups. The surgical procedure was performed as follows: male mice were fasted for at least 12 h and then anesthetized by intraperitoneal injection of tribromoethanol (10 mg/kg). For the sepsis and the activator intervention groups, the cecum was exposed after mid-line laparotomy and ligated immediately below the ileo-cecal valve without causing intestinal obstruction. After being punctured twice with an 18G needle, the cecum was placed back in the peritoneal cavity, and the abdominal wall was closed in two layers. SALI+activator group and activator group were administered with the small molecular compound 7460-0250 (25 and 100 mg/kg) by intraperitoneal injection at 2 h before the CLP operation. For the sham group, the cecum was exposed, and then the abdominal wall was closed in two layers. All the three groups were treated with normal saline just after operation to mimic clinical therapy. At 6 h after the operation, six mice from each group were sacrificed, and inferior lobe of right lung was used as the study sample. And the survival of these four groups at 7 days was recorded. All animal experiments were conducted under the rules approved by the Ethics Committee of Beijing Tsinghua Changung Hospital (protocol code NCT05095324).

### Drug

Small molecule compound 7460-0250 and MK-2206 were obtained from Shanghai Topscience Limited Corporation (Shanghai, China). The powder was stored at −20°C and was dissolved in DMSO adjusted to pH 4.5 with 1 N acetic acid for *in vitro* studies before use.

## Methods

### Schrodinger

Schrodinger software was used to preprocess the protein to generate the docker grid file, and construct the pharmacophore model of the small molecule compound database and the pharmacophore model of AKT agonist SC79. The pharmacophore model of SC79 was used to match the ChemDiv pharmacophore database model. In addition, ADMET screening high-throughput screening (HTVS) standard precision screening (SP) ultra-high precision screening (XP) was performed, and MMGBSA was used to score and sort, and the top five binding energies were selected for binding mode analysis. The detailed steps and results are shown in the Results section.

### Molecular dynamics simulation

The docking results were selected as the initial structure, Gromacs was used as the dynamics simulation software, AMBER14SB was selected as the protein position, and Gaff2 was selected as the small molecule position. TIP3P water model was used to add solvent to the protein-ligand system to establish the water box, and sodium ion equilibrium system was added. The PME handles electrostatic interactions under elastic simulations using Verlet and CG algorithms, respectively, and minimizes energy for a maximum number of steps (50,000) using the steepest descent method. The Coulomb force cutoff distance and Van der Waals radius cutoff distance are both 1.4 nm. Finally, the canonical system (NVT) and isothermal isobaric system (NPT) equilibrium systems are used, and then 100ns MD simulation is carried out at room temperature and pressure.

### CCK-8

HUVECs were cultured in 96-well plates to 80% confluence, then incubated with the new compound for indicated hours. Cell viability was detected with CCK-8 according to the manufacturer's instruction. Briefly, after new compound treatment, cells were incubated with 10 mL CCK-8 solution at 37 °C for 2 h and were measured the absorbance of each well at 450 nm.

### Flow cytometry analysis

Cell apoptosis was tested by flow cytometry using an annexin V-FITC apoptosis detection kit. HUVECs were washed twice with phosphate-buffered saline (PBS) and resuspended in 100 µl of 1× binding buffer mixed with 5 µl of

annexin-V-FITC and 2.5 µl of 7-AAD staining solution for 15 min in the dark at room temperature. After 15 min of incubation, an additional 400 µl of binding buffer was added, and then the cells were analyzed using a flow cytometer (BD, USA). The production of ROS was tested by flow cytometry using an DCFH-DA probe. HUVECs were washed twice with PBS and resuspended in 100 µl PBS mixed with 10µM DCFH-DA for 30 min in the dark at room temperature. Then, the cells were washed with PBS three times, and 300 µl PBS was added before analysis by flow cytometry. 7- AAD and annexin-V assay Q2 + Q3 were used to perform the apoptosis rate (Kepp et al., 2011).

### Western blot

Apoptosis-mediated proteins were analyzed by western blot. The total protein was extracted by radio-immunoprecipitation assay and phenylmethane sulfonylfluoride following the standard protocols for extracting protein. The protein concentrations were quantified using the BCA Protein Assay kit. Samples were electrophoresed in 10 or 8% SDS-PAGE gel and transferred onto a polyvinylidene fluoride membrane. Then, the membrane was blocked in 5% dried milk at 4°C overnight. The membrane was washed with Tris-buffered saline Tween-20 (TBST) three times, followed by incubation with a secondary antibody at room temperature for 40 min. After washing with TBST again, to observe protein signals, substrate luminol reagent and HRP substrate solution were added onto the membrane, 1 ml/membrane, and membrane signals were revealed by an enhanced chemiluminescence immunoblot detection system. The staining intensity of the bands was quantitated by densitometry through ImageJ software. The antibodies used in our study are described above in the "Reagents". Protein expression levels were defined as gray value, standardized to the housekeeping gene GAPDH, and expressed as a fold of control. All experiments were performed in triplicate and three times independently.

### Immunoprecipitation

For pre-clearance of G protein sugar beads, a total of 25µl of G protein sugar beads (GE Healthcare, Mississauga, ON, Canada) were incubated with primary antibody for 50 min at 4°C. The beads were then mixed with protein from 500µg of cell lysate and spun overnight at 4° C on a spinner. The following day, the beads were centrifuged at 10000 g for 5 min and the supernatant was discarded. The plates were washed 3 times with 1X PBS, mixed with 25µl of 2X SDS buffer, and then boiled at 95°C. The SDS-PAGE and western blot protocols were then followed as mentioned above.

## Hematoxylin-eosin (HE) staining

The lung tissues fixed with paraformaldehyde were embedded in paraffin and sectioned (thickness 5  $\mu\text{m}$ ) for HE staining. The pathological changes of lung tissue were observed under the light microscope at 200  $\times$ , and according to the pulmonary interstitial edema, alveolar hemorrhage, medium Lung histopathological injury score (0 = normal, 1 = mild, 2 was classified as moderate, 3 as severe, and 4 as extremely severe), and the total score was calculated.

## Results

### The existing AKT activator SC79 was used to screen small molecule compounds

#### AKT1 protein pretreatment

Schrodinger's Protein Preparation module was used for AKT1 Protein (PDB ID Code: 1UNR) pretreatment, that is, water molecules and excess ions were deleted, missing side chains and loop regions were completed, and energy minimization was achieved (Figure 1A). Studies have shown that AKT1 activator SC79 binds to the PH region of AKT through interaction with residue R25. According to the sites reported in literature, Arg25 of AKT1 protein is set as the docking center, and the distance 20Å around Arg25 is taken as the docking box (Figure 1B). Schrodinger's Glide Grid module is used to generate the docking Grid file. Use of Schrodinger LigPrep module of small molecule ChemDiv database ([https://](https://www.chemdiv.com/complete-list/)

[www.chemdiv.com/complete-list/](https://www.chemdiv.com/complete-list/)) protons, desalination, hydrogenation, generate tautomer, pretreatment of generating three-dimensional conformation and energy minimization.

#### Construction of pharmacophore model of small molecule compound database

Schrodinger's Create Phase Database module was used to preprocess tautomers, ionization, etc. The original ChemDiv Database contained 2091084 compounds, and after preprocessing, it contained 2465124 compounds. ChemDiv pharmacophore database model was constructed by using each molecule of ChemDiv database to generate pharmacophore model. There were 120988286 pharmacophore models in total (49.08 pharmacophore models per molecule on average).

#### Construction of AKT agonist SC79 pharmacophore model

According to the molecular structure of AKT activator SC79, the above pretreatment was performed and the pharmacophore model was generated (Figure 1C). The pharmacophore model was generated as a total of 7 elements, 1 aromatic ring pharmacophore, 3 hydrogen bond acceptor pharmacophore, 1 hydrogen bond donor pharmacophore, and 2 hydrophobic center pharmacophore.

#### Screening effective pharmacophore

The ChemDiv pharmacophore database model was matched with the pharmacophore model of SC79 in Schrodinger's Phase Ligand Screening module. A total of 250789 molecules met the criteria of at least six elements of the pharmacophore model and would be screened for the next round of molecular docking.

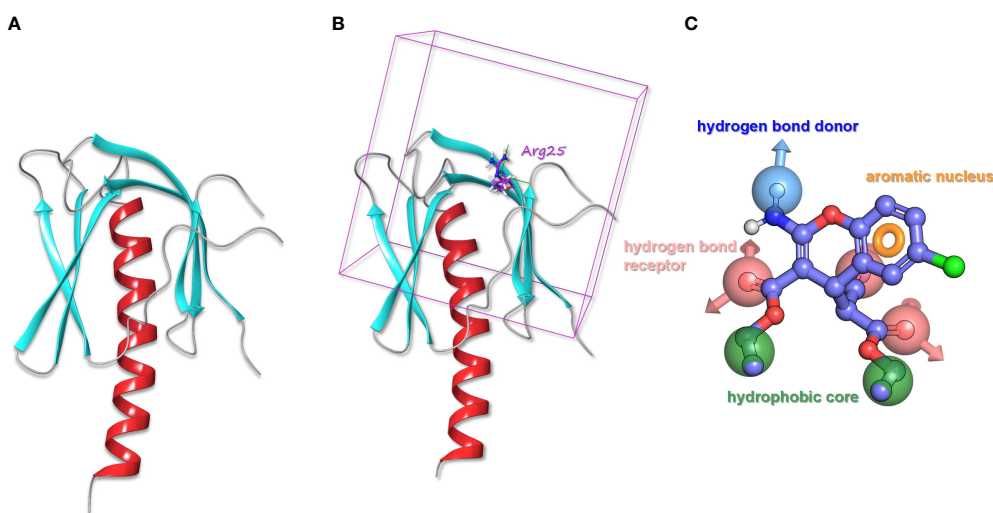


FIGURE 1

(A) The processed structure of AKT1 protein. (B) AKT1 protein with the docking box. (C) The pharmacophore model of SC79.

Schrodinger's QickProp module was used for ADMET screening. A total of 237609 molecules that met the five rules of drug-like properties and did not contain reactivity fragments were retained for the next round of docking screening. Because the last round of pharmacophore screening molecules meet the pharmacophore of positive drug SC79, so the last round of pharmacophore screening 237609 molecules could all docking into the cavity of AKT1, using Schrodinger Glide module high throughput screening (HTVS). The top 10% of the scoring 23761 molecules were selected for the next round of precision screening (SP) docking screening. Schrodinger's Glide module standard was used for precision screening SP, and the top 10% (2376 molecules) were selected according to the score for the next round of ultra-precision (XP) screening. Schrodinger's Glide module was used for XP screening, and the top 10% (237 molecules) were scored according to the score for MMGBSA. The top five scores were selected for binding mode analysis (Table 1), and molecular dynamics simulation was performed on them.

### Docking results of small molecule compounds with AKT1 protein molecules

In order to compare with the positive compounds, we used the same parameter settings, first performed XP docking on SC79, and calculated the MMGBS binding free energy of SC79: MMGBSA score: -63.21kcal/mol. The results were consistent with those reported in the literature, in which ARG25 was a key amino acid and formed a halogen bond interaction with SC79 and N-PI interaction (Figure 2A). Compound 1 binds to the corresponding binding site reported in the literature and forms hydrogen bond interactions with ARG25, a key amino acid reported in the literature. In addition, it can also form hydrogen bond interactions with LYS14, TYR18 and ASN53, and form a salt bridge with ARG86 (Figure 2B). Compound 2 forms hydrogen bond interactions with LYS14, TYR18, ILE19 and ASN53 of ATK1, and can also form N-PI interactions with ARG25 (Figure 2C). Compound 3 forms hydrogen bond interactions with LYS14, TYR18, ILE19 and ASN53 of ATK1,

and can also form N-PI interactions with ARG25 (Figure 2D). Compound 4 forms hydrogen bond interactions with LYS14, ALA50, and ASN53 of ATK1, and can also form N-PI interactions with ARG25 (Figure 2E). Compound 5 and ARG25 of ATK1 can form hydrogen bond interaction on the one hand and N-PI interaction on the other hand. In addition, it can also form hydrogen bond interaction with LYS14, GLU17, TYR18, ILE19, ASN53 and ASN54. N-pi interaction is formed with ARG86 (Figure 2F). The interaction modes and hydrogen bonds between each small molecule compound and AKT1 protein are shown in Table 2.

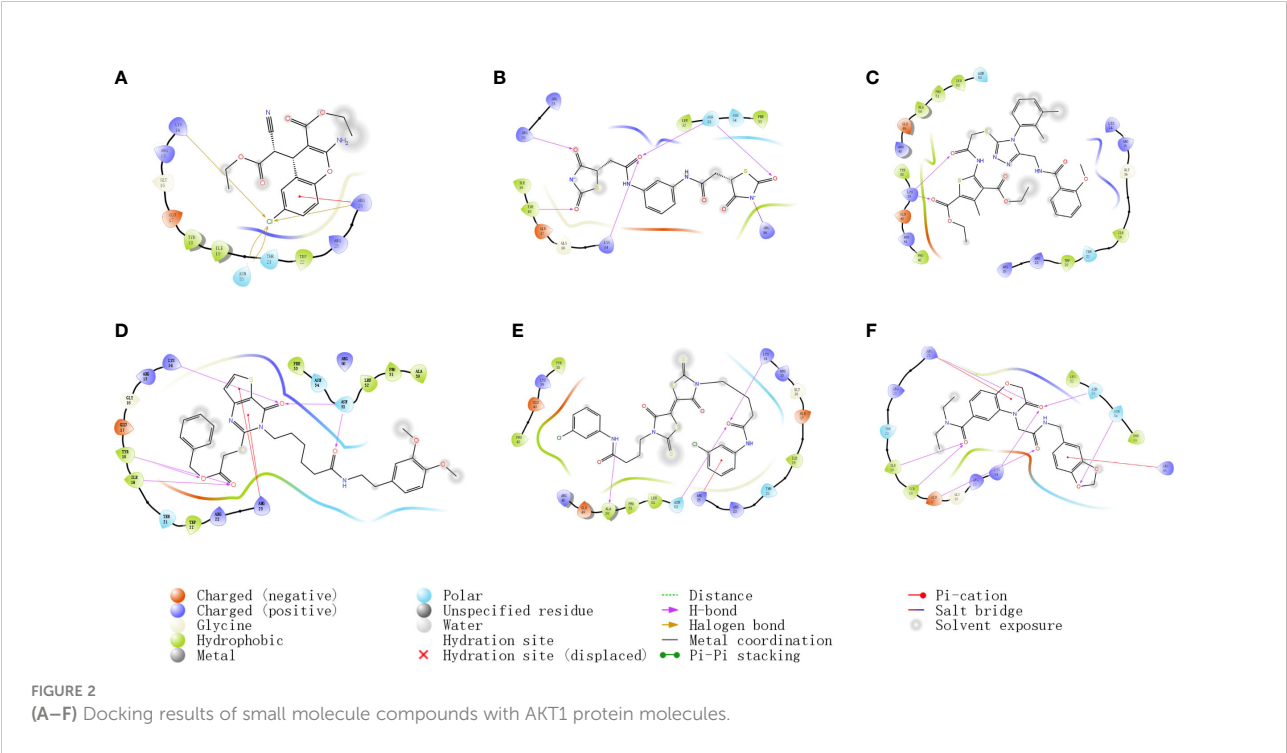
### Molecular dynamics simulation results of small molecule compound 7460-0250 and AKT1 protein

After 100ns molecular dynamics simulation of small molecule compound 7460-0250 and AKT1 protein, trajectory analysis was carried out. Firstly, RMSD of trajectory protein and small molecule were extracted. As shown in Figure 3A, protein and small molecule were in a mutually stable state after 10ns. So we could do the following analysis for trajectories from 10 to 100ns. The RMSF of track proteins and small molecules was extracted, as shown in Figures 3B, C. There were five places with large RMSF values, namely N segment, C segment and the middle three loop regions. For example, in the RMSF diagram of small molecules (Figure 3D), all amino acids of small molecules are basically in a stable state. The interaction mode of the stability interval (10-100ns) of the kinetic trajectory was analyzed, as shown in Figure 3E. Amino acids that play important roles in small molecule binding include Lys14, Glu17, Tyr18, Ile19, Arg25, Asn53 and Arg86, whose main roles are hydrogen bonding, water bridge and hydrophobic interaction. The occupancy of interactions formed by 10-100ns (number of frames forming interactions/total number of frames) was counted. As shown in Figure 3F, binding of small molecules to proteins mainly depends on 2, 4-thiazolidinediones at both ends.

TABLE 1 MMGBSA scores for selected compounds.

Hits	Title	ID number	Smile	MMGBSAdG Bind(kcal/mol)
Compound1	2-(2,4-dioxo-1,3-thiazolidin-5-yl)-N-((2,4-dioxo-1,3-thiazolidin-5-yl)acetyl)amino}phenyl}acetamide	7460-0250	<chem>c1c(NC(CC2C(NC(=O)S2)=O)=O)cc(NC(CC2C(NC(=O)S2)=O)=O)cc1</chem>	-67.46
Compound2	diethyl 5-(((4-(2,3-dimethylphenyl)-5-((2-methoxybenzoyl)amino)methyl)-4H-1,2,4-triazol-3-yl)thio)acetyl)amino)-3-methylthiophene-2,4-dicarboxylate	K403-0776	<chem>c1cc(c(C(NC2[nH0](c3c(c(ccc3)C)C)c(SCC(NC3=C(C(C)=C(C(=O)OCC)S3)=O)OCC)=O)[nH0][nH0]2)=O)cc1)OC</chem>	-62.71
Compound3	benzyl {[3-(6-([2-(3,4-dimethoxyphenyl)ethyl]amino)-6-oxohexyl)-4-oxo-3,4-dihydrothieno[3,2-d]pyrimidin-2-yl]thio}acetate	K292-1366	<chem>c1ccc(COC(CSc2[nH0](CCCCC(=O)NCCc3cc(c(cc3)OC)OC)c(c3c([nH0]2)C=CS3)=O)=O)cc1</chem>	-62.54
Compound4	N-(3-Chloro-phenyl)-4-{3'-[3-(3-chloro-phenylcarbonyl)-propyl]-4,4'-dioxo-2,2'-	2159-2999	<chem>c1c(cc(NC(CCCN2C(SC(C2=O)=C2C(N(C(=S)S2)CCCC(Nc2cc(Cl)ccc2)=O)=O)=S)=O)cc1)Cl</chem>	-61.13
Compound5	4-[2-[(1,3-benzodioxol-5-ylmethyl)amino]-2-oxoethyl]-N,N-diethyl-3-oxo-3,4-dihydro-2H-1,4-benzoxazine-6-carboxamide	F118-0638	<chem>CCN(C(c1ccc2c(N(CC(NC3cc4c(cc3)OCO4)=O)C(CO2)=O)c1)=O)CC</chem>	-60.12





Small molecule compound 7460-0250 could specifically activate AKT1 phosphorylation

We used different concentrations of small molecule compound 7460-0250 to induce HUVECs for 8h. As shown in Figures 4A, B, with the increase of the concentration of small molecule compound 7460-0250, the p-AKT1/AKT ratio gradually increased in a dose-dependent manner ( $P < 0.001$ ). The expression of p-AKT2/AKT was significantly increased only when the concentration of small molecule compound 7460-0250 was 8 $\mu$ g/ml ( $P > 0.05$ ). When the concentration of 7460-0250 was 2  $\mu$ g/ml and 4 $\mu$ g/ml, there was no significant difference in the expression of p-AKT2/AKT compared with control group ( $P >$

0.05). The p-AKT3/AKT ratio increased slightly when the induction concentration of 7460-0250 was 4  $\mu$ g/ml and 8 $\mu$ g/ml, which was critically lower than the expression of p-AKT1/AKT at the lowest induction concentration of 7460-0250 ( $P < 0.001$ ). There was no significant difference in p-AKT3/AKT ratio between the control group and 2 $\mu$ g/ml 7460-0250 group ( $P > 0.05$ ).

To further verify the activation effect of the new compound in other cell lines, we used different concentrations of small molecule compound 7460-0250 to induce Raw264.7 cells for 8h. As shown in Figure 4C, the p-AKT1/AKT ratio increased significantly when the induction concentration of 7460-0250 was 8  $\mu$ g/ml. The p-AKT3/AKT ratio enhanced slightly when the induction concentration of 7460-0250 was 8  $\mu$ g/ml. The p-AKT2/AKT ratio could not be up-regulated in these groups.

TABLE 2 Interaction of compounds with AKT1.

Compound	IDNUMBER	MMGBSA dG Bind	Interaction				Interacting amino acids
			Hydrogen bonding	n-Pi Interaction	Halogen bond	Salt bridge	
Compound1	7460-0250	-67.46	4	0	0	1	LYS14, TYR18, ARG25, ASN53, ARG86
Compound2	K403-0776	-62.71	2	0	0	0	LYS39
Compound3	K292-1366	-62.54	6	2	0	0	LYS14, TYR18, ILE19, ARG25, ASN53
Compound4	2159-2999	-61.13	3	1	0	0	LYS14, ARG25, ALA50, ASN53
Compound5	F118-0638	-60.12	7	2	0	0	LYS14, GLU17, TYR18, ILE19, ARG25, ASN53, ASN54, ARG86

Bold values means the predicted bonding bond between the compound and the AKT1 protein.

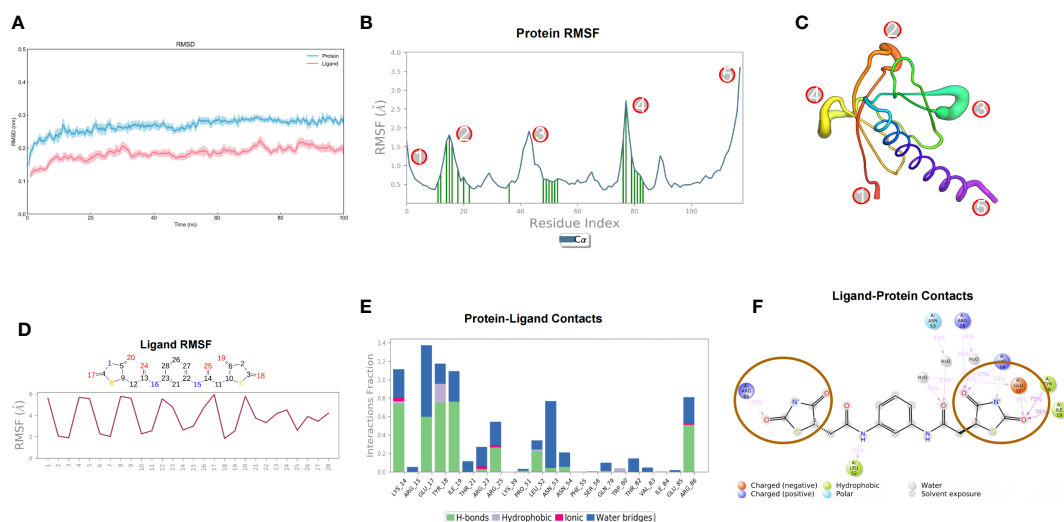


FIGURE 3

Molecular dynamics simulation results of small molecule compound 7460-0250 and AKT1 protein. (A) RMSD; (B, C) Protein RMSF; (D) Ligand RMSF; (E, F) The connection between ligand and protein.

To determine whether AKT inhibitor could inhibit the AKT-mTOR pathway activated by the new selectively compound or not, western blot was applied. MK-2206 was used as the AKT inhibitor. As shown in Figures 4D, E, compared with control group, the expression level of p-AKT and mTOR were enhanced in activator group, and were decreased by MK-2206 in a dose-dependent manner ( $p < 0.001$ ).

Meanwhile, to detect the cytotoxicity and effective concentration of the new compound, CCK-8 was employed. As shown in Figure 4F, the cytotoxicity of the new highly selective compound was also measured to identify an effective and safe dose. The new highly selective compound at 2  $\mu\text{g/ml}$ , 4  $\mu\text{g/ml}$ , and 8  $\mu\text{g/ml}$  had no influence on cell proliferation ( $p > 0.05$ ). However, the compound at 16  $\mu\text{g/ml}$  could reduced the cell proliferation ( $p < 0.001$ ).

## Small molecule compound 7460-0250 could activate AKT-mTOR pathway and down-regulate Bax protein expression

As previously mentioned, stimulation of HUVECs with 1  $\mu\text{g/ml}$  LPS for 6h could successfully induce septic cell model. So we divided cells into four groups: control group, LPS group (1  $\mu\text{g/ml}$  LPS), activator group (8  $\mu\text{g/ml}$  small molecule compound 7460-0250), and LPS (1  $\mu\text{g/ml}$  LPS)+activator (8  $\mu\text{g/ml}$  small molecule compound 7460-0250) group. 7460-0250 was added 2h in

advance. As shown in Figures 5A, C, the expression of p-AKT and mTOR increased slightly after stimulation with LPS or small molecule compound 7460-0250. The expressions of p-AKT and mTOR in LPS+small molecule compound 7460-0250 group were significantly higher than those in single molecule stimulation group ( $P < 0.05$ ). As shown in Figures 5B, D, the expression of Bax in LPS+activator group was significantly increased compared with the control group, and the expression of Bax in LPS+activator group was significantly decreased compared with the LPS group ( $P < 0.05$ ). There was no significant difference in Bax expression in activator group compared with the control group ( $P > 0.05$ ). CoIP was applied to investigate whether mTOR binds to Bax in HUVECs. The expressions of mTOR and Bax proteins were detected by Input WB (Figure 5E). Empty GFP plasmid failed to bind to Bax, whereas GFP-tagged mTOR bound to Bax in HUVECs (Figure 5F).

## The small molecule compound 7460-0250 could down-regulate the apoptosis of LPS-induced HUVECs

As shown in Figures 6A, B, the apoptosis rate of HUVECs in LPS group was significantly higher than that of the control group ( $P < 0.001$ ), and the apoptosis rate of HUVECs in activator group was not statistically different from that of the control group ( $P > 0.05$ ), while the apoptosis rate in the LPS+activator

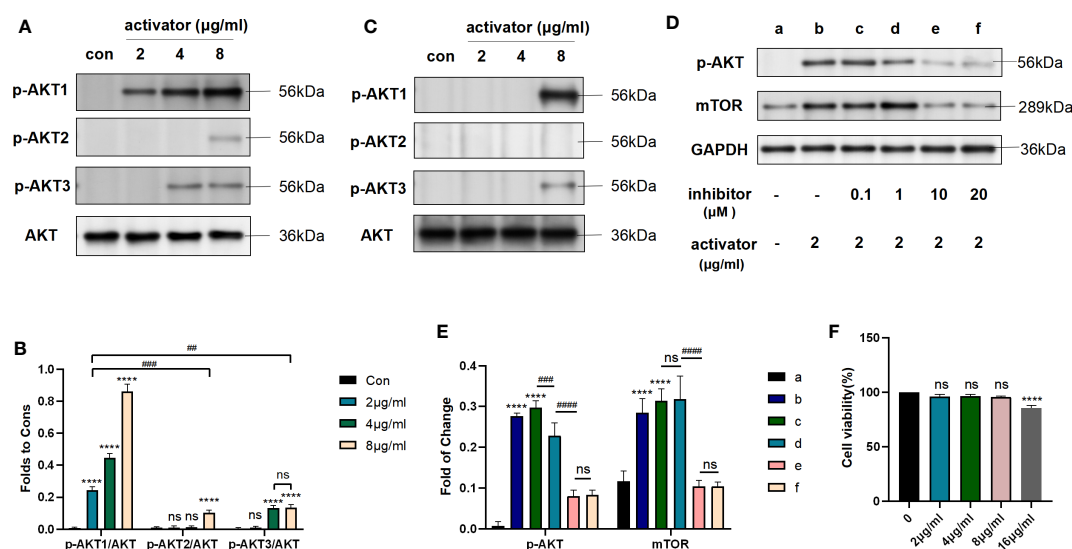


FIGURE 4

Small molecule compound 7460-0250 could specifically activate AKT1 phosphorylation. (A, B) The protein expression of AKT phosphorylation and AKT in HUVECs. (C) The protein expression of AKT phosphorylation and AKT in Raw264.7 cells. (D, E) AKT inhibitor could inhibit the AKT mTOR pathway activated by the new selectively compound (F) Effects of MK2206 on cell viability. Data are presented as mean  $\pm$  SD (n = 3 per group) of the representative data from three independent experiments;  $P^{##} < 0.01$ ,  $P^{####} < 0.001$ ,  $P^{****} < 0.001$ . The asterisk (\*) represents the group is statistically different from the Con group. ns, no significant difference.

group was significantly lower ( $P < 0.001$ ). Apoptosis rates (%) of control group, LPS group, activator group, and LPS+activator group were  $3.763 \pm 0.281$ ,  $43.33 \pm 2.068$ ,  $4.5 \pm 0.51$ ,  $15.97 \pm 0.65$ , respectively.

### The small molecule compound 7460-0250 could improve the survival rate of SALI mice induced by CLP

Mice were divided into 6 groups: sham group, 25mg/kg activator group, 100mg/kg activator group, SALI group, SALI +25mg/kg activator group, and SALI+100mg/kg activator group. The small molecule compound 7460-0250 was administered by intraperitoneal injection at 2 h before the CLP operation. The 7-day survival rate of the four groups was monitored in our study. As illustrated in Figure 7A, while all sham-operated mice and 7460-0250-administrated mice survived to the end of the observation period, half of mice in the SALI group died within 3 days. The survival rate of mice in SALI group were lower than that in the sham group ( $P < 0.001$ ). The survival rate of mice in the SALI+100mg/kg activator group was essentially improved compared with that in the SALI group ( $P < 0.001$ ). There was no significant difference in survival rate between SALI+25mg/kg activator group and SALI group ( $P > 0.05$ ).

### The small molecule compound 7460-0250 could alleviate SALI mice induced by CLP

As shown in Figures 7B, C, at 6 h after operation, mice in sham group, 100mg/kg activator group, and 25mg/kg activator group had no obvious congestion, bleeding and inflammatory cell infiltration in lung interstitium. In SALI group, pulmonary interstitial hyperemia, hemorrhage, edema, severe rupture of alveolar capillary wall, and a large number of inflammatory cell infiltration were observed. Mice in SALI+100mg/kg activator group had mild pulmonary interstitial edema, alveolar capillary congestion with a small amount of cleft bleeding, and inflammatory cell infiltration was reduced compared with those in SALI group. Compared with SALI group, SALI+25mg/kg activator group had no significant changes. The lung histopathological injury scores of mice in Sham group, 100mg/kg activator group, 100mg/kg activator group, SALI group, SALI +25mg/kg activator group and SALI+100mg/kg activator group were  $0.333 \pm 0.21$ ,  $0.167 \pm 0.167$ ,  $0.2 \pm 0.2$ ,  $6.0 \pm 0.365$ ,  $5.833 \pm 0.307$ ,  $2.167 \pm 0.167$ , respectively. Overall, the difference was statistically significant ( $P < 0.001$ ). There was no significant difference in the pathological score of lung tissue injury between 25mg/kg Activator group and 100mg/kg Activator group and sham group ( $P > 0.05$ ), while the pathological score of lung

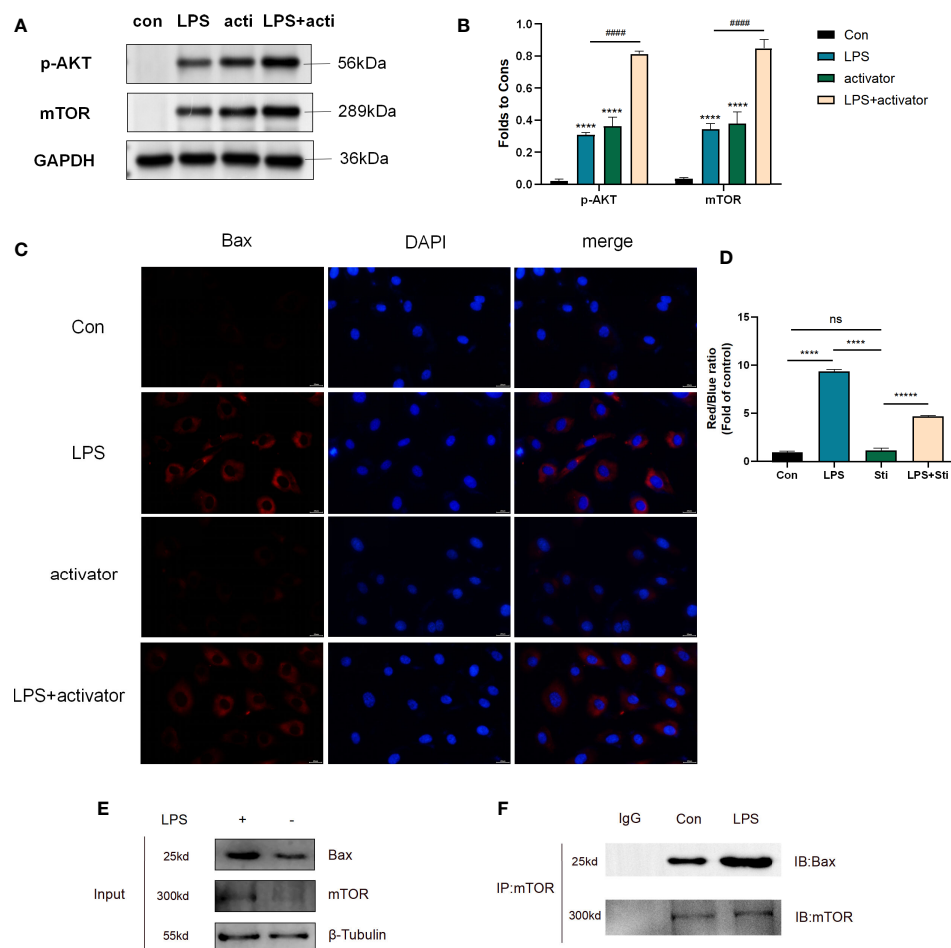


FIGURE 5

(A, C) The protein expression of p-AKT and mTOR in control group, LPS group, activator group, and LPS+activator group. (B, D) The protein expression of Bax in control group, LPS group, activator group, and LPS+activator group. (E, F) CoIP of mTOR and Bax in control and LPS group. Data are presented as mean  $\pm$  SD ( $n = 3$  per group) of the representative data from three independent experiments;  $p^{####} < 0.001$ ,  $p^{****} < 0.001$ . The asterisk (\*) represents the group is statistically different from the Con group. activator group: compound 7460-0250 group; LPS+activator group: LPS+compound 7460-0250 group. ns, no significant difference.

tissue injury in SALI group was significantly higher than that in Sham group ( $P < 0.001$ ). The pathological injury score of lung tissue in SALI+100mg/kg activator group was significantly lower than that in SALI group ( $P < 0.001$ ), but there was no significant difference between SALI+25mg/kg activator group and SALI group ( $P > 0.05$ ).

## The small molecule compound 7460-0250 could activate AKT-mTOR pathway in lung tissue *in vivo*

To verify the effect of the new compound *in vivo*, CLP-induced sepsis mice model was employed. As shown in

Figures 8A, B, compared with sham group, the expressions of p-AKT and mTOR in lung tissue increased slightly in SALI group. Compared with SALI group, the expressions of p-AKT and mTOR in lung tissue in SALI+activator group were significantly higher ( $P < 0.001$ ).

## Discussion

The systemic inflammatory reaction in sepsis could damage the alveoli, causing alveolar edema and exudation, pulmonary capillary dilatation, congestion, and inflammatory cell infiltration, and could eventually lead to decreased oxygenation capacity of patients, with ALI resulting from

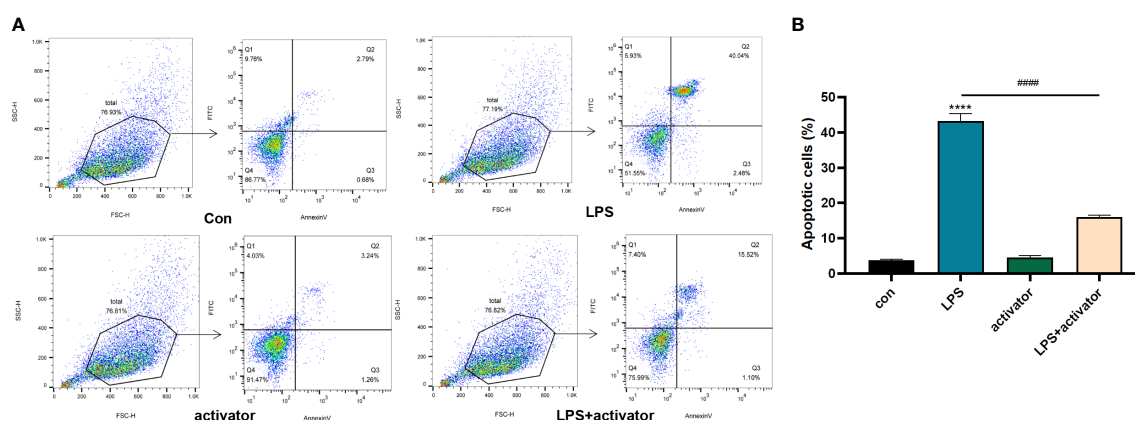


FIGURE 6

(A, B) The flow cytometry results in control group, LPS group, activator group, and LPS+activator group. The small molecule compound 7460-0250 could down-regulate the apoptosis of LPS-induced HUVECs. Data are presented as mean  $\pm$  SD ( $n = 3$  per group) of the representative data from three independent experiments;  $P^{###} < 0.001$ ,  $P^{***} < 0.001$ . The asterisk (\*) represents the group is statistically different from the Con group. activator group: compound 7460-0250 group; LPS+activator group: LPS+compound 7460-0250 group.

progression of the disease (Wang et al., 2019). Although there are numerous predisposing clinical factors for ALI, sepsis is the most common cause, and ALI in patients with sepsis is termed SALI. The main treatments for SALI are anti-infectives, dilatation, diuresis, use of ventilator, and endotracheal intubation. These treatments could save lives and reduce mortality in patients with SALI, but the efficacy is unsatisfactory. Consequently, there is an urgent need to find drugs to prevent and block sepsis (Gotts and Matthay, 2016).

The homeostasis of intercutaneous junctions in alveolar capillary vessels is a key factor for maintaining normal alveolar homeostasis and lung repair after injury (Mehta and Malik, 2006). The alveoli contain abundant pulmonary microvascular endothelial cells, which mediate the transport of molecules from the blood vessels to the lung interstitium. LPS and other activators of lung injury could induce vascular endothelial cell injury (Hou et al., 2019). The most important pathological change of SALI is diffuse alveolar epithelial injury (Mokra, 2020). Under pathological conditions, the destruction of vascular endothelial connections leads to an increase in vascular permeability, the infiltration of inflammatory factors and inflammatory cells, and the production of a cascade reaction to expand the inflammatory effect, resulting in or aggravating SALI (Li et al., 2020). Scholars have found that inducing macrophage polarization from the proinflammatory M1 type to the anti-inflammatory M2 type could reduce ALI caused by sepsis (Jiao et al., 2021). In addition, inhibition of PD-L1 protein expression in neutrophils could promote neutrophil apoptosis and reduce SALI (Wang et al., 2021). These findings demonstrate that the neutrophils and macrophages that exude

from the alveolar capillary endothelium then accumulate around alveolar epithelial cells and release numerous inflammatory factors are instrumental in promoting the development of SALI. Therefore maintaining the stability of vascular barrier function and reducing the damage to endothelial cells are vital for the prevention and treatment of SALI.

Activation of the PI3K-AKT-mTOR pathway could alleviate the apoptosis of HUVECs (Lin et al., 2020; Chen et al., 2021). In addition, our previous study revealed that various active components in Reduning, a traditional Chinese medicine, could alleviate LPS-induced apoptosis of HUVECs by targeting AKT1 and activating AKT phosphorylation (Wang et al., 2022). The discovery of AKT dates back to the 1970s, when an oncogene sequence, named AKT8, was identified in murine leukemia viruses, and two homologous oncogenes of AKT8, named AKT1 and AKT2 (also known as PKKB  $\alpha$  and PKKB  $\beta$ , respectively), were subsequently identified in human chromosomes (Pastorino et al., 2005). Later, an oncogene called AKT3 (also known as PKB $\gamma$ ) was identified in mammalian cells and was classified as a third isoform of AKT (Gogvadze et al., 2008). Studies of AKT gene subtypes revealed that AKT1 is predominantly involved in apoptosis (Gao et al., 2004), AKT2 is mainly involved in glucose metabolism (Wang et al., 2014), and AKT3 plays a role in the development of the nervous system (Ong et al., 2010).

The existing AKT activator SC79 has the ability to activate all three subtypes of AKT (AKT1, AKT2, and AKT3) (Jo et al., 2012). The current study employed HTS (Kalwat, 2021; Cretin et al., 2021; Tian et al., 2021) to screen out specific activators of AKT1, and more specifically identify those that could protect



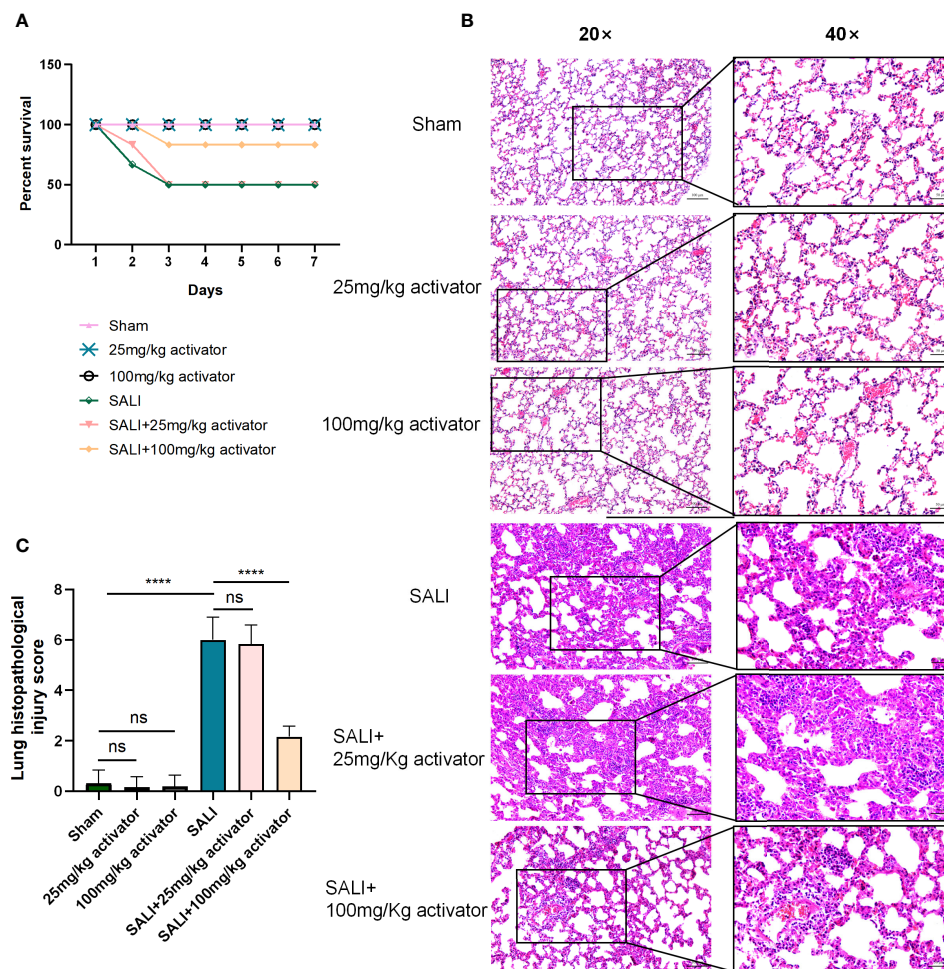


FIGURE 7

(A) The survival rate of sham group, 25mg/kg activator group, 100mg/kg activator group, SALI group, SALI+25mg/kg activator group, and SALI+100mg/kg activator group. (B, C) lung issue HE of sham group, 25mg/kg activator group, 100mg/kg activator group, SALI group, SALI+25mg/kg activator group, and SALI+100mg/kg activator group. Data are presented as mean  $\pm$  SD ( $n = 3$  per group) of the representative data from three independent experiments; Magnification $\times 40$ , scale bar 50 $\mu$ m. Magnification $\times 20$ , scale bar 100 $\mu$ m.  $P^{****} < 0.001$ . 25mg/kg activator group: 25mg/kg compound 7460-0250 group; 100mg/kg activator group: 100mg/kg compound 7460-0250 group; SALI+25mg/kg activator group: SALI+25mg/kg compound 7460-0250 group; SALI+100mg/kg activator group: SALI+100mg/kg compound 7460-0250 group. ns, no significant difference.

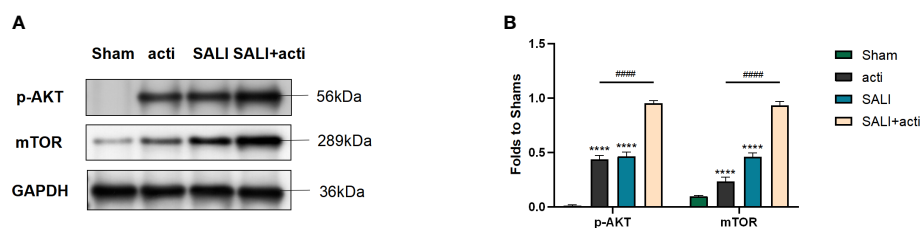


FIGURE 8

Small molecule compound 7460-0250 could alleviate AKT phosphorylation and mTOR in lung tissue of CLP-induced sepsis mice model (A, B). The protein expression of AKT phosphorylation and mTOR in Sham group, activator group, SALI group, and SALI+activator group. Data are presented as mean  $\pm$  SD ( $n = 3$  per group) of the representative data from three independent experiments.  $P^{####} < 0.001$ ,  $P^{****} < 0.001$ . The asterisk (\*) represents the group is statistically different from the Con group. activator group: compound 7460-0250 group; SALI+activator group: SALI+compound 7460-0250 group.

LPS-induced HUVECs. The small-molecule compound 7460-0250 was identified by HTS of the ChemDiv database using Schrodinger software based on the structure of the existing AKT activator SC79. Compared with the positive control SC79, the novel compound 7460-0250 had a higher MMGBSA score and also formed more hydrogen bond interactions. This indicated that the small-molecule compound 7460-0250 may potentially have improved activity compared with SC79. Therefore, a molecular dynamics simulation was performed on compound 7460-0250 to study the dynamic binding mode of compound 7460-0250 and AKT1, which would provide a theoretical basis for subsequent structural modification. The results of molecular dynamics simulation showed that the small-molecule compound 7460-0250 could stably bind to AKT1 protein, and its binding characteristics were explained.

In molecular biological validation experiments, western blot revealed that small-molecule compound 7460-0250 could specifically activate AKT1 in a dose-dependent manner. Moreover, the protective effect of compound 7460-0250 on LPS-induced HUVECs was subsequently verified. It was found that compound 7460-0250 could downregulate the level of apoptosis-related protein Bax in LPS-induced HUVECs by activating the AKT-mTOR pathway. We therefore investigated the interaction between mTOR and Bax by CoIP. Empty GFP plasmid failed to bind to Bax, whereas GFP-tagged mTOR bound to Bax in HUVECs. Taken together, these data suggest that mTOR interacts with Bax to delay LPS-induced HUVECs apoptosis. Then, we tested the protective effect of compound 7460-0250 in SALI mice induced by CLP. Compound 7460-0250 could up-regulated the survival rate and alleviate pulmonary interstitial hyperemia, hemorrhage, edema, and inflammatory cells infiltration. It was demonstrated that compound 7460-0250 maintained endothelial barrier function by protecting HUVECs

from apoptosis, reducing immune cell leakage into the interstitial space and improving further inflammatory responses. This study also demonstrated that HTS is a simple and effective way to explore new therapeutic agents, and our discovery of this novel AKT1 activator may provide a new treatment for sepsis.

## Conclusion

Based on the literature and previous mechanism studies, this study established and optimized a HTS system for activators of AKT1. Through HTS of the ChemDiv database, new highly selective AKT1 activator compound 7460-0250 was identified, and subsequent *in vitro* and *in vivo* experiments confirmed that compound 7460-0250 could attenuate SALI through activating the AKT-mTOR signaling pathway (Figure 9). These findings provided a theoretical basis for the research and development of new drugs for sepsis.

## Limitation

As with most studies, the design of the current study is apt to limitations. This study provide a new option for the prevention and treatment of SALI, which has been verified *in vivo* and *in vitro* experiments, but fell short of investigating whether the efficiency of new highly selected small molecule compound is better than SC79 in molecular biological experiments. However, we have demonstrated the advantages of the new highly selective AKT1 activator in molecular docking analysis, so this limitation will not cause a very large bias in the results of the study. We will make further efforts to unearth the role of compound 7460-0250.

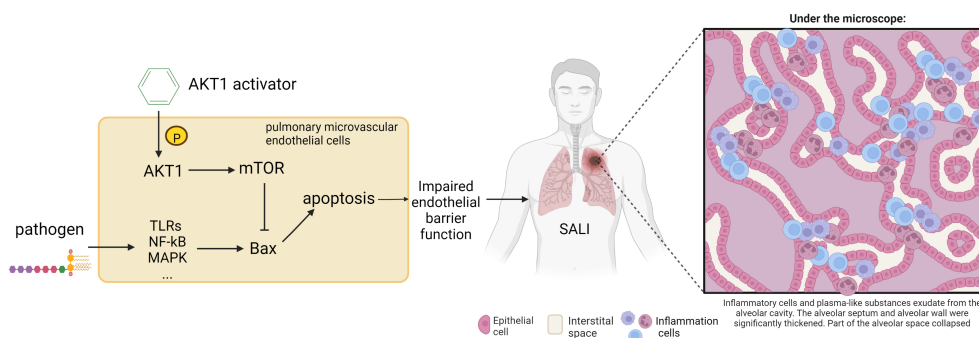


FIGURE 9

Schematic illustration of the mechanism of the protective effect of AKT1 activator on SALI. The destruction of the endothelial vascular barrier by pathogens leads to the leakage of inflammatory cells into the lung interstitium, resulting in SALI. Compound 7460-0250 may attenuate SALI by activating AKT-mTOR signaling pathway to bind Bax and thereby alleviate alveolar capillary cell apoptosis.

## Data availability statement

The original contributions presented in the study are included in the article/Supplementary Material. Further inquiries can be directed to the corresponding author.

## Ethics statement

The animal study was reviewed and approved by Beijing Tsinghua Changgung Hospital (protocol code NCT05095324).

## Author contributions

ZYW conducted to design and writing; XW contributed to cell culture and animal surgery; ZG conducted to western blot; HL contributed to immunofluorescence and flow cytometry; ZWW and YC contributed to HE and results assessment; ZW contributed to supervise this study. All authors contributed to the article and approved the submitted version.

## References

- Cao, Y. Y., Wang, Z., Yu, T., Zhang, Y., Wang, Z. H., Lu, Z. M., et al. (2021). Sepsis induces muscle atrophy by inhibiting proliferation and promoting apoptosis via PI3K-AKT signalling. *J. Cell Mol. Med.* 25 (20), 9724–9739. doi: 10.1111/jcmm.16921
- Chen, X., Zhang, W., Sun, L., and Lian, Y. (2021). Tectorigenin protect HUVECs from H2O2-induced oxidative stress injury by regulating PI3K/Akt pathway. *Tissue Cell* 68, 101475. doi: 10.1016/j.tice.2020.101475
- Cretin, E., Lopes, P., Vimont, E., Tatsuta, T., Langer, T., Gazi, A., et al. (2021). High-throughput screening identifies suppressors of mitochondrial fragmentation in OPA1 fibroblasts. *EMBO Mol. Med.* 13 (6), e13579. doi: 10.15252/emmm.202013579
- Gao, N., Flynn, D. C., Zhang, Z., Zhong, X. S., Walker, V., Liu, K. J., et al. (2004). G1 cell cycle progression and the expression of G1 cyclins are regulated by PI3K/AKT/mTOR/p70S6K1 signaling in human ovarian cancer cells. *Am. J. Physiol. Cell Physiol.* 287 (2), C281–C291. doi: 10.1152/ajpcell.00422.2003
- Gogvadze, V., Orrenius, S., and Zhivotovsky, B. (2008). Mitochondria in cancer cells: What is so special about them? *Trends Cell Biol.* 18 (4), 165–173. doi: 10.1016/j.tcb.2008.01.006
- Gong, H., Cao, Y., Han, G., Zhang, Y., You, Q., Wang, Y., et al. (2017). p53/microRNA-374b/AKT1 regulates colorectal cancer cell apoptosis in response to DNA damage. *Int. J. Oncol.* 50 (5), 1785–1791. doi: 10.3892/ijo.2017.3922
- Gotts, J. E., and Matthay, M. A. (2016). Sepsis: pathophysiology and clinical management. *BMJ* 353, i1585. doi: 10.1136/bmj.i1585
- Green, B. D., Jabbar, A. M., Sandow, J. J., Rifkin, C. D., Masouras, D., Daunt, C. P., et al. (2013). Akt1 is the principal akt isoform regulating apoptosis in limiting cytokine concentrations. *Cell Death Differ.* 20 (10), 1341–1349. doi: 10.1038/cdd.2013.63
- Hou, X., Yang, S., and Yin, J. (2019). Blocking the REDD1/TXNIP axis ameliorates LPS-induced vascular endothelial cell injury through repressing oxidative stress and apoptosis. *Am. J. Physiol. Cell Physiol.* 316 (1), C104–C110. doi: 10.1152/ajpcell.00313.2018
- Hua, H., Zhang, H., Chen, J., Wang, J., Liu, J., and Jiang, Y. (2021). Targeting akt in cancer for precision therapy. *J. Hematol. Oncol.* 14 (1), 128. doi: 10.1186/s13045-021-01137-8
- Hussman, J. P. (2020). Cellular and molecular pathways of COVID-19 and potential points of therapeutic intervention. *Front. Pharmacol.* 11, 1169. doi: 10.3389/fphar.2020.01169
- Jiao, Y., Zhang, T., Zhang, C., Ji, H., Tong, X., Xia, R., et al. (2021). Exosomal miR-30d-5p of neutrophils induces M1 macrophage polarization and primes macrophage pyroptosis in sepsis-related acute lung injury. *Crit. Care* 25 (1), 356. doi: 10.1186/s13054-021-03775-3
- Jo, H., Mondal, S., Tan, D., Nagata, E., Takizawa, S., Sharma, A. K., et al. (2012). Small molecule-induced cytosolic activation of protein kinase akt rescues ischemia-elicited neuronal death. *Proc. Natl. Acad. Sci. U.S.A.* 109 (26), 10581–10586. doi: 10.1073/pnas.1202810109
- Kalwat, M. A. (2021). High-throughput screening for insulin secretion modulators. *Methods Mol. Biol.* 2233, 131–138. doi: 10.1007/978-1-0716-1044-2\_9
- Kepp, O., Galluzzi, L., Lipinski, M., Yuan, J., and Kroemer, G. (2011). Cell death assays for drug discovery. *Nat. Rev. Drug Discov.* 10 (3), 221–237. doi: 10.1038/nrd3373
- Kim, I. Y., Park, Y. K., Song, S. H., Seong, E. Y., Lee, D. W., Bae, S. S., et al. (2020). Akt1 is involved in tubular apoptosis and inflammatory response during renal ischemia-reperfusion injury. *Mol. Biol. Rep.* 47 (12), 9511–9520. doi: 10.1007/s11033-020-06021-1
- Kumar, V. (2020). Pulmonary innate immune response determines the outcome of inflammation during pneumonia and sepsis-associated acute lung injury. *Front. Immunol.* 11, 1722. doi: 10.3389/fimmu.2020.01722
- Li, H., Hao, Y., Yang, L. L., Wang, X. Y., Li, X. Y., Bhandari, S., et al. (2020). MCTRI alleviates lipopolysaccharide-induced acute lung injury by protecting lung endothelial glycocalyx. *J. Cell Physiol.* 235 (10), 7283–7294. doi: 10.1002/jcp.29628
- Li, X., Wei, S., Niu, S., Ma, X., Li, H., Jing, M., et al. (2022). Network pharmacology prediction and molecular docking-based strategy to explore the potential mechanism of huanglian jiedu decoction against sepsis. *Comput. Biol. Med.* 144, 105389. doi: 10.1016/j.compbiomed.2022.105389
- Lin, F., Yang, Y., Wei, S., Huang, X., Peng, Z., Ke, X., et al. (2020). Hydrogen sulfide protects against high glucose-induced human umbilical vein endothelial cell injury through activating PI3K/Akt/eNOS pathway. *Drug Des. Devel. Ther.* 14, 621–633. doi: 10.2147/DDDT.S242521
- Mehta, D., and Malik, A. B. (2006). Signaling mechanisms regulating endothelial permeability. *Physiol. Rev.* 86 (1), 279–367. doi: 10.1152/physrev.00012.2005
- Mokra, D. (2020). Acute lung injury - from pathophysiology to treatment. *Physiol. Res.* 69 (Suppl 3), S353–S366. doi: 10.33549/physiolres.934602

## Funding

This article is supported by Tsinghua University Education Foundation, Sepsis Prevention Program (Funding number: 202002).

## Conflict of interest

The authors declare that the research was conducted in the absence of any commercial or financial relationships that could be construed as a potential conflict of interest.

## Publisher's note

All claims expressed in this article are solely those of the authors and do not necessarily represent those of their affiliated organizations, or those of the publisher, the editors and the reviewers. Any product that may be evaluated in this article, or claim that may be made by its manufacturer, is not guaranteed or endorsed by the publisher.

- Ong, C. S., Zhou, J., Ong, C. N., and Shen, H. M. (2010). Luteolin induces G1 arrest in human nasopharyngeal carcinoma cells *via* the akt-GSK-3beta-Cyclin D1 pathway. *Cancer Lett.* 298 (2), 167–175. doi: 10.1016/j.canlet.2010.07.001
- Pan, X., Xu, S., Zhou, Z., Wang, F., Mao, L., Li, H., et al. (2020). Fibroblast growth factor-2 alleviates the capillary leakage and inflammation in sepsis. *Mol. Med.* 26 (1), 108. doi: 10.1186/s10020-020-00221-y
- Pastorino, J. G., Hoek, J. B., and Shulga, N. (2005). Activation of glycogen synthase kinase 3beta disrupts the binding of hexokinase II to mitochondria by phosphorylating voltage-dependent anion channel and potentiates chemotherapy-induced cytotoxicity. *Cancer Res.* 65 (22), 10545–10554. doi: 10.1158/0008-5472.CAN-05-1925
- Singer, M., Deutschman, C. S., Seymour, C. W., Shankar-Hari, M., Annane, D., Bauer, M., et al. (2016). The third international consensus definitions for sepsis and septic shock (Sepsis-3). *JAMA* 315 (8), 801–810. doi: 10.1001/jama.2016.0287
- Tian, S., Jin, S., Wu, Y., Liu, T., Luo, M., Ou, J., et al. (2021). High-throughput screening of functional deubiquitinating enzymes in autophagy. *Autophagy* 17 (6), 1367–1378. doi: 10.1080/15548627.2020.1761652
- Wang, C. D., Yuan, C. F., Bu, Y. Q., Wu, X. M., Wan, J. Y., Zhang, L., et al. (2014). Fangchinoline inhibits cell proliferation *via* Akt/GSK-3beta/ cyclin D1 signaling and induces apoptosis in MDA-MB-231 breast cancer cells. *Asian Pac J. Cancer Prev.* 15 (2), 769–773. doi: 10.7314/APJCP.2014.15.2.769
- Wang, Y. M., Wang, Y. P., Xie, J., Zhao, Z. Z., Gupta, S., Guo, Y., et al. (2019). Paclitaxel alleviated sepsis-induced acute lung injury by activating MUC1 and suppressing TLR-4/NF-kappaB pathway. *Drug Des. Devel Ther.* 13, 3391–3404. doi: 10.2147/DDDT.S222296
- Wang, J. F., Ji, R., Chen, W. W., Huang, S. W., Zheng, Y. J., Yang, Z. T., et al. (2021). Upregulated PD-L1 delays human neutrophil apoptosis and promotes lung injury in an experimental mouse model of sepsis. *Blood* 138 (9), 806–810. doi: 10.1182/blood.2020009417
- Wang, Z., Wang, X., Guo, Z., Liao, H., Chai, Y., Wang, Z., et al. (2022). Reduning attenuates LPS-induced human umbilical vein endothelial cells (HUVECs) apoptosis through PI3K-AKT signaling pathway. *Front. Pharmacol.* 13, 921337. doi: 10.3389/fphar.2022.921337



## OPEN ACCESS

## EDITED BY

Parth Sarthi Sen Gupta,  
Indian Institute of Science Education and  
Research Berhampur (IISER), India

## REVIEWED BY

Sunil Kumar Tripathi,  
Georgia State University, United States  
Gopal L. Khatik,  
National Institute of Pharmaceutical  
Education and Research, India

## \*CORRESPONDENCE

Neha S. Gandhi  
✉ neha.gandhi@qut.edu.au  
Roger Woodgate  
✉ woodgate@mail.nih.gov

## SPECIALTY SECTION

This article was submitted to  
Clinical Microbiology,  
a section of the journal  
Frontiers in Cellular and  
Infection Microbiology

RECEIVED 23 September 2022

ACCEPTED 14 February 2023

PUBLISHED 03 March 2023

## CITATION

Schuurs ZP, McDonald JP, Croft LV,  
Richard DJ, Woodgate R and Gandhi NS  
(2023) Integration of molecular modelling  
and *in vitro* studies to inhibit  
LexA proteolysis.  
*Front. Cell. Infect. Microbiol.* 13:1051602.  
doi: 10.3389/fcimb.2023.1051602

## COPYRIGHT

© 2023 Schuurs, McDonald, Croft, Richard,  
Woodgate and Gandhi. This is an open-  
access article distributed under the terms of  
the [Creative Commons Attribution License](#)  
(CC BY). The use, distribution or  
reproduction in other forums is permitted,  
provided the original author(s) and the  
copyright owner(s) are credited and that  
the original publication in this journal is  
cited, in accordance with accepted  
academic practice. No use, distribution or  
reproduction is permitted which does not  
comply with these terms.

# Integration of molecular modelling and *in vitro* studies to inhibit LexA proteolysis

Zachariah P. Schuurs <sup>1,2</sup>, John P. McDonald <sup>3</sup>,  
Laura V. Croft <sup>1</sup>, Derek J. Richard <sup>1</sup>, Roger Woodgate <sup>3\*</sup>  
and Neha S. Gandhi <sup>1,2\*</sup>

<sup>1</sup>Cancer and Ageing Research Program, Centre for Genomics and Personalised Health, Queensland University of Technology (QUT), Translational Research Institute (TRI), Brisbane, QLD, Australia,

<sup>2</sup>School of Chemistry and Physics, Queensland University of Technology (QUT), Brisbane,

QLD, Australia, <sup>3</sup>Laboratory of Genomic Integrity, National Institute of Child Health and Human Development, National Institutes of Health, Bethesda, MD, United States

**Introduction:** As antibiotic resistance has become more prevalent, the social and economic impacts are increasingly pressing. Indeed, bacteria have developed the SOS response which facilitates the evolution of resistance under genotoxic stress. The transcriptional repressor, LexA, plays a key role in this response. Mutation of LexA to a non-cleavable form that prevents the induction of the SOS response sensitizes bacteria to antibiotics. Achieving the same inhibition of proteolysis with small molecules also increases antibiotic susceptibility and reduces drug resistance acquisition. The availability of multiple LexA crystal structures, and the unique Ser-119 and Lys-156 catalytic dyad in the protein enables the rational design of inhibitors.

**Methods:** We pursued a binary approach to inhibit proteolysis; we first investigated  $\beta$ -turn mimetics, and in the second approach we tested covalent warheads targeting the Ser-119 residue. We found that the cleavage site region (CSR) of the LexA protein is a classical Type II  $\beta$ -turn, and that published 1,2,3-triazole compounds mimic the  $\beta$ -turn. Generic covalent molecule libraries and a  $\beta$ -turn mimetic library were docked to the LexA C-terminal domain using molecular modelling methods in FlexX and CovDock respectively. The 133 highest-scoring molecules were screened for their ability to inhibit LexA cleavage under alkaline conditions. The top molecules were then tested using a RecA-mediated cleavage assay.

**Results:** The  $\beta$ -turn library screen did not produce any hit compounds that inhibited RecA-mediated cleavage. The covalent screen discovered an electrophilic serine warhead that can inhibit LexA proteolysis, reacting with Ser-119 via a nitrile moiety.

**Discussion:** This research presents a starting point for hit-to-lead optimisation, which could lead to inhibition of the SOS response and prevent the acquisition of antibiotic resistance.

## KEYWORDS

LexA, antibiotic resistance, covalent inhibitors, molecular docking, proteolysis



## 1 Introduction

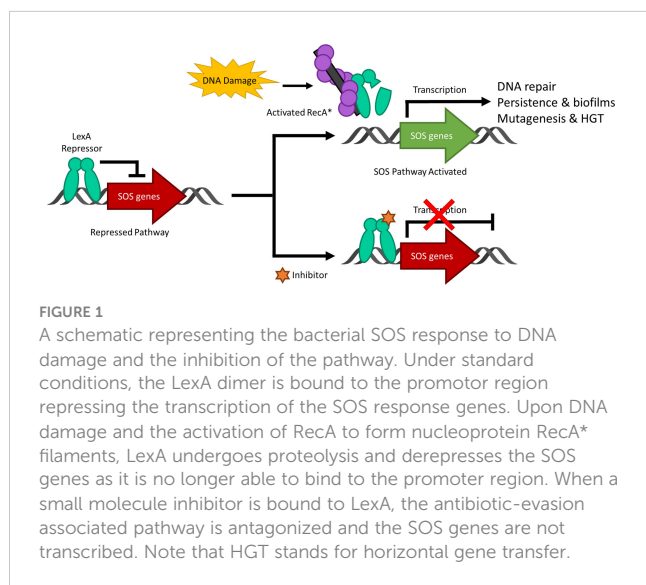
Antimicrobial resistance is a prevailing problem, threatening to undermine the progress of healthcare in the last century since the discovery of antibiotics. Infections that were previously treatable no longer respond to traditional antibiotics. Quiescent populations of bacterial pathogens resistant to antibiotics can lead to a higher risk of mortality from the infection and an increased risk of disease dissemination (Founou et al., 2017). Bacteria can acquire this resistance through three main mechanisms – transformation, transduction and conjugation (Munita and Arias, 2016). While some bacteria acquire resistance through genetic exchange, others acquire it as the result of chromosomal mutations that inactivate drug-activating enzymes or targets of the drugs. Where it has previously been unprofitable to develop new antibiotics, the social and economic implications are now beginning to outweigh that criterion (Aslam et al., 2018). It is therefore no surprise that alternative antibiotic targets, like the SOS pathway, have emerged (Cirz et al., 2005; Smith and Romesberg, 2007; Culyba et al., 2015).

DNA damage to a bacterium compromises the chromosomal integrity and can threaten cell survival. As a countermeasure, bacteria have evolved the damage-inducible “SOS response” (Radman, 1974). The SOS response is regulated by two proteins; LexA, which serves as a transcriptional repressor of >40 genes in *E. coli* (Fernández de Henestrosa et al., 2000) and RecA, which upon DNA damage, forms a RecA nucleoprotein filament (RecA\*) that mediates the self-cleavage of LexA. Upon proteolysis, LexA is inactivated as a transcriptional repressor and the SOS response is derepressed (Figure 1) (Little, 1984). The LexA NTD (Figure 2) normally binds to a 16–19 bp palindromic recognition site in the promoter region of genes in the SOS regulon (Fernández de Henestrosa et al., 2000). The affinity of LexA to this promoter region creates a finely tuned regulator of the SOS response. Genes that have weak LexA binding sites are induced first, while those with tighter binding sites are induced later in the SOS response (Fernández de Henestrosa et al., 2000). Of the more than 40 genes in the SOS regulation, three encode DNA polymerases (pols

II, IV and V). In particular, polV is responsible for the majority of damage-induced mutagenesis in *E. coli* (Kato and Shinoura, 1977). Previous studies have reported that the SOS response can be attenuated by genetically inactivating the RecA\*/LexA interaction (Mo et al., 2016) and antibiotic-associated mutagenesis is decreased, re-sensitizing resistant strains to DNA damaging antibiotics with the latter being dependent on functional polys II, IV and V (Cirz et al., 2006; Cirz et al., 2007; Li et al., 2010). As a consequence, previous studies have investigated the SOS pathway as target to prevent the acquisition of antibiotic resistance (Cirz et al., 2006; Cirz et al., 2007; Mo et al., 2018; Selwood et al., 2018; Bellio et al., 2020).

LexA is a dimeric protein in solution (Mohana-Borges et al., 2000), with each monomer joined by a short flexible linker called the cleavage site region (CSR) between residues 79–95 (Figure 2). This linker region undergoes a conformational change from the non-cleavable (NC) form to the cleavable (C) form when LexA binds to RecA\*. Figure 3 illustrates the conformational movement of the CSR. The CSR region of LexA has been described as a  $\beta$ -turn in several instances (Mo et al., 2014; Jaramillo et al., 2022), but is not yet categorised. The N-terminal domain (NTD) binds to the LexA-binding box, while the C-terminal domain contains the protease active site. LexA is a serine protease, in the endopeptidase clan SF, and part of family S24 (Slilaty and Little, 1987; Polgár, 2013) defined by the Ser-119 and Lys-156 catalytic dyad (Figure 2). Located in a hydrophobic cleft (Figure 3), the Ser-119 of the dyad acts as a nucleophile and the lysine as the acid/base. Over the pH range 7.15–11.77 LexA, undergoes a linear rate of autodigestion, reaching a plateau above pH 10 (Slilaty et al., 1986). In this case, the Lys-156 is deprotonated, and the protein undergoes autocleavage (Slilaty and Little, 1987). In the presence of RecA\* nucleoprotein filaments, the CSR loop changes conformation, shifting into the hydrophobic cleft (Figure 3) and causing the  $pK_a$  of the Lys-156 to change, deprotonating it (Polgár, 2013). This forms a transient tetrahedral intermediate between the Ser-119, Ala-84 and Gly-85 (Figure 2 insert). Cleavage of the protein occurs when the bond between Ala-84 and Glu-85 is hydrolysed by the nucleophilic Ser-119.

LexA was the first of a superfamily of enzymes that have been shown to undergo autoproteolysis (Little, 1984; Slilaty et al., 1986; Burckhardt et al., 1988; McDonald et al., 1999; Luo et al., 2001; Cezairliyan and Sauer, 2009; Gonzalez et al., 2019). This family of enzymes are subjected to RecA-mediated cleavage and are therefore close structural homologs to LexA. This includes UmuD (Burckhardt et al., 1988; McDonald et al., 1999), DinR (Hajjema et al., 1996; Winterling et al., 1997), SetR<sub>ICE391</sub> (Gonzalez et al., 2019) and  $\lambda$  cI (Gimble and Sauer, 1985), all of which are involved in the mutagenic SOS response. The scissile Ala-Gly or Cys-Gly residues, along with the catalytic dyad of Ser and Lys are conserved across these proteins. While all of them undergo proteolysis, what sets them apart is the rate at which they undergo cleavage. Point mutations of the residues around the CSR have found that they are essential to mediating the rate at which members of this family undergo cleavage, from speeding it up to preventing cleavage altogether (Gimble and Sauer, 1985; Lin and Little, 1988; Shepley and Little, 1996; McDonald et al., 1998; Beuning et al., 2006; Mo et al., 2014).



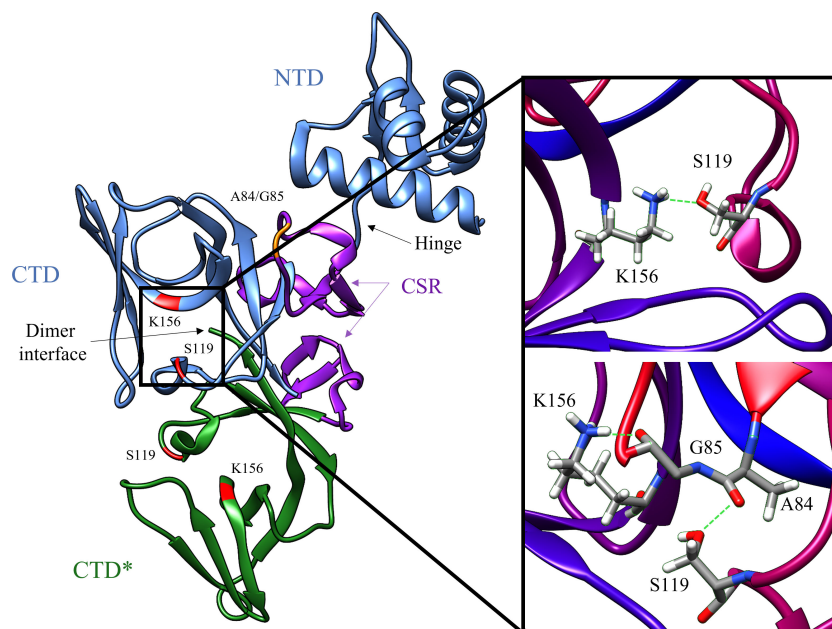


FIGURE 2

Key structural features of the LexA dimer (PDB ID: 1JHF). One of the monomers is depicted in blue, and the other is in green. The catalytic dyad Ser-119 and Lys-156 are highlighted in red, and the scissile bond Ala-84 – Glu-85 is in orange. The CSR which undergoes the conformational shift upon binding to RecA is shown in purple. The insert depicts the transition from the catalytic S119-K156 dyad to the tetrahedral intermediate (PDB ID: 1JHE) as the scissile Ala-84 – Glu-85 moves into the hydrophobic pocket. This conformational change activates LexA from the NC form into the C form. The green dashed lines in the insert represent the hydrogen bonds between residues in the crystal structure. Note that the crystal structure does not contain the NTD of the second monomer in the dimer, due to poor electron density (Luo et al., 2001).

While prior work has attempted to develop inhibitors to LexA cleavage, none are potent enough to take to market. A major campaign in a partnership between industry and academia (Mo et al., 2018) reported five molecules with micromolar cytotoxicity. The 1,2,3-triazole lead (GSK-C1) from this first iteration was

advanced by Selwood et al. (Selwood et al., 2018) and an analogue of the initial hit was reported to have an IC<sub>50</sub> of 9  $\mu$ M against LexA. Further modifications to the 1,2,3-triazole core scaffold have been investigated by Jaramillo et al. (Jaramillo et al., 2022), however, none of the compounds had an IC<sub>50</sub> below 48  $\mu$ M.

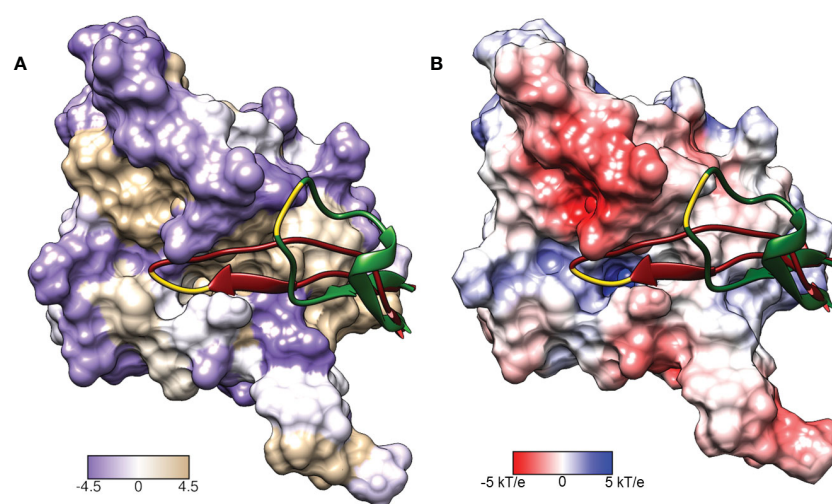


FIGURE 3

Surface representations of the LexA repressor protein. The ribbon represents the CSR in the cleavable (red, PDB: 1JHE) and non-cleavable (green, PDB: 1JHC) forms. The key scissile bond (Ala-84 – Gly-85) is in yellow. (A) depicts the amino acid hydrophobicity using the Kyte-Doolittle scale. (B) illustrates the electrostatic potential (kT/e) of the surface, calculated using DelPhi Webserver (Sarkar et al., 2013). These representations depict the catalytic pocket that the CSR moves into when the protein is activated. As the surface representations indicate, the pocket is highly hydrophobic and electrostatically positive.

To aid in the discovery of novel inhibitors, an understanding of these compounds' molecular recognition is necessary. Molecular modelling has proven to be a vital tool in the determination of a structure-activity relationship (SAR) without the need to perform resource-intensive mutagenesis studies (dos Santos et al., 2014). These approaches have also facilitated the ability to screen large chemical spaces in a relatively short amount of time and at little cost compared to their counterpart *in vitro* screening techniques (Bender et al., 2021). A common approach to novel proteins is to virtually screen large libraries of compounds, sometimes reaching into millions of compounds. When there are existing compounds known to bind to a protein it can be appropriate to use them as a rationale to perform a targeted screen of smaller libraries (Sarnpitak et al., 2015). This reduces the computational resources required and speeds up how long the screening campaign takes.

In recent times, covalent inhibitors have gained momentum owing to their potency, selectivity and extended duration of action (Kim et al., 2021; Gao et al., 2022). Covalent inhibitors have an electrophilic warhead that reacts with nucleophilic residues, both reversibly and irreversibly (Kumalo et al., 2015; Ábrányi-Balogh and Keserű, 2022). Selectivity is achieved through non-covalent interactions with the scaffold. Serine is one of the most commonly targeted residues due to its catalytic role in many proteases, and common covalent inhibitors such as penicillin and aspirin are examples of serine warheads (Martin et al., 2019). A recent study explored boronic acids as covalent inhibitors of LexA autocleavage (Bellio et al., 2020). This study found (3-aminophenyl)boronic acid had a  $K_d$  of 1.07 mM, and that it is predicted to form an acyl-enzyme intermediate with the Ser-119 and form hydrogen bonds with the Lys-156 and Val-153 (Bellio et al., 2020). The same study developed a new equation for describing the inhibition potency of autoproteolytic enzymes (Bellio et al., 2020).

This investigation uses a two-fold approach to find a novel inhibitor scaffold. First, we established the SAR of current non-covalent inhibitors, which was used as a rationale to dock a selected molecule libraries –  $\beta$ -turn mimetics and covalent serine warheads. A small library of the top binding molecules from each of the two libraries was screened *in vitro* after establishing a pseudo high-throughput approach. A  $K_d$  for the identified covalent proteolytic antagonist was determined, and the unsuccessful nature of the  $\beta$ -turn mimetic screen was discussed. Herein, we describe the discovery of a covalent inhibitor scaffold that inhibits the cleavage of the LexA transcriptional repressor.

## 2 Materials and methods

### 2.1 Hydrophobic and electrostatic potential surface

The hydrophobicity of LexA (Figure 3A) was represented according to the Kyte and Doolittle scale (Kyte and Doolittle, 1982) which assigns a hydrophobicity value to each residue, and was visualised with UCSF Chimera version 1.13.1 (Pettersen et al., 2004). The Adaptive Poisson-Boltzmann Solver (APBS) (Jurrus et al., 2018) webserver was used to calculate the electrostatic

potential surface of the LexA CTD wild-type monomer. The C-terminal wild type (WT) was prepared by downloading the structural file (PDB: 1JHC) and mutating the Ala-119 to a serine before adding hydrogens. The PDB file was converted to PQR format at pH 7.0 and using PROPKA (Olsson et al., 2011; Søndergaard et al., 2011) to assign protonation states. The PARSE forcefield (Sitkoff et al., 1994; Tang et al., 2007) was used for the conversion. To run APBS, the dielectric constant set to 2.00  $\text{Fm}^{-1}$ , and the solvent dielectric constant to 78.5400  $\text{Fm}^{-1}$ . The output electrostatic potential surface was visualised with UCSF Chimera version 1.13.1 (Pettersen et al., 2004) (Figure 3B).

### 2.2 Molecular docking with BioSolveIT

The mutant *E. coli* LexA C-terminal fragment (PDB ID: 1JHC) (Luo et al., 2001) was obtained from the Protein Data Bank (Berman et al., 2000). The A119 presented in the 3D structure was changed to serine using Chimera version 1.13.1 (Pettersen et al., 2004) to represent the WT LexA sequence. As there are no structures of LexA co-crystallized with ligands, a comparative assessment of docking programs could not be conducted. We used the FlexX (Rarey et al., 1996) module of SeeSAR version 10.1 (BioSolveIT GmBH, 2020) to dock the three molecules from Mo et al. that bound directly to LexA (Mo et al., 2018). We docked these three to determine their binding modes and use them as a point of comparison (Figure S1). HYDE (Reulecke et al., 2008) was used to re-score the docked poses and calculate predicted binding affinities. This scoring function involves the fragmentation of the ligand and selection of a base fragment, which is placed in the active site. A free energy is assigned to each atom depending on the emerging hydrogen bond and dehydration energies of the complex. A tree-search algorithm is then used to incrementally build upon the base fragment. SeeSAR (BioSolveIT GmBH, 2020) was used as it offers a unique suite of tools to understand binding recognition from per-atom scoring and overall concentration ranges for the ligand dissociation constant (Pagadala et al., 2017). The analysis of the  $\beta$ -turn in LexA was accomplished using RamachanDraw v0.2.3 (Cirilo, 2022) and visualised using BIOVIA Discovery Studio version 10.1.0.19295 (Biovia, 2019).

### 2.3 Virtual Screening of $\beta$ -turn mimetics with BioSolveIT

Having determined the type of  $\beta$ -turn present in the LexA structure, we theorised that the catalytic site would molecularly recognise  $\beta$ -turn mimetics. A structure-based virtual screening was performed with the ChemDiv library peptidomimetics of  $\beta$ -turn motifs (ChemDiv, 2019). The 2276 molecules were docked to the full-length, wild-type LexA CTD protein using FlexX (Rarey et al., 1996). The binding site was automatically identified by SeeSAR (BioSolveIT GmBH, 2020), matching the predicted hydrophobic cleft. Each ligand was docked with 10 poses per molecule generated, and a score was generated for each pose using the HYDE scoring function (Schneider et al., 2013). The top 53 compounds



were subsequently ordered from ChemDiv to test *in vitro*. Docking poses were visualised using Chimera version 1.13.1 (Pettersen et al., 2004) and 2D residue interaction plots were generated with BIOVIA Discovery Studio version 20.1.0.19295 (Biovia, 2019).

## 2.4 Virtual screening of covalent inhibitors with CovDock

The ChemDiv libraries Covalent Generic and Smart Inhibitors (ChemDiv, 2020) was docked to the WT LexA using the CovDock (Toledo Warshaviak et al., 2014; Zhu et al., 2014) workflow in the Schrödinger Maestro suite 2019-4. This was used as Maestro Suite is considered to have one of the best high-throughput covalent docking implementations (Kumalo et al., 2015; Scarpino et al., 2018). The WT LexA protein structure was prepared using the Schrödinger protein preparation wizard, and the 8607 molecules were prepared using LigPrep (Schrodinger, 2020). The OPLS3e forcefield (Roos et al., 2019) was used to dock both compound libraries. The cubic grid used to select the search space, with an inner box equal to 15 Å and outer box of 25 Å. The grid box was centred on the catalytic Ser-119, which was selected as the active residue. CovDock automatically sorts the input library based on the possible covalent reactions between the warhead functional groups and the selected catalytic residues. The sub libraries were docked with beta-lactam addition; boronic acid addition; conjugate addition to an alkyne (aryl and carbonyl activated), alkene (nitrile activated); epoxide opening, Michael addition, nucleophilic addition to a double and triple bond and nucleophilic substitution. The CovDock module consists of five distinct steps (Zhu et al., 2014). ConfGen (Watts et al., 2010) generated conformations of each molecule, and the three conformations with the lowest conformational energies were selected for Glide docking. CovDock mutated the Ser-119 to an alanine, removing potential interference of the sidechain, and the molecules are docked within 8 Å of the C-beta atom of the S119A. Poses of each molecule scored within 2.5 kcal/mol of the lowest score sampled were retained. Secondly, the Ser-119 was restored, and the side chain conformations were sampled with a rotamer library. The binding modes from step one was sampled to see if the two atoms that would form the covalent bond were within 5 Å of each other. If so, the covalent bond was then formed, and all the changes in bond order, ionization state and chirality were adjusted. Stereoisomers were retained for further optimisation. Next the complexes were minimised in a vacuum to restore standard bond lengths and avoid steric clashes. The molecule cartesian coordinates were clustered with a k-means algorithm and poses were selected and minimised to obtain a Prime energy used to rank poses and select favourable binding geometry. Lastly, the poses were assigned a docking score based on the empirical scoring function that Zhu et al. developed. This score is the average of the pre-reactive Glide score and the Glide score of the ligand in the final complex. This score aims to capture the key elements during the covalent docking process (Zhu et al., 2014; Delre et al., 2020). Of the 8607 input compounds, the top scoring compounds across the reaction types were ranked by docking score and analyzed visually. The 80 top scoring compounds were ordered from ChemDiv (San Diego, CA).

## 2.5 Expression and purification of native *E. coli* LexA and RecA proteins

Native, untagged LexA protein, was expressed from an IPTG-inducible T7 promoter from plasmid pJWL288 (Roland et al., 1992) in the *E. coli* strain, RW644 (Karata et al., 2012). LexA was purified to more than 95% purity by standard protocols (Little, 1984). Native, untagged RecA, protein was expressed from an IPTG-inducible T7 promoter from plasmid pAIR79 (Lusetti et al., 2003) in the *E. coli* strain, EAW68 (Norais et al., 2009), that was also transformed with pT7pol26 (Mertens et al., 1995). RecA was purified to greater than 95% purity by standard protocols (Cox et al., 1981; Lusetti et al., 2003; Ojha et al., 2022).

## 2.6 *In vitro* screen LexA autocleavage reactions

A total of 133 compounds from the two screens were ordered from ChemDiv (San Diego, CA), which consisted of 80 molecules from the covalent screen, and 53 molecules from the  $\beta$ -turn library. An assay that takes advantage of the autocleavage that the protein undergoes in alkaline conditions was based on previously described methods (Mo et al., 2018; Gonzalez et al., 2019). To establish the optimal pH for the screen, a pH response curve was made with the *E. coli* LexA protein. In each reaction 0.4  $\mu$ g of LexA was used, which was diluted in 10 mM Tris-HCl, 150mM NaCl (4.5  $\mu$ L). Cleavage buffer consisting of 50 mM CAPS-NaOH (pH 10.00, pH 10.22, pH 10.42, pH 10.60), 150 mM NaCl was added (4.5  $\mu$ L) to begin autoproteolysis. After 30 min, reactions were terminated by the appropriate addition of 4X SDS sample buffer and freezing on dry ice.

For the screen, 0.4  $\mu$ g of LexA was used per reaction, which was diluted in 10 mM Tris-HCl, 150mM NaCl (4  $\mu$ L/sample). To this, compound suspended in DMSO was added to a final concentration of 20  $\mu$ M (0.5  $\mu$ L/5.55%) and incubated for 10 min at 37°C. Cleavage buffer consisting of 50 mM CAPS-NaOH (pH 10.00) was then added (4.5  $\mu$ L) and the mix incubated for 30 min. The reactions were terminated with 4X SDS sample buffer and frozen on dry ice.

The products of the autocleavage reactions were subjected to electrophoresis in SDS-PAGE gels containing 4-12% polyacrylamide (ThermoFisher Bis-Tris, Bolt™). Proteins were stained with Coomassie brilliant blue using a Bio-Rad Trans-Blot Turbo. The gels were imaged on an Odyssey CLx and quantified with Image Studio.

## 2.7 *In vitro* RecA-mediated LexA cleavage reactions

The RecA-mediated cleavage assay was based upon a previously described procedure for the cleavage of SetR<sub>ICE391</sub> (Gonzalez et al., 2019) with modifications. Two 50  $\mu$ L master mixes were made in a buffer consisting of 40 mM Tris-HCl (pH 7.4), 10 mM MgCl<sub>2</sub>, 1mM DTT and 30 mM NaCl. One mix contained 2.5  $\mu$ g of RecA, 200 ng

$\Phi$ X174 virion (ssDNA) (New England Biolabs; cat; N3023S) and 1 mM ATP $\gamma$ S. The other mix contained 15  $\mu$ g of LexA and either DMSO (5% of total) or the compound of interest in DMSO (5% of total). These master mixes were pre-incubated at 37°C for 10 minutes to activate RecA and allow the compound to interact with LexA. Afterwards, the mixes were combined and further incubated at 37°C. 14  $\mu$ L aliquots were taken at 5-minute intervals. The reaction at each timepoint was terminated by the addition of 4 x SDS sample buffer and freezing on dry ice. After electrophoresis of the timepoint samples in SDS-PAGE gels containing 4-12% polyacrylamide (Invitrogen NuPAGE 4-12% Bis-Tris), the gels were stained with Coomassie brilliant blue. Subsequently, the gels were imaged and quantified using Image StudioLite.

## 2.8 Homology with superfamily members

We conducted a protein sequence alignment of *E. coli* LexA (A0A418GQD6), *B. subtilis* DinR (P31080), *E. coli* UmuD (E7BTC7), *S. typhimurium* UmuD (A0A648F2G5) and SetR<sub>ICE391</sub> (A0A6G8F0T0) from UniProt using the Bio3D package (Grant et al., 2006) implemented in R version 4.2.2 (R Core Team, 2022). The alignment was visualised using ESPript 3.0, and the *E. coli* LexA structural features with the docked compound **1** was visualised with ENDscript 2.0 (Robert and Gouet, 2014).

## 3 Results

### 3.1 $\beta$ -turn definition

As the LexA CSR is a  $\beta$ -turn, we hypothesized that  $\beta$ -turn peptidomimetics would bind to the same region of the LexA CTD, thereby preventing cleavage from occurring. It was recently predicted (Jaramillo et al., 2022) that the current 5-amino-1-(carbamoylmethyl)-1H-1,2,3-triazole-4-carboxamide scaffold (Selwood et al., 2018) was a  $\beta$ -turn mimetic, as the 1,2,3-triazole ring provides a geometry similar to a  $\beta$ -turn (Mo et al., 2018). Therefore, we were interested in classifying the  $\beta$ -turn of LexA, which would facilitate a visual comparison between the LexA  $\beta$ -turn and the conformation that docked compounds would take.  $\beta$ -turns are classified according to the dihedral torsion angles ( $\Phi$  and  $\Psi$ ) between the amino acid residues  $i+1$  and  $i+2$  (Venkatachalam, 1968). The standard nomenclature for  $\beta$ -turn types are: I, I', II, II', VIII, VIa1, VIa2, VIb and IV (Hutchinson and Thornton, 1994). As more protein structures are being elucidated, these classifications are being changed, with new turns being defined. This gives definitions to turns that previously were considered “non-standard” but occur with a high frequency. We have analyzed the  $\beta$ -turn in LexA (residues 83-86) to classify it. According to the standard classification, it falls into type II (de Brevern, 2016), however a more recent classification puts it under the SC2-SC10 turn. This is classified according to the dihedral torsions in Table 1. In approximately 68% of the turns that fall into this new classifier, glycines occur at the  $i+2$  position (Zhang et al., 2022). The distance

between the  $\alpha$ -carbons of the  $i$  and  $i+3$  is 5.405 Å, and the 2.610 Å distance between the  $i$  oxygen and  $i+3$  hydrogen indicate a hydrogen bond between the molecules (Figure 4B). This is narrower than most standard  $\beta$ -turns, which have distances up to 7 Å (de Brevern, 2016; Ahn et al., 2017).

When the compound GSK-C1 was docked to the hydrophobic cleft, we found it to take on a conformation reminiscent of a  $\beta$ -turn. One of the classifications of a  $\beta$ -turn is that the  $i$  and  $i+3$  residues are less than 7.0 Å (Ahn et al., 2017) from each other. In the case of GSK-C1, there is 5.608 Å (Figure 4C) between the aromatic rings, occupying a slightly larger space in the pocket than the  $\beta$ -turn does. Based on this modelling we decided to screen a library of  $\beta$ -turn mimetics.

### 3.2 $\beta$ -turn peptidomimetics screen

A common approach to inhibiting proteases is the use of peptidomimetics (Amblard et al., 2018; Capasso et al., 2021; Bai et al., 2022). Peptidomimetics are slightly modified backbones or sidechains, possibly sharing topological similarities with peptide features. These modifications can be used to hone the properties such as cell permeability, target specificity, and stability. Based on the results of the GSK molecule QSAR assessment and our analysis of the CSR  $\beta$ -turn, we performed a structure-based virtual screen of the 2276 molecules of the ChemDiv  $\beta$ -turn peptidomimetics library (Table 2) using the FlexX implementation in SeeSAR version 10.1 (BioSolveIT GmbH, 2020). The results of the docking campaign showed that the mimetics occupied the binding site with a similar conformation to GSK-C1, the  $\beta$ -turn mimetic, and some extended down to bind in regions closer to the CSR. The main point of differentiation between the docked compounds was the structural features used to mimic a  $\beta$ -turn. Where there are a variety of  $\beta$ -turn types, denoted by the torsions between residues, these structural features change the turn of a mimetic. Looking at Table 2, most of these top compounds contain heterocyclic spiro groups (2, 3, 4, 5, 8, 10). The results also indicate the importance of strong hydrogen donor/acceptor groups in the compounds as they can stabilise the compound within the hydrophobic pocket. The only compound in this library that when docked, took a conformation like that of a  $\beta$ -turn is compared in Figure 4D. Molecules were selected based on their score when compared to the benchmark molecules and included an enriched scaffold diversity. We selected the 53 top scoring compounds from the screen to test *in vitro*.

TABLE 1 Dihedral torsions of the CSR  $\beta$ -turn.

Residue	$\Phi$	$\Psi$
Glu-83 ( $i$ )	-62.5°	145.65°
Gly-84 ( $i+1$ )	-58.86°	126.78°
Ala-85 ( $i+2$ )	79.02°	-24.45°
Ala-86 ( $i+3$ )	-68.97°	136.73°

These torsions were calculated from PDB 1JHF (Luo et al., 2001) using BIOVIA Discovery Studio (Biovia, 2019). Torsions are between four atoms and are used to classify  $\beta$ -turns.



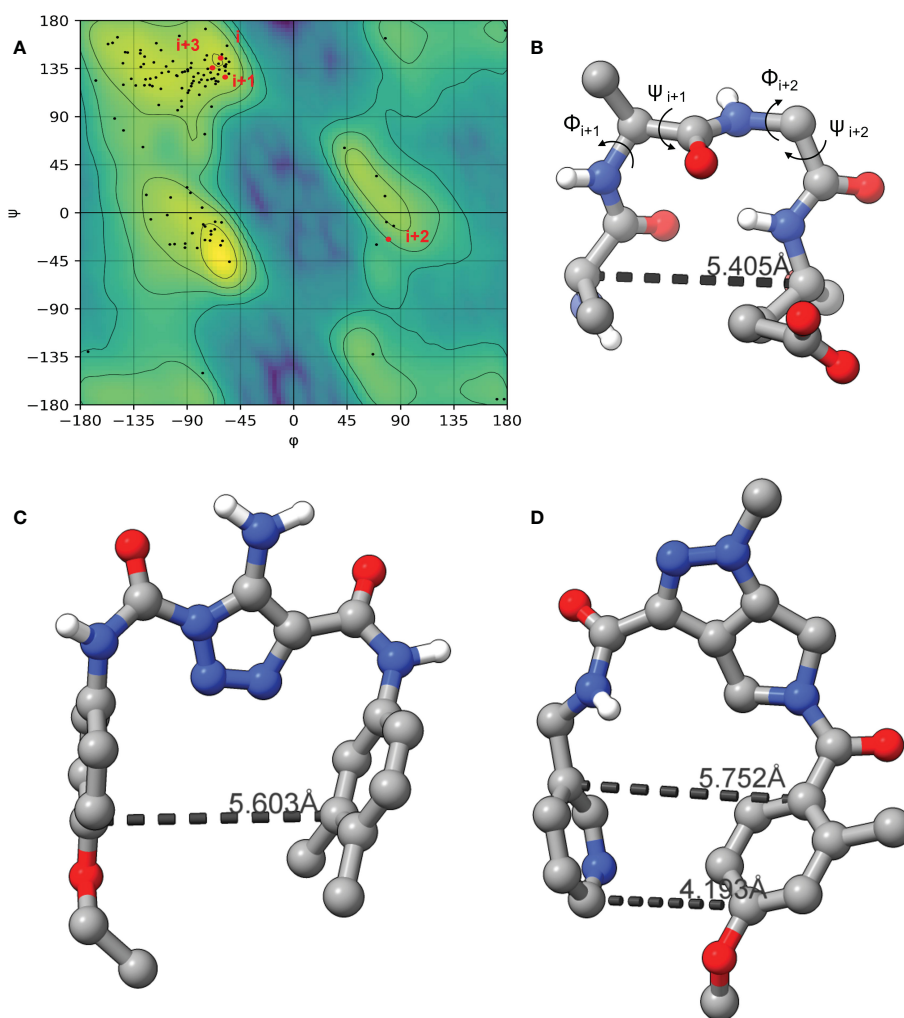


FIGURE 4

The Ramachandran plot of LexA highlighting the dihedral torsions between  $\beta$ -turn residues of the CSR region are presented in (A). The key atoms in the  $\beta$ -turn of the CSR that contains scissile bond between Ala-84 and Gly-85 are shown in (B). The dihedral torsions of the CSR  $\beta$ -turn are detailed in Table 1. These torsions determine the classification of the  $\beta$ -turn. The docked model of the compound GSK-C1 is shown in (C), (D) is the only  $\beta$ -turn mimetic compound from our screen that took a conformation reminiscent of the  $\beta$ -turn.

### 3.3 Covalent warhead screen

We performed a structure-based covalent screening protocol after it was shown that it was possible to prevent the cleavage of LexA by targeting the catalytic Ser-119 with covalent warheads (Bellio et al., 2020). Using Schrödinger's CovDock feature, the ChemDiv Generic and Smart covalent inhibitor libraries were docked. This revealed scaffolds that demonstrated improved binding scores over the boronic acids tested by Bellio et al. (Bellio et al., 2020). The top ten scoring compounds using the OPLS3e forcefield are in Table 3. These are predicted to bind by a series of different reactions, dependent on the functional group chemistries available.

### 3.4 *In vitro* screen

The *in vitro* screen carried out was based on the LexA's ability to undergo autoproteolysis in alkaline conditions. Our initial

development of the assay determined the optimal conditions for the screen to be pH 10.00 for 30 min. Using this property, we screened the 133 compounds for inhibition activity. Of these, 12 compound exhibited some inhibitory effect under autocleavage conditions (Table S1), however once tested in the RecA-mediated counter assay, only one compound exhibited an inhibitory effect on LexA proteolysis. Compound 1 (ChemDiv ID: 2381-1036, Figure 5A) covalently bound to the catalytic Ser-119, thereby inhibiting LexA cleavage. This compound reacts with the serine *via* a nitrile-activated conjugate addition, where the alkene reacts to bind to the serine. In docking this compound scored -4.841, worse than the top scoring compounds.

Analysis of the top scoring docked pose of this compound shows that there are three main ways that compound 1 interacts with the LexA hydrophobic pocket (Figure 5). The primary interaction is the covalent bond with the oxygen of the catalytic Ser-119. The second essential interaction is the hydrogen bond between the donating Lys-156 and the hydrogen bond accepting

TABLE 2 The top 10 compounds docked to LexA using BioSolveIT, with HYDE rescoring predicted affinities (Schneider et al., 2013).

Ranking	Compound ID	Molecular Weight	Predicted Affinity [μM]	Structure
1	CM1461-0224	397.467	18.48	
2	T787-5165	398.544	26.51	
3	S635-3152	355.317	83.81	
4	S635-2320	357.515	97.81	
5	S635-4217	398.495	98.84	
6	L871-0125	522.6	107.81	
7	CM1461-0349	430.377	118.36	

(Continued)

TABLE 2 Continued

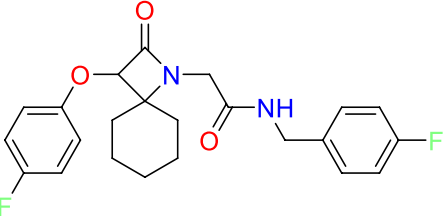
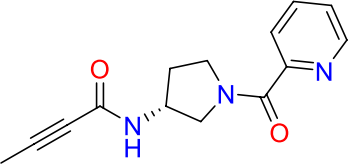
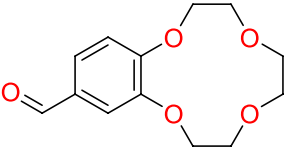
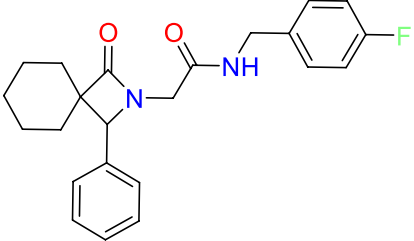
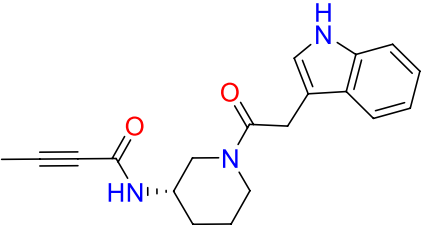
Ranking	Compound ID	Molecular Weight	Predicted Affinity [ $\mu$ M]	Structure
8	T655-0553	397.516	122.96	
9	S398-2187	405.456	130.07	
10	S635-2899	368.293	157.31	

TABLE 3 Top-ranked serine covalent warheads from structure-based virtual screening against LexA, predicted with Schrödinger Covdock.

Compound ID	Molecular Weight	Structure	Docking score	Reaction
T002-1796	270.33		-6.22	Conjugate Addition to Alkyne (carbonyl activated)
T002-1859	274.30		-6.13	Conjugate Addition to Alkyne (carbonyl activated)
T002-1864	284.36		-5.98	Conjugate Addition to Alkyne (carbonyl activated)
M074-0516	244.30		-5.97	Nucleophilic Addition to a Double Bond
ZE09-1281	282.30		-5.87	Conjugate Addition to Alkyne (carbonyl activated)

(Continued)

TABLE 3 Continued

Compound ID	Molecular Weight	Structure	Docking score	Reaction
S644-0079	414.46		-5.78	Beta Lactam Addition
T002-1895	257.29		-5.71	Conjugate Addition to Alkyne (carbonyl activated)
0682-0046	252.27		-5.64	Nucleophilic Addition to a Double Bond
S642-0048	380.47		-5.64	Beta Lactam Addition
T002-2908	323.40		-5.64	Nucleophilic Addition to a Double Bond

oxygen of the acetamide. Thirdly, the terminal aromatic hydroxyl group on compound **1** acts as a hydrogen bond donor to the glutamic acid carboxyl group. This compound takes a conformation that is in line with the LexA CSR when the protease is in the C-form (Figure 6B). The hit rate of the virtual screen was 1.22%, the hit rate of the *in vitro* screen was 0.75% calculated according to the methods outlined by Zhu et al. (Zhu et al., 2013). In cases such as this when a novel scaffold is identified, a low hit rate is considered preferable to a high one (Sotriffer, 2011).

We did not find any  $\beta$ -turn mimetics from the ChemDiv  $\beta$ -turn mimetic library that inhibited the RecA-mediated cleavage of LexA. While some demonstration mild inhibition of LexA autoproteolysis under alkaline conditions, when tested with RecA they did not

exhibit the same inhibitory effect. An analysis of the  $\beta$ -turn mimetics conformations reveals that most of them do not take the same tight hairpin turn that GSK-C1 or the CSR  $\beta$ -turn does (Figures 4, S2). In the top 10 scoring  $\beta$ -turn mimetics from the virtual screen, we only see one that takes a hairpin conformation (Figures 4D, S2I) close to that of the CSR  $\beta$ -turn or the conformation that GSK-C1 takes (Figure 4C). The compound ranked at 9 in Table 2 has a distance of 4.193 Å between the terminal carbons of the pyridine and aromatic rings at each end, and 5.752 Å between the carbons at the para positions. This is close to the 5.405 Å between the  $\beta$ -turn *i* and *i*+3  $\alpha$  carbons, and the 5.603 Å at the narrowest point of GSK-C1. This compound bound in the reverse position, as the central methylated double heterocycle would

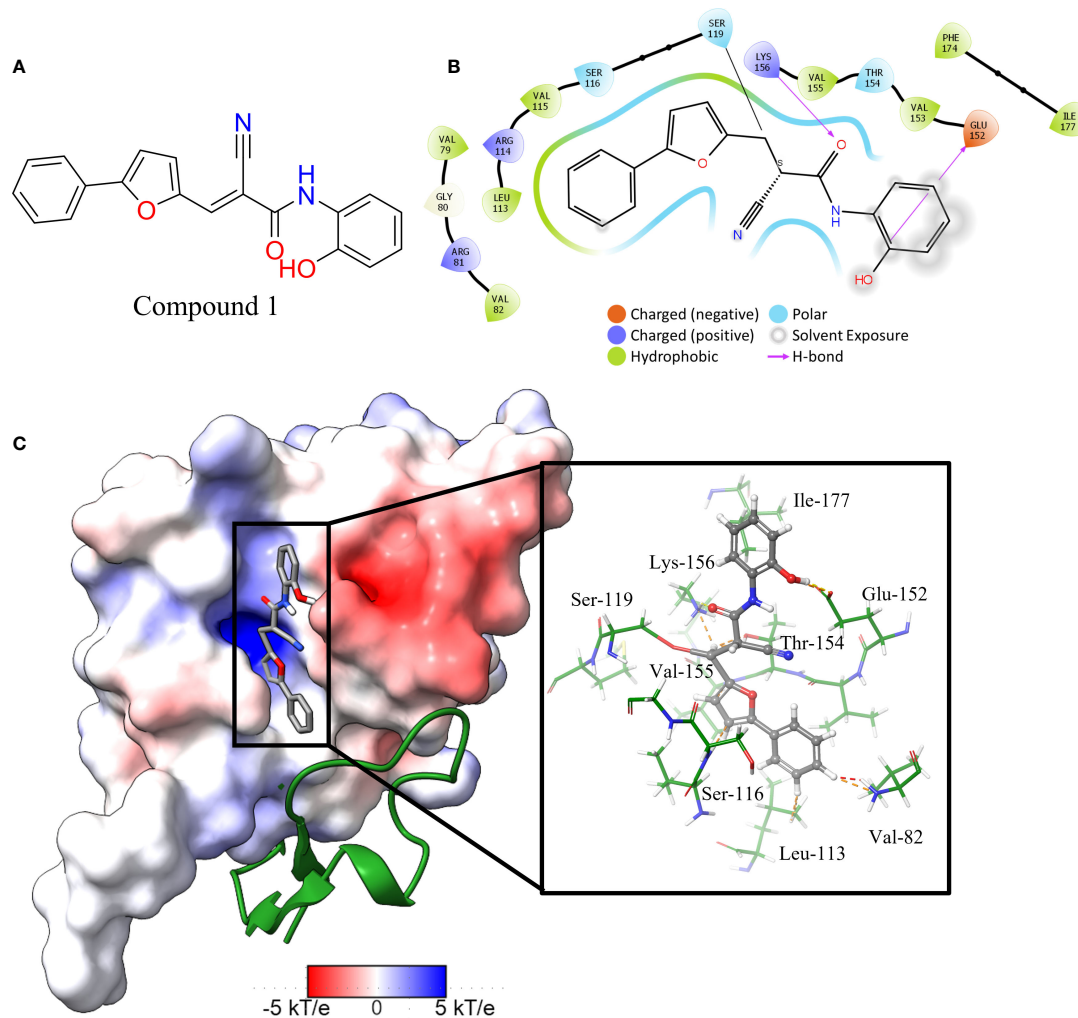


FIGURE 5

Interaction profile of compound 1. (A) 2D structure of compound 1. (B) 2D representation of the amino acid residues directly interacting with the compound. Residue color is based on the type, grey atom background is the solvent-accessible surface area. (C) The full LexA CTD with the bound compound and the same electrostatic surface as in Figure 3, with the DelPhi Webserver generated electrostatic surface. The ribbon also denotes the CSR of LexA. The insert shows the 3-D orientation of the molecule with the surrounding interacting residues.

have larger steric clashes than those of GSK-C1. GSK-C1 binds in the opposite direction in a manner closer to the CSR  $\beta$ -turn (Figure S2K).

### 3.5 Pharmacophore of top hit

Exploring the pharmacophore of compound 1 reveals its similarities to previous hit compounds. Using Cresset's FieldTemplater software in Flare v6.0 (Cheeseright et al., 2006; Kuhn et al., 2020), we developed a pharmacophore of these active compounds. In Figure 6A, the major electropositive and electronegative fields of the inhibitors overlap or are close in position. The same can be observed in the overlapping aromatic rings. Despite the new compound being a covalent inhibitor, it was revealed to have a similarity of 0.768 to the other three compounds, combining the field (electrostatic and hydrostatic) similarity and the shape similarity of the molecules. The similarity to previous

inhibitors of LexA cleavage further supports the non-covalent interactions that compound 1 has with the catalytic site of LexA.

### 3.6 *In vitro* inhibitor cleavage profile

To understand how compound 1 inhibits LexA cleavage over time, a series of RecA-mediated cleavage reactions were conducted. Between 0 and 25 minutes, compound 1 demonstrated inhibition at a series of concentrations (Figure 7A, gels in Figure S3). Testing between 1 mM and 0.0625 mM concentrations, compound 1 demonstrated inhibitory activity at all these concentrations, with significantly higher activity at 0.5 mM and 1 mM of inhibitor. To compare the inhibition of compound 1 with the other covalent inhibitors of LexA cleavage we used the kinetic model described by Bellio et al. (Bellio et al., 2020) to determine dissociation constant  $K_d$ . LexA proteolysis behaves in a non-Michaelian manner as it is unimolecular, and the protein is consumed during the reaction. As



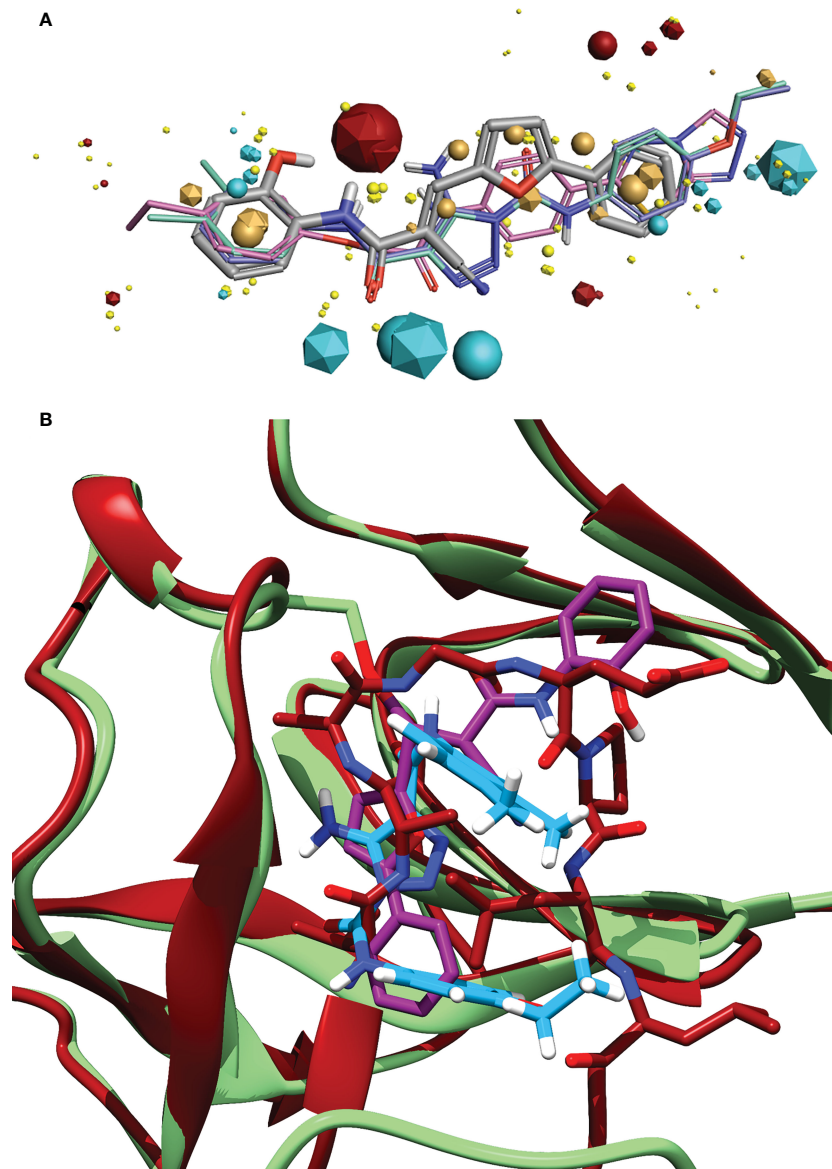


FIGURE 6

(A) Alignment of the identified compound to three previously identified inhibitors, showing the similarity of features between the ligands. The key features are represented by the spheres (Compound 1) and icosahedrons (previous inhibitors). Compound 1 is denoted by the grey carbons, and thick bonds. The previous inhibitors GSK-D1 (pink), GSK-C1 (lilac) and the lead from Selwood et al. (Selwood et al., 2018) are represented by thin lines. Red features are electropositive regions, cyan are electronegative, tan are hydrophobicity fields and yellow van der Waals fields. The size of the field corresponds to the size of the effect. Image generated using Flare™ from Cresset®. (B) An alignment of the C-form of LexA (red) with GSK-C1 (blue) and compound 1 (purple) bound to the NC-form of LexA (green). This shows the similarity of these compound conformations to the β-turn of the C-form.

RecA theoretically binds in a 1:1 ratio, as does the inhibitor, we assumed that the proteolysis reaction could be described as:



We assume that  $[\text{LexA}]$  is the concentration at any time during the reaction and  $[\text{LexA}]_0$  is the initial concentration of LexA. In the case of our experiments, these values were the band intensities, and the ratio was between the initial aliquot and then each subsequent aliquot. As the cleavage occurs as an exponential decay, the integrated rate law that applies to this equation is:

$$\frac{[\text{LexA}]}{[\text{LexA}]_0} = e^{-kt} \quad (2)$$

where  $k$  is the first order rate constant, and  $t$  is the time. We fit this equation to the LexA cleavage without inhibitor, to obtain the rate constant  $k_0$  (Figure 7). By calculating the  $k_i$  for each molar ratio ( $[\text{LexA}]/[\text{LexA}]_0$ ) the effectiveness of these inhibitors can then be described with the equation:

$$k_i = \frac{k_0}{1 + \frac{[I]:[\text{LexA}]}{\Phi}} \quad (3)$$

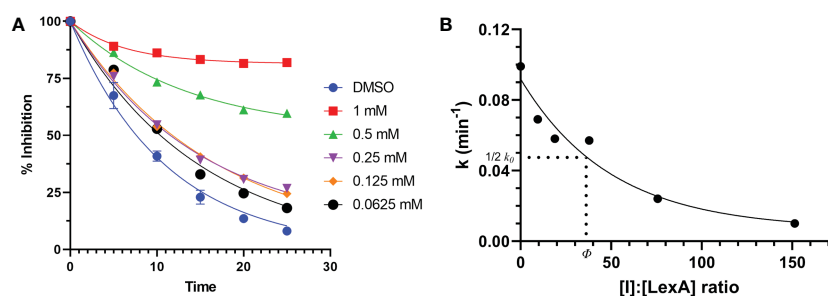


FIGURE 7

Time course of RecA-mediated LexA proteolysis in the presence of different concentrations of compound 1 (A). Example gels are in Supplementary Material Figure S4. This was used to derive values of  $k$  for each concentration. The second graph (B) plots the values of  $k$  derived from graph (A) as a function of the [I]:[LexA] ratio. The value of  $\phi$  is the ratio that is half of the rate constant  $k_0$ .

where [I] is the inhibitor concentration and  $\phi$  is the effectiveness at half of the first order rate constant ( $k_0$ ). Plotting the  $k_i$  values against the molar ratios, it is possible to determine how effective the inhibitor is at inhibiting LexA cleavage (Figures 7, 7B). In the case of compound 1, the effectiveness was determined to be 43.422, which equates to a  $K_d$  of 286.36  $\mu$ M – significantly lower than those of the boronic acid compounds published by Bellio et al. (Bellio et al., 2020).

### 3.7 Comparison of compound 1 binding pocket and related proteins

An analysis of the amino acids interacting with compound 1 from the docking reveals the residues that stabilise the compound in the binding pocket (Figure 5), we see the Lys-156 forming hydrogen bond with the oxygen of the acetamide group. The interaction diagram further depicts the residues that stabilise compound 1 in the pocket (Figure 5B) and the orientation of the compound in the hydrophobic pocket (Figure 5C).

While we determined that compound 1 bound to LexA *in vitro*, it was of interest to investigate if it potentially would bind to structurally similar proteins in other species. We investigated *B. subtilis* DinR, *E. coli* UmuD, *S. typhimurium* UmuD, and SetR<sub>ICE391</sub> as they share structural homology with LexA. A multiple sequence alignment showed that not only are Ala-84, Glu-85, Ser-119, and Lys-156 conserved (Figure S5), but other residues in the catalytic cleft are as well, an expected occurrence due to the retention of function by these proteins (Burckhardt et al., 1988; Haijema et al., 1996; Gonzalez et al., 2019). Using ENDScript 2.0 (Robert and Gouet, 2014), residues within 3.2 Å and 3.2–5 Å of the compound were evaluated (Figure S5). Several of these residues, particularly Glu-152 – Lys-156 are mildly conserved across species.

## 4 Discussion

The goal of this study was to continue the search for novel inhibitors of the SOS response in *E. coli* by inhibiting the transcriptional repressor LexA. We approached this through a targeted campaign combining *in silico* and *in vitro* techniques. In

this approach, we hypothesized a binary approach searching  $\beta$ -turn peptidomimetics and covalent compound libraries for a molecule that binds to the hydrophobic cleft of LexA and prevent the proteolysis of the protein. The cleavage of this dimer is regulated by the Ser-119 in the active site, which in the NC conformation is in a catalytic dyad with Lys-156. The formation of the transient tetrahedral with Ala-84 and Gly-85 and subsequent hydrolysis of the amide bond regulates the cleavage rate.

Our workflow resulted in the discovery of one compound – (2E)-2-cyano-N-(2-hydroxyphenyl)-3-(5-phenyl-2-furyl) acrylamide – that exhibited inhibitory activity against LexA. This compound, while not as effective as the non-covalent inhibitor that has been published by Selwood et al. (Selwood et al., 2018), further demonstrates the possibility of using covalent inhibitors against RecA-mediated LexA cleavage. The resulting compound shares some similarities, such as the aromatic end-groups and the presence of acetamides in the chains. Using SwissADME (Daina et al., 2017), the pharmacokinetic properties of compound 1 were estimated. Based on the predicted WLOGP and TPSA, the molecule would be absorbed into the GI tract (Daina and Zoete, 2016). Optimization of the compound would seek to improve the pharmacokinetic profile and the inhibitory activity.

We reasoned that the previous 1,2,3-triazole inhibitors (Mo et al., 2018; Selwood et al., 2018) acted as  $\beta$ -turn mimetics. This was supported by the recent paper by Jaramillo et al. (Jaramillo et al., 2022). When comparing the docked structure of GSK-C1 to the CSR turn we determined that it appeared to take a  $\beta$ -turn-like conformation, but in a different orientation to that of the CSR, instead interacting with residues on the CSR (Figure 6). While the current lead inhibitors mimic  $\beta$ -turns, our *in silico* screen did not result in any  $\beta$ -turn mimetics that were active in RecA-mediated LexA proteolysis. The limited library selection may have caused this, as the mimetics copied wider  $\beta$ -turns than the LexA CSR; a greater range of protein mimetics and an increased scaffold diversity may have resulted in an improved outcome.

Covalent docking techniques have only recently emerged. Molecular modelling programs are still in the process of implementing tools that facilitate this type of docking. Subsequently, the scoring functions of these programs are still being optimized, and each program takes a different approach to how the docking is done. Instances such as ours are not uncommon

- where the lead compounds after a covalent screening campaign are not necessarily the compounds that scored highest in the virtual screen (Shen et al., 2022).

Covalent inhibitors require two main features to be effective. The first is the need for a reactive warhead on the molecule that reacts with the catalytic residue. In the case of compound **1**, there are two electrophilic groups – the alkene and the nitrile. CovDock predicted that the alkene group in the middle of the compound, activated by the nitrile group, is how the compound binds to the catalytic Ser-119. While this is the most likely mechanism, the nitrile group on the compound might also be directly reacting with the serine. The second key feature are the functional groups that denote the non-covalent interactions with the binding pocket. These interactions both position the compound to facilitate the covalent binding, and they also stabilize the molecule in the binding pocket after the fact, slowing or preventing a reversible reaction. Based on our docking, the binding of compound **1** to the LexA pocket is stabilized by the Val-82, Leu-113, Ser-116, Glu-152, Thr-154, Lys-156 and Ile-177 (Figure 5B), leaving space to develop the molecule to target interactions with other residues in the hydrophobic pocket. A larger scaffold would theoretically interact more strongly with residues in the binding pocket. When compared to the prior best covalent inhibitor with a  $K_d$  of 1.09 mM (Bellio et al., 2020), this compound has one 238.36  $\mu$ M. Molecular modelling shows that the orientation of compound **1** in the catalytic pocket lines up with *i* and *i*+2 residues of the CSR in the activated C-form (Figure 6).

Other members of the LexA superfamily have a low sequence homology (Figure S5). Despite this, they have a highly conserved structure, and serve closely related roles in different species. The residues interacting with compound **1** (Figures 5, S6) are conserved across several of the other proteins of the superfamily which suggests that the molecule may have a similar antagonistic effect. Testing these compounds with proteins in the LexA superfamily to determine if it could be applied as a broad-spectrum treatment would be another step in the further development of this compound but was outside the scope of this investigation.

Future development of compound **1** needs to address the solubility in aqueous solutions. Presently, it has a relatively poor solubility in water, with precipitate observable in 0.5 mM concentrations. Rational modification of the molecule would require improving interactions with the other amino-acid residues in the binding pocket to increase target specificity and affinity, improve the bioavailability of the compound, and improve the aqueous solubility. Importantly, it would need to be determined whether compound **1** is able to permeate the bacterial cell wall, and if not, then what modifications would facilitate such movements. To achieve this, *in vivo* assays testing the compound with a bacterial model is necessary.

The major limitation of this investigation is the lack of studies confirming and improving our understanding of the compound activity; extensive mass spectrometry to show the covalent bond formation, cell-based SOS reporter assays (Selwood et al., 2018) or filamentation assays (Bellio et al., 2020). While these would further confirm binding is occurring it would be more appropriate to deal with the solubility issue and improve the binding first. Despite these caveats, we can make a reasonable assumption that the covalent reaction is indeed occurring due to the catalytic dyad within the

catalytic pocket. Ser-119 is the most reactive serine on the protein, as the  $\beta$ -hydroxy group of the serine is polarized due to the presence of the Lys-156 thereby increasing the nucleophilicity of the residue (Bellio et al., 2020).

Where previous papers on LexA kinetics have investigated the kinetic relationship between RecA concentrations and LexA cleavage rates, only one study (Bellio et al., 2020) has defined an approach to kinetically studying the effectiveness of inhibitors against LexA. We were able to adapt this to our approach when defining how effective a compound is at inhibiting LexA cleavage. Moving forward, this robust method is well suited to quantitatively comparing inhibitor effectiveness.

## 5 Conclusion

This work is the first binary approach to finding novel LexA inhibitors – investigating both  $\beta$ -turn mimetics and covalent warheads. The combined *in silico* and *in vitro* workflow based on rational library selection eliminated the need to physically test millions of compounds to identify novel scaffolds against the LexA transcriptional repressor. In studying the  $\beta$ -turn of the CSR, we determined that  $\beta$ -turn mimetics need to take conformations close to that of the protein's native  $\beta$ -turn, with limited bulky functional groups so that the compound can form a narrow turn. This is why none of the  $\beta$ -turns in the selected library inhibited the RecA-mediated cleavage of LexA. A previously unidentified covalent scaffold that inhibits RecA-mediated LexA cleavage was identified. This scaffold binds the catalytic Ser-119 *via* a different mechanism compared to the boronic acids published by Bellio et al. (Bellio et al., 2020) and does so with a stronger effect. Further optimization of this scaffold is required, to improve solubility and increase non-covalent interactions within the binding pocket. While molecular modelling indicates that the novel compound forms a covalent bond with the catalytic Ser-119, experimental confirmation of this reaction would strengthen these results. Assays that determine the potency of this compound on *E. coli* strains would determine if this compound antagonizes the bacterial SOS response.

## Data availability statement

The original contributions presented in the study are included in the article/Supplementary Material. Further inquiries can be directed to the corresponding authors.

## Author contributions

ZS, NG, RW, DR, and LC contributed to conceptualisation of the study and discussion of implications. ZS, NG conceptualised and carried out *in silico* experiments. ZS, RW, DR contributed to *in vitro* methodologies and performing the analysis. ZS and JM performed *in vitro* assays. ZS performed data analysis and prepared the manuscript. RW, JM, DR and NG provided advice and editing of the manuscript and analysis. All authors contributed to the article and approved the submitted version.

## Funding

This work was supported by funds from the NIH/NICHD Intramural Research Program to RW; and the Advance Queensland Industry Research Fellowship support Dr. NG and ZS.

## Acknowledgments

We would like to acknowledge QUT eResearch, Brisbane, Australia for the use of the Lyra HPC cluster. We would like to thank colleagues at the Cancer and Ageing Research Program for their constructive feedback and discussions, with particular thanks to Dr. Alexander Martyn for running QC tests on compounds, and Dr. David Marshall at the QUT Central Analytical Research Facility for the assistance and advice with trying to develop a screening protocol. We thank John W. Little (University of Arizona) for sharing the LexA overproducing plasmid, pJWL288 and Mike M. Cox (University of Wisconsin) for sharing the RecA overproducing plasmid, pAIR79. We would also like to thank BioSolveIT for the free license to SeeSAR during the Summer Challenge.

## References

- Ábrányi-Balogh, P., and Keserű, G. M. (2022). "Chapter 2 - Warheads for designing covalent inhibitors and chemical probes," in *Advances in chemical proteomics developments in organic chemistry*. Ed. Yao, (Elsevier), 47–73. doi: 10.1016/B978-0-12-821433-6.00007-6
- Ahn, J.-M., Kassees, K., Lee, T.-K., Manandhar, B., and Yousif, A. M. (2017). "6.03 - strategy and tactics for designing analogs: Biochemical characterization of the large molecules," in *Comprehensive medicinal chemistry III*. Eds. S. Chackalamannil, D. Rotella and S. E. Ward (Oxford: Elsevier), 66–115. doi: 10.1016/B978-0-12-409547-2.12413-8
- Amblard, F., Zhou, S., Liu, P., Yoon, J., Cox, B., Muzzarelli, K., et al. (2018). Synthesis and antiviral evaluation of novel peptidomimetics as norovirus protease inhibitors. *Bioorg. Med. Chem. Lett.* 28, 2165–2170. doi: 10.1016/j.bmcl.2018.05.012
- Aslam, B., Wang, W., Arshad, M. I., Khurshid, M., Muzammil, S., Rasool, M. H., et al. (2018). Antibiotic resistance: a rundown of a global crisis. *Infect. Drug Resist.* 11, 1645–1658. doi: 10.2147/IDR.S173867
- Bai, B., Belovodskiy, A., Hena, M., Kandadai, A. S., Joyce, M. A., Saffran, H. A., et al. (2022). Peptidomimetic  $\alpha$ -acyloxymethylketone warheads with six-membered lactam P1 glutamine mimic: SARS-CoV-2 3CL protease inhibition, coronavirus antiviral activity, and *in vitro* biological stability. *J. Med. Chem.* 65, 2905–2925. doi: 10.1021/acs.jmedchem.1c00616
- Bellio, P., Mancini, A., Di Pietro, L., Cracchiolo, S., Franceschini, N., Reale, S., et al. (2020). Inhibition of the transcriptional repressor LexA: Withstanding drug resistance by inhibiting the bacterial mechanisms of adaptation to antimicrobials. *Life Sci.* 241, 117116. doi: 10.1016/j.lfs.2019.117116
- Bender, B. J., Gahbauer, S., Luttens, A., Lyu, J., Webb, C. M., Stein, R. M., et al. (2021). A practical guide to large-scale docking. *Nat. Protoc.* 16, 4799–4832. doi: 10.1038/s41596-021-00597-z
- Berman, H. M., Westbrook, J., Feng, Z., Gilliland, G., Bhat, T. N., Weissig, H., et al. (2000). The protein data bank. *Nucleic Acids Res.* 28, 235–242. doi: 10.1093/nar/28.1.235
- Beuning, P., Simon, S., Zemla, A., Barsky, D., and Walker, G. (2006). A non-cleavable UmuD variant that acts as a UmuD' mimic. *J. Biol. Chem.* 281, 9633–9640. doi: 10.1074/jbc.M511101200
- BioSolveIT GmBH (2020). *SeeSAR version 10.1* (Sankt Augustin, Germany). Available at: [www.biosolveit.de/SeeSAR](http://www.biosolveit.de/SeeSAR).
- Biovia, D. S. (2019) *Discovery studio 2019 client*. Available at: <https://www.3dsbiovia.com/products/collaborative-science/biovia-discovery-studio/>.
- Burckhardt, S. E., Woodgate, R., Scheuermann, R. H., and Echols, H. (1988). UmuD mutagenesis protein of *Escherichia coli*: overproduction, purification, and cleavage by RecA. *Proc. Natl. Acad. Sci. U. S. A.* 85, 1811–1815. doi: 10.1073/pnas.85.6.1811
- Capasso, C., Nocentini, A., and Supuran, C. T. (2021). Protease inhibitors targeting the main protease and papain-like protease of coronaviruses. *Expert Opin. Ther. Pat.* 31, 309–324. doi: 10.1080/13543776.2021.1857726
- Cezairliyan, B. O., and Sauer, R. T. (2009). Control of *Pseudomonas aeruginosa* AlgW protease cleavage of MucA by peptide signals and MucB. *Mol. Microbiol.* 72, 368–379. doi: 10.1111/j.1365-2958.2009.06654.x
- Cheeseright, T., Mackey, M., Rose, S., and Vinter, A. (2006). Molecular field extrema as descriptors of biological activity: definition and validation. *J. Chem. Inf. Model.* 46, 665–676. doi: 10.1021/ci050357s
- ChemDiv. (2020). *Covalent inhibitors library*. Available at: <https://www.chemdiv.com/catalog/focused-and-targeted-libraries/covalent-inhibitors-library/> (Accessed February 7, 2020).
- ChemDiv. (2019). *Peptidomimetics of beta-turn motifs library*. Available at: <https://www.chemdiv.com/catalog/focused-and-targeted-libraries/peptidomimetics-of-beta-turn-motifs-library/> (Accessed September 1, 2019).
- Cirilo, A. D. (2022) *RamachanDraw: Ramachandran plotting tool*. Available at: <https://github.com/alxdrcirilo/RamachanDraw> (Accessed August 19, 2022).
- Cirz, R. T., Chin, J. K., Andes, D. R., de Crécy-Lagard, V., Craig, W. A., and Romesberg, F. E. (2005). Inhibition of mutation and combating the evolution of antibiotic resistance. *PLoS Biol.* 3, e176. doi: 10.1371/journal.pbio.0030176
- Cirz, R. T., Jones, M. B., Gingles, N. A., Minogue, T. D., Jarrahi, B., Peterson, S. N., et al. (2007). Complete and SOS-mediated response of *Staphylococcus aureus* to the antibiotic ciprofloxacin. *J. Bacteriol.* 189, 531–539. doi: 10.1128/JB.01464-06
- Cirz, R. T., O'Neill, B. M., Hammond, J. A., Head, S. R., and Romesberg, F. E. (2006). Defining the *Pseudomonas aeruginosa* SOS response and its role in the global response to the antibiotic ciprofloxacin. *J. Bacteriol.* 188, 7101–7110. doi: 10.1128/JB.00807-06
- Cox, M. M., McEntee, K., and Lehman, I. R. (1981). A simple and rapid procedure for the large scale purification of the RecA protein of *Escherichia coli*. *J. Biol. Chem.* 256, 4676–4678.
- Culyba, M. J., Mo, C. Y., and Kohli, R. M. (2015). Targets for combating the evolution of acquired antibiotic resistance. *Biochemistry* 54, 3573–3582. doi: 10.1021/acs.biochem.5b00109
- Daina, A., Michielin, O., and Zoete, V. (2017). SwissADME: a free web tool to evaluate pharmacokinetics, drug-likeness and medicinal chemistry friendliness of small molecules. *Sci. Rep.* 7, 42717. doi: 10.1038/srep42717
- Daina, A., and Zoete, V. (2016). A BOILED-egg to predict gastrointestinal absorption and brain penetration of small molecules. *ChemMedChem* 11, 1117–1121. doi: 10.1002/cmdc.201600182
- de Brevern, A. G. (2016). Extension of the classical classification of  $\beta$ -turns. *Sci. Rep.* 6, 33191. doi: 10.1038/srep33191

## Conflict of interest

The authors declare that the research was conducted in the absence of any commercial or financial relationships that could be construed as a potential conflict of interest.

## Publisher's note

All claims expressed in this article are solely those of the authors and do not necessarily represent those of their affiliated organizations, or those of the publisher, the editors and the reviewers. Any product that may be evaluated in this article, or claim that may be made by its manufacturer, is not guaranteed or endorsed by the publisher.

## Supplementary material

The Supplementary Material for this article can be found online at: <https://www.frontiersin.org/articles/10.3389/fcimb.2023.1051602/full#supplementary-material>



- Delre, P., Caporuscio, F., Saviano, M., and Mangiatordi, G. F. (2020). Repurposing known drugs as covalent and non-covalent inhibitors of the SARS-CoV-2 papain-like protease. *Front. Chem.* 8. doi: 10.3389/fchem.2020.594009
- dos Santos, C. B. R., Lobato, C. C., de Sousa, M. A. C., da Cruz Macêdo, W. J., and Carvalho, J. C. T. (2014). Molecular modeling: Origin, fundamental concepts and applications using structure-activity relationship and quantitative structure-activity relationship. *Rev. Theor. Sci.* 2, 91–115. doi: 10.1166/rits.2014.1016
- Fernández de Henestrosa, A. R., Ogi, T., Aoyagi, S., Chafin, D., Hayes, J. J., Ohmori, H., et al. (2000). Identification of additional genes belonging to the LexA regulon in *Escherichia coli*. *Mol. Microbiol.* 35, 1560–1572. doi: 10.1046/j.1365-2958.2000.01826.x
- Founou, R. C., Founou, L. L., and Essack, S. Y. (2017). Clinical and economic impact of antibiotic resistance in developing countries: A systematic review and meta-analysis. *PLoS One* 12, e0189621. doi: 10.1371/journal.pone.0189621
- Gao, M., Moumbock, A. F. A., Qaseem, A., Xu, Q., and Günther, S. (2022). CovPDB: a high-resolution coverage of the covalent protein-ligand interactome. *Nucleic Acids Res.* 50, D445–D450. doi: 10.1093/nar/gkab868
- Gimble, F. S., and Sauer, R. T. (1985). Mutations in bacteriophage  $\lambda$  repressor that prevent RecA-mediated cleavage. *J. Bacteriol.* 162, 147–154. doi: 10.1128/jb.162.1.147-154.1985
- Gonzalez, M., Huston, D., McLenigan, M. P., McDonald, J. P., Garcia, A. M., Borden, K. S., et al. (2019). SetR<sub>ICE391</sub>, a negative transcriptional regulator of the integrating conjugative element 391 mutagenic response. *DNA Repair* 73, 99–109. doi: 10.1016/j.dnarep.2018.11.007
- Grant, B. J., Rodrigues, A. P. C., ElSawy, K. M., McCammon, J. A., and Caves, L. S. D. (2006). Bio3d: an r package for the comparative analysis of protein structures. *Bioinformatics* 22, 2695–2696. doi: 10.1093/bioinformatics/btl461
- Haijema, B. J., van Sinderen, D., Winterling, K., Kooistra, J., Venema, G., and Hamoen, L. W. (1996). Regulated expression of the *dinR* and *recA* genes during competence development and SOS induction in *Bacillus subtilis*. *Mol. Microbiol.* 22, 75–85. doi: 10.1111/j.1365-2958.1996.tb02657.x
- Hutchinson, E. G., and Thornton, J. M. (1994). A revised set of potentials for  $\beta$ -turn formation in proteins. *Protein Sci.* 3, 2207–2216. doi: 10.1002/pro.5560031206
- Jaramillo, A. V. C., Cory, M. B., Li, A., Kohli, R. M., and Wuest, W. M. (2022). Exploration of inhibitors of the bacterial LexA repressor-protease. *Bioorg. Med. Chem. Lett.* 65, 128702. doi: 10.1016/j.bmcl.2022.128702
- Jurrus, E., Engel, D., Star, K., Monson, K., Brandi, J., Felberg, L. E., et al. (2018). Improvements to the APBS biomolecular solvation software suite. *Protein Sci.* 27, 112–128. doi: 10.1002/pro.3280
- Karata, K., Vaisman, A., Goodman, M. F., and Woodgate, R. (2012). Simple and efficient purification of *Escherichia coli* DNA polymerase V: cofactor requirements for optimal activity and processivity *in vitro*. *DNA Repair* 11, 431–440. doi: 10.1016/j.dnarep.2012.01.012
- Kato, T., and Shinoura, Y. (1977). Isolation and characterization of mutants of *Escherichia coli* deficient in induction of mutations by ultraviolet light. *Mol. Genet. Genomics* 156, 121–131. doi: 10.1007/bf00283484
- Kim, H.-R., Tagirasa, R., and Yoo, E. (2021). Covalent small molecule immunomodulators targeting the protease active site. *J. Med. Chem.* 64, 5291–5322. doi: 10.1021/acs.jmedchem.1c00172
- Kuhn, M., Firth-Clark, S., Tosco, P., Mey, A. S. J. S., Mackey, M., and Michel, J. (2020). Assessment of binding affinity *via* alchemical free-energy calculations. *J. Chem. Inf. Model.* 60, 3120–3130. doi: 10.1021/acs.jcim.0c00165
- Kumalo, H. M., Bhakat, S., and Soliman, M. E. S. (2015). Theory and applications of covalent docking in drug discovery: Merits and pitfalls. *Molecules* 20, 1984–2000. doi: 10.3390/molecules20021984
- Kyte, J., and Doolittle, R. F. (1982). A simple method for displaying the hydropathic character of a protein. *J. Mol. Biol.* 157, 105–132. doi: 10.1016/0022-2836(82)90515-0
- Li, B., Smith, P., Horvath, D. J., Romesberg, F. E., and Justice, S. S. (2010). SOS Regulatory elements are essential for UPEC pathogenesis. *Microbes Infect.* 12, 662–668. doi: 10.1016/j.micinf.2010.04.009
- Lin, L. L., and Little, J. W. (1988). Isolation and characterization of noncleavable (Ind<sup>r</sup>) mutants of the LexA repressor of *Escherichia coli* K-12. *J. Bacteriol.* 170, 2163–2173. doi: 10.1128/jb.170.5.2163-2173.1988
- Little, J. W. (1984). Autodigestion of LexA and phage  $\lambda$  repressors. *Proc. Natl. Acad. Sci. U. S. A.* 81, 1375–1379. doi: 10.1073/pnas.81.5.1375
- Luo, Y., Pfuetzner, R. A., Mosimann, S., Paetzel, M., Frey, E. A., Cherney, M., et al. (2001). Crystal structure of LexA: A conformational switch for regulation of self-cleavage. *Cell* 106, 585–594. doi: 10.1016/S0092-8674(01)00479-2
- Lusetti, S. L., Wood, E. A., Fleming, C. D., Modica, M. J., Korth, J., Abbott, L., et al. (2003). C-terminal deletions of the *Escherichia coli* RecA protein. characterization *in vivo* and *in vitro* effects. *J. Biol. Chem.* 278, 16372–16380. doi: 10.1074/jbc.M212917200
- Martin, J. S., MacKenzie, C. J., Fletcher, D., and Gilbert, I. H. (2019). Characterising covalent warhead reactivity. *Bioorg. Med. Chem.* 27, 2066–2074. doi: 10.1016/j.bmc.2019.04.002
- McDonald, J. P., Maury, E. E., Levine, A. S., and Woodgate, R. (1998). Regulation of UmuD cleavage: role of the amino-terminal tail. *J. Mol. Biol.* 282, 721–730. doi: 10.1006/jmbi.1998.2044
- McDonald, J. P., Peat, T. S., Levine, A. S., and Woodgate, R. (1999). Intermolecular cleavage by UmuD-like enzymes: identification of residues required for cleavage and substrate specificity. *J. Mol. Biol.* 285, 2199–2209. doi: 10.1006/jmbi.1998.2433
- Mertens, N., Remaut, E., and Fiers, W. (1995). Tight transcriptional control mechanism ensures stable high-level expression from T7 promoter-based expression plasmids. *Biotechnol. Nat. Publ. Co.* 13, 175–179. doi: 10.1038/nbt0295-175
- Mo, C. Y., Birdwell, L. D., and Kohli, R. M. (2014). Specificity determinants for autoproteolysis of LexA, a key regulator of bacterial SOS mutagenesis. *Biochemistry* 53, 3158–3168. doi: 10.1021/bi500026e
- Mo, C. Y., Culyba, M. J., Selwood, T., Kubiak, J. M., Hostettler, Z. M., Jurewicz, A. J., et al. (2018). Inhibitors of LexA autoproteolysis and the bacterial SOS response discovered by an academic-industry partnership. *ACS Infect. Dis.* 4, 349–359. doi: 10.1021/acsinfecdis.7b00122
- Mo, C. Y., Manning, S. A., Roggiani, M., Culyba, M. J., Samuels, A. N., Sniegowski, P. D., et al. (2016). Systematically altering bacterial SOS activity under stress reveals therapeutic strategies for potentiating antibiotics. *mSphere* 1, e00163–e00116. doi: 10.1128/mSphere.00163-16
- Mohana-Borges, R., Pacheco, A. B. F., Sousa, F. J. R., Foguel, D., Almeida, D. F., and Silva, J. L. (2000). LexA repressor forms stable dimers in solution: the role of specific DNA in tightening protein-protein interactions. *J. Biol. Chem.* 275, 4708–4712. doi: 10.1074/jbc.275.7.4708
- Munita, J. M., and Arias, C. A. (2016). Mechanisms of antibiotic resistance. *Microbiol. Spectr.* 4:487–511. doi: 10.1128/microbiolspec.VMBF-0016-2015
- Norais, C. A., Chittani-Pattu, S., Wood, E. A., Inman, R. B., and Cox, M. M. (2009). DdrB protein, an alternative *Deinococcus radiodurans* SSB induced by ionizing radiation. *J. Biol. Chem.* 284, 21402–21411. doi: 10.1074/jbc.M109.010454
- Ojha, D., Jaszczur, M. M., Sikand, A., McDonald, J. P., Robinson, A., van Oijen, A. M., et al. (2022). Host cell RecA activates a mobile element-encoded mutagenic DNA polymerase. *Nucleic Acids Res.* 50, 6854–6869. doi: 10.1093/nar/gkac515
- Olsson, M. H. M., Søndergaard, C. R., Rostkowski, M., and Jensen, J. H. (2011). PROPKA3: Consistent treatment of internal and surface residues in empirical pKa predictions. *J. Chem. Theory Comput.* 7, 525–537. doi: 10.1021/ct100578z
- Pagadala, N. S., Syed, K., and Tuszyński, J. (2017). Software for molecular docking: a review. *Biophys. Rev.* 9, 91–102. doi: 10.1007/s12551-016-0247-1
- Petersen, E. F., Goddard, T. D., Huang, C. C., Couch, G. S., Greenblatt, D. M., Meng, E. C., et al. (2004). UCSF chimera—a visualization system for exploratory research and analysis. *J. Comput. Chem.* 25, 1605–1612. doi: 10.1002/jcc.20084
- Polgár, L. (2013). “Catalytic mechanisms of serine and threonine peptidases,” in *Handbook of proteolytic enzymes*. Eds. G. Salvesen and N. D. Rawlings (Elsevier Science & Technology), 2524–2533. doi: 10.1016/B978-0-12-382219-2.00560-3
- Radman, M. (1974). “Phenomenology of an inducible mutagenic DNA repair pathway in *Escherichia coli*: SOS repair hypothesis,” in *Molecular and environmental aspects of mutagenesis basic life series*. Eds. P. C. Hanawalt and R. B. Setlow (United States: Charles C Thomas Publisher).
- Rarey, M., Kramer, B., Lengauer, T., and Klebe, G. (1996). A fast flexible docking method using an incremental construction algorithm. *J. Mol. Biol.* 261, 470–489. doi: 10.1006/jmbi.1996.0477
- R Core Team (2022) R: A language and environment for statistical computing. Available at: <https://www.R-project.org/> (Accessed November 22, 2022).
- Reulecke, I., Lange, G., Albrecht, J., Klein, R., and Rarey, M. (2008). Towards an integrated description of hydrogen bonding and dehydration: Decreasing false positives in virtual screening with the HYDE scoring function. *ChemMedChem* 3, 885–897. doi: 10.1002/cmdc.200700319
- Robert, X., and Gouet, P. (2014). Deciphering key features in protein structures with the new ENDscript server. *Nucleic Acids Res.* 42, W320–W324. doi: 10.1093/nar/gku316
- Roland, K. L., Smith, M. H., Rupley, J. A., and Little, J. W. (1992). *In vitro* analysis of mutant LexA proteins with an increased rate of specific cleavage. *J. Mol. Biol.* 228, 395–408. doi: 10.1016/0022-2836(92)90829-9
- Roos, K., Wu, C., Damm, W., Reboul, M., Stevenson, J. M., Lu, C., et al. (2019). OPLS3e: Extending force field coverage for drug-like small molecules. *J. Chem. Theory Comput.* 15, 1863–1874. doi: 10.1021/acs.jctc.8b01026
- Søndergaard, C. R., Olsson, M. H. M., Rostkowski, M., and Jensen, J. H. (2011). Improved treatment of ligands and coupling effects in empirical calculation and rationalization of pKa values. *J. Chem. Theory Comput.* 7, 2284–2295. doi: 10.1021/ct200133y
- Sarkar, S., Witham, S., Zhang, J., Zhenirovskyy, M., Rocchia, W., and Alexov, E. (2013). DelPhi web server: A comprehensive online suite for electrostatic calculations of biological macromolecules and their complexes. *Commun. Comput. Phys.* 13, 269–284. doi: 10.4208/cicp.300611.201011s
- Sampitak, P., Mujumdar, P., Taylor, P., Cross, M., Coster, M. J., Gorse, A.-D., et al. (2015). Panel docking of small-molecule libraries — prospects to improve efficiency of lead compound discovery. *Biotechnol. Adv.* 33, 941–947. doi: 10.1016/j.biotechadv.2015.05.006
- Scarpino, A., Ferenczy, G. G., and Keserü, G. M. (2018). Comparative evaluation of covalent docking tools. *J. Chem. Inf. Model.* 58, 1441–1458. doi: 10.1021/acs.jcim.8b00228
- Schneider, N., Lange, G., Hindle, S., Klein, R., and Rarey, M. (2013). A consistent description of hydrogen bond and dehydration energies in protein-ligand complexes: methods behind the HYDE scoring function. *J. Comput. Aided Mol. Des.* 27, 15–29. doi: 10.1007/s10822-012-9626-2
- Schrodinger, L. (2020). *LigPrep release 2020-2* (New York: Schrödinger LLC). Available at: <https://www.schrodinger.com/products/ligprep>.



- Schrödinger, (2019) *Maestro*. Available at: <https://www.schrodinger.com/>
- Selwood, T., Larsen, B. J., Mo, C. Y., Culyba, M. J., Hostetler, Z. M., Kohli, R. M., et al. (2018). Advancement of the 5-amino-1-(carbamoylmethyl)-1H-1,2,3-triazole-4-carboxamide scaffold to disarm the bacterial SOS response. *Front. Microbiol.* 9. doi: 10.3389/fmicb.2018.02961
- Shen, Z., Zhuang, W., Li, K., Guo, Y., Qu, B., Chen, S., et al. (2022). Identification of novel covalent XPO1 inhibitors based on a hybrid virtual screening strategy. *Molecules* 27, 2543. doi: 10.3390/molecules27082543
- Shepley, D. P., and Little, J. W. (1996). Mutant LexA proteins with specific defects in autodigestion. *Proc. Natl. Acad. Sci.* 93, 11528–11533. doi: 10.1073/pnas.93.21.11528
- Sitkoff, D., Sharp, K. A., and Honig, B. (1994). Accurate calculation of hydration free energies using macroscopic solvent models. *J. Phys. Chem.* 98, 1978–1988. doi: 10.1021/j100058a043
- Slilaty, S. N., and Little, J. W. (1987). Lysine-156 and serine-119 are required for LexA repressor cleavage: a possible mechanism. *Proc. Natl. Acad. Sci.* 84, 3987–3991. doi: 10.1073/pnas.84.12.3987
- Slilaty, S. N., Rupley, J. A., and Little, J. W. (1986). Intramolecular cleavage of *lexA* and phage  $\lambda$  repressors: dependence of kinetics on repressor concentration, pH, temperature, and solvent. *Biochemistry* 25, 6866–6875. doi: 10.1021/bi00370a020
- Smith, P. A., and Romesberg, F. E. (2007). Combating bacteria and drug resistance by inhibiting mechanisms of persistence and adaptation. *Nat. Chem. Biol.* 3, 549–556. doi: 10.1038/nchembio.2007.27
- Sottriffer, C. (2011). *Virtual screening: Principles, challenges, and practical guidelines* (John Wiley & Sons). doi: 10.1002/9783527633326.ch2
- Tang, C. L., Alexov, E., Pyle, A. M., and Honig, B. (2007). Calculation of pK<sub>a</sub>s in RNA: On the structural origins and functional roles of protonated nucleotides. *J. Mol. Biol.* 366, 1475–1496. doi: 10.1016/j.jmb.2006.12.001
- Toledo Warshaviak, D., Golan, G., Borrelli, K. W., Zhu, K., and Kalid, O. (2014). Structure-based virtual screening approach for discovery of covalently bound ligands. *J. Chem. Inf. Model.* 54, 1941–1950. doi: 10.1021/ci500175r
- Venkatachalam, C. M. (1968). Stereochemical criteria for polypeptides and proteins. v. conformation of a system of three linked peptide units. *Biopolymers* 6, 1425–1436. doi: 10.1002/bip.1968.360061006
- Watts, K. S., Dalal, P., Murphy, R. B., Sherman, W., Friesner, R. A., and Shelley, J. C. (2010). ConfGen: A conformational search method for efficient generation of bioactive conformers. *J. Chem. Inf. Model.* 50, 534–546. doi: 10.1021/ci100015j
- Winterling, K. W., Levine, A. S., Yasbin, R. E., and Woodgate, R. (1997). Characterization of DinR, the *Bacillus subtilis* SOS repressor. *J. Bacteriol.* 179, 1698–1703. doi: 10.1128/jb.179.5.1698-1703.1997
- Zhang, R., Stahr, M. C., and Kennedy, M. A. (2022). Introduction of a new scheme for classifying  $\beta$ -turns in protein structures. *Proteins Struct. Funct. Bioinforma.* 90, 110–122. doi: 10.1002/prot.26190
- Zhu, T., Cao, S., Su, P.-C., Patel, R., Shah, D., Chokshi, H. B., et al. (2013). Hit identification and optimization in virtual screening: Practical recommendations based upon a critical literature analysis. *J. Chem.* 56, 6560–6572. doi: 10.1021/jm301916b
- Zhu, K., Borrelli, K. W., Greenwood, J. R., Day, T., Abel, R., Farid, R. S., et al. (2014). Docking covalent inhibitors: A parameter free approach to pose prediction and scoring. *J. Chem. Inf. Model.* 54, 1932–1940. doi: 10.1021/ci500118s



## OPEN ACCESS

## EDITED BY

Parth Sarthi Sen Gupta,  
Indian Institute of Science Education and  
Research Berhampur (IISER), India

## REVIEWED BY

Kaixia Mi,  
Institute of Microbiology, Chinese  
Academy of Sciences, China  
José Hélio Costa,  
Federal University of Ceara, Brazil

## \*CORRESPONDENCE

Suvash Chandra Ojha  
✉ suvash\_ojha@swmu.edu.cn  
Mohibullah Shah  
✉ mohib@bzu.edu.pk  
mohibusb@gmail.com

<sup>†</sup>These authors have contributed  
equally to this work and share  
first authorship

## SPECIALTY SECTION

This article was submitted to  
Clinical Microbiology,  
a section of the journal  
Frontiers in Cellular and  
Infection Microbiology

RECEIVED 11 August 2022

ACCEPTED 02 March 2023

PUBLISHED 24 March 2023

## CITATION

Qasim A, Jaan S, Wara TU, Shehroz M,  
Nishan U, Shams S, Shah M and Ojha SC  
(2023) Computer-aided genomic data  
analysis of drug-resistant *Neisseria*  
*gonorrhoeae* for the Identification of  
alternative therapeutic targets.  
*Front. Cell. Infect. Microbiol.* 13:1017315.  
doi: 10.3389/fcimb.2023.1017315

## COPYRIGHT

© 2023 Qasim, Jaan, Wara, Shehroz, Nishan,  
Shams, Shah and Ojha. This is an open-  
access article distributed under the terms of  
the [Creative Commons Attribution License](https://creativecommons.org/licenses/by/4.0/)  
(CC BY). The use, distribution or  
reproduction in other forums is permitted,  
provided the original author(s) and the  
copyright owner(s) are credited and that  
the original publication in this journal is  
cited, in accordance with accepted  
academic practice. No use, distribution or  
reproduction is permitted which does not  
comply with these terms.

# Computer-aided genomic data analysis of drug-resistant *Neisseria gonorrhoeae* for the Identification of alternative therapeutic targets

Aqsa Qasim<sup>1†</sup>, Samavia Jaan<sup>1</sup>, Tehreem Ul Wara<sup>1</sup>,  
Muhammad Shehroz<sup>2</sup>, Umar Nishan<sup>3</sup>, Sulaiman Shams<sup>4</sup>,  
Mohibullah Shah<sup>1\*†</sup> and Suvash Chandra Ojha<sup>5\*</sup>

<sup>1</sup>Department of Biochemistry, Bahauddin Zakariya University, Multan, Pakistan, <sup>2</sup>Department of Bioinformatics, Kohsar University, Murree, Pakistan, <sup>3</sup>Department of Chemistry, Kohat University of Science & Technology, Kohat, Pakistan, <sup>4</sup>Department of Biochemistry, Abdul Wali Khan University Mardan, Mardan, Pakistan, <sup>5</sup>Department of Infectious Diseases, The Affiliated Hospital of Southwest Medical University, Luzhou, China

*Neisseria gonorrhoeae* is an emerging multidrug resistance pathogen that causes sexually transmitted infections in men and women. The *N. gonorrhoeae* has demonstrated an emerging antimicrobial resistance against reported antibiotics, hence fetching the attention of researchers to address this problem. The present *in-silico* study aimed to find putative novel drug and vaccine targets against *N. gonorrhoeae* infection by the application of bioinformatics approaches. Core genes set of 69 *N. gonorrhoeae* strains was acquired from complete genome sequences. The essential and non-homologous metabolic pathway proteins of *N. gonorrhoeae* were identified. Moreover, different bioinformatics databases were used for the downstream analysis. The DrugBank database scanning identified 12 novel drug targets in the prioritized list. They were preferred as drug targets against this bacterium. A viable vaccine is unavailable so far against *N. gonorrhoeae* infection. In the current study, two outer-membrane proteins were prioritized as vaccine candidates *via* reverse vaccinology approach. The top lead B and T-cells overlapped epitopes were utilized to generate a chimeric vaccine construct combined with immune-modulating adjuvants, linkers, and PADRE sequences. The top ranked prioritized vaccine construct (V7) showed stable molecular interaction with human immune cell receptors as inferred during the molecular docking and MD simulation analyses. Considerable response for immune cells was interpreted by *in-silico* immune studies. Additional tentative validation is required to ensure the effectiveness of the prioritized vaccine construct against *N. gonorrhoeae* infection. The identified proteins can be used for further rational drug and vaccine designing to develop potential therapeutic entities against the multi-drug resistant *N. gonorrhoeae*.

## KEYWORDS

*Neisseria gonorrhoeae*, epitope, chimaric vaccine, novel drug target, multi-drug resistant

## Introduction

Gonorrhoeae is the second most reported sexually transmitted disease caused by the gram-negative, coffee bean-shaped intracellular bacterium, *Neisseria gonorrhoeae*. After chlamydia trachomatis, gonorrhoeae is the second most common sexually transmitted infection (STI) in the world (Jefferson et al., 2021). Unsafe sex practice is the most common cause of gonorrhoeae. If it remains untreated, it can lead to sterility, swelling, ectopic gestation, and maternal death (Yeshanew and Geremew, 2018). Urethral infection in men and the endocervix infection in women are the common causes of gonorrhoeae. This damage the columnar epithelium of the endocervix and cause pain during sexual contact, an aching feeling while urinating and abdominal vaginal emission (Sahile et al., 2020). Additionally, the infection enhances the chances of sexually transmitted diseases, including human immunodeficiency virus (HIV) (Sahile et al., 2020). Likewise, suppurative arthritis can also be caused by a disseminated gonococcal infection in both men and women (Bar-On et al., 1990).

The *N. gonorrhoeae* has posed a significant health threat to the world, specifically asymptomatic individuals. Due to inefficient therapies and the asymptomatic nature of the disease, the number of untreated and new cases increased, according to the world health organization (WHO) (Newman et al., 2015). A trend of antimicrobial resistance for *N. gonorrhoeae* is increasing and becoming a serious health burden. This bacterium has the ability to resist different available antibiotics (Lin et al., 2021). Sulfonamides and penicillin were formerly most effective drugs to treat gonorrhoeae, however, bacteria have developed resistance to these antibiotics over time. It has become resistant to many other antibiotics like aminocyclitol, spectinomycin, fluoroquinolone, ciprofloxacin, azithromycin, vancomycin, trimethoprim, and colistin in the recent years. This extensive drug resistance (XDR) nature of *N. gonorrhoeae* is posing a threat of untreatable gonorrhoeae in the near future (Yang and Yan, 2020).

There is no single consistent class of antimicrobials appropriate for the treatment of *N. gonorrhoeae*. Therefore, some dual treatments approaches are applied to treat gonorrhoeae, however failure to these treatments has shown the severity of the infections (Vincent and Jerse, 2019). These gonococcal infections can persist and reinfect the host with the evidence that this bacterium can dodge and overwhelm the immune responses of the individual (Jefferson et al., 2021). Some efficient control measures should be taken to resolve the complicated situation, including safe-sex counseling, appropriate diagnostic and alternative antimicrobial treatment (Vincent and Jerse, 2019).

The continued resistance of this bacterium to all available antibiotics has developed a need to design novel drug and vaccine targets to deal with the urgent impediment and treatment of gonorrhoeae (Jefferson et al., 2021). Moreover, *N. gonorrhoeae* can lower the affinity of drugs and enhance resistance levels by evolving specific mutations in the target sites of antimicrobials (Yang and Yan, 2020). *N. gonorrhoeae* shares much of its genome with *Neisseria meningitidis*, 4CMenB vaccine was found to have potential cross-protection against *N. gonorrhoeae* which was 40%

effective with two doses. Although, the vaccine antigen selection becomes problematic due to gonorrhoeal strains which can be overcome by introducing core genome studies to target all the mutant strains of *N. gonorrhoeae*. Preclinical phase of vaccine development against *N. gonorrhoeae* is still going on. Favorable vaccine candidates are still under study, however, no information has so far been gathered about vaccine efficacy in humans (Soltan et al., 2021). The current study aims to unveil alternative therapeutic targets against *N. gonorrhoeae* and to design vaccine constructs based on reverse vaccinology.

## Materials and methods

Subtractive proteomics and reverse vaccinology approaches were utilized to determine the drug and vaccine targets against *N. gonorrhoeae* pathogen. which divides the proteins into two pathways i.e; cytoplasmic proteins and membrane proteins Depicted in Figure 1).

### Core proteome retrieval and paralogous proteins removal

The core genes sequences of 69 complete genome sequences of *N. gonorrhoeae* strains were retrieved from EDGAR version 2.0 (Blom et al., 2016). During this analysis, *N. gonorrhoeae* strain 35\_02\_CP012028 was used as reference genome for the analysis. The first step includes removal of paralogous proteins as they may result in duplication and complexity in data analysis. The CD-HIT (Li and Godzik, 2006) server was used to obtain these non-paralogous proteins based on 60% sequence similarity as according to former studies (Hizbullah et al., 2018; Aslam et al., 2020; Aslam et al., 2021; Shah et al., 2021).

### Identification of host non-homologous proteins

Non-paralogous proteins were checked against human proteome by comparative BLASTp analysis (Johnson et al., 2008) with threshold values of bitscore  $\leq 100$ , E-value  $< 1e-4$ , query coverage  $\leq 35\%$  and sequence identity  $\leq 35\%$  (Hizbullah et al., 2018; Aslam et al., 2020; Shah et al., 2021). The human proteome data was obtained from UniProt database (Shah et al., 2021). Additionally, the human host non-homologous proteins were subtracted from 75,176 non-redundant gut microbiome proteins. Standalone BLASTp was used for the comparative analysis with criteria i.e. E.value  $< 1e-4$  and sequence identity of 50%.

### Prediction of metabolic pathways

The pathogen non-homologous proteins of above step were proceeded for KEGG metabolic pathway analysis using KAAS

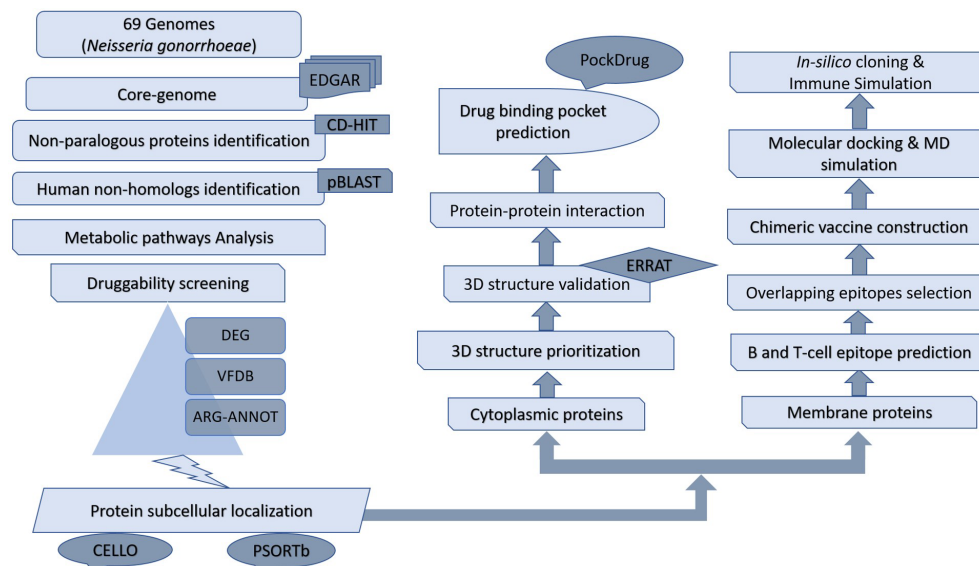


**FIGURE 1**  
Flowchart of subtractive proteomics and reverse vaccinology approach followed for the potential drug and vaccine identifications.

(KEGG Automatic Annotation Server) server (Moriya et al., 2007). Manual comparison with human metabolic pathways was performed to identify pathogen unique and common pathways (Hizbullah et al., 2018). The pathogen pathways were searched for unique and common proteins. The proteins not mapped to metabolic pathways were proceeded as KEGG independent proteins.

## Novel drug targets identification

A customized database specific for all the FDA approved drug targets was retrieved from Drugbank. The shortlisted proteins from the previous step were searched against Drugbank entries using BLASTp with parameters as criteria bitscore > 100 and E-value < 1e-4. The targets not showing any significant sequences match with drugbank entries were prioritized for additional analyses to predict novel targets.

## Identification of pathogen essential proteins

A promising drug target is necessary to be a pathogen key protein essential for basic cellular survival (Shah et al., 2021). Database of essential genes (DEG) (Luo et al., 2021) was used for the curation of essential proteins sequences. The DEG database has empirically authorized data holding genes necessary for the survival of an organism. Pathogen proteins were scanned against DEG database using BLASTp (Aslam et al., 2020). The criteria for BLASTp was set as E-value  $< 1e-4$  and bitscore  $\geq 100$  (Nogueira et al., 2021).

## Virulence and antibiotic resistant proteins identification

The virulent and antibiotic resistance proteins were determined by scanning pathogen proteins against BLASTp with parameters, i.e. E-value < 1e-4 and bitscore  $\geq$  100 as performed earlier (Aslam et al., 2020; Aslam et al., 2021). Virulence Factor Database (VFDB) was employed for the identification of putative virulence factors to better interpret the pathogenesis and host defense system (Liu et al., 2019). There is an emerging trend of antibiotic resistance in bacterial pathogens and ARG-ANNOT database contains the information about these resistant drug targets. Antibiotic resistant targets were predicted by screening the pathogen proteins against the ARG-ANNOT *via* BLASTp (Gupta et al., 2014).

### Subcellular localization prediction, protein-protein interaction and transmembrane proteins analysis

It is essential to determine subcellular localization of proteins for the identification of appropriate drug targets. Subcellular localization was assessed using two different web servers i.e., PSORTb version 3.0 (<http://www.psort.org/psortb/>) (Hossain et al., 2017) and CELLO version 2.5 (<http://cello.life.nctu.edu.tw/>) (Yu et al., 2014). Cytoplasmic and membrane proteins prediction is mainly done by PSORTb. CELLO is used for further validation of protein subcellular localization (Shah et al., 2021). Cytoplasmic proteins were selected as probable drug targets while outermembrane and membrane proteins were proceeded for vaccine target analysis. STRING database v10.5 (<http://string-db.org>) was used to perform PPI analysis with default parameters (Szklarczyk et al., 2017). TMHMM v0.2 server was employed to

evaluate the transmembrane topology of the proteins (Krogh et al., 2001).

## Druggability screening of target proteins

The prioritized list of proteins were additionally assessed for basic druggability features, including small drug-like molecules anchoring pocket prediction etc. For this purpose, the proteins were subjected to I-TASSER server (<http://zhang.bioinformatics.ku.edu/I-TASSER>) to generate 3D structures. Analysis was done based on defined parameters like C-score where five models were obtained as output (Zhang, 2008). Higher C-score indicates the model with high confidence which is frequently in the range of -5 to 2. Quality of the proteins 3D structure was checked by ERRAT protein verification tool. For non-bonded atomic interactions, 'overall quality factor' is determined by ERRAT where maximum score, i.e.  $\geq 50$  indicates a good quality of 3D structure (Colovos and Yeates, 1993). The models were downstream analyzed using Pock-Drug server (Hussein et al., 2015). The Pock-Drug server holds various pocket assessment methods to predict a protein druggability feature based on 3D structure evidences and ligand proximity evaluation.

## Reverse vaccinology for potential vaccine targets identification

From the subtractive proteomics analysis, outer membrane and extracellular proteins were selected for evaluation of antigenicity by VaxiJen server v2.0 with criteria set as 70-89% accuracy rate and  $> 0.4$  probability score. AllergenFP was employed to check the allergenicity of the shortlisted proteins. The proteins predicted to cause allergy in the host were discarded (Dimitrov et al., 2014). Furthermore, the parameters including the theoretical PI, instability index, aliphatic index, half life, number of amino acids and GRAVY (Grand Average of Hydropathicity) of proteins were assessed using ExPasy ProtParam tool (Gasteiger et al., 2005).

## Prediction of T-cell epitopes

Immune responses are majorly elicited by T-Cells. It is therefore helpful to predict T-cell epitopes for effective vaccine construct prioritization. Cytotoxic or helper T-cells are stimulated by MHC binding molecule (Jaan et al., 2022). Immune Epitope Database server (IEDB) (Fleri et al., 2017b) was employed for the prediction of MHC binding epitopes with criteria of lower percentile rank i.e.  $< 0.2$ . NetMHCpan EL 4.0 web server was used for MHC-I binding. For the prediction of MHC-II epitopes binding, IEDB recommended 2.22 method, where percentile rank was set as  $< 10$  for the selection of epitopes. Moreover, SMM-Align (netMHCII-1.1) (Nielsen et al., 2007) method was used for the prediction of MHC class II, where top binding was based on cut-off value of  $IC_{50} < 100$  nM (Fleri et al., 2017a). Epitopes having lowest percentile ranks were preferred for further evaluation.

## Prediction of B-cell epitopes

An antigenic portion binding to the immunoglobulin is known as B-Cell epitope. Solvent exposed antigens can be recognized by B-Cells specific receptors (BCR). Sequence based methods are used for the prediction of Linear B-Cell epitopes (Sanchez-Trincado et al., 2017). Linear B-Cell epitope prediction was performed by BCPreds, FBCPred and BepiPred (El-Manzalawy et al., 2008) servers. Prioritization was given in the downstream analyses to B-cell, MHC-1 and MHC-2 overlapping epitopes (Jaan et al., 2022).

## Immunogenicity, antigenicity, toxicity and conservancy analysis

For further filtration, immunogenicity of the predicted MHC-I epitopes was assessed by IEDB server where negative values were discarded. For all the predicted epitopes, the Auto cross covariance (ACC) transformation and alignment-independent prediction of the protected antigens was performed by VaxiJen server 2.0 at a default value  $> 0.5$  (Doytchinova and Flower, 2007). ToxinPred server was employed for the evaluation of toxicity of all the epitopes (Svanberg Frisinger et al., 2021). IEDB conservancy evaluation was performed to determine the conservancy level of epitopes within genotype sequences by setting parameters to default. Conservancy or variability of epitopes within a protein can be assessed by this tool (Bui et al., 2007).

## Construction of chimeric vaccine and physicochemical properties analysis

Amino acid linkers i.e. EAAAK, GGGS and KK were utilized to join the overlapped epitopes of MHC-1, MHC-2 and B-Cells to generate chimera vaccine constructs. To improve the potency and effectiveness of peptide vaccines, adjuvants were added to the constructs. Four distinct adjuvants i.e. HBHA protein, beta defensin, L7/L12 50 ribosomal protein and HBHA conserved sequences were added (Aslam et al., 2020). For the activation of CD4+ T-cells, a synthetic universal peptide PADRE containing 13 amino acids was added. Effective CD4+ response and problems of polymorphism can be overwhelmed by PADRE sequences. PADRE sequence (i.e. AKFVAAWTLKAAA) was used for the better efficacy of peptide vaccine (Ghaffari-Nazari et al., 2015). Toxicity, allergenicity and antigenicity of these chimera constructs were analyzed by different tools. AlgPred server was used to evaluate the allergic and non-allergic behavior of chimeric vaccine subunits (Bui et al., 2006). A sequence based prediction method by SOLpro server was also employed to check the solubility of the constructs (Magnan et al., 2009). Physicochemical properties including number of amino acids, aliphatic index, instability index, estimated half-life, molecular weight, theoretical PI and GRAVY (Grand Average of Hydropathicity) of vaccine constructs were evaluated by ProtParam tool (Kumar et al., 2021).



## Secondary and tertiary structure prediction

PSIPRED (<http://bioinf.cs.ucl.ac.uk/psipred/>) was employed for the prediction of the secondary structures of the chimeric vaccine constructs. For tertiary structure prediction, Phyre2 was used and refinement of models was performed by GalaxyRefine server tested in CASP10. In this method, side chains are rebuilt and their repacking was performed. Validation of refined 3D model was done by ERRAT (quality 90%) and ProSA-web (Wiederstein and Sippl, 2007). ProSA-web is commonly used to check the probable errors of 3D models. PROCHECK server was used for obtaining Ramachandran plot (Maxwell and Popelier, 2017). Ramachandran plot was used to assess the phi/psi angles for a comprehensive understanding of protein conformation.

## Molecular docking of vaccine constructs

PatchDock is a shape complimentary algorithmic tool to evaluate structural interactions of novel vaccine targets with the ligands (Jaan et al., 2022). Two final vaccine constructs were docked with six commonly occurring HLA alleles by PatchDock server to exhibit HLA-Peptide interactions (Solanki and Tiwari, 2018). FireDock server was employed for refinement and re-scoring of docked complex and ten best models were acquired for refinement as output (Mashiach et al., 2008). Vaccine construct 7 (V7) showed best results prioritized in accordance with lowest binding energy. Therefore, the V7 construct was additionally docked within TLR4. The 3D structure information of TLR4 was acquired from PDB (ID: 2Z65). The docking and structural refinements were performed through PatchDock server and FireDock server, respectively. Binding score and global binding energies of the refined models were examined to analyze the docked complexes.

## Molecular dynamic simulation

GROMACS, a command-line Linux-based software, was utilized for molecular dynamics assessment of the docked complex (V7-TLR4) (Van Der Spoel et al., 2005). The vaccine construct was put through molecular simulations to mimic the biological context in which protein structures operate. A Gromos87 file format) was created from the vaccine structure using pdb2gmX to obtain a topology compatible with the OPLS-AA (Optimized Potential for Liquid Simulation-All Atom) force field (Kaminski et al., 2001). To fill water molecules, the structure was contained in a rhombic cube and was placed in the center of the box, 1 nm from the cube's edge, to generate its periodic picture, which was 2 nm apart. The vaccine was simulated with water, which had a force constant of 1000 kJ mol<sup>-1</sup>nm<sup>-2</sup> and was spatially arranged. The vaccine's overall charge was calculated. The charge was used to neutralize the system. The energy minimization method was carried out, and the energy-minimized structure was obtained. NVT

equilibration for 100 ps was used to keep the temperature stable. Several simulations were run at various beginning speeds, with V-rescale applied and temperature changes noticed on the temperature graph. The NPT ensemble made it possible to calculate pressure and density. For 10 nanoseconds, the resultant structure was subjected to molecular dynamics (MD) simulation. The RMSD of the energy-minimized structure's backbone was anticipated, and the results were graphed. The radius of gyration (Rg) was determined for the structure's compactness analysis. The qtgrace tool was used to examine simulation graphs.

## Codon optimization, *in-silico* expression and immune simulation

The codon optimization of the vaccine constructs was performed by Java Codon Adaptation tool (JCat) in *E. coli* (strain K12). Back translation of the vaccine amino acid sequences to DNA was done by JCat which employs an algorithm to obtain Codon adaption index (CAI) values (Chung and Lee, 2012). The expression level in *E. coli* was predicted by average GC content and CAI values of the adapted sequences. GC content ranges from 30 to 70% and CAI value of 1.0 is considered best. The rho-independent transcription terminators, cleavage sites of some restriction enzymes and prokaryotic ribosomes binding sites were avoided. To construct recombinant plasmid sequence, codon adapted sequences were introduced into plasmid vector pET28a (+). SnapGene software was employed for this purpose.

The immune response by vaccine was predicted using C-Immsim server. Herein, the random seeds were selected as "12345" and the number of Ag to inject was kept at 1000. The simulation volume, simulation steps, Host HLA selection and type of injection were kept as default per reference. A total of two doses were given at steps 1 and 84. The immune profile was generated for analysis of vaccine construct activity.

## Results

### Human host non-homologous core proteins identification

A Total of 1294 core proteins were retrieved from the 69 complete genomes of *N. gonorrhoeae* species (Table S1). Three paralogous proteins were removed using CD\_HIT tool having sequence similarity of >60%. To prevent the likelihood of adverse effects, proteins homologous to the host were discarded by subjecting pathogen proteins to standalone BLASTp against human proteome. The 1137 human non-homologous pathogen proteins were additionally subtracted from the human gut microbiome. The microbes that colonize the human body are also known to be involved in metabolic reactions like development, homeostasis of immunity, and different physiological functions (Kho and Lal, 2018).

## Pathogen metabolic pathways analysis and druggability screening

A total of 549 pathogen proteins, non-homologous to human as well as human gut proteome were prioritized for KEGG metabolic pathway analysis to understand their key cellular functioning (Table S2). A preferable drug target is promising to involve in unique metabolic pathways of pathogens. The prioritized list of proteins were identified to enrich in 100 of metabolic pathways of *N. gonorrhoeae*. Among these about 28 metabolic pathways were identified specific to the pathogen during comparison with human host metabolic network.

Human-host non-homologous proteins were mapped to the KEGG metabolic pathways involving 262 proteins in different metabolic pathways, of which 99 proteins were involved in common while 59 were engaged in unique metabolic pathways of the pathogen (Table S3). Only nine proteins were identified as KEGG dependent proteins which were unique to both the pathways (Table 1). Remaining 450 proteins were categorized as KEGG independent. Both KEGG dependent and independent proteins were used for further analysis of drug target prioritization. Screening proteins against the drug bank revealed 6 KEGG dependent proteins as novel drug targets (Table S4). All these novel drug targets were subjected to further analyses for determination of the potential drug and vaccine targets.

## Identification of pathogen essential, virulent and antibiotic resistant proteins

Different analysis were employed to obtain the minimal number of the proteins as potential targets. DEG analysis showed that 1 protein in KEGG dependent and 79 proteins in KEGG independent pathway were essential for the bacterial survival. Moreover, the pathogenic capacity of bacteria to overwhelm the host is enhanced by the virulence factors (Shah et al., 2021; Jaan et al., 2022). Thus, virulence factor analysis was performed by VFDB where 1 and 28

proteins were found to be virulent as in KEGG pathways dependent and independent, respectively.

The survival evolution in the pathogens is based on mechanism of antibiotic resistance. These genes were collected in ARG-ANNOT database that was used to identify the antibiotic resistance by subjecting prioritized proteins to BLASTp scanning. It was found that only 1 KEGG independent protein was involved in antibiotic resistance. These essential, virulent and antibiotic resistance genes could pave ways for further investigations and studies to design novel drug targets.

### Subcellular localization and final drug targets prioritization

It is important to predict subcellular location of a protein for better understanding of its functions, disease mechanism and it is also valuable for developing new drug and vaccine targets (Yao et al., 2019). For potential drug targets, proteins located in the cytoplasm were prioritized while remaining proteins having sublocations that are extracellular or outer membrane were preferred as vaccine targets as they would more likely elicit greater immune responses (Nogueira et al., 2021). The subcellular location prediction of both the pathways dependent and independent revealed that 1 and 41 proteins were cytoplasmic, respectively. Similarly, 1 and 18 proteins were found to be outer membrane and extracellular, respectively.

STRING analysis for checking protein-protein interactions was performed which minimized the number of proteins as hub proteins. The 12 proteins were prioritized to be potent drug targets (Figure S1). Furthermore, for prediction of transmembrane helices proteins were subjected to TMHMM server. The finalized 12 proteins were submitted to I-TASSER server for the prediction of 3D structure. Models with higher C-score were selected which show the more accurate alignment of our model (Zhang, 2008). For binding small molecules, a protein must have ability to hold a pocket known as pocket druggability being considered as a crucial step during drug development. All the druggable targets were considered potent drug targets with drug value >0.5. Moreover, all the models showed high quality factor >85% analyzed by ERRAT server (Table 2).

TABLE 1 *Neisseria gonorrhoeae* proteins involved in the unique metabolic pathways with their respective pathway IDs.

Sr No.	Protein IDs	Protein names	KO Identifiers	Unique Pathway names	Pathway IDs
1	AKP15425.1	D-alanyl-D-alanine carboxypeptidase DacC precursor	K07259	Peptidoglycan biosynthesis	NGK00550
2	AKP14613.1	Penicillin-binding protein 2	K03587	beta-Lactam resistance	NGK01501
3	AKP14672.1	Penicillin-binding protein 1F	K03814	Peptidoglycan biosynthesis	NGK00550
4	AKP15153.1	Major outer membrane protein P.IB precursor	K03587	beta-Lactam resistance	NGK01501
5	AKP14619.1	Thiol:disulfide interchange protein DsbA precursor	K03673	Cationic antimicrobial peptide (CAMP) resistance	NGK01503
6	AKP16189.1	Nitrate/nitrite sensor protein NarX	K07673	Two-component system	NGK02020
7	AKP14248.1	Zinc uptake regulation protein	K09823	Quorum sensing	NGK02024
8	AKP14928.1	Phosphoenolpyruvate-protein phosphotransferase	K08483	Phosphotransferase system (PTS)	NGK02060
9	AKP14929.1	Phosphocarrier protein HPr	K02784	Phosphotransferase system (PTS)	NGK02060

TABLE 2 Analysis of shortlisted druggable proteins.

Sr No.	Protein ID	Protein Names	TMHMM	M. wt (Da)	Query length	STRING (K>5)	ERRAT scores	Pocket residues (PockDrug >0.5)
Pathways Dependent Proteins								
1	AKP14928.1	Phosphoenolpyruvate-protein phosphotransferase	0	64	131	6.18	97	0.96
Pathways Independent Proteins								
1	AKP14242.1	tRNA-modifying protein YgfZ	0	31	81	8.18	87	0.98
2	AKP14617.1	hypothetical protein	0	43	101	6.18	92	0.95
3	AKP15484.1	Ribosome maturation factor RimM	0	18	41	10	66	0.77
4	AKP15723.1	hypothetical protein	0	12	21	6.91	92	0.96
5	AKP15740.1	Modification methylase BspRI	0	42	72	6.91	94	0.91
6	AKP15765.1	Ribosomal large subunit pseudouridine synthase F	0	28	53	5.64	91	0.95
7	AKP15987.1	putative FAD-linked oxidoreductase	0	50	97	5.09	96	0.95
8	AKP16026.1	Elongation factor P	0	20	82	8.36	87	0.5
9	AKP16115.1	DnaA regulatory inactivator Hda	0	25	45	5.09	92	0.82
10	AKP16132.1	tRNA(Ile)-lysine synthase	0	48	103	5.27	91	0.81
11	AKP14182.1	Ribosomal small subunit pseudouridine synthase A	0	26	49	5.09	95	0.5

## Vaccine target screening of membrane proteins

VaxiJen server was used for the antigenicity analysis of 18 outer membrane proteins with antigenicity probability score > 0.4. Further analysis of these proteins by AllergenFp was performed to check the allergenicity. A potent vaccine candidate must be non-allergic in nature. Moreover, ProtParam tool was used to check different parameters of these outer membrane proteins such as molecular weight (30-70 KDa), theoretical PI (<9), instability index (<30), aliphatic index (>70), estimated half life (>10 hr) and GRAVY (Table S5). Two proteins (IDs: AKP15153.1 and AKP15828.1) were prioritized as potent vaccine targets for further deep analysis.

## Prediction of T-cell and B-cell epitopes

T and B-Cells recognized as immune cell are capable of mediating adaptive immunity. Pathogen-specific memory is developed by these cells that induces immunological protection. Pathogens have specialized receptors for specific antigens presented by MHC molecules

(Sanchez-Trincado et al., 2017). A cellular immune response mediated by B-Cell and T-Cell can be triggered by regions of proteins known as epitope. Epitope prediction is one of the major corner stones in the development of novel vaccine targets (Li et al., 2014). In cell mediated immunity, two types of cells are involved (a) cytotoxic T-cells (b) helper T-cells. MHC-I and MHC-II molecules

provide these cells with epitopes. IEDB database was employed to analyze the MHC binding epitopes of shortlisted two vaccine candidates. High binding affinity epitopes were selected. NetMHCpan EL 4.0 web server with criteria set at IC<sub>50</sub> <100 nm and percentile rank <0.2 was employed for MHC-I binding where peptide can attach with just nine amino acids because of shallow binding pockets with tight physicochemical bias (Hizbullah et al., 2018). Therefore, several alleles of human host having 9mer length were set as reference and total 42 epitopes from both the candidates were selected to proceed further (Table S6). Moreover, filtration of these epitopes with different servers confirmed 7 and 4 final MHC-I binding epitopes (Table 3).

For MHC-II molecules binding epitopes, IEDB recommended method with percentile rank <10 was set to predict peptides interacting with possible MHC-II alleles where prediction is less accurate and due to shallow binding pockets, 15mer length was employed. MHC class-II alleles prediction confirmed 5 and 3 final epitopes after antigenicity, allergenicity, toxicity and conservancy analysis. Furthermore, IFN gamma, IL-4 and IL-10 Induction ability was also calculated by respective servers.

Humoral immunity is induced by B-cell epitopes which are present on the surface of B lymphocytes (Soltan et al., 2021). After prediction of linear B-cell epitopes by different servers, (Table S7) binding of B-cell epitopes with HLA alleles was checked by IEDB server. For final epitope selection, predicted T-cell and B-cell epitopes were compared to obtain overlapped epitopes (Table S8). The 11 overlapped epitopes of two shortlisted antigenic proteins were prioritized as they may prove successful for potential vaccine preparation against *N. gonorrhoeae*. Structure-function association

TABLE 3 MHC-I interacting T-cell epitopes for the two potential vaccine candidate proteins.

Protein ID	Peptide	Start	End	MHC-I alleles	Score	Rank	Toxicity	Antigenicity	Conservancy
AKP15153.1	EVAATAAYR	267	275	HLA-A*68:01	0.987267	0.01	Non-Toxin	Antigen	100.00%
	AQYAGLFQR	193	201	HLA-A*31:01	0.93643	0.01	Non-Toxin	Non-Antigen	77.78%
	NTKDNVNAW	118	126	HLA-A*25:01	0.907364	0.01	Non-Toxin	Non-Antigen	100.00%
	ESYHVGLNY	178	186	HLA-A*26:01	0.900357	0.02	Non-Toxin	Antigen	100.00%
	DQVVVGAEY	303	311	HLA-B*15:02	0.895167	0.02	Non-Toxin	Antigen	100.00%
	SVAGTNTGW	83	91	HLA-A*25:01	0.791029	0.02	Non-Toxin	Non-Antigen	100.00%
	YAHGFKGTV	285	293	HLA-C*12:03	0.695197	0.02	Non-Toxin	Antigen	88.89%
	VAATADVTL	15	23	HLA-C*03:03	0.812732	0.03	Non-Toxin	Antigen	88.89%
	RSVEHTKGK	35	43	HLA-A*30:01	0.746071	0.03	Non-Toxin	Antigen	100.00%
	KKSLIALTL	2	10	HLA-B*48:01	0.558335	0.03	Non-Toxin	Non-Antigen	66.67%
	HSADYDNTY	294	302	HLA-A*01:01	0.864001	0.05	Non-Toxin	Non-Antigen	100.00%
	GGYDNNALY	233	241	HLA-A*30:02	0.615879	0.1	Non-Toxin	Non-Antigen	100.00%
	GLKGFGFTI	99	107	HLA-A*02:03	0.585985	0.16	Non-Toxin	Antigen	100.00%
AKP15828.1	DVFFGVVTQK	91	99	HLA-A*68:01	0.975893	0.01	Non-Toxin	Non-Antigen	33.33%
	IPIAESPNI	116	124	HLA-B*51:01	0.944744	0.01	Non-Toxin	Antigen	66.67%
	RLNALIFQY	132	140	HLA-A*30:02	0.899966	0.01	Non-Toxin	Antigen	55.56%
	RQRHVVNAY	192	200	HLA-B*15:01	0.991112	0.01	Non-Toxin	Non-Antigen	88.89%
	KRMDVRYIY	234	242	HLA-B*27:05	0.976768	0.01	Non-Toxin	Antigen	66.67%
	TPAGVEVLL	269	277	HLA-B*35:03	0.93623	0.01	Non-Toxin	Non-Antigen	88.89%
	SSDNIIYAY	288	296	HLA-A*01:01	0.989534	0.01	Non-Toxin	Non-Antigen	88.89%
	EEGLFRFQL	209	217	HLA-B*18:01	0.447957	0.18	Non-Toxin	Antigen	88.89%

among antigen and antibody can be predicted by conformational B-cell epitope prediction. Due to unavailability of 3D structures, conformational B-cell epitope cannot be predicted (Shah et al., 2021; Jaan et al., 2022).

## Construction of multi-epitope chimeric vaccine

Final epitopes were linked by using linkers, i.e., EAAAK, GGGS, and KK. Adjuvant was added to enhance the immunogenic nature of the designed vaccine to the N-terminal of prioritized epitopes. An adjuvant is taken as a vaccine component to elicit more robust immune responses. Different adjuvants, i.e., HBHA protein, HBHA conserved sequences, beta-defensin, and L7/L12 50-ribosomal protein, were added to enhance the vaccine potential. Moreover, PADRE sequences containing 13 amino acids (AKFVAAWTLKAAA) was also included to resolve the problem triggered by polymorphism of HLA-DR molecules. It was noted that PADRE sequences provided vaccine constructs with improved cytotoxic T lymphocyte responses and immune protection (Aslam et al., 2020). Total eight vaccine constructs (V1 to V8) with different combinations of epitopes and adjuvants were designed (Table S9).

SOLPro server with a solubility score >0.5 was employed to check the solubility of vaccine constructs. The solubility core determines the High soluble property of vaccine constructs over expression. All the constructs showed a high solubility score indicating their soluble nature in biological system. Antigenicity analysis with antigenicity score >0.90 exhibiting considerable antigenic behavior of constructs. The three constructs, i.e. V4, V5, and V7 were confirmed to exhibit the antigenic behavior. Vaccine constructs were also subjected to a VexiJen server analysis with a threshold of 0.75 to validate the antigenic behavior. The AllergenFP server was employed which indicated that all the constructs were non-allergen. CAI value (ranges between 0.92-0.99) and GC content (30-70%) were checked for cloning characteristics (Table S10A). Further analysis of vaccine constructs was performed by ProtParam tool. Two vaccine constructs with standard values were selected by this analysis (Table S10B).

## Structure prediction and validation

Vaccine constructs, i.e., V5 and V7 were prioritized for secondary structure prediction by PSIPRED. The overall vaccine sequence was estimated to have 39.44%  $\alpha$ -helix, 9.48%  $\beta$ -strands, 18.32% extended strand, and 32.76% random coils for the V5

construct. V7 construct contains 27.37%  $\alpha$ -helix, 8.95%  $\beta$ -strands, 21.84% extended strand and 41.84% random coils. Tertiary structure prediction of vaccine constructs by Phyre2 showed 93.8%, 2.7%, 2.7%, and 0.9% of residues for V5 construct and 76.3%, 13.2%, 10.5%, and 0.0% residues for V7 construct in favored, additional allowed, allowed and disallowed regions, respectively. Orientation of dihedral angles and combination of angles that are not in favored regions on account of steric hindrance can be estimated *via* Ramachandran plot assessment (Maxwell and Popelier, 2017). The ProSA web server was used to validate the stereochemical stability of models. Quality-based parameters validate models in both the servers where ProSA shows the results in graphical form (Shah et al., 2021). The Z-score (assessed by ProSA server) of the constructs V5 and V7 was -4.98 and -4.75, respectively, indicating that these models needed to be refined. The refinement of these 3D models was performed by GalaxyRefine, where the quality of models improved. Z-score improved from -4.98 to -5.21 for V5 and -4.75 to -4.33 for V7, respectively. Ramachandran plot analysis improved to show 96.5%, 2.7%, 0%, and 0.9% of residues for V5 and 92.1%, 7.9%, 0%, 0% of residues for V7 constructs in favored, additionally allowed, allowed and disallowed regions (Figure 2). In addition, ERRAT server showed the quality of predicted models (>90%).

## Molecular docking analysis of vaccine constructs

PatchDock server was employed for protein-protein docking of two vaccine constructs (V5 and V7) with six different commonly occurring HLA alleles, i.e., 1A6A, 1AQD, 2Q6W, 3C5J, 4MD4, 5NI9 acquired from PDB. The FireDock server refined docked complexes to achieve top ten best models. Among them, a model was selected with the best docking score. The V7 vaccine construct met the best selection standards with the least global energy of -39.22, and highest affinity with docking score of 13406. As vaccine

contains beta-defensin adjuvant, the docking of selected vaccine construct V7 was further performed with TLR4 to validate the immune responses. Primary innate immune responses are activated by vaccines containing beta defensin as adjuvants. Moreover, other immunomodulatory immune responses are mediated by these. Based on binding energy -27.91 of docked complex, the V7-TLR4 complex showed overall good interaction. It is speculated that for destroying viral antigens, docked complex V7-TLR4 will elicit immune cascades (Table 4).

## Molecular dynamic simulation and immune simulation

In order to further validate the interaction of the vaccine construct with the corresponding HLA allele, the complex was subjected to molecular dynamic simulation. Using GROMACS' built-in Spectro tool, a total of 19,574 water molecules were introduced to the system. The construct has a total charge of -11, according to calculations. Two positive sodium ions were supplied to the solution to neutralize it, replacing two existing water molecules at atoms 14274 and 20388. Energy minimization was carried out for 50000 steps; when the steepest descents converged at 1734 steps, the force reached 1098 KJ/mol.

While the average density was determined to be 1017.19 kg/m<sup>3</sup>. After a 100 ns simulation time, a trajectory analysis was performed. The gyration radius reached roughly 3.15 nm throughout MD simulation, indicating that the three-dimensional protein structure remained stable. A plot of the RMSD backbone indicated that RMSD levels rise to 0.45 nm and stay there for the majority of the simulation time, indicating that the vaccine is stable. On the other hand, RMSF explains regions with a lot of flexibility (Figure 3).

The initial responses generated by vaccine include IgM and IgG production. As IgM is the main antibody response, it started to rise by the administration of 1<sup>st</sup> dose whereas its amount boosts up until

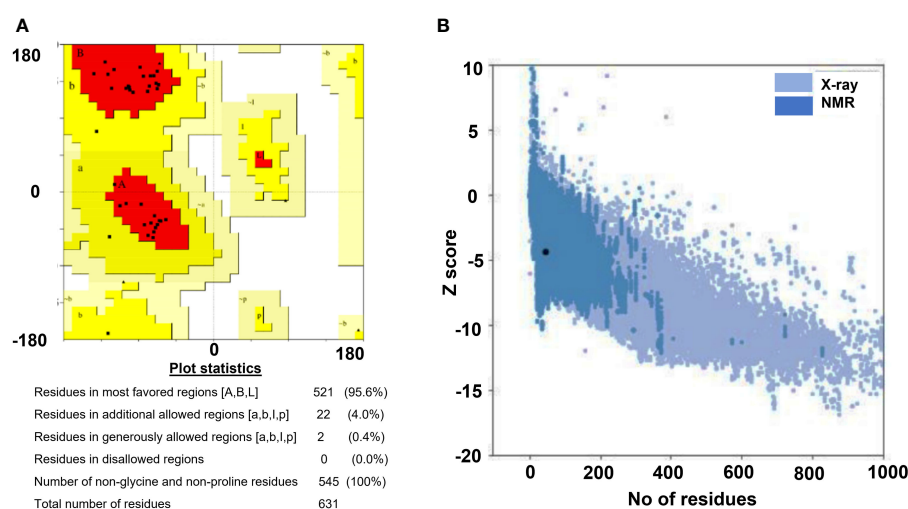


FIGURE 2

Tertiary structure validation results for the designed construct (V7). (A) Ramachandran plot, (B) ProSA web graph.



TABLE 4 Docking analysis of prioritized vaccine constructs (V5 and V7) with different HLA alleles.

Vaccine constructs	HLA alleles PDB ID's	Score	Area	Hydrogen bond energy	Global energy	ACE
V5	1A6A	15292	2131	0	-38.87	-8.46
	1AQD	16202	2194	0	5.14	0.54
	2Q6W	15638	2490	-0.99	4.49	15.71
	3C5J	15364	2107	-0.95	-27.27	-19.94
	4MD4	16112	2308	-6.58	-20.58	3.97
	5NI9	17136	2291	-0.44	1.74	1.6
V7	1A6A	12728	1744	-4.55	6.26	9.6
	1AQD	12186	1621	-2.42	-28.28	5.5
	2Q6W	12134	1575	-7.12	-24	11.51
	3C5J	12832	1859	-2.58	-21.97	5.11
	4MD4	13406	1858	-2.63	-39.22	7.99
	5NI9	12840	1920	-3.63	-24.68	9.41

the second dose followed by robust increase in the levels of IgM +IgG and IgG1 and IgG2. This indicated the ability of vaccine construct to bind with B-cells directly and create strong humoral antibody response. In the case of cytotoxic(CTLs) and Helper (HTLs) T-cells, there was a strong response in the different types of cells, which was highly accompanied by memory cells

production. The later graph represents the danger levels as “D” and Interleukin-2 levels as “IL”. The results show very minute amount of both factors that indicate the safety of vaccine while administration. In summary, the vaccine construct (V7) has shown great potential to generate adaptive immune response in a safe limit (Figure 4).

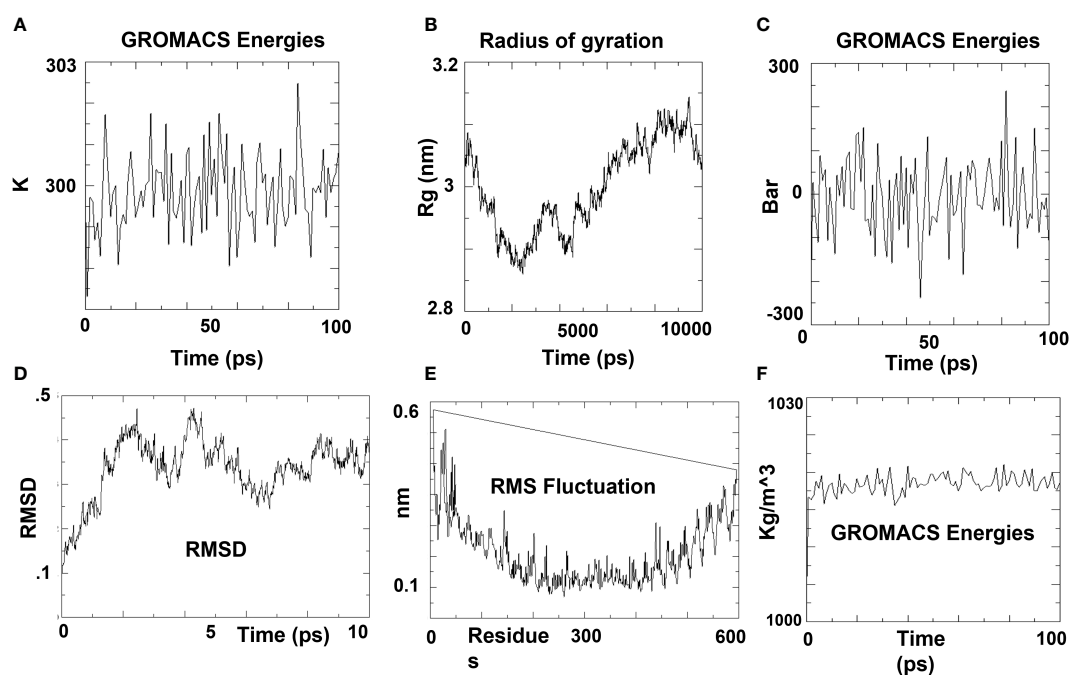


FIGURE 3

MD simulation plots of V7-TLR4 docked complex. (A) Variations in temperature during the simulation. During 100 ps, the system temperature reached 300 K and showed little variations. (B) During simulation time, the radius of gyration vaccine construct is stable in its compact form. (C) Pressure variations during simulation. During 100 ps, the average pressure is 2.73710 bar, according to the pressure plot. (D) RMSD plot of backbone. The RMSD graph demonstrates that the RMSD of the protein backbone reaches ~0.4 nm and is generally maintained, indicating that the vaccine construct has few structural aberrations. (E) RMSF (Root Mean Square Fluctuation) plot. The RMSF plot of side chains illustrates the regions in peaks that have a lot of flexibility. (F) The expected density is 1017.19 kg/m<sup>3</sup> on average.

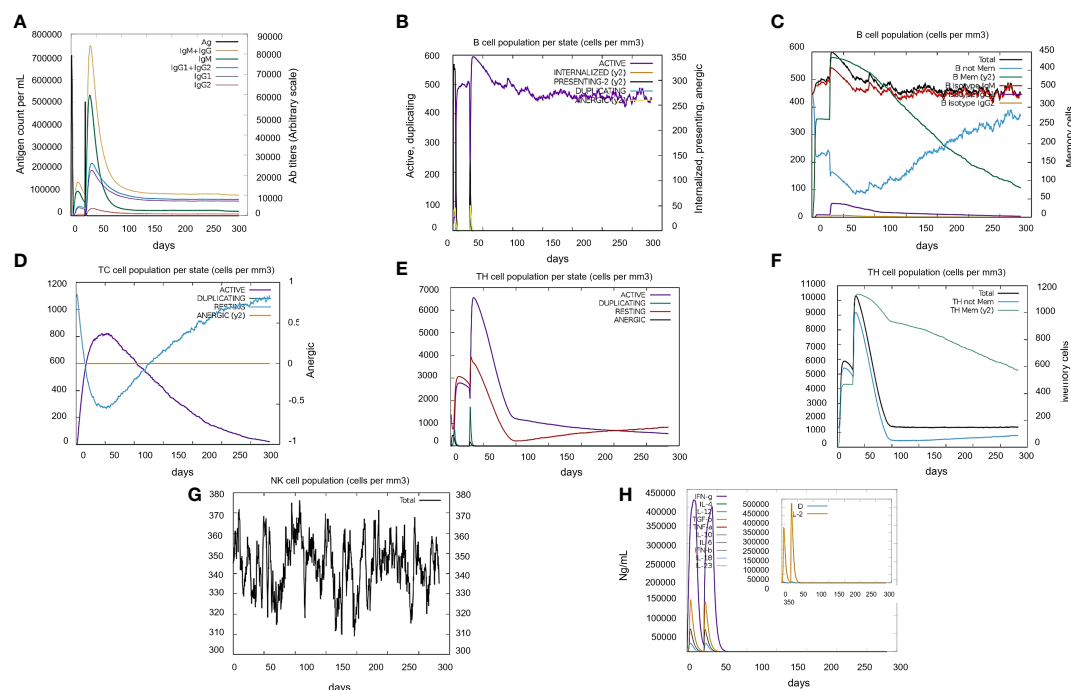


FIGURE 4

Immune simulation profile of vaccine construct (V7) in two injections by C-immSim server. (A) High primary response of IgM and IgG antibodies by antigen exposure. (B) B-cells immune reaction where active B-cells are produced in constant amount after second injection. (C) Total B-cell antibodies immune response. (D) Cytotoxic T-cells immune reaction with high active T-cell production. (E) Helper T-cell response with significant increase at second injection. (F) Total Helper T-cells immune response. (G) Natural Killer immune cells profile. (H) Simpson Index D graph representing cytokines and Interleukin levels where "D" indicates the danger level.

## Reverse translation and *In-silico* cloning of vaccine construct

The vaccine construct showed GC content up to 70% and CAI value of 1.0 which ensured high cloning in *E. coli* (strain K12). In addition, for heterologous cloning of vaccine construct (V7) in *E. coli*, the adapted codon sequences were introduced into the plasmid vector pET 28a (+) employing SnapGene software. A 6490 bp recombinant vector (Figure 5) was acquired by cloning vaccine DNA sequences into the vector. It was found that our vaccine construct (V7) was capable of cloning in pET 28a (+) which ensured its heterologous cloning and expression in cellular environment.

## Discussion

Prevention against the extensive-drug resistant *N. gonorrhoeae* is thought-provoking because of its serious health problems. Identification of potential therapeutic targets might be promising by targeting core genes of bacteria due to increasing resistance, the antibiotics which were earlier efficient against this bacterium, are no longer suggested for the treatment of infection caused by *N. gonorrhoeae*. This includes resistance to penicillin, quinolones, tetracyclines, macrolides and cephalosporins (Jefferson et al., 2021). In the current study, we utilized state of the art computational biology approaches to investigate the core genes from the 69 complete genomes of the *N. gonorrhoeae* to identify

potent drug and vaccine targets. The ultimate results may apply to diverse bacterial strains because of the conservancy of core proteins throughout a species (Aslam et al., 2020; Jaan et al., 2022). Analyzing the 69 complete genomes, essential core genes, non-homologous to human and virulent proteins were prioritized as potent drug candidates, used for further analyses. Hub proteins were identified by PPI network analysis. According to sub-cellular localization, cytoplasmic proteins were prioritized for novel drug targets and outer membrane proteins as potential vaccine candidates. Membrane localized proteins are difficult to isolate and purify, so cytoplasmic proteins were used as putative drug candidates (Mondal et al., 2015). Druggability screening of proteins shortlisted the 12 drug candidates being novel drug targets against *N. gonorrhoeae* species (Table 2). Out of twelve prioritized drug targets, Phosphoenolpyruvate protein phosphotransferase (AKP14928.1) involves in glucose transport system. Further, this system can hinder strain productivity by imposing metabolic and regulatory modifications (Gosset, 2005). tRNAs are important targets for a large number of antibiotics playing major role in translational machinery. tRNA-modifying protein YgfZ (AKP14242.1) may prove to be a prominent target as used in previous studies (Chopra and Reader, 2015). Hypothetical protein (AKP14617.1) often involved in resistivity mechanism can be a suitable drug target (Osuntokun and Cristina, 2019). Another protein Ribosome maturation factor RimM (AKP15484.1) which is a chaperon protein, involved in ribosome maturation was also prioritized as potential drug target (Zhang et al., 2021).



FIGURE 5

*In-silico* restriction cloning of final vaccine construct (V7) into the *E. coli* pET28a (+) expression vector where red color shows the cloned vaccine construct.

Double stranded sequence GGCC is recognized by Modification methylase BspRI (AKP15740.1) and DNA is protected by this methylase. Putative FAD-linked oxidoreductase (AKP15987.1) was previously not found in literature as a drug target. Elongation factor P (AKP16026.1) is required to maintain peptide formation during translation which is a conserved factor (Tollerson et al., 2018). DnaA regulatory inactivator Hda (AKP16115.1) is a major regulator which interacts with ATP bound DnaA and inactivates DnaA by the hydrolysis of ATP. Bacterial pathogens have an important, conserved, ATP dependent and tRNA modifying enzyme, tRNA(Ile)-lysidine synthase (AKP16132.1) by which cytidine base I anticodon loop of Ile 2 tRNA is modified (Shapiro et al., 2014). Ribosomal small subunit pseudouridine synthase A (AKP14182.1) could be an alternative drug target.

According to centrality-lethality rule, infections of *N. gonorrhoeae* can be prevented by targeting these prioritized drug candidates. Subtractive proteomics works with the combination of reverse vaccinology to find out potential vaccine candidates due to increased antimicrobial resistance in different clinical isolates of *N. gonorrhoeae*. Host-pathogen interactions are majorly controlled by outer membrane proteins. So, two outer membrane proteins (IDs: AKP15153.1 and AKP15828.1) were prioritized as therapeutic vaccine candidates against *N. gonorrhoeae* infection. Major outer membrane protein P. IB precursor (AKP15153.1) was found to involve in adherence, entry and intracellular processing of bacteria in infected epithelial cells which proved to be a potent vaccine candidate. While, hypothetical protein (AKP15828.1) was

considered best to estimate novel therapeutic inventions. Bacterial outer membrane proteins have a direct exposure to host cells, involved in elicitation of better immune responses (Rizwan et al., 2017). These proteins are prioritized due to their role in bacterial survival and pathogenesis (Mishra et al., 2020). Implementation of immunoinformatics approach in epitope mapping worked efficiently in the identification of potential vaccine targets which uses only antigenic portion of protein for the stimulation of B and T-cell immunity (Majid and Andleeb, 2019). Chimeric subunit vaccine constructs were generated from the leading T and B-cell overlapped epitopes. Out of eight vaccine constructs, a prioritized vaccine construct (V7) with appropriate adjuvant was able to clone in pET 28a (+) by ensuring its optimal expression (Figure 5). Molecular docking of vaccine construct V7 with HLAs and TL4 predicting a stable interaction between ligand and receptor. PAMPs (pathogen associated molecular patterns) on pathogen's surface are recognized by TLR4 (tool like receptors) found on immune cells. TLR4 produces cytokines and chemokines to mediate immune responses (Aslam et al., 2020). Molecular dynamic simulation was performed to check the stability of docked complex V7-TLR4 in the presence of water molecules, speculating the stable molecular interaction between vaccine construct V7 and toll like receptor (TLR4). Typical immune responses with reliable results were symbolized by immune investigations. Greater immune responses were observed as a result of repeated exposure of vaccine construct to the antigens. Memory B-cells and T-cells were developed and stimulation of helper T cells was evident. Humoral immune

responses were supported by significant production of Ig and T H cells. Practical implementation of all the proposed therapeutic targets is certainly required to explore their efficacies.

## Conclusions

In the current study, state of the art computational approaches were utilized to find appropriate, novel drug and vaccine targets against *N. gonorrhoeae* as no viable vaccine is reported to prevent the infection of this pathogen. The computational screening of the core genome extracted from 69 complete genomes, by multiple updated biological databases identified twelve cytoplasmic novel drug targets not reported previously. After a vigorous analysis, two outer membrane vaccine candidate proteins (AKP15153.1, AKP15828.1) were selected, followed by T-cell and B-cell epitope prediction, used to generate a vaccine construct. As a result, eight different vaccine constructs (V1-V8) with different combinations of epitopes and adjuvants were designed. Of these, one of the constructs (V7) was found as the best candidate capable of eliciting the human immune response. The elicitation of the human immune response by this construct was confirmed through docking and MD simulation analysis with four distinct HLA alleles. The *in-silico* cloning of this construct was performed in the bacterial system (*E. coli*-K12) to verify further the cloning ability of the vaccine construct. The immune simulation analysis confirmed that immunoglobulins have a higher binding affinity for this construct. Further experimental validation of the proposed vaccine construct in animal models will be auspicious.

## Data availability statement

The datasets presented in this study can be found in online repositories. The names of the repository/repositories and accession number(s) can be found in the article/[Supplementary Material](#).

## Author contributions

SCO, and MoS performed the conceptualization and manuscript writing. AQ, SJ, TW and MuS executed the study. UN, and SS participated in the critical revision of the manuscript for intellectual content. SCO and MoS did the final revision and editing of the manuscript. All authors have read and approved the manuscript.

## References

- Aslam, M., Shehroz, M., Ali, F., Zia, A., Pervaiz, S., Shah, M., et al. (2021). Chlamydia trachomatis core genome data mining for promising novel drug targets and chimeric vaccine candidates identification. *Comput. Biol. Med.* 136. doi: 10.1016/j.combiomed.2021.104701
- Aslam, M., Shehroz, M., Hizbullah, Shah, M., Khan, M. A., Afridi, S. G., et al. (2020). Potential druggable proteins and chimeric vaccine construct prioritization against brucella melitensis from species core genome data. *Genomics* 112, 1734–1745. doi: 10.1016/j.ygeno.2019.10.009
- Bar-On, E., Sagiv, S., and Malkin, C. (1990). Disseminated gonococcal infection. *J. Am. Geriatr. Soc.* 38, 678–679. doi: 10.1111/j.1532-5415.1990.tb01429.x
- Blom, J., Kreis, J., Spänig, S., Juhre, T., Bertelli, C., Ernst, C., et al. (2016). EDGAR 2.0: an enhanced software platform for comparative gene content analyses. *Nucleic Acids Res.* 44, W22–W28. doi: 10.1093/nar/gkw255
- Bui, H. H., Sidney, J., Dinh, K., Southwood, S., Newman, M. J., and Sette, A. (2006). Predicting population coverage of T-cell epitope-based diagnostics and vaccines. *BMC Bioinf.* 7, 1–5. doi: 10.1186/1471-2105-7-153
- Bui, H. H., Sidney, J., Li, W., Fusseder, N., and Sette, A. (2007). Development of an epitope conservancy analysis tool to facilitate the design of epitope-based diagnostics and vaccines. *BMC Bioinf.* 8, 1–6. doi: 10.1186/1471-2105-8-361

## Funding

This study was funded by the Doctoral Research Fund awarded to SCO.

## Acknowledgments

The authors would like to acknowledge the Bahauddin Zakariya University Multan, Pakistan and The Affiliated Hospital of Southwest Medical University, China, for providing the necessary infrastructure to perform this study.

## Conflict of interests

The authors declare that the research was conducted in the absence of any commercial or financial relationships that could be construed as a potential conflict of interest.

## Publisher's note

All claims expressed in this article are solely those of the authors and do not necessarily represent those of their affiliated organizations, or those of the publisher, the editors and the reviewers. Any product that may be evaluated in this article, or claim that may be made by its manufacturer, is not guaranteed or endorsed by the publisher.

## Supplementary material

The Supplementary Material for this article can be found online at: <https://www.frontiersin.org/articles/10.3389/fcimb.2023.1017315/full#supplementary-material>

### SUPPLEMENTARY FIGURE 1

Interaction analysis of predicted drug targets with other proteins using STRING database where query proteins are indicated by red color. The proteins with the best predicted three-dimensional structures are shown to summarize the drug target's PPI list.

- Chopra, S., and Reader, J. (2015). tRNAs as antibiotic targets. *Int. J. Mol. Sci.* 16, 321–349. doi: 10.3390/ijms16010321
- Chung, B. K. S., and Lee, D. Y. (2012). Computational codon optimization of synthetic gene for protein expression. *BMC Syst. Biol.* 6. doi: 10.1186/1752-0509-6-134
- Colovos, C., and Yeates, T. O. (1993). Verification of protein structures: Patterns of nonbonded atomic interactions. *Protein Sci.* 2, 1511–1519. doi: 10.1002/pro.5560020916
- Dimitrov, I., Naneva, L., Doytchinova, I., and Bangov, I. (2014). AllergenFP: Allergenicity prediction by descriptor fingerprints. *Bioinformatics* 30, 846–851. doi: 10.1093/bioinformatics/btt619
- Doytchinova, I. A., and Flower, D. R. (2007). VaxiJen: A server for prediction of protective antigens, tumour antigens and subunit vaccines. *BMC Bioinf.* 8. doi: 10.1186/1471-2105-8-4
- El-Manzalawy, Y., Dobbs, D., and Honavar, V. (2008). Predicting linear b-cell epitopes using string kernels. *J. Mol. Recognit.* 21, 243–255. doi: 10.1002/jmr.893
- Fleri, W., Paul, S., Dhanda, S. K., Mahajan, S., Xu, X., Peters, B., et al. (2017a). The immune epitope database and analysis resource in epitope discovery and synthetic vaccine design. *Front. Immunol.* 8. doi: 10.3389/fimmu.2017.00278
- Fleri, W., Paul, S., Dhanda, S. K., Mahajan, S., Xu, X., Peters, B., et al. (2017b). The immune epitope database and analysis resource in epitope discovery and synthetic vaccine design. *Front. Immunol.* 0. doi: 10.3389/FIMMU.2017.00278
- Gasteiger, E., Hoogland, C., Gattiker, A., Duvaud, S., Wilkins, M. R., Appel, R. D., et al. (2005). The proteomics protocols handbook. *Proteomics Protoc. Handb.*, 571–608. doi: 10.1385/1592598900
- Ghaffari-Nazari, H., Tavakkol-Afshari, J., Jaafari, M. R., Tahaghoghi-Hajghorbani, S., Masoumi, E., and Jalali, S. A. (2015). Improving multi-epitope long peptide vaccine potency by using a strategy that enhances CD4+ T help in BALB/c mice. *PLoS One* 10, 1–12. doi: 10.1371/journal.pone.0142563
- Gosset, G. (2005). Improvement of escherichia coli production strains by modification of the phosphoenolpyruvate:sugar phosphotransferase system. *Microb. Cell Fact.* 4, 1–11. doi: 10.1186/1475-2859-4-14
- Gupta, S. K., Padmanabhan, B. R., Diene, S. M., Lopez-Rojas, R., Kempf, M., Landraud, L., et al. (2014). ARG-annot, a new bioinformatic tool to discover antibiotic resistance genes in bacterial genomes. *Antimicrob. Agents Chemother.* 58, 212–220. doi: 10.1128/AAC.01310-13
- Hizbullah, Nazir, Z., Afridi, S. G., Shah, M., Shams, S., and Khan, A. (2018). Reverse vaccinology and subtractive genomics-based putative vaccine targets identification for burkholderia pseudomallei Bp1651. *Microb. Pathog.* 125, 219–229. doi: 10.1016/j.micpath.2018.09.033
- Hossain, T., Kamruzzaman, M., Choudhury, T. Z., Mahmood, H. N., Nabi, A. H. M. N., and Hosen, I. (2017). Application of the subtractive genomics and molecular docking analysis for the identification of novel putative drug targets against salmonella enterica subsp. enterica serovar poona. *Biomed Res. Int.* 2017, 3783714. doi: 10.1155/2017/3783714
- Hussein, H. A., Borrel, A., Geneix, C., Petitjean, M., Regad, L., and Camproux, A. C. (2015). PockDrug-server: A new web server for predicting pocket druggability on holo and apo proteins. *Nucleic Acids Res.* 43 (W1), W436–42. doi: 10.1093/nar/gkv462
- Jaan, S., Shah, M., Ullah, N., Amjad, A., Javed, M. S., Nishan, U., et al. (2022). Multi-epitope chimeric vaccine designing and novel drug targets prioritization against multi-drug resistant staphylococcus pseudintermedius. *Front. Microbiol.* 13, 3022. doi: 10.3389/FMICB.2022.971263
- Jefferson, A., Smith, A., Fasinu, P. S., and Thompson, D. K. (2021). Sexually transmitted neisseria gonorrhoeae infections—update on drug treatment and vaccine development. *Medicines* 8, 11. doi: 10.3390/medicines8020011
- Johnson, M., Zaretskaya, I., Raytelis, Y., Merezuk, Y., McGinnis, S., and Madden, T. L. (2008). NCBI BLAST: a better web interface. *Nucleic Acids Res.* 36, 5–9. doi: 10.1093/nar/gkn201
- Kaminski, G. A., Friesner, R. A., Tirado-rives, J., and Jorgensen, W. L. (2001). Comparison with accurate quantum chemical calculations on peptides †. *Quantum* 2, 6474–6487.
- Kho, Z. Y., and Lal, S. K. (2018). The human gut microbiome - a potential controller of wellness and disease. *Front. Microbiol.* 9. doi: 10.3389/fmicb.2018.01835
- Krogh, A., Larsson, B., Von Heijne, G., and Sonnhammer, E. L. L. (2001). Predicting transmembrane protein topology with a hidden Markov model: Application to complete genomes. *J. Mol. Biol.* 305, 567–580. doi: 10.1006/jmbi.2000.4315
- Kumar, A., Rathi, E., and Kini, S. G. (2021). Immunoinformatics approach for a novel multi-epitope vaccine construct against spike protein of human coronaviruses abstract. *bioRxiv* 2021.05.02.442313. doi: 10.1101/2021.05.02.442313
- Li, W., and Godzik, A. (2006). Cd-hit: A fast program for clustering and comparing large sets of protein or nucleotide sequences. *Bioinformatics* 22, 1658–1659. doi: 10.1093/bioinformatics/btl158
- Li, X., Yang, H. W., Chen, H., Wu, J., Liu, Y., and Wei, J. F. (2014). In silico prediction of T and b cell epitopes of der f 25 in dermatophagoides farinae. *Int. J. Genomics* 2014. doi: 10.1155/2014/483905
- Lin, E. Y., Adamson, P. C., and Klausner, J. D. (2021). Epidemiology, treatments, and vaccine development for antimicrobial-resistant neisseria gonorrhoeae: Current strategies and future directions. *Drugs* 81, 1153–1169. doi: 10.1007/s40265-021-01530-0
- Liu, B., Zheng, D., Jin, Q., Chen, L., and Yang, J. (2019). VFDB 2019: A comparative pathogenomic platform with an interactive web interface. *Nucleic Acids Res.* 47, D687–D692. doi: 10.1093/nar/gky1080
- Luo, H., Lin, Y., Zhang, R., Liu, T., Lai, F., Zhang, C., et al. (2021). DEG 15 , an update of the database of essential genes that includes built-in analysis tools. *Nucleic Acids Res.* 49, 677–686. doi: 10.1093/nar/gkaa917
- Magnan, C. N., Randall, A., and Baldi, P. (2009). SOLpro: accurate sequence-based prediction of protein solubility. *Bioinformatics* 25, 2200–2207. doi: 10.1093/bioinformatics/btp386
- Majid, M., and Andleeb, S. (2019). Designing a multi-epitopic vaccine against the enterotoxigenic bacteroides fragilis based on immunoinformatics approach. *Sci. Rep.* 9, 1–15. doi: 10.1038/s41598-019-55613-w
- Mashiach, E., Schneidman-Duhovny, D., Andrusier, N., Nussinov, R., and Wolfson, H. J. (2008). FireDock: a web server for fast interaction refinement in molecular docking. *Nucleic Acids Res.* 36 (Web Server issue), W229–232. doi: 10.1093/nar/gkn186
- Maxwell, P. I., and Popelier, P. L. A. (2017). Unfavorable regions in the ramachandran plot: Is it really steric hindrance? the interacting quantum atoms perspective. *J. Comput. Chem.* 38, 2459–2474. doi: 10.1002/jcc.24904
- Mishra, M., Panda, S., Barik, S., Sarkar, A., Singh, D. V., and Mohapatra, H. (2020). Antibiotic resistance profile, outer membrane proteins, virulence factors and genome sequence analysis reveal clinical isolates of enterobacter are potential pathogens compared to environmental isolates. *Front. Cell. Infect. Microbiol.* 10. doi: 10.3389/fcimb.2020.00054
- Mondal, S. I., Ferdous, S., Jewel, N. A., Akter, A., Mahmud, Z., Islam, M. M., et al. (2015). Identification of potential drug targets by subtractive genome analysis of escherichia coli O157:H7: An in silico approach. *Adv. Appl. Bioinform. Chem.* 8, 49–63. doi: 10.2147/AABC.S88522
- Moriya, Y., Itoh, M., Okuda, S., Yoshizawa, A. C., and Kanehisa, M. (2007). KAAS: an automatic genome annotation and pathway reconstruction server. *Nucleic Acids Res.* 35, 182–185. doi: 10.1093/nar/gkm321
- Newman, L., Rowley, J., Hoorn, S. V., Wijesooriya, N. S., Unemo, M., Low, N., et al. (2015). Global estimates of the prevalence and incidence of four curable sexually transmitted infections in 2012 based on systematic review and global reporting. *PLoS One* 10. doi: 10.1371/journal.pone.0143304
- Nielsen, M., Lundegaard, C., and Lund, O. (2007). Prediction of MHC class II binding affinity using SMM-align, a novel stabilization matrix alignment method. *BMC Bioinf.* 8, 1–12. doi: 10.1186/1471-2105-8-238
- Nogueira, W. G., Jaiswal, A. K., Tiwari, S., Ramos, R. T. J., Ghosh, P., Barh, D., et al. (2021). Computational identification of putative common genomic drug and vaccine targets in mycoplasma genitalium. *Genomics* 113, 2730–2743. doi: 10.1016/j.jygeno.2021.06.011
- Osuntokun, O. T., and Cristina, G. M. (2019). Bio isolation, chemical purification, identification, antimicrobial and synergistic efficacy of extracted essential oils from stem bark extract of spondias mombin(Linn). *Int. J. Mol. Biol.* 4, 135–143. doi: 10.15406/ijmboa.2019.04.00110
- Rizwan, M., Naz, A., Ahmad, J., Naz, K., Obaid, A., Parveen, T., et al. (2017). VacSol: A high throughput in silico pipeline to predict potential therapeutic targets in prokaryotic pathogens using subtractive reverse vaccinology. *BMC Bioinf.* 18, 1–7. doi: 10.1186/s12859-017-1540-0
- Sahile, A., Teshager, L., Fekadie, M., and Gashaw, M. (2020). Prevalence and antimicrobial susceptibility patterns of neisseria gonorrhoeae among suspected patients attending private clinics in jimma, Ethiopia. *Int. J. Microbiol.* 2020. doi: 10.1155/2020/7672024
- Sanchez-Trincado, J. L., Gomez-Perosanz, M., and Reche, P. A. (2017). Fundamentals and methods for T- and b-cell epitope prediction. *J. Immunol. Res.* 2017, 1–14. doi: 10.1155/2017/2680160
- Shah, M., Jaan, S., Fatima, B., Javed, M. S., Amjad, A., Khan, A., et al. (2021). Delineating novel therapeutic drug and vaccine targets for staphylococcus cornubiensis NW1T through computational analysis. *Int. J. Pept. Res. Ther.* 27, 181–195. doi: 10.1007/s10989-020-10076-w
- Shapiro, A. B., Plant, H., Walsh, J., Sylvester, M., Hu, J., Gao, N., et al. (2014). Discovery of ATP-competitive inhibitors of tRNA<sup>Ala</sup> lysine synthetase (TilS) by high-throughput screening. *J. Biomol. Screen.* 19, 1137–1146. doi: 10.1177/1087057114534981
- Solanki, V., and Tiwari, V. (2018). Subtractive proteomics to identify novel drug targets and reverse vaccinology for the development of chimeric vaccine against acinetobacter baumannii. *Sci. Rep.* 8, 1–19. doi: 10.1038/s41598-018-26689-7
- Soltan, M. A., Elbassiony, N., Gamal, H., Elkadee, E. B., Eid, R. A., Eldeen, M. A., et al. (2021). In silico prediction of a multipot vaccine against moraxella catarrhalis: Reverse vaccinology and immunoinformatics. *Vaccines* 9, 1–13. doi: 10.3390/vaccines9060669
- Svanberg Frisinger, F., Jana, B., Donadio, S., and Guardabassi, L. (2021). In silico prediction and prioritization of novel selective antimicrobial drug targets in escherichia coli. *Antibiotics* 10. doi: 10.3390/antibiotics10060632
- Szklarczyk, D., Morris, J. H., Cook, H., Kuhn, M., Wyder, S., Simonovic, M., et al. (2017). The STRING database in 2017: Quality-controlled protein-protein association networks, made broadly accessible. *Nucleic Acids Res.* 45, D362–D368. doi: 10.1093/nar/gkw937



- Tollerson, R., Witzky, A., and Ibba, M. (2018). Elongation factor p is required to maintain proteome homeostasis at high growth rate. *Proc. Natl. Acad. Sci. U. S. A.* 115, 11072–11077. doi: 10.1073/pnas.1812025115
- Van Der Spoel, D., Lindahl, E., Hess, B., Groenhof, G., Mark, A. E., and Berendsen, H. J. C. (2005). GROMACS: Fast, flexible, and free. *J. Comput. Chem.* 26, 1701–1718. doi: 10.1002/jcc.20291
- Vincent, L. R., and Jerse, A. E. (2019). Biological feasibility and importance of a gonorrhea vaccine for global public health. *Vaccine* 37, 7419–7426. doi: 10.1016/j.vaccine.2018.02.081
- Wiederstein, M., and Sippl, M. J. (2007). ProSA-web: Interactive web service for the recognition of errors in three-dimensional structures of proteins. *Nucleic Acids Res.* 35, 407–410. doi: 10.1093/nar/gkm290
- Yang, F., and Yan, J. (2020). Antibiotic resistance and treatment options for multidrug-resistant gonorrhea. *Infect. Microbes Dis.* 2, 67–76. doi: 10.1097/im9.0000000000000024
- Yao, Y. H., Lv, Y. P., Li, L., Xu, H. M., Ji, B. B., Chen, J., et al. (2019). Protein sequence information extraction and subcellular localization prediction with gapped k-mer method. *BMC Bioinf.* 20, 1–8. doi: 10.1186/s12859-019-3232-4
- Yeshanew, A. G., and Geremew, R. A. (2018). *Neisseria gonorrhoeae* and their antimicrobial susceptibility patterns among symptomatic patients from gondar town, north West Ethiopia. *Antimicrob. Resist. Infect. Control* 7, 1–7. doi: 10.1186/s13756-018-0376-3
- Yu, C. S., Cheng, C. W., Su, W. C., Chang, K. C., Huang, S. W., Hwang, J. K., et al. (2014). CELLO2GO: a web server for protein subCELLular LOcalization prediction with functional gene ontology annotation. *PLoS One* 9 (6), e99368. doi: 10.1371/journal.pone.0099368
- Zhang, Y. (2008). I-TASSER server for protein 3D structure prediction. *BMC Bioinf.* 9, 1–8. doi: 10.1186/1471-2105-9-40
- Zhang, H., Zhou, Q., Guo, C., Feng, L., Wang, H., Liao, X., et al. (2021). Structural basis for the c-terminal domain of mycobacterium tuberculosis ribosome maturation factor rimm to bind ribosomal protein s19. *Biomolecules* 11. doi: 10.3390/biom11040597



## OPEN ACCESS

## EDITED BY

Parth Sarthi Sen Gupta,  
Indian Institute of Science Education and  
Research Berhampur (IISER), India

## REVIEWED BY

Huahao Fan,  
Beijing University of Chemical Technology,  
China  
Sohan Sengupta,  
Patanjali Research Foundation, India

## \*CORRESPONDENCE

Rohit Sharma

✉ rohitsharma@bhu.ac.in

Kow-Tong Chen

✉ ktchen@mail.ncku.edu.tw

## SPECIALTY SECTION

This article was submitted to  
Clinical Microbiology,  
a section of the journal  
Frontiers in Cellular and  
Infection Microbiology

RECEIVED 30 December 2022

ACCEPTED 20 February 2023

PUBLISHED 19 April 2023

## CITATION

Sharma R, Chen K-T and Sharma R (2023)  
Emerging evidence on Monkeypox:  
resurgence, global burden, molecular  
insights, genomics and possible  
management.  
*Front. Cell. Infect. Microbiol.* 13:1134712.  
doi: 10.3389/fcimb.2023.1134712

## COPYRIGHT

© 2023 Sharma, Chen and Sharma. This is  
an open-access article distributed under the  
terms of the [Creative Commons Attribution  
License \(CC BY\)](#). The use, distribution or  
reproduction in other forums is permitted,  
provided the original author(s) and the  
copyright owner(s) are credited and that  
the original publication in this journal is  
cited, in accordance with accepted  
academic practice. No use, distribution or  
reproduction is permitted which does not  
comply with these terms.

# Emerging evidence on Monkeypox: resurgence, global burden, molecular insights, genomics and possible management

Ruchi Sharma<sup>1</sup>, Kow-Tong Chen<sup>2,3\*</sup> and Rohit Sharma<sup>1\*</sup>

<sup>1</sup>Department of Rasa Shastra and Bhaishajya Kalpana, Faculty of Ayurveda, Institute of Medical  
Sciences, Banaras Hindu University (BHU), Varanasi, Uttar Pradesh, India, <sup>2</sup>Department of  
Occupational Medicine, Tainan Municipal Hospital (managed by Show Chwan Medical Care  
Corporation), Tainan, Taiwan, <sup>3</sup>Department of Public Health, College of Medicine, National Cheng  
Kung University, Tainan, Taiwan

An outbreak of monkeypox (encoded enveloped double stranded DNA), resurgence and expansion has emerged in early 2022, posing a new threat to global health. Even though, many reports are available on monkeypox, still a comprehensive updated review is needed. Present updated review is focused to fill the research gaps pertaining to the monkeypox, and an extensive search was conducted in a number of databases, including Google Scholar, Scopus, Web of Science, and Science Direct. Although the disease usually progresses self-limiting, some patients require admission for kidney injury, pharyngitis, myocarditis, and soft tissue super infections. There is no well-known treatment available yet; still there has been a push for the use of antiviral therapy and tecovirimat as a promising option when dealing with co-morbidities. In this study, we mapped and discussed the updates and scientific developments surrounding monkeypox, including its potential molecular mechanisms, genomics, transmission, risk factors, diagnosis, prevention, vaccines, treatment, possible plant-based treatment along with their proposed mechanisms. Each day, a growing number of monkeypox cases are reported, and more cases are expected in the near future. As of now, monkeypox does not have a well-established and proven treatment, and several investigations are underway to find the best possible treatment from natural or synthetic drug sources. Multiple molecular mechanisms on pathophysiological cascades of monkeypox virus infection are discussed here along with updates on genomics, and possible preventive and therapeutic strategies.

## KEYWORDS

monkeypox, infection, genomics, molecular insights, vaccines, herbs, treatment

## 1 Introduction

An evolving zoonotic disease, monkeypox occurs due to a virus belonging to poxviridae family and orthopoxvirus genus (Lai et al., 2022). Along with cowpox virus, variola virus, and vaccinia virus, the monkeypox virus is one of four orthopox virus species that causes disease in humans (Shchelkunov et al., 2005). A monkeypox infection causes few symptoms identical to those of smallpox, but is less severe, and rarely causes death compared to that of smallpox (Petersen et al., 2019). Two outbreaks of a disease that appeared like pox, led to the discovery of monkeypox in 1958 which spread across colonies of monkeys (Mileto et al., 2022). Monkeypox may have been named so, due to its first-time appearance in monkeys and pox like symptoms, but its origin remains mysterious (Begum et al., 2023). The virus can, however, also be carried by African rodents and nonhuman primates (such as monkeys) and infect humans (Begum et al., 2023). Later an instance of monkeypox in a human was first reported in 1970 (Sejvar et al., 2004). By the time, number of countries in Central and Western Africa had already reported the monkeypox cases before the outbreak of 2022 (Simões and Bhagani, 2022). Prior to recently, nearly all monkeypox cases aside from Africa were associated with traveling overseas countries or importing animals that frequently suffer from the disease (Al-Tawfiq et al., 2022). It has been determined that the monkeypox outbreak has resulted in a public health emergency of International concern in multiple countries (Formenty et al., 2010).

Several mammalian species are known to be susceptible to monkeypox, however the native host of the disease is unidentified (Khodakevich et al., 1986). From times monkeypox virus isolates have known of two wild animal origins: a rope squirrel and a sooty mangabey from Ivory Coast and the Democratic Republic of Congo (DRC) places respectively (Khodakevich et al., 1986; Jezek et al., 1988; Hutson et al., 2009; Radonić et al., 2014). Monkeypox has a similar clinical picture to smallpox, but the major difference is the swelling of lymph nodes that begins early, often during fever

(Sklenovská and Van Ranst, 2018) and has a lower mortality rate (Centers for Disease Control and Prevention (CDC), 2022). There can be a period of infection of up to four weeks before the lesion of monkeypox desquamates (Fenner et al., 1998). It is likely that patients will experience complications such as second level bacterial infections, bronchopneumonia, respiratory distress, dehydration, gastrointestinal complications, encephalitis, sepsis, and infection of cornea with blindness as a result (Elsevier – clinical overviews, 2022). At present, no specific treatment exists for monkeypox virus infections, instead patients being treated with symptomatic treatment and supportive care (Otu et al., 2022).

Even though many short studies are present, there is a need of study which covers the detailed explanation of the disease along with mechanism involved in it. So, this study was conducted in order to map and summarize upcoming scientific developments surrounding monkeypox, such as its potential molecular insights, genomic patterns, diagnosis, prevention, vaccines, treatment and possible plant-based leads of monkeypox. Presented below is a comprehensive updated review that illustrates a better understanding on monkeypox virus. Understanding the mechanisms involved in monkeypox infection will strengthen the disease preventive and therapeutic strategies along with the discovery of new drugs.

## 2 Methodology

We conducted a review based on scientific articles that addressed monkeypox and its diagnostic method or treatment, especially pharmacological properties (Figure 1). Science Direct, SciFinder, Google Scholar, MEDLINE, EMBASE, and Scopus were the search engines used to search for published articles (till 24, November, 2022). For extracting information about the effects of monkeypox on global transmission and treatment, we used keywords such as “monkeypox”, “transmission”, “mode of

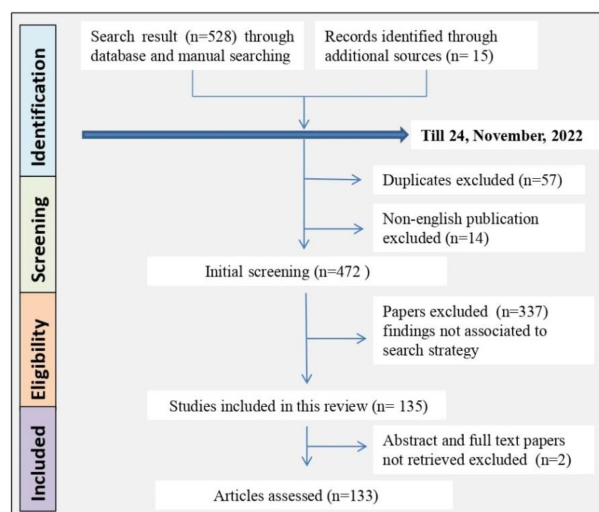


FIGURE 1  
Flowchart showing screening methodology for the review.

spread”, “fatality”, “incidence rate”, “prevention”, “diagnosis”, “vaccine”, “genomics”, “molecular mechanism”, “treatment”, “clinical trial”, “case study”, “traditional medicine”, and “mechanism of action”, along with their corresponding MeSH terms and conjunctions OR/AND. To understand the severity of disease and possible treatment options, we searched the available reports for scientific claims. All searches were limited to English. We excluded conference proceedings, gray literature, unpublished data, newspaper articles, preliminary reports without substantial proof of the claim, abstracts and full texts that could not be retrieved, and studies not relevant to this review. The graphs were generated using the GraphPad software version 6 for analysis.

### 3 Timeline recapped

A non-fatal pox outbreak was first reported in 1958 by Von Magnus in Copenhagen in *Cynomolgus* macaque (*C. macaque*). Prior to 1970, no human infection with monkeypox virus had been documented (Breman et al., 1980; Sejvar et al., 2004). The following cases of human monkeypox have been reported worldwide since 1970 (Figure 2, Table 1) (World Health Organization, 1996; Merouze and Lesoin, 1983; World Health Organization, 2022; McConnell et al., 1962; Ladnyj et al., 1972; Breman et al., 1980; Massung et al., 1994; Centers for Disease Control and Prevention (CDC), 1997; Mukinda et al., 1997; Anderson et al., 2003; Centers for Disease Control and Prevention (CDC), 2003a; Centers for Disease Control and Prevention (CDC), 2003b; Huhn et al., 2005; Learned et al., 2005; Likos et al., 2005; Nalca et al., 2005; Reynolds et al., 2006; Hutson et al., 2007; Rimoin et al., 2010; Kantele et al., 2016; Kozlov, 2018; Beer and Bhargavi Rao, 2019; Bhattacharya et al., 2022; Luo and Han, 2022; Tomori and Ogoina, 2022). On

June 23, 2022, the WHO declared monkeypox as an “evolving threat of moderate public health concern” (Reed et al., 2004). In a WHO report published on 23 July 2022, there were more than 16,000 cases with five deaths reported from 75 countries and territories (World Health Organisation, 2022). The outbreak of monkeypox in 2022 gained global attention when WHO declared it an “International Health Emergency” on July 27, 2022 (As monkeypox surges, WHO urges reducing number of sexual partners, 2022). Recently, in nearly 110 countries, 80,850 confirmed cases (79,877 in areas where monkeypox has not been reported historically and 973 in areas where monkeypox has been reported historically) and 55 deaths (42 in areas where monkeypox have not reported historically and 13 in areas where monkeypox have been reported historically) were reported till 24, November, 2022 (Monkeypox data explorer - our world in data, 2022).

### 4 Monkeypox virus strains: Genomic perspective

Figure 3A shows structure of the double stranded DNA virus (monkeypox virus), which causes monkeypox to occur in humans and animals (Figure 3B). This virus belonged to the poxviridae family and referred to as orthopoxviruses. As with variola, cowpox, and vaccinia, monkeypox virus belongs to the orthopoxvirus genus. It is not related to, nor is it descended from, the variola virus, which is responsible for smallpox (von Magnus et al., 1959; Breman et al., 1980; Shchelkunov et al., 2002; Alkhalil et al., 2010).

Two genetic clades have been identified in monkeypox virus, namely Central African clade (recently renamed as Clade I) and West African clade (recently renamed as Clade II). Furthermore, Clade II has two subclades: IIa and IIb, referring to the set of

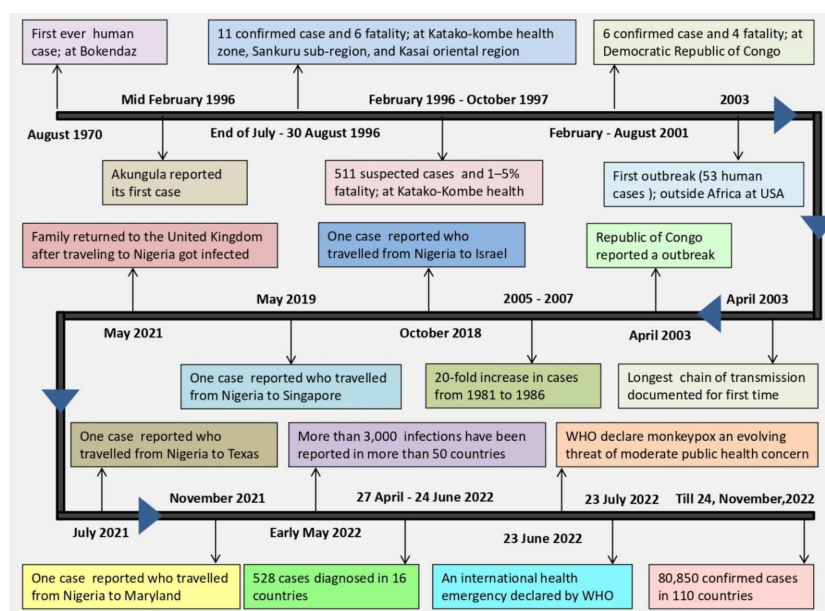


FIGURE 2  
Timeline of events in monkeypox's global transmission.

TABLE 1 An overview of monkeypox outbreaks cases between August, 1970 and 24, November, 2022.

Year Country	1970– 1979	1980– 1989	1990– 1999	2000– 2009	2010– 2019	2020– 2021	24 May, 2022	Till 24, November, 2022
Andorra	–	–	–	–	–	–	–	4
Argentina	–	–	–	–	–	–	–	894
Aruba	–	–	–	–	–	–	–	3
Australia	–	–	–	–	–	–	2	141
Austria	–	–	–	–	–	–	1	326
Bahamas	–	–	–	–	–	–	–	2
Bahrain	–	–	–	–	–	–	–	1
Barbados	–	–	–	–	–	–	–	1
Belgium	–	–	–	–	–	–	4	789
Benin	–	–	–	–	–	–	–	3
Bermuda	–	–	–	–	–	–	–	1
Bolivia	–	–	–	–	–	–	–	252
Bosnia and Herzegovina	–	–	–	–	–	–	–	9
Brazil	–	–	–	–	–	–	–	<b>9876</b>
Bulgaria	–	–	–	–	–	–	–	6
Cameroon	1	1	–	–	16	–	–	16
Canada	–	–	–	–	–	–	15	<b>1449</b>
Central African Republic	–	8	–	–	61	–	2	12
Chile	–	–	–	–	–	–	–	<b>1259</b>
China	–	–	–	–	–	–	–	1
Colombia	–	–	–	–	–	–	–	<b>3803</b>
Costa Rica	–	–	–	–	–	–	–	23
Croatia	–	–	–	–	–	–	–	29
Cuba	–	–	–	–	–	–	–	8
Curaçao	–	–	–	–	–	–	–	3
Cyprus	–	–	–	–	–	–	–	5
Czechia	–	–	–	–	–	–	1	70
DRC	38	343	511	10,027	18,788	7,374	10	206
Denmark	–	–	–	–	–	–	2	191
Dominican Republic	–	–	–	–	–	–	–	52
Ecuador	–	–	–	–	–	–	–	346
Egypt	–	–	–	–	–	–	–	1
El Salvador	–	–	–	–	–	–	–	21
Estonia	–	–	–	–	–	–	–	11
Finland	–	–	–	–	–	–	–	42
France	–	–	–	–	–	–	5	<b>4104</b>

(Continued)



TABLE 1 Continued

Year Country	1970– 1979	1980– 1989	1990– 1999	2000– 2009	2010– 2019	2020– 2021	24 May, 2022	Till 24, November, 2022
Georgia	–	–	–	–	–	–	–	2
Germany	–	–	–	–	–	–	12	3672
Ghana	–	–	–	–	–	–	–	107
Gibraltar	–	–	–	–	–	–	–	6
Greece	–	–	–	–	–	–	–	85
Greenland	–	–	–	–	–	–	–	2
Guadeloupe	–	–	–	–	–	–	–	1
Guatemala	–	–	–	–	–	–	–	141
Guyana	–	–	–	–	–	–	–	2
Honduras	–	–	–	–	–	–	–	11
Hong Kong	–	–	–	–	–	–	–	1
Hungary	–	–	–	–	–	–	–	80
Iceland	–	–	–	–	–	–	–	16
India	–	–	–	–	–	–	–	17
Indonesia	–	–	–	–	–	–	–	1
Iran	–	–	–	–	–	–	–	1
Ireland	–	–	–	–	–	–	–	217
Israel	–	–	–	–	1	–	1	262
Italy	–	–	–	–	–	–	5	917
Jamaica	–	–	–	–	–	–	–	16
Japan	–	–	–	–	–	–	–	7
Jordan	–	–	–	–	–	–	–	1
Latvia	–	–	–	–	–	–	–	6
Lebanon	–	–	–	–	–	–	–	18
Liberia	4	–	–	–	6	–	–	3
Lithuania	–	–	–	–	–	–	–	5
Luxembourg	–	–	–	–	–	–	–	57
Malta	–	–	–	–	–	–	–	33
Martinique	–	–	–	–	–	–	–	1
Mexico	–	–	–	–	–	–	–	3145
Moldova	–	–	–	–	–	–	–	2
Monaco	–	–	–	–	–	–	–	3
Montenegro	–	–	–	–	–	–	–	2
Morocco	–	–	–	–	–	–	–	3
Mozambique	–	–	–	–	–	–	–	1
Netherlands	–	–	–	–	–	–	6	1248
New Caledonia	–	–	–	–	–	–	–	1
New Zealand	–	–	–	–	–	–	–	35

(Continued)

TABLE 1 Continued

Year Country	1970– 1979	1980– 1989	1990– 1999	2000– 2009	2010– 2019	2020– 2021	24 May, 2022	Till 24, November, 2022
Nigeria	4	–	–	–	228	42	–	624
Norway	–	–	–	–	–	–	–	93
Panama	–	–	–	–	–	–	–	40
Paraguay	–	–	–	–	–	–	–	17
Peru	–	–	–	–	–	–	–	<b>3444</b>
Philippines	–	–	–	–	–	–	–	4
Poland	–	–	–	–	–	–	–	213
Portugal	–	–	–	–	–	–	39	948
Qatar	–	–	–	–	–	–	–	5
Republic of the Congo	–	–	–	73	24	–	–	5
Romania	–	–	–	–	–	–	–	45
Russia	–	–	–	–	–	–	–	2
Saint Martin	–	–	–	–	–	–	–	1
San Marino	–	–	–	–	–	–	–	1
Saudi Arabia	–	–	–	–	–	–	–	8
Serbia	–	–	–	–	–	–	–	40
Singapore	–	–	–	–	1	–	–	19
Slovakia	–	–	–	–	–	–	–	14
Slovenia	–	–	–	–	–	–	1	47
South Africa	–	–	–	–	–	–	–	5
South Korea	–	–	–	–	–	–	–	3
South Sudan	–	–	–	–	19	–	–	18
Spain	–	–	–	–	–	–	45	<b>7405</b>
Srilanka	–	–	–	–	–	–	–	1
Sweden	–	–	–	–	–	–	1	220
Switzerland	–	–	–	–	–	–	2	546
Taiwan	–	–	–	–	–	–	–	4
Thailand	–	–	–	–	–	–	–	12
Turkey	–	–	–	–	–	–	–	12
Ukraine								5
United Arab Emirates	–	–	–	–	–	–	1	16
United Kingdom	–	–	–	–	4	–	71	<b>3720</b>
United States	–	–	–	47	–	2	4	<b>29199</b>
Uruguay	–	–	–	–	–	–	–	14
Venezuela	–	–	–	–	–	–	–	10
Vietnam	–	–	–	–	–	–	–	2
Total cases (till 24, November,2022)								80,850

\*Countries with more than 1000 cases are bold.

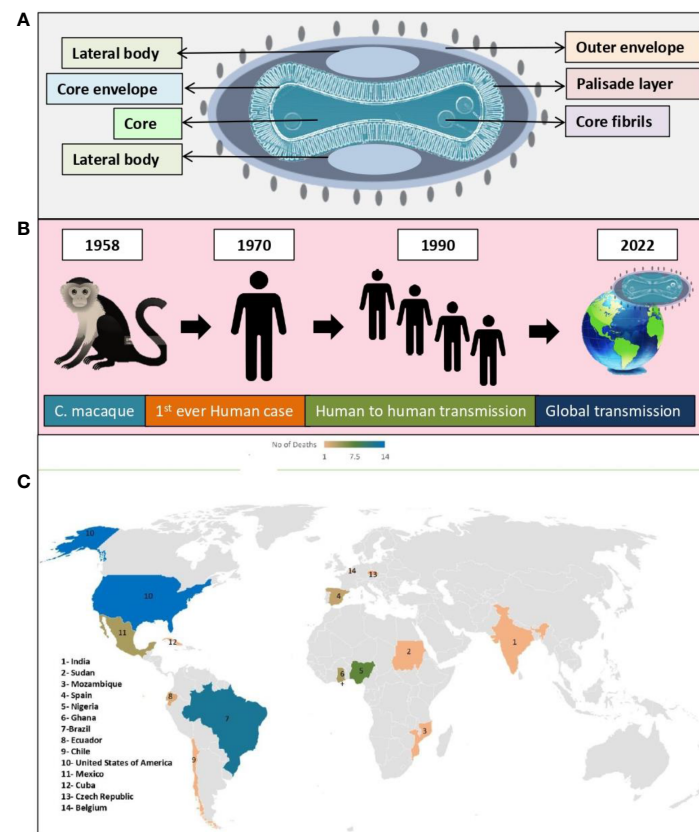


FIGURE 3  
Monkeypox virus; (A) Structure, (B) Global transmission, (C) Reported death cases of different geographical areas (till 24, November, 2022).

mutations that are circulating in the 2022 worldwide pandemic. There is a geographic separation between these two clades, as well as a distinction between their epidemiological and clinical characteristics. It has never been documented that West African clade transmits from case to case, and there is a case fatality rate (CFR) of 1%. As a contrast, the Congo Basin clade (aka Central African clade) exhibits a CFR of 11%, and transmission has been documented up to six times sequentially. It is believed that isolates from West African clade came from Nigeria, Ivory Coast, Liberia, USA, and Sierra Leone (imported from Ghana). On the other hand, isolates from Central African clade come from Congo, Gabon, Central African Republic, Cameroon, Sudan, and DRC. Non-vaccinated individuals of Central African encountered a 10% death rate in the 1980s, while cases occurring in West African strains were not fatal. It has been confirmed that the 2022 monkeypox virus is of West African origin based on preliminary genetic data. Various studies were conducted to compare genomes and was found that nucleotide sequences of the Central African strain (ZAI-96) differ by 0.55-0.56% from those of 3 West African strains (SL-V70, WRAIR-61 and COP-58). Central and West African strains have 173 and 171 unique functional genes, respectively. In terms of protein sequence, they have about 99.4% identity and share 170 orthologs. Transcription regulatory sequences between the two genomes did not differ significantly.

In order to determine which virulence genes are present in both strains, researchers studied 56 virulence genes to determine which are present in both strains, 53 of which were found common to both. 276 substitutions have been found in these 53 genes, accounting for 93 non-conservative changes, 61 conservative changes, and 121 silent changes in amino acid. In total, 16 proteins have extended their N- and C-termini, altering their predicted size. A study reported that BR-203, COP-C3L, and BR-209 orthologs accounted for significant virulence differences between the two strains, which is supported by another study reporting similar gene candidates (Jezek and Fenner, 1988; von Magnus et al., 1959; Ladnyj et al., 1972; Ježek et al., 1987; Chen et al., 2005; Likos et al., 2005; Osorio and Yuill, 2008; Weaver and Isaacs, 2008; Monkeypox: experts give virus variants new names, 2022; Comparative pathology of north American and central African strains of monkeypox virus in a ground squirrel model of the disease, 2022; Multi-country monkeypox outbreak: situation update, 2022).

Monkeypox virus encoded of all the orthopoxvirus genes known so far, but have only small subsets of the genes related to host range and immunomodulation (Shchelkunov et al., 2002). Monkeypox may adapt further to become a more effective human pathogen by a series of extended person-to-person transmissions. Moreover, as the human population changes, ecological

disturbances occurs and new infections emerges such as the HIV and COVID-19, which can be a possible cause of decreased immunity and further contributing towards more spreading of monkeypox virus (Chen et al., 2005; Likos et al., 2005; Weaver and Isaacs, 2008).

Also, an analysis of publicly available genomes from the current human monkeypox virus outbreak of 2022 was conducted to determine the phylogenetic diversity. As compared to previous monkeypox virus outbreaks, this outbreak reveals a distinct monophyletic lineage. Virus outbreaks in Europe may have started as early as March 2022, according to studies. As compared to its related viral predecessors from 2018 and 2019, monkeypox virus 2022 exhibits a marked divergence. In contrast to what is normally observed in orthopoxviruses, the heightened mutational signature this time indicates an accelerated evolutionary path. There has been an increase in cases reported across multiple regions, suggesting that some of these changes in genomics have led to more efficient transmission and dispersal mechanisms, which are compatible with sexual transmission, but research is needed to confirm this assertion. In addition, host-specific mechanisms, like APOBEC enzymatic editing, may be driving this rapid evolution of virus in favor of emergence of a host-specific clade that has enhanced human-to-human transmission capabilities. In light of its continuous spread across different countries and the increasing number of cases reported globally, genomic variability is likely to increase continuously its transmission efficiency (Kraemer et al., 2022; Luna et al., 2022).

In another study on monkeypox virus genome comparisons, indicate that COP-C3L ortholog, a gene that codes for a complement control protein associated to innate immune response, may play a role in determining the degree of virulence among those strains. One SCR domain is truncated in the Central African ortholog of COP-C3L, which is likely to affect its function, particularly its decay-accelerating ability. The monkeypox strain of Central Africa also contains truncated COP-E3L and COP-K3L, which is similar to the proteins in variola and vaccinia and allows the organism to resist interferons (IFN). Unlike COP-E3L and COP-K3L, monkeypox virus has a full-length ortholog of BR-203 (protein that prevents lymphocytes apoptosis), but variola virus lacks it and vaccinia virus has fragments. The differences between these three orthopoxviruses in terms of virulence may be explained by their proteins differences which affect the host immune system. Research is needed to determine whether genes encoding of proteins fragments with known functions influence its virulence. It may be possible to develop safer vaccines and better therapeutics with such knowledge (Carter et al., 2005; Reynolds et al., 2017).

## 5 Molecular perspective

As molecular biology has advanced, we have gained a deeper understanding of how viruses replicate and infect cells. The genome of this organism is relatively larger containing approximately 1,96,858 number of base pairs, which encodes for 190 open reading frames (Shchelkunov et al., 2002). These open reading

frames of virus make up most of the replication material in the infected cell. Viral entry into cells depends on the cell type and viral strain and is initiated once the virus attaches to the cell surface through the interaction between multiple viral ligands and cell receptors (Carter et al., 2005).

An apoptosis is a natural mechanism that occurs when a variety of stimuli trigger the death of cells for maintaining homeostasis in tissue and removal of abnormal or infected cells (Hengartner, 2000). Due to the importance of apoptosis in the immune response, poxviruses developed several anti-apoptotic strategies to disrupt it (Everett and McFadden, 2002). In order to survive, viruses contain many proteins that interfere with apoptosis at various points (Elmore, 2007). Previous study data however indicate that NOXA and caspase-3 were upregulated, while Bcl-2, PUMA, and PAK2 were downregulated in monkeypox virus, which is consistent with apoptosis induction (Alkhalil et al., 2010). Apoptosis-specific genes are underregulated in cells infected with monkeypox virus, whereas anti-apoptotic outcomes are observed in other poxvirus infected cells, suggesting that monkeypox virus infects cells in a way that is anti-apoptotic *via* a mechanism downstream from apoptosis initiation (Nichols et al., 2017). Although monkeypox virus genes involved in blocking apoptosis are unknown, still data suggest that an orthologs of the vaccinia virus (F1L) gene functions in the same manner as Bcl-2 by directly targeting mitochondria (Alkhalil et al., 2010).

Also, studies suggest that expression of histone, modification in histone posttranslational, and chromatin dynamic exchanges play an important role in host-poxvirus interactions (Alkhalil et al., 2010; Nichols et al., 2017). Moreover, studies introduced signaling components that regulate actin cytoskeletal dynamics as infection-regulated genes which further helps in regulating microtubule signaling. A membrane-associated protein encoded by the intersection 1 gene (SH3 domain protein) is said to be closely related to actin assembly machinery that controls endocytic membrane traffic. Morphological differentiation and cell motility are also affected by Rho-effector ROCK1, which is also closely related to cytoskeletal dynamics. As well as RAS p21 protein activator, homolog of oncogene from v-Ki-rat sarcoma virus and SOS2 are found essential in polymerizing actin filaments and reorganizing the cytoskeleton (McGlade et al., 1993; Giancotti and Ruoslahti, 1999; Pawlak and Helfman, 2002; Scaife et al., 2003; Alkhalil et al., 2010).

Studies also suggest that genes related to ion channels were impacted by monkeypox virus infection in an intriguing and novel manner. A total of ten genes that encode nine ion channels and a transporter were suppressed as infection progressed. A large number of these channels are located on the membrane of the cell in order to maintain its osmolarity homeostasis and cell membrane potential. Modulation mechanisms of transport, such as indirect consequences of Ras, Rho, and Rab GTPases, have been described, but their impact on viral infections and global cell biology continues to be unclear. However, there has been a report found describing how myxoma poxvirus protein M11L hinders apoptosis by interacting with mitochondrial permeability transition pores (Everett et al., 2002; Pochynyuk et al., 2007).

## 6 Monkeypox: A serious global health threat?

The monkeypox virus, is a public health concern since it can be transmitted from infected individuals, animals and contaminated substances. A number of countries that are non-endemic were reported to have monkeypox in May 2022 (Bunge et al., 2022). According to our discussion above, monkeypox lethality varies across Africa, suggesting its growing threat. Also, the current outbreak of monkeypox virus infection in humans suggests that biological aspects of virus, human behavior or both, have changed (Quarleri et al., 2022). A number of factors may have contributed to these changes, including the decline in smallpox immunity, the relaxed prevention measures for COVID -19, the resumption of international travel, the change in sexual interaction, and the presence of large gatherings in large numbers (Vaughan et al., 2018; Monkeypox update from AR Dept. of health - Arkansas medical society, 2022; Sharma V. et al., 2022; Thornhill et al., 2022). In the course of time, all viruses change and evolve despite this, monkeypox viruses mutate more slowly than COVID-19 virus (León-Figueroa et al., 2022). Currently, many studies are being conducted to understand the epidemiology, sources, and patterns of infection (Centers for Disease Control and Prevention, 2022; Ligon, 2004; Erez et al., 2019; Yong et al., 2020). Out of which study conducted in African countries by the European Centre for Disease Prevention and Control estimates that immunocompromised people, children, and young adults are at higher risk of death (Dhawan et al., 2022). This outbreak reported total of 55 deaths until know among various geographical areas (Figure 3C).

Policy makers and government officials also need to understand public opinion regarding the health crisis in order to develop health policies for monitoring and controlling it. So, in order to determine public attitudes towards the monkeypox virus, an analysis was conducted on 27, June, 2022 using techniques of advanced machine learning, particularly technique of Natural Language Processing (NLP). Intriguingly, the analysis results indicate that more people are posting positively about the monkeypox virus on social media (28.82%) than posting negatively about it (23.11%). When examining the tweets more closely, most positive tweets about monkeypox was that this virus is not severe and there is a low death rate caused by the disease. There are only few tweets about monkeypox that have negative sentiments suggesting that public hasn't panicked that much about the virus, and that too negative comments are of people discussing death caused by monkeypox, virus severity, infections caused due to it, whether it can be transmitted, vaccines available, whether it will be the next pandemic after COVID-19, if it is safe to travel, if it will affect the schools functioning, and whether it will affect the people lives. In light of the early stages of this epidemic, researchers and policymakers can use this study to better understand public concerns about monkeypox and develop effective awareness programs and control the outbreak so that general public concerns can be addressed. In order to raise awareness about the ongoing outbreak, it is imperative to teach the general public what

the disease symptoms are and when to seek medical attention (Farahat et al., 2022; Sv and Ittamalla, 2022).

## 7 Transmission

Over the past several years, numerous outbreaks of emerging infectious viral diseases originating from zoonotic animals including MERS-CoV, SARS-CoV-2, H7N9 (avian influenza), chikungunya virus, ebola virus, dengue virus, and Japanese encephalitis virus, which all are highly pathogenic have been reported. From time to time, international travelers reported to spread these viruses. SARS-CoV-2 was spread across countries largely due to international travel. In some non-African countries, monkeypox outbreaks have been reported recently. As of now, there are no links between monkeypox endemic areas and travel found in the current scenario. It is imperative to investigate the root cause of the current outbreaks as soon as possible. Furthermore, the focus must be placed on determining the zoonotic reservoir, zoonosis, spill overs from the host, etc., of this virus. Despite a lack of association between monkeypox outbreaks and air travel, it might be more likely that the disease will spread as a result of air travel as it is a contagious disease (Morens and Fauci, 2020; Wells et al., 2020; Bhattacharya et al., 2022; Bryer et al., 2022; Sharma R. et al., 2022; Begum et al., 2023; Varghese et al., 2023a).

A person who suffers from monkeypox can transmit it to others from the time period of beginning of symptoms until the complete healing of rash and formation of fresh skin layer (Farahat et al., 2022; Soriano and Corral, 2022; Vivancos et al., 2022; Zambrano et al., 2022). The possible causes for anyone to contract monkeypox up to its clinical manifestation are described in Figure 4. In addition to it, placental transmission can also spread the virus to a fetus while a mother is pregnant. Current spread has disproportionately affected gay, men who have sexual relations with men and bisexual men by developing a vesicular pustular rash or lesions on genital, suggesting that sexual networks are amplifying transmission and close contact is believed to constitute a reason of disease transmission (Farahat et al., 2022). This rash typically occurs on the perennial area and genitals, suggesting that it was transmitted sexually, but it can be mistaken for molluscum contagiosum, chancre, herpes simplex infection or granuloma inguinale (Farahat et al., 2022; Soriano and Corral, 2022; Vivancos et al., 2022; Zambrano et al., 2022).

Moreover, infected human fecal sample can also contain monkeypox virus DNA, according to a recent small study, which may provide yet another potential route for viral transmission. Since some animals (such as rodents) might be infected with the virus as they consume human waste that is laden with the virus, thus causing new infected wild animal populations to establish themselves in traditionally non-endemic areas (Murphy and Ly, 2022; Peiro-Mestres et al., 2022).

Researchers are investigating whether monkeypox can be spread when a person does not have symptoms, or if people with monkeypox symptoms are more likely to spread the virus, and also



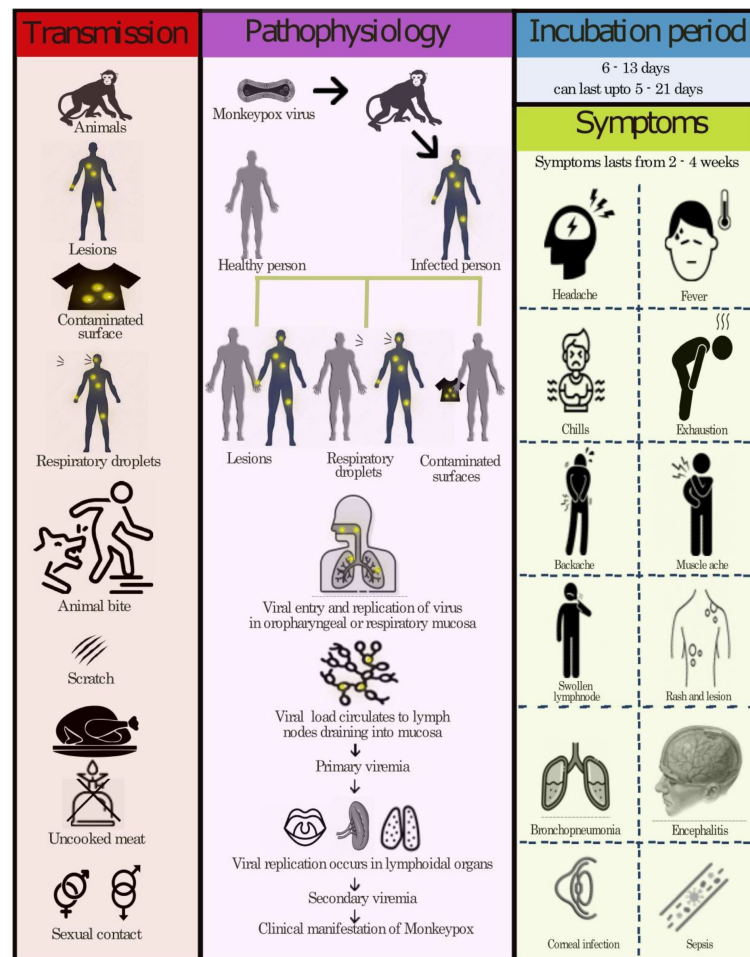


FIGURE 4  
Transmission, pathophysiology and symptoms of monkeypox.

to determine if the virus is spread more easily through feces, semen, vaginal fluid, or urine of symptomatic patient. To date, the disease seems to be having difficulties spreading effectively, however, the possibility that it can be transmitted through intimate or sexual contact ought to alarm infectious disease specialists in conducting further research to determine how the disease spreads so it can be prevented from spreading worldwide (Zambrano et al., 2022).

## 8 Clinical manifestation

Most monkeypox cases are self-limiting, with clinical manifestation as detailed in Figure 4. In children, complications are more likely to occur if they have been exposed to a high level of virus exposure, they have a poor health status, and they have complications of a severe nature. There is a possibility that underlying immune deficiencies will result in worse outcomes. In spite of vaccination against smallpox being protective in the past, now that campaigns of smallpox vaccination have stopped since the disease was eradicated globally, young people may be more susceptible to monkeypox. In monkeypox, lymphadenopathy

distinguishes it from other similar diseases (chickenpox, measles, smallpox) and the skin eruption usually appears within 1-3 days of the fever onset. The rash can manifest as a pimple or blister and may be itchy or painful. Some patients may experience all symptoms at once, whereas others may experience only a few. Also, it affects the mucous membranes of the oral cavity, the genitalia and the conjunctiva. The disease begins with macules (flat lesions) then progresses to papules (slightly raised firm lesions), pustules (fluid filled yellow lesions), vesicles (fluid-filled clear lesions) and crusts that fall off over time. In some cases, there can be few to several thousand lesions. Severe cases can result in large areas of skin sloughing off caused by the coalescence of lesions (MacNeil et al., 2009; Adler et al., 2022; European Medicines Agency, 2022; Gilbourne et al., 2022; Monkeypox: What to know, 2022).

Asymptomatic infection may occur in some cases, but it is not known to what extent. In the general population, monkeypox has historically had a case fatality rate between 0 and 11%, with a higher rate among younger children. Recent years have seen a 3–6% case fatality rate (Ministry of Health and Family Welfare, 2020).

As a result of monkeypox associated encephalitis, patients often experience pharyngitis, fever, anorexia, headache, weakness,

adenopathy, and a vesiculo-papular rash. A very slow electroencephalogram and diffuse oedema found on cortical magnetic resonance imaging were associated with amplification of meninges in the thalamus and partial cortex as well as signal abnormalities. However, within 5-6 days polymorphonuclear pleocytosis in cerebrospinal fluid (CSF) may decrease and primarily consist of lymphocytes (Shafaati and Zandi, 2022).

## 9 Differential diagnosis

When considering the differential diagnosis, other rash illnesses should also be considered, such as measles, chickenpox, scabies, bacterial infections, and medications associated allergies. When monkeypox is in its prodromal stage, lymphadenopathy distinguishes it from chickenpox or smallpox (World Health Organization, 2022).

A monkeypox sample must be collected by health workers and transported safely to a laboratory that has the necessary capabilities if monkeypox is suspected. A laboratory test and the type of specimen determine whether monkeypox is confirmed or not. It is therefore imperative that specimens are packaged and shipped must comply with international and national regulations. In terms of accuracy and sensitivity, polymerase chain reaction (PCR) is the preferred laboratory test. Ideally, monkeypox diagnostic samples should come from skin lesions such as vesicles, pustules, and crusts. Biopsies can be performed where feasible. Keeping lesions cold and storing them in dry and sterile tubes (no viral transport media) is essential. But, due to the short duration of viremia, blood tests for PCR are usually inconclusive and should not be routinely conducted in patients of monkeypox after symptoms begin (Ministry of Health and Family Welfare, 2020).

Also, serological cross-reactivity between orthopoxviruses makes antibody and antigen detection method ineffective from providing monkeypox specific confirmation. Hence it is not recommended to use serology or antigen detection methods for case investigation where resources are limited. Furthermore, a false positive result may also result from recent vaccination with an orthopoxvirus vaccine (e.g. those vaccinated before smallpox eradication or more recently due to a higher risk). So, for interpretation of test results, patient symptoms information must be included with specimens (Reed et al., 2004; Reynolds et al., 2006; Dubois and Slifka, 2008). It may be helpful to detect orthopoxvirus induced encephalitis. A CSF IgM reaction against orthopoxvirus may help detect encephalitis caused by orthopoxvirus (Sejvar et al., 2004).

## 10 Prevention strategies

Educating people about risk factors and ways to reduce exposure is the primary strategy for preventing monkeypox (Figure 5). Research is currently being conducted to determine whether vaccination is an appropriate and feasible preventative or

control measure against monkeypox. To protect the public's health, it is important to investigate all possible modes of transmission since the source of this outbreak is still being investigated. Many countries have or developing policies that offer vaccines to health workers, laboratory personnel, and rapid response teams who may be at risk (Health ministry issues guidelines for monkeypox management - the statesman, 2022).

Also to reduce the risk of transmission between humans, surveillance and rapid detection of new cases are crucial for outbreak containment. Standard infection control precautions should be followed by health workers caring for patients or handling specimens from those patients with monkeypox virus infection. The patient should be cared for by persons previously vaccinated against smallpox if possible. Make sure you are using appropriate personal protective equipment (PPE) when caring for those with symptoms, including gloves, a mask, and a gown. Personnel who are trained and equipped with the proper equipment should handle samples suspected of being infected with monkeypox virus. According to WHO guidelines for transporting infectious substances, patient specimens must be packaged triple to ensure their safety (Health ministry issues guidelines for monkeypox management - the statesman, 2022). Keep your sexual partner/s informed about any recent illness, including sores or rashes, and avoid close contact with anyone who has symptoms such as sores or rashes. To reduce the risk of a resurgence of infection, a 21-day self-isolation period and other preventive measures have been implemented (UK Health Security Agency, 2022).

Furthermore to prevent monkeypox, some countries have enacted regulations restricting rodent and non-human primate importation. Monkeypox infected captive animals or that might have come into contact with them should be quarantined immediately, handle with standard precautions, and observed for 30 days to monitor monkeypox symptoms (Health ministry issues guidelines for monkeypox management - the statesman, 2022).

## 11 Therapeutics

A specific treatment does not exist for monkeypox viral infections. Monkeypox and smallpox viruses have genetic similarities, so smallpox related antiviral drugs and vaccines may be effective against monkeypox. It is essential that patients receive fluids and food in order to maintain a healthy nutritional status and infections caused by secondary bacteria should be treated accordingly (Health ministry issues guidelines for monkeypox management - the statesman, 2022).

Tecovirimat, an antiviral agent previously approved by the United States Food and Drug Administration (FDA) for smallpox, has been now approved by the European Medicines Agency (EMA) for treatment of monkeypox after animal and human studies. Tecovirimat (previously ST-246), a small molecule that inhibits viral egress, has been demonstrated to be

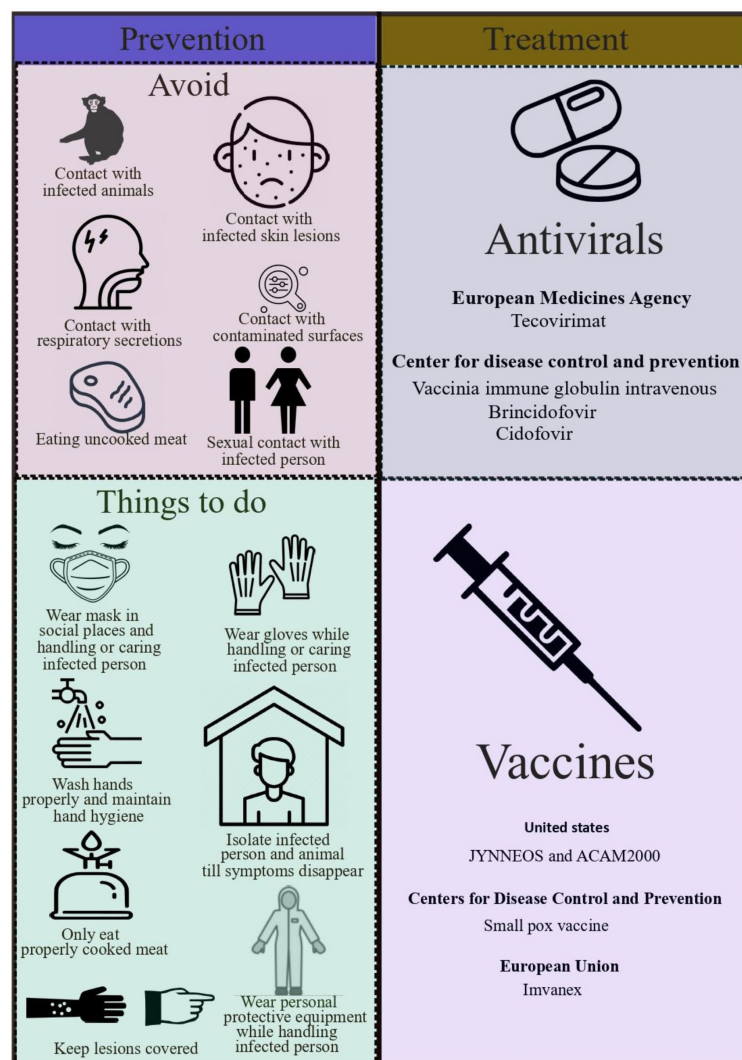


FIGURE 5  
Representing prevention and treatment of monkeypox.

effective against vaccinia, cowpox, camelpox, ectromelia (mousepox), and variola viruses (Yang et al., 2005). Through screening of more than 350,000 compounds, tecovirimat was discovered to target a gene that produces p37, an envelope protein essential for extracellular virus production (Bolken and Hruby, 2010). In mice, tecovirimat was proven to be effective and safe when administered orally twice daily at 50 mg/kg of body weight for 14 days before or shortly after infection. When used at a concentration (EC50) of  $\leq 0.07 \mu\text{M}$ , it suppresses viral multiplication by 50% in *in vitro* (Quenelle et al., 2007). In a ground squirrel model of disease, tecovirimat was effective in saving all animals that were given the drug on days 0, 1, 2, and 3; in contrast, all animals in the placebo group died (Nalca et al., 2008). It was clear from these findings that further human studies were necessary. In patients with weakened immune systems, antivirals such as tecovirimat may be helpful in preventing severe

illness. If tecovirimat will be used for patient care, WHO recommends monitoring it in a clinical research setting and have prospective data collection (Centers for Disease Control and Prevention, 2022; World Health Organization, 2022). Recently, Phase 1 and Phase 2 clinical trials involving an oral formulation of it was funded by National Institute of Allergy and Infectious Disease (NIAID and Biomedical Advanced Research and Development Authority (BARDA), part of the USA Department of Health and Human Services (NIH: National Institute of Allergy and Infectious Diseases, 2022).

Monkeypox can be prevented through vaccination if administered before or soon after exposure. There are currently two monkeypox vaccines available in the USA through the Strategic National Stockpile: JYNNEOS and ACAM2000. For adults 18 years and older, JYNNEOS is licensed. At least four weeks apart, two doses have to be administered in the upper arm. Itching, redness

and swelling are the most common reactions people have at the injection site after receiving the JYNNEOS vaccine. Public health has prioritized the JYNNEOS vaccine for the following groups: known close contacts of monkeypox cases identified by case investigations, tracing of contact, and assessments of risk exposure, and for individuals who attended an event where monkeypox was present. Advisory committee on immunization practices (ACIP) also recommends monkeypox vaccinations for laboratory and clinical workers who conduct monkeypox testing and collect monkeypox specimens (Centers for Disease Control and Prevention, 2022). Moreover, European Union (EU) has also approved Imvanex as a vaccine against monkeypox disease as of 22 July 2022. Later, Imvanex has been authorized for the treatment of smallpox and vaccinia virus in the EU (European Medicines Agency, 2022).

Furthermore, the Center for Disease Control and Prevention (CDC) recommends administration of vaccinia immune globulin intravenous (VIGIV), cidofovir and Brincidofovir to treat monkeypox. Earlier, VIGIV was used for treating complications caused by vaccinating against vaccinia, such as generalized vaccinia severe, eczema vaccinatum, vaccinia infections among skin diseases, progressive vaccinia and aberrant infections caused by vaccinia virus (except in isolated cases of keratitis). And as an antiviral, FDA has approved cidofovir to treat cytomegalovirus (CMV) retinitis among AIDS patients and Brincidofovir for treating smallpox in adults and children, including neonates since June, 4, 2021. There is a possibility that Brincidofovir has a better safety profile than cidofovir. There have been no serious renal toxic effects or other adverse reactions associated with Brincidofovir treatment for cytomegalovirus infection (Figure 5). Dose and possible

mechanism of these vaccines are represented in Figure 6 (Centers for Disease Control and Prevention, 2022).

Despite their effectiveness in animal studies against orthopoxviruses, no data indicate that they are effective in humans infected with monkeypox virus. Patients with severe T-cell deficiencies and who are contraindicated from smallpox vaccination after monkeypox exposure should take VIGIV. Cidofovir or brincidofovir should be given to treat monkeypox outbreaks in patients who have severe immunodeficiency (Kugelman et al., 2014; Centers for Disease Control and Prevention, 2022). All these vaccines suggested to be used in monkeypox should be further clinically proved.

## 12 In silico findings: Possible drug targets

In silico studies have shown that the genome of monkeypox are identical to the central regions that encode essential enzymes and proteins to the genome of smallpox. Despite the fact that monkeypox genome nomenclature resembles universal nomenclature, certain regions differ encoding for virulence. There is a great deal of research being done on the vaccinia virus, as it is used in vaccinations against other types of poxviruses and has lower risk than smallpox. Each of the three agents of monkeypox, smallpox, and vaccinia has nearly 197, 186, and 190kb of genome size respectively. The genomes of all poxviruses are linear and have double-stranded DNAs. Since other poxvirus homologues have similar characteristics and naming problems, the authors of that study refer to their targets by the universal nomenclature gene name based on the vaccinia

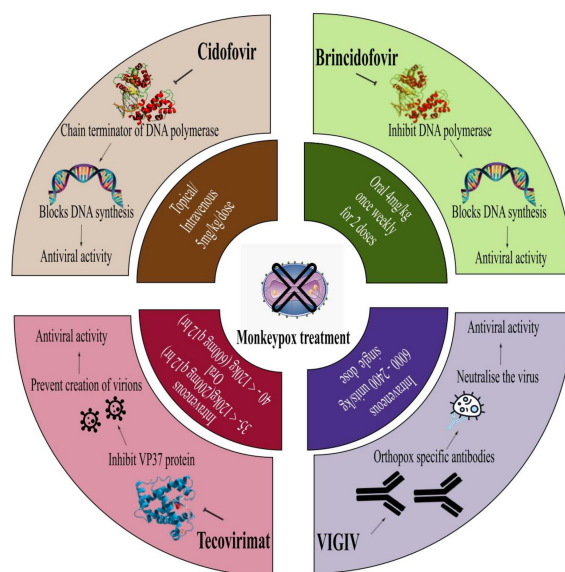


FIGURE 6  
Representing mechanism and dose of various monkeypox treatments.

TABLE 2 Overview of the clinical course and outcome of cases from recent outbreak of monkeypox.

Country	Age (years)	Gender	Comorbidity	Treatment	Clinical presentation	Infection site	Outcome	Hospitalization require (days)	References
Romania	26	Male	HIV	.*	Vesicular and pustular rash, few lesions, hyperemia of pharynx, pseudo-membranous appearance, thrush, enlarged lymph nodes	Rash & lesion- Buttocks, neck, trunk, sole, upper and lower limbs; Lymph nodes- cervical and inguinal region	.*	.*	(Oprea et al., 2022)
Italy	34	Male	HIV	Cephalosporins	Painless ulceration after sex with men, high fever, chills, painful enlargement, papulovesicles, itchy rashes,	Lymph node- left inguinal; Rashes- forehead, perianal, left tonsil	.*	.*	(Bířová et al., 2022)
Italy	33	Male	HIV	.*	Asthenia, malaise, anorexia, papular lesion, ulceration, respiratory symptoms, fever	Elbow, perianal	.*	.*	(Bířová et al., 2022)
Italy	26	Male	.*	Amoxicillin potassium clavunate 3 g/d for 8 days and cidofovir 5 mg/kg day 1 and 7	Chills, sweats, lesion followed by high fever, lymphadenopathy	Nose, limb	Recovery	Yes(8)	(Moschese et al., 2022)
Italy	35	Male	.*	Analgesic therapy	Vesicular rash followed by fever, lymphadenopathy	Head, trunk, limbs	Recovery	Yes (5)	(Moschese et al., 2022)
Italy	34	Male	HIV	None	Lesion followed by fever, lymphadenopathy	Perianal, face, foot, arm	Recovery	Yes(8)	(Moschese et al., 2022)
Italy	37	Male	HIV	Ceftriaxone 2 g/d for 7 days and daptomycin 500 mg/d for 5 days	Skin lesion followed by fever, headache, lymphadenopathy	Inguinal, scrotum, penis, face	Recovery	Yes(13)	(Moschese et al., 2022)
France	.*	Male	.*	No specific treatment	Fever, intense fatigue, chills, myalgia, several anal pain, lymphadenopathy and sore throat	.*	Recovery	No	(Vallée et al., 2022)
Taiwan	20	Male	.*	.*	Fever, muscle pain, sore throat, skin rash and lymph node swelling in the groin	.*	Recovery	No	(Yang et al., 2022)



TABLE 3 Representing data of case studies on monkeypox registered with [clinicaltrials.gov](https://clinicaltrials.gov).

NCT05476744	Viral clearance and epidemiological characteristics in patients with monkeypox	Observational	Cohort, prospective	Spain	No	100	Recruiting	Viral clearance in skin lesions, blood and oropharyngeal swabs
NCT05443867	Monkeypox a symptomatic shedding: evaluation by self-sampling MPX-ASSESS	Observational	Cohort, prospective	Belgium	No	140	Recruiting	Secondary attack rate of monkeypox virus infection in contacts, defined by PCR positivity on any sample, rate of seroconversion in contacts, defined as a positive IgG (immunoglobulineG) for monkeypox and proportion of seroconversion in PCR positive contacts vs PCR negative.
NCT05438953	Follow-up of contact at risk of monkeypox infection: a prospective cohort study	Interventional	Non-randomized, parallel assignment, open label, prevention	France	MVA vaccine (IMVANEX® and JYNNEOS®)	226	Recruiting	Proportion of failure of MVA vaccine, assess early vaccine humoral immunogenicity and early vaccine humoral immunogenicity after one, two doses
NCT02977715	IMVAMUNE® smallpox vaccine in adult healthcare personnel at risk for monkeypox in the DRC	Interventional	Single group, open label, prevention	DRC	IMVAMUNE®	1600	Active, not recruiting	Proportion of participants who develop suspected or confirmed monkeypox virus infection following receipt of IMVAMUNE and proportion of participants who have Orthopoxvirus antibody responses on days 0, 14, 28, 42, 180, 365, 545, and 730 days after the receipt of the first dose of vaccine
NCT05058898	A one health study of monkeypox human infection	Observational	Case-control, prospective	Central African Republic	Blood samples, scabs and pus samples	280	Recruiting	Proportion of monkeypox cases occurring following interhuman exposures, zoonotic exposures, measurement of the effective reproduction rate R in CAR according to the level of immunity (smallpox vaccine immunity or Orthopoxvirus-related post disease immunity)
NCT03745131	Cohort study of healthcare workers receiving Imvanex®	Observational	Cohort, prospective	United kingdom	Blood draw	120	Completed	Antibody responses to first dose of Imvanex®, antibody titres following first dose of Imvanex® and antibody responses to second dose of Imvanex®
NCT02080767	Tecovirimat (ST-246) treatment for orthopox virus exposure	Expanded access	–	–	Tecovirimat	–	Available	–
NCT00728689	Phase I trial of an investigational small pox medication	Interventional	Randomized, crossover, triple masking, treatment	United states	ST-246 Days 1 - 3	12	Completed and has results	Pharmacokinetic Parameters for a Single Dose of ST-246 form I vs. form V: $t_{1/2}$ , form I vs. form V: AUC <sub>0-τ</sub> and form I vs. form V: AUC <sub>0-∞</sub>
NCT number	Study title	Study type	Study design	Country	Interventions	Number enrolled	Status	Outcome measures

nomenclature. A50R, A48R, D13L protein trimer complex, F13L, and E are five poxvirus targets examined in that study. A number of studies and reviews have proposed that I7L be used as a useful target for intervention. Based on these targets, an in silico study was conducted on the active residues of monkeypox and eight potential repurposable drugs were identified. In this list of eight drugs, they find nilotinib for A50R, rutaecarpine and NMCT for A48R, naldemedine and hypericin for F13L, simeprevir for D13L, and lixivaptan and fosdagrocorat for I7L. As the drugs show promise in an in silico model, they should also be tested in clinical trials to see if they can combat disease effectively (Prazsák et al., 2018; Senkevich et al., 2021; Akash et al., 2023; Varghese et al., 2023b).

## 13 Case studies and therapeutic intervention

Few case studies cases pertaining to this outbreak of monkeypox available online are discussed below in Table 2 to understand the presentation and treatment provided. It is crucial for health authorities and clinicians to take into account the diagnosis of monkeypox in all patients, as cases in which patients have other sexually transmitted infections make it difficult to diagnose. For this reason, clinicians should always test suspected cases for monkeypox as part of their differential diagnosis. Further, it was noticed that antibiotics, antivirals and analgesics are given to these patients and recovery is shown. Although, this data is insufficient to propose any valid treatment, but these leads can be taken in consideration and validate in more number of patients. Also there are 8 studies yet found to be registered at clinicaltrial.gov that are related to monkeypox. The studies are compiled in Table 3. Among them are three interventional studies (IMVAMUNE<sup>®</sup>, ST-246, MVA vaccine (IMVANEX<sup>®</sup> and JYNNEOS<sup>®</sup>)), four observational studies, and one study to expand access to tecovirimat. Recruitment of patients are still ongoing for the studies (Search of: Monkeypox - list results - ClinicalTrials.gov, 2022). In future, the findings of these studies will hopefully provide some scientific results.

## 14 Possible plant-based strategies and probable mechanism involved to manage upcoming monkeypox cases

Besides providing scaffolding for cells and facilitating cellular long-distance traffic, microtubules serve as important components of multiple biological processes. It is astounding that viruses are often able to move actively into cells by using the cytoskeleton transportation machinery. As part of their replication cycle, viruses often interact with the cytoskeleton and require an intact microtubule network. Microtubule-dependent motors are involved in transporting intact virions and capsids to replication sites and exiting replication sites to the plasma membrane for some viruses. Upon maturation of the

endosomes, some viruses move along microtubules with a characteristic vesicular motion that targets either kinesins or dyneins. Pharmacological modulation of microtubules has been hypothesized to interfere with virus replication and spread, demonstrating their potential as broad-spectrum antivirals. In contrast, an pharmacological interventions against viral infections must be tightly controlled in order to prevent the compromise of physiological functions of cells. Therefore, we suggest microtubule targeting agents to inhibit viral replication in monkeypox (Figure 7) (Vale, 1987; Gundersen and Cook, 1999; Ridley et al., 2003; Khodjakov and Rieder, 2009; Mogilner and Keren, 2009; van der Vaart et al., 2009; Stehbens and Wittmann, 2012; Zulkipli et al., 2015).

Compounds targeted at microtubules from natural sources and synthetic compounds such as Colchicine, Nocodazole, Vinblastine, Paclitaxel, Vincristine, Podophyllotoxin, Combretastatins, Noscapine, Vindesine, Vinorelbine, Vinflunine, Docetaxel, Cabazitaxel, Larotaxel, Tesetaxel, Ombrabulin, Fosbretabulin, Crolibulin and Verubulin are potent antiviral leads that can also be an effective treatment for monkeypox (Kaul et al., 2019).

Also, the traditional use of several plant species and their extracts investigated for their antiviral properties has been documented. An array of plant extracts including *Pterocaulon sphacelatum*, *Dianella longifolia* var. *grandis*, *Euphorbia australis*, *Scaevola spinescens*, *Pittosporum phylliraeoides* var. *Microcarpa*, *Azadirachta indica*, *Eremophila latrobei* subsp. *Glabra*, *Opuntia streptacantha*, *Nerium indicum*, *Bergenia ligulata* and *Holoptelia integrifolia* exhibited antiviral effects towards a variety of DNA viruses in experimental models. The fact that monkeypox is a DNA virus makes it a viable candidate for inhibiting actions of these herbs (Semple et al., 1998; Abubakar et al., 2022). Furthermore, a study suggests that *Acacia nilotica* (L.) Delile, *Adansonia digitata* L., *Aframomum melegueta* K. Schum., *Allium sativum* L., *Alstonia boonei* De Wild, *Anogeissus leiocarpus* (DC.) Guill. & Perr., *Azadirachta indica* A. Juss., *Balanites aegyptiaca* (L.) Delile, *Calotropis procera* (Aiton) Dryand, *Carica papaya*, *Cissus populnea* Guill. & Perr., *Citrullus lanatus* (Thunb.) Matsum. & Nakai, *Combretum micranthum* G. Don., *Detarium senegalense* J.F. Gmel., *Diospyros mespiliformis* Hochst. ex A.DC., *Eleusine coracana* (L.) Gaertn., *Euphorbia hirta* L., *Ficus platyphylla* Delile, *Ficus polita* Vahl, *Guiera senegalensis* J.F. Gmel., *Lagenaria breviflora* (Benth.) Roberty, *Lawsonia inermis* L., *Mangifera indica*, *Maytenus senegalensis* (Lam.) Exell, *Momordica charantia* L., *Moringa oleifera* Lam., *Nigella sativa* L., *Olea europea* L., *Parinari macrophylla* Sabine, *Piper guineense* Schumach. & Thonn., *Sterculia setigera* Delile, *Tamarindus indica*, *Terminalia avicenoides* Guill. & Perr., *Vernonia amygdalina*, *Vitellaria paradoxa* C.F. Gaertn, *Viscum album* L. and *Ziziphus mauritiana* Lam. were among the most commonly used plants for treating monkey pox in different country regions. As of now, monkeypox does not have a well-established and proven treatment. It is therefore essential to evaluate the molecular mechanism underlying these plant-based treatments and to verify their

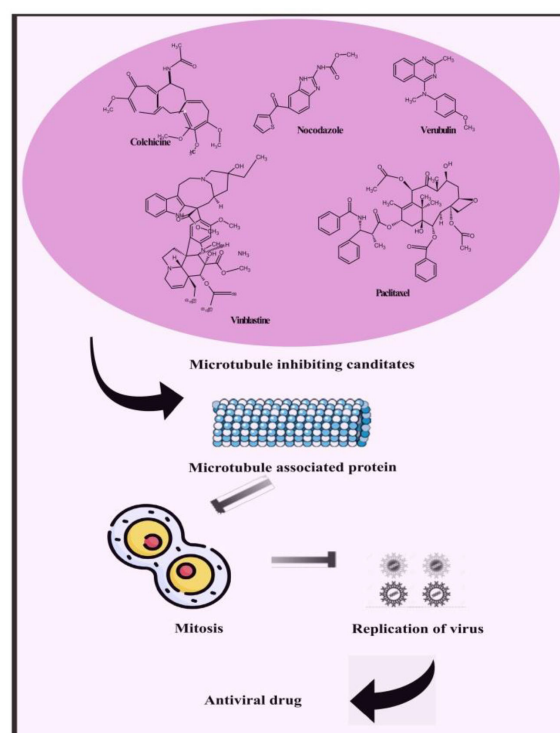


FIGURE 7

Representing possible leads constituents to mitigate monkeypox by microtubule inhibiting candidate.

pharmacological claims in different experimental models as to their ability to mitigate monkeypox virus (Jassim and Naji, 2003).

## 15 Conclusion and future perspectives

Each day, a growing number of monkeypox cases are reported, and more cases are expected in the near future. Most cases have been found among men, of whom several are gay or bisexual. A rash was the most common symptom that drove patients to seek medical attention. For the first time, a chain of transmission has been reported in Europe without any epidemiological connection to West or Central Africa. As compared to the Central African strain (ZAI-96), the nucleotide sequences of the three West African strains (SL-V70, COP-58, and WRAIR-61) differ by only 0.55–0.56%. BR-203, BR-209, and COP-C3L orthologs may play a role in the virulence differences between the strains. Multiple molecular mechanisms are stated in this study which explain how monkeypox viruses produce symptoms such as apoptosis by NOXA and caspase-3 upregulation, Bcl-2, PUMA, and PAK2 downregulation, targeting mitochondria, expression of histone, modification of histone posttranslational, dynamic exchanges of chromatin, packaging of DNA, ROCK1 and actin components regulating cytoskeletal dynamics. In order to reduce the risk of future outbreaks, it is imperative to act quickly and stop community transmission.

Several key features need to be acknowledged and addressed if we hope to prevent monkeypox and minimize unintentional harms. Additionally, it is likely that an early cluster is responsible for the most cases among men who have sexual relationship with men in the current outbreak. It is important to identify monkeypox cases early so that officials of public health can identify potential contacts, their vulnerability, isolate them appropriately, keep track of symptoms, and possibly administer vaccinations. Whenever dermatologists are able to evaluate a patient with papulo-vesiculo-pustular or vesiculo-pustular lesions, should be evaluated for presence of monkeypox. If a diagnosis is suspected or confirmed, public health systems should be contacted quickly. Public health authorities should therefore support those exposed to monkeypox or quarantined monkeypox patients, especially because the pathogen has a prolonged incubation period and is infectious for a long period of time. Studies have revealed the possible plants-based leads to mitigate the monkeypox. These leads should attract the attention and more studies to validate these treatments to help mitigating monkeypox pandemic.

## Author contributions

RuS, writing – original draft and formal analysis. K-TC, editing. RoS, conceptualization, editing and supervision.

All authors contributed to the article and approved the submitted version.

## Funding

This study was supported by a grant (no. RA112001) from the Tainan Municipal Hospital (managed by Show Chwan Medical Care Corporation), Tainan, Taiwan.

## Acknowledgments

We acknowledge Banaras Hindu University for their kind support and facilities provided.

## References

- Abubakar, I. B., Kankara, S. S., Malami, I., Danjuma, J. B., Muhammad, Y. Z., Yahaya, H., et al. (2022). Traditional medicinal plants used for treating emerging and re-emerging viral diseases in northern Nigeria. *Eur. J. Integr. Med.* 49, 102094. doi: 10.1016/j.eujim.2021.102094
- Adler, H., Gould, S., Hine, P., Snell, L. B., Wong, W., Houlihan, C. F., et al. (2022). Clinical features and management of human monkeypox: a retrospective observational study in the UK. *Lancet Infect. Dis.* 22(8), 1153–1162. doi: 10.1016/s1473-3099(22)00228-6
- Akash, S., Islam, M. R., Rahman, M. M., Hossain, M. S., Azad, M. A. K., and Sharma, R. (2023). Investigation of the new inhibitors by modified derivatives of pinocembrin for the treatment of monkeypox and marburg virus with different computational approaches. *Biointerface. Res. Appl. Chem.* 13(6), 534. doi: 10.33263/BRIAC136.534
- Alkhalil, A., Hammamieh, R., Hardick, J., Ichou, M. A., Jett, M., and Ibrahim, S. (2010). "Gene expression profiling of monkeypox virus-infected cells reveals novel interfaces for host-virus interactions." *Virol. J.* 7, 173. doi: 10.1186/1743-422X-7-173
- Al-Tawfiq, J. A., Barry, M., and Memish, Z. A. (2022). International outbreaks of monkeypox virus infection with no established travel: A public health concern with significant knowledge gap. *Travel. Med. Infect. Dis.* 49, 102364. doi: 10.1016/j.tmaid.2022.102364
- Anderson, M. G., Frenkel, L. D., Homann, S., and Guffey, J. (2003). A case of severe monkeypox virus disease in an American child: emerging infections and changing professional values. *Pediatr. Infect. Dis. J.* 22 (12), 1093–1096. doi: 10.1097/01.INF.0000101821.61387.A5
- As monkeypox surges, WHO urges reducing number of sexual partners. (2022). *Health news | Al Jazeera*. Available at: <https://www.aljazeera.com/news/2022/7/27/as-monkeypox-surges-who-urges-reducing-number-of-sexual-partners> (Accessed Aug. 13, 2022).
- Search of: Monkeypox - list results - ClinicalTrials.gov. (2022). Available at: <https://clinicaltrials.gov/ct2/results?cond=Monkeypox&term=&cntry=&state=&city=&dist> (Accessed Aug. 12, 2022).
- Beer, E. M., and Bhargavi Rao, V. (2019). A systematic review of the epidemiology of human monkeypox outbreaks and implications for outbreak strategy. *PLoS Negl. Trop. Dis.* 13 (10), e0007791. doi: 10.1371/JOURNAL.PNTD.0007791
- Begum, J. P. S., Ngangom, L., Semwal, P., Painuli, S., Sharma, R., and Gupta, A. (2023). Emergence of monkeypox: a worldwide public health crisis. *Hum. Cell.* 7, 1–17. doi: 10.1007/s13577-023-00870-1
- Bhattacharya, M., Dhama, K., and Chakraborty, C. (2022). Recently spreading human monkeypox virus infection and its transmission during COVID-19 pandemic period: A travelers' prospective. *Travel. Med. Infect. Dis.* 49, 102398. doi: 10.1016/j.tmaid.2022.102398
- Bířová, B., Veselý, D., and Trojánec, M. (2022). And f. rob, "Coinfection of syphilis and monkeypox in HIV positive man in Prague, Czech republic." *Travel. Med. Infect. Dis.* 49, 102368. doi: 10.1016/j.tmaid.2022.102368
- Bolken, T. C., and Hruby, D. E. (2010). Tecovirimat for smallpox infections." *Drugs Today (Barc)*. 46 (2), 109–117. doi: 10.1358/DOT.2010.46.2.1437244
- Breman, J. G., Kalisa-Ruti, Steniowski, M. V., Zanolto, E., Gromyko, A. I., and Arita, I. (1980). Human monkeypox, 1970–79. *Bull. World Health Organ* 58 (2), 165.
- Bryer, J. S., Freeman, E. E., and Rosenbach, M. (2022). Monkeypox emerges on a global scale: A historical review and dermatologic primer. *J. Am. Acad. Dermatol.* 87(5), 1069–1074. doi: 10.1016/j.jaad.2022.07.007
- Bunge, E. M., Hoet, B., Chen, L., Lienert, F., Weidenthaler, H., Baer, L. R., et al. (2022). The changing epidemiology of human monkeypox—a potential threat? a systematic review. *PLoS Negl. Trop. Dis.* 16 (2), e0010141. doi: 10.1371/JOURNAL.PNTD.0010141
- Carter, G. C., Law, M., Hollinshead, M., and Smith, G. L. (2005). Entry of the vaccinia virus intracellular mature virion and its interactions with glycosaminoglycans. *J. Gen. Virol.* 86 (5), 1279–1290. doi: 10.1099/VIR.0.80831-0
- Centers for Disease Control and Prevention (CDC) (1997). Human monkeypox – Kasai oriental, democratic republic of Congo, February 1996–October 1997. *MMWR. Morb. Mortal. Wkly. Rep.* 46 (49), 1168–1171.
- Centers for Disease Control and Prevention (CDC). (2003a). Multistate outbreak of monkeypox—Illinois, Indiana, and Wisconsin, 2003. *MMWR Morb Mortal Wkly Rep.* 52 (23), 537–40.
- Centers for Disease Control and Prevention (CDC). (2003b) Update: Multistate outbreak of monkeypox — Illinois, Indiana, Kansas, Missouri, Ohio, and Wisconsin, 2003. *MMWR Morb Mortal Wkly Rep* 52 (27), 642–646.
- Centers for Disease Control and Prevention (CDC). (2022). *Clinical recognition*. Available at: <https://www.cdc.gov/poxvirus/monkeypox/clinicians/clinical-recognition.html> (Accessed Aug. 13, 2022).
- Centers for Disease Control and Prevention. (2022). U.S. monkeypox outbreak. Available at: <https://www.cdc.gov/poxvirus/monkeypox/response/2022/index.html> (Accessed Aug. 12, 2022).
- Centers for Disease Control and Prevention. (2022). Patient's Guide to Mpox Treatment with Tecovirimat. Available at: <https://www.cdc.gov/poxvirus/monkeypox/treatment.html> (Accessed Aug. 14, 2022).
- Chen, N., Li, G., Liszewski, M. K., Atkinson, J. P., Jahrling, P. B., Feng, Z., et al. (2005). Virulence differences between monkeypox virus isolates from West Africa and the Congo basin. *Virology* 340 (1), 46–63. doi: 10.1016/j.virol.2005.05.030
- Comparative pathology of north American and central African strains of monkeypox virus in a ground squirrel model of the disease. (2022). *PubMed*. (Accessed Aug. 13, 2022).
- Dhawan, M., Priyanka, and Choudhary, O. P. (2022). Emergence of monkeypox: Risk assessment and containment measures. *Travel. Med. Infect. Dis.* 49, 102392. doi: 10.1016/j.tmaid.2022.102392
- Dubois, M. E., and Slifka, M. K. (2008). Retrospective analysis of monkeypox infection. *Emerg. Infect. Dis.* 14 (4), 592. doi: 10.3201/EID1404.071044
- Elmore, S. (2007). Apoptosis: A review of programmed cell death. *Toxicol. Pathol.* 35 (4), 495. doi: 10.1080/01926230701320337
- Elsevier – clinical overviews. (2022). *Monkeypox*. Available at: <https://elsevier.health/en-US/preview/monkeypox-co> (Accessed Aug. 13, 2022).
- Erez, N., Achdout, H., Milrot, E., Schwartz, Y., Wiener-Well, Y., Paran, N., et al. (2019). Diagnosis of imported monkeypox, Israel, 2018. *Emerg. Infect. Dis.* 25 (5), 980–983. doi: 10.3201/EID2505.190076

## Conflict of interest

The authors declare that the research was conducted in the absence of any commercial or financial relationships that could be construed as a potential conflict of interest.

## Publisher's note

All claims expressed in this article are solely those of the authors and do not necessarily represent those of their affiliated organizations, or those of the publisher, the editors and the reviewers. Any product that may be evaluated in this article, or claim that may be made by its manufacturer, is not guaranteed or endorsed by the publisher.



- European Medicines Agency. (2022). Monkeypox | European Medicines Agency. Available at: [https://www.ema.europa.eu/en/human-regulatory/overview/public-health-threats/monkeypox#availability-of-critical-medicines-\(new\)-section](https://www.ema.europa.eu/en/human-regulatory/overview/public-health-threats/monkeypox#availability-of-critical-medicines-(new)-section) (Accessed Aug. 12, 2022).
- Everett, H., Barry, M., Sun, X., Lee, S. F., Frantz, C., Berthiaume, L. G., et al. (2002). The myxoma poxvirus protein, M11L, prevents apoptosis by direct interaction with the mitochondrial permeability transition pore. *J. Exp. Med.* 196 (9), 1127–1139. doi: 10.1084/JEM.20011247
- Everett, H., and McFadden, G. (2002). Poxviruses and apoptosis: a time to die. *Curr. Opin. Microbiol.* 5 (4), 395–402. doi: 10.1016/S1369-5274(02)00340-5
- Farahat, R. A., Ali, I., Al-Ahdal, T., Benmelouka, A. Y., Albakri, K., El-Sakka, A. A., et al. (2022). Monkeypox and human transmission: Are we on the verge of another pandemic? *Travel. Med. Infect. Dis.* 49, 102387. doi: 10.1016/J.TMAID.2022.102387
- Farahat, R. A., Sah, R., El-Sakka, A. A., Benmelouka, A. Y., Kundu, M., Labieb, F., et al. (2022). Human monkeypox disease (MPX). *Infez Med.* 30 (3), 372–391. doi: 10.53854/liim-3003-6
- Fenner, F., Henderson, D. A., Arita, I., Jezek, Z., and Ladnyi, I. D. (1988). Smallpox and its eradication. World Health Organization. Available at: <https://apps.who.int/iris/handle/10665/39485> (Accessed Aug. 12, 2022).
- Formenty, P., Muntasir, M. O., Damon, I., Chowdhary, V., Opoka, M. L., Monimart, C., et al. (2010). Human monkeypox outbreak caused by novel virus belonging to Congo basin clade, Sudan, 2005. *Emerg. Infect. Dis.* 16 (10), 1539–1545. doi: 10.3201/eid1610.100713
- Giancotti, F. G., and Ruoslahti, E. (1999). Integrin signaling. *Sci.* (80-). 285 (5430), 1028–1032. doi: 10.1126/SCIENCE.285.5430.1028
- Gilbourne, M., Coulson, L., and Mitchell, G. (2022). *Monkeypox: Symptoms, treatment, and outcome* — DermNet. Available at: <https://dermnetnz.org/topics/monkeypox> (Accessed Aug. 12, 2022).
- Gundersen, G. G., and Cook, T. A. (1999). Microtubules and signal transduction. *Curr. Opin. Cell Biol.* 11 (1), 81–94. doi: 10.1016/S0955-0674(99)80010-6
- Health ministry issues guidelines for monkeypox management - the statesman. (2022). Available at: <https://www.thestatesman.com/india/health-ministry-issues-guidelines-monkeypox-management-1503090385.html> (Accessed Aug. 13, 2022).
- Hengartner, M. O. (2000). The biochemistry of apoptosis. *Nat* 407 (6805), 770–776. doi: 10.1038/35037710
- Huhn, G. D., Bauer, A. M., Yorita, K., Graham, M. B., Sejvar, J., Likos, A., et al. (2005). Clinical characteristics of human monkeypox, and risk factors for severe disease. *Clin. Infect. Dis.* 41 (12), 1742–1751. doi: 10.1086/498115
- Hutson, C. L., Lee, K. N., Abel, J., Carroll, D. S., Montgomery, J. M., Olson, V. A., et al. (2007). Monkeypox zoonotic associations: insights from laboratory evaluation of animals associated with the multi-state US outbreak. *Am. J. Trop. Med. Hyg.* 76 (4), 757–68.
- Hutson, C. L., Olson, V. A., Carroll, D. S., Abel, J. A., Hughes, C. M., Braden, Z. H., et al. (2009). A prairie dog animal model of systemic orthopoxvirus disease using West African and Congo basin strains of monkeypox virus. *J. Gen. Virol.* 90 (Pt 2), 323–333. doi: 10.1099/VIR.0.005108-0
- Jassim, S. A. A., and Naji, M. A. (2003). Novel antiviral agents: a medicinal plant perspective. *J. Appl. Microbiol.* 95 (3), 412–427. doi: 10.1046/J.1365-2672.2003.02026.X
- Jezek, Z., and Fenner, F. (1988). Human monkeypox, monographs in virology. *Monographs Virol.* 17, 127–134.
- Jezek, Z., Grab, B., Szczeniowski, M. V., Paluku, K. M., and Mutombo, M. (1988). Human monkeypox: secondary attack rates. *Bull. World Health Organ.* 66 (4), 465.
- Jezek, Z., Szczeniowski, M., Paluku, K. M., and Mutombo, M. (1987). Human monkeypox: clinical features of 282 patients. *J. Infect. Dis.* 156 (2), 293–298. doi: 10.1093/INFDIS/156.2.293
- Kantele, A., Chickering, K., Vapalahti, O., and Rimoin, A. W. (2016). Emerging diseases—the monkeypox epidemic in the democratic republic of the Congo. *Clin. Microbiol. Infect.* 22 (8), 658–659. doi: 10.1016/J.CMI.2016.07.004
- Kaul, R., Risinger, A. L., and Mooberry, S. L. (2019). Microtubule-targeting drugs: More than antimetabolites. *J. Nat. Prod.* 82 (3), 680–685. doi: 10.1021/ACS.JNATPROD.9B00105/ASSET/IMAGES/MEDIUM/NP-2019-00105P\_0002.GIF
- Khodakevich, L., Jezek, Z., and Kinzanzka, K. (1986). ISOLATION OF MONKEYPOX VIRUS FROM WILD SQUIRREL INFECTED IN NATURE. *Lancet* 327 (8472), 98–99. doi: 10.1016/S0140-6736(86)90748-8
- Khodjakov, A., and Rieder, C. L. L. (2009). Mitosis: too much of a good thing (can be bad). *Curr. Biol.* 19 (22), R1032–R1034. doi: 10.1016/J.CUB.2009.10.013
- Kozlov, M. (2018). 1053131562.
- Kraemer, M. U. G., Tegally, H., Pigott, D. M., Dasgupta, A., Sheldon, J., Wilkinson, E., et al. (2022). Tracking the 2022 monkeypox outbreak with epidemiological data in real-time. *Lancet Infect. Dis.* 22 (7), 941–942. doi: 10.1016/S1473-3099(22)00359-0
- Kugelman, J. R., Johnston, S. C., Mulembakani, P. M., Kisaal, N., Lee, M. S., Koroleva, G., et al. (2014). Genomic variability of monkeypox virus among humans, democratic republic of the Congo - volume 20, number 2-February 2014 - emerging infectious diseases journal - CDC. *Emerg. Infect. Dis.* 20 (2), 232–239. doi: 10.3201/EID2002.130118
- Ladnyi, I. D., Ziegler, P., and Kima, E. (1972). A human infection caused by monkeypox virus in basankusu territory, democratic republic of the Congo. *Bull. World Health Organ.* 46 (5), 593.
- Lai, C.-C., Hsu, C.-K., Yen, M.-Y., Lee, P.-I., Ko, W.-C., and Hsueh, P.-R. (2022). Monkeypox: An emerging global threat during the COVID-19 pandemic. *J. Microbiol. Immunol. Infect.* 5(5), 787–794. doi: 10.1016/J.JMII.2022.07.004
- Learned, L. A., Reynolds, M. G., Wass, D. W., Li, Y., Olson, V. A., Karem, K., et al. (2005). Extended interhuman transmission of monkeypox in a hospital community in the republic of the congo, 2003. *Am. J. Trop. Med. Hyg.* 73 (2), 428–434. doi: 10.4269/AJTMH.2005.73.428
- León-Figueroa, D. A., Bonilla-Aldana, D. K., Pachar, M., Romani, L., Saldaña-Cumpa, H. M., Anchay-Zuloeta, C., et al. (2022). The never-ending global emergence of viral zoonoses after COVID-19? the rising concern of monkeypox in Europe, north America and beyond. *Travel. Med. Infect. Dis.* 49, 102362. doi: 10.1016/J.TMAID.2022.102362
- Ligon, B. L. (2004). Monkeypox: A review of the history and emergence in the Western hemisphere. *Semin. Pediatr. Infect. Dis.* 15 (4), 280. doi: 10.1053/JSPID.2004.09.001
- Likos, A. M., Sammons, S. A., Olson, V. A., Frace, A. M., Li, Y., Olsen-Rasmussen, M., et al. (2005). A tale of two clades: monkeypox viruses. *J. Gen. Virol.* 86 (Pt 10), 2661–2672. doi: 10.1099/VIR.0.81215-0
- Luna, N., Ramírez, A. L., Muñoz, M., Ballesteros, N., Patiño, L. H., Castañeda, S. A., et al. (2022). Phylogenomic analysis of the monkeypox virus (MPXV) 2022 outbreak: Emergence of a novel viral lineage? *Travel. Med. Infect. Dis.* 49, 102402. doi: 10.1016/J.TMAID.2022.102402
- Luo, Q., and Han, J. (2022). Preparedness for a monkeypox outbreak. *Infect. Med.* 1 (2), 124–134. doi: 10.1016/J.IMJ.2022.07.001
- MacNeil, A., Reynolds, M. G., and Damon, I. K. (2009). Risks associated with vaccinia virus in the laboratory. *Virology* 385 (1), 1–4. doi: 10.1016/J.VIROL.2008.11.045
- Massung, R. F., Liu, L. I., Qi, J., Knight, , et al. (1994). Analysis of the complete genome of smallpox variola major virus strain Bangladesh-1975. *Virology* 201 (2), 215–240. doi: 10.1006/VIRO.1994.1288
- McConnell, S. J., Herman, Y. F., Mattson, D. E., and Erickson, L. (1962). Monkey pox disease in irradiated cynomolgous monkeys. *Nat* 195 (4846), 1128–1129. doi: 10.1038/1951128a0
- McGlade, J., Brunkhorst, B., Anderson, D., Mbamalu, G., Settleman, J., Dedhar, S., et al. (1993). The n-terminal region of GAP regulates cytoskeletal structure and cell adhesion. *EMBO J.* 12 (8), 3073–3081. doi: 10.1002/J.1460-2075.1993.TB05976.X
- Merouze, F., and Lesoin, J. J. (1983). [Monkeypox: second human case observed in Ivory Coast (rural health sector of Daloa)]. *Medecine tropicale : Revue du Corps de sante colonial* 43 (2), 145–7.
- Mileto, D., Riva, A., Cutrera, M., Moschese, D., Mancon, A., Meroni, L., et al. (2022). New challenges in human monkeypox outside Africa: A review and case report from Italy. *Travel. Med. Infect. Dis.* 49, 102386. doi: 10.1016/J.TMAID.2022.102386
- Ministry of Health and Family Welfare, Government of India. (2020). Guidelines for management of monkeypox disease. Available at: Guidelines for Management of Monkeypox Disease.pdf (<https://mohfw.gov.in>).
- Mogilner, A., and Keren, K. (2009). The shape of motile cells. *Curr. Biol.* 19 (17), PR762–R771. doi: 10.1016/J.CUB.2009.06.053
- Monkeypox data explorer - our world in data. (2022). Available at: [https://ourworldindata.org/explorers/monkeypox?tab=table&time=2025-08-04&facet=none&Metric=Confirmed+cases&Frequency=Cumulative&Relative+to+population=false&country=~OWID\\_WRL](https://ourworldindata.org/explorers/monkeypox?tab=table&time=2025-08-04&facet=none&Metric=Confirmed+cases&Frequency=Cumulative&Relative+to+population=false&country=~OWID_WRL) (Accessed Aug. 12, 2022).
- Monkeypox: experts give virus variants new names. (2022). Available at: <https://www.who.int/news/item/12-08-2022-monkeypox-experts-give-virus-variants-new-names> (Accessed Oct. 31, 2022).
- Multi-country monkeypox outbreak: situation update. (2022). Available at: <https://www.who.int/emergencies/disease-outbreak-news/item/2022-DON396> (Accessed Aug. 12, 2022).
- Monkeypox update from AR Dept. of health - Arkansas medical society. (2022). Available at: <https://www.arkmed.org/news/2022/08/monkeypox-update-from-arkdept-of-health/> (Accessed Aug. 13, 2022).
- Monkeypox: What to know. (2022). Available at: <https://www.webmd.com/a-to-z-guides/monkeypox-what-know> (Accessed Aug. 12, 2022).
- Morens, D. M., and Fauci, A. S. (2020). Emerging pandemic diseases: How we got to COVID-19. *Cell* 182 (5), 1077–1092. doi: 10.1016/J.CELL.2020.08.021
- Moschese, D., Giacomelli, A., Beltrami, M., Pozza, G., Mileto, D., Reato, S., et al. (2022). Hospitalisation for monkeypox in Milan, Italy. *Travel. Med. Infect. Dis.* 49, 102417. doi: 10.1016/J.TMAID.2022.102417
- Mukinda, V., Mwema, G., Kilundu, M., Heymann, D., Khan, A. S., Esposito, J. J., et al. (1997). Re-emergence of human monkeypox in Zaire in 1996. *Lancet* 349 (9063), 1449–1450. doi: 10.1016/S0140-6736(05)63725-7
- Murphy, H., and Ly, H. (2022). The potential risks posed by inter- and intraspecies transmissions of monkeypox virus. *Virulence* 13 (1), 1681–1683. doi: 10.1080/21505594.2022.2127199



- Nalca, A., et al. (2008). Evaluation of orally delivered ST-246 as postexposure prophylactic and antiviral therapeutic in an aerosolized rabbitpox rabbit model. *Antiviral Res.* 79 (2), 121–127. doi: 10.1016/j.antiviral.2008.03.005
- Nalca, A., Rimoin, A. W., Bavari, S., and Whitehouse, C. A. (2005). Reemergence of monkeypox: prevalence, diagnostics, and countermeasures. *Clin. Infect. Dis.* 41 (12), 1765–1771. doi: 10.1086/498155
- Nichols, D. B., De Martini, W., and Cottrell, J. (2017). Poxviruses utilize multiple strategies to inhibit apoptosis. *Viruses* 9 (8), 215. doi: 10.3390/V9080215
- NIH: National Institute of Allergy and Infectious Diseases. (2022). Mpox (Formerly Monkeypox) Treatment. Available at: <https://www.niaid.nih.gov/diseases-conditions/monkeypox-treatment> (Accessed Oct. 31, 2022).
- Oprea, C., Ianache, I., Piscu, S., Tardei, G., Nica, M., Ceausu, E., et al. (2022). First report of monkeypox in a patient living with HIV from Romania. *Travel. Med. Infect. Dis.* 49, 102395. doi: 10.1016/j.TMAID.2022.102395
- Osorio, J. E., and Yuill, T. M. (2008). *Zoonoses* In: B. Mahy and M. van Regenmortel, editors. *Encyclopedia of Virology 3rd ed.* Elsevier Academic Press 485–495.
- Otu, A., Ebenso, B., Walley, J., Barceló, J. M., and Ochu, C. L. (2022). Global human monkeypox outbreak: atypical presentation demanding urgent public health action. *Lancet Microbe.* 3(8), e554–e555. doi: 10.1016/s2666-5247(22)00153-7
- Pawlak, G., and Helfman, D. M. (2002). Post-transcriptional down-regulation of ROCK1/Rho-kinase through an MEK-dependent pathway leads to cytoskeleton disruption in ras-transformed fibroblasts. *Mol. Biol. Cell* 13 (1), 336–347. doi: 10.1091/MBC.01-06-0302
- Peiró-Mestres, A., Fuertes, I., Camprubi-Ferrer, D., Marcos, M. Á., Vilella, A., Navarro, M., et al. (2022). Frequent detection of monkeypox virus DNA in saliva, semen, and other clinical samples from 12 patients, Barcelona, Spain, may to June 2022. *Euro. Surveill.* 27 (28), 2200503. doi: 10.2807/1560-7917.ES.2022.27.28.2200503
- Petersen, E., Kantele, A., Koopmans, M., Asogun, D., Yinka-Ogunleye, A., Ihekweazu, C., et al. (2019). Human monkeypox: Epidemiologic and clinical characteristics, diagnosis, and prevention. *Infect. Dis. Clin. North Am.* 33 (4), 1027–1043. doi: 10.1016/j.IDC.2019.03.001
- Pochynyuk, O., Stockand, J. D., and Staruschenko, A. (2007). Ion channel regulation by ras, rho, and rab small GTPases. *Exp. Biol. Med. (Maywood)*. 232 (10), 1258–1265. doi: 10.3181/0703-MR-76
- Prazsák, I., Tombácz, D., Szucs, A., Dénes, B., Snyder, M., and Boldogkoi, Z. (2018). Full genome sequence of the Western reserve strain of vaccinia virus determined by third-generation sequencing. *Genome Announc.* 6 (11), e01570-17. doi: 10.1128/GENOMEA.01570-17
- Quarleri, J., Victoria Delpino, M., and Galvan, V. (2022). Monkeypox: considerations for the understanding and containment of the current outbreak in non-endemic countries. *GeroScience* 2022, 1–9. doi: 10.1007/S11357-022-00611-6
- Quenelle, D. C., Buller, R. M., Parker, S., Keith, K. A., Hraby, D. E., Jordan, R., et al. (2007). Efficacy of delayed treatment with ST-246 given orally against systemic orthopoxvirus infections in mice. *Antimicrob. Agents Chemother.* 51 (2), 689–695. doi: 10.1128/AAC.00879-06
- Radonić, A., Metzger, S., Dabrowski, P. W., Couacy-Hymann, E., Schuenadel, L., Kurth, A., et al. (2014). “Fatal monkeypox in wild-living sooty mangabey, côte d’Ivoire, 2012.”. *Emerg. Infect. Dis.* 20 (6), 1009–1011. doi: 10.3201/EID2006.131329
- Reed, K. D., Melski, J. W., Graham, M. B., Regnery, R. L., Sotir, M. J., Wegner, M. V., et al. (2004). The detection of monkeypox in humans in the Western hemisphere. *N. Engl. J. Med.* 350 (4), 342–350. doi: 10.1056/NEJM04032299
- Reynolds, M. G., Yorita, K. L., Kuehnert, M. J., Davidson, W. B., Huhn, G. D., Holman, R. C., et al. (2006). Clinical manifestations of human monkeypox influenced by route of infection. *J. Infect. Dis.* 194 (6), 773–780. doi: 10.1086/505880
- Reynolds, M. G., McCollum, A. M., Nguete, B., Lushima, R. S., and Petersen, B. W. (2017). Improving the care and treatment of monkeypox patients in low-resource settings: Applying evidence from contemporary biomedical and smallpox biodefense research. *Viruses* 9 (12), 380. doi: 10.3390/V9120380
- Ridley, A. J., Schwartz, M. A., Burridge, K., Firtel, R. A., Ginsberg, M. H., Borisy, G., et al. (2003). Cell migration: integrating signals from front to back. *Science* 302 (5651), 1704–1709. doi: 10.1126/SCIENCE.1092053
- Rimoin, A. W., Mulembakani, P. M., Johnston, S. C., Lloyd Smith, J. O., Kitalu, N. K., Kinkela, T. L., et al. (2010). Major increase in human monkeypox incidence 30 years after smallpox vaccination campaigns cease in the democratic republic of congo.”. *Proc. Natl. Acad. Sci. U. S. A.* 107 (37), 16262–16267. doi: 10.1073/PNAS.1005769107/-/DCSUPPLEMENTAL
- Scaife, R. M., Job, D., and Langdon, W. Y. (2003). Rapid microtubule-dependent induction of neurite-like extensions in NIH 3T3 fibroblasts by inhibition of ROCK and cbl. *Mol. Biol. Cell* 14 (11), 4605. doi: 10.1091/MBC.E02-11-0739
- Sejvar, J. J., Chowdary, Y., Schomogyi, M., Stevens, J., Patel, J., Karem, K., et al. (2004). Human monkeypox infection: a family cluster in the midwestern united states. *J. Infect. Dis.* 190 (10), 1833–1840. doi: 10.1086/425039
- Semple, S. J., Reynolds, G. D., O’Leary, M. C., and Flower, R. L. P. (1998). Screening of Australian medicinal plants for antiviral activity. *J. Ethnopharmacol.* 60 (2), 163–172. doi: 10.1016/S0378-8741(97)00152-9
- Senkevich, T. G., Yutin, N., Wolf, Y. I., Koonin, E. V., and Moss, B. (2021). Ancient gene capture and recent gene loss shape the evolution of orthopoxvirus-host interaction genes. *MBio* 12 (4), e0149521. doi: 10.1128/MBIO.01495-21
- Shafaati, M., and Zandi, M. (2022). Monkeypox virus neurological manifestations in comparison to other orthopoxviruses. *Travel. Med. Infect. Dis.* 49, 102414. doi: 10.1016/J.TMAID.2022.102414
- Sharma, R., Kumar, P., Rauf, A., Chaudhary, A., Prajapati, P. K., Emran, T. B., et al. (2022). Mucormycosis in the COVID-19 environment: a multifaceted complication. *Front. Cell. Infect. Microbiol.* 964. doi: 10.3389/fcimb.2022.937481
- Sharma, V., Rai, H., Gautam, D. N. S., Prajapati, P. K., and Sharma, R. (2022). “Emerging evidence on omicron (B.1.1.529) SARS-CoV-2 variant.”. *J. Med. Virol.* 94 (5), 1876–1885. doi: 10.1002/JMV.27626
- Shchelkunov, S. N., Totmenin, A. V., Safronov, P. F., Mikheev, M. V., Gutorov, V. V., and Ryazankina, O. I. (2002). Analysis of the monkeypox virus genome. *Virology* 297 (2), 172–194. doi: 10.1006/VIRO.2002.1446
- Shchelkunov, S. N., Marennikova, S. S., and Moyer, R. W. (2005). Orthopoxviruses pathogenic for humans. *Orthopoxviruses. Pathog. Humans.*, 1–425. doi: 10.1007/B107126/COVER
- Simões, P., and Bhagani, S. (2022). A viewpoint: The 2022 monkeypox outbreak. *J. Virus Res.* 8 (2), 100078. doi: 10.1016/J.JVE.2022.100078
- Sklenovská, N., and Van Ranst, M. (2018). Emergence of monkeypox as the most important orthopoxvirus infection in humans. *Front. Public Heal.* 6. doi: 10.3389/FPUBH.2018.00241/PDF
- Soriano, V., and Corral, O. (2022). International outbreak of monkeypox in men having sex with men. *AIDS Rev.* 24 (2), 101–103. doi: 10.24875/AIDSREV.M22000051
- Stehbens, S., and Wittmann, T. (2012). Targeting and transport: how microtubules control focal adhesion dynamics. *J. Cell Biol.* 198 (4), 481–489. doi: 10.1083/JCB.201206050
- Sv, P., and Ittamalla, R. (2022). What concerns the general public the most about monkeypox virus? - a text analytics study based on natural language processing (NLP). *Travel. Med. Infect. Dis.* 49, 102404. doi: 10.1016/J.TMAID.2022.102404
- Thornhill, J. P., Barkati, S., Walmsley, S., Rockstroh, J., Antinori, A., Harrison, L. B., et al. (2022). Monkeypox virus infection in humans across 16 countries - April-June 2022. *N. Engl. J. Med.* 387(8), 679–691. doi: 10.1056/NEJM0A2207323
- Tomori, O., and Ogoina, D. (2022). Monkeypox: The consequences of neglecting a disease, anywhere. *Science* 377 (6612), 1261–1263. doi: 10.1126/SCIENCE.ADD3668
- Vale, R. D. (1987). Intracellular transport using microtubule-based motors. *Annu. Rev. Cell Biol.* 3, 347–378. doi: 10.1146/ANNUREV.CB.03.110187.002023
- UK Health Security Agency. (2022). Recommendations for the use of pre and post exposure vaccination during a monkeypox incident. Available at: <https://www.in.gr/wp-content/uploads/2022/05/Recommendations-for-use-of-pre-and-post-exposure-vaccination-during-a-monkeypox-incident.pdf>.
- Vallée, A., Farfour, E., and Zucman, D. (2022). Monkeypox virus: A novel sexually transmitted disease? a case report from France. *Travel. Med. Infect. Dis.* 49, 102394. doi: 10.1016/J.TMAID.2022.102394
- van der Vaart, B., Akhmanova, A., and Straube, A. (2009). Regulation of microtubule dynamic instability. *Biochem. Soc. Trans.* 37 (Pt 5), 1007–1013. doi: 10.1042/BST0371007
- Varghese, R., Patel, P., Kumar, D., and Sharma, R. (2023a). Climate change and glacier melting: risks for unusual outbreaks? *J. Travel. Med.* 31, taad015. doi: 10.1093/jtm/taad015
- Varghese, R., Patel, P., Kumar, D., and Sharma, R. (2023b). Monkeypox and drug repurposing: Seven potential antivirals to combat the viral disease. *Rev. Environ. Health.* 30(2), 1–3. doi: 10.1515/revh-2023-0001
- Vaughan, A., Aarons, E., Astbury, J., Balasegaram, S., Beadsworth, M., Beck, C. R., et al. (2018). Two cases of monkeypox imported to the united kingdom, September 2018. *Euro. Surveill.* 23 (38), 2018. doi: 10.2807/1560-7917.ES.2018.23.38.1800509
- Vivancos, R., Anderson, C., Blomquist, P., Balasegaram, S., Bell, A., Bishop, L., et al. (2022). Community transmission of monkeypox in the united kingdom, April to may 2022. *Euro. Surveill.* 27 (22), 2200422. doi: 10.2807/1560-7917.ES.2022.27.22.2200422
- von Magnus, P., Andersen, E. K., Petersen, K. B., and Birch-Andersen, A. (1959). A POX-LIKE DISEASE IN CYNOMOLGUS MONKEYS. *Acta Pathol. Microbiol. Scand.* 46 (2), 156–176. doi: 10.1111/J.1699-0463.1959.TB00328.X
- Weaver, J. R., and Isaacs, S. N. (2008). Monkeypox virus and insights into its immunomodulatory proteins. *Immunol. Rev.* 225 (1), 96–113. doi: 10.1111/J.1600-065X.2008.00691.X
- Wells, C. R., Sah, P., Moghadas, S. M., Pandey, A., Shoukat, A., Wang, Y., et al. (2020). Impact of international travel and border control measures on the global spread of the novel 2019 coronavirus outbreak. *Proc. Natl. Acad. Sci. U. S. A.* 117 (13), 7504–7509. doi: 10.1073/PNAS.2002616117
- World Health Organization. (2022). *Disease Outbreak News; Multi-country monkeypox outbreak in non-endemic countries*. Available at: <https://www.who.int/emergencies/disease-outbreak-news/item/2022-DON385> (Accessed Aug. 12, 2022).

World Health Organisation. (2022). *WHO director-general's statement at the press conference following IHR emergency committee regarding the multi-country outbreak of monkeypox - 23 July 2022*. Available at: <https://www.who.int/director-general/speeches/detail/who-director-general-s-statement-on-the-press-conference-following-IHR-emergency-committee-regarding-the-multi-country-outbreak-of-monkeypox-23-july-2022> (Accessed Aug. 12, 2022).

World Health Organization. (1996). *Weekly epidemiological record*. 71 (23), 180–173. Available at: <https://apps.who.int/iris/handle/10665/229796> (Accessed Aug. 12, 2022).

World Health Organization. (2022). Monkeypox. Available at: <https://www.who.int/news-room/fact-sheets/detail/monkeypox> (Accessed Aug. 14, 2022).

Yang, G., Pevear, D. C., Davies, M. H., Collett, M. S., Bailey, T., Rippen, S., et al. (2005). An orally bioavailable antipoxvirus compound (ST-246) inhibits extracellular virus formation and protects mice from lethal orthopoxvirus challenge. *J. Virol.* 79 (20), 13139–13149. doi: 10.1128/JVI.79.20.13139-13149.2005

Yang, Z. S., Lin, C. Y., Urbina, A. N., Wang, W. H., Assavalapsakul, W., Tseng, S. P., et al. (2022). The first case of monkeypox virus infection detected in Taiwan: awareness and preparation. *Int. J. Infect. Dis.* 122, 991–995. doi: 10.1016/J.IJID.2022.07.051

Yong, S. E.F., Ng, O. T., Ho, Z. J.M., Mak, T. M., Marimuthu, K., Vasoo, S., et al. (2020). Imported monkeypox, Singapore. *Emerg. Infect. Dis.* 26 (8), 1826–1830. doi: 10.3201/EID2608.191387

Zambrano, P. G., Acosta-España, J. D., Mosquera Moyano, F., and Altamirano Jara, J. B. (2022). Sexually or intimately transmitted infections: A look at the current outbreak of monkeypox in 2022. *Travel. Med. Infect. Dis.* 49, 102383. doi: 10.1016/J.TMAID.2022.102383

Zulkipli, I. N., David, S. R., Rajabalaya, R., and Idris, A. (2015). Medicinal plants: A potential source of compounds for targeting cell division. *Drug Target. Insights* 9, 9. doi: 10.4137/DTI.S24946



## OPEN ACCESS

## EDITED BY

Dr. Parth Sarthi Sen Gupta,  
Indian Institute of Science Education and  
Research Berhampur (IISER), India

## REVIEWED BY

Muhammad Bilal Azmi,  
Dow University of Health Sciences,  
Pakistan  
Suprabhat Mukherjee,  
Kazi Nazrul University, India

## \*CORRESPONDENCE

Sheikh Arslan Sehgal  
✉ arslansehgal@yahoo.com  
Kow-Tong Chen  
✉ ktchen@mail.ncku.edu.tw

RECEIVED 30 December 2022

ACCEPTED 29 April 2023

PUBLISHED 24 May 2023

## CITATION

Marriam S, Afghan MS, Nadeem M, Sajid M,  
Ahsan M, Basit A, Wajid M, Sabri S, Sajid M,  
Zafar I, Rashid S, Sehgal SA,  
Alkhalifah DHM, Hozzein WN, Chen K-T  
and Sharma R (2023) Elucidation of novel  
compounds and epitope-based peptide  
vaccine design against C30 endopeptidase  
regions of SARS-CoV-2 using  
immunoinformatics approaches.  
*Front. Cell. Infect. Microbiol.* 13:1134802.  
doi: 10.3389/fcimb.2023.1134802

## COPYRIGHT

© 2023 Marriam, Afghan, Nadeem, Sajid,  
Ahsan, Basit, Wajid, Sabri, Sajid, Zafar, Rashid,  
Sehgal, Alkhalifah, Hozzein, Chen and  
Sharma. This is an open-access article  
distributed under the terms of the [Creative  
Commons Attribution License \(CC BY\)](#). The  
use, distribution or reproduction in other  
forums is permitted, provided the original  
author(s) and the copyright owner(s) are  
credited and that the original publication in  
this journal is cited, in accordance with  
accepted academic practice. No use,  
distribution or reproduction is permitted  
which does not comply with these terms.

# Elucidation of novel compounds and epitope-based peptide vaccine design against C30 endopeptidase regions of SARS-CoV-2 using immunoinformatics approaches

Saigha Marriam<sup>1</sup>, Muhammad Sher Afghan<sup>2</sup>, Mazhar Nadeem<sup>2</sup>,  
Muhammad Sajid<sup>3</sup>, Muhammad Ahsan<sup>4</sup>, Abdul Basit<sup>5</sup>,  
Muhammad Wajid<sup>6</sup>, Sabeen Sabri<sup>1</sup>, Muhammad Sajid<sup>3</sup>,  
Imran Zafar<sup>7</sup>, Summya Rashid<sup>8</sup>, Sheikh Arslan Sehgal<sup>9,10\*</sup>,  
Dalal Hussien M. Alkhalifah<sup>11</sup>, Wael N. Hozzein<sup>12</sup>,  
Kow-Tong Chen<sup>13,14\*</sup> and Rohit Sharma<sup>15</sup>

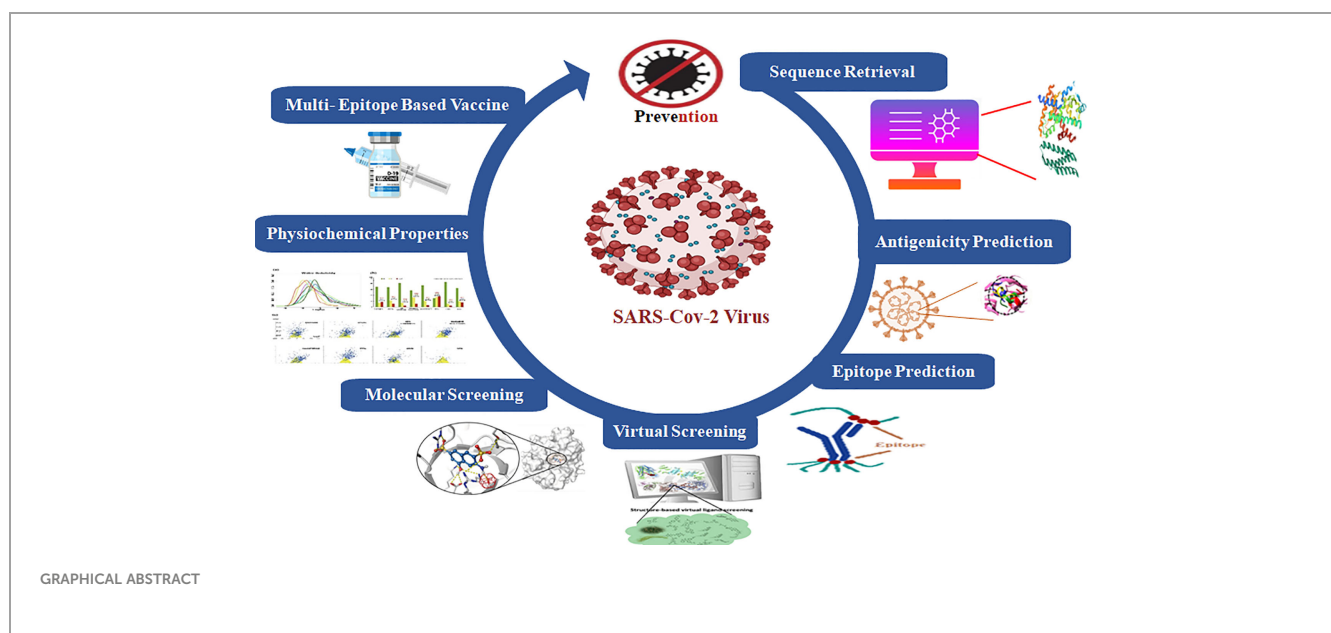
<sup>1</sup>Department of Microbiology and Molecular Genetics, Faculty of Life Sciences, University of Okara, Okara, Pakistan, <sup>2</sup>Department of Ear, Nose, and Throat (ENT), District Headquarter (DHQ) Teaching Hospital Faisalabad, Faisalabad, Punjab, Pakistan, <sup>3</sup>Department of Biotechnology, Faculty of Life Sciences, University of Okara, Okara, Pakistan, <sup>4</sup>Institute of Environmental and Agricultural Sciences, University of Okara, Okara, Pakistan, <sup>5</sup>Department of Microbiology, University of Jhang, Jhang, Pakistan, <sup>6</sup>Department of Zoology, Faculty of Life Sciences, University of Okara, Okara, Pakistan, <sup>7</sup>Department of Bioinformatics and Computational Biology, Virtual University, Punjab, Pakistan, <sup>8</sup>Department of Pharmacology and Toxicology, College of Pharmacy, Prince Sattam Bin Abdulaziz University, Al-Kharj, Saudi Arabia, <sup>9</sup>Department of Bioinformatics, Faculty of Life Sciences, University of Okara, Okara, Pakistan, <sup>10</sup>Department of Bioinformatics, Institute of Biochemistry, Biotechnology and Bioinformatics, The Islamia University of Bahawalpur, Bahawalpur, Pakistan, <sup>11</sup>Department of Biology, College of Science, Princess Nourah Bint Abdulrahman University, Riyadh, Saudi Arabia, <sup>12</sup>Botany and Microbiology Department, Faculty of Science, Beni-Suef University, Beni-Suef, Egypt, <sup>13</sup>Department of Occupational Medicine, Tainan Municipal Hospital (managed by ShowChwan Medical Care Corporation), Tainan, Taiwan, <sup>14</sup>Department of Public Health, College of Medicine, National Cheng Kung University, Tainan, Taiwan, <sup>15</sup>Department of Rasa Shastra and Bhaishajya Kalpana, Faculty of Ayurveda, Institute of Medical Sciences, Banaras Hindu University, Varanasi, India

There has been progressive improvement in immunoinformatics approaches for epitope-based peptide design. Computational-based immune-informatics approaches were applied to identify the epitopes of SARS-CoV-2 to develop vaccines. The accessibility of the SARS-CoV-2 protein surface was analyzed, and hexa-peptide sequences (KTPKYK) were observed having a maximum score of 8.254, located between amino acids 97 and 102, whereas the FSVLAC at amino acids 112 to 117 showed the lowest score of 0.114. The surface flexibility of the target protein ranged from 0.864 to 1.099 having amino acid ranges of 159 to 165 and 118 to 124, respectively, harboring the FCYMHMM and YNGSPSG hepta-peptide sequences. The surface flexibility was predicted, and a 0.864 score was observed from amino acids 159 to 165 with the hepta-peptide (FCYMHMM) sequence. Moreover, the highest score of 1.099 was observed between amino acids 118 and 124 against YNGSPSG. B-cell epitopes and cytotoxic T-lymphocyte (CTL) epitopes were also identified against SARS-CoV-2. In molecular docking

analyses,  $-0.54$  to  $-26.21$  kcal/mol global energy was observed against the selected CTL epitopes, exhibiting binding solid energies of  $-3.33$  to  $-26.36$  kcal/mol. Based on optimization, eight epitopes (SEDMLNPNY, GSVGFNIDY, LLEDEFTPF, DYDCVSFCY, GTDLEGNFY, QTFSVLACY, TVNVLAWLY, and TANPKTPKY) showed reliable findings. The study calculated the associated HLA alleles with MHC-I and MHC-II and found that MHC-I epitopes had higher population coverage (0.9019% and 0.5639%) than MHC-II epitopes, which ranged from 58.49% to 34.71% in Italy and China, respectively. The CTL epitopes were docked with antigenic sites and analyzed with MHC-I HLA protein. In addition, virtual screening was conducted using the ZINC database library, which contained 3,447 compounds. The 10 top-ranked scrutinized molecules (ZINC222731806, ZINC077293241, ZINC014880001, ZINC003830427, ZINC030731133, ZINC003932831, ZINC003816514, ZINC004245650, ZINC000057255, and ZINC011592639) exhibited the least binding energy ( $-8.8$  to  $-7.5$  kcal/mol). The molecular dynamics (MD) and immune simulation data suggest that these epitopes could be used to design an effective SARS-CoV-2 vaccine in the form of a peptide-based vaccine. Our identified CTL epitopes have the potential to inhibit SARS-CoV-2 replication.

## KEYWORDS

SARS-CoV-2, 3CL pro, CTL epitopes, immunoinformatics, peptide-based vaccine, computational immunology, C30 endopeptidase



## Introduction

A newly discovered human coronavirus (HCoV) becomes the deadliest pandemic of the 21st century. On December 31st, in Wuhan, China, numerous patients have been identified as asymptomatic carriers of the Severe Acute Respiratory Syndrome-2 (SARS-CoV-2) virus (Agarwal et al., 2022; Rayan et al., 2022). Comparative molecular analyses of SARS-CoV-2 against SARS-

CoV-1, SARS-CoV-2, MERS-CoV, and bat-CoV showed 80% to 95% similarity (Ahmad et al., 2022). The World Health Organization (WHO) has declared SARS-CoV-2 disease as COVID-19 (Kannan et al., 2020). SARS-CoV-2 has impacted individuals from diverse nations including Thailand, Japan, and South Korea, who had not previously travelled to the epicenter of the outbreak in Wuhan, China. Based on these outcomes, the researcher emphasizes that diagnosed individuals contracted the



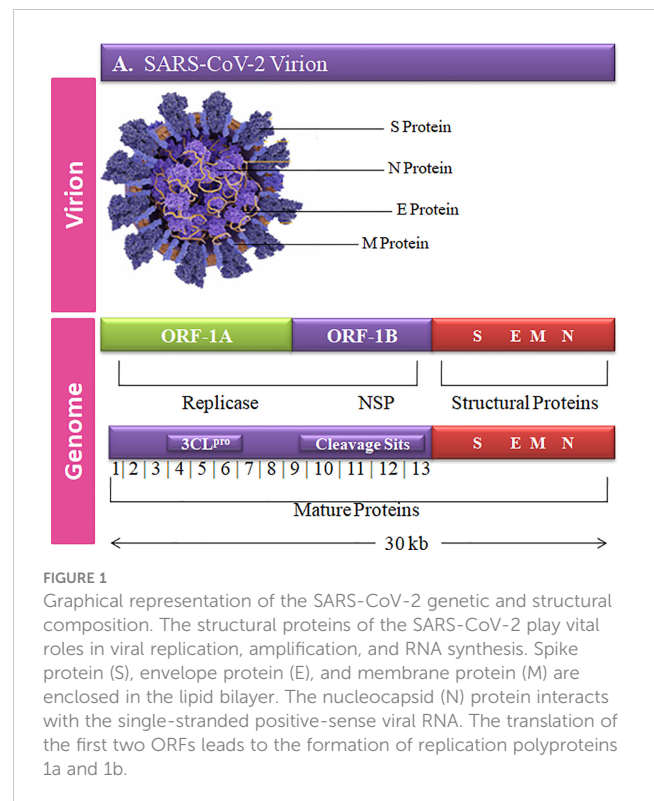
virus through anthropogenic actions (Bastola et al., 2020; Huang et al., 2020).

The genomic determinants of pathogenicity and computational analyses of MERS and SARS coronaviruses highlighted the importance of SARS-CoV-2 as a causative agent (Fehr et al., 2017). In January 2020, the Chinese institutes submitted SARS-CoV-2 sequences for conformations and sequence homology targets and predicted a vast reality by using bioinformatics approaches (Riva et al., 2020). In China, researchers emphasized the implications of the novel mutations and mutational diversification of SARS-CoV-2 from rapid genome sequencing of ~30,000 nucleotides (Beniac et al., 2006). Comparative sequence analyses and whole-genome phylogenetic guidelines showed that SARS-CoV-2 has 80% similarity with previously known SARS-CoV (Waqas et al., 2020).

SARS-CoV-2 viral proteins interact with various human proteins, including regulatory proteins (Chen et al., 2021). Specifically, the Nsp1, Nsp5, Nsp8, Nsp13, E, S, ORF3a, ORF8, M, ORF9b, N, and Nsp15 proteins have been identified as affecting critical cellular processes (Li et al., 2021), such as posttranscriptional and epigenetic regulation, epithelial trafficking, lipid changes, and RNA translation and transcription. Additionally, the Nsp1, Nsp4, Nsp8, Nsp9, Nsp13, Nsp15, ORF6, ORF9C, S, E, and ORF proteins also disturb the cytoskeleton, mitochondria, and extracellular matrix (O'Meara et al., 2020). To overcome the SARS-CoV-2, current therapeutic strategies focus to inhibit the 3-chymotrypsin-like protease of SARS-CoV-2. However, there is a critical need to develop novel antiviral drugs and vaccines that specifically target the Nsp, S, E, and ORF proteins to prevent viral replication and proliferation.

The complete genome sequence of HCoV is more complex than other viruses with ~30-kb size and a unique club-shaped spike morphology (Figure 1). The coronavirus (CoV) genome has significant loops to provide genetic evidence at the beginning of the untranslated region (UTR region). The 3' end of poly-A contain a ladder sequence with unique structures required for genome synthesis and replication and reveal an additional 5' capped end ladder sequence (Zhao et al., 2012). The genomic variation of the human SARS-CoV-2 viral genome comprises 14 open reading frames (ORFs) and 29,891 nucleotides encoding for 9,860 amino acids (Guan et al., 2020). The cross-functional analyses of CoV assessed to evolve 5' terminal contain 1–16 non-structural protein (nsp) and 2 key ORFs (ORF1a and ORF1b) translated into polyproteins (pp) 1a (pp1a; nsp 1–11) and 1ab (pp1ab; nsp1–16) (Lu et al., 2020).

Non-structural proteins (nsp) are released from the multimeric complex during viral transcription and replication by cysteine proteases (Oanca et al., 2020). The conserved 3-chymotrypsin-like protease (3CL<sup>pro</sup>), also known as the main protease (M-pro), originates in the polyprotein ORF1ab of SARS-CoV-2 and found within Nsp5. In contrast, the papain-like protease (PLpro) is found inside nsp3 (Chen et al., 2020). 3CL<sup>pro</sup> is a crucial SARS-CoV-2 receptor that regulates the transcription and viral replication (Jin et al., 2020). 3CL<sup>pro</sup> cuts the pp at 11 diverse regions to produce numerous parts for viral replication. Proteinases are required for proteolytic processing degradation, and they inhibit the host



interpretation by interacting the 40S subunits' extended head shape (Way, 2021). The C-terminus attaches to prevent the ribosomal mRNA entry tunnels from forming (Schubert et al., 2020). As a result, it suppresses the antiviral activity induced by adaptive immunity. The nsp1–40S ribosome complex also causes endonuclease breaking at the 5'UTR of host mRNAs, resulting in their elimination based on similarities. Viral mRNAs are less vulnerable to nsp1-mediated translational inhibition due to their 5'-end ladder sequence (Crow, 2021). 3CL<sup>pro</sup> nsp5 causes a conformational shift at the C-terminus of the reverse transcription protein complex (Dai et al., 2020).

SARS-CoV-2 is more lethal than SARS and MERS, so precautionary measures have been taken against the novel SARS-CoV-2 disease globally (Douglas et al., 2018). COVID-19 prevention techniques mostly rely on peptide-based vaccines, and researchers have tried to develop a variety of vaccines against SARS-CoV-2 (Tahir ul Qamar et al., 2020). Bioinformatics techniques, virtual screening, molecular docking, and bioactive compounds have been utilized to inhibit SARS-CoV-2 (Xiao et al., 2021). B-cell and conservation of cytotoxic T lymphocyte (CTL) epitopes are time consuming (Ip et al., 2015). The identification of protein specific peptides which can bind to the major histocompatibility complex (MHC) is a critical step in peptide-based vaccine design. The peptide and MHC molecule binding depends at the association of T-cell immunogenicity (Lazarski et al., 2005). The peptide-based vaccines can activate specific immune responses accurately (Purcell et al., 2007).

The present study was aimed to employ advanced computational analyses and immunoinformatics methodologies to design epitope-based vaccine and to scrutinize novel compounds



against SARS-CoV-2. The primary objective was to investigate the linear and conformational B-cell and T-cell potential antigens of 3CL<sup>pro</sup>. This study was performed to identify peptide-based vaccines against SARS-CoV-2. Through elucidating the current findings, the researchers aspire to make a significant and valuable contribution toward developing a workable vaccine.

## Materials and methods

The genomic and proteomic data of SARS-CoV-2 were retrieved from publicly accessible databases including GISAID, NCBI, GenBank, and UniProtKB. 3CL<sup>pro</sup> was selected and plays a critical role in transcription and replication processes of SARS-CoV2 and has the potential to be an extremely effective therapeutic target.

### Sequence retrieval and alignment

UniProtKB was utilized to retrieve the amino acid sequence of 3CL<sup>pro</sup> having accession number P0DTD1 ( ). The specific section of non-structural 3CL<sup>pro</sup> was selected consisting of 306 amino acids, whereas the entire P0DTD1-R1AB\_SARS2 has a total number of 7,096 amino acids. The 3D structure of the selected protein was determined by X-ray crystallography (PDB ID: 6W63) and was retrieved from PDB to visualize the atomic level of the selected structure. Additionally, ProtParam was utilized to examine the physiochemical properties of 3CL<sup>pro</sup> and the data were extracted from SWISS-PROT and TrEMBL (O'Donovan et al., 2002).

Comparative genomic analyses of SARS-CoV (NC 004718), MERS-CoV (NC 019843.3), and SARS-CoV-2 (NC 045512.2) were performed by applying the multiple-sequence alignment (MSA) approach. The genomic sequences of the selected viral strains were retrieved from NCBI GenBank (Benson et al., 2018) and GISAID databases (Shu and McCauley, 2017). Clustal Omega (Sievers and Higgins, 2014) was employed to perform MSA. WebLogo3 (<https://weblogo.threeplusone.com/>) was used to visualize the conserved domain of the selected protein. MSA was cross verified by using pair-score matrices, including the Hidden Markov Model (HMM) (Blunsom, 2004) and OXBench (Raghava et al., 2003). MacVector (Rastogi, 1999) sequence application was used to examine the selected genomes and translated proteins.

### *In silico* prediction of linear and conformational B- and T-cell epitope prediction

Linear B-cell epitope peptides are potential candidates for antigens in vaccine design and immunological regulation. The immune epitope database and analysis resource (IEDB) (Fleri et al., 2016) was applied to conduct *in silico* analyses followed by Karplus and Schulz's flexibility prediction and the Kolaskar antigenicity scale (Alexander et al., 2011). The surface accessibility predictions were also calculated by using Emini and

Parker's and Hopp and Wood's hydrophilicity prediction methods (Parker et al., 1986). ElliPro was utilized to predict the B-cell epitope conformation ranges from 0.5 to 6 Å. To ensure the reliability of epitope prediction within 95.5% and 99.5%, a cut-off value of 0.85 was used. The protrusion index (pI), adjacent residues, and protein shape approximation algorithms were employed for further analyses (Nain et al., 2020). The 3CL<sup>pro</sup> 3D structure was visualized through PyMOL and UCSC Chimera visualization tools. Moreover, the anticipated epitopes as spheres to determine the surface accessibility of potential peptides were removed.

### Prediction of CTL epitopes

The NetCTL 1.2 server (<https://services.healthtech.dtu.dk/service.php?NetCTL-1.2>) was used to predict the cytotoxic T-lymphocyte (CTL) epitopes. CTLs are immune cells that recognize and kill the infected cells by binding to short peptide fragments (epitopes) presented by MHC molecules on the cell surface. A combination of algorithms was utilized to evaluate the MHC-I binding affinity, transporter associated with antigen processing (TAP), transport efficiency (with a threshold of 0.05), and proteasomal C-terminal cleavage (with a threshold of 0.15), at an epitope identification threshold of 0.75 (Larsen et al., 2007). The amino acid sequences of the target protein were submitted to the NetCTL 1.2 server in FASTA format to predict the peptide lengths and human leukocyte antigen (HLA) alleles. To predict TAP utilization, weight matrix, T-cell epitope prediction, and artificial neural network approaches, proteasomal C-terminal cleavage and MHC class-I binding were used.

### Prediction of antigenicity

In order to design an effective antigen construct, it is important to identify potential epitopes with high antigenicity. Initially, the B-cell epitopes were screened and MHC-I and II epitopes were subsequently determined by using ProPred (<http://crdd.osdd.net/raghava/propred/>, accessed on 10 April 2023) and ProPred 1 (<http://crdd.osdd.net/raghava/propred1/>, accessed on 10 April 2023) servers. The VaxiJen v2.0 server was used to evaluate the antigenicity of the predicted MHC-I and II epitopes having a threshold value of 0.5. The alignment-independent prediction method was utilized to identify the possible epitopes of 3CL<sup>pro</sup>. The virus cell line was selected as the target organism for vaccine development. The utilized methodology helped to identify the potential epitopes with high antigenicity, which can be incorporated into an optimized antigen construct for the development of a vaccine against SARS-CoV-2.

### An epidemiological strategic and world population coverage analyses

The world population coverage assessments were conducted by using the IEDB server (<https://www.iedb.org/>) and CTL epitopes

against the relevant allele sets to determine whether the chosen candidates were suitable for coverage. Major population coverage evaluations were conducted on China, Japan, Iran, and Korea (Vita et al., 2019).

## Molecular docking and bioinformatics analysis for the peptide–MHC protein complex

SARS-CoV-2-predicted CTL epitope peptides and virulent residues were selected for the molecular docking analyses. For 100 simulation runs, the PEP-FOLD3 server was used to forecast the ideal model configurations and to simulate the 3D structure of selected peptides (Lamiable et al., 2016) and were assessed by SOPEP energy scores (Maupetit et al., 2007). For molecular docking analyses, the score peptides were selected by PatchDock with a clustering RMSD value of 4. Furthermore, the unwanted docked complexes with receptor atom penetrations into ligands were removed (Schneidman-Duhovny et al., 2005). FireDock was used to cross verify and screen the suitable docked complexes (Mashiach et al., 2008). The fast rigid-body docking with clear flexibility and scoring issues were used for docking calculations (Kingsford et al., 2005). The PyMOL (Alexander et al., 2011) and UCSF Chimera 1.15 (Pettersen et al., 2004) were employed to identify the docked complexes having hydrogen-bonding interactions.

## Structure-based molecular docking analyses of potential compounds

The library of 3,447 compounds (FDA, DrugBank approved) from the ZINC database was used for virtual screening through molecular docking analyses. All the compounds were minimized to get stable results through ChemDraw and UCSF Chimera. The molecular docking analyses was performed through AutoDock Vina (Dallakyan and Olson, 2015) and AutoDock Tools. The RMSD values were also calculated based on suitable hits. The admetSAR server (Shen et al., 2010) and ADMETlab 2.0 (Xiong et al., 2021) were used to calculate the drug-like physical and chemical properties of the selected compounds. BIOVIA Discovery studio (Sievers and Higgins, 2014) and Ligplot were used to analyze the resultant interacting residues (Wallace et al., 1995).

## Molecular dynamics simulation

Desmond software from Schrödinger LLC was used to perform the molecular dynamics (MD) simulation of the receptor and ligand complexes for 100 ns (Manandhar et al., 2022). To simulate atomic movements over time, MD simulations with Newton's classical equation of motion was utilized. For the ligand binding status in physiological conditions, simulation predictions were generated.

Maestro's Protein Preparation Wizard was used to incorporate the complex optimization and minimization, and the receptor–ligand complex was preprocessed (Tabti et al., 2023). Using the OPLS\_2005 force field and TIP3P orthorhombic box solvent model, the System Builder tool generated each system. The models were neutralized by using the counter ions. The physiological conditions were simulated by adding 0.15 M sodium chloride (NaCl). For the duration of the simulation, the NPT ensemble at 300 K temperature and 1 atm pressure was used. Before running the simulation, the models were unloaded and trajectories were saved every 100 ns to analyze the stability of the simulation analyses. By contrasting the root mean square deviation (RMSD) of the protein and ligand with time, stability was verified (Knapp et al., 2011; Rather et al., 2020). To assess the stability of the MD simulations, RMSD, radius of gyration (Rg), hydrogen bond number, and solvent accessible surface (SASA) were calculated.

## Immune simulation

To evaluate the immunogenicity and immune responses of *in silico* vaccine design, an agent-based immune simulation technique was utilized. The C-ImmSim webserver was used to simulate the molecular interactions between immunogenic molecules at a mesoscopic level (Rapin et al., 2010). The amino acid sequence of each vaccine was used to conduct the simulation process, and the machine learning method was used to design the epitope constructs for injection. The ability of the vaccine was predicted by using the C-ImmSim web server to induce the differentiation and proliferation of various immune cells. The default algorithm was used, and the refined 3-C-like protease was tested for its efficacy to induce an immune response. Three doses of the designed vaccine were administered through three injections at intervals of 28 days in the immune simulation experiment. The time steps were fixed at 1, 91, and 181, which were equal to 8 h of real-life time, and all other parameters were kept at their default values (Das et al., 2021).

## Results

A recent outbreak of a new type of viral pneumonia has emerged at an alarming pace, causing widespread concern and fear. Surprisingly, this pneumonia is distinct from other highly infectious and disease-causing viruses such as MERS, SARS, adenovirus, and influenza viruses. The implications of this outbreak are still being studied, and much research is being conducted to understand the nature and transmission (Lu et al., 2020). WHO identified the cause of the pneumonia outbreak as a new coronavirus and named it COVID-19. The virus quickly spread across borders and international travel, posing a significant threat to countries with inadequate healthcare systems. The global health emergency declaration was made to prevent the further spread of the disease, and various measures were taken to control its transmission, including social distancing, travel restrictions, and wearing masks. The scientific community also swiftly mobilized to

develop vaccines and treatments to combat the deadly virus. Despite the challenges faced, the world has united to fight against COVID-19, highlighting the importance of global cooperation in addressing such health crises (W. H. Organization, 2019). The swift infection of host cells by the emerging virus, SARS-CoV-2, has created an air of uncertainty surrounding its final dimensions and impact (De Wilde et al., 2017). A surveillance system is required, and preventive measures should be taken to combat the rapidly increasing burden of SARS-CoV-2 infections globally.

Peptide-based vaccine mechanisms were extensively utilized to prevent the COVID-19 (Tahir ul Qamar et al., 2020). Immunoinformatics has played a significant role to predict the effective vaccines that lessen the manufacturing costs and consume less time. Developing an effective epitope-based peptide vaccine with the proper selection of immune-dominant epitopes and suitable antigen candidates is difficult. However, predicting the right epitopes of the target protein for designing epitope-based peptide vaccines via approaching immunoinformatics tools was necessary (Nain et al., 2020). The main target of immunoinformatics approaches is to predict the epitope-based peptide vaccines by recognizing 3CL<sup>Pro</sup>. The pathogenic analyses help to discover the novel vaccines at the genomic level; however, these experimental tools have multiple limitations (Vilela Rodrigues et al., 2019).

Immunoinformatics approaches help *in vitro* expressions of the potential antigen, complete spectrum analysis, and observe pathogen culturing. Researchers have observed many vaccine candidates by using computational methods with promising preclinical outputs (Davies and Flower, 2007). CTL epitopes help to design peptide-based vaccines against human leukocyte antigen-B protein (Tahir et al., 2018). SARS-CoV-2 epitope-based vaccine development targets structural proteins of the virus and CTL epitopes of the selected protein. CTL epitopes support the host immune responses; moreover, the PBD ID 6W63-tagged non-structural protein of SARS-CoV-2 is linked to viral replication (Waqas et al., 2021).

The selected CTL epitopes or allergenicity and antigenicity were optimized (Dimitrov et al., 2014). In China, the predicted epitope population coverage analyses for MHC-I were reported to be 0.0373 with average hits of 0.3. Eight epitopes promising peptides were designed, and molecular docking analyses were performed to identify the effective binding sites (Huang et al., 2010).

## Surface accessibility analysis

A peptide of >1.0 surface accessibility has more probability of being found on the surface (Parker et al., 1986). SARS-CoV-2 top-ranked predicted peptides among numerous peptides were selected for further analyses. The peptide surface probability and sequence position were represented by the y-axis and x-axis (Figure 2A). The maximum 8.254 scores of surface probability were observed in hexa-peptide sequence KTPKYK (97 to 102), and the lowest score of 0.114 was observed in hexa-peptide sequence FSVLAC (112 to 117) (Supplementary S1, S1.1).

## Surface flexibility prediction

The Schulz and Karplus flexibility method was utilized to calculate the atomic vibrational motions of the protein structure. The selection was made on temperature value and B-factor as the organization of the predicted structure, stability. The quality of the predicted structure was observed proportional to the B-factor. The lower range is more effective as compared to the higher range of the B-factor. SARS-CoV-2 surface flexibility outputs were observed (Figure 2B), and the minimum flexibility score of 0.864 ranging from 159 to 165 amino acids with the FCYMHMH hepta-peptide sequence was observed. The maximum flexibility score of 1.099 ranging from 118 to 124 amino acids with the YNGSPSG hepta-peptide sequence was observed (Supplementary S2).

## Parker hydrophilicity prediction

Parker's hydrophilicity scale analysis was performed to find the hydrophilicity of the peptides associated with peptide retention times using HPLC on the reversed-phase column. Hydrophilic regions and associated antigenic sites have been observed through immunological analyses (Parker et al., 1986). Parker's hydrophilicity method-predicted peptides were visualized (Figure 2C), and the residues were positioned along the x-axis and hydrophilicity was positioned along the y-axis. The maximum hydrophilicity score of 5.329 was observed to range from 92 to 98 having a hepta-peptide (DTANPKT) sequence. However, the minimum hydrophilicity score was observed—4.257 ranging from 204 to 210 with the hepta-peptide (VLAWLYA) sequence (Supplementary S3).

## Kolaskar and Tongaonkar antigenicity prediction

The Kolaskar and Tongaonkar process was used to measure the antigenicity (Figure 2D); the highest antigenicity value of 1.220 was observed in two hepta-peptide sequences, CVLKLKV (85 to 91) and CPRHVIC (38 to 41). The predicted amino acid residues results along with CTL epitopes of SARS-CoV-2 are mentioned in Table 1. The minimum antigenicity value of 0.844 was observed for hepta-peptide sequence NGMNGRT from 274 to 280 amino acid positions (Supplementary S4).

## Structure-based epitope prediction

ElliPro was used to determine the association of the predicted epitopes, protein structure antigenicity, flexibility, and accessibility within the 3D structure (Ponomarenko et al., 2008). The protein antibody interactions were observed to distinguish the predicted epitopes. The top-ranked four conformational epitopes with  $\geq 0.5$  scores were selected. The isoelectric point (pI) (Lamiable et al., 2016) was observed to analyze the atom percentage and molecular

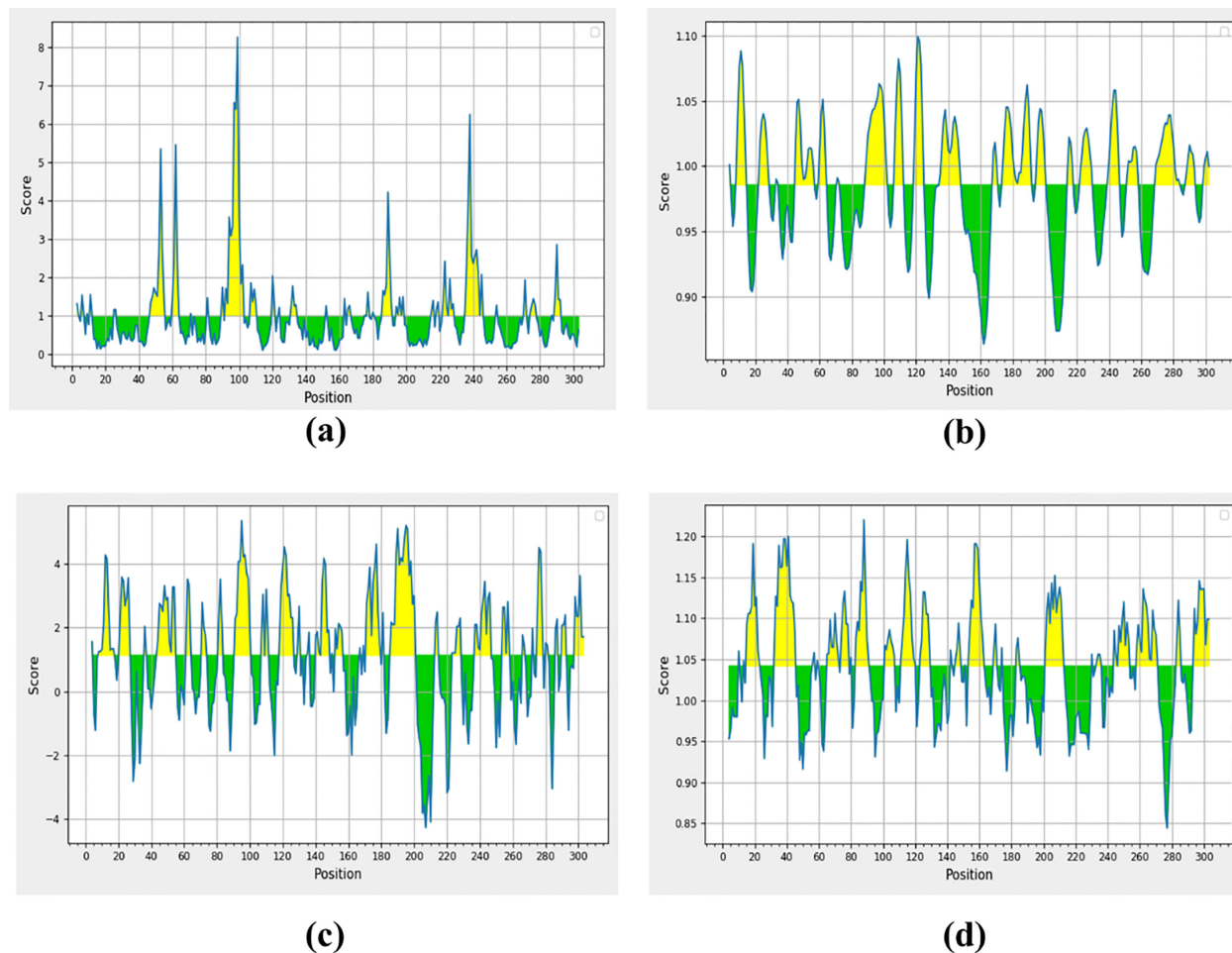


FIGURE 2

Non-structural protein (PDB: 6W63), (A) Parker's predictions for hydrophilicity, (B) surface accessibility, (C) flexibility, and (D) antigenicity were evaluated. The all figure shows the results as scores, with the x-axis showing sequence positions and the y-axis showing probability values.

TABLE 1 Predicted amino acid residues along with CTL epitopes of SARS-CoV-2.

Residue number	Peptide sequence	MHC binding affinity prediction	Rescale binding affinity	C-terminal cleavage affinity	TAP transport efficiency
146	GSVGFNIDY	0.3112	1.3211	0.9565	2.8570
1	SGFRKMAFP	0.0549	0.2332	0.0275	0.0010
5	KMAFPGSKV	0.0729	0.3094	0.9651	0.6920
110	QTFSVLACY	0.2625	1.1146	0.9725	2.9980
9	PSGKVEGCM	0.0574	0.2438	0.1230	-0.4030
16	CMVQVTCGT	0.0649	0.2754	0.0334	-0.5770
17	MVQVTCGTT	0.0672	0.2853	0.0501	-0.5590
10	SGKVEGCMV	0.0541	0.2297	0.4221	-0.0460
201	TVNVLAWLY	0.6255	2.6559	0.8852	2.9570
4	RKMAFPGSK	0.0597	0.2533	0.1516	0.7180
12	KVEGCMVQV	0.0775	0.3290	0.5447	0.3860
153	DYDCVSFCY	0.2097	0.8905	0.9722	2.7060

(Continued)

TABLE 1 Continued

Residue number	Peptide sequence	MHC binding affinity prediction	Rescale binding affinity	C-terminal cleavage affinity	TAP transport efficiency
174	GTDLEGNFY	0.7930	3.3669	0.6229	2.7020
2	GFRKMAFPS	0.0512	0.2174	0.0246	-2.1540
15	GCMVQVTCG	0.0499	0.2118	0.0306	-1.6560
6	MAFPSGKVE	0.0476	0.2021	0.0253	-1.2530
46	SEDMLNPNY	0.1528	0.6489	0.8406	2.6760
3	FRKMAFPSG	0.0505	0.2146	0.0527	-1.3160
13	VEGCMVQVT	0.0535	0.2272	0.0339	-0.8410
93	TANPKTPKY	0.1676	0.7118	0.9755	2.7230
7	AFPSGKVEG	0.0551	0.2341	0.1583	-1.0630
14	EGCMVQVC	0.0548	0.2326	0.0285	-0.4000
8	FPSGKVEGC	0.0537	0.2278	0.0300	-0.2350
11	GKVEGCMVQ	0.0455	0.1932	0.2424	-0.1030
286	LLEDEFTPF	0.1132	0.4807	0.9503	2.5680

bulk responsible for the antibody binding. The pI value of 5.95 was observed for the selected target protein. The name of the residue, lengths, and locations of the top-ranked four conformational predicted epitopes were critically analyzed (Table 2), and a 0.517–0.719 score was observed.

## Molecular docking analyses with HLA-B

Molecular docking analyses were performed on the selected CTL epitopes of designed peptides. The global energy of the selected CTL epitopes was observed between -0.54 and -26.21 kcal/mol. Moreover, the binding affinities were also observed with Van der Waals (VdW) energy values of -3.33 to -26.36 kcal/mol (Table 3). The HLA-B effective binding affinities were observed through molecular docking of the selected CTL-predicted epitopes (SEDMLNPNY, GSVGFNIDY, LLEDEFTPF,

DYDCVSFCY, GTDLEGNFY, QTFSVLACY, TVNVLAFLY, and TANPKTPKY).

## Population coverage analyses

The population coverage analyses were performed on MHC-I, MHC-II, and associated HLA alleles. MHC-I epitopes resulted in the highest population coverage in Italy and China as 0.9019% and 0.5639% respectively. MHC-II selected epitopes had shown population coverage of 58.49% in Italy and 34.71% in China (Supplementary S5)

## Multiple-sequence alignment

The conserved residues of three selected coronavirus genomes (NC\_045512.2, NC\_004718.3, and NC\_006577.2) were analyzed

TABLE 2 Selected scores and interacted residues of top-ranked discontinuous epitopes.

Serial no.	Predicted discontinuous epitopes residues	Residues	Score
1	A:Q244, A:D245, A:V247, A:D248	4	0.719
2	A:S1, A:G2, A:F3, A:T198, A:A211, A:V212, A:I213, A:N214, A:G215, A:D216, A:R217, A:W218, A:F219, A:L220, A:N221, A:R222, A:F223, A:T225, A:T226, A:L227, A:N228, A:D229, A:F230, A:N231, A:L232, A:V233, A:A234, A:M235, A:K236, A:Y237, A:N238, A:Y239, A:E240, A:P241, A:L242, A:T243, A:G251, A:P252, A:S254, A:A255, A:Q256, A:T257, A:G258, A:I259, A:A260, A:L262, A:D263, A:A266, A:S267, A:K269, A:E270, A:L271, A:L272, A:Q273, A:N274, A:G275, A:M276, A:N277, A:G278, A:R279, A:T280, A:I281, A:L282, A:G283, A:S284, A:A285, A:L286, A:C300, A:S301, A:G302, A:V303, A:T304, A:F305	73	0.709
3	A:G11, A:K12, A:G15, A:C16, A:T21, A:C22, A:G23, A:T24, A:D33, A:D34, A:R40, A:C44, A:T45, A:S46, A:E47, A:D48, A:M49, A:L50, A:N51, A:P52, A:N53, A:Y54, A:E55, A:D56, A:L57, A:L58, A:I59, A:R60, A:K61, A:S62, A:N63, A:H64, A:N65, A:L67, A:Q69, A:A70, A:G71, A:N72, A:V73, A:Q74, A:L75, A:R76, A:V77, A:I78, A:G79, A:H80, A:S81, A:M82, A:K90, A:V91, A:D92, A:T93, A:A94, A:N95, A:P96, A:K97, A:T98, A:P99, A:K100, A:N133, A:T135, A:D155, A:C156, A:G183, A:P184, A:F185, A:V186, A:D187, A:R188, A:Q189, A:T190, A:A191, A:Q192, A:A193, A:A194, A:G195, A:T196, A:D197	78	0.699
4	A:L167, A:P168, A:T169, A:V171	4	0.517



TABLE 3 Peptides-MHC class I, HLA-B interaction characteristics of designed peptides against SARS-CoV-2.

Peptide sequence	Global energy (kcal/mol)	Attractive VDW energy (kcal/mol)	H-bond energy (kcal/mol)	Peptidase-MHC pair	Bond distance (Å)	Conserved residues
<b>GTDLEGNFY</b>	-1.65	-5.52	0.36	ASN 7 CB-PRO 168.A CB ASN 7 CA-PRO 168.A CB ASN 7 N-PRO 168.A CG ASN 7 N-PRO 168.A CB PHE 8 N-PRO 168.A CA	1.557 1.755 1.880 1.956 2.286	GLN189 ASN142 MET49 GLU166 PRO168
<b>TVNVLAFLY</b>	-5.53	-3.33	0.00	TRP 7 O-SER 46.A CB TRP 7 NE1-SER 46.A TRP 7 CH2-GLU 47.A OE1 ASN 3 O-HOH 711.A O TRP 7 N-HOH 711.A O	2.433 2.377 2.711 2.426 2.675	GLN189 ASN142 MET49 GLU166 PRO168
<b>GSVGFNIDY</b>	-26.21	-21.80	15.63	YR 9 O2-LEU 27.A CD1 TYR 9 CA-CYS 145.A SG ILE 7 O-HOH 671.A O ASP 8 CG-ASN 142.A CA TYR 9 O2-LEU 27.A	2.172 2.606 1.881 2.779 2.355	GLN189 ASN142 MET49 GLU166 PRO168
<b>QTFSVLACY</b>	-17.39	-21.55	20.78	TYR 9 O2-SER 46.A OG TYR 9 O2-SER 46.A CB	2.616 3.049	GLU166 PRO168
<b>DYDCVSFCY</b>	-14.90	-5.82	2.72	TYR 2 CZ-GLN 189.A NE2 PHE 7 CG-ASN 142.A ND2 TYR 2 CD2-HOH 711.A O PHE 7 CD2-ASN 142.A PHE 7 CE2-ASN 142.A CB	2.394 2.406 2.411 2.597 2.959	GLN189 ASN142 MET49 GLU166 PRO168
<b>TANPKTPKY</b>	-15.11	-26.36	33.19	PRO 7 CB-GLU 166.A CB THR 6 CG2-HOH 650.A O LYS 8 CG-HOH 515.A O TYR 9 O2-HOH 650.A O PRO 7 CB-GLU 166.A CD	2.529 2.132 2.155 1.728 2.654	GLN189 ASN142 MET49 GLU166 PRO168
<b>SEDMLNPY</b>	-17.58	-19.77	25.28	GLU 2 CD-MET 49.A SD TYR 9 C-HOH 671.A O ASN 6 OD1-GLN 189.A ASN 6 CG-GLN 189.A NE2	2.089 1.865 1.863 2.128 2.079	GLN189 ASN142 MET49 GLU166 PRO168

(Continued)

TABLE 3 Continued

Peptide sequence	Global energy (kcal/mol)	Attractive VDW energy (kcal/mol)	H-bond energy (kcal/mol)	Peptidase-MHC pair	Bond distance (Å)	Conserved residues
				GLU 2 OE2-MET 49.A SD		
LLEDEFTPF	-0.54	-3.54	0.37	PHE 6 CA-GLU 166.A CB PHE 6 C-GLU 166.A CG THR 7 CG2-HOH 515.A O GLU 5 O-LEU 167.A N LEU 1 CD2-THR 190.A	0.854 0.598 0.610 0.394 0.940	GLN189 ASN142 MET49 GLU166 PRO168

and detected through MSA. MSA has shown conserved domains in all selected strains of the coronavirus restored with a strain of novel SARS-CoV-2 outbreak. Moreover, the binding domains of the previously reported MERS and SARS strains were similar to the novel SARS-CoV-2 outbreak.

## Molecular docking analyses

The compound library (FDA drugs) was used for virtual screening. Molecular docking analyses revealed the significant values of the selected peptides (Irwin and Shoichet, 2005). There were 3,447 compounds screened, and molecular docking analyses showed variations in binding energy. Molecular docking was performed against the selected library, and the top-ranked docked compounds based on higher binding affinities, interacting residues, least binding energies, and drug properties were selected for further analyses. The top 10 complexes were selected, visualized, and analyzed. The top four interacting docked compounds were analyzed, and their similar binding pockets were observed (Figure 3). Met-49, Asn-

142, Pro-168, Glu-166, and Gln-189 were observed as conserved residues.

The chemical library was used, and ZINC222731806, ZINC014880001, ZINC077293241, ZINC003830427, ZINC030731133, ZINC003816514, ZINC003932831, ZINC004245650, ZINC000057255, and ZINC011592639 compounds were selected with least binding energy ranges from -7.5 to -8.8 kcal/mol, and we draw their promising structure as mentioned in Figure 4, at similar binding pocket and common binding sites (Table 4). The FDA-approved compounds play a vital role in different diseases and the top-ranked 10 docked complexes bound at the similar binding region. The selected compounds may predict the replication inhibition at observed residues (Pro-168, His-41, Arg-188, Gln-189, Cys-145, Glu-166, Met-49, Asp-187, Met-165, His-164, and CYS44). A plot was generated to analyze the docked complexes (Figures 5A–C).

The drug compounds were selected with the goal that they could inhibit SARS-CoV-2 replication without consuming much time. For toxicity, absorption, excretion, metabolism, and distribution analyses of the selected docked complexes were performed (Table 4). All the selected complexes had shown the

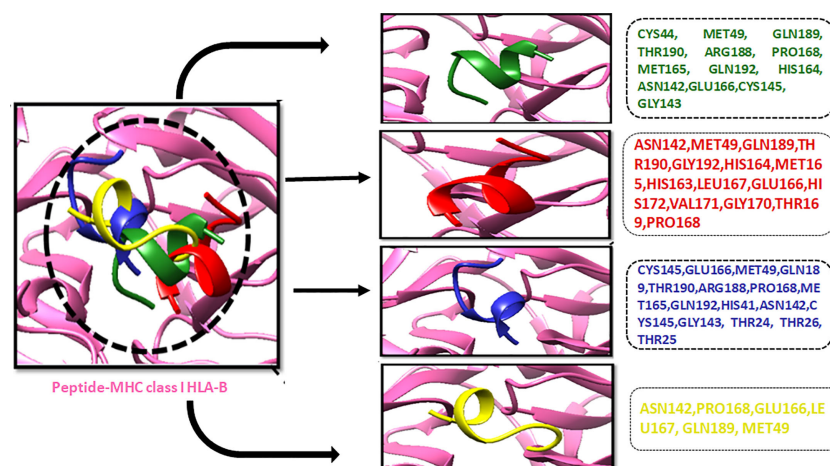


FIGURE 3

The four top-ranked peptides of MHC class I, HLA-B binding residues, and sequences are displayed in different colors.

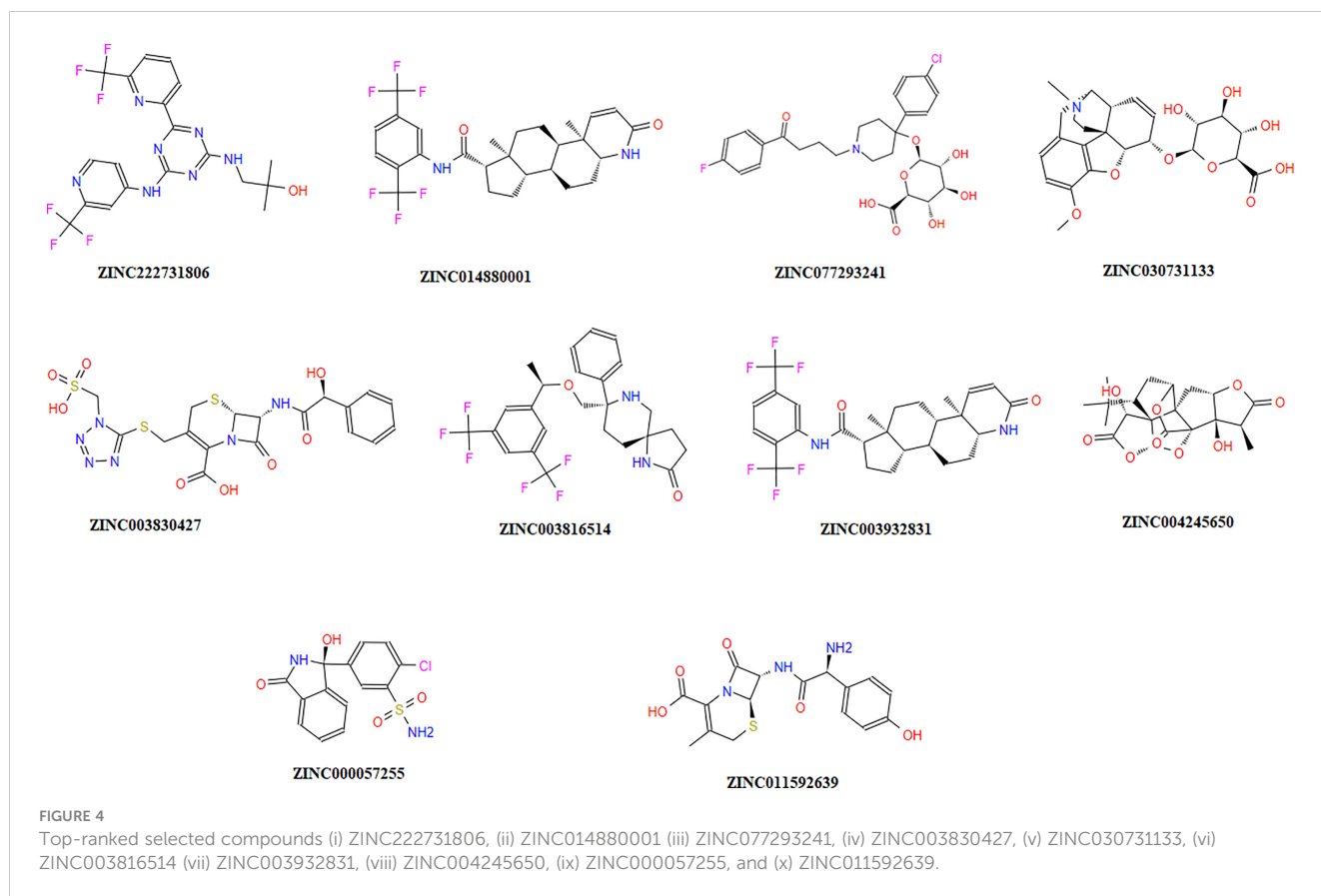


TABLE 4 Drug like properties and molecular docking analyses of the selected ten top-ranked compounds.

Ligands	Binding energy (kcal/Mol)	RMSD value	M. weight (g/Mol)	A-Log P value	Water solubility (logS)	H-Bond acceptor	H-Bond donor	Interacting residues	Lipinski rule
ZINC222731806	-8.8	2.284	473.38	4.29	-3.182	8	3	Cys44, Gln192, Pro168, Arg188, Gln189, Thr190, Cys145, Glu166, Asn142, Phe140, Met165, His41	Accepted
ZINC077293241	-8.1	2.247	552.00	2.34	-3.419	8	4	Met165, His41, Gln189, Glu166, Pro168, Asn142, Ser144, Cys145	Accepted
ZINC014880001	-8	2.207	528.54	6.58	-4.341	2	2	Cys145, Glu166, Met165, Gln189, Pro168, Arg188	Rejected
ZINC003830427	-8	2.074	542.58	-0.92	-3.133	12	4	Glu166, Leu167, Pro168, Gln189, Cys44	Rejected
ZINC030731133	-7.9	2.32	475.49	-0.58	-2.351	9	4	Asp187, Arg188, Gln189, Glu166, Cys44, His41, Asn142	Accepted
ZINC003932831	-7.8	1.815		6.58	-4.341	2	2	Asp187, Arg188, Gln189, Cys44, His41, Met49, Glu166, Met165, Pro168	Rejected
ZINC003816514	-7.7	2.812	500.48	5.73	-3.766	3	2	Glu166, Met165, Pro168, Gln192, Thr190, Arg188, Gln189, Met49, Asn142, Leu141	Accepted
ZINC004245650	-7.6	1.252	408.40	-0.34	-2.412	9	2	Met49, Gln189, Cys44	Accepted

(Continued)

TABLE 4 Continued

Ligands	Binding energy (kcal/Mol)	RMSD value	M. weight (g/Mol)	A-Log P value	Water solubility (logS)	H-Bond acceptor	H-Bond donor	Interacting residues	Lipinski rule
ZINC000057255	-7.5	0.306	318.35	0.58	-3.513	4	3	His164, Met165, Glu166, Gln189, His41, Met49, Cys44, Arg188	Accepted
ZINC011592639	-7.5	0.555	363.40	0.15	-3.082	6	4	His163, Met165, Glu166, Asn142, His41, Asp187	Accepted

highest binding affinities with close binding sites. The aqueous solubility prediction of the selected compounds defined water at 25°C and disclosed that selected molecules can dissolve in water. The selected molecules may have inadequate oral bioavailability and lower LogP values following the Lipinski’s rule of five (Supplementary S6).

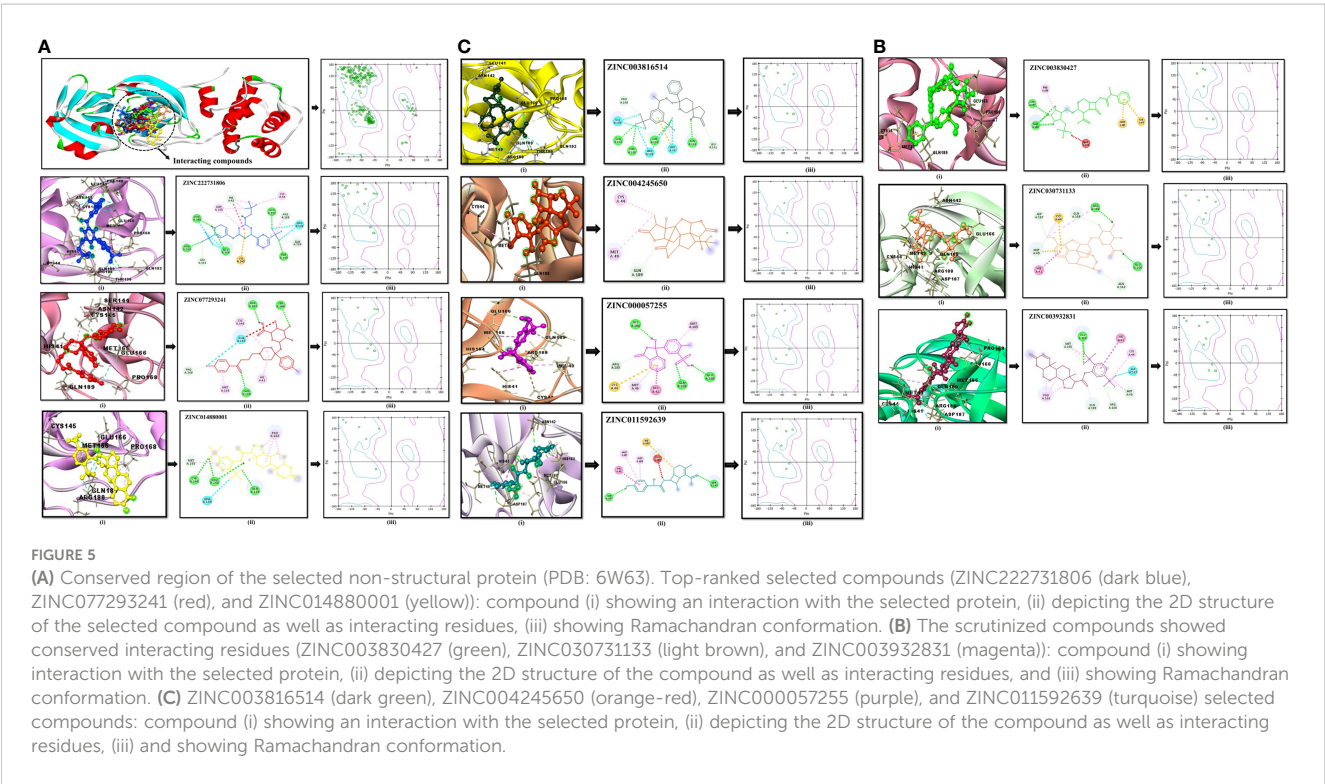
Molecular dynamics simulation

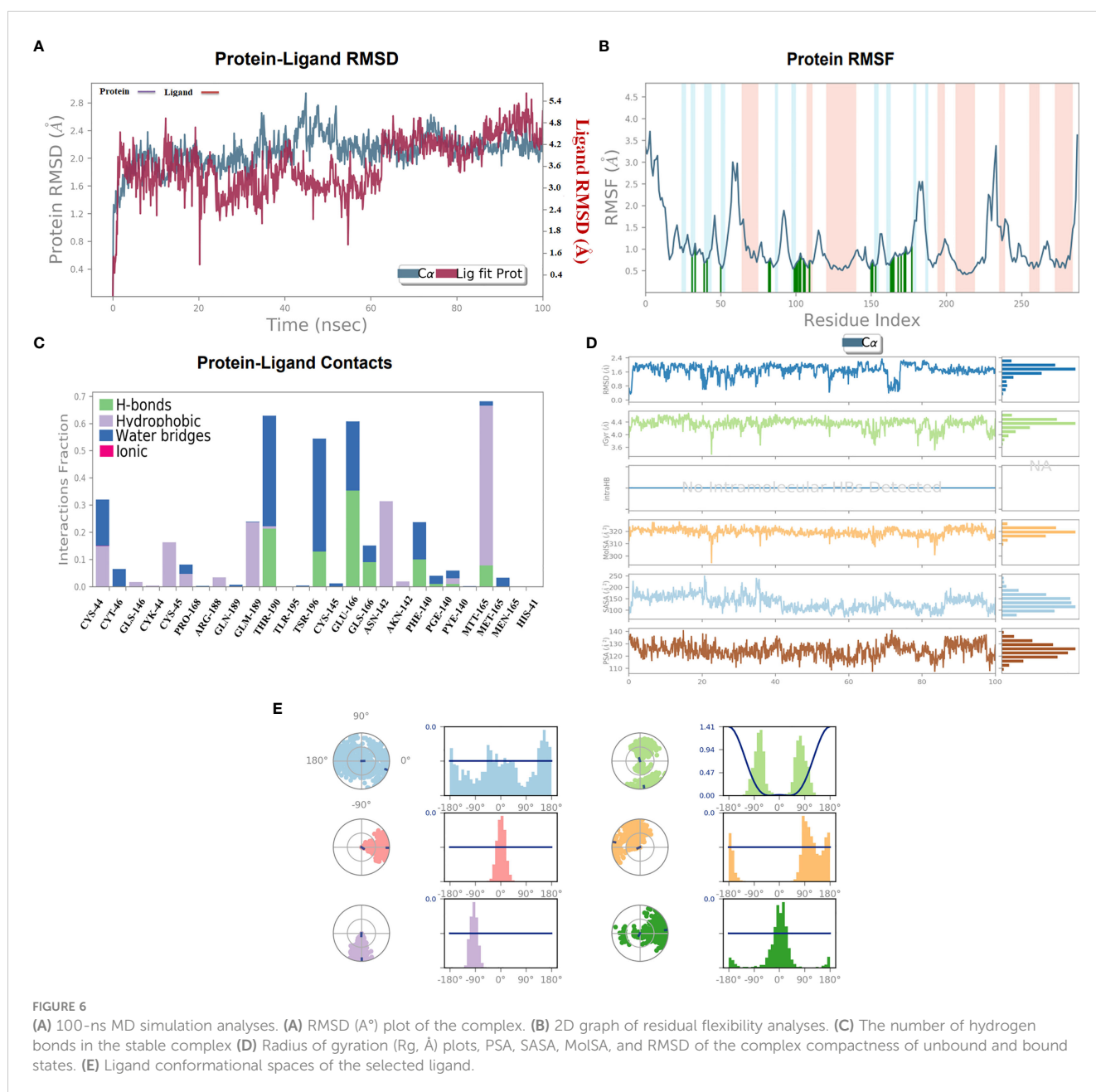
The stability of the top-ranked complex with non-structural proteins (PDB: 6W63) was investigated through MD simulation. A 100-ns MD simulation was performed, and the RMSD of the protein–ligand complex was analyzed to evaluate the conformational stability of the complex. The RMSD plot showed fluctuations in the conformation of the protein and ligand complexes, with an initial rapid change until 60 ns, after which the complex stabilized with the minimal fluctuations. The RMSD value of the stable conformations of the complex exhibited a high degree of conformational stability, with an average deviation of 2.4 Å due to the conformational change necessary

for the protein to interact with the ligand. The ligand remained within the binding pocket, making significant interactions, whereas the backbone remained coherent, with a deviation of 1.6–2.6 Å (Figure 6A).

To investigate the flexibility of the complexes and the role of each amino acid in contributing to the overall flexibility, an RMSF analysis was conducted. The utilized methodology is widely used to study the dynamic behavior of protein–protein interactions. The observed results showed that the generated complex had a low RMSF range for most of the residues, indicating high flexibility in binding with the C30 endopeptidase (Figure 6B). The finding suggested that the efficacy of the vaccine candidates in enhancing C30 endopeptidase responses may be correlated with their ability to adapt to different conformational states.

The RMSF analysis provided the valuable insights into the dynamic behavior of the complex, which could aid in optimizing the vaccine design and enhancing its efficacy. The generated findings were consistent with earlier research (Padma et al., 2023), which emphasized the importance of flexibility in interactions. Therefore, the RMSF analysis presented the significance of flexibility in the design of effective vaccines.





The formation of the hydrogen bonds between a ligand and the amino acid plays a crucial role in the stabilizing of the protein–ligand complexes. The number of hydrogen bonds present between the protein and the ligand can be calculated through simulation studies, which also allow investigating the variation in the number of changes over time. The simulation analyses indicated that the number of hydrogen bonds formed between the protein and the ligand remained relatively constant during the simulation period indicating a high degree of stability. The stability can be attributed to the critical number of hydrogen bonds that form between the two entities. A substantial number of hydrogen bonds between the protein and the complex were observed with an average of one hydrogen bond being formed throughout the simulation time. It was observed that the formation of the stable complexes may be facilitated by the presence of the observed hydrogen bonds.

The stability of the protein–ligand complex was achieved through a diverse set of interactions, including hydrogen bonds, hydrophobic interactions, and water bridges. Specifically, the ligand formed hydrogen bonds with Thr-190, Tys-145, Phe-140, and Met-165 residues (Figure 6C). Moreover, the ligand also participated in hydrophobic interactions with Lys-44, Pro-168, Ans-142, and Met-165. Additionally, a water bridge was established between the ligand positively charged nitrogen atom and the negatively charged side chain of the selected protein.

In order to assess the stability and compactness of the protein–ligand complex (Figure 6D), SASA plots were generated to determine the area accessible to the solvent. The SASA of the protein complex displayed minimal fluctuation, indicating a high degree of stability. Moreover, the SASA of the ligand in its bound state was lower (150 Å<sup>2</sup>) than in its unbound state (220 Å<sup>2</sup>),



indicating a more compact conformation upon the binding. Additionally, the MolSA of the ligand in its bound state was higher (330 Å<sup>2</sup>) than in its unbound state (310 Å<sup>2</sup>). The compactness of the protein in the complex was assessed through the measurement of its Radius of Gyration (Rg). During the early stages, Rg values fluctuated up to 60 ns; however, it became stable between 65 and 100 ns. The Rg values observed between 4.0 Å and 4.4 Å suggested a compact protein–ligand-bound state. Moreover, the stable Rg values between 12 and 16 Å suggested that the overall shape and size of the complex remained constant over a certain range of concentration. The observed results indicated that the docked complex possessed strong interactions between its components, which contributed to its greater compactness. Furthermore, the PSA of the ligand in its bound state was lower (130 Å<sup>2</sup>) than in its unbound state, further indicating a more compact conformation upon binding. Overall, the observed results demonstrated the stability and compactness of the protein–ligand complex and the strong interactions between its components.

The torsion profile is a powerful tool that sheds light on the flexibility of the ligand and the ability to conform the binding site of the protein. The ligand torsion profile of the top-ranked ligands (Figure 6E) was analyzed, and the x-axis denoted the torsion angle in degrees and the y-axis represented the associated energy. The distinct energy minima were observed in the plot, indicating the presence of multiple low-energy conformations of the ligand. Further analysis of the torsion profile revealed that the ligand adopts a planar orientation at a torsion angle of approximately -90°, with specific functional group orientations. The second lowest energy conformation occurred at a torsion angle of 180°, where the ligand takes on a twisted orientation. In essence, the torsion profile provided information about the flexibility and behavior of the ligand molecules in bound state.

The changes in protein conformation during and after the interaction were important for the stability of the complex. The conformational changes of the non-structural protein were observed through superimposition of the unbound structure with the vaccine-bound structures over the 100 ns course of MD simulation. The study also utilized a torsion profile to identify the energetically favorable conformations of the ligand, providing insight into ligand behavior and protein–ligand interactions.

## Antibody-mediated immune response

First, we predict Kolaskar and Tongaonkar process-based antigenicity (Figure 2D), where we observed two hepta-peptide sequences CVLKLKV (85 to 91) and CPRHVIC (38 to 41) with 1.220 values, and a minimum antigenicity value of 0.844 was observed for hepta-peptide sequence NGMNGRT from 274 to 280 amino acid positions, as mentioned in Supplementary S4. Then, we performed immune simulation and examined the immune responses generated in response to repeat the exposure to refined C30 endopeptidase. The simulation analyses revealed that the C30 endopeptidase induces high humoral immune response in the mammalian system. The refined C30 endopeptidase induced weak primary immunoglobulin response after first immunogen

exposure; however, the second exposure demonstrated the elevated immunoglobulin response with a high IgM+IgG response. The major share of immune response during this stage was apparently mediated by IgM. Subsequently, the exposure to refined C30 endopeptidase further raised IgM+IgG titers and the intensity of IgM and IgG responses was observed to be similar. IgG response was mainly due to IgG1, whereas the contribution of IgG2 was negligible. Such high IgM+IgG response was further supported by an amplified population of diverse B-cell subpopulations, memory B cells, and B cells expressing IgM and IgG1 isotypes. The simulation assay also suggested persistence of active antibody-producing B cells for a prolonged period.

## Discussion

Animal-derived coronaviruses can traverse species boundaries and transmit illnesses that can be fatal, in contrast to the less severe human viral diseases that are constantly prevalent in the human population (Agarwal et al., 2022; Ahmad et al., 2022). All three SARS-CoVs have caused problems with the outbreak, the original from 2003, the MERS-CoV from 2012, and the current SARS-CoV-2. The present pandemic calls for urgently developing innovative and cost-effective preventative measures (Rayan et al., 2022). Coronaviruses are massive enclosed particles that contain a considerable size of positive-sense single-stranded RNA (+ssRNA), have a genetic code of around 30 kb, and resemble a crown, as identified in numerous studies (Dutta et al., 2022; Chaitanya, 2019; Lythgoe et al., 2022). Coronaviruses play a critical role in the viral replication cycle (Lythgoe et al., 2022). The viral 3CL<sup>Pro</sup> enzyme regulates the life cycle and replication of the virus (Cabero Pérez, 2020; Hu et al., 2022). As per our frontier consequence and identification, 3CL<sup>Pro</sup> has been regarded as a possible target to develop antiviral drugs against SARS-CoV-2.

In contrast to conventional vaccine design, bioinformatics analyses enable the prediction of potent epitopes, which streamlines and expedites the vaccine design (Sajid et al., 2022). A suitable target for the B-cell epitope study might have been 3CL<sup>Pro</sup> since most of it is available outside the virion. Vaccination is a standard method for strengthening the host immune system against a particular infection. Various vaccinations, including natural or recombinant, remain costly and time-consuming and require a very long period to be launched (de Pinho Favaro et al., 2022). The immature vaccine-poor adaptive immunity and high antigenic load also result in allergic reactions. Developing multi-omics and immunoinformatics techniques have made it simpler to identify the epitopes that trigger a potent immune response.

The peptide-based vaccines are essential due to their ultra-fast mechanism of action, fewer side effects, and less toxicity (Albekairi et al., 2022). The peptide-based vaccinations are anticipated to offer a safer option to conventional immunizations. The large-scale manufacture of the peptide-based products would be more straightforward due to their chemical synthesis and high repeatability rate. Scientists have made many efforts as an immediate response to design peptide-based vaccines. The peptide inhibitors play an exciting role in developing the peptide-

based vaccines. The immunoinformatics approaches are constructive, reduce the workload of laboratory trials, and are time-saving and cost-effective compared with traditional drug design approaches (Vanhee et al., 2011). The researchers have identified several vaccine candidates by utilizing the computational techniques with promising preclinical results (Davies and Flower, 2007). CTL epitopes help to design the peptide-based vaccines against human leukocyte antigen-B protein (Tahir et al., 2018).

Extensive *in silico* analyses were performed to design epitope-based vaccine by targeting CL<sup>Pro</sup> for CTL epitopes. The current study revealed four epitopes having an immunogenic, non-toxic, and non-allergenic response. The top 25 epitopes showed 97.87% worldwide population coverage. For validation of results, CTL epitopes were optimized for all ergenicity and antigenicity as per the method of an earlier study (Dimitrov et al., 2014). Furthermore, we hypothesized epitope population coverage analyses for MHC-I (Table 3) indicating 0.0373 with an estimated hit rate of 0.3. Based on an *in silico* investigation, we predict the peptide designs in contrast to eight epitopes and HLA-B interaction characteristics of designed peptides for effective binding residues. The generated results were reconciled with literature (Rezaei and Nazari, 2022). The pI value was observed 5.95, and top-ranked four conformational predicted epitopes were used to predict the names of the residues, lengths, and locations (Table 2) and reconciled with previous literature (Sajid et al., 2022).

Surface accessibility was analyzed, and the hexa-peptide sequence KTPKYK displayed the highest score of 8.254. On the other hand, the lowest score of 0.114 was found in the 97- to 102-amino acid regions. Another sequence, FSVLAC, showed up in the 112- to 117-a.a. region. The surface flexibility analysis revealed that the hepta-peptides FCYMHHM and YNGSPSG had a score of 0.864, with amino acid ranges of 159 to 165 and 118 to 124, respectively, as shown in Figure 2B. For surface flexibility prediction, the lowest score was 0.864, ranging from 159 to 165 aa with the FCYMHHM heptapeptide sequence, and the highest score was 1.099, spanning from 118 to 124 aa with the YNGSPSG heptapeptide sequence. Parker's hydrophilicity scale analyses were also done for the hydrophilicity of peptides associated with peptide retention times using HPLC on a reversed-phase column as per the method of earlier researchers (Iranparast et al., 2022; Sajid et al., 2022). Hydrophilic regions and associated antigenic sites have been observed through immunological analysis (Parker et al., 1986) based on Parker's hydrophilicity, as shown in Figure 2C. Between 204 and 210 amino acids, the VLAWLYA hepta-peptide sequence was observed with a minimum hydrophilicity score of -4.257 and reconciled with earlier research (Sajid et al., 2022). The highest antigenicity value of 1.220 was observed in two hepta-peptide sequences, CVLKLKV (85 to 91) and CPRHVIC (38 to 41). The minimum antigenicity value of 0.844 was reported for hepta-peptide sequence NGMNGRT from 274 to 280, and results were matched with (Adhikari et al., 2022).

The global energy of the CTL epitopes selected for this study ranged from -0.54 to -26.21 kcal/mol, and results were matched with (Joshi et al., 2023). The binding solid affinities were also determined, with binding energies ranging from -3.33 to -26.36 kcal/mol, as

mentioned in Table 3. HLA-B binding affinities were calculated for the CTL-predicted epitopes, namely, SEDMLNPY, GSVGFNIDY, LLEDEFTPF, DYDCVSFCY, GTDLEGNFY, QTFSVLACY, TVNVLAWL, and TANPKTPKY. We selected top 10 complexes and top four interacting docked compounds and their similar binding pockets as shown in Figure 4, where we explored Met-49, Asn-142, Pro-168, Glu-166, and Gln-189 residues and observed that Pro-168, His-41, Arg-188, Gln-189, Cys-145, Glu-166, Met-49, Asp-187, Met-165, His-164, and Cys-44 residues are effective binding interactions (Figures 5A–C). The virtual screening of potential compounds was performed, and top 10 compounds showing binding affinities between -7.5 and -8.8 kcal/mol were observed. Our MD simulation study results showed that 3CL<sup>Pro</sup>-vaccine is complex and highly stable throughout the simulation time. The interaction between the protein and the vaccine was primarily stabilized by electrostatic configurations. During the dynamics, the docked complex also showed increased rigidity in the motion of residues. The immune simulation data suggested that using the epitopes of 3CL<sup>Pro</sup> could lead to the design of an effective SARS-CoV-2 vaccine.

Our study explored the potential of C30 endopeptidase to elicit an immune response in humans using immunoinformatics and immune simulation techniques. We found that C30 endopeptidase has multiple B-cell and T-cell epitopes, indicating its potential to stimulate high-titered antibody responses and reduce infections, including SARS-CoV-2. The immune simulation data predicted a strong immune response dominated by IgM and IgG1, with long-lived B-cell responses. Therefore, we suggest that refined C30 endopeptidase could be used in immunotherapeutic approaches to provide long-term protection against infections in the population. Moreover, in our experimental study, we identified 10 promising compounds, namely, ZINC222731806, ZINC077293241, ZINC014880001, ZINC003830427, ZINC030731133, ZINC003932831, ZINC003816514, ZINC004245650, ZINC000057255, and ZINC011592639, that could be used in C30 endopeptidase-based antibody therapy to treat infections, including SARS-CoV-2. Additionally, the epitopes of C30 endopeptidase could be used in the design of a potential vaccine against infections. These findings provide a promising avenue for the use of these compounds to target 3CL<sup>Pro</sup> and treat infections caused by SARS-CoV-2.

## Conclusion

Our study formulates a multi-epitope-based peptide vaccine using both T-cell and B-cell epitopes occurring in the 3CL<sup>Pro</sup> protein that efficiently target the SARS-CoV-2-mediated immune response. Extensive *in silico* analyses were performed to scrutinize potential peptide-based inhibitors. CTL epitopes showed potential targets for a peptide-based vaccine. An *in silico* study designed 10 different vaccine candidates' compounds, which (ZINC222731806, ZINC077293241, ZINC014880001, ZINC003830427, ZINC030731133, ZINC003932831, ZINC003816514, ZINC004245650, ZINC000057255, and ZINC011592639) showed least binding energy and high binding affinity. Molecular dynamics (MD) study of the docked 3CL<sup>Pro</sup>-vaccine complex delineated it to

be highly stable during simulation time, and the stabilization of interaction was majorly contributed by electrostatic energy. The docked complex also showed low deformation and increased rigidity in motion of residues during dynamics. The immune simulation data indicated toward the possibility of designing an effective SARS-CoV-2 vaccine using the epitopes of 3CLpro. However, this claim needs additional experimental validation in non-human primates for further preclinical development.

## Data availability statement

The original contributions presented in the study are included in the article/Supplementary Material. Further inquiries can be directed to the corresponding authors.

## Author contributions

Conceptualization, Methodology, Investigation, data collection and Writing-original manuscript: SM, MSA, MN, MS, MA, AB. Investigation, data collection: MW, SS, IZ. Editing and proof reading: SR, SAS, RS, MS, DA, WH, K-TC. Supervision: IZ, SAS, RS. All authors contributed to the article and approved the submitted version.

## Funding

This study was supported by a grant (no. RA112001) from the Tainan Municipal Hospital (managed by Show Chwan Medical Care Corporation), Tainan, Taiwan.

## References

- Adhikari, P., Jawad, B., Podgornik, R., and Ching, W.-Y. (2022). Mutations of omicron variant at the interface of the receptor domain motif and human angiotensin-converting enzyme-2. *Int. J. Mol. Sci.* 23, 2870. doi: 10.3390/ijms23052870
- Agarwal, D., Zafar, I., Ahmad, S. U., Kumar, S., Sundaray, J. K., and Rather, M. A. (2022). Structural, genomic information and computational analysis of emerging coronavirus (SARS-CoV-2). *Bull. Natl. Res. Centre* 46, 1–16. doi: 10.1186/s42269-022-00861-6
- Ahmad, S. U., Kiani, B. H., Abrar, M., Jan, Z., Zafar, I., Ali, Y., et al. (2022). A comprehensive genomic study, mutation screening, phylogenetic and statistical analysis of SARS-CoV-2 and its variant omicron among different countries. *J. Infection Public Health* 15, 878–891. doi: 10.1016/j.jiph.2022.07.002
- Albekairi, T. H., Alshammari, A., Alharbi, M., Alshammari, A. F., Tahir ul Qamar, M., Anwar, T., et al. (2022). Design of a multi-epitope vaccine against tropheryma whipplei using immunoinformatics and molecular dynamics simulation techniques. *Vaccines* 10, 691. doi: 10.3390/vaccines10050691
- Alexander, N., Woetzel, N., and Meiler, J. (2011). “Bcl: cluster: a method for clustering biological molecules coupled with visualization in the pymol molecular graphics system,” in *2011 IEEE 1st international conference on computational advances in bio and medical sciences (ICCBMS)*. (Orlando, FL, USA: IEEE), 13–18.
- Bastola, A., Sah, R., Rodriguez-Morales, A. J., Lal, B. K., Jha, R., Ojha, H. C., et al. (2020). The first 2019 novel coronavirus case in Nepal. *Lancet Infect. Dis.* 20, 279–280. doi: 10.1016/S1473-3099(20)30067-0
- Beniac, D. R., Andonov, A., Grudeski, E., and Booth, T. F. (2006). Architecture of the SARS coronavirus prefusion spike. *Nat. Struct. Mol. Biol.* 13, 751–752. doi: 10.1038/nsmb1123
- Benson, D. A., Cavanaugh, M., Clark, K., Karsch-Mizrachi, I., Ostell, J., Pruitt, K. D., et al. (2018). GenBank. *Nucleic Acids Res.* 46, D41. doi: 10.1093/nar/gkx1094
- Blunsom, P. (2004). Hidden markov models. *Lecture Notes* 15, 48.
- Cabero Pérez, M. J. (2020). Exploring the catalytic reaction of cysteine proteases. *J. Phys. Chem. B* 124, 11349–11356. doi: 10.1021/acs.jpcc.0c08192
- Chaitanya, K. (2019). “Structure and organization of virus genomes,” in *Genome and genomics* (Switzerland: Springer), 1–30.
- Chen, Z., Wang, C., Feng, X., Nie, L., Tang, M., Zhang, H., et al. (2021). Interactomes of SARS-CoV-2 and human coronaviruses reveal host factors potentially affecting pathogenesis. *EMBO J.* 40, e107776. doi: 10.15252/embj.2021107776
- Chen, Y. W., Yiu, C.-P. B., and Wong, K.-Y. (2020). Prediction of the SARS-CoV-2 (2019-nCoV) 3C-like protease (3CL pro) structure: virtual screening reveals velpatasvir, ledipasvir, and other drug repurposing candidates. *F1000Research* 9. doi: 10.12688/f1000research.22457.1
- Crow, M. K. (2021). Charles I Christian: model physician scientist and mentor. *Ann. Rheumatic Dis.* 80, 685–688. doi: 10.1136/annrheumdis-2019-216630
- Dai, W., Zhang, B., Jiang, X.-M., Su, H., Li, J., Zhao, Y., et al. (2020). Structure-based design of antiviral drug candidates targeting the SARS-CoV-2 main protease. *Science* 368, 1331–1335. doi: 10.1126/science.abb4489
- Dallakyan, S., and Olson, A. J. (2015). “Small-molecule library screening by docking with PyRx,” in *Chemical biology* (Heidelberg Dordrecht London: Springer New York), 243–250.
- Das, N. C., Ray, A. S., Bayry, J., and Mukherjee, S. (2021). Therapeutic efficacy of anti-betstrophin antibodies against experimental filariasis: immunological, immune-informatics and immune simulation investigations. *Antibodies* 10, 14. doi: 10.3390/antib10020014
- Davies, M. N., and Flower, D. R. (2007). Harnessing bioinformatics to discover new vaccines. *Drug Discovery Today* 12, 389–395. doi: 10.1016/j.drudis.2007.03.010
- de Pinho Favaro, M. T., Atienza-Garriga, J., Martínez-Torró, C., Parladé, E., Vázquez, E., Corchero, J. L., et al. (2022). Recombinant vaccines in 2022: a perspective from the cell factory. *Microbial Cell Factories* 21, 1–17. doi: 10.1186/s12934-022-01929-8

## Acknowledgments

The authors acknowledge the support from Princess Nourah bint Abdulrahman University researchers supporting project number (PNURSP2023R15) and Princess Nourah bint Abdulrahman University, Riyadh, Saudi Arabia.

## Conflict of interest

The authors declare that the research was conducted in the absence of any commercial or financial relationships that could be construed as a potential conflict of interest.

## Publisher's note

All claims expressed in this article are solely those of the authors and do not necessarily represent those of their affiliated organizations, or those of the publisher, the editors and the reviewers. Any product that may be evaluated in this article, or claim that may be made by its manufacturer, is not guaranteed or endorsed by the publisher.

## Supplementary material

The Supplementary Material for this article can be found online at: <https://www.frontiersin.org/articles/10.3389/fcimb.2023.1134802/full#supplementary-material>



- De Wilde, A. H., Snijder, E. J., Kikkert, M., and van Hemert, M. J. (2017). Host factors in coronavirus replication. *Roles Host Gene non-coding RNA Expression Virus infection* 419, 1–42. doi: 10.1007/978-3-030-05369-7
- Dimitrov, I., Naneva, L., Doytchinova, I., and Bangov, I. (2014). AllergenFP: allergenicity prediction by descriptor fingerprints. *Bioinformatics* 30, 846–851. doi: 10.1093/bioinformatics/btt619
- Douglas, M. G., Kocher, J. F., Scobey, T., Baric, R. S., and Cockrell, A. S. (2018). Adaptive evolution influences the infectious dose of MERS-CoV necessary to achieve severe respiratory disease. *Virology* 517, 98–107. doi: 10.1016/j.virol.2017.12.006
- Dutta, S., Ghosh, R., Ghosh, D., Santra, P., and Daw, S. (2022). A detailed study of covid-19 (Emphasizing its genomic variants, pathogenicity, phylogenetic analysis, epidemiology, and clinical measures). *International Healthcare Res. J.* 6, 8–30. doi: 10.26440/IHRJ/0605.08556
- Fehr, A. R., Channappanavar, R., and Perlman, S. (2017). Middle East respiratory syndrome: emergence of a pathogenic human coronavirus. *Annu. Rev. Med.* 68, 387–399. doi: 10.1146/annurev-med-051215-031152
- Fleri, W., Salimi, N., Vita, R., Peters, B., and Sette, A. (2016). *Immune epitope database and analysis resource*. (La Jolla, CA, USA: Jolla Institute for Allergy and Immunology). doi: 10.1016/B978-0-12-374279-7.06004-5
- Guan, W.-j., Ni, Z.-y., Hu, Y., Liang, W.-h., Ou, C.-q., He, J.-x., et al. (2020). Clinical characteristics of coronavirus disease 2019 in China. *New Engl. J. Med.* 382, 1708–1720. doi: 10.1056/NEJMoa2002032
- Hu, Q., Xiong, Y., Zhu, G. H., Zhang, Y. N., Zhang, Y. W., Huang, P., et al. (2022). The SARS-CoV-2 main protease (Mpro): structure, function, and emerging therapies for COVID-19. *MedComm* 3, e151. doi: 10.1002/mco.2151
- Huang, P.-T., Lo, P.-H., Wang, C.-H., Pang, C.-T., and Lou, K.-L. (2010). “PPDock-port patch dock: a web server for drug virtual screen and visualizing the docking structure by GP and X-score,” in *ACTA CRYSTALLOGRAPHICA a-FOUNDATION AND ADVANCES*. (Taiwan: Institutes of Biochemistry and Molecular Biology, College of Medicine, National Taiwan University) (Acta Cryst). S233–S234.
- Huang, C., Wang, Y., Li, X., Ren, L., Zhao, J., Hu, Y., et al. (2020). “Clinical features of patients infected with 2019 novel coronavirus in wuhan, China. *Lancet* 395, 497–506. doi: 10.1016/S0140-6736(20)30183-5
- Ip, P. P., Nijman, H. W., and Daemen, T. (2015). Epitope prediction assays combined with validation assays strongly narrows down putative cytotoxic T lymphocyte epitopes. *Vaccines* 3, 203–220. doi: 10.3390/vaccines3020203
- Iranparast, S., Ghafourian, M., and Tahmasebi Birgani, M. (2022). Protein e-peptide driven vaccine for novel coronavirus: immunoinformatics. *J. Kerman Univ. Med. Sci.* 29, 368–377. doi: 10.22062/jkmu.2022.92012
- Irwin, J. J., and Shoichet, B. K. (2005). ZINC— a free database of commercially available compounds for virtual screening. *J. Chem. Inf. modeling* 45, 177–182. doi: 10.1021/ci049714+
- Jin, Z., Du, X., Xu, Y., Deng, Y., Liu, M., Zhao, Y., et al. (2020). Structure of m pro from SARS-CoV-2 and discovery of its inhibitors. *Nature* 582, 289–293. doi: 10.1038/s41586-020-2223-y
- Joshi, A., Akhtar, N., Sharma, N. R., Kaushik, V., and Borkotoky, S. (2023). MERS virus spike protein HTL-epitopes selection and multi-epitope vaccine design using computational biology. *J. Biomolecular Structure Dynamics* 1–16. doi: 10.1080/07391102.2023.2191137
- Kannan, S., Subbaram, K., Ali, S., and Kannan, H. (2020). Protein in SARS-CoV-1, SARS-CoV-2, MERS-CoV, and bat coronavirus. *J. Pure Appl. Microbiol.* 14, 757–763. doi: 10.22207/JPAM.14.SPL1.13
- Kingsford, C. L., Chazelle, B., and Singh, M. (2005). Solving and analyzing side-chain positioning problems using linear and integer programming. *Bioinformatics* 21, 1028–1039. doi: 10.1093/bioinformatics/bti144
- Knapp, B., Frantal, S., Cibena, M., Schreiner, W., and Bauer, P. (2011). Is an intuitive convergence definition of molecular dynamics simulations solely based on the root mean square deviation possible? *J. Comput. Biol.* 18, 997–1005. doi: 10.1089/cmb.2010.0237
- Lamiable, A., Thévenet, P., Rey, J., Vavrusa, M., Derreumaux, P., and Tuffery, P. (2016). PEP-FOLD3: faster de novo structure prediction for linear peptides in solution and in complex. *Nucleic Acids Res.* 44, W449–W454. doi: 10.1093/nar/gkw329
- Larsen, M. V., Lundegaard, C., Lamberth, K., Buus, S., Lund, O., and Nielsen, M. (2007). Large-Scale validation of methods for cytotoxic T-lymphocyte epitope prediction. *BMC Bioinf.* 8, 1–12. doi: 10.1186/1471-2105-8-424
- Lazarski, C. A., Chaves, F. A., Jenks, S. A., Wu, S., Richards, K. A., Weaver, J., et al. (2005). The kinetic stability of MHC class II: peptide complexes is a key parameter that dictates immunodominance. *Immunity* 23, 29–40. doi: 10.1016/j.immuni.2005.05.009
- Li, J., Guo, M., Tian, X., Wang, X., Yang, X., Wu, P., et al. (2021). Virus-host interactome and proteomic survey reveal potential virulence factors influencing SARS-CoV-2 pathogenesis. *Med* 2, 99–112. doi: 10.1016/j.medj.2020.07.002
- Lu, H., Stratton, C. W., and Tang, Y. W. (2020). Outbreak of pneumonia of unknown etiology in wuhan, China: the mystery and the miracle. *J. Med. Virol.* 92, 401. doi: 10.1002/jmv.25678
- Lythgoe, K. A., Golubchik, T., Hall, M., House, T., MacIntyre-Cockett, G., Fryer, H., et al. (2022). Lineage replacement and evolution captured by the united kingdom covid infection survey. *MedRxiv*. doi: 10.1101/2022.01.05.21268323
- Manandhar, S., Pai, K. S. R., Krishnamurthy, P. T., Kiran, A. V. R., and Kumari, G. K. (2022). Identification of novel TMPRSS2 inhibitors against SARS-CoV-2 infection: a structure-based virtual screening and molecular dynamics study. *Struct. Chem.* 33, 1529–1541. doi: 10.1007/s11224-022-01921-3
- Mashiach, E., Schneidman-Duhovny, D., Andrusier, N., Nussinov, R., and Wolfson, H. J. (2008). FireDock: a web server for fast interaction refinement in molecular docking. *Nucleic Acids Res.* 36, W229–W232. doi: 10.1093/nar/gkn186
- Maupetit, J., Tuffery, P., and Derreumaux, P. (2007). A coarse-grained protein force field for folding and structure prediction. *Proteins: Structure Function Bioinf.* 69, 394–408. doi: 10.1002/prot.21505
- Nain, Z., Abdulla, F., Rahman, M. M., Karim, M. M., Khan, M. S. A., Sayed, S. B., et al. (2020). Proteome-wide screening for designing a multi-epitope vaccine against emerging pathogen elizabethkingia anophelis using immunoinformatic approaches. *J. Biomolecular Structure Dynamics* 38, 4850–4867. doi: 10.1080/07391102.2019.1692072
- O'Donovan, C., Martin, M. J., Gattiker, A., Gasteiger, E., Bairoch, A., and Apweiler, R. (2002). High-quality protein knowledge resource: SWISS-PROT and TrEMBL. *Briefings Bioinf.* 3, 275–284. doi: 10.1093/bib/3.3.275
- Oanca, G., Asadi, M., Saha, A., Ramachandran, B., and Warshel, A. (2020). Exploring the catalytic reaction of cysteine proteases. *J. Phys. Chem. B* 124, 11349–11356. doi: 10.1021/acs.jpcc.0c08192
- O'Meara, M. J., Guo, J. Z., Swaney, D. L., Tummino, T. A., and Hüttenhain, R. (2020). A SARS-CoV-2-human protein-protein interaction map reveals drug targets and potential drug-repurposing. *BioRxiv* 2020, 123. doi: 10.1101/2020.03.22.002386
- Padma, S., Patra, R., Sen Gupta, P. S., Panda, S. K., Rana, M. K., and Mukherjee, S. (2023). Cell surface fibroblast activation protein-2 (Fap2) of fusobacterium nucleatum as a vaccine candidate for therapeutic intervention of human colorectal cancer: an immunoinformatics approach. *Vaccines* 11, 525. doi: 10.3390/vaccines11030525
- Parker, J., Guo, D., and Hodges, R. (1986). New hydrophobicity scale derived from high-performance liquid chromatography peptide retention data: correlation of predicted surface residues with antigenicity and X-ray-derived accessible sites. *Biochemistry* 25, 5425–5432. doi: 10.1021/bi00367a013
- Petersen, E. F., Goddard, T. D., Huang, C. C., Couch, G. S., Greenblatt, D. M., Meng, E. C., et al. (2004). UCSF chimera—a visualization system for exploratory research and analysis. *J. Comput. Chem.* 25, 1605–1612. doi: 10.1002/jcc.20084
- Ponomarenko, J., Bui, H.-H., Li, W., Fusseder, N., Bourne, P. E., Sette, A., et al. (2008). ElliPro: a new structure-based tool for the prediction of antibody epitopes. *BMC Bioinf.* 9, 1–8. doi: 10.1186/1471-2105-9-514
- Purcell, A. W., McCluskey, J., and Rossjohn, J. (2007). More than one reason to rethink the use of peptides in vaccine design. *Nat. Rev. Drug Discovery* 6, 404–414. doi: 10.1038/nrd2224
- Raghava, G., Searle, S. M., Audley, P. C., Barber, J. D., and Barton, G. J. (2003). OXBench: a benchmark for evaluation of protein multiple sequence alignment accuracy. *BMC Bioinf.* 4, 1–23. doi: 10.1186/1471-2105-4-47
- Rapin, N., Lund, O., Bernaschi, M., and Castiglione, F. (2010). Computational immunology meets bioinformatics: the use of prediction tools for molecular binding in the simulation of the immune system. *PLoS One* 5, e9862. doi: 10.1371/journal.pone.0009862
- Rastogi, P. A. (1999). MacVector: integrated sequence analysis for the macintosh. *Bioinf. Methods Protoc.* 132, 47–69. doi: 10.1385/1-59259-192-2:47
- Rather, M. A., Dutta, S., Guttula, P. K., Dhandare, B. C., Yusufzai, S., and Zafar, M. I. (2020). Structural analysis, molecular docking and molecular dynamics simulations of G-protein-coupled receptor (kisspeptin) in fish. *J. Biomolecular Structure Dynamics* 38, 2422–2439. doi: 10.1080/07391102.2019.1633407
- Rayan, R. A., Tsagkaris, C., Zafar, I., and Tata, A. (2022). “Epidemiology of COVID-19,” in *COVID-19 and SARS-CoV-2* (UK: CRC Press), 63–78.
- Rezaei, M., and Nazari, M. (2022). New generation vaccines for COVID-19 based on peptide, viral vector, artificial antigen presenting cell, DNA or mRNA. *Avicenna J. Med. Biotechnol.* 14, 30. doi: 10.18502/ajmb.v14i1.8167
- Riva, L., Yuan, S., Yin, X., Martin-Sancho, L., Matsunaga, N., Pache, L., et al. (2020). Discovery of SARS-CoV-2 antiviral drugs through large-scale compound repurposing. *Nature* 586, 113–119. doi: 10.1038/s41586-020-2577-1
- Sajid, M., Marriam, S., Mukhtar, H., Sohail, S., Sajid, M., and Sehgal, S. A. (2022). Epitope-based peptide vaccine design and elucidation of novel compounds against 3C like protein of SARS-CoV-2. *PLoS One* 17, e0264700. doi: 10.1371/journal.pone.0264700
- Schneidman-Duhovny, D., Inbar, Y., Nussinov, R., and Wolfson, H. J. (2005). PatchDock and SymmDock: servers for rigid and symmetric docking. *Nucleic Acids Res.* 33, W363–W367. doi: 10.1093/nar/gki481
- Schubert, K., Karousis, E. D., Jomaa, A., Scaiola, A., Echeverria, B., Gurzeler, L.-A., et al. (2020). SARS-CoV-2 Nsp1 binds the ribosomal mRNA channel to inhibit translation. *Nat. Struct. Mol. Biol.* 27, 959–966. doi: 10.1038/s41594-020-0511-8
- Shen, J., Cheng, F., Xu, Y., Li, W., and Tang, Y. (2010). Estimation of ADME properties with substructure pattern recognition. *J. Chem. Inf. modeling* 50, 1034–1041. doi: 10.1021/ci100104j
- Shu, Y., and McCauley, J. (2017). GISAID: global initiative on sharing all influenza data—from vision to reality. *Eurosurveillance* 22, 30494. doi: 10.2807/1560-7917.ES.2017.22.13.30494
- Sievers, F., and Higgins, D. G. (2014). Clustal omega. *Curr. Protoc. Bioinf.* 48, 3.13.1–3.13.16. doi: 10.1002/0471250953.bi0313s48
- Tabti, K., Ahmad, I., Zafar, I., Sbati, A., Maghat, H., Bouachrine, M., et al. (2023). Profiling the structural determinants of pyrrolidine derivative as gelatinases (MMP-2 and MMP-9) inhibitors using in silico approaches. *Comput. Biol. Chem.* 104, 107855. doi: 10.1016/j.compbiolchem.2023.107855

- Tahir, R. A., Wu, H., Rizwan, M. A., Jafar, T. H., Saleem, S., and Sehgal, S. A. (2018). Immunoinformatics and molecular docking studies reveal potential epitope-based peptide vaccine against DENV-NS3 protein. *J. Theor. Biol.* 459, 162–170. doi: 10.1016/j.jtbi.2018.10.005
- Tahir ul Qamar, M., Rehman, A., Tusleem, K., Ashfaq, U. A., Qasim, M., Zhu, X., et al. (2020). Designing of a next generation multi-epitope based vaccine (MEV) against SARS-CoV-2: immunoinformatics and in silico approaches. *PLoS One* 15, e0244176. doi: 10.1371/journal.pone.0244176
- The UniProt Consortium. (2022). The Universal Protein Knowledgebase in 2023. *Nucleic Acids Res.* 51 (D1), D523–D531. doi: 10.1093/nar/gkac1052
- Vanhee, P., van der Sloot, A. M., Verschuere, E., Serrano, L., Rousseau, F., and Schymkowitz, J. (2011). Computational design of peptide ligands. *Trends Biotechnol.* 29, 231–239. doi: 10.1016/j.tibtech.2011.01.004
- Vilela Rodrigues, T. C., Jaiswal, A. K., de Sarom, A., de Castro Oliveira, L., Freire Oliveira, C. J., Ghosh, P., et al. (2019). Reverse vaccinology and subtractive genomics reveal new therapeutic targets against mycoplasma pneumoniae: a causative agent of pneumonia. *R. Soc. Open Sci.* 6, 190907. doi: 10.1098/rsos.190907
- Vita, R., Mahajan, S., Overton, J. A., Dhanda, S. K., Martini, S., Cantrell, J. R., et al. (2019). The immune epitope database (IEDB): 2018 update. *Nucleic Acids Res.* 47, D339–D343. doi: 10.1093/nar/gky1006
- Wallace, A. C., Laskowski, R. A., and Thornton, J. M. (1995). LIGPLOT: a program to generate schematic diagrams of protein-ligand interactions. *Protein engineering design selection* 8, 127–134. doi: 10.1093/protein/8.2.127
- Waqas, M., Haider, A., Rehman, A., Qasim, M., Umar, A., Sufyan, M., et al. (2021). Immunoinformatics and molecular docking studies predicted potential multi-epitope-based peptide vaccine and novel compounds against novel SARS-CoV-2 through virtual screening. *BioMed. Res. Int.* 2021. doi: 10.1155/2021/1596834
- Waqas, M., Haider, A., Sufyan, M., Siraj, S., and Sehgal, S. A. (2020). Determine the potential epitope based peptide vaccine against novel SARS-CoV-2 targeting structural proteins using immunoinformatics approaches. *Front. Mol. Biosci.* 7. doi: 10.3389/fmolb.2020.00227
- Way, G. (2021). *Pushing the limits: increasing the speed and specificity of SARS-CoV-2 testing*. (United States: VCU Scholars Compass)
- W. H. Organization (2019) *Coronavirus*. Available at: <https://www.who.int/health-topics/coronavirus> (Accessed July, 12, 2020).
- Xiao, Y., Li, Z., Wang, X., Wang, Y., Wang, Y., Wang, G., et al. (2021). Comparison of three TaqMan real-time reverse transcription-PCR assays in detecting SARS-CoV-2. *J. Virological Methods* 288, 114030. doi: 10.1016/j.jviromet.2020.114030
- Xiong, G., Wu, Z., Yi, J., Fu, L., Yang, Z., Hsieh, C., et al. (2021). ADMETlab 2.0: an integrated online platform for accurate and comprehensive predictions of ADMET properties. *Nucleic Acids Res.* 49. doi: 10.1093/nar/gkab255
- Zhao, L., Jha, B. K., Wu, A., Elliott, R., Ziebuhr, J., Gorbalenya, A. E., et al. (2012). Antagonism of the interferon-induced OAS-RNase I pathway by murine coronavirus ns2 protein is required for virus replication and liver pathology. *Cell Host Microbe* 11, 607–616. doi: 10.1016/j.chom.2012.04.011





## OPEN ACCESS

## EDITED BY

Parth Sarthi Sen Gupta,  
D Y Patil International University, India

## REVIEWED BY

Giuseppe Losurdo,  
University of Bari Medical School, Italy  
Gargi Mishra,  
Fred Hutchinson Cancer Research Center,  
United States

## \*CORRESPONDENCE

Pengyuan Zheng  
✉ pyzheng@zzu.edu.cn  
Yang Mi  
✉ yangmi198@zzu.edu.cn

RECEIVED 29 March 2023

ACCEPTED 07 July 2023

PUBLISHED 09 August 2023

## CITATION

Shen S, Ren F, Qin H, Bukhari I, Yang J,  
Gao D, Ouwehand AC, Lehtinen MJ,  
Zheng P and Mi Y (2023) *Lactobacillus*  
*acidophilus* NCFM and *Lactiplantibacillus*  
*plantarum* Lp-115 inhibit *Helicobacter*  
*pylori* colonization and gastric  
inflammation in a murine model.  
*Front. Cell. Infect. Microbiol.* 13:1196084.  
doi: 10.3389/fcimb.2023.1196084

## COPYRIGHT

© 2023 Shen, Ren, Qin, Bukhari, Yang, Gao,  
Ouwehand, Lehtinen, Zheng and Mi. This is  
an open-access article distributed under the  
terms of the [Creative Commons Attribution](#)  
[License \(CC BY\)](#). The use, distribution or  
reproduction in other forums is permitted,  
provided the original author(s) and the  
copyright owner(s) are credited and that  
the original publication in this journal is  
cited, in accordance with accepted  
academic practice. No use, distribution or  
reproduction is permitted which does not  
comply with these terms.

# *Lactobacillus acidophilus* NCFM and *Lactiplantibacillus plantarum* Lp-115 inhibit *Helicobacter pylori* colonization and gastric inflammation in a murine model

Siqi Shen<sup>1,2</sup>, FeiFei Ren<sup>1,2</sup>, Haiming Qin<sup>1,2</sup>, Ihtisham Bukhari<sup>1,2</sup>,  
Jing Yang<sup>3</sup>, Dafang Gao<sup>3</sup>, Arthur C. Ouwehand<sup>4</sup>,  
Markus J. Lehtinen<sup>4</sup>, Pengyuan Zheng<sup>1,2\*</sup> and Yang Mi<sup>1,2\*</sup>

<sup>1</sup>Henan Key Laboratory of *Helicobacter pylori* & Microbiota and Gastrointestinal Cancer, Marshall  
Medical Research Center, The Fifth Affiliated Hospital of Zhengzhou University, Zhengzhou, China,

<sup>2</sup>Department of Gastroenterology, The Fifth Affiliated Hospital of Zhengzhou University, Zhengzhou,  
Henan, China, <sup>3</sup>R&D Health & Biosciences, Danisco (China) Holding Co. Ltd, Shanghai, China, <sup>4</sup>IFF  
Health & Biosciences, Global Health and Nutrition Science, Kantvik, Finland

**Purpose:** To determine the role of *Lactobacillus* strains and their combinations in  
inhibiting the colonization of *H. pylori* and gastric mucosa inflammation.

**Methods:** Human gastric adenocarcinoma AGS cells were incubated with *H.*  
*pylori* and six probiotic strains (*Lactobacillus acidophilus* NCFM, *L. acidophilus*  
La-14, *Lactiplantibacillus plantarum* Lp-115, *Lactocaseibacillus paracasei* Lpc-37,  
*Lactocaseibacillus rhamnosus* Lr-32, and *L. rhamnosus* GG) and the adhesion  
ability of *H. pylori* in different combinations was evaluated by fluorescence  
microscopy and urease activity assay. Male C57BL/6 mice were randomly  
divided into five groups (uninfected, *H. pylori*, *H. pylori*+NCFM, *H. pylori*+Lp-  
115, and *H. pylori*+NCFM+Lp-115) and treated with two lactobacilli strains (NCFM  
and Lp-115) for six weeks. *H. pylori* colonization and tissue inflammation statuses  
were determined by rapid urease test, Hematoxylin-Eosin (HE) staining,  
immunohistochemistry, and qRT-PCR and ELISA.

**Results:** *L. acidophilus* NCFM, *L. acidophilus* La-14, *L. plantarum* Lp-115, *L.*  
*paracasei* Lpc-37, *L. rhamnosus* Lr-32, and *L. rhamnosus* GG reduced *H. pylori*  
adhesion and inflammation caused by *H. pylori* infection in AGS cells and mice.  
Among all probiotics *L. acidophilus* NCFM and *L. plantarum*, Lp-115 showed  
significant effects on the *H. pylori* eradication and reduction of inflammation *in-*  
*vitro* and *in-vivo*. Compared with the *H. pylori* infection group, the mRNA and  
protein expression levels of IL-8 and TNF- $\alpha$  in the six *Lactobacillus* intervention  
groups were significantly reduced. The changes in the urease activity (*ureA* and  
*ureB*) for 1-7h in each group showed that *L. acidophilus* NCFM, *L. acidophilus*  
La-14, *L. plantarum* Lp-115, and *L. rhamnosus* GG effectively reduced the  
colonization of *H. pylori*. We observed a higher ratio of lymphocyte and  
plasma cell infiltration into the lamina propria of the gastric mucosa and  
neutrophil infiltration in *H. pylori*+NCFM+Lp-115 mice. The infiltration of  
inflammatory cells in lamina propria of the gastric mucosa was reduced in the

*H. pylori*+NCFM+Lp-115 group. Additionally, the expression of IFN- $\gamma$  was decreased significantly in the NCFM and Lp-115 treated C57BL/6 mice.

**Conclusions:** *L. acidophilus* NCFM and *L. plantarum* Lp-115 can reduce the adhesion of *H. pylori* and inhibit the gastric inflammatory response caused by *H. pylori* infection.

#### KEYWORDS

*Helicobacter pylori*, *Lactobacillus*, adhesion, inflammation, probiotic

## 1 Introduction

*Helicobacter pylori* infect over 50% of the population worldwide, and the World Health Organization (WHO) has listed *H. pylori* as a class I carcinogen since 1994 (Hooi et al., 2017; Shah et al., 2021). *H. pylori* infection is closely related to the occurrence and development of various gastrointestinal diseases, such as chronic gastritis, peptic ulcer, gastric cancer, and gastric mucosa associated lymphoid tissue lymphoma (Sugano et al., 2015; Liu et al., 2018; Liou et al., 2020; Robinson and Atherton, 2021). Currently, the primary method to eradicate *H. pylori* is a quadruple therapy based on a proton pump inhibitor, two antibiotics, and a bismuth agent (Fallone et al., 2016; Chey et al., 2017). However, the antibiotic resistance rate of *H. pylori* has increased, and the side effects of the eradication therapy can be severe (Savoldi et al., 2018). Therefore, searching for novel and efficient *H. pylori* management options has become an urgent aim (Fallone et al., 2019).

Studies on probiotics and *H. pylori* have made significant progress recently, thus, increasingly being used in routine clinics (Suez et al., 2019; Sousa et al., 2022). Currently, blends of probiotics are the most widely studied, but little is known about the antagonistic or synergistic effects of the different probiotic strains (Vieira et al., 2013; Ouwehand et al., 2018; Simon et al., 2021). To manage *H. pylori* infection, the Maastricht VI/Florence Consensus Report mentioned that only some probiotics could effectively reduce gastrointestinal side effects in *H. pylori* eradication therapy, suggesting strain-specific efficacy (Malfertheiner et al., 2022). However, the European Society of Paediatric Gastroenterology and Hepatology later updated the guidelines. They considered that the existing evidence was insufficient to support the routine use of single or compound probiotic strains in treating *H. pylori* to reduce adverse reactions and improve the eradication rate (Jones et al., 2017). Therefore, probiotics are mainly used as an adjunct to *H. pylori* eradication therapy, and only a few reports are available for using probiotics as a single treatment for *H. pylori* infection, and further investigations are warranted.

The applications of certain probiotics, such as lactobacilli, fecal bacteria, *Bifidobacterium* spp., *Saccharomyces* spp., and *Bacillus licheniformis*, to assist in *H. pylori* eradication have been incorporated into *H. pylori* treatment guidelines (Shi et al., 2019). These probiotics attenuate the gastrointestinal adverse effects of

*H. pylori* eradication therapy, but whether they can improve *H. pylori* eradication rates is controversial (Liu et al., 2018). Meta-analyses on the efficacy of multiple probiotic strains in treating *H. pylori* have shown the most significant effects with lactobacilli (Lu et al., 2016; McFarland et al., 2016). In related studies of using lactobacilli for treating *H. pylori* infection, certain lactobacilli such as *Lactobacillus acidophilus*, *Lacticaseibacillus rhamnosus*, *Lactiplantibacillus plantarum*, *Lacticaseibacillus paracasei*, *Limosilactobacillus reuteri* and *Lactobacillus delbrueckii* subsp. *bulgaricus* can effectively manage *H. pylori* infection (Zhao et al., 2018; Chen et al., 2019; Yoon et al., 2019; Asgari et al., 2020; Lin et al., 2020; Dargenio et al., 2021) but underlying mechanisms are not well explained. However, it has been speculated that lactobacilli interfere with the adhesion of *H. pylori* to the mucosa and down-regulate the immune and inflammatory mediators (Keikha and Karbalaee, 2021).

In this study, six lactobacilli strains with good acid, bile salt, and digestive enzyme resistance, combined with good mucosal adhesion were used in screening experiments to identify probiotics that inhibit the adhesion and inflammatory response to *H. pylori*. We tested the selected probiotics in the *H. pylori* infected AGS cell line and mouse models. The results of the cell model experiments provided a basis for probiotic strain selection for the eradication of *H. pylori* in the mouse model.

## 2 Materials and methods

### 2.1 Bacterial strains, cell lines and animals

*H. pylori* P12 and *H. pylori* P12-GFP strains were provided by the Max Planck Institute for Infection Biology and *H. pylori* SS1 (ATCC 43504) (Lee et al., 1997) was provided by the University of Western Australia (UWA), Australia. *H. pylori* strains were cultured on Columbia agar containing 7% sterile defibrinated sheep blood (Bianzhen, Nanjing, China), 20 $\mu$ g/ml vancomycin (Meilunbio, Dalian, China), 10 $\mu$ g/ml polymyxin (Meilunbio), 10 $\mu$ g/ml amphotericin B (Meilunbio), 10 $\mu$ g/ml trimethoprim (Sigma, St. Louis, USA), then placed in an incubator containing 5% O<sub>2</sub> and 10% CO<sub>2</sub>, cultured at 37°C, subcultured once every three days, and used for the experiment after subculture. The tested lactobacilli were provided by Danisco China (Shanghai, China):

*Lactobacillus acidophilus* NCFM (ATCC 7003969), *L. acidophilus* La-14 (ATCC SD5212), *Lactiplantibacillus plantarum* Lp-115 (ATCC SD5209), *Lacticaseibacillus paracasei* Lpc-37 (ATCC SD5275), *Lacticaseibacillus rhamnosus* Lr-32 (ATCC SD5217) and *L. rhamnosus* GG (ATCC 53103). After the Gram Staining Kit (Solarbio, Beijing, China) was used to identify the bacterial morphology, the lactobacilli were cultured anaerobically in MRS broth (Solarbio) at 37 °C 48 hours and then subcultured (Figure S1).

The human gastric adenocarcinoma cell line (AGS) was purchased from the Institute of Biochemistry and Cell Biology of the Chinese Academy of Sciences (Shanghai, China) and cultured in RPMI 1640 medium (Thermo Fisher, Waltham, MA, USA) supplemented with 10% fetal bovine serum at 37°C and 5% CO<sub>2</sub> in a humidified incubator.

Fifty male C57BL/6 mice, Specific Pathogen Free (SPF), four weeks old, were purchased from Zhejiang Vital River Laboratory Animal Technology Co. Ltd. (Zhejiang, China). All the animals were housed under standard conditions (SPF grade animal room with individually ventilated cages; temperature range from 23°C to 25°C, humidity range from 50% to 60%, 12/12 hours light/dark cycle, food and water were provided ad libitum). The experimental steps and ethics were approved by the ethics committee of the Fifth Affiliated Hospital of Zhengzhou University (KY2022002).

## 2.2 Cytokine profiles quantification by ELISA

After infection, the culture medium was collected by centrifugation at 12000x rpm for 5 min to remove cell debris and bacteria and collect the supernatant. The concentration of interleukin (IL)-8 and tumor necrosis factor (TNF)- $\alpha$  were detected by human IL-8 ELISA Kit (Elabscience, Wuhan, China) and human TNF- $\alpha$  ELISA Kit (Elabscience, Houston, TX, USA) respectively, by following the guidelines of the manufacturer. All experiments were performed in triplicate.

## 2.3 *H. pylori* and lactobacilli co-infection model *in vitro*

*H. pylori* P12 and lactobacilli were cultured overnight in BHI (Thermo Fisher) and MRS broth. After centrifugation at 5000 x rpm for 8 min and 4000 x rpm for 5 min, the supernatant was discarded, and bacteria were harvested and resuspended in 1 ml serum-free RPMI 1640 medium.

Overnight cultured AGS cells were co-incubated with lactobacilli (multiplicity of infection (MOI) = 100) and *H. pylori* P12 (MOI = 100) for 6h. After the incubation period, the supernatant was harvested for ELISA and cells were harvested for RNA isolation.

## 2.4 Adhesion of *H. pylori* on AGS cell

AGS cells were cultured in two 12 well plates and incubated with lactobacilli (MOI = 100) and *H. pylori* P12-GFP (MOI = 100)

for 6h. At the end of incubation, one plate of the cells was washed thrice with PBS and photographed by fluorescence and white light. A urease detection reagent was prepared by adding concentrated hydrochloric acid into the PBS (pH=7.4) to adjust the solution to pH=6.8. Urea (Solarbio) and phenol red (Solarbio) were weighed and added to reach concentrations of 110mmol/L and 10mg/L, respectively, and then dissolved by vigorously shaking. To the other 12well plates, 1 ml urease detection reagent was added. After 1-7 hours of reaction, 80 $\mu$ l medium was withdrawn to record the absorbance value at 540nm (Shmueli et al., 2004; Rokka et al., 2008; Tharmalingam et al., 2014; Yang et al., 2020).

## 2.5 Quantitative reverse transcription PCR (qRT-PCR)

AGS cells and mouse gastric mucosal tissue were lysed with RNAiso plus (TaKaRa, Kyoto, Japan), and gastric mucosal tissue needed to be assisted by an ultrasonic crusher. According to the manufacturer's instructions, cDNA was converted using the ReverTra Ace qPCR RT Kit (TOYOBO, Shanghai, China). qRT-PCR was performed using 2 $\times$ ChamQ Universal SYBR qPCR Master Mix (Vazyme, Nanjing, China) in a Roche Lightcycler480II system based on the manufacturer's recommendations. Primer sequences were designed in NCBI Primer-BLAST (Table 1). The relative gene expression was determined using the 2<sup>- $\Delta\Delta$ Ct</sup> method. All experiments were repeated thrice.

## 2.6 Establishing the model of *H. pylori* infection and lactobacilli intervention in mice

SPF C57BL/6 mice (male 4 weeks old) were obtained from Zhejiang Vital River Laboratory Animal Technology Co., Ltd. (Zhejiang, China) and fed on Laboratory Rodent Diet 5001. The mice were randomly divided into 5 groups (Uninfected, *H. pylori* SS1, *H. pylori* SS1+*L. acidophilus* NCFM, *H. pylori* SS1+*L. plantarum* Lp-115, *H. pylori* SS1+*L. acidophilus* NCFM and *L. plantarum* Lp-115) of 10 individuals each after one week of adaptation. The control group was gavaged with PBS, and the experimental groups were gavaged with *H. pylori* SS1 (1 $\times$ 10<sup>9</sup> CFU, 0.2ml/piece) only or combined with the corresponding lactobacilli (1 $\times$ 10<sup>9</sup> CFU, 0.2ml/piece) (1:1) or together (1:1:1) once every other day for 6 weeks (Figure 1A).

## 2.7 Rapid urease test (RUT)

Mouse gastric mucosa was analyzed for urease activity using the rapid urease Kit (Sanqiang, Fujian, China) as instructed by the manufacturer. The color change was determined, when the solution turns pink or red, the urease test is positive; when it remains yellow, the urease test is negative.

TABLE 1 Primers for the quantification of inflammatory factors in AGS cells and mouse gastric tissue.

Species	Gene	Primer	Nucleotide Sequence(5'-3')
Human	<i>TNF</i>	Forward	CCCAGGGACCTCTCTCTAATCA
	<i>TNF</i>	Reverse	GCTACAGGCTTGTCACTCGG
	<i>Cxcl8</i>	Forward	ACTGAGAGTGATTGAGAGTGGAC
	<i>Cxcl8</i>	Reverse	AACCCTCTGCACCCAGTTTTC
	<i>GAPDH</i>	Forward	GGTATCGTGGAAGGACTCATGAC
	<i>GAPDH</i>	Reverse	ATGCCAGTGAGCTTCCCGTTTCAG
Mouse	<i>ureA</i>	Forward	GCTGGTGCATTGGCTTTA
	<i>ureA</i>	Reverse	GGATAGCGACTTGCACATCGT
	<i>ureB</i>	Forward	GCCCACTTCTACAGAACCGACATAC
	<i>ureB</i>	Reverse	AGGCGATAACGACAACCTCAGGATC
	<i>Il10</i>	Forward	CCAGGGAGATCCTTTTGATGA
	<i>Il10</i>	Reverse	AACTGGCCACAGTTTTCAGG
	<i>Il4</i>	Forward	GGTCTCAACCCCGAGTAGT
	<i>Il4</i>	Reverse	GCCGATGATCTCTCTCAAGTGAT
	<i>Ifng</i>	Forward	CAGGCCATCAGCAACAACATAAGC
	<i>Ifng</i>	Reverse	AGCTGGTGGACCACTCGGATG
	<i>Cxcl15</i>	Forward	CGGCAATGAAGCTTCTGTAT
	<i>Cxcl15</i>	Reverse	CCTTGAAACTCTTTGCCTCA
	<i>GAPDH</i>	Forward	GCTGAGTATGTCGTGGAG
	<i>GAPDH</i>	Reverse	TCTTCTGAGTGGCAGTGAT

## 2.8 Hematoxylin-eosin (HE) staining and immunohistochemistry (IHC)

Gastric tissues were fixed with 4% paraformaldehyde, embedded in paraffin, cut into 4mm sections, and stained by HE and immunohistochemical methods. The Chronic gastritis histological grade scale was used to evaluate the samples (Fang et al., 2018). Five histological changes were graded: *H. pylori*, chronic inflammation, activity, atrophy, and intestinal metaplasia. Each histological change was classified into one of four grades: none, mild, moderate, and severe. According to the new Sydney system, the degree of inflammation and lymphocyte infiltration of gastric tissue after *H. pylori* infection were evaluated (Kim et al., 2020; Maluf et al., 2020). Immunohistochemistry for *H. pylori* was performed using a Rabbit anti-*H. pylori* polyclonal antibody (Cell Marque) (ZSGB, Beijing, China), and the colonies of *H. pylori* in mouse gastric mucosa were identified.

## 2.9 Statistics

All statistical analyses were performed using GraphPad Prism 9 software. During the processing of experimental data, the values whose deviation from the average value of the same group of data exceeded three times the standard deviation were considered

outliers and eliminated. We performed one-way ANOVA on raw and lg-converted data to compare the multi groups. The Bonferroni and Tukey tests were conducted to calculate the statistical significance among the groups. P-value < 0.05 was considered significant for all statistical analyses.

## 3 Results

### 3.1 Six lactobacilli strains inhibit the adhesion of *H. pylori* with AGS cells

To compare the effect of the six selected lactobacilli interfering with *H. pylori* adhesion, AGS cells were co-infected with *H. pylori* P12-GFP and the six lactobacilli strains (MOI=100) respectively for 6 hours. After infection, cells and GFP-positive *H. pylori* were measured under fluorescence microscopy. Upon comparative observation under fluoroscopy, the amount of GFP-positive *H. pylori* in the lactobacilli groups was less than in the *H. pylori* only infected group. Furthermore, the morphology of AGS cells was relatively normal in the *L. acidophilus* NCFM and *L. plantarum* Lp-115 treated cells compared with the other lactobacilli treated cells, indicating less cell stress on the AGS cells compared with other lactobacilli strains (Figure 2A).



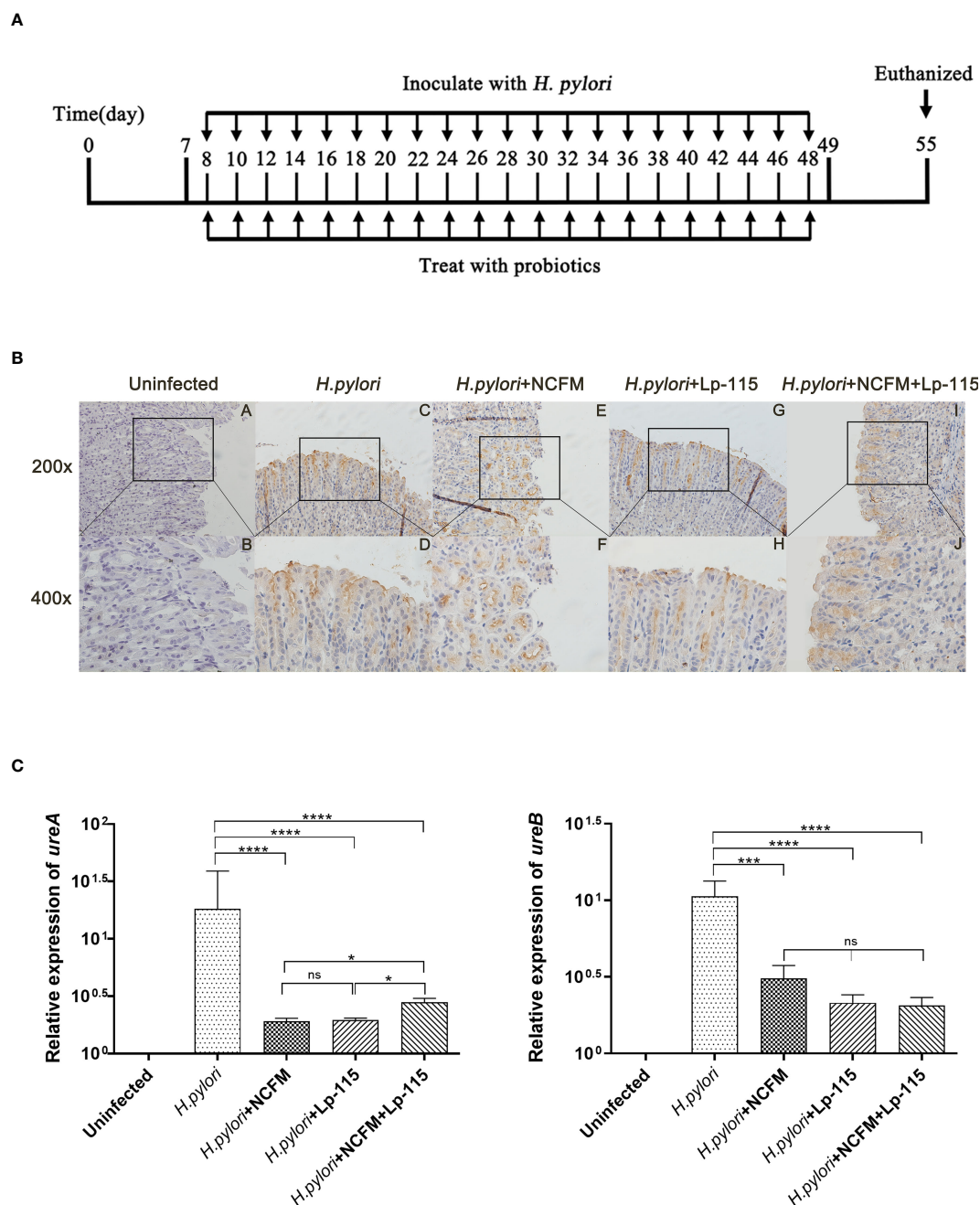


FIGURE 1

*Lactobacillus acidophilus* NCFM and *Lactiplantibacillus plantarum* Lp-115 suppress *Helicobacter pylori* adhesion in mice. (A) Mice were fed with *H. pylori* SS1 only or with *L. acidophilus* NCFM and/or *L. plantarum* Lp-115 for 6 weeks. (B) The colonization of *H. pylori* was identified by immune histochemistry. Uninfected group; *H. pylori* group; *H. pylori* + NCFM group; *H. pylori* + Lp-115 group; *H. pylori* +NCFM+Lp-115 group. (C) The colonization of *H. pylori* was identified by the expression of *ureA* and *ureB* by qRT-PCR. Mice were coinfected with *H. pylori* SS1 and *L. acidophilus* NCFM and/or *L. plantarum* Lp-115. The mRNA levels of *ureA* and *ureB* were determined as described. Each experiment result shows the mean  $\pm$  standard deviation of three independent experiments. \* ( $P < 0.05$ ); \*\* ( $P < 0.01$ ); \*\*\* ( $P < 0.001$ ); ns, not significant.

To further quantify the inhibition effect between different lactobacilli, we used a urease activity assay for the co-infection plate and recorded the absorbance at 540nm. The absorbance values of the six intervention groups were decreased to different degrees from 1 to 7 hours compared with that of the *H. pylori* infected group. For further quantification analysis, the absorbance values at each group's 7h time point were taken into a bar chart for statistical

analysis. The absorbance values of the seventh hour were statistically analyzed. The data suggest that samples of *L. acidophilus* NCFM, *L. acidophilus* La-14, *L. plantarum* Lp-115 and *L. rhamnosus* GG had significant differences compared with samples of *H. pylori* ( $P < 0.05$ ), indicating that these four lactobacilli strains can effectively reduce the colonization of *H. pylori* (Figure 2B).



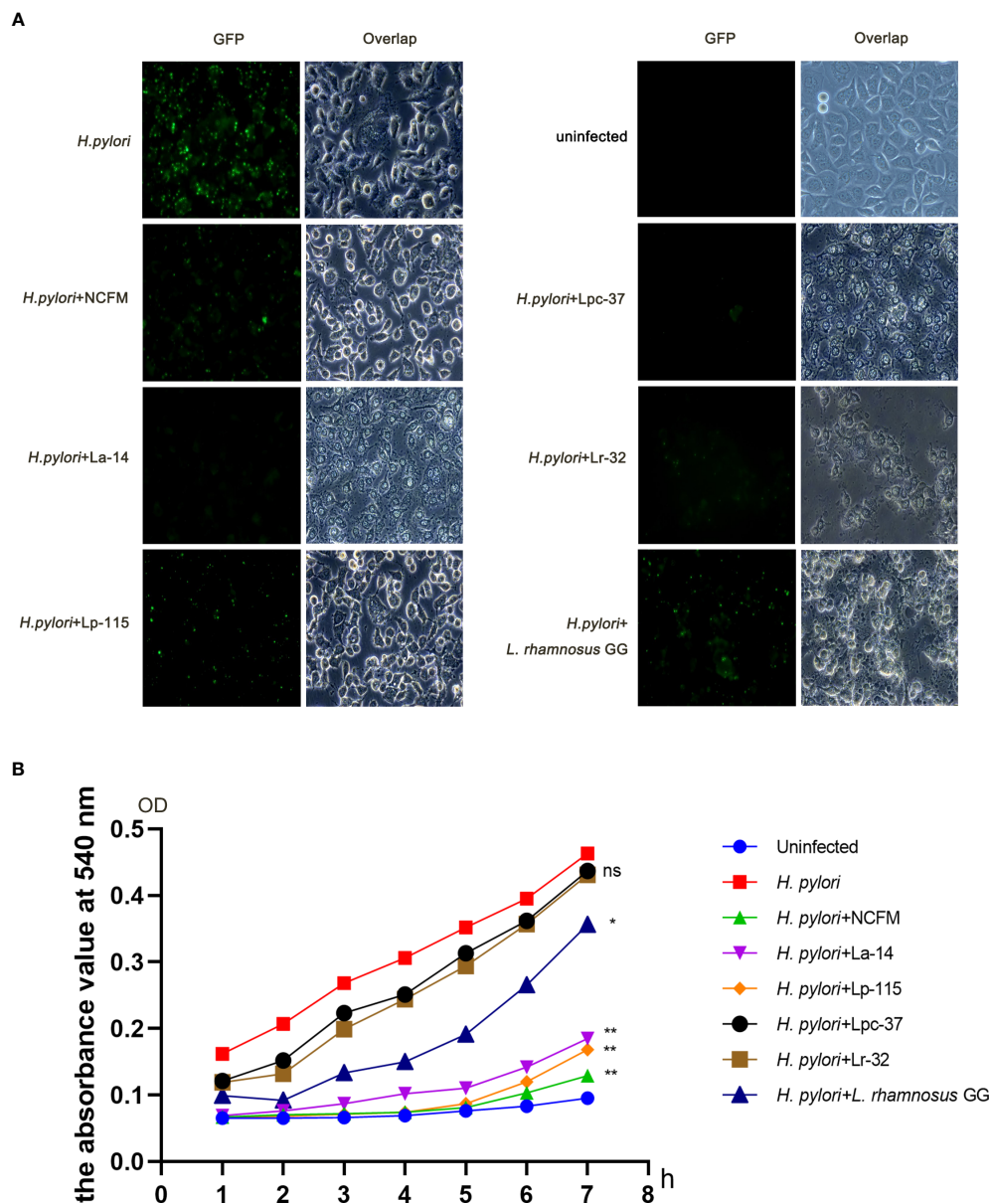


FIGURE 2

Six lactobacilli strains inhibit the adherence of *Helicobacter pylori* to AGS cells. (A) Fluorescence microscope images showing the colonization of *H. pylori* P12-GFP on AGS cells alone or upon intervention with six lactobacilli: *Lactobacillus acidophilus* NCFM, *L. acidophilus* La-14, *Lactiplantibacillus plantarum* Lp-115, *Lactocaseibacillus paracasei* Lpc-37, *Lactocaseibacillus rhamnosus* Lr-32 and *L. rhamnosus* GG. (B) Urease activity assay shows interference with the colonization of *H. pylori* P12-GFP on AGS cells in 1–7 hours by the six tested probiotic strains. (\* $P < 0.05$ ); \*\*( $P < 0.01$ ), compared to *H. pylori*. ns, not significant.

### 3.2 Six probiotic strains inhibit *H. pylori* induced inflammation in AGS cells

To compare the inhibitory effect between the six probiotic strains, we performed a co-infection model of *H. pylori* and the strains (MOI=100) in AGS cell culture for 6 hours. We analyzed the mRNA and protein levels of IL-8 (Cxl8) and TNF- $\alpha$  (TNF) to determine whether these probiotic strains transcriptionally regulate the inflammatory markers. The expression of these markers is commonly altered upon *H. pylori* infection. Expression of Cxl8 and TNF mRNA with all six probiotic strains was significantly reduced compared with the *H. pylori* infected group ( $P < 0.001$ ). In

Cxl8, Lp-115 showed significant difference than other probiotics except NCFM, while pattern of NCFM was significantly lower than La-14 and Lpc-37 ( $P < 0.01$ ). The comparison of other probiotics including La-14, Lpc-37, Lr32 and GG did not show any significant difference ( $P > 0.01$ ). In TNF, only Lpc-37 was found to have significant difference than other probiotics in the group ( $P < 0.01$ ) (Figure 3A).

Consistent with the mRNA results, IL-8 and TNF- $\alpha$  in the cell supernatant were significantly decreased in the probiotic treatments compared with the *H. pylori*-infected group ( $P < 0.001$ ). In IL-8, NCFM was significantly lower than La-14, while Lp-115 showed significant difference than the La-14 and Lpc-37 ( $P < 0.01$ ). In

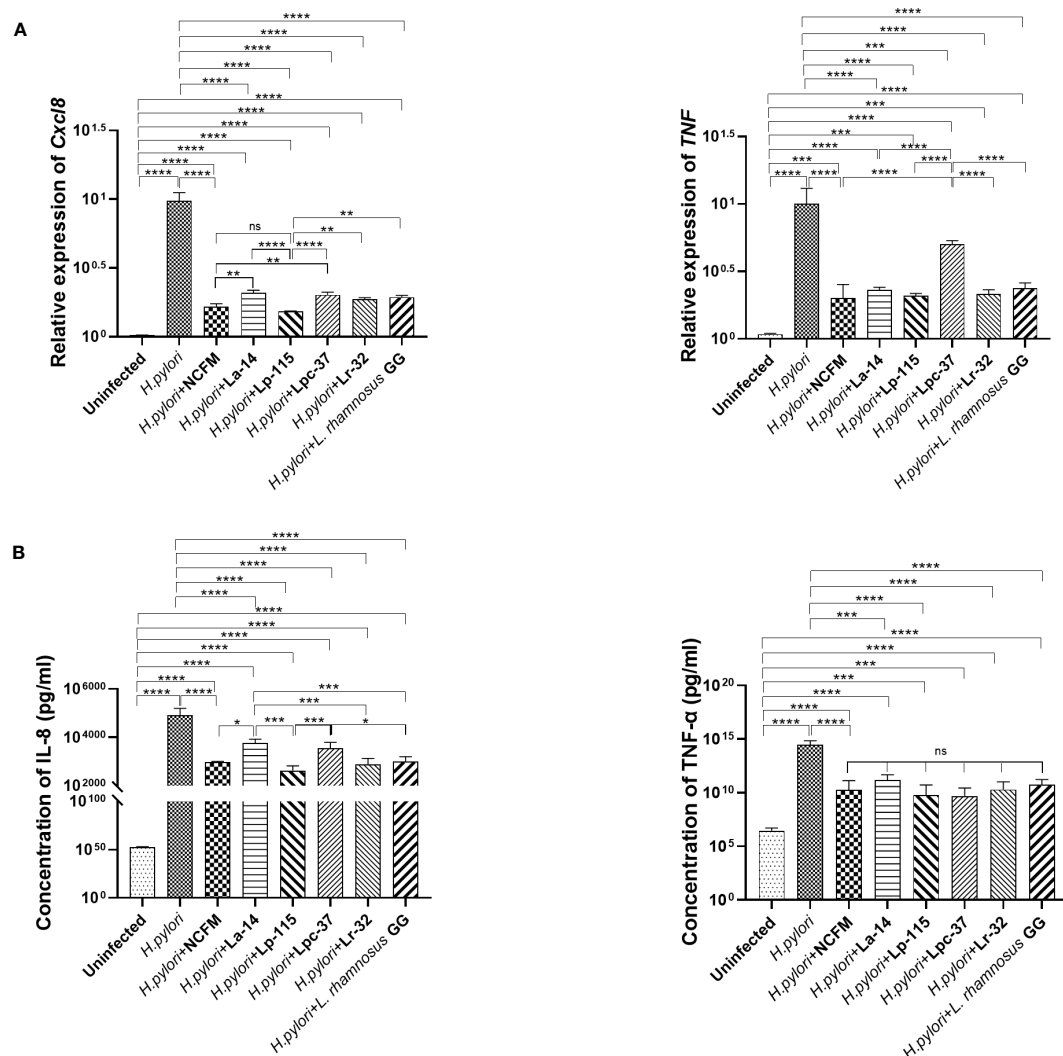


FIGURE 3

Inhibitory effects of the six probiotic strains on *Helicobacter pylori*-induced inflammation in AGS cell line. AGS cells were co-infected with the probiotic strains: *Lactobacillus acidophilus* NCFM, *L. acidophilus* La-14, *Lactiplantibacillus plantarum* Lp-115, *Lacticaseibacillus paracasei* Lpc-37, *Lacticaseibacillus rhamnosus* Lr-32 and *L. rhamnosus* GG and *H. pylori* P12 at a multiplicity of infection (MOI) 100 for 6 hours. (A) The mRNA levels of Cxcl8 and TNF the cells and (B) the protein concentrations of IL-8 and TNF-α in the supernatant. The results of each experiment are shown as mean  $\pm$  standard deviation of three independent experiments. \* ( $P < 0.05$ ); \*\* ( $P < 0.01$ ); \*\*\* ( $P < 0.001$ ); \*\*\*\* ( $p < 0.0001$ ); ns, not significant.

TNF-α, the inhibitory effect of the six selected probiotic strains did not show significant differences (Figure 3B). Combined with the anti-adhesion results, *L. acidophilus* NCFM and *L. plantarum* Lp-115 had a good effect and less cell stress. Therefore, *L. acidophilus* NCFM and *L. plantarum* Lp-115 were further selected for validation in the *H. pylori* infected mouse model.

### 3.3 *L. acidophilus* NCFM and *L. plantarum* Lp-115 suppress *H. pylori* colonization in mice

To further validate whether *L. acidophilus* NCFM and *L. plantarum* Lp-115 alone or in combination can counteract *H. pylori* colonization and attenuate gastric inflammation *in vivo*, C57BL/6 mice were infected with *H. pylori* SS1 and co-

administered *L. acidophilus* NCFM and *L. plantarum* Lp-115 with for 6 weeks (Figure 1A). After co-administration the mice were euthanized, and the gastric tissues were assessed for *H. pylori* infection by the rapid urease test (Figure S2). The *H. pylori* adhesion on gastric tissues was then analyzed by immunohistochemistry (IHC) assays (Figure 1B), which showed that *L. acidophilus* NCFM and/or *L. plantarum* Lp-115 intervention groups had comparably less *H. pylori* adhesion than the *H. pylori* infected group. To further validate the *H. pylori* colonization in different groups, the mRNA expression of *ureA* and *ureB* was tested from gastric tissues of all groups (Figure 1C), which showed that *L. acidophilus* NCFM and/or *L. plantarum* Lp-115 intervention groups had less expression of *ureA* and *ureB* compared with *H. pylori* infected group ( $P < 0.001$ ). These results show that *L. acidophilus* NCFM and *L. plantarum* Lp-115 alone or combined can reduce *H. pylori* colonization on gastric mucosa in mice.

### 3.4 *L. acidophilus* NCFM and *L. plantarum* Lp-115 suppress *H. pylori* induced inflammation in mice

To further investigate whether *L. acidophilus* NCFM and *L. plantarum* Lp-115 can attenuate *H. pylori* colonization and gastric inflammation *in vivo*, gastric tissues from the five study groups were analyzed by Hematoxylin-Eosin staining (HE stain). Compared with the uninfected group, the gastric lamina propria of mice in the *H. pylori* infected group showed more lymphocyte, plasma cell, and neutrophil infiltration in the active phase. Incidentally, the mice also had local thinning of the mucosal layer, reduction of the glands propria, and thickening of the muscularis mucosae (Figure 4A). Compared with the *H. pylori* group, the inflammatory cells infiltrating the lamina propria of the gastric mucosa in the *H. pylori* + NCFM group, *H. pylori* + Lp-115 group, and *H. pylori* + NCFM+Lp-115 group were reduced to different degrees, which indicated that *L. acidophilus* NCFM and *L. plantarum* Lp-115 could ameliorate the *H. pylori* induced gastric inflammation (Figure 4A).

To further verify if NCFM and/or Lp-115 can inhibit *H. pylori* induced Th1 type inflammation, the mRNA expression of *Il4* (IL-4), *Cxcl15* (CXCL15), *Il10* (IL-10), and *Ifng* (IFN- $\gamma$ ) was measured by qRT-PCR from mouse gastric mucosal tissue. The results showed that NCFM and Lp-115 reduced the expression of *Ifng* and promoted the expression of *Il4* induced by *H. pylori* in C57BL/6 mice. In *Il4* expression, the difference between the Lp-115 and *H. pylori* groups was the most significant ( $P < 0.001$ ). In *Cxcl15*, only the Lp-115 group was significantly different from the *H. pylori* group ( $P < 0.01$ ); therefore, the overall anti-inflammatory effect of Lp-115 was more pronounced than that of NCFM. The expression of *Cxcl15* in the group receiving the combination of Lp-115 and NCFM was not significantly different from that in the *H. pylori* group. The expression of *Il4* was lower than that in the Lp-115 group (Figure 4B), indicating that the two LAB strains had no compound effect in improving inflammation caused by *H. pylori* infection. In conclusion, NCFM and/or Lp-115 can reduce *H. pylori* induced Th1 type inflammation (*Ifng* expression) in C57BL/6 mice and tend to transform Th2 type inflammation (*Il4* expression).

## 4 Discussion

Currently, quadruple therapy is the standard treatment for *H. pylori* eradication, but it has drawbacks. There is an increasing incidence of drug resistance and the misuse of antibiotics for *H. pylori* eradication can cause gastrointestinal disorders, gastrointestinal microbiota dysbiosis and other adverse effects (Hu et al., 2017). Modulation of the gastrointestinal microecology by microbial agents could represent a novel therapy or adjunct therapy for the current quadruple treatment. Furthermore, previous studies have shown that probiotics can modulate immune function, balance normal gastrointestinal microbiota, and reduce the side effects of antibiotics (Lu et al., 2016; Wang et al., 2017; Goderska et al., 2018), but may also inhibit *H. pylori* adhesion and gastric inflammation, suggesting beneficial effects. Although probiotics have advantages in aiding the eradication of *H. pylori* infection

during conventional therapy, potential risks still exist. For some immunocompromised people, some strains of lactobacilli under certain rare conditions can cause infections (Liong, 2008). Therefore, selecting safe and suitable probiotic strains to support *H. pylori* eradication and management therapy is necessary.

Previous studies have shown that selected strains of lactobacilli can inhibit adherence of *H. pylori* to the gastric mucosa (Song et al., 2019; Zuo et al., 2019). In our study, we screened six probiotic strains and found that *L. acidophilus* NCFM and/or *L. plantarum* Lp-115 can inhibit *H. pylori* adhesion in an *in vitro* AGS cell line model and *in vivo* gastric mucosa of C57BL/6 mice, indicating preclinical evidence of these two strains for potential clinical use. However, the mechanisms by which NCFM and Lp-115 inhibit *H. pylori* colonization remains to be explored. Some studies have reported that probiotics' effects are strain specific in inhibiting the colonization of *H. pylori*. For example, some *Lactobacillus* spp. such as *L. acidophilus* and *L. bulgaricus* have a high affinity for gastric epithelial cells, and they can protect the gastric mucosa by blocking or inhibiting the adhesion of *H. pylori* to gastric epithelial cells (de Klerk et al., 2016; Takeda et al., 2017; Zhao et al., 2018; Song et al., 2019). Some lactobacilli, such as *L. plantarum* and *Ligilactobacillus salivarius*, cannot compete with *H. pylori* for the binding site on the gastric mucosa but inhibit the activity of *H. pylori* through the antibacterial properties of metabolites, including Lactic acid and hydrogen peroxide (de Klerk et al., 2016; Takeda et al., 2017; Zhao et al., 2018; Song et al., 2019). Therefore, the immune system's independent effects of probiotics against *H. pylori* infection may include affecting *H. pylori* gastric adhesive colonization or inhibiting *H. pylori* activity through the bacteriostatic properties of metabolites. These effects and other specific mechanisms need to be explored further.

*H. pylori* infection induces inflammation of gastric mucosa and expression of cytokines such as TNF- $\alpha$  or chemokines like CXCL8 (also known as IL-8) (Panpetch et al., 2016; Zhao et al., 2020; Tang et al., 2021). Previous studies have shown that *L. rhamnosus* GMNL-74 and *L. acidophilus* GMNL-185 reduce *H. pylori* induced gastric inflammation (Chen et al., 2019; Song et al., 2019). In the current study, we are showing for the first that *L. acidophilus* NCFM and/or *L. plantarum* Lp-115 inhibit *H. pylori* P12 induced IL-8 and TNF- $\alpha$  expression *in vitro*, which is consistent with previous studies analyzed other *L. acidophilus* strains (Ryan et al., 2009; Hwang et al., 2012). Previous studies have shown that *H. pylori* SS1 can induce T-helper cell type 1 (Th1) driven inflammation in C57BL/6 mice and that lactobacilli can suppress this response and may thus be involved in modulating Th1/Th2 balance (Boltin, 2016; Asgari et al., 2018; Asgari et al., 2020). In the *H. pylori* SS1 infected C57BL/6 mouse model, our study also confirmed that *L. acidophilus* NCFM and/or *L. plantarum* Lp-115 could inhibit *Ifng* but increase *Il4* expression, consistent with the previous report that *L. acidophilus* can turn *H. pylori* induced Th1 type inflammation into Th2 type inflammation in C57BL/6 mice (Boltin, 2016). Helper T cells (Th1, Th2) are essential factors in immunity and the main effector molecules of Th1 are IFN- $\gamma$  and IL-12, but IL-8 (CXCL15 in mice) may also contribute to the inflammation. The primary effector molecule of Th2 mediated inflammation is IL-4, whereas IL-10 may contribute

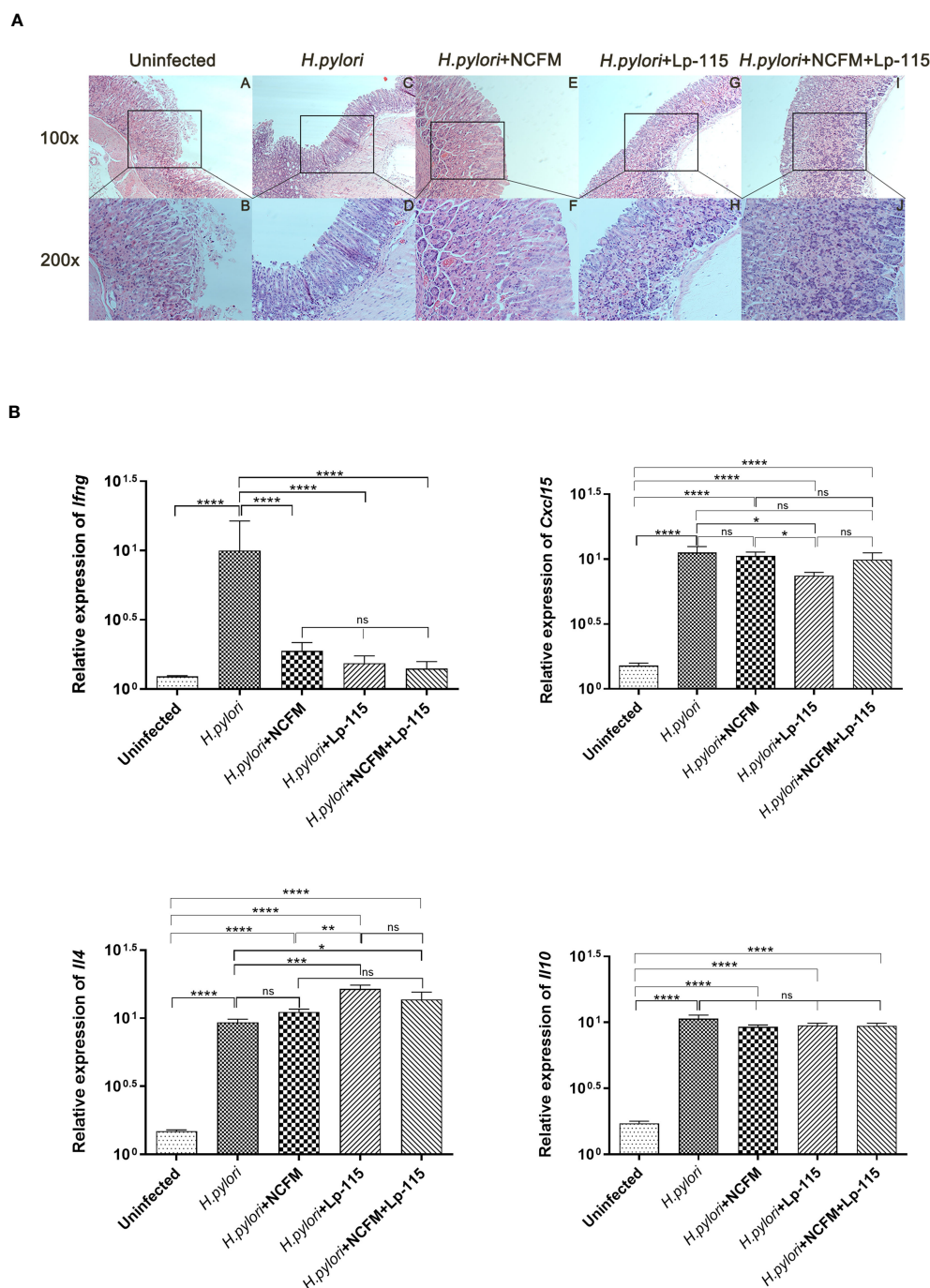


FIGURE 4

*Lactobacillus acidophilus* NCFM and *Lactiplantibacillus plantarum* Lp-115 suppress *Helicobacter pylori* inflammation in mice. (A) The inflammation of *H. pylori* was identified by HE. Uninfected group; *H. pylori* group; *H. pylori*+ NCFM group; *H. pylori* + Lp-115 group; *H. pylori* + NCFM+Lp-115 group. (B) The mRNA expression level of *Il4*, *Cxcl15*, *Il10*, and *Ifng* in each group. ns( $P \geq 0.05$ ); \*( $P < 0.05$ ); \*\*( $P < 0.01$ ); \*\*\*( $P < 0.001$ ); \*\*\*\*( $P < 0.0001$ ); ns, not significant.

to inhibiting Th2 responses. The two kinds of helper T-cells regulate and inhibit each other by secreting different factors to maintain the balance of the Th1 and Th2 (Schmitt and Ueno, 2015; Jafarzadeh et al., 2018; Saravia et al., 2019). Previous studies demonstrated that lactobacilli strains could balance the Th1/Th2 immune response. Certain *L. plantarum* strains can maintain normal intestinal immune function by stimulating the secretion of cytokines and regulating the Th1/Th2 balance (Xie et al., 2015; Boltin, 2016; Meng

et al., 2019). Conversely, one study showed that *L. rhamnosus* GG could increase the number of CD4<sup>+</sup> T lymphocytes, assist in differentiating Th cells and enhance Th1 immune responses (Shi et al., 2020). In this study, the intervention of *L. acidophilus* NCFM and *L. plantarum* Lp-115 might alleviate *H. pylori* infection induced host inflammatory response by down regulating local Th1 immune response in the gastric mucosa (inhibiting proinflammatory factor IFN- $\gamma$ ) while promoting Th2 response to produce the anti-Th1



cytokine IL-4. Thus, *L. acidophilus* NCFM and *L. plantarum* Lp-115 may play an essential role in promoting the differentiation of T cells into Th2 cells to balance *H. pylori* induced Th1 inflammation.

Although the focus of the study was not safety related, it shows that while the tested strains have different efficacy, they are not negatively affecting the AGS cell line or the *H. pylori* infected mice, which is in line with earlier reports (Daniel et al., 2006; Morovic et al., 2017). Thus, their choice of probiotic strain and rational application must be seriously considered. Based on the classification of risk factors posed by individuals, the safest, most effective, and most affordable lactobacilli to manage *H. pylori* infection should be selected for further investigation.

In conclusion, probiotic health benefits are strain-specific; thus, data specific for strain and health benefits should be investigated. After screening several strains, we chose two safe lactobacilli candidate strains: *L. acidophilus* NCFM and *L. plantarum* Lp-115, which inhibit *H. pylori* adhesion and host inflammatory responses in cell line and mouse models. *H. pylori* has a high infection rate and high prevalence of drug resistance worldwide. The current study presented a unique value in managing *H. pylori* *in vitro* and *in vivo*. The clinical intervention study with the two probiotic strains or their combination is warranted.

## Data availability statement

The raw data supporting the conclusions of this article will be made available by the authors, without undue reservation.

## Ethics statement

The animal study was reviewed and approved by The Fifth Affiliated Hospital of Zhengzhou University.

## Author contributions

SS: Data curation; Formal analysis; Investigation; Software; Validation; Visualization; Writing—original draft. FR: Formal analysis; Software; Investigation; Validation. HQ: Formal analysis; Software; Investigation; Validation. IB: Formal analysis; Writing—review & editing. JY: Funding acquisition. DG: Funding acquisition. ACO: Writing—review & editing. MJL: Writing—review & editing.

## References

- Asgari, B., Kermanian, F., Derakhshan, N., Asna-Ashari, M., Sadat, Z. R. N., and Yaslianifard, S. (2018). Honey-derived lactobacillus rhamnosus alleviates helicobacter pylori-induced gastro-intestinal infection and gastric inflammation in C57bl/6 mice: an immuno-histologic study. *Arq. Gastroenterol.* 55 (3), 279–282. doi: 10.1590/S0004-2803.201800000-70
- Asgari, B., Kermanian, F., Hedayat Yaghoobi, M., Vaezi, A., Soleimanifar, F., and Yaslianifard, S. (2020). The Anti-Helicobacter pylori Effects of Lactobacillus acidophilus, L. plantarum and L. rhamnosus in Stomach Tissue of C57BL/6 Mice. *Visc Med.* 36 (2), 137–143. doi: 10.1159/000500616
- Boltin, D. (2016). Probiotics in Helicobacter pylori-induced peptic ulcer disease. *Best Pract. Res. Clin. Gastroenterol.* 30 (1), 99–109. doi: 10.1016/j.bpg.2015.12.003
- Chen, Y. H., Tsai, W. H., Wu, H. Y., Chen, C. Y., Yeh, W. L., Chen, Y. H., et al. (2019). Probiotic Lactobacillus spp. act Against Helicobacter pylori-induced Inflammation. *J. Clin. Med.* 8 (1), 90. doi: 10.3390/jcm8010090
- Chey, W. D., Leontiadis, G. I., Howden, C. W., and Moss, S. F. (2017). ACG clinical guideline: treatment of helicobacter pylori infection. *Am. J. Gastroenterol.* 112 (2), 212–239. doi: 10.1038/ajg.2016.563

PZ: Conceptualization; Project administration; Resources; Supervision. YM: Methodology; Project administration; Formal analysis; Writing—review & editing. All authors contributed to the article and approved the submitted version.

## Funding

This study was fully funded by Danisco (China) Holding Co., Ltd. (a subsidiary of International Flavors & Fragrances, IFF), Shanghai, China, which was the study sponsor. No public funding was received to conduct this study.

## Conflict of interest

JY and DG are former employees of Danisco (China) Holding Co. Ltd., part of International Flavors & Fragrances, IFF. ACO and MJL are employees of Danisco Sweeteners Oy, part of IFF. YM and PZ (principal investigators), SS, and FR are employed by The Fifth Affiliated Hospital of Zhengzhou University.

The remaining authors declare that the research was conducted in the absence of any commercial or financial relationships that could be construed as a potential conflict of interest.

The sponsor participated in the design of the study, the interpretation of data, In review writing of the manuscript, and in the decision to publish the results.

## Publisher's note

All claims expressed in this article are solely those of the authors and do not necessarily represent those of their affiliated organizations, or those of the publisher, the editors and the reviewers. Any product that may be evaluated in this article, or claim that may be made by its manufacturer, is not guaranteed or endorsed by the publisher.

## Supplementary material

The Supplementary Material for this article can be found online at: <https://www.frontiersin.org/articles/10.3389/fcimb.2023.1196084/full#supplementary-material>



- Daniel, C., Poiret, S., Goudercourt, D., Dennin, V., Leyer, G., and Pot, B. (2006). Selecting lactic acid bacteria for their safety and functionality by use of a mouse colitis model. *Appl. Environ. Microbiol.* 72 (9), 5799–5805. doi: 10.1128/AEM.00109-06
- Dargenio, C., Dargenio, V. N., Bizzoco, F., Indrio, F., Francavilla, R., and Cristofori, F. (2021). Limosilactobacillus reuteri Strains as Adjuvants in the Management of Helicobacter pylori Infection. *Medicina (Kaunas)* 57 (7), 733. doi: 10.3390/medicina57070733
- de Klerk, N., Maudsdotter, L., Gebreegziabher, H., Saroj, S. D., Eriksson, B., Eriksson, O. S., et al. (2016). Lactobacilli reduce helicobacter pylori attachment to host gastric epithelial cells by inhibiting adhesion gene expression. *Infect. Immun.* 84 (5), 1526–1535. doi: 10.1128/IAI.00163-16
- Fallone, C. A., Chiba, N., van Zanten, S. V., Fischbach, L., Gisbert, J. P., Hunt, R. H., et al. (2016). The toronto consensus for the treatment of helicobacter pylori infection in adults. *Gastroenterology* 151 (1), 51–69 e14. doi: 10.1053/j.gastro.2016.04.006
- Fallone, C. A., Moss, S. F., and Malfertheiner, P. (2019). Reconciliation of recent helicobacter pylori treatment guidelines in a time of increasing resistance to antibiotics. *Gastroenterology* 157 (1), 44–53. doi: 10.1053/j.gastro.2019.04.011
- Fang, J. Y., Du, Y. Q., Liu, W. Z., Ren, J. L., Li, Y. Q., Chen, X. Y., et al. (2018). Chinese consensus on chronic gastritis, (2017, shanghai). *J. Dig. Dis.* 19 (4), 182–203. doi: 10.1111/1751-2980.12593
- Goderska, K., Agudo Pena, S., and Alarcon, T. (2018). Helicobacter pylori treatment: antibiotics or probiotics. *Appl. Microbiol. Biotechnol.* 102 (1), 1–7. doi: 10.1007/s00253-017-8535-7
- Hooi, J. K. Y., Lai, W. Y., Ng, W. K., Suen, M. M. Y., Underwood, F. E., Tanyingoh, D., et al. (2017). Global prevalence of helicobacter pylori infection: systematic review and meta-analysis. *Gastroenterology* 153 (2), 420–429. doi: 10.1053/j.gastro.2017.04.022
- Hu, Y., Zhu, Y., and Lu, N. H. (2017). Novel and effective therapeutic regimens for helicobacter pylori in an era of increasing antibiotic resistance. *Front. Cell Infect. Microbiol.* 7. doi: 10.3389/fcimb.2017.00168
- Hwang, S. W., Kim, N., Kim, J. M., Huh, C. S., Ahn, Y. T., Park, S. H., et al. (2012). Probiotic suppression of the H. pylori-induced responses by conjugated linoleic acids in a gastric epithelial cell line. *Prostaglandins Leukot. Essent. Fatty Acids* 86 (6), 225–231. doi: 10.1016/j.plefa.2012.04.002
- Jafarzadeh, A., Larussa, T., Nemat, M., and Jalapour, S. (2018). T cell subsets play an important role in the determination of the clinical outcome of Helicobacter pylori infection. *Microb. Pathog.* 116, 227–236. doi: 10.1016/j.micpath.2018.01.040
- Jones, N. L., Koletzko, S., Goodman, K., Bontems, P., Cadranet, S., Casswall, T., et al. (2017). Joint ESPGHAN/NASPGHAN guidelines for the management of helicobacter pylori in children and adolescents (Update 2016). *J. Pediatr. Gastroenterol. Nutr.* 64 (6), 991–1003. doi: 10.1097/MPG.0000000000001594
- Keikha, M., and Karbalaee, M. (2021). Probiotics as the live microscopic fighters against Helicobacter pylori gastric infections. *BMC Gastroenterol.* 21 (1), 388. doi: 10.1186/s12876-021-01977-1
- Kim, D. H., Son, B. K., Min, K. W., Han, S. K., Na, J. U., Choi, P. C., et al. (2020). Chronic gastritis is associated with a decreased high-density lipid level: histological features of gastritis based on the updated sydney system. *J. Clin. Med.* 9 (6), 1856. doi: 10.3390/jcm9061856
- Lee, A., O'Rourke, J., De Ungria, M. C., Robertson, B., Daskalopoulos, G., and Dixon, M. F. (1997). A standardized mouse model of Helicobacter pylori infection: introducing the Sydney strain. *Gastroenterology* 112 (4), 1386–1397. doi: 10.1016/s0016-5085(97)70155-0
- Lin, C. C., Huang, W. C., Su, C. H., Lin, W. D., Wu, W. T., Yu, B., et al. (2020). Effects of multi-strain probiotics on immune responses and metabolic balance in helicobacter pylori-infected mice. *Nutrients* 12 (8), 2476. doi: 10.3390/nu12082476
- Liong, M. T. (2008). Safety of probiotics: translocation and infection. *Nutr. Rev.* 66 (4), 192–202. doi: 10.1111/j.1753-4887.2008.00024.x
- Liou, J. M., Malfertheiner, P., Lee, Y. C., Sheu, B. S., Sugano, K., Cheng, H. C., et al. (2020). Screening and eradication of Helicobacter pylori for gastric cancer prevention: the Taipei global consensus. *Gut* 69 (12), 2093–2112. doi: 10.1136/gutjnl-2020-322368
- Liu, W. Z., Xie, Y., Lu, H., Cheng, H., Zeng, Z. R., Zhou, L. Y., et al. (2018). Fifth Chinese National Consensus Report on the management of Helicobacter pylori infection. *Helicobacter* 23 (2), e12475. doi: 10.1111/hel.12475
- Lu, M., Yu, S., Deng, J., Yan, Q., Yang, C., Xia, G., et al. (2016). Efficacy of probiotic supplementation therapy for helicobacter pylori eradication: A meta-analysis of randomized controlled trials. *PLoS One* 11 (10), e0163743. doi: 10.1371/journal.pone.0163743
- Malfertheiner, P., Megraud, F., Rokkas, T., Gisbert, J. P., Liou, J. M., Schulz, C., et al. (2022). Management of Helicobacter pylori infection: the Maastricht VI/Florence consensus report. *Gut* 71, 17247–1762. doi: 10.1136/gutjnl-2022-327745
- Maluf, S., Salgado, J. V., Cysne, D. N., Camelo, D. M. F., Nascimento, J. R., Maluf, B. V. T., et al. (2020). Increased glycated hemoglobin levels in patients with helicobacter pylori infection are associated with the grading of chronic gastritis. *Front. Immunol.* 11. doi: 10.3389/fimmu.2020.02121
- McFarland, L. V., Huang, Y., Wang, L., and Malfertheiner, P. (2016). Systematic review and meta-analysis: Multi-strain probiotics as adjunct therapy for Helicobacter pylori eradication and prevention of adverse events. *United Eur. Gastroenterol. J.* 4 (4), 546–561. doi: 10.1177/2050640615617358
- Meng, Y., Wang, J., Wang, Z., Zhang, G., Liu, L., Huo, G., et al. (2019). Lactobacillus plantarum KLD51.0318 ameliorates impaired intestinal immunity and metabolic disorders in cyclophosphamide-treated mice. *Front. Microbiol.* 10. doi: 10.3389/fmicb.2019.00731
- Morovic, W., Roper, J. M., Smith, A. B., Mukerji, P., Stahl, B., Rae, J. C., et al. (2017). Safety evaluation of HOWARU((R)) Restore (Lactobacillus acidophilus NCFM, Lactobacillus paracasei Lpc-37, Bifidobacterium animalis subsp. lactis BI-04 and B. lactis BI-07) for antibiotic resistance, genomic risk factors, and acute toxicity. *Food Chem. Toxicol.* 110, 316–324. doi: 10.1016/j.fct.2017.10.037
- Ouweland, A. C., Invernici, M. M., Furlaneto, F. A. C., and Messoria, M. R. (2018). Effectiveness of multistrain versus single-strain probiotics: current status and recommendations for the future. *J. Clin. Gastroenterol.* 52 Suppl 1, S35–S40. doi: 10.1097/MCG.0000000000001052
- Panpetch, W., Spinler, J. K., Versalovic, J., and Tumwasorn, S. (2016). Characterization of Lactobacillus salivarius strains B37 and B60 capable of inhibiting IL-8 production in Helicobacter pylori-stimulated gastric epithelial cells. *BMC Microbiol.* 16 (1), 242. doi: 10.1186/s12866-016-0861-x
- Robinson, K., and Atherton, J. C. (2021). The spectrum of helicobacter-mediated diseases. *Annu. Rev. Pathol.* 16, 123–144. doi: 10.1146/annurev-pathol-032520-024949
- Rokka, S., Myllykangas, S., and Joutsjoki, V. (2008). Effect of specific colostral antibodies and selected lactobacilli on the adhesion of Helicobacter pylori on AGS cells and the Helicobacter-induced IL-8 production. *Scand. J. Immunol.* 68 (3), 280–286. doi: 10.1111/j.1365-3083.2008.02138.x
- Ryan, K. A., O'Hara, A. M., van Pijkeren, J. P., Douillard, F. P., and O'Toole, P. W. (2009). Lactobacillus salivarius modulates cytokine induction and virulence factor gene expression in Helicobacter pylori. *J. Med. Microbiol.* 58 (Pt 8), 996–1005. doi: 10.1099/jmm.0.009407-0
- Saravia, J., Chapman, N. M., and Chi, H. (2019). Helper T cell differentiation. *Cell Mol. Immunol.* 16 (7), 634–643. doi: 10.1038/s41423-019-0220-6
- Savoldi, A., Carrara, E., Graham, D. Y., Conti, M., and Tacconelli, E. (2018). Prevalence of antibiotic resistance in helicobacter pylori: A systematic review and meta-analysis in world health organization regions. *Gastroenterology* 155 (5), 1372–1382 e17. doi: 10.1053/j.gastro.2018.07.007
- Schmitt, N., and Ueno, H. (2015). Regulation of human helper T cell subset differentiation by cytokines. *Curr. Opin. Immunol.* 34, 130–136. doi: 10.1016/j.coi.2015.03.007
- Shah, S. C., Tepler, A., Chung, C. P., Suarez, G., Peek, R. M. Jr., Hung, A., et al. (2021). Host genetic determinants associated with helicobacter pylori eradication treatment failure: A systematic review and meta-analysis. *Gastroenterology* 161 (5), 1443–1459. doi: 10.1053/j.gastro.2021.07.043
- Shi, C. W., Cheng, M. Y., Yang, X., Lu, Y. Y., Yin, H. D., Zeng, Y., et al. (2020). Probiotic lactobacillus rhamnosus GG promotes mouse gut microbiota diversity and T cell differentiation. *Front. Microbiol.* 11. doi: 10.3389/fmicb.2020.607735
- Shi, X., Zhang, J., Mo, L., Shi, J., Qin, M., and Huang, X. (2019). Efficacy and safety of probiotics in eradicating Helicobacter pylori: A network meta-analysis. *Med. (Baltimore)* 98 (15), e15180. doi: 10.1097/MD.00000000000015180
- Shmueli, H., Burger, O., Neeman, I., Yahav, J., Samra, Z., Niv, Y., et al. (2004). Susceptibility of Helicobacter pylori isolates to the antiadhesion activity of a high-molecular-weight constituent of cranberry. *Diagn. Microbiol. Infect. Dis.* 50 (4), 231–235. doi: 10.1016/j.diagmicrobio.2004.08.011
- Simon, E., Calinoniu, L. F., Mitrea, L., and Vodnar, D. C. (2021). Probiotics, prebiotics, and synbiotics: implications and beneficial effects against irritable bowel syndrome. *Nutrients* 13 (6), 2112. doi: 10.3390/nu13062112
- Song, H., Zhou, L., Liu, D., Ge, L., and Li, Y. (2019). Probiotic effect on Helicobacter pylori attachment and inhibition of inflammation in human gastric epithelial cells. *Exp. Ther. Med.* 18 (3), 1551–1562. doi: 10.3892/etm.2019.7742
- Sousa, C., Ferreira, R., Azevedo, N. F., Oleastro, M., Azeredo, J., Figueiredo, C., et al. (2022). Helicobacter pylori infection: from standard to alternative treatment strategies. *Crit. Rev. Microbiol.* 48 (3), 376–396. doi: 10.1080/1040841X.2021.1975643
- Suez, J., Zmora, N., Segal, E., and Elinav, E. (2019). The pros, cons, and many unknowns of probiotics. *Nat. Med.* 25 (5), 716–729. doi: 10.1038/s41591-019-0439-x
- Sugano, K., Tack, J., Kuipers, E. J., Graham, D. Y., El-Omar, E. M., Miura, S., et al. (2015). Kyoto global consensus report on Helicobacter pylori gastritis. *Gut* 64 (9), 1353–1367. doi: 10.1136/gutjnl-2015-309252
- Takeda, S., Igoshi, K., Tsend-Ayush, C., Oyunsuren, T., Sakata, R., Koga, Y., et al. (2017). Lactobacillus paracasei strain 06Tca19 suppresses inflammatory chemokine induced by Helicobacter pylori in human gastric epithelial cells. *Hum. Cell* 30 (4), 258–266. doi: 10.1007/s13577-017-0172-z
- Tang, L., Tang, B., Lei, Y., Yang, M., Wang, S., Hu, S., et al. (2021). Helicobacter pylori-Induced Heparanase Promotes H. pylori Colonization and Gastritis. *Front. Immunol.* 12. doi: 10.3389/fimmu.2021.675747
- Tharmalingam, N., Kim, S. H., Park, M., Woo, H. J., Kim, H. W., Yang, J. Y., et al. (2014). Inhibitory effect of piperine on Helicobacter pylori growth and adhesion to gastric adenocarcinoma cells. *Infect. Agent Cancer* 9 (1), 43. doi: 10.1186/1750-9378-9-43
- Vieira, A. T., Teixeira, M. M., and Martins, F. S. (2013). The role of probiotics and prebiotics in inducing gut immunity. *Front. Immunol.* 4. doi: 10.3389/fimmu.2013.00445
- Wang, F., Feng, J., Chen, P., Liu, X., Ma, M., Zhou, R., et al. (2017). Probiotics in Helicobacter pylori eradication therapy: Systematic review and network meta-analysis. *Clin. Res. Hepatol. Gastroenterol.* 41 (4), 466–475. doi: 10.1016/j.clinre.2017.04.004

- Xie, J., Yu, Q., Nie, S., Fan, S., Xiong, T., and Xie, M. (2015). Effects of lactobacillus plantarum NCU116 on intestine mucosal immunity in immunosuppressed mice. *J. Agric. Food Chem.* 63 (51), 10914–10920. doi: 10.1021/acs.jafc.5b04757
- Yang, J. Y., Kim, P., Jeong, S. H., Lee, S. W., Myung, Y. S., Baeg, M. K., et al. (2020). The effects of sulglycotide on the adhesion and the inflammation of helicobacter pylori. *Int. J. Environ. Res. Public Health* 17 (8), 2918. doi: 10.3390/ijerph17082918
- Yoon, J. Y., Cha, J. M., Hong, S. S., Kim, H. K., Kwak, M. S., Jeon, J. W., et al. (2019). Fermented milk containing Lactobacillus paracasei and Glycyrrhiza glabra has a beneficial effect in patients with Helicobacter pylori infection: A randomized, double-blind, placebo-controlled study. *Med. (Baltimore)* 98 (35), e16601. doi: 10.1097/MD.00000000000016601
- Zhao, K., Xie, Q., Xu, D., Guo, Y., Tao, X., Wei, H., et al. (2018). Antagonistics of Lactobacillus plantarum ZDY2013 against Helicobacter pylori SS1 and its infection in vitro in human gastric epithelial AGS cells. *J. Biosci. Bioeng* 126 (4), 458–463. doi: 10.1016/j.jbiosc.2018.04.003
- Zhao, Q., Yin, W., Zhao, R., Wang, Y., Song, C., Wang, H., et al. (2020). Outer inflammatory protein of Helicobacter pylori impacts IL-8 expression, adherence, cell apoptosis and cell cycle of gastric cells independent of its copy number. *Med. Microbiol. Immunol.* 209 (5), 621–630. doi: 10.1007/s00430-020-00688-w
- Zuo, F., Appaswamy, A., Gebremariam, H. G., and Jonsson, A. B. (2019). Role of Sortase A in Lactobacillus gasseri Kx110A1 Adhesion to Gastric Epithelial Cells and Competitive Exclusion of Helicobacter pylori. *Front. Microbiol.* 10. doi: 10.3389/fmicb.2019.02770



## OPEN ACCESS

## EDITED BY

Parth Sarthi Sen Gupta,  
D Y Patil International University, India

## REVIEWED BY

Vicky Mody,  
Philadelphia College of Osteopathic  
Medicine (PCOM), United States  
Shweta Saraswat,  
Amity University, India

## \*CORRESPONDENCE

Shilpa Borehalli Mayegowda  
✉ shilpa.borehalli@christuniversity.in  
Arpita Roy  
✉ arbt2014@gmail.com

RECEIVED 18 May 2023

ACCEPTED 18 July 2023

PUBLISHED 16 August 2023

## CITATION

Borehalli Mayegowda S, Roy A, N. G. M,  
Pandit S, Alghamdi S, Almeahmadi M,  
Allahyani M, Awwad NS and Sharma R  
(2023) Eco-friendly synthesized  
nanoparticles as antimicrobial agents: an  
updated review.  
*Front. Cell. Infect. Microbiol.* 13:1224778.  
doi: 10.3389/fcimb.2023.1224778

## COPYRIGHT

© 2023 Borehalli Mayegowda, Roy, N. G.,  
Pandit, Alghamdi, Almeahmadi, Allahyani,  
Awwad and Sharma. This is an open-access  
article distributed under the terms of the  
[Creative Commons Attribution License  
\(CC BY\)](https://creativecommons.org/licenses/by/4.0/). The use, distribution or  
reproduction in other forums is permitted,  
provided the original author(s) and the  
copyright owner(s) are credited and that  
the original publication in this journal is  
cited, in accordance with accepted  
academic practice. No use, distribution or  
reproduction is permitted which does not  
comply with these terms.

# Eco-friendly synthesized nanoparticles as antimicrobial agents: an updated review

Shilpa Borehalli Mayegowda<sup>1\*</sup>, Arpita Roy<sup>2\*</sup>, Manjula N. G.<sup>3</sup>,  
Soumya Pandit<sup>4,5</sup>, Saad Alghamdi<sup>6</sup>, Mazen Almeahmadi<sup>7</sup>,  
Mamdouh Allahyani<sup>7</sup>, Nasser S. Awwad<sup>8</sup> and Rohit Sharma<sup>9</sup>

<sup>1</sup>Department of Psychology, CHRIST (Deemed to be University), Bangalore, India, <sup>2</sup>Department of Biotechnology, School of Engineering & Technology, Sharda University, Greater Noida, India, <sup>3</sup>Department of Microbiology, School of Basic and Applied Sciences, Dayananda Sagar University, Bengaluru, India, <sup>4</sup>Department of Life Sciences, School of Basic Science and Research, Sharda University, Greater Noida, India, <sup>5</sup>Department of Biotechnology, Graphic Era Deemed to be University, Dehradun, Uttarakhand, India, <sup>6</sup>Laboratory Medicine Department, Faculty of Applied Medical Sciences, Umm Al-Qura University, Makkah, Saudi Arabia, <sup>7</sup>Department of Clinical Laboratory Sciences, College of Applied Medical Sciences, Taif University, Taif, Saudi Arabia, <sup>8</sup>Department of Chemistry, King Khalid University, Abha, Saudi Arabia, <sup>9</sup>Department of Rasa Shastra and Bhaishajya Kalpana, Faculty of Ayurveda, Institute of Medical Sciences, Banaras Hindu University, Varanasi, India

Green synthesis of NPs has gained extensive acceptance as they are reliable, eco-friendly, sustainable, and stable. Chemically synthesized NPs cause lung inflammation, heart problems, liver dysfunction, immune suppression, organ accumulation, and altered metabolism, leading to organ-specific toxicity. NPs synthesized from plants and microbes are biologically safe and cost-effective. These microbes and plant sources can consume and accumulate inorganic metal ions from their adjacent niches, thus synthesizing extracellular and intracellular NPs. These inherent characteristics of biological cells to process and modify inorganic metal ions into NPs have helped explore an area of biochemical analysis. Biological entities or their extracts used in NPs include algae, bacteria, fungi, actinomycetes, viruses, yeasts, and plants, with varying capabilities through the bioreduction of metallic NPs. These biosynthesized NPs have a wide range of pharmaceutical applications, such as tissue engineering, detection of pathogens or proteins, antimicrobial agents, anticancer mediators, vehicles for drug delivery, formulations for functional foods, and identification of pathogens, which can contribute to translational research in medical applications. NPs have various applications in the food and drug packaging industry, agriculture, and environmental remediation.

## KEYWORDS

green synthesis, antimicrobial agents, anticancer agents, antioxidant activity, drug delivery, DNA damage, eco-friendly

## Introduction

Nanoparticles (NP) vary in size from 1 to 100 nm with a large surface-to-volume ratio and are currently used in translation research technology. The biological NPs employed are ecofriendly, cost effective, and have attracted substantial attention. Nanotechnology comprises various fields, including biological sciences, chemistry, physics, material science, engineering, and computational science. It has applications in various fields, such as optics, space industries, cosmetics, biomedical, chemical industries, electronics, mechanics, environmental remediation, food and feed, health care, photoelectron chemistry, numerous engineering fields, and material science (Christian et al., 2008). Nanotechnology is the most promising field in integrated engineering, physics, medicine, chemistry, and biology, and has widespread applications with increased demand for industrial-scale production of nanomaterials (NMs). However, concerns have been raised regarding the environmental safety of chemically synthesized NPs. The origin and synthesis of these chemical NPs have caused an enormous burden on the environment because of their toxins, which have harmful effects on animals and humans (Wiley et al., 2005; Vo-Dinh, 2007). Physiochemical techniques to produce NPs of metals and metal oxides require the use of corrosive and toxic reducing agents such as sodium borohydride and hydrazine hydrate, which adversely affect the atmosphere (Mandal et al., 2006). Thus, alternative methods for synthesizing harmless NPs using moderate solvents are eco-friendly reducers and stabilizers with experimental parameters or biological material applications. The most eco-friendly are the use of plants, fungal or bacterial extracts, lysates, or biomolecules, which are widely used due to their minimal side effects (Figure 1). Numerous microbes act as potential sustainable precursors that are eco-friendly and can produce stable and well-functionalized NPs (Baroumand

Moghaddam et al., 2015). Thus, such environmentally safe techniques used for the synthesis of NPs are also referred to as 'green nanotechnology' or "clean-technology" that are feasible alternatives to chemical methods. Furthermore, nanoparticles conjugated with natural biomolecules exhibit improved bioavailability and minimal side effects. They are not only smaller in size with higher permeability, but are also important reducing and stabilizing agents and show excellent antioxidant activity. Nanoparticles serve as potential antimicrobial agents because of their affinity toward sulfur-rich amino acids, adherence to the microbial cell wall by electrostatic attraction, and disruption of the microbial cytoplasmic membrane and nucleic acids. They possess anticancer activity owing to the initiation of oxidative stress, cellular DNA damage, and lipid peroxidation. Additionally, biological synthesis is eco-friendly, cost-effective, and fast, and unlike compounds or their derivatives, it is not harmful, thus minimizing pollution. Therefore, the use of green synthetic methods holds promise as safe alternatives for healthcare and bioremediation applications. Currently, nanotechnology, being an indispensable part of the healthcare, research and innovation sector in recent years is used extensively (Manjula et al., 2022). Nanocompounds have been promising antimicrobial agents, anti-cancer mediators, vehicles for drug delivery, formulations for functional foods, in the identification of pathogens, and in the food and drug packaging industry.

## Sustainable green nanotechnology

### Advantage

Engineered nanomaterials (NMs) have gained the utmost importance in daily life and have been used in cosmetics, food



FIGURE 1  
Implication of green nanotechnology.

packaging materials, biosensors, drug delivery systems, and therapies. Subsequently, their size is similar to that of biological macromolecules with antibacterial and anti-odor properties, which can be widely used in wound dressing, antimicrobial coatings, and detergents. However, despite innumerable applications, the biodegradation of NPs and the effect of their accumulation in the environment remain questionable. The accumulation of bio-degraded NPs within cells leads to intracellular changes, causing alterations in organelle integrity or gene alterations. Although NMs continue to be used extensively, it is important to address their toxicity, environmental impact, and possible undesirable side effects (Figure 1). In cancer nanotechnology, monoclonal antibodies, peptides, or small molecules targeting tumor ligands can be induced using NPs to target tumor antigens and tumor vasculature with high specificity and affinity. Recent developments have used bioaffinity NP probes for cellular and molecular imaging to target NP drugs for the treatment of cancers and integrated nanodevices for the early detection of cancers (Gao et al., 2004). Currently, green synthesis of nanoparticles is a novel alternative method. In addition, nanoparticles conjugated with natural biomolecules, which are easily taken up by human cells, have been reported to be more efficacious. In parallel, they act as reducers and stabilizers with smaller sizes and higher penetrating capacities proving themselves to have excellent therapeutic activity.

## Types of green synthesis of nanoparticles

### Biocompatible green reagents

#### Biopolymers

The synthesis of magnetic NPs has attracted a great deal of research interest owing to the utilization of synthetic, non-toxic, and biocompatible materials. The hydrophilic polymer, starch (~20% amylase) plays a substantial role in stabilizing and dispersing NPs, as observed in the synthesis of magnetite NPs (Fe<sub>3</sub>O<sub>4</sub>) NPs achieved by sodium alginate biopolymer with a redox-based hydrothermal process using FeCl<sub>3</sub>·6H<sub>2</sub>O and urea as a precursor (Jegan et al., 2011).

#### Ascorbic acid functionalizes and stabilizes

NP synthesis. The use of ascorbic acid as a super-paramagnetic iron oxide NPs results in a stable dispersion with an advantage in medical applications. The coated NPs were spherical with a mean particle size of 5 nm, as observed by transmission electron microscopy (TEM) (Sreeja et al., 2014).

#### Amino acids

Biological amines such as L-cysteine, L-arginine, L-glutamine, and L-glutamic acid are functionalized by magnetite NPs to produce FeNPs by a method that involves wet chemical co-precipitation along with the effect of pH (Siskova et al., 2013) (Table 1).

The synthesis of Fe-NPs from natural precursors of Fe, such as hemoglobin and myoglobin, by a single-phase chemical reaction produces Fe-NPs that are stable at room temperature (RT). This strategy is an important approach for the fabrication of bioconjugated NP for biological applications (Sayyad et al., 2012) (Figure 2).

#### Sugar and glucose

A reducing agent, D-glucose and gluconic acid as a stabilizer are used for the synthesis of polycrystalline Fe<sub>3</sub>O<sub>4</sub>-NPs (Table 1). Synthesis of Fe<sub>3</sub>O<sub>4</sub>- NP is coated with glucose and gluconic acid by hydrothermal reduction of Fe<sup>3+</sup> ions to Fe<sup>2+</sup> followed by capping of NPs to enhance and stabilize the properties (Ramakrishna et al., 2022).

#### Synthetic tannic and gallic acid

Fe<sub>3</sub>O<sub>4</sub>-NPs are exceedingly crystalline and monodispersed and are synthesized by ultrasonication of an aqueous suspension of tannic acid at an optimal pH of 10. These synthesized NPs were spherical with a size less than 10 nm, as revealed by high-resolution transmission electron microscopy (HR-TEM) (Herrera-Becerra et al., 2010). Figure 2 shows the green synthesis of nanomaterials from different biological agents.

## By microorganisms

### Bacteria

Iron nanomaterials (Fe-NPs) are biosynthesized most commonly by iron-reducing bacteria, such as *Actinobacteria* sp., under aerobic conditions that form spherical iron oxide nanoparticles (FeO-NPs). These microbes synthesized magnetic NPs when exposed to an aqueous ferric salt solution under aerobic conditions within 48–72 h. The FeO-NPs that exhibited a color change from medium to brown were analyzed by TEM, X-ray diffraction (XRD), Fourier Transform Infrared Spectroscopy (FTIR), magnetic measurements, and other methods. The synthesis of magnetic NPs in bacteria such as *Actinobacter* sp. is a highly complex phenomenon that involves iron reductase enzymes in the presence of excess iron salts (Bharde et al., 2008). Iron reductase reduces Fe<sup>3+</sup> to Fe<sup>2+</sup> extracellularly to produce magnetic NPs. Additionally, the activity of Fe<sup>3+</sup> reductase was confirmed by a ferrisiderophore reductase assay, indicating extracellular synthesis (Bharde et al., 2005) (Table 2).

### Fungi

Magnetic NPs are produced extracellularly by a combination of fungi of different sizes, such as *Fusarium oxysporum* and *Verticillium* sp., using ferric and ferrous salts at room temperature. These microbes secrete extracellular cationic proteins that hydrolyze anionic iron complexes to crystalline magnetite particles at low temperatures via means of spontaneous magnetization and ferrimagnetic transition signatures (Bharde et al., 2006). Various species of fungal and bacterial strains, such



TABLE 1 Biosynthetic methods of various kinds of nanoparticles along with their morphology, size, and applications.

Sl. No.	Different types of nanoparticles	Chemical and Biological Agents used	Size/Morphology	Various Applications	References
1.	Bimetallic Fe/Pd-NPs	Starch	14.1 nm	Water purification, degradation of chlorinated hydrocarbons	(He and Zhao, 2005)
2.	Fe <sub>3</sub> O <sub>4</sub>	Sodium alginate	27.2 nm/ Spherical	Pollutant removal	(Gao et al., 2008)
3.	Polymer composite-Fe <sub>3</sub> O <sub>4</sub>	Agar	50–200 nm/ Hexagonal, Spherical	Biosensors, Bio-analysis, gene delivery	(Jegan et al., 2011)
4.	Fe nano-shell	Ascorbic acid (Vitamin C)	<100 nm/cube	Nanomaterial field	(Nadagouda and Varma, 2007)
5.	nZVI (Nano zero-valent iron)	Ascorbic acid	20–75 nm/Spherical	Bioremediation of Cd	(Savasari et al., 2015)
6.	Superparamagnetic Iron oxide (Coating and functionalisation)	Ascorbic acid	5 nm and 30 nm	Environmental sensing, imaging, and remediation	(Sreeja et al., 2014)
7.	Fe <sub>3</sub> O <sub>4</sub>	L-lysine, L-glutamic acid.	17.5 nm/crystalline and spherical	Thermal therapy of cancer	(Vines et al., 2019)
8.	nZVI (Nano zero-valent iron)	L-glutamic acid. L-cysteine L-arginine	–	Bioremediation of Cd	(Siskova et al., 2013)
9.	Fe NPs	Haemoglobin, myoglobin	2–5 nm	Environmental remediation	(Saif et al., 2016)
10.	Fe <sub>3</sub> O <sub>4</sub>	Gluconic acid, D-glucose	12.5 nm/Spherical crystalline	Waste water purification	(Lu et al., 2010)
11.	Fe <sub>3</sub> O <sub>4</sub>	Gluconic acid, D-glucose	4–16 nm/Crystalline	Drug delivery	(Ramakrishnappa et al., 2022)
12.	Iron NPs encapsulating carbon	Sugars derived from woods	100–150 nm/ Nanosphere	To confer extreme chemical stability	(Yan et al., 2015)
13.	Iron oxide	Tannic acid	<10 nm	Drug targeting and Separation of biomolecules	(Herrera-Becerra et al., 2010)
14.	Fe-core shell	Chitosan- Gallic acid	~11 nm/cubic	Molecular bio-imaging and cancer therapy	(Dorniani et al., 2012)

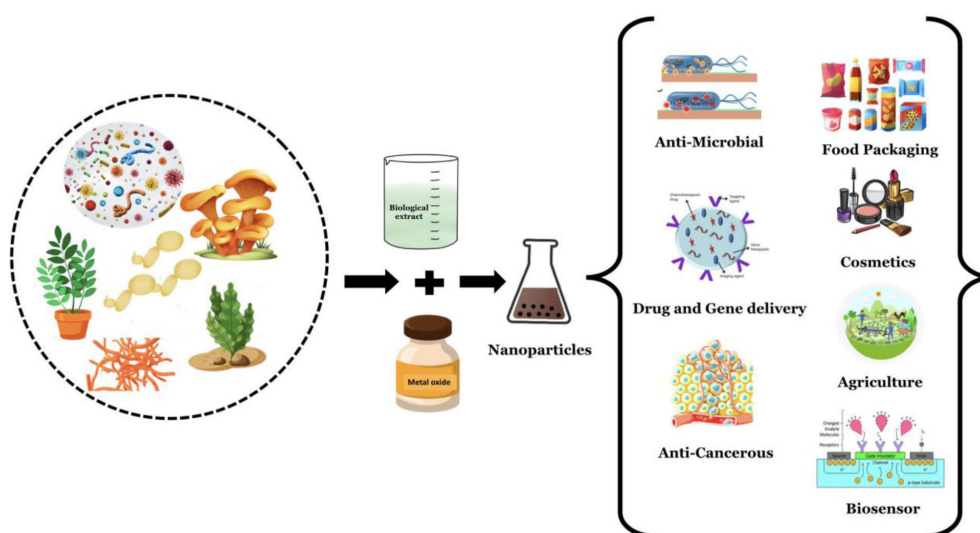


FIGURE 2

Green synthesis of nanomaterials using various biological components and their applications.

TABLE 2 List of environmental applications involving various microbial-derived NPs.

Sl.No.	Type of Nanoparticles	Type of Microorganisms used	Species Name	Size	Environmental Applications	References
1.	Iron Oxide NP	Bacteria	<i>Actinobacter</i> sp. <i>Bacillus subtilis</i>	10–40 nm cubic <50 nm 60–80 nm Spherical	–Removal of plant biomass –Microbial enhanced oil recovery, bio-remediation of oil spills	(Bharde et al., 2005; Bharde et al., 2008; Sundaram et al., 2012)
2.	Magnetite NP And Iron NP	Fungi	<i>Fusarium oxysporum</i> , <i>Verticillium</i> sp. <i>Aspergillus</i> <i>Alternaria alternata</i>	20–50 nm Spherical 50–200 nm –9 nm	–Fungicides –Visualizing root infections in plants –Antibacterial activity	(Bharde et al., 2006; Pavani and Kumar, 2013; Mohamed et al., 2015)
3.	Iron Oxide NP and Iron NP	Algae	<i>Sargassum muticum</i> <i>Chlorococcum</i> sp.	18 ± 4 nm, cubic 20–50 nm, spherical	–To treat beach erosion –reduction of chromium	(Mahdavi et al., 2013; Subramaniam et al., 2015)

as *Pochonia chlamydosporium*, *Aspergillus fumigatus*, *A. wentii*, *Curvularia lunata*, *Chaetomium globosum*, *Alcaligenes faecalis*, *Bacillus faecalis*, and *Bacillus coagulans*, have been tested to produce iron NP (Kaul et al., 2012) (Table 2).

## Algae

The biosynthesis of Fe<sub>3</sub>O<sub>4</sub> NP involves ferric chloride reduction in macroalgae of brown seaweed, *Sargassum muticum* extracts containing sulfated polysaccharides that help facilitate the reduction of iron salt. XRD analysis of the NPs synthesized using this method indicated the presence of crystalline and cube-shaped particles (Table 2). The TEM images of these microalgae revealed the presence of intracellular and extracellular iron. FTIR analysis confirmed that carbonyl and amine groups reduced the iron salts (Mahdavi et al., 2013). Algae are potential phototrophic organisms known for the greater production of several metabolites, pigments, polysaccharides, fibers, and secondary metabolites, yielding larger production of NPs. Hence, these biofactories are expected to contribute more competent and harmless bioactive compounds for various applications.

## Nanoparticles synthesized by plants

Green synthesis of metallic NPs from various plant parts, such as leaves, stems, roots, and seeds, is the simple, inexpensive, and reproducible. However, plants as natural sources will certainly produce the added advantage of stable metal NPs. Hence, green-synthesized NPs have proven to be the best candidates for fast and large-scale production in comparison to microbes that require specific environmental conditions (Kalaierasi et al., 2010). Extracts from the seeds, fruits, leaves, stems of different herbs and higher plants are rich in antioxidants that help boost the capacity of NPs. Therefore, the use of plant-based phytochemicals for the synthesis of NPs unites natural/plant sciences and

nanotechnology, and enables safe, environmentally friendly, justifiable, and economically feasible green technologies (Mayegowda et al., 2022a; Mayegowda et al., 2023).

## Synthesis from leaf extract

Fe-NPs were produced using green tea (*Camellia sinensis*) extracts, which are rich in polyphenols. Polyphenols are excellent reducing and capping agents, resulting in the formation of stable, green, nanoscale zero-valent iron particles (Rotti et al., 2023). Similarly, crystalline monodisperse magnetite [Fe<sub>3</sub>O<sub>4</sub>] NPs were synthesized using the carob leaf in a one-step reaction (Awwad and Salem, 2012). FeO/Fe<sub>3</sub>O<sub>4</sub> NPs were synthesized using pomegranate (*Punica granatum*) leaf extract and heat-killed yeast (*Yarrowia lipolytica*), as biosorbents to remove hexavalent chromium. Mössbauer spectroscopy revealed the presence of FeO/Fe<sub>3</sub>O<sub>4</sub>, and SEM images displayed even the dispersal of Fe-NPs on the outer surface of yeast cells (Rao et al., 2013).

## By fruit extract

Pd and Fe-NPs were prepared using aqueous fruit extracts of *Terminalia chebula*. Stable Fe-NPs were synthesized by the reduction of a FeSO<sub>4</sub>·7H<sub>2</sub>O solution by *T. chebula* extract (Kumar et al., 2013). Fe<sub>3</sub>O<sub>4</sub> NPs were synthesized from the fruit extracts of *Passiflora tripartita* var. *mollissima* are 22.3 nm in size and show significant nanocatalytic activity (Kumar et al., 2014).

## Seed extract

A previous study demonstrated the production of FeO NPs using *Syzygium cumini* (Malabar plum) as a stabilizing agent. The seed extract was used as a reducing agent, and sodium acetate was used as an electrostatic stabilizing agent. The presence of polyphenols, such as flavonoids, was confirmed by FTIR spectroscopy, which is important in serving the role as reducing agents (Venkateswarlu et al., 2014).

## Mechanism of antimicrobial action

### Bacteria

NPs also exhibit antibacterial properties. Silver (Ag) NPs continuously release Ag ions that adhere to the bacterial cell wall and cell membrane, leading to disruption of the bacterial envelope (Khorrami et al., 2018). Once inside the cell, Ag deactivates respiratory enzymes by producing reactive oxygen species (ROS) (Ramkumar et al., 2017). The accumulation of ROS causes damage to DNA, RNA, and proteins, resulting in cell death. The Ag released from NPs binds the sulfur and phosphorus of DNA and blocks replication and cell division, eventually leading to cell death. Ag ions also cause denaturation of ribosomes in the cytoplasm, leading to inhibition of protein synthesis (Durán et al., 2016; Jadimurthy et al., 2022) (Figure 3).

The accumulation of AgNPs alters the structure of the cell membrane and promotes cell lysis (Liao et al., 2019). The surface charge of the NP plays a significant role in determining its interaction with the cell membrane. Cationic NPs infiltrate cells and cause extensive damage. Although anionic NPs do not penetrate the plasma membrane, they destabilize at specific concentrations. While this property of charged NPs suggests potential damage to human cells, it offers opportunities for use as a vehicle for drug delivery to cancerous cells. Denaturation of the cytoplasmic membrane often leads to the rupture of organelles, which ultimately results in cell lysis. Bacterial signal transduction involves phosphorylation events that enable bacteria to sense, adapt, and respond to environmental changes. NPs cause dephosphorylation and disruption of signal transduction, leading to apoptosis (Li et al., 2019). Ag NPs are spherical or quasi spherical and can easily release Ag ions owing to their large surface (Shanmuganathan et al., 2018). To avoid agglomeration, capping agents are used to coat the NPs, which modifies their surfaces and

affects their dissolution. The presence of organic or inorganic in the medium can also be responsible for the dissolution of NPs by aggregation.

It has been demonstrated that Ag NPs release Ag ions in the aqueous solution and this is quite faster when the pH is acidic (below 5) than in neutral solution (Jacob et al., 2019). Differential mode of action for NPs has been reported for Gram-positive and Gram-negative bacteria and has been attributed to the presence of peptidoglycan in Gram-positive bacteria which hinders efficient penetration (Meikle et al., 2020). NPs with a size less than 10 nm can directly penetrate the cell and alter cell permeability, enter bacteria, and cause cellular destruction, suggesting a direct correlation between NP uptake and antibacterial properties (Noronha et al., 2017). Hence, Ag NPs have a great potential as antibacterial agents. However, the application of Ag NPs as biofilm inhibitors warrants further investigation (Pugazhendhi et al., 2018). Magnesium oxide NPs have been reported to possess anti-biofilm and anti-adhesion potential, which are efficient against drug-resistant bacteria (Hayat et al., 2018).

### Fungi

Repetitive damage to the environment due to hazardous chemicals, such as excessive use of pesticides, poses a great threat to agriculture worldwide. The use of NPs to target plant pathogens appears to be a safe alternative to chemically synthesized pesticides (Kim et al., 2012). Ag NPs, with varied modes of action, are suggested to be safe agents against plant pathogens, particularly commercially relevant fungal pathogens, as compared to artificial antifungal agent (Manjula et al., 2023). Metal NPs are non-toxic, eco-friendly, and widely used as disinfectants and investigational antifungal mediators (Borehalli Mayegowda et al., 2022). Zinc NPs have potential applications in the pharmaceutical sector, as

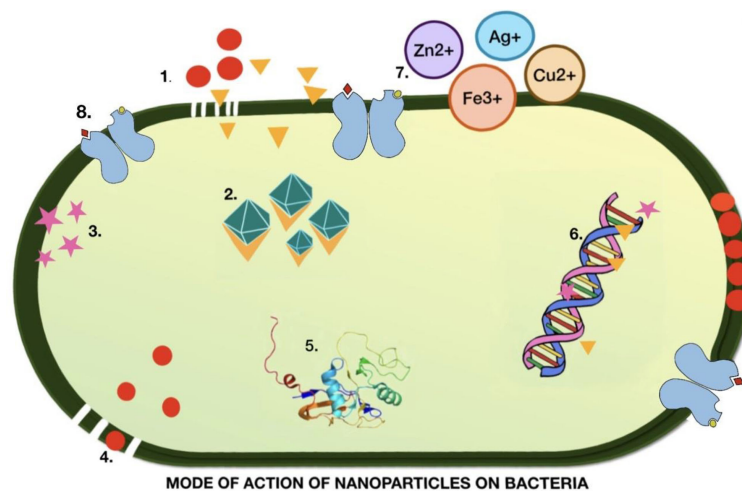


FIGURE 3

Illustration of the mechanism of action of nanoparticles in the destruction of bacterial cells. 1. Metal nanoparticles destroyed the cell wall and cell membrane. 2. Ions generated from metal NP bind to and denature ribosomes. 3. ROS production. 4. Accumulation of nanoparticles rupturing the cell membrane. 5. Alteration of the protein structure leading to damage. 6. DNA denaturation. 7. Metal ions that inhibit the electron transport chain. 8. Metal NPs bind to the receptor, causing a change in conformation.

potent antimicrobial agents and in water disinfection. Studies demonstrating the antifungal activity of Ag NPs are limited. Kim and colleagues have however, suggested a concentration dependent inhibitory activity, probably due to saturation of fungal hyphae with higher density NPs leading to deactivation of the disease-causing fungi (Kim et al., 2012).

While the effect of Ag ions on fungi is limited, reports suggest their inhibitory effect on DNA replication (Feng et al., 2000) and impairment of ribosomal attachment, blocking protein synthesis, enzymes, and additional proteins involved in the production of ATP (Yamanaka et al., 2005). Ag NPs synthesized using ribose sugar and sodium dodecyl sulfate acting like reducing agent and capping agent, respectively demonstrating antifungal activity against highly resistant human pathogenic fungi such as *Candida albicans* and *Candida tropicalis* (Mallmann et al., 2015). Similar results have been reported by other researchers (Kim et al., 2009). Fungal cells maintain an ion gradient, trehalose and glucose protects the biological viability of cells from protein denaturation caused by environmental stress such as heat, cold, high pH, dehydration, oxidative stress, and lethal agents (Alvarez-Peral et al., 2002). NPs disrupt the membrane structure and permeability, leading to leakage of intracellular contents and loss of membrane potential. TEM observations revealed the formation of pits in the fungal membrane when treated with Ag ions, leading to cell cycle arrest and cell death in *C. albicans*. Additionally, destruction of the membrane and inhibition of budding have been noted (Endo et al., 1997). Palladium NPs demonstrated effective antifungal activity against *Colletotrichum gloeosporioides* and *F. oxysporum* although in a size-dependent manner (Osonga et al., 2020). Therefore, NPs may induce antifungal activity by disrupting cellular integrity, generating reactive species, and creating osmotic imbalances in pathogens.

## Virus

While several viral diseases have been eradicated, emerging threats from novel viruses cannot be ignored because of their adaptability and mutagenic ability (Esteban, 2010). Hence, these viruses pose a continuous challenge to the scientific community. Enfuvirtide is a synthetic peptide drug, approved by the US Food and Drug Administration that targets a specific HIV protein named the gp41 coding envelope protein and prevents its fusion (Galdiero et al., 2011).

Under such challenging circumstances, NPs have been developed as promising antiviral agents owing to their increased surface area and unique chemical and physical properties (Elechiguerra et al., 2005). NPs block viral infections by having their mode of action at the time of attachment as well as entry by obstructing polyvalent interactions across viral surface components in interaction with host cell membrane receptors (Figure 4) (Helenius, 2007). Previous studies have demonstrated the efficacy of NPs against HIV-1 (Lara et al., 2010a; Lara et al., 2010b), hepatitis B virus (Lu et al., 2008), herpes simplex virus type 1 (Baram-Pinto et al., 2009), monkey pox virus (Rogers et al., 2008), and influenza virus (Papp et al., 2010). While the interaction and efficacy of NPs against viruses were largely dependent on NP size, they also interacted at specific sites. NPs also bind strongly to the sulfur-containing residues of GP120 (Lara et al., 2010a). Both Ag and Au NPs have promising antiviral properties, particularly against enveloped DNA/RNA viruses. A recent study on COVID-19 viral disease explains about the neurotropism property demonstrating the application of NPs by inhibiting replication by cellular transcytosis blockade when given in the form of encapsulated particles (Ren et al., 2021).

## Characterization of nanoparticles

NPs are classified based on their composition into three classes: a) organic-based, which comprises proteins, lipids, carbohydrates, polymers, or any other organic compounds that are nontoxic, ecofriendly, such as dendrimers, liposomes, micelles, and protein complexes (Bharde et al., 2005; Bharde et al., 2008; Rotti et al., 2023), and carbon-based are solely made of carbon such as fullerenes, carbon black NPs, and quantum dots (Savasari et al., 2015). Inorganic nanoparticles (NPs) including metals, ceramics, and semiconductors. These inorganic metal NPs can be synthesized from monometallic or bimetallic alloys (Mayegowda et al., 2022b). Owing to the varying properties of NPs, different techniques can be used for characterization and analysis to determine their potential applications. Morphological and topological features were established to check the size, shape, dispersity, localized, surface topography, surface area and porosity of NPs, which can be determined by TEM and SEM (Herrera-Becerra et al., 2010; Sreeja et al., 2014). Other techniques include dynamic light scattering (DLS) and nanoparticle tracking analysis (NTA), which involve the light interference measured on the suspended NPs for Brownian motion with the

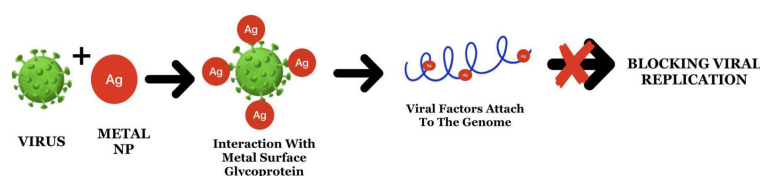


FIGURE 4

The mode of action of Ag nanoparticles through attachment to the surface proteins and viral genome leads to the blockage of replication.

correlation of its velocity with their size using the Stokes–Einstein equation (Bharde et al., 2008). However, the structural and chemical characterization of NPs can be carried out by XRD, energy-dispersive X-ray spectroscopy (EDX), high-angle annular dark-field imaging (HAADF), and FTIR for the phase, composition, crystallinity, chemical state (oxidation), functional groups, surface charges, and electrochemical characteristics. Zeta potential analysis can be used to determine the surface charge of NPs (Manjula et al., 2023; Mayegowda et al., 2023). The characterization of NPs for optical, electronic, and electrical properties was carried out by Raman spectroscopy and SERS for absorption, luminescence, electronic state, photoactivity, and electrical conductivities. UV–vis and photoluminescence spectroscopy, which transitions electrons from the ground to an excited state, as measured by absorption spectroscopy (Manjula et al., 2023). Magnetic properties have great advantages and are quantified by magnetic force microscopy or electron spin resonance spectroscopy.

## Application of nanoparticles

Although NPs hold tremendous promise owing to their ease of synthesis and wide industrial applications, their synthesis using chemical approaches results in toxic side effects. Therefore, green synthesis is promising as an alternative and safe process. The following section highlights the commercial, medicinal, and other applications of green synthetic NPs.

### Agriculture

In agriculture, nanotechnology is primarily used for the synthesis of pesticides and fertilizers. NPs can be used as fertilizers to facilitate crop improvement, seed germination, and root growth, while also reducing eco-toxicity. Ag NPs were shown to improve wheat growth and yield. One of the essential micronutrients for plant metabolic processes is zinc, which is involved in the synthesis of auxins such as indole acetic acid and carbohydrates, and in the formation of chlorophyll. Many NPs have been used in the form of pesticides, such as green peach aphids (Ghidan et al., 2018; Mayegowda et al., 2022b). Decreased plant mortality for granulomatosis with polyangiitis (GPA), a condition in which the blood vessels become swollen, was achieved by the synthesis of NPs using aqueous peel extracts of *Punica granatum*, leaf extracts of *Olea europaea*, and flower extract of *Chamaemelum nobile*. GPA infection and the absence of metal accumulation suggest the advantages of bio-NPs (Ghidan et al., 2017). Ag NPs also function as fungicides and have been effective against *C. gloeosporioides* which causes bitter rot in various crops (Aguilar-Méndez et al., 2010).

### Food industry

Nanotechnology in the food industry can escalate their shelf life of various foods and reduce their depletion due to contagious

infestation (Pradhan et al., 2015). Encapsulation of biomolecules, such as lipids proteins, carbohydrates, and vitamins, using NPs can protect them from the acidic environment of the stomach and intestine and can improve their assimilation (Singh et al., 2017). However, the use of NPs in food packaging materials aids in the preservation and protection from several of these issues.

Essential oils obtained from organic compounds, organic acids, and bacteriocins have been extensively studied for use in polymeric matrices as antimicrobial packaging material (Gálvez et al., 2007). Many NPs, such as Ag, copper, biopolymer chitosan, and metal-oxide derived NPs, such as titanium oxide (TiO<sub>2</sub>) and zinc oxide (ZnO), have been shown to have antibacterial activity (Manjula et al., 2022). Nanobiosensors are used in the food industry for pathogen detection during processing (Mayegowda et al., 2022). Nano-biosensor can detect changes in the environment, such as moisture content or temperature fluctuations in storage rooms, microbial contamination, or product deprivation. NPs play a vital role in the food industry, and their green synthesis offers additional advantages.

### Cosmetics

The use of NPs is most popular in the cosmetic industry. Leading brands such as L'Oreal, Avon, and Johnson and Johnson have patents on nanoparticles. NPs are employed in sunscreens, skin creams, skin lotions, and dye-based products such as fabric colors, skin tanning, and whitening lotions. Sunscreens are used as UV filters and provide broad UV protection with minimal or no adverse effects. NMs labeled in cosmetics can be similar to vesicles in cells, such as liposomes, nano-emulsions, and nano-capsules. Other solid lipid NP conjugates, include nanocrystals and NP with metal-like nanosilver and nanogold, dendrimers, cubosomes, liquid-based hydrogels, and buckyballs (Raj et al., 2012; Ananda et al., 2022). NPs utilized in cosmetics are generally chemically synthesized, but there is an emerging shift towards green synthesis. Xia et al. demonstrated the use of ivy plant-derived NPs as an alternative to oxide particles in blocking UV rays (Bezbaruah et al., 2022).

### Healthcare

Recently, NPs have been used for detection, diagnosis, and tumor therapy. NPs are excellent tools for cancer drug delivery because of their small size, which facilitates targeted delivery. NPs have also been used to mitigate adverse effects of photodynamic cancer therapy. The hydrophilic antigenic drug Mosquirix<sup>®</sup> is used to treat malaria caused by *Plasmodium falciparum* and hepatitis B virus. This liposomal drug, modified as a phospholipid intrinsic adjuvant, has greater stability in the gastrointestinal tract for absorption. A nanogel made up of polyethylenimine along with cationic coated alginate, which is given intraperitoneally, produces anti-ovalbumin IgG, which is promising for drug delivery (Adarsha et al., 2022). A dye used in photodynamic therapy migrates to the skin and eyes, leading to sensitivity. Partial encapsulation of the dye



in NPs helped reduce sensitivity (Roy et al., 2003). Furthermore, NPs, such as gold NPs, have research applications, such as immunohistochemistry and identification of protein–protein interactions. Cao et al. (2003) synthesized a AuNP probe with catalytic activity for protein identification (Cao et al., 2003; Yadav et al., 2021). The extensive medical use of chemically made NPs has been reported to have adverse effects. Therefore, there has been a shift toward safer green synthetic bio-NPs. A study reported the use of nano-encapsulated AgNPs by green-synthesized pcDNA3.1/H5 for immunization through humoral and cell-mediated immune responses. Thus, green NPs can be used as an alternative DNA vaccine through nanotechnology for the oral administration of vaccines in a more effective way. AgNPs are an attractive and unique alternative delivery method for oral DNA vaccinations. NP-based vaccination showed a similar effect in the elucidation of the immune response as traditional vaccination procedures. In addition, it exhibits greater stability, cost-effectiveness, and target specificity in minimizing various disease types (Jazayeri et al., 2012).

Fungal based synthesized ZnNPs showed excellent antimicrobial property against pathogenic fish bacteria in comparison with chemical ZnNPs. This study also highlights the increase in immune response in organisms by the released  $\text{Zn}^{2+}$  hindering active transport as well as inhibiting bacterial enzymes in metabolism, leading to the release of ROS, causing death of the organism (El-Saadony et al., 2021). Similarly, biosynthesis of NPs from microbes and plant extracts has also shown vast application in modulating immune responses through innate and adaptive immunity across conditions, such as inflammation, cell differentiation and signaling during cancer, autoimmune disease, and allergic reactions. Hence, describing the ecofriendly and safer

approach to green NPs is a novel therapeutic approach in drug delivery and therapeutics (Cai et al., 2022).

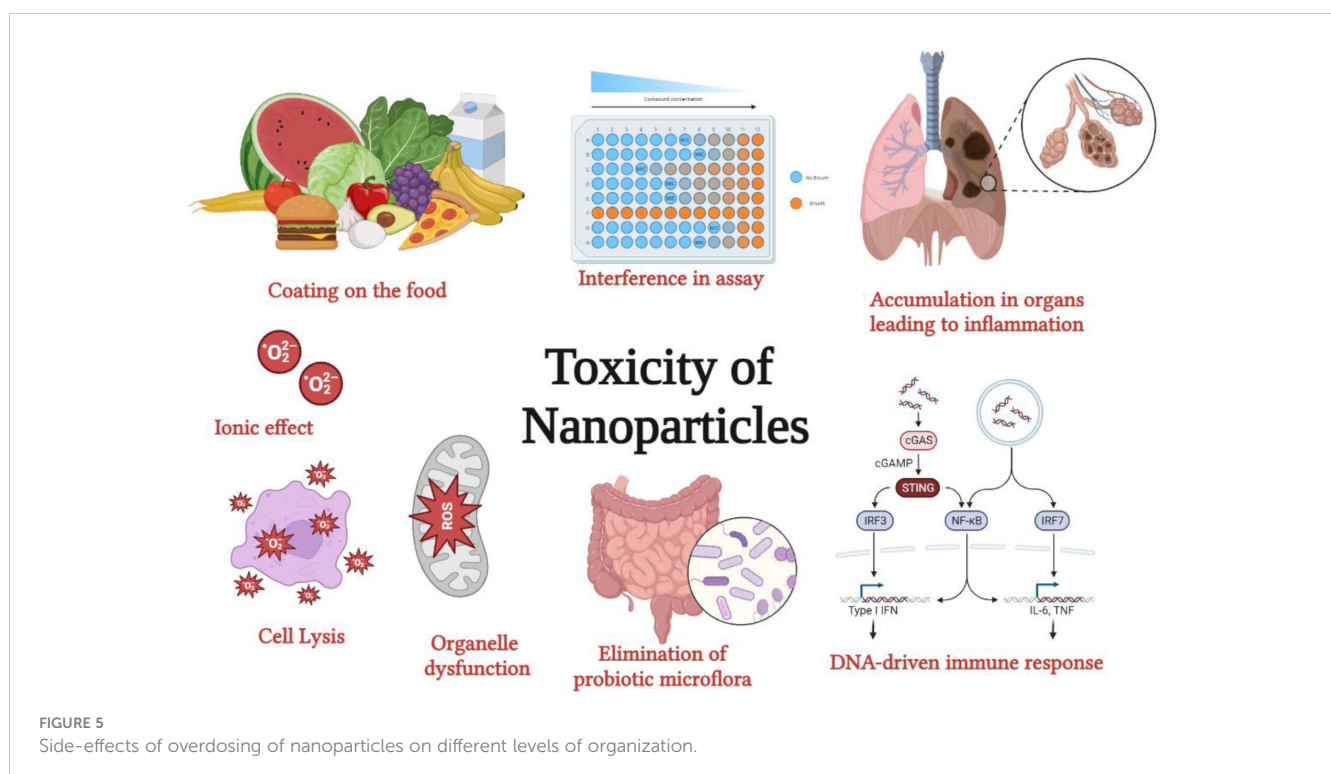
## Toxicity of nanoparticles

Despite the innumerable advantages of NPs, as listed above, they can still be toxic at higher concentrations, if overused, or accumulate within the system. However, the toxicity levels in the environment depend largely on the type of NPs and the properties that have been used.

## Toxicity to humans

The size of the NP decreased from 30 to 3 nm, and the number of surface molecules increased from 10% to 50%. Metal NPs are the most common type of NPs employed in all industries. Studies on cellular uptake of gold NPs indicated their extracellular aggregation followed by enmass transport into the cells with resultant reactive species production and cytotoxicity (Figure 5) (Goodman et al., 2004; Chithrani et al., 2006). Studies have shown that the formation of abnormal actin filaments results in decreased cell adhesion, proliferation, and motility (Pernodet et al., 2006). While gold nanospheres capped with citrate were non-toxic to baby hamster kidney and human hepatocellular liver carcinoma cells, they were toxic to human carcinoma lung cell lines at certain concentrations, signifying their effect on cell type (Pernodet et al., 2006).

Large concentrations of Ag in atmospheric air led to breathing abnormalities and lung, throat, and stomach discomforts. Ag in skin



contact can occasionally lead to insignificant allergic conditions, such as rashes, swelling, and inflammation. However, several studies have been conducted (Carlson et al., 2008). However, studies have not proven the toxicity of spherical AgNPs and Ag nano-prisms in human skin keratinocytes. TiO<sub>2</sub> NPs induce oxidative stress by inducing changes in gene expression (Park et al., 2008). ZnO also induced toxicity by generating reactive oxygen species, oxidant injury, and inflammation, leading to cell death (El-Saadony et al., 2021).

## Toxicity to the environment

In addition to humans, other animals and microbes such as zebra fish, daphnids, and algal species were exposed to silver, copper, aluminum, nickel, cobalt, and TiO<sub>2</sub> nanoparticles. Griffith et al. (2008) detected toxicity levels in aquatic organisms owing to the presence of metallic NPs. In contrast, no toxicity was observed for TiO<sub>2</sub> NPs. These results were corroborated by another study on zebrafish embryos that suggested the dose-dependent developmental toxicity of Ag NPs (Asharani et al., 2008). The toxicity level of AgNPs in the aquatic environment can be denoted by the concentration accumulated by aquatic organisms. The liver is the initial accumulator organ for NPs in these aquatic organisms, followed by the gills, intestine, and muscles, causing cell necrosis and lysis in the intestinal villi, followed by progressive release of Ag ions (Liu et al., 2015). AgNPs are frequently used in apparel owing to their antimicrobial properties. However, the release of Ag, in both colloidal and ionic forms, from the fabric during washing causes its accumulation in the wastewater, leading to toxicity (Benn and Westerhoff, 2008).

ZnO NPs are readily used in cosmetics and, as such, are a large constituent of factory run off from the cosmetic industries. These NPs are toxic to *Lolium perenne* (ryegrass). ZnO-NP, along with the ryegrass biomass, has been able to suggestively reduce, characterized by shrinking the root tips, and highly vacuolated or collapsed epidermal or cortical cells (Lin and Xing, 2008). However, a minor reduction in root cells was detected upon exposure to uncoated alumina NPs (Yang and Watts, 2005).

## Future prospects

Recently, there has been a burst of commercial applications for NPs. However, green synthesis of NPs is still in its infancy. Green synthesis offers a safe mechanism for producing nontoxic NPs with additional beneficial effects. Green synthesis has already been applied in several fields owing to the use of natural alternatives. Bio-NPs have been used as artificial food colors, strengthening agents for skincare products, antimicrobial agents embedded in fabrics, core molecules for drugs, and therapeutic molecules. However, their global application is limited by technology. Further research in this nascent field is warranted. Thus, green

synthesis has the potential to reduce environmental pollution by employing commercially viable yet safe biomaterials.

## Conclusion

NPs are generally used for their antimicrobial properties, which can act against bacteria, fungi, and certain viruses. This generally results from the metal component, but bio-NPs also contain other biomolecules as vital components. The antimicrobial properties of NPs are used in various industries, such as food packaging, active agents in skincare products, disease treatment, and drug delivery. It should be noted that the overuse and extensive deployment of NPs could lead to toxicity owing to the accumulation of metals and ions being released. However, lethal effects on humans at the currently used concentrations have not been reported. In conclusion, green synthesis is a largely positive and significant venture in all fields of science, in which the use of environmentally friendly resources and biodegradable materials in the synthesis of NPs will undoubtedly lead to an eco-friendly era with reduced industrial and environmental pollution.

## Author contributions

SB, AR, and MG conceptualized, designed, and wrote the initial manuscript draft the manuscript. SP, SA, MAlm, MAlI, NSA and RS prepared the figures and tables, edited, and revised the manuscript critically. Final manuscript has been approved by all the authors.

## Acknowledgments

The authors extend their appreciation to the Deanship of Scientific Research at King Khalid University for supporting this work through research groups program under grant number RGP.2/273/44.

## Conflict of interest

The authors declare that the research was conducted in the absence of any commercial or financial relationships that could be construed as a potential conflict of interest.

## Publisher's note

All claims expressed in this article are solely those of the authors and do not necessarily represent those of their affiliated organizations, or those of the publisher, the editors and the reviewers. Any product that may be evaluated in this article, or claim that may be made by its manufacturer, is not guaranteed or endorsed by the publisher.

## References

- Adarsha, J. R., Ravishankar, T. N., Ananda, A., Manjunatha, C. R., Shilpa, B. M., and Ramakrishnapa, T. (2022). Hydrothermal synthesis of novel heterostructured Ag/TiO<sub>2</sub>/CuFe<sub>2</sub>O<sub>4</sub> nanocomposite: Characterization, enhanced photocatalytic degradation of methylene blue dye, and efficient antibacterial studies. *Water Environ. Res.* 94 (6), e10744. doi: 10.1002/wer.10744
- Aguilar-Méndez, M. A., Martín-Martínez, E. S., Ortega-Arroyo, L., Coblan-Portillo, G., and Sanchez-Espindola, E. (2010). Synthesis and Characterization of silver nanoparticles: effect on phytopathogen *Colletotrichum gloeosporoides*. *J. Nanoparticle Res.* 12, 404–416. doi: 10.1007/s11051-010-0145-6
- Alvarez-Peral, F. J., Zaragoza, O., Pedreno, Y., and Argüelles, J. (2002). Protective role of trehalose during severe oxidative stress caused by hydrogen peroxide and the adaptive oxidative stress response in *Candida albicans*. *Microbiology* 148, 2599–2606. doi: 10.1099/00221287-148-8-2599
- Ananda, A., Ramakrishnapa, T., Archana, S., Reddy Yadav, L. S., Shilpa, B. M., Nagaraju, G., et al. (2022). Green synthesis of MgO nanoparticles using *Phyllanthus emblica* for Evans blue degradation and antibacterial activity. *Materials Today: Proc.* 49, 801–810. doi: 10.1016/j.matpr.2021.05.340
- Asharani, P. V., Wu, Y. L., Gong, Z., and Valiyaveetil, S. (2008). Toxicity of silver nanoparticles in zebrafish models. *Nanotechnology* 19, 255102. doi: 10.1088/0957-4484/19/25/255102
- Awad, A. M., and Salem, N. M. (2012). A green and facile approach for synthesis of magnetite nanoparticles. *Nanoscience Nanotechnology* 2, 208–213. doi: 10.5923/j.nn.20120206.09
- Baram-Pinto, D., Shukla, S., Perkash, N., Gedanken, A., and Sarid, R. (2009). Inhibition of herpes simplex virus type 1 infection by silver nanoparticles capped with mercaptoethane sulfonate. *Bioconjug. Bioconjugate Chem.* 20, 1497–1502. doi: 10.1021/bc900215b
- Baroumand Moghaddam, A., Namvar, F., Moniri, M., Azizi, S., and Mohammad, R. (2015). Nanoparticles biosynthesized by fungi and yeast: A review of their preparation, properties, and medical application. *Molecules* 20, 16540–16565. doi: 10.3390/molecules200916540
- Benn, T. M., and Westerhoff, P. (2008). Nanoparticle silver released into water from commercially available sock fabrics. *Environ. Sci. Technol.* 42, 4133–4139. doi: 10.1021/es7032718
- Bezbaruah, R., Chavda, V. P., Nongrang, L., Alom, S., Deka, K., Kalita, T., et al. (2022). Nanoparticle-based delivery systems for vaccines. *Vaccines (Basel)* 10, 1946. doi: 10.3390/vaccines10111946
- Bharde, A. A., Parikh, R. Y., Baidakova, M., Jouen, S., Hannoyer, B., Enoki, T., et al. (2008). Bacteria-mediated precursor-dependent biosynthesis of superparamagnetic iron oxide and iron sulfide nanoparticles. *Langmuir* 24, 5787–5794. doi: 10.1021/la704019p
- Bharde, A., Rautaray, D., Bansal, V., Ahmad, A., Sarkar, I., Yusuf, S. M., et al. (2006). Extracellular biosynthesis of magnetite using fungi. *Small* 2, 135–141. doi: 10.1002/sml.200500180
- Bharde, A., Wani, A., Shouche, Y., Joy, P. A., Prasad, B. L. V., and Sastry, M. (2005). Bacterial aerobic synthesis of nanocrystalline magnetite. *J. Am. Chem. Soc.* 127, 9326–9327. doi: 10.1021/ja0508469
- Borehalli Mayegowda, S., Rashmi, R., Manjula, N. G., and Sreekantha, A. (2022). “Bioremediation of Heavy Metal Contaminated Sites Using Phytoengineered Nanoparticles,” in *Phytotechnology*. Eds. M. P. Shah and A. Roy (Singapore: Springer Nature), 227–253. doi: 10.1007/978-981-19-4811-4\_11
- Cai, F., Li, S., Huang, H., Iqbal, J., Wang, C., and Jiang, X. (2022). Green synthesis of gold nanoparticles for immune response regulation: Mechanisms, applications, and perspectives. *J. Biomed. Materials Res.* 110, 424–442. doi: 10.1002/jbm.a.37281
- Cao, Y. C., Jin, R., Nam, J. M., Thaxton, C. S., and Mirkin, C. A. (2003). Raman dye labeled nanoparticle probes for proteins. *J. Am. Chem. Soc.* 125, 14676–14677. doi: 10.1021/ja0366235
- Carlson, C., Hussain, S. M., Schrand, A. M., Braydich-Stolle, L. K., Hess, K. L., Jones, R. L., et al. (2008). Unique cellular interaction of silver nanoparticles: size-dependent generation of reactive oxygen species. *J. Phys. Chem. B.* 112 (43), 13608–13619. doi: 10.1021/jp712087m
- Chithrani, B. D., Ghazani, A. A., and Chan, W. C. W. (2006). Determining the size and shape dependence of gold nanoparticle uptake into mammalian cells. *Nano Lett.* 6, 662–668. doi: 10.1021/nl052396o
- Christian, P., Von der Kammer, F., Baalousha, M., and Hofmann, T. (2008). Nanoparticles: Structure, properties, preparation and behaviour in environmental media. *Ecotoxicology* 17, 326–343. doi: 10.1007/s10646-008-0213-1
- Dorniani, D., Hussein, M. Z., Kura, A. U., Fakurazi, S., Shaari, A. H., and Ahmad, Z. (2012). Preparation of Fe<sub>3</sub>O<sub>4</sub> magnetic nanoparticles coated with gallic acid for drug delivery. *Int. J. Nanomedicine* 7, 5745–5756. doi: 10.2147/IJN.S35746
- Durán, N., Nakazato, G., and Seabra, A. (2016). Antimicrobial activity of biogenic silver nanoparticles, and silver chloride nanoparticles: an overview and comments. *Appl. Microbiol. Biotechnol.* 100 (15), 6555–6570. doi: 10.1007/s00253-016-7657-7
- Elechiguerra, J. L., Burt, J. L., Morones, J. R., Camacho-Bragado, A., Gao, X., Lara, H. H., et al. (2005). Interaction of silver nanoparticles with HIV-1. *J. Nanobiotechnology* 29, 3–6. doi: 10.1186/1477-3155-3-6
- El-Saadony, M. T., Alkhatib, F. M., Alzahrani, S. O., Shafi, M. E., El Abdel-Hamid, S., Taha, T. F., et al. (2021). Impact of mycogenic zinc nanoparticles on performance, behavior, immune response, and microbial load in *Oreochromis niloticus*. *Saudi J. Biol. Sci.* 28, 4592–4604. doi: 10.1016/j.sjbs.2021.04.066
- Endo, M., Takesako, K., Kato, I., and Yamaguchi, H. (1997). Fungicidal action of aureobasidin A, a cyclic depsipeptide antifungal antibiotic, against *Saccharomyces cerevisiae*. *Antimicrobial Agents Chemotherapy* 41, 672–676. doi: 10.1128/AAC.41.3.672
- Esteban, D. (2010). Mechanisms of viral emergence. *Veterinary Res.* 41, 38. doi: 10.1051/vetres/2010010
- Feng, Q. L., Wu, J., Chen, G. Q., Cui, F. Z., Kim, T. N., and Kim, J. O. (2000). A mechanistic study of the antibacterial effect of silver ions on *Escherichia coli* and *Staphylococcus aureus*. *J. Biomed. Material Res.* 52, 662–668. doi: 10.1002/1097-4636(20001215)52:4<662::aid-jbm10>3.0.co;2-3
- Galdiero, S., Falanga, A., Vitiello, M., Cantisani, M., Marra, V., and Galdiero, M. (2011). Silver nanoparticles as potential antiviral agent. *Molecules* 16 (10), 8894–8918. doi: 10.3390/molecules16108894
- Gálvez, A., Abriouel, H., López, R. L., and Omar, N. B. (2007). Bacteriocin-based strategies for food biopreservation. *Int. J. Food Microbiol.* 120, 51–70. doi: 10.1016/j.jifoodmicro.2007.06.001
- Gao, X., Cui, Y., Levenson, R. M., Chung, L. W. K., and Nie, S. (2004). In vivo cancer targeting and imaging with semiconductor quantum dots. *Nat. Biotechnol.* 22, 969–977. doi: 10.1038/nbt994
- Gao, S., Shi, Y., Zhang, S., Jiang, K., Yang, S., Li, Z., et al. (2008). Biopolymer-assisted green synthesis of iron oxide nanoparticles and their magnetic properties. *J. Phys. Chem. C* 112, 10398–10401. doi: 10.1021/jp802500a
- Ghidan, A. Y., Al-Antary, T. M., Awwad, A. M., and Ayad, J. Y. (2018). Physiological effect of some nanomaterials on pepper (*Capsicum annum* L.) plants. *Fresenius Environ. Bull.* 27 (11), 7872–7878.
- Ghidan, A. Y., Al-Antary, T. M., Salem, N. M., and Awwad, A. M. (2017). Facile green synthetic route to the zinc oxide (ZnONPs) nanoparticles: Effect on green peach aphid and antibacterial activity. *J. Agric. Sci.* 9 (2), 131–138. doi: 10.5539/jas.v9n2p131
- Goodman, C. M., McCusker, C. D., Yilmaz, T., and Rotello, V. M. (2004). Toxicity of gold nanoparticles functionalized with cationic and anionic side chains. *Bioconjugate Chem.* 15, 897–900. doi: 10.1021/bc049951i
- Griffith, R. J., Luo, J., Gao, J., Bonzongo, J.-C., and Barber, D. S. (2008). Effects of particle composition and species on toxicity of metallic nanomaterials in aquatic organisms. *Environ. Toxicol. Chem.* 27, 1972–1978. doi: 10.1897/08-002.1
- Hayat, S., Muzammil, S., Rasool, M. H., Nisar, Z., Hussain, S. Z., Sabri, A. N., et al. (2018). In vitro antibiofilm and anti-adhesion effects of magnesium oxide nanoparticles against antibiotic resistant bacteria. *Microbiol. Immunol.* 62, 211–220. doi: 10.1111/1348-0421.12580
- He, F., and Zhao, D. (2005). Preparation and characterization of a new class of starch-stabilized bimetallic nanoparticles for degradation of chlorinated hydrocarbons in water. *Environ. Sci. Technol.* 39, 3314–3320. doi: 10.1021/es048743y
- Helenius, A. (2007). “Virus Entry and Uncoating,” in *Fields “Virology”, Fifth Edition* (London, UK: LWW), 99–118.
- Herrera-Becerra, R., Rius, J. L., and Zorrilla, C. (2010). Tannin Biosynthesis of iron oxide nanoparticles. *Appl. Phys. A* 100, 453–459. doi: 10.1007/s00339-010-5903-x
- Jadimurthy, R., Mayegowda, S. B., Nayak, S. C., Mohan, C. D., and Rangappa, K. S. (2022). Escaping mechanisms of ESKAPE pathogens from antibiotics and their targeting by natural compounds. *Biotechnol. Rep.* 34, e00728. doi: 10.1016/j.btre.2022.e00728
- Jazayeri, S. D., Ideris, A., Zakaria, Z., Shameli, K., Moeini, H., and Omar, A. R. (2012). Cytotoxicity and immunological responses following oral vaccination of nanoencapsulated avian influenza virus H5 DNA vaccine with green synthesized silver nanoparticles. *J. Controlled Release* 161, 116–123. doi: 10.1016/j.jconrel.2012.04.015
- Jegan, A., Ramasubbu, A., Saravanan, S., and Vasanthkumar, S. (2011). One-pot synthesis and characterization of biopolymer–Iron oxide nanocomposite. *Int. J. Nano Dimension* 2, 105–110. doi: 10.7508/IJND.2011.02.002
- Kalaierasi, R., Jayalakshmi, N., and Venkatachalam, P. (2010). Phytosynthesis of nanoparticles and its applications. *Plant Cell Biotechnol. Mol. Biol.* 11, 1–16.
- Kaul, R. K., Kumar, P., Burman, U., Joshi, P., Agrawal, A., Raliya, R., et al. (2012). Magnesium and iron nanoparticles production using microorganisms and various salts. *Material Sci. Poland* 30, 254–258. doi: 10.2478/s13536-012-0028-x
- Khorrami, S., Zarrabi, A., Khaleghi, M., Danaei, M., and Mozafari, M. (2018). Selective cytotoxicity of green synthesized silver nanoparticles against the MCF-7 tumor cell line and their enhanced antioxidant and antimicrobial properties. *Int. J. Nanomedicine* 13, 8013–8024. doi: 10.2147/IJN.S189295
- Kim, S. W., Jung, J. H., Lamsal, K., Kim, Y. S., and Min JS and Lee, Y. S. (2012). Antifungal effects of silver nanoparticles (AgNPs) against various plant pathogenic fungi. *Mycobiology*. 40 (1), 53–58. doi: 10.5941/MYCO.2012.40.1.053



- Kim, K. J., Sung, W. S., Suh, B. K., Moon, S.-K., Choi, J.-S., and Kim JG and Lee, D. G. (2009). Antifungal activity and mode of action of silver nano-particles on *Candida albicans*. *Biometals* 22 (2), 235–242. doi: 10.1007/s10534-008-9159-2
- Kumar, B., Smita, K., Cumbal, L., and Debut, A. (2014). Biogenic synthesis of iron oxide nanoparticles for 2-arylbenzimidazole fabrication. *J. Saudi Chem. Soc.* 18, 364–369. doi: 10.1016/j.jscs.2014.01.003
- Lara, H. H., Ayala-Núñez, N. V., Ixtapan-Turrent, L., and Rodríguez-Padilla, C. (2010a). Mode of antiviral action of silver nanoparticles against HIV-1. *J. Nanobiotechnology* 8, 1–10. doi: 10.1186/1477-3155-8-1
- Lara, H. H., Ixtapan-Turrent, L., Garza-Treviño, E. N., and Rodríguez-Padilla, C. (2010b). PVP-coated silver nanoparticles block the transmission of cell-free and cell-associated HIV-1 in human cervical culture. *J. Nanobiotechnology* 8, 15–25. doi: 10.1186/1477-3155-8-150son
- Li, L., Li, L., Zhou, X., Yu, Y., Li, Z., Zuo, D., et al. (2019). Silver nanoparticles induce protective autophagy via Ca<sup>2+</sup>/CAMKK $\beta$ /AMPK/mTOR pathway in SH-SY5Y cells and rat brains. *Nanotoxicology* 13 (3), 369–391. doi: 10.1080/17435390.2018.1550226
- Liao, C., Li, Y., and Tjong, S. C. (2019). Bactericidal and cytotoxic properties of silver nanoparticles. *Int. J. Mol. Sci.* 20 (2), 449. doi: 10.3390/ijms20020449
- Lin, D., and Xing, B. (2008). Root uptake and phytotoxicity of ZnO nanoparticles. *Environ. Sci. Technol.* 42, 5580. doi: 10.1021/es800422x
- Liu, J., Hwang, Y. S., and Lenhart, J. J. (2015). Heteroaggregation of bare silver nanoparticles with clay minerals. *Environmental Science. Nano* 2, 528–540. doi: 10.1039/C5EN00130G
- Lu, W., Shen, Y., Xie, A., and Zhang, W. (2010). Green synthesis and characterization of superparamagnetic Fe<sub>3</sub>O<sub>4</sub> nanoparticles. *J. Magnetism Magnetic Materials* 322, 1828–1833. doi: 10.1016/j.jmmm.2009.12.035
- Lu, L., Sun, R. W., Chen, R., Hui, C. K., Ho, C. M., Luk, J. M., et al. (2008). Silver nanoparticles inhibit hepatitis B virus replication. *Antiviral Ther.* 13, 253–262. doi: 10.1177/135965350801300210
- Mahdavi, M., Namvar, F., Ahmad, M. B., and Mohamad, R. (2013). Green biosynthesis and characterization of magnetic iron oxide (Fe<sub>3</sub>O<sub>4</sub>) nanoparticles using seaweed (*Sargassum muticum*) aqueous extract. *Molecules* 18, 5954–5964. doi: 10.3390/molecules18055954
- Mallmann, E. J. J., Cunha, F. A., Castra, B. N. M. F., Maciel, A. M., Menezes, E. A., and Fecine, P. B. A. (2015). Antifungal activity of silver nanoparticles obtained by green synthesis. *Rev. do Instituto Medicina Trop. São Paulo* 57 (2), 165–167. doi: 10.1590/S0036-46652015000200011
- Mandal, D., Bolander, M. E., Mukhopadhyay, D., Sarkar, G., and Mukherjee, P. (2006). The use of microorganisms for the formation of metal nanoparticles and their application. *Appl. Microbiol. Biotechnol.* 69, 485–492. doi: 10.1007/s00253-005-0179-3
- Manjula, S. B. M., Bhoomika, S., and Kavita Nagshetty, N. G. (2022). “Environmental Adequacy of Green Polymers and Biomaterials,” in *Polymeric Biomaterials* (United States: CRC Press).
- Manjula, N. G., Sarma, G., Shilpa, B. M., and Suresh Kumar, K. (2022). “Environmental Applications of Green Engineered Copper Nanoparticles,” in *hytonanotechnology*. Eds. M. P. Shah and A. Roy (Singapore: Springer Nature Singapore), 255–276.
- Manjula, N. G., Tajunnisa, Mamani, V., McGhana, C. A., and Mayegowda, S. B. (2023). “Fungal-Based Synthesis to Generate Nanoparticles for Nanobioremediation,” in *Green Nanoremediation: Sustainable Management of Environmental Pollution*. Eds. F. M. Policarpo Tonelli, A. Roy and H. C. Ananda Murthy (Cham: Springer International Publishing), 83–108. doi: 10.1007/978-3-031-30558-0\_4
- Mayegowda, S. B., Ng, M., Alghamdi, S., Atwah, B., Alhindi, Z., and Islam, F. (2022a). Role of antimicrobial drug in the development of potential therapeutics. *Evidence-Based Complementary Altern. Med.* 2022, 1–17. doi: 10.1155/2022/2500613
- Mayegowda, S. B., Sarma, G., Gadilingappa, M. N., Alghamdi, S., Aslam, A., Refaat, B., et al. (2023). Green-synthesized nanoparticles and their therapeutic applications: A review. *Green Process. Synthesis* 12, 20230001. doi: 10.1515/gps-2023-0001
- Mayegowda, K. M. K., Shristi Ram, N. G., and Shilpa Borehalli, M. (2022). “Biopolymers and Their Applications in Biomedicine,” in *Polymeric Biomaterials* (United States: CRC Press).
- Mayegowda, S. B., Sureshkumar, K., Yashaswini, R., and Ramakrishnapa, T. (2022b). “Phytonanotechnology for the Removal of Pollutants from the Contaminated Soil Environment,” in *Phytonanotechnology*. Eds. M. P. Shah and A. Roy (Singapore: Springer Nature Singapore), 319–336.
- Meikle, T., Dyett, B. P., Strachan, J. B., White, J., Drummond, C. J., and Conn, C. E. V. (2020). Preparation, characterization, and antimicrobial activity of cubosome encapsulated metal nanocrystals. *ACS Appl. Materials Interfaces* 12 (6), 6944–6954. doi: 10.1021/acsami.9b21783
- Mohamed, Y. M., Azzam, A. M., Amin, B. H., and Safwat, N. A. (2015). Mycosynthesis of iron nanoparticles by *Alternaria alternata* and its antibacterial activity. *Afr. J. Biotechnol.* 14, 1234–1241. doi: 10.5897/AJB2014.14286
- Nadagouda, M. N., and Varma, R. S. (2007). A greener synthesis of core (Fe, Cu)-shell (Au, Pt, Pd, and Ag) nanocrystals using aqueous Vitamin C. *Crystal Growth Design* 7, 2582–2587. doi: 10.1021/cg070554e
- Noronha, V. T., Paula, A. J., Durán, G., Galembeck, A., Cogo-Muller, K., Franz-Montan, M., et al. (2017). Silver nanoparticles in dentistry. *Dental Materials* 33 (10), 1110–1126. doi: 10.1016/j.dental.2017.07.002
- Osonga, F. J., Kalra, S., Miller, R. M., Isika, D., and Sadik, O. A. (2020). Synthesis, characterization and antifungal activities of eco-friendly palladium nanoparticles. *RSC Adv.* 10, 5894–5904. doi: 10.1039/C9RA07800B
- Papp, I., Sieben, C., Ludwig, K., Roskamp, M., Böttcher, C., Schlecht, S., et al. (2010). Inhibition of influenza virus infection by multivalent sialic-acid-functionalized gold nanoparticles. *Small* 6, 2900–2906. doi: 10.1002/smll.201001349
- Park, E.-J., Yi, J., Chung, K.-H., Rye, D.-Y., Choi, J., and Park, K. (2008). Oxidative stress and apoptosis induced by titanium dioxide nanoparticles in cultured BEAS-2B cells. *Toxicol. Lett.* 180, 222–229. doi: 10.1016/j.toxlet.2008.06.869
- Pernodet, N., Fang, X., Sun, Y., Bakhtina, A., Ramakrishnan, A., Sokolov, J., et al. (2006). Adverse effects of citrate/gold nanoparticles on human dermal fibroblasts. *Small* 6, 766–773. doi: 10.1002/smll.200500492
- Pradhan, N., Singh, S., Ojha, N., Srivastava, A., Barla, A., Rai, V., et al. (2015). Facets of nanotechnology as seen in food processing, packaging, and preservation industry. *BioMed. Res. Int.*, 365672. doi: 10.1155/2015/365672
- Pugazhendhi, A., Prabakar, D., Jacob, J. M., Karuppusamy, I., and Saratale, R. G. (2018). Synthesis and characterization of silver nanoparticles using *Gelidium amansii* and its antimicrobial property against various pathogenic bacteria. *Microbial Pathogenesis* 114, 41–45. doi: 10.1016/j.micpath.2017.11.013
- Raj, S., Jose, S., Sumod, U. S., and Sabitha, M. (2012). Nanotechnology in cosmetics: Opportunities and challenges. *J. Pharm. BioAllied Sci.* 4 (3), 186–193. doi: 10.4103/0975-7406.99016
- Ramakrishnapa, S. B. M., Kempahanumakkagari Sureshkumar, M., and Thippeswamy, S. (2022). “pH and Thermo-responsive Systems,” in *Polymeric Biomaterials* (United States: CRC Press).
- Ramkumar, V. S., Pugazhendhi, A., Gopalakrishnan, K., Sivagurunathan, P., Saratale, G. D., Dung, T. N. B., et al. (2017). Biofabrication and characterization of silver nanoparticles using aqueous extract of seaweed *Enteromorpha compressa* and its biomedical properties. *Biotechnol. Rep.* 14, 1–7. doi: 10.1016/j.btre.2017.02.001
- Rao, A., Bankar, A., Kumar, A. R., Gosavi, S., and Zinjarde, S. (2013). Removal of hexavalent chromium ions by *Yarrowia lipolytica* cells modified with phyto-inspired FeO/Fe<sub>3</sub>O<sub>4</sub> nanoparticles. *J. Contaminant Hydrology* 146, 63–73. doi: 10.1016/j.jconhyd.2012.12.008
- Ren, M., Wang, Y., Luo, Y., Yao, X., Yang, Z., Zhang, P., et al. (2021). Functionalized nanoparticles in prevention and targeted therapy of viral diseases with neurotropism properties, special insight on COVID-19. *Front. Microbiol.* 12. doi: 10.3389/fmicb.2021.767104
- Rogers, J. V., Parkinson, C. V., Choi, Y. W., Speshock, J. L., and Hussain, S. M. (2008). A preliminary assessment of silver nanoparticles inhibition of monkeypox virus plaque formation. *Nanoscale Res. Lett.* 3, 129–133. doi: 10.1007/s11671-008-9128-2
- Rotti, R. B., Sunitha, D. V., Manjunath, R., Roy, A., Mayegowda, S. B., Gnanaprakash, A. P., et al. (2023). Green synthesis of MgO nanoparticles and its antibacterial properties. *Front. Chem.* 11. doi: 10.3389/fchem.2023.1143614
- Roy, I., Ohulchanskyy, T. Y., Pudavar, H. E., Bergey, E. J., Oseroff, A. R., Morgan, J., et al. (2003). Ceramic-based nanoparticles entrapping water-insoluble photosensitizing anticancer drugs: a novel drug-carrier system for photodynamic therapy. *J. Am. Chem. Soc.* 125, 7860–7865. doi: 10.1021/ja0343095
- Saif, S., Tahir, A., and Chen, Y. (2016). Green synthesis of iron nanoparticles and their environmental applications and implications. *Nanomaterials* 6 (11), 209. doi: 10.3390/nano6110209
- Savasari, M., Emadi, M., Bahmanyar, M. A., and Biparva, P. (2015). Optimization of Cd(II) removal from aqueous solution by ascorbic acid-stabilized zero valent iron nanoparticles using response surface methodology. *J. Ind. Engineering Chem.* 21, 1403–1409. doi: 10.1016/j.jiec.2014.06.014
- Sayyad, A. S., Balakrishnan, K., Ci, L., Kabbani, A. T., Vajtai, R., and Ajayan, P. M. (2012). Synthesis of iron nanoparticles from hemoglobin and myoglobin. *Nanotechnology* 23, 55602. doi: 10.1088/0957-4484/23/5/055602
- Shanmuganathan, R., MubarakAli, D., Prabakar, D., Muthukumar, H., Thajuddin, N., Kumar, S. S., et al. (2018). An enhancement of antimicrobial efficacy of biogenic and ceftriaxone-conjugated silver nanoparticles: green approach. *Environ. Sci. Pollut. Res. Int.* 25 (11), 10362–10370. doi: 10.1007/s11356-017-9367-9
- Singh, T., Shukla, S., Kumar, P., Wahla, V., Bajpai, V. K., and Rather, I. A. (2017). Application of nanotechnology in food science: Perception and overview. *Front. Microbiology* 8. doi: 10.3389/fmicb.2017.01501
- Siskova, K. M., Straska, J., Krizek, M., Tucek, J., Machala, L., and Zboril, R. (2013). Formation of zero-valent iron nanoparticles mediated by amino acids. *Proc. Environ. Sci.* 18, 809–817. doi: 10.1016/j.proenv.2013.04.109
- Sreeja, V., Jayaprabha, K. N., and Joy, P. A. (2014). Water-dispersible ascorbic-acid-coated magnetite nanoparticles for contrast enhancement in MRI. *Appl. Nanoscience* 5, 435–441. doi: 10.1007/s13204-014-0335-0
- Subramaniam, V., Subashchandrabose, S. R., Thavamani, P., Megharaj, M., Chen, Z., and Naidu, R. (2015). *Chlorococcum* sp. MM11—A novel phyco-nanofactory for the synthesis of iron nanoparticles. *J. Appl. Phycol.* 27, 1861–1869. doi: 10.1007/s10811-014-0492-2
- Sundaram, P. A., Augustine, R., and Kannan, M. (2012). Extracellular biosynthesis of iron oxide nanoparticles by *Bacillus subtilis* strains isolated from rhizosphere soil. *Biotechnol. Bioprocess Eng.* 17, 835–840. doi: 10.1007/s12257-011-0582-9

- Venkateswarlu, S., Natesh Kumar, B., Prasad, C. H., Venkateswarlu, P., and Jyothi, N. V. V. (2014). Bio-inspired green synthesis of Fe<sub>3</sub>O<sub>4</sub> spherical magnetic nanoparticles using *Syzygium cumini* seed extract. *Physica B Condensed Matter* 449, 67–71. doi: 10.1016/j.physb.2014.04.031
- Vines, J. B., Yoon, J.-H., Ryu, N.-E., Lim, D.-J., and Park, H. (2019). Gold nanoparticles for photothermal cancer therapy. *Front. Chem.* 7 (April). doi: 10.3389/fchem.2019.00167
- Vo-Dinh, T. (2007). *Nanotechnology in Biology and Medicine: Methods, Devices, and Applications* (Boca Raton, FL: CRC Press).
- Wiley, B. Y., Mayers, B., and Xia, Y. (2005). shape-Controlled. The case of silver. *Chem. Eur. J* 11, 454–463. doi: 10.1002/chem.200400927
- Yadav, L. S. R., Shilpa, B. M., Suma, B. P., Venkatesh, R., and Nagaraju, G. (2021). Synergistic effect of photocatalytic, antibacterial and electrochemical activities on biosynthesized zirconium oxide nanoparticles. *Eur. Phys. J. Plus* 136 (7), 764. doi: 10.1140/epjp/s13360-021-01606-6
- Yamanaka, M., Hara, K., and Kudo, J. (2005). Bactericidal actions of a silver ion solution on *Escherichia coli*, studied by energy-filtering transmission electron microscopy and proteomic analysis. *Appl. Environ. Microbiology* 71, 7589–7593. doi: 10.1128/AEM.71.11.7589-7593.2005
- Yan, Q., Street, J., and Yu, F. (2015). Synthesis of carbon-encapsulated iron nanoparticles from wood derived sugars by hydrothermal carbonization (HTC) and their application to convert bio-syngas into liquid hydrocarbons. *Biomass Bioenergy* 83, 85–95. doi: 10.1016/j.biombioe.2015.09.002
- Yang, L., and Watts, D. J. (2005). Particle surface characteristics may play an important role in phytotoxicity of alumina nanoparticles. *Toxicol. Lett.* 158, 122–132. doi: 10.1016/j.toxlet.2005.03.003





## OPEN ACCESS

## EDITED BY

Simone Brogi,  
University of Pisa, Italy

## REVIEWED BY

Katrin Ehrhardt,  
Hannover Medical School, Germany  
Mohana Priya Arumugam,  
Vellore Institute of Technology, India

## \*CORRESPONDENCE

Seyed Fazlollah Mousavi

✉ mousavi@pasteur.ac.ir

Ali Akbar Shabani

✉ shabani@semums.ac.ir

<sup>†</sup>These authors have contributed equally to this work

RECEIVED 01 August 2023

ACCEPTED 26 October 2023

PUBLISHED 15 November 2023

## CITATION

Shafaghi M, Bahadori Z, Barzi SM, Afshari E, Madanchi H, Mousavi SF and Shabani AA (2023) A new candidate epitope-based vaccine against PspA PhtD of *Streptococcus pneumoniae*: a computational experimental approach. *Front. Cell. Infect. Microbiol.* 13:1271143. doi: 10.3389/fcimb.2023.1271143

## COPYRIGHT

© 2023 Shafaghi, Bahadori, Barzi, Afshari, Madanchi, Mousavi and Shabani. This is an open-access article distributed under the terms of the [Creative Commons Attribution License \(CC BY\)](#). The use, distribution or reproduction in other forums is permitted, provided the original author(s) and the copyright owner(s) are credited and that the original publication in this journal is cited, in accordance with accepted academic practice. No use, distribution or reproduction is permitted which does not comply with these terms.

# A new candidate epitope-based vaccine against PspA PhtD of *Streptococcus pneumoniae*: a computational experimental approach

Mona Shafaghi<sup>1,2†</sup>, Zohreh Bahadori<sup>1,2†</sup>,  
Seyed Mahmoud Barzi<sup>2</sup>, Elnaz Afshari<sup>2,3</sup>, Hamid Madanchi<sup>1,4</sup>,  
Seyed Fazlollah Mousavi<sup>2\*</sup> and Ali Akbar Shabani<sup>1\*</sup>

<sup>1</sup>Department of Medical Biotechnology, faculty of Medicine, Semnan University of Medical Sciences, Semnan, Iran, <sup>2</sup>Department of Bacteriology, Pasteur Institute of Iran, Tehran, Iran, <sup>3</sup>Department of Biology, Science and Research Branch, Islamic Azad University, Tehran, Iran, <sup>4</sup>Drug Design and Bioinformatics Unit, Department of Medical Biotechnology, Biotechnology Research Center, Pasteur Institute of Iran, Tehran, Iran

**Introduction:** Pneumococcus is an important respiratory pathogen that is associated with high rates of death in newborn children and the elderly. Given the disadvantages of current polysaccharide-based vaccines, the most promising alternative for developing improved vaccines may be to use protein antigens with different roles in pneumococcus virulence. PspA and PhtD, highly immunogenic surface proteins expressed by almost all pneumococcal strains, are capable of eliciting protective immunity against lethal infections.

**Methods:** In this study using immunoinformatics approaches, we constructed one fusion construct (called PAD) by fusing the immunodominant regions of PspA from families 1 & 2 (PA) to the immunodominant regions of PhtD (PD). The objective of this project was to test the immunogenicity of the fusion protein PAD and to compare its protective activity against *S. pneumoniae* infection with PA or PD alone and a combination of PA and PD. The prediction of physicochemical properties, antigenicity, allergenicity, toxicity, and 3D-structure of the constructs, as well as molecular docking with HLA receptor and immune simulation were performed using computational tools. Finally, mice were immunized and the serum levels of antibodies/cytokines and functionality of antibodies *in vitro* were evaluated after immunization. The mice survival rates and decrease of bacterial loads in the blood/spleen were examined following the challenge.

**Results:** The computational analyses indicated the proposed constructs could be antigenic, non-allergenic, non-toxic, soluble and able to elicit robust immune responses. The results of actual animal experiments revealed the candidate vaccines could induce the mice to produce high levels of antibodies and cytokines. The complement-mediated bactericidal activity of antibodies was confirmed and the antibodies provided favorable survival in immunized mice after bacterial challenge. In general, the experimental results verified the immunoinformatics studies.

**Conclusion:** For the first time this report presents novel peptide-based vaccine candidates consisting of immunodominant regions of PspA and PhtD antigens. The obtained findings confirmed that the fusion formulation could be relatively more efficient than the individual and combination formulations. The results propose that the fusion protein alone could be used as a serotype-independent pneumococcal vaccine or as an effective partner protein for a conjugate polysaccharide vaccine.

#### KEYWORDS

*Streptococcus pneumoniae*, pneumococcal surface protein A (PspA), pneumococcal histidine triad protein D (PhtD), pneumococcal epitope-based vaccine, immunodominant B and T cell epitopes, immunoinformatics, actual animal experiments, fusion protein

## 1 Introduction

*Streptococcus pneumoniae* (pneumococcus) has remained one of the main causes of lethal diseases such as pneumonia and meningitis, and of secondary infections following respiratory viral diseases including influenza and COVID-19 (Bahadori et al., 2022). The high morbidity and mortality rates in more than 1 million cases, particularly in children under 2 years old and the elderly above 65 years old, are the major driving force for the development of pneumococcal vaccines (Shafaghi et al., 2023). There are currently two types of commercial pneumococcal vaccines comprising of unconjugated or protein-conjugated polysaccharides, both of which have advantages and disadvantages (Goulart et al., 2017). The 23-valent polysaccharide vaccine has the potential to cover many serotypes. However, this vaccine is weakly immunogenic in high-risk groups of young children due to the poor immunogenicity of the T cell-independent antigens (Nguyen et al., 2011). The protein-polysaccharide conjugate vaccines have been in use for many years and could lead to more effective immune responses even in the high-risk populations, but there are many limitations including high cost, limited serotype coverage, and serotype replacement following vaccination with these vaccines (Lu et al., 2015). The antigenic proteins of pneumococcus that are highly conserved and are expressed on the bacterial surface at different stages of pathogenesis are expected to be particularly useful as vaccine antigens. Two of the well-characterized protein candidates are pneumococcal surface protein A (PspA) and pneumococcal histidine triad protein D (PhtD) (Plumptre et al., 2013a; Lu et al., 2015).

PspA is one of the key virulence factors in all clinical isolates of pneumococcus, which plays important roles including preventing the deposition of complement and the bactericidal activity of lactoferrin (Shaper et al., 2004; Mukerji et al., 2012). The PspA protein possesses 3 main domains: alpha helix domain consisting of the regions A, A', and B ( $\alpha$ -HD, residues 1-288), proline-rich domain (region C, residues 289-370), and choline binding domain (residues 371-571) (Hollingshead et al., 2000). The N-terminal

alpha helix domain and proline-rich domain are exposed on the surface and are capable of interacting with the host's immune system (Daniels et al., 2010; Vadesilho et al., 2014). The alpha helical domain is highly immunogenic and variable in sequence among different strains. The protection appears to be mediated by epitopes within 100 residues at the N-terminus (region A) and about 100 residues at the C-terminus (region B) of this domain (McDaniel et al., 1994; Roche et al., 2003; Vadesilho et al., 2014). PspA is divided into 3 families including 6 clades according to the sequence diversity in the B region or clade-defining region (CDR) (Hollingshead et al., 2000). Family one includes clades 1 & 2, family two includes classes 3, 4 & 5, and family three includes the rare clade 6 (Hollingshead et al., 2000). The studies have shown that more than 95% of the isolated pneumococcal strains belong to families 1 & 2, which is why efforts for developing PspA-based vaccines are focused on these 2 families (Converso et al., 2017b; Mukerji et al., 2018). The cross-reactivity level among different PspAs depends on the degree of sequence similarity so that there is a higher degree of cross-reactivity in the same clade (Miyaji et al., 2002). It has found that the immunity elicited by the 2 main PspA families are clade dependent (Miyaji et al., 2002; Darrieux et al., 2008; Goulart et al., 2011), thus it is suggested that the highly antigenic fragments of all clades should be included in the PspA-based vaccine (Akbari et al., 2019). Moreover, the A and C regions of PspA, which possess the more conserved domains, could help to expand the cross protection (Darrieux et al., 2008; Kristian et al., 2016).

PhtD is one of the known polyhistidine triad proteins expressed by all pneumococcal strains and is distinguished by the presence of 5 copies of the His triad motif (Plumptre et al., 2012). It has been shown that this protein mediates bacterial adhesion due to its high affinity with zinc, and also can inhibit complement deposition (Lagousi et al., 2019). The C-terminal segment of protein PhtD (PhtD-C) is exposed on the bacterial surface, making it a more immunogenic region (Malekan et al., 2019; Bahadori et al., 2022). The studies have revealed that vaccination with the truncated derivatives of PhtD-C was more effective in inducing antibodies and protective immune responses

in comparison to vaccination with the full length protein (Plumprtre et al., 2013b).

Bioinformatics techniques could help scientists in different biological areas (Shafaghi et al., 2019; Nabizadeh et al., 2020; Bahadori et al., 2021), especially for anticipation of potential immunoprotective epitopes to develop vaccine candidates (Tapia et al., 2016; Fereshteh et al., 2022). In fact, the tools of immunoinformatics provide benefits in comparison with traditional vaccinology methods such as lower costs and faster outcomes (Afshari et al., 2023a). In this study, immunoinformatics and computational tools were used to design a novel fusion protein with several peptides from different domains of PspA and PhtD; peptides from PspA (region A, region B for both families 1 & 2, and region C) and PhtD-C. In addition to the fusion construct, two individual constructs corresponding to PspA or PhtD were also constructed. Then, we investigated whether vaccination with the peptide-based fusion construct is able to induce more effective protective responses than vaccination with each of the individual constructs alone or a combination of them.

## 2 Materials and methods

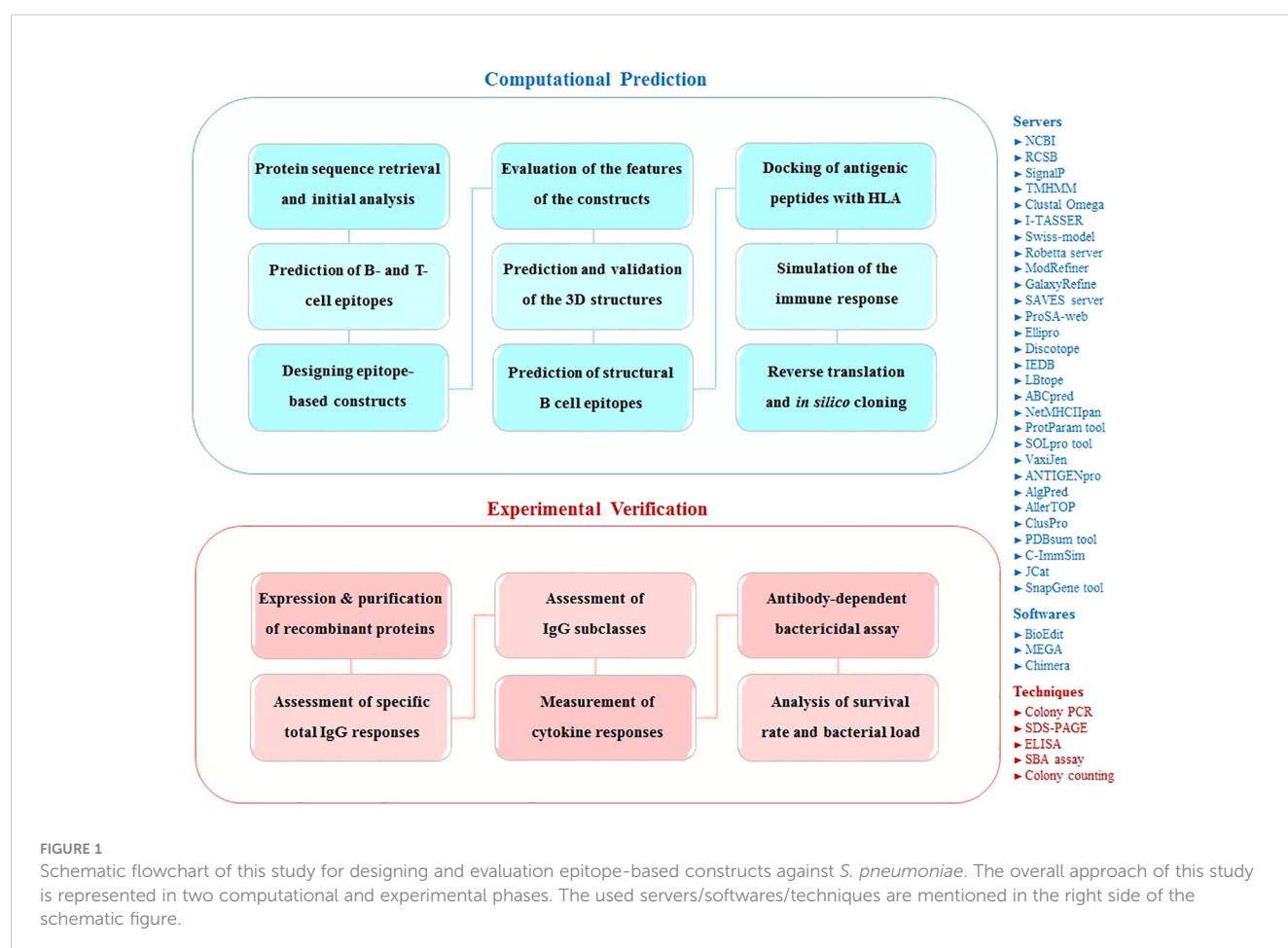
The present study was performed in two phases: computational prediction and experimental verification. Figure 1 shows the schematic flowchart of this study.

### 2.1 Computational prediction

#### 2.1.1 Retrieval of amino acid sequences of PspA and PhtD, and preliminary analysis

The amino acid sequences of PspA and PhtD proteins were extracted from the National Center for Biotechnology Information (NCBI) database ([www.ncbi.nlm.nih.gov/protein](http://www.ncbi.nlm.nih.gov/protein)). Due to the diversity of the PspA molecule in different pneumococcal strains, the amino acid sequences of PspA were retrieved from 123 pneumococcal strains which had unique sequences (Mukerji et al., 2018). The retrieved accession numbers of PspA protein sequences are given in Supplementary Table S1. The PhtD protein sequence from strain R6 (accession number: AAK99711) was also stored in FASTA format. The possible signal peptide of the proteins was identified using SignalP server (<http://www.cbs.dtu.dk/services/SignalP/>) (Nielsen, 2017). Moreover, the presence of transmembrane regions in PspA and PhtD-C proteins were investigated using the TransMembrane Hidden Markov Models (TMHMM) server ([www.cbs.dtu.dk/services/TMHMM-2.0](http://www.cbs.dtu.dk/services/TMHMM-2.0)) (Krogh et al., 2001).

The PspA sequences from 123 strains were classified and aligned using the Clustal Omega web server (<https://www.ebi.ac.uk/Tools/msa/clustalo/>) (Sievers et al., 2011) to identify sequence similarities and differences. The alignment results were edited in BioEdit software version 7.1.3.0 and



ambiguous aligned points were corrected. The phylogenetic tree was drawn using Molecular Evolutionary Genetics Analysis (MEGA) software with Maximum likelihood and Neighbor-Joining methods (Saitou and Nei, 1987) to investigate the relationship between different strains. Before computational predictions to design a potential epitope-based vaccine, the Immune Epitope Database (IEDB; <https://www.iedb.org/>) was used to find the experimentally identified epitopes.

### 2.1.2 Prediction of conformational (discontinuous) B cell epitopes

Prediction of conformational B cell epitopes requires the three-dimensional structure of a protein. Since there is no 3D structure for PspA and PhtD-C proteins in the PDB database, the 3D models of the proteins were predicted by different servers. These proteins were modeled in the best way using the iterative threading assembly refinement (I-TASSER) server (<https://zhanglab.ccmb.med.umich.edu/I-TASSER/>) (Yang et al., 2015) or SWISS-MODEL server (<http://swissmodel.expasy.org/>) (Waterhouse et al., 2018). The protein structure was constructed with the help of homology/comparative modeling according to the existence of homologous templates with sequence identity less than 30% using I-TASSER server and sequence identity more than 30% with SWISS-MODEL. The low-quality modeled structures were refined by the servers ModRefiner (<https://zhanglab.ccmb.med.umich.edu/ModRefiner/>) (Xu and Zhang, 2011) and GalaxyRefine (<http://galaxy.seoklab.org/cgi-bin/submit.cgi?type=REFINE>) (Shin et al., 2014). The validation of 3D structures was done using PROCHECK (Laskowski et al., 1993) and ERRAT (Colovos and Yeates, 1993) programs in SAVES server (<https://saves.mbi.ucla.edu/>). BIOVIA Discovery Studio Visualizer was used to display the 3D structure of proteins. Eventually the conformational epitopes were anticipated based on the 3D protein structure using the servers Ellipro (<http://tools.iedb.org/ellipro/>) (Ponomarenko et al., 2008) and DiscoTope (<http://www.cbs.dtu.dk/services/DiscoTope/>) (Kringelum et al., 2012). The Ellipro server uses the solvent accessibility and flexibility to identify linear and structural epitopes, and the higher score indicates more solvent accessibility. The DiscoTope server uses half-sphere exposure and propensity scores to identify structural B-cell epitopes.

### 2.1.3 Prediction of linear B cell and linear T cell epitopes

Unlike conformational epitopes, which are only recognized by B cells, linear epitopes are recognized by both B and T lymphocytes. The linear or continuous B cell epitope is characterized based on properties such as hydrophilicity, accessibility, flexibility and antigenicity in a beta-turn region. In the present study, prediction of linear B-cell epitopes in PspA and PhtD-C proteins were done using web servers LBTope (<http://crdd.osdd.net/raghava/lbtope/protein.php>) (Singh et al., 2013), ABCpred (<http://crdd.osdd.net/raghava/abcpred/>) (Saha and Raghava, 2006), IEDB Emini surface accessibility tool (<http://tools.immuneepitope.org/bcell/>) (Emini et al., 1985) and Ellipro. The LBTope server with a prediction

accuracy of 81% and the ABCpred server with an overall accuracy of 65.93% predict linear B cell epitopes. The LBTope assigns a value ranging from 0 to 100% for each predicted epitope, and a higher value indicates a higher probability of being an epitope. In the ABCPred, a score closer to 1 indicates a higher probability that the peptide sequence is an epitope.

Since helper T cells play a role in immunity against extracellular pathogens such as pneumococci, the prediction of CD4+ T cell epitopes (MHC-II binding peptides) was performed using MHC-II prediction tool in IEDB server (<http://tools.immuneepitope.org/mhcii>) (Wang et al., 2008) and NetMHCIIpan 4.0 server (<http://www.cbs.dtu.dk/services/NetMHCIIpan/>) (Jensen et al., 2018). To evaluate the immune response against the vaccine candidate in a mouse model, mouse alleles were investigated in addition to human alleles. The predictions were performed for 8 common human alleles HLA-DRB1 (\*01:01, \*03:01, \*04:01, \*07:01, \*08:01, \*11:01, \*13:01, \*15:01) and mouse alleles H-2-IAb, H-2-IAd and H-2-IEd. The IEDB peptides with percentile rank <10.0 and the NetMHCIIpan peptides with rank value <1.0 were considered for further analysis.

### 2.1.4 Analysis of epitopic areas of B region of PspA in different strains: to obtain consensus epitope sequences

In the consensus sequence approach, the homologous sequences are analyzed to reach the target sequence. Substitution of amino acids with similar chemical features (such as positively charged Lys & Arg or hydrophobic Leu & Val) often does not significantly affect the structure/function of a protein (Zhang et al., 2013; Jones et al., 2020). The epitopic areas of B region of PspA in different families or clades were evaluated to obtain consensus sequences providing epitopes that facilitate the induction of cross-reactive antibodies. Consensus sequences for each clade or family were obtained using the threshold and majority-based selection methods in BioEdit software. In the threshold-based method, the residue that has a greater frequency than the user's chosen threshold is selected while in the majority-based method, the most common residue at each position is selected regardless of any threshold. Swiss-Model server was used for modeling of the initial peptide and the final peptide containing the consensus sequences. Superimposition and Root Mean Square Deviation (RMSD) calculations were carried out with UCSF Chimera software (Pettersen et al., 2004) to evaluate possible errors in the models.

### 2.1.5 Designing peptide-based constructs consisting of PspA and PhtD epitopes

The peptides predicted by different servers consisting of higher scoring B cell epitopes overlapped with immunodominant T-helper (Th) cell epitopes were analyzed and eventually the selected peptide sequences were linked together using flexible linkers (Gly-Gly-Gly-Ser and Gly-Gly-Ser-Ser-Gly-Gly). In order to efficiently separate and preserve the independent folding and immunological activities, flexible linkers were considered to connect adjacent epitopes (Tian et al., 2013). In addition, the 6xHis-Tag was added at the C-terminal of the constructs to aid protein purification. Finally, three



constructs were designed and named PAD (rPspA-PhtD, a recombinant fusion peptide consisting of PspA and PhtD epitopes), PA (rPspA, the recombinant peptide consisting of PspA epitopes), PD (rPhtD, the recombinant peptide consisting of PhtD epitopes).

### 2.1.6 Evaluation of the characteristics of the final constructs

Following designing peptide-based constructs PAD, PA, and PD, their various physicochemical properties, such as molecular weight (MW), total number of positive and negative amino acids, theoretical isoelectric point, instability index, *in vitro/in vivo* half-life, average aliphatic index, and average hydropathicity, were evaluated using ProtParam tool in ExPASy server (<http://web.expasy.org/protparam/>) (Gasteiger et al., 2005). Moreover, antigenicity, solubility, allergenicity, and toxicity were investigated for the designed constructs. The recombinant protein solubility on overexpression in *Escherichia coli* was predicted by SOLpro tool in SCRATCH server (<https://scratch.proteomics.ics.uci.edu/>) (Magnan et al., 2009). VaxiJen v2.0 (<http://www.ddg-pharmfac.net/vaxijen/VaxiJen/VaxiJen.html>) (Doytchinova and Flower, 2007) and ANTIGENpro tool of SCRATCH server (<http://scratch.proteomics.ics.uci.edu/>) (Magnan et al., 2010) were utilized for prediction of the antigenicity of peptides. The servers AllerTOP (<http://www.ddg-pharmfac.net/AllerTOP/>) (Dimitrov et al., 2014) and AlgPred (<https://www.imtech.res.in/raghava/algpred/>) (Saha and Raghava, 2007) were used for prediction of the allergenicity of the vaccine candidates. ToxinPred server was employed to predict toxicity of the constructs (<https://webs.iitd.edu.in/raghava/toxinpred/index.html>) (Gupta et al., 2013).

### 2.1.7 Prediction and validation of the tertiary structure of vaccine candidates

3D structure modeling of the protein constructs was performed in the best way by Robetta server (<http://robeta.bakerlab.org/>) (Kim et al., 2004) based on comparative and ab-initio modeling. The GalaxyRefine server (<http://galaxy.seoklab.org/cgi-bin/submit.cgi?type=REFINE>) (Shin et al., 2014) was used to refine the structure of the best model. The validation of the models was carried out by PROCHECK (Laskowski et al., 1993) and ERRAT (Colovos and Yeates, 1993) at the SAVES server (<https://saves.mbi.ucla.edu/>), as well as the ProSA web server (<https://prosa.services.came.sbg.ac.at/prosa.php>) (Wiederstein and Sippl, 2007).

### 2.1.8 Identification of conformational B cell epitopes in peptide-based constructs

The structural epitopes which are recognized by antibodies play a major role in the humoral immunity. Therefore, the developed protein constructs should have effective conformational epitopes in their protein domains to induce stronger immunity. The ElliPro server was employed to identify the structural B-cell epitopes in the refined models of the epitope-based vaccine candidates, keeping the default parameters.

### 2.1.9 Molecular docking of immunogenic peptides with HLA-DRB1\_01:01

To confirm the binding affinity of the selected immunogenic regions with MHC-II, molecular docking was performed by ClusPro web server (<https://cluspro.org/login.php>) (Kozakov et al., 2017). The 3D structures of ≤30-mer peptides corresponding to the selected epitope-rich regions as the ligand and the crystal structure of one of the most common alleles, HLA-DRB1\*01:01 (PDB ID: 1AQD), as the receptor were submitted to the server. The docked complexes were visualized by UCSF Chimera software. The PDBsum tool (<http://www.ebi.ac.uk/thornton-srv/databases/pdbsum/Generate.html>) (Laskowski et al., 2018) was utilized to obtain details of the interactions between the peptides and HLA.

### 2.1.10 Simulation of the immune response against epitope-based constructs

To evaluate the immune responses to the designed constructs, the immune-simulation was done with the help of the C-ImmSim server (<https://kraken.iac.rm.cnr.it/C-IMMSIM/>) (Rapin et al., 2010). This server predicts immune interactions in three parts of the mammalian immune system (bone marrow, thymus, and tertiary lymphatic organs), using machine learning techniques and a position-specific scoring matrix (PSSM). Four injections of the construct were performed at 2-week intervals (on days 0, 14, 28, and 42). Each time step is 8 hours and the first injection step is at zero time. The production of cytokines and antibodies as well as the responses of Th1 and Th2 cells were predicted by the server.

### 2.1.11 Reverse translation, codon optimization and *in silico* cloning of the constructs in pET28a vector

The codon optimization approach was used to enhance the expression of PAD, PA and PD recombinant proteins. The Java Codon Adaptation Tool (JCat) (<http://www.jcat.de/>) (Grote et al., 2005) online server was used for reverse translation and codon optimization based on codon preference of the expression host *E. coli* (K12 strain). In addition, this server prevents unwanted sites for restriction enzymes, Rho-independent transcription termination, and prokaryotic ribosome binding. Finally, the optimized gene sequences for the PAD, PA, and PD, with restriction sites *Nco*I and *Xho*I respectively added to the 5' and 3' ends, were cloned in pET28a vectors using SnapGene tool (<https://www.snapgene.com/try-snapgene/>).

## 2.2 Experimental verification

### 2.2.1 *E. coli* transformation, expression and purification of recombinant proteins

The pET28a vector harboring the sequence encoding PAD, PA or PD was synthesized by Biomartik Corporation (Cambridge, Ont., Canada). The recombinant expression vectors (pET28a-PAD, pET28a-PA, and pET28a-PD) were transferred into *E. coli* BL21 (DE3) cells, and recombinant clones were identified by colony PCR



using T7 universal primers (<https://www.addgene.org/mol-bio-reference/sequencing-primers/>). Expression of the recombinant proteins was induced by the addition of 1 mM isopropyl- $\beta$ -thiogalactopyranoside (IPTG) for 18 h, and examined by running on 15% SDS-PAGE and Coomassie Brilliant Blue staining R-250. The expressed recombinant proteins PAD, PA and PD were purified using Ni-NTA chromatography under native conditions, according to the manufacturer's manual (Qiagen, Hilden, Germany). Finally, the purified proteins were dialyzed overnight and then quantified by NanoDrop spectrophotometer at 280 nm.

## 2.2.2 Immunization of mice

Vaccination schedule and timeline of experimental procedures are presented in Figure 2. Six- to eight-week old female BALB/c mice were randomly divided into 5 groups PA, PD, PA+PD, PAD, and control (n = 5 per group). The mice were immunized subcutaneously on days 0, 14, 28 and 42 with 10  $\mu$ g PA or PD peptide (PA or PD group), 10  $\mu$ g PA combined with 10  $\mu$ g PD peptide (PA+PD group), or 20  $\mu$ g PAD fusion peptide (PAD group) formulated in PBS containing Alum adjuvant (1:1 v/v) in a final volume 100  $\mu$ l per mouse. The negative control group was injected with the Alum adjuvant in PBS (1:1 v/v). The sera were collected before each immunization and two weeks after the last immunization (on days 0, 14, 28, 42, and 56) and stored for further analysis.

## 2.2.3 Assessment of the levels of specific total immunoglobulin G (IgG) and IgG isotypes

The levels of anti-recombinant protein IgG on days 0, 14, 28, 42, and 56, and the levels of immunoglobulin G1 and G2a (IgG1 and IgG2a) isotypes two weeks after the 3<sup>rd</sup> injection were evaluated by indirect enzyme-linked immunosorbent assay (ELISA) (Fereshteh et al., 2023). In brief, ELISA microtiter plates (Nanc MaxiSorp, Thermo Fisher, USA) were coated with 100  $\mu$ l of purified recombinant protein PA or PD (0.2  $\mu$ g/well) and incubated at 4 °C overnight. After blocking the plates, 100  $\mu$ l of diluted anti-sera (1:100) were added to the wells and then the 1:100,000 dilution of HRP-conjugated secondary antibodies (Sigma Chemical, St. Louis, MO, USA) were applied and incubated for one hour. Finally, TMB substrate (Seramun, Dolgenbrodt, Germany) was added to each well and the absorbance was read by an ELISA reader (BioTek Company) at 450 nm.

## 2.2.4 Evaluation of the levels of cytokines induced by the vaccine candidates

The titers of cytokines interferon-gamma (IFN- $\gamma$ ), interleukin-4 (IL-4), and interleukin-17A (IL-17A) in the mouse sera two weeks after the 3<sup>rd</sup> injection were determined using ELISA kits (Mabtech, Sweden) in accordance with manufacturers' guidelines.

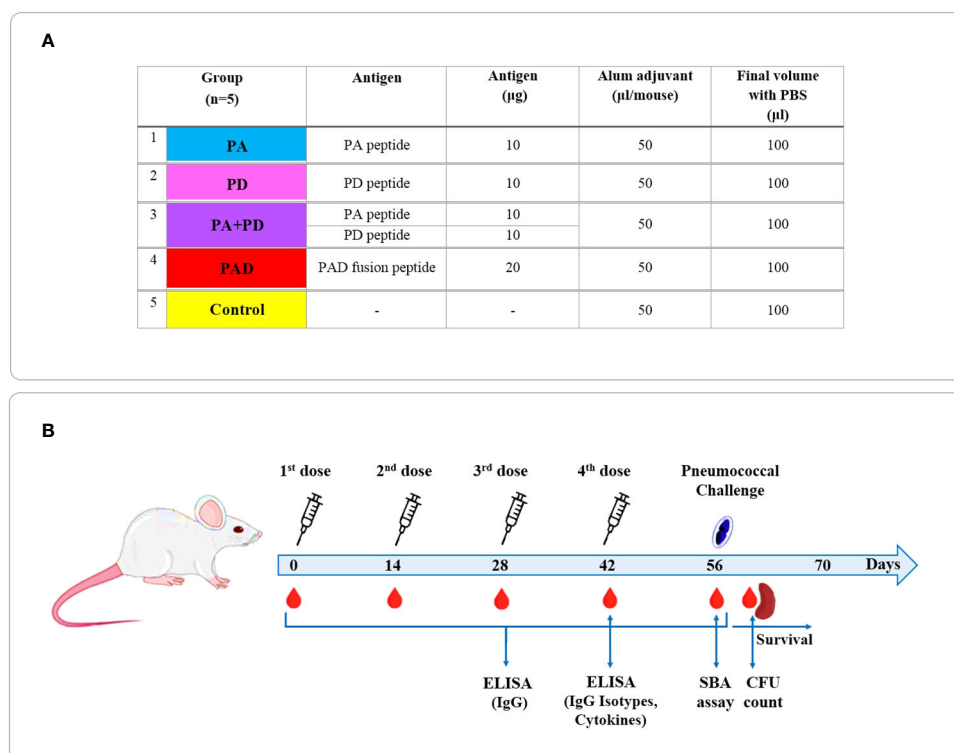


FIGURE 2

Vaccination schedule and timeline of experimental procedures. (A) BALB/c mice were divided into 5 groups PA, PD, PA+PD, PAD, and control (n = 5 per group). (B) The mice were immunized subcutaneously on days 0, 14, 28 and 42. The sera were collected before each injection and 2 weeks after the last injection and used for further analysis.

### 2.2.5 Evaluation of serum bactericidal activity

Two weeks after the 4<sup>th</sup> injection, the SBA assay was used to evaluate the activity of anti-recombinant protein antibodies in killing of pneumococcal strain ATCC 6303. At first the sera of immunized mice were decomplexed at 56°C for 30 min. Then, 12.5 µl of the bacterial suspension at 10<sup>5</sup> CFU/ml and 12.5 µl of infant rabbit serum as a source of the complement were added to the 96-well microtiter plates containing serially diluted inactivated serum sample (1:2 to 1:64). After 1 h incubation at 37°C in 5% CO<sub>2</sub>, 10 µl of each well was cultured on a blood agar plate and incubated for 24 h at 37°C in 5% CO<sub>2</sub>. The SBA titer was reported as the reciprocal of the serum dilution at which ≥50% of bacteria were lysed in comparison to the negative control without Ab (Fereshteh et al., 2023).

### 2.2.6 Challenge of immunized mice with *S. pneumoniae*

After the final immunization, challenge was performed intraperitoneally with a lethal dose of pneumococcal strain ATCC 6303 and the mortality of mice was monitored for about one week. One day after the challenge, two mice from each experimental group were euthanized and blood and spleen samples were collected to subject to bacterial colony counting on blood agar plates.

### 2.2.7 Statistical investigations

GraphPad Prism 8 software was used to perform statistical analysis. Differences in antibody levels were analyzed using two-way ANOVA and cytokine concentration, bacterial loads, and serum bactericidal activity were analyzed using one-way ANOVA followed by Tukey's multiple comparison test. Kaplan–Meier survival curves was used for comparison between the control and the immunized groups (Guyot et al., 2012). P-values of ≤0.05 were considered significant.

## 3 Results

### 3.1 Immunoinformatics studies

#### 3.1.1 Protein sequences retrieval and initial analysis

The amino acid sequences of the target proteins were extracted from the database for computational epitope mapping. Due to the diversity of the PspA molecule in different strains, PspA amino acid sequences were retrieved from 123 strains in FASTA format. The signal peptide of the proteins was separated from the sequences after prediction using the SignalP server. The TMHMM server results showed that the candidate sequences did not have any transmembrane domain. Following aligning of the sequences of A region of PspAs and drawing the phylogenetic tree, the A region from the reference strain AC122 was selected as a representative to determine epitopes of the A region (Supplementary Figure S1, Supplementary Table S2). CDR sequences of 123 strains were grouped into clades 1 to 5, and after alignment of the sequences of each clade, the required corrections were made using BioEdit

software. Strains with duplicated CDRs were excluded and the remaining strains with non-duplicated CDRs were used for further evaluations (Supplementary Table S3). The amino acid sequence of PhtD strain R6 was extracted in FASTA format (Supplementary Table S4), and its C-terminal from aa 383 to 853 was chosen for the prediction of epitopes. The investigations showed that there are experimental epitopes for N-terminal of PspA protein, while there is no experimental data for C-terminal of PhtD. The epitopes of the A, B, and C regions of PspAs previously experimentally identified (Daniels et al., 2010; Singh et al., 2010; Vadesilho et al., 2014; Tamborrini et al., 2015) were extracted from IEDB database (Supplementary Tables S5–S7, respectively).

#### 3.1.2 Prediction of B-cell and helper T-cell epitopes

Before the prediction of the conformational epitopes, the 3D structure of PspA from strain AC122 was modeled through I-TASSER server and refined with GalaxyRefine server. Validation of the model was performed using ProSA Z-score and the result showed that the Z-score of the structure is -3.88 near to natural proteins of similar size (Supplementary Figure S2). Strains DBL6A (Clade1), R6 (Clade2), AC122 (Clade3), EF5668 (Clade4) and ATCC 6303 (Clade5) were selected as representatives of the 123 strains to determine the range of B region epitopes. Tertiary structure modeling of B regions of PspA clades 1-5 was performed using Swiss-Model server based on PMS2 template with sequence similarity more than 30% (Supplementary Figure S3). The 3D structure of PhtD-C was predicted through I-TASSER server and refined with ModRefiner and GalaxyRefine servers (Supplementary Figure S4). Ramachandran plot demonstrated that 87.2% of amino acids were located in favorable regions, and the ERRAT result showed the overall quality factor was 85.23% (Supplementary Figure S5).

The predicted linear/conformational B cell epitopes and MHC-II binding epitopes for A region of PspA are shown in Supplementary Tables S8–S9, respectively. For B region of PspAs in clades 1 to 5, B cell epitopes (Supplementary Tables S10–S14) and MHC-II binding epitopes (Supplementary Table S15) were predicted and considered for further analysis. The predicted linear and structural B-cell epitopes, and MHC class II epitopes for PhtD-C are listed in Supplementary Tables S16–S18, respectively. In this way, the epitopes were collected to check and finally select the immune-dominant epitopic regions.

#### 3.1.3 Obtaining the consensus epitope sequences for B region of PspA in different pneumococcal strains

Since the B region of PspA varies in different families/clades, the recognition of consensus epitope sequences capable to cover all strains from each family or clade could be an ideal immunization strategy. These consensus antigens could provide epitopes that facilitate the elicitation of cross-reactive Abs (Nachbagauer and Palese, 2020). For this purpose, the sequences of B region in different families/clades were aligned using Clustal Omega

software and the results were edited in BioEdit software. The aligned and modified sequences were evaluated to identify common epitope regions and the 3D structures were considered to select the final suitable domains. As an example, the selected epitope locations of the B region of Clade 1 (strain DBL6A) on the three-dimensional structure are shown in [Supplementary Figure S6](#). The selection of consensus epitope sequence of region B of Clade 1 and 2 with the help of BioEdit software is given as an example in [Supplementary Figure S7A](#). Since there was overlap between different strains of clades 1 and 2 in the amino acids 1-29 of region B, the consensus sequence was selected for strains of clades 1 and 2 (Cons-Clade 1 + 2; [Supplementary Table S19](#)). Another consensus sequence of the B region only for strains in Clade 1 is shown as another example in [Supplementary Figure S7B](#). Since there was no overlap between strains of clades 1 and 2 in the amino acids 51-76 of B region, the consensus sequence was chosen only for Clade 1 strains (Cons-Clade 1; [Supplementary Table S19](#)). In the same way, for the other clades, the consensus epitope sequences of B region were selected, and in the area where there was overlap between the strains of two clades, the consensus sequence was considered common ([Supplementary Table S19](#)).

The initial peptide and the final peptide containing the consensus sequence were modeled using the Swiss-Model server and then structurally checked by the UCSF Chimera program. The superimposition of the primary structure and the structure containing consensus sequence was done to avoid the structural problems of the final peptide ([Supplementary Figure S8](#)). The RMSD between primary and consensus sequence structures was close to zero, which indicates that despite the amino acid differences

there is an overall structural similarity between the peptides and the structure and folding of the resulting antigen is reliable.

### 3.1.4 Designing epitope-based constructs PAD, PA, and PD

The high-scoring B- and T-cell epitopes shared between several computational prediction servers were considered to predict immunodominant peptide sequences, and 3D models were analyzed to select the most suitable domains. The selected final peptides from PspA (region A, region B for both families 1 & 2, and region C) and PhtD-C antigens are listed in [Table 1](#). Due to the size limitation of the final construct, only four of the seven consensus sequences, which could target different clades, were considered for the B region of the PspA protein. The selected peptides were linked by the linkers GGGS (for peptides related to one protein) and GGSSGG (between peptides related to two proteins PspA and PhtD), which provide the possibility of rotation. The immunodominant peptides were placed next to each other in different positions and the features were evaluated with various servers. Ultimately, the sequences that had the best characteristics among the different positions of the peptides were selected for further analysis. Three final constructs named PAD (fusion construct consisting of PspA and PhtD epitopes), PA (consisting of PspA epitopes) and PD (consisting of PhtD epitopes) were designed. A histidine tag was added by a glycine to the C-terminal end of the designed constructs, which could be useful for protein purification. The schematic picture of how the peptides are placed in the final constructs PAD, PA and PD is shown in [Figure 3](#). The total sequence length of PAD, PA, and PD constructs was 329, 222 and 109 amino acids, respectively ([Table 2](#)).

TABLE 1 Final selected immunodominant peptides of PspA and PhtD for designing the vaccine candidates.

Protein	Antigenic region	Peptide name & sequence	Length
PspA	A Region	<b>A Peptide</b>	
		EAPVASQSKAEKDYDAAVKKSEAAKKHYEEVKKKAEDAQKKYDEGQKKTVAKREKEASEKIA	64
	B Region	<b>Cons-Clade 1 + 2</b>	
		LKEIDESDSEDIKEGFRVPLQSEDAKR	29
		<b>Cons-Clade 1</b>	
		KLEKDVEYFKNTDGEYTEQYLEAAEK	26
		<b>Cons-Clade 3 + 4</b>	
		ELEKLLDTLDPEGKTQDELDKEAAEAELDKKV	32
		<b>Cons-Clade 4 + 5</b>	
		LTRLEDNLKDAEENNVEDYIKEGLEKAI	28
	C Region	<b>C Peptide</b>	
		PAPAPKPEQPAPAPK	15
PhtD	C-terminal of PhtD	<b>PhtD-C Peptide</b>	
		SLEDLLATVKYYVEHPNERPHSDNGFGNASDHVQRNKGQADTNQTEKPNEEK	53
		<b>PhtD-C' Peptide</b>	
		EKVTDSSIRQNAVETLTGLKSSLLGTGKDNNTISAIEVDSLALLK	45

### 3.1.5 Evaluation of the various properties of the designed constructs

The designed constructs were evaluated and compared with respect to their physicochemical and immunological properties. Various features of the constructs were predicted using the ProtParam tool as represented in Table 2. The molecular weight of PAD, PA, and PD vaccine constructs was 35.66, 24.34, and 11.94 kDa, with theoretical pI about 5.05, 5.00, and 5.94, respectively. The instability index of PAD, PA, and PD were predicted as 39.88, 49.82, and 15.6, respectively. Proteins with an instability index below 40 are taken into account stable and vice versa (Gasteiger et al., 2005). For epitope-based proteins PAD, PA, and PD, the aliphatic index respectively was 61.76, 56.40 and 71.56 (indicating that they could be thermostable), and the GRAVY index respectively was -1.148, -1.285, and -0.982 (indicating that they are hydrophilic). The half-life of the protein constructs was calculated to be 30 hours in *E. coli*, more than 20 hours in yeast and more than 10 hours in mammals. Moreover, the antigenicity, solubility, allergenicity and toxicity of the constructs were investigated as shown in Table 2. The sequences were analyzed by Vaxijen and ANTIGENpro servers, and the scores above the threshold indicated that the proteins were antigenic in nature. Based on the prediction of the solubility upon overexpression in *E. coli*, the designed recombinant proteins were soluble. AlgPred and AllerTOP servers demonstrated that the protein constructs were non-allergen. The ToxinPred server showed the non-toxicity of the constructs for humans and

animals. The output of these computational analyses revealed that the proposed constructs passed the evaluations with satisfactory results.

### 3.1.6 Modeling and quality assessment of 3D structures of the constructs

The three-dimensional structures of the protein constructs PAD, PA, and PD were predicted by Robetta server and refined by the GalaxyRefine server. The quality evaluation of the models was accomplished using Ramachandran plot, ERRAT value and ProSA Z-score. The predicted 3D structures and validation of the models before and after refinement are represented in Table 3. The Ramachandran, ProSA Z-score, and ERRAT plots before refinement and after refinement are depicted in Supplementary Figure S9 and Figure 4, respectively. The Ramachandran plots demonstrated that in the primary models PAD, PA, and PD, 89.6%, 92.3%, and 84.9% of residues were in the favored regions, while in the refined models, 92.5%, 95.6% and 90.3% of residues were in the favored regions, respectively. The ERRAT values of the crude models PAD, PA, and PD were predicted as 93.96, 95.14, and 89.24, while the values of the refined models were calculated as 93.31, 95.54, and 92.13, respectively (higher score represents the higher quality). The Z-scores obtained by the ProSA were found to be -5.38, -3.48, and -6.63 in the primary models PAD, PA, and PD, compared to -5.33, -3.46, and -6.55 in the refined models, respectively (within the range of scores for natural proteins). The modeled and validated structures were used for further analysis.

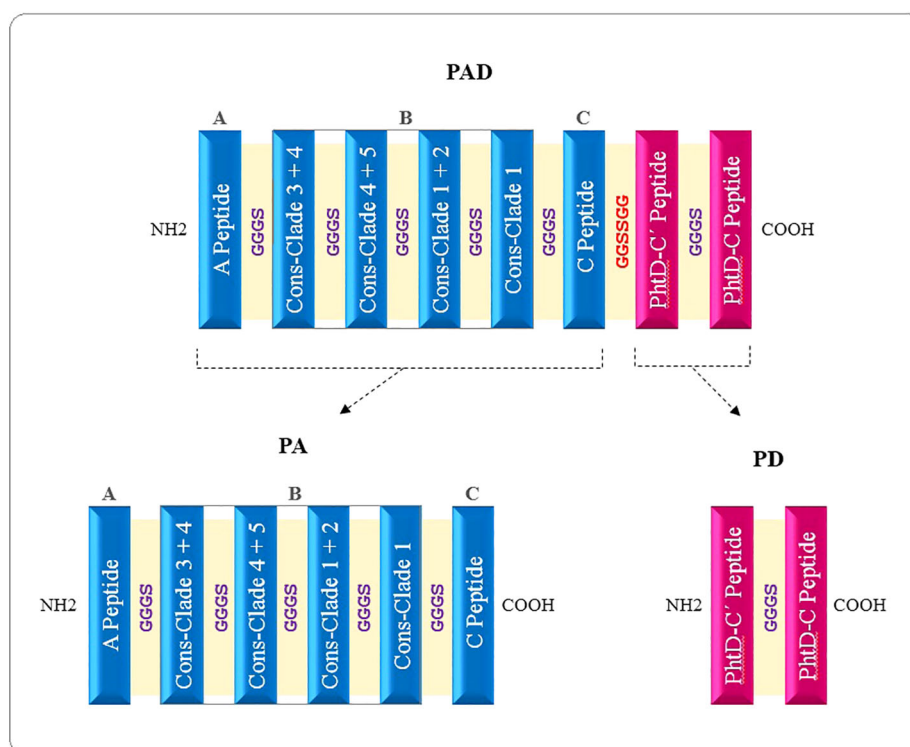


FIGURE 3

Schematic diagram of vaccine candidates. PAD, fusion peptide consisting of PspA and PhtD epitopes; PA, peptide consisting of epitopes of PspA protein; PD, Peptide consisting of epitopes of PhtD protein.

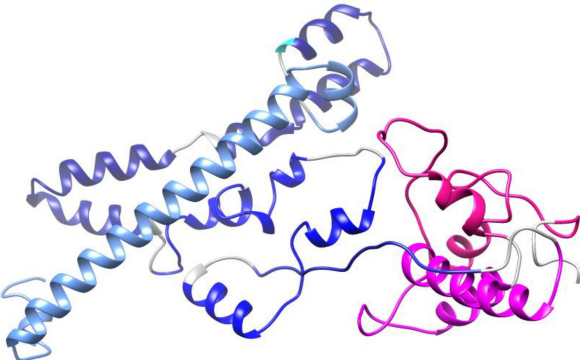
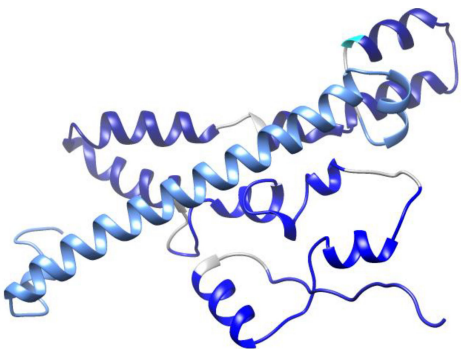

TABLE 2 Evaluation of physicochemical and immunological properties of the designed constructs.

Name	Sequence	Num.	MW (kDa)	pI	+R	−R	II	Aliphatic index	GRAVY	Antigenicity (VaxiJen)	Antigenicity (ANTIGENpro)	Solubility (SOLpro)	Allergenicity (AlgPred/ AllerTOP)	Toxicity (ToxinPred)
<b>PAD</b>	MEAPVASQSKAEKDYDAAVK KSEA AKKHYYEVKKKAEDAQKKY DEGQKKTVEKAKREKEASEKIAgggsEL EKLLDTLDPEGKTQDELKAAEAELD KKVgggsLTRLEDNLKDAEENNVEDIKE GLEKAIgggsLKEIDESDSEDIKEGFRVPL QSELDAKRgggsKLEKDVEYFKNTDGEYT EQYLEAAEKgggsPAPAPKPEQPAPAPKg gssggEKVTDSSIRQNAVETLTGLKSSLLGT KDNNTISA EVDLLALLKgggsLEDLLATVKY YVEHPNERPHSDNGFGNASDHVQRNKNG QADTNQTEKPNEEKgHHHHHH	329	35.69	5.05	49	70	39.88	61.76	-1.148	1.0069	0.887445	0.918234	non- allergenic	non- toxic
<b>PA</b>	MEAPVASQSKAEKDYDAAVKKSEAAKKHY EEVKKKAEDAQKKYDEGQKKTVEKAKRE KEASEKIAgggsELEKLLDTLDPEGKTQDELKKEA AEAELDKKVgggsLTRLEDNLKDAEENNVEDIKE GLEKAIgggsLKEIDESDSEDIKEGFRVPLQSEL AKRgggsKLEKDVEYFKNTDGEYTEQYLEAAEKgg gsPAPAPKPEQPAPAPKgHHHHHH	222	24.34	5.00	38	54	49.82	56.40	-1.285	1.0392	0.689983	0.896574	non- allergenic	non- toxic
<b>PD</b>	MEKVTDSIRQNAVETLTGLKSSLLGTGKDNNTISA EVDLLALLKgggsLEDLLATVKYYYVEHPNERPHSD NGFGNASDHVQRNKNGQADTNQTEKPNEEKgHHHHHH	109	11.97	5.94	11	16	15.6	71.56	-0.982	0.7390	0.893044	0.876282	non- allergenic	non- toxic

The linker gggs for peptides related to one protein and the linker ggssgg between peptides related to two proteins (PspA and PhtD) are shown in blue and red, respectively.



TABLE 3 Predicted 3D structures and quality evaluation of the models before refinement (B.R.) and after refinement (A.R.).

Name	Structure	Step	Ramachandran plot			ProSA Z-Score	ERRAT
			Most favored regions (%)	Allowed regions (%)	Disallowed regions (%)		
PAD		B.R.	89.6	10.4	0.0	-5.38	93.96
		A.R.	92.5	7.1	0.4	-5.33	93.31
PA		B. R.	92.3	7.7	0.0	-3.48	95.14
		A.R.	95.6	4.3	0.0	-3.46	95.54
PD		B.R.	84.9	15.1	0.0	-6.63	89.24
		A.R.	90.3	9.7	0.0	-6.55	92.13

### 3.1.7 Prediction of structural B cell epitopes in engineered constructs

Since most of B cell epitopes are discontinuous, the 3D models of the final designed constructs were analyzed for identification of the conformational epitopes by the ElliPro server. It was found that the PAD construct possessed five new epitopes, comprising 20 to 63 residues with the score values of 0.531 to 0.887 (protrusion index). The PA construct had five new epitopes, comprising 4 to 39 residues with the score values of 0.592 to 0.792. For the PD construct, three new epitopes, comprising 19–22 residues were found with a score value of 0.636–0.717. The details of the identified structural epitopes of the constructs PAD, PA, and PD are given in [Supplementary Table S20](#). The three-dimensional representation of the epitopes in the PAD, PA, and PD constructs are shown in [Figure 5](#), and [Supplementary Figures S10–S11](#), respectively.

### 3.1.8 Further validation using molecular docking with HLA

The selected immunogenic regions were further validated using molecular docking with MHC Class II (DRB1\*01:01) receptor. Since the optimal size of peptides binding to the cleft of MHC-II molecules is approximately 30 residues, the ≤30-mer peptides of the selected epitope-rich regions were considered for the molecular docking. Following the docking process, the complex models ranked according to the energy level were generated by the ClusPro 2.0 server. The best docked complexes were visualized by Chimera software as shown in [Figure 6](#). According to the results it appeared that the peptides interacted favorably with the receptor groove. For each complex, the lowest interaction energy scores, the number of salt bridges, hydrogen bonds, and non-bonded contacts formed between the peptides and the receptor are given in [Supplementary Table S21](#).

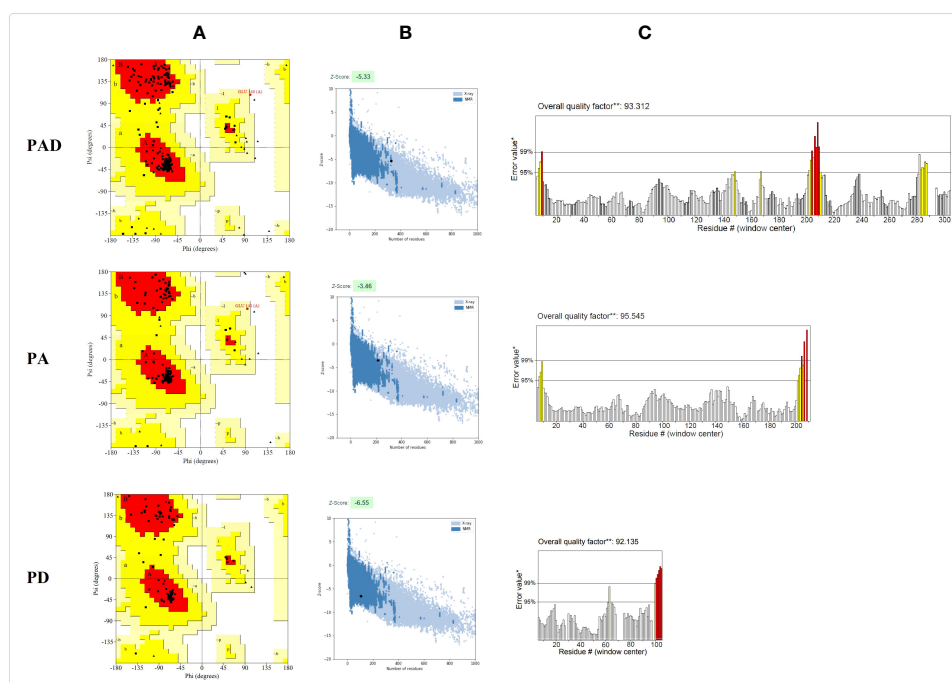


FIGURE 4

Validation of the final models PAD, PA, and PD after refinement. (A) The Ramachandran plots show that in the refined models PAD, PA, and PD, 92.5%, 95.6% and 90.3% of the residues are located in the favorable areas, respectively. The most favored, allowed, generously allowed and disallowed regions are shown in red, dark yellow, lighter yellow and white, respectively. (B) The ProSA Z-scores are found to be -5.33, -3.46, and -6.55 in the refined models PAD, PA, and PD, respectively. The z-scores of proteins determined by NMR or X ray are represented in dark or light blue, respectively. (C) In the ERRAT plots, the overall quality factors of the refined structures PAD, PA, and PD are 93.31, 95.54, and 92.13, respectively. The red and yellow colours show the problematic parts while the white colour shows the normal parts in the structure.

### 3.1.9 Immune simulations

*In silico* immune simulations were performed for the evaluation of immunogenic profile of the constructs in real life. Based on the immune-simulation results, the designed constructs are able to generate appropriate primary, secondary and tertiary responses (Figure 7 and Supplementary Figures S12-S13 respectively for the PAD, PA and PD constructs). After the first injection, the initial response was characterized by an increase in the titer of IgM antibodies. After the injection of the booster dose, secondary and tertiary responses were characterized by increased B cell population, isotype switching, and memory cell formation, as well as increased immunoglobulin expression (IgM, IgM + IgG, and IgG1 + IgG2). Moreover, an increase in T helper cells with the development of memory was observed. The Immune simulations also demonstrated that the immunizations were able to induce production of IFN- $\gamma$  which increases the activity of macrophages.

### 3.1.10 Reverse translation and *in silico* cloning of the constructs

To achieve a high-level expression of recombinant proteins, the codon optimization of the designed constructs was done using the JCat server based on the codon preference of *E. coli* strain K12. Codon optimization can increase protein production by affecting mRNA stability. The CAI values for the optimized sequences of PAD, PA and PD were 0.98, 0.98 and 1.0, respectively. As much as this number is close to 1.0, it indicates a high level of expression in

the bacterial system. The predicted GC contents for PAD, PA and PD were 47.82%, 46.54% and 51.07%, respectively, which are in the optimum range (30-70%) and show the possibility of high expression of the constructs in *E. coli* strain K12. The *Nco*I (CCATGG) and *Xho*I (CTCGAG) cleavage sites were inserted into the 5' and 3' ends of the optimized PAD, PA and PD sequences, respectively (Supplementary Table S22). The total length of the gene sequences of PAD, PA and PD were 998, 677 and 338 nucleotides, respectively. Finally, the adapted vaccine sequences were placed in the expression vectors pET28a(+) between the restriction enzymes *Nco*I and *Xho*I using the SnapGene tool. The developed plasmids were designated as pET28a-PAD, pET28a-PA, and pET28a-PD plasmids (Supplementary Figures S14).

## 3.2 Experimental analysis

### 3.2.1 Expression and purification of recombinant epitope-based proteins PAD, PA, and PD

The optimized sequences of PAD, PA and PD were synthesized and cloned into the *Nco*I and *Xho*I restriction sites of pET28a plasmids by Biomatik Company (Canada). The recombinant plasmids were transferred into *E. coli* BL21 and the positive clones were detected by colony PCR using T7 universal primers (Supplementary Figures S15). The protein expression was

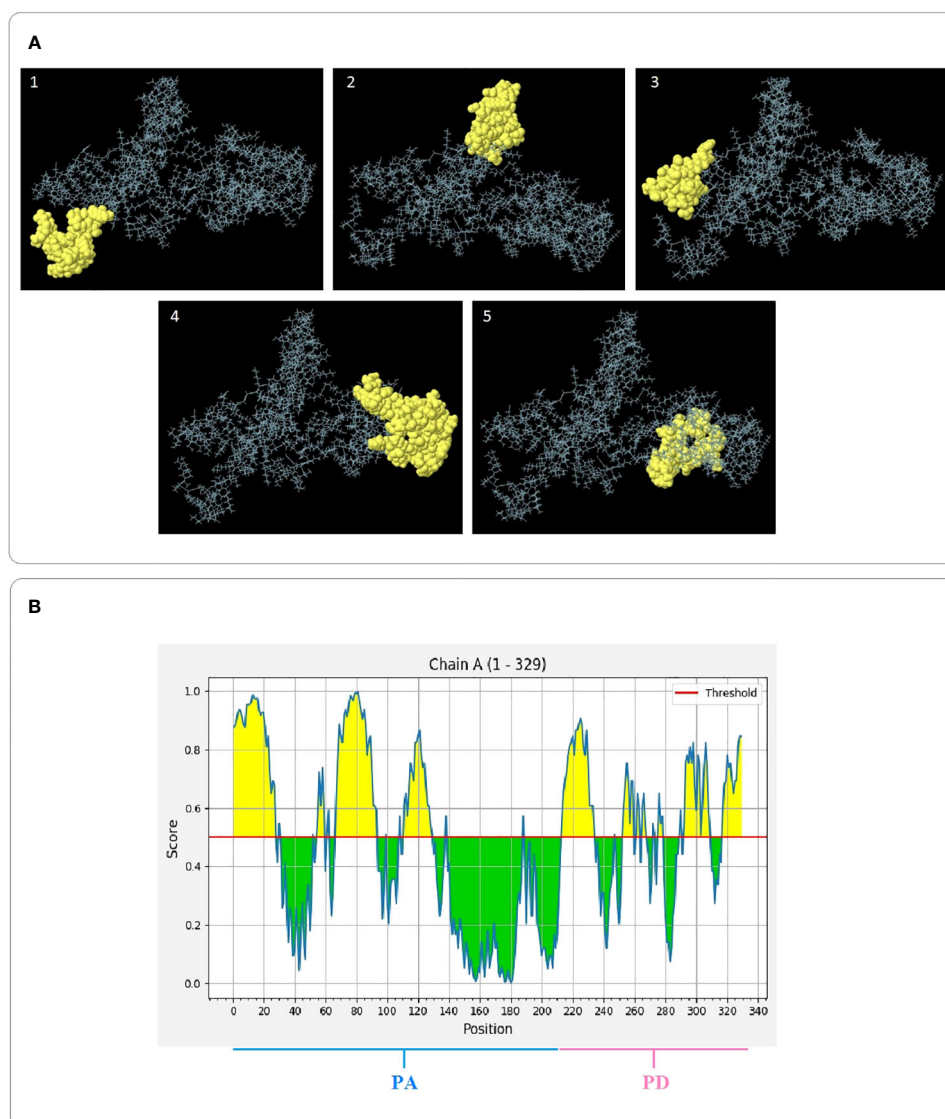


FIGURE 5

3D images of structural B cell epitopes of the PAD construct and 2D score chart. (A) The yellow and gray areas represent the structural epitopes and the other protein segments, respectively. (B) Yellow areas with values above a threshold of 0.5 indicate potential B-cell epitopes.

successfully performed in *E. coli* and the protein purification was carried out by Ni-NTA chromatography under native conditions. As shown in Figure 8, the presence of proteins was monitored by SDS-PAGE, although the proteins PAD and PA showed a little different mobility on the gel. The calculated MW of PAD and PA was lower than the MW observed on the SDS-PAGE gel, indicating that these proteins move more slowly. These differences can be caused by the different protein characteristics such as the amino acid composition (high percentage of acidic AA), increased hydrophilicity (lower GRAVY), or the presence of proline in the protein. It has been found that the discrepancy between the calculated and observed MW on the gel reveals a linear relationship with the content of acidic residues, glutamate (Glu) and aspartate (Asp), that fits the equation  $y = 276.5x - 31.33$  ( $x$  presents the content of Glu and Asp and  $y$  presents the average

$\Delta$ MW per residue) (Guan et al., 2015). The PA and PAD proteins consist of 222 and 329 residues with 24.32% and 21.27% acidic residues, respectively. Using the mentioned equation, it may be possible to conclude that the MW of PA and PAD proteins on SDS-PAGE gel is approximately 8 and 9 kDa higher than their predicted MW. In the next step, the purified recombinant proteins PAD, PA, and PD were used for subsequent *In vivo* immunogenicity assessments in mice.

### 3.2.2 Specific total IgG responses induced by the vaccine candidates

After the injection with the PAD fusion peptide, the mixture of PA and PD, and PA or PD alone, the levels of specific IgG produced against PA or PD were evaluated by indirect ELISA method. The Figures 9A, B shows IgG titers at 2 weeks after every 4 injections, i.e.

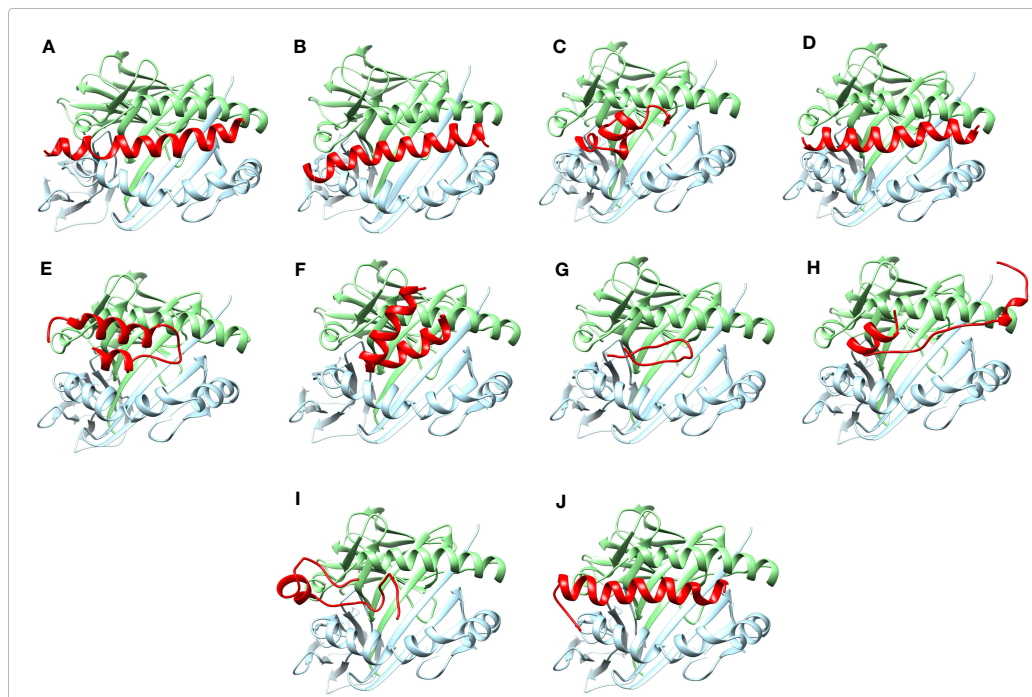


FIGURE 6

Molecular docking of immunogenic peptides with HLA-DRB1\_01:01 molecule (chains A and B). Schematic images of peptide-HLA complexes were shown using Chimera software. The  $\leq 30$ -mer peptides from the selected epitope-rich regions are shown in red. The A and B chains of HLA molecule are indicated in light green and light blue colors, respectively. The results displayed that the peptides had a favorable interaction with the receptor groove. (A, B) The peptides are related to the selected immunogenic part of A region of PspA. (C-F) The peptides are the selected B regions of PspA. (G) The peptide is the selected C region of PspA. (H-J) The peptides are related to the selected immunogenic regions of C-terminal of PhtD.

on days 14, 28, 42, and 56, in the test mice groups compared to each other and the control group (A1). The results of anti-PA IgG responses (Figure 9A) showed that 2 weeks after the first injection on day 14, the groups PA, PA+PD and PAD had significant increases in the Ab levels compared to the control group. Also on day 14, the PA+PD and PAD groups exhibited 0.2- and 0.9-fold increases in the levels of anti-PA IgG compared to the PA group, respectively. In addition, there was a difference in term of anti-PA IgG level on day 14 between the PA+PD and PAD groups with an average of 0.6, indicating the superiority of the PAD group. Anti-PA IgG levels on day 28 had significant differences compared to the levels on day 14, while no significant differences were observed between days 28, 42, and 56 in the test groups.

The data of anti-PD IgG responses (Figure 9B) demonstrated that 2 weeks after the second injection on day 28, the groups PD, PA+PD and PAD had significant increases in the Ab levels compared to the control group. Also on day 28, the PA+PD and PAD groups showed a 0.2- and 0.4-fold increase in anti-PD IgG responses compared to the PD group, respectively. There was a slight difference in term of anti-PD IgG level among the PA+PD and the PAD groups which showed the superiority of the PAD group. Anti-PD responses on day 42 showed an increase compared to the responses on day 28 only in the PA+PD group. On day 56 compared to day 42, there was increases in the anti-PD IgG levels in the groups PD, PA+D and PAD. These results showed that the

antibody responses against PD were increased after the second injection, and these increases continued following the next injections.

### 3.2.3 Assessment of IgG subclasses

To determine the induction of Th1/Th2 immune responses, the levels of specific IgG1 and IgG2a against PA or PD were evaluated two weeks after the third injection. No significant differences were observed between IgG1 and IgG2a anti-PA antibodies in the mice groups PA, PA+PD and PAD (Figure 9C). Also, no significant differences were observed between IgG1 and IgG2a anti-PD antibodies in the PD and PA+PD groups, while in the PAD group a significant increase was observed in the level of IgG1 compared to IgG2a (\*\* $p < 0.01$ ; Figure 9D). The IgG1/IgG2a ratio against PA in the groups PA, PA+PD and PAD is almost equal to one, showing the induction of a balanced Th1 and Th2 response (Supplementary Table S23). The ratio of anti-PD IgG isotypes in the groups PD, PA+PD and PAD is more than one, indicating the dominance of Th2 immune response (Supplementary Table S23).

### 3.2.4 Measurement of cytokine responses

To confirm the induction of Th1/Th2/Th17 responses, evaluation of the levels of cytokines IFN- $\gamma$ , IL-4 and IL-17 in the serum of mice groups PD, PA, PA+PD, PAD and control A1 was done two weeks after the third immunization by sandwich ELISA



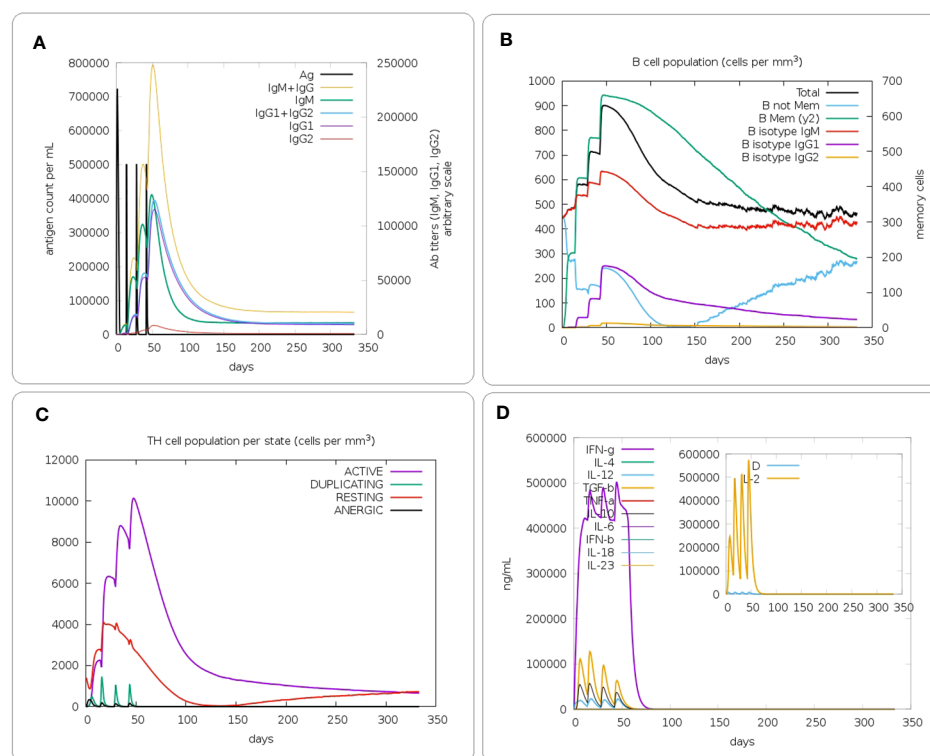


FIGURE 7

*In silico* immune simulation of the PAD construct. (A) Immunoglobulin production in response to injection of the PAD construct (antigens and immunoglobulin subclasses are represented as black and colored peaks, respectively). (B) Evolution of the B cell population after 4 injections. (C) Evolution of the T-helper cell population. (D) Analysis of the levels of different cytokines induced by the construct. The cytokines were distinguished by different colours and the concentration was expressed as ng/mL.

method. As shown in the Figure 10A, the mice groups PD, PA, PA +PD and PAD showed ~1.4-, 2-, 1.5-, and 1.7-fold increases in IFN- $\gamma$  levels compared to the control group, respectively. The levels of IFN- $\gamma$  in the PA group were increased by 1.4- and 1.2-fold compared to those in the PD and PA+PD groups, respectively. However, no significant differences were observed between the PA and PAD groups, as well as between the PA+PD and PAD groups. From the results it follows that Th1 cell responses could be activated by subcutaneous immunization with PA, PD (individually as well as in combination) and PAD proteins.

As illustrated in Figure 10B, the groups PD, PA, PA+PD and PAD showed significant (more than 2.5-fold) increases in IL-4 levels compared to the control group. The superiority of the fusion peptide group among the test groups was observed in terms of IL-4 production. PAD group showed about more than 1-fold increase in IL-4 level compared to PD and PA+PD groups. As seen in Figure 10C, the cytokine IL-17A also showed significant increases in all test groups compared to that in the control group. Among the test groups, the superiority of the fusion group was also observed in terms of IL-17A production. The level of IL-17A in the PAD fusion group showed an increase of more than 1.3-fold compared to that in the PD and PA+PD groups. According to the results, it was found that the constructs PA, PD (individually and in combination) and PAD could activate Th2 and Th17 responses, and among them, the fusion peptide could enhance these responses more favorably.

### 3.2.5 Antibody-dependent bactericidal assay

The complement-mediated bactericidal activity of antibodies created against the recombinant proteins in the serum of mice groups PA, PD, PA+PD and PAD was evaluated by SBA assay 2 weeks after the 4th immunization (Figure 10D). The specific antibodies in the serum of PA, PA+PD and PAD mice groups were more effective than those in serum of the PD group. The bactericidal activity of antibodies in the serum of PD group was considered in 1:4 dilution in which approximately 50% of the bacteria are killed compared to the control. The bactericidal activity of the serum of groups PA, PAD and PA+PD was considered in 1:16 dilution.

### 3.2.6 Analysis of mice survival rates and bacterial loads in the blood and spleen

To assess whether the recombinant proteins are capable of inducing protective immunity and decreasing bacterial burden in blood and spleen, an intraperitoneally challenge with a lethal dose of the ATCC 6303 bacteria was conducted in the mice groups after the final immunization. The survival of mice was monitored up to seven days after challenge. The mice of the control group died one day after the challenge. In the PD group, one mouse died, while all mice survived in the PA, PA+PD, and PAD groups, as shown in Figures 11A-D, respectively.



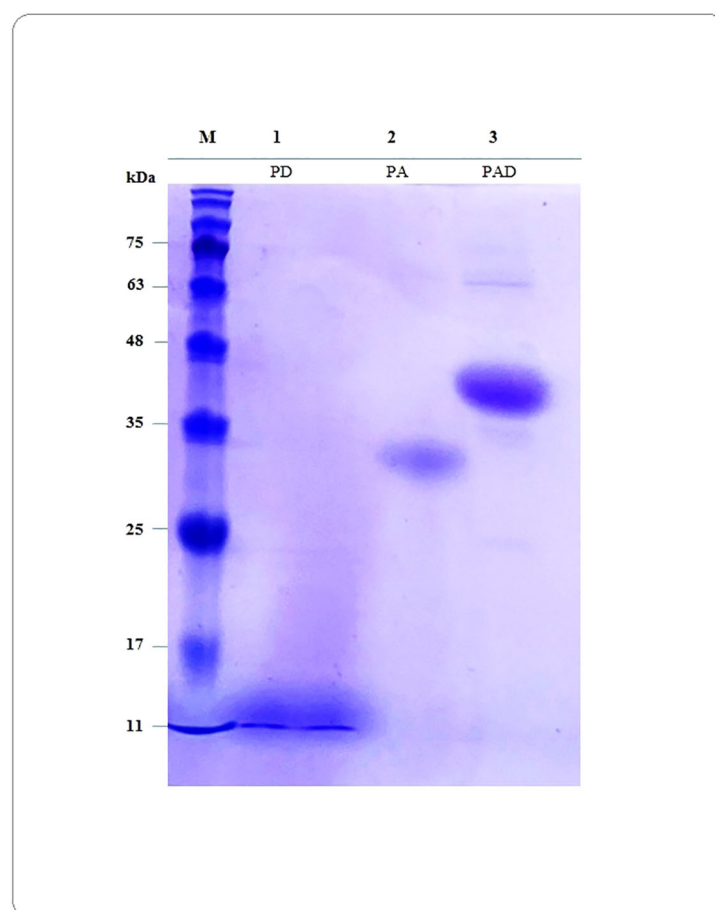


FIGURE 8

Verification of presence of purified proteins by SDS-PAGE electrophoresis. The calculated MW for the peptide constructs PAD, PA and PD are 35.69, 24.34 and 11.97 kDa, respectively. The calculated MW of PAD and PA is lower than the MW observed on the gel, indicating these proteins move more slowly. Lane M: protein marker; Lanes 1 to 3: Proteins PD, PA and PAD, respectively.

One day after the challenge, the number of bacteria in the blood and spleen of the mice were counted and a significant decrease of bacterial loads (DLs; log<sub>10</sub> CFU/ml or g) was seen in the test groups compared to the control group. The bacterial loads in the blood of control mice were about 10<sup>8</sup> CFU/ml, while there were 10<sup>1</sup> CFU/ml of bacteria in the blood of the PD group (DL=7.0; Figure 11E) and no bacteria in the blood of PA, PA+PD and PAD groups (DL=8.0; Figure 11E). The results show that PA, PA+D and PAD groups were more effective in reducing the blood bacterial loads. The bacterial loads in the spleen of control mice were about 10<sup>3</sup> CFU/g, while there were no bacteria in the spleen of the mice groups immunized with PD, PA, PA+PD and PAD (DL=3.0; Figure 11F).

## 4 Discussion

The commercial polysaccharide-based pneumococcal vaccines are expensive and serotype-dependent, and their immunogenicity is limited to the serotypes included in the vaccines (Norolahi et al., 2020; Bahadori et al., 2022). Therefore, pneumococcal protein vaccines providing serotype-independent immunity at low cost

have been considered as interesting alternatives to existing vaccines (Converso et al., 2020; Masomian et al., 2020). The use of several protein antigens in a single vaccine, targeting multiple major bacterial virulence factors, can be a very attractive strategy to prevent infection (Lu et al., 2015). So far, different studies have demonstrated that fusion proteins containing several antigens are more efficient compared with combination formulations and could facilitate the production/purification process and product quality control (Nguyen et al., 2011; Goulart et al., 2013).

Recent improvements in immunoinformatics tools could aid in identifying possible B and T cell epitopes in protein candidates and speed up the process of developing epitope-based vaccines (Oli et al., 2020). In recent years, many research groups have developed innovative vaccine candidates employing immunoinformatics against various types of pathogens including viruses, bacteria, and parasites (such as SARS-CoV-2 (Marriam et al., 2023), *Mycobacterium tuberculosis* (Cheng et al., 2022), and *Leishmania donovani* (Saha et al., 2022)). The peptide-based vaccines are attractive alternatives to conventional vaccines since they have a lower production cost, save time, do not contain the whole pathogen, and are safer and more specific (Naz et al., 2020).

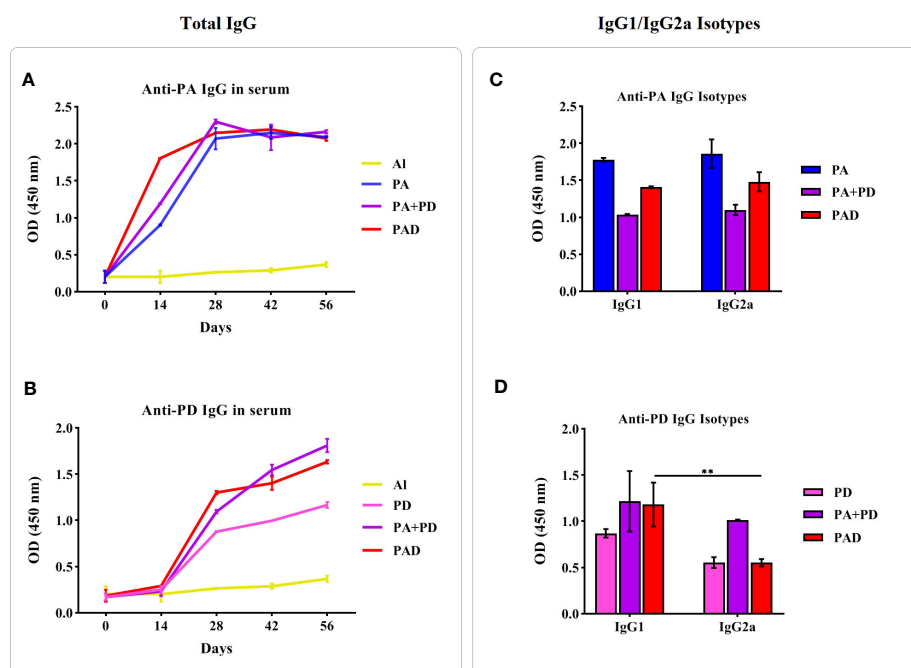


FIGURE 9

Immunogenicity of the recombinant proteins. Left figures: The comparison of specific total IgG responses in test and control groups was done before each injection and 2 weeks after the last injection (days 0, 14, 28, 42, and 56). Mice ( $n = 5$  per group) were vaccinated with PA or PD alone, PA+PD, PAD or AI adjuvant, and then antisera were examined against PA or PD separately. (A) Anti-PA responses in the groups PA, PA+PD and PAD were significantly increased after the second, third, or fourth immunization compared to the first immunization. (B) Anti-PD responses in the groups PD, PA+PD and PAD after each immunization showed significant increases compared to the preceding phase. Right figures: The responses of IgG isotypes against the peptide PA or PD in the tested mice groups ( $n = 5$ ) were examined 2 weeks after the third injection. (C) Specific IgG1 and IgG2a subclasses against the PA peptide in the groups PA, PA+PD and PAD did not show significant differences from each other. (D) The IgG1 subclass against the PD peptide showed 0.6-fold increase compared to IgG2a subclass in the PAD group. Statistical analysis was done using two-way ANOVA. \*\* $p < 0.01$ .

The PspA and PhtD proteins, among the pneumococcal virulence proteins, are highly immunogenic which are expressed on all serotypes and have shown very promising results in clinical studies as vaccine candidates (Converso et al., 2020; Masomian et al., 2020). The fact that PspAs are diverse in different clinical isolates may restrict the broad coverage of PspA-derived vaccines (Goulart et al., 2011). It has been found that the levels of cross-reactivity among PspAs depends on sequence similarity which is high within a PspA family and low among different families. In addition, some studies have shown that the levels of cross-reactivity and protection depends on the PspA clade (Darrieux et al., 2008; Goulart et al., 2011; Akbari et al., 2019). Recently, Akbari and colleagues have produced a PspA-derived fusion vaccine that contains fragments of the B region of PspA from the five most common clades (PspAB1-5). The vaccine would appear to have a significant protective effect against various pneumococcal strains, suggesting that using fusion proteins harboring B regions from clades 1-5 may be an effective vaccination strategy. Also, it has been proposed that the inclusion of the A and C regions of PspA protein in the vaccine construct could help elicit broadly cross-reactive antibodies (Akbari et al., 2019). The C-terminal fragment of PhtD protein is placed on the bacterial surface and Plumptre et al. showed that recombinant truncated derivatives of this fragment are highly immunogenic and capable of inducing very high titers of antibodies

in comparison with the full-length PhtD protein (Plumptre et al., 2013a; Plumptre et al., 2013b).

According to our knowledge, the proteins PspA and PhtD have not been studied in a fusion form until today, and this study is the first report evaluating the fusion form of these two proteins as a vaccine candidate against *Streptococcus pneumoniae*. In the present study, the computational approaches were applied for designing potential peptide-based vaccines including the immunodominant regions of PspA (from different families) and PhtD proteins. We assessed the A, B and C regions of the PspA protein to predict the B and T cell epitopes. B regions from clades 1 to 5 were analyzed to provide wider protective coverage and decrease the possibility of PspA variants escaping host immune responses. In addition, the C-terminal of PhtD was analyzed as a promising immunogenic region for predicting B and Th cell epitopes. None of the selected epitope-rich regions of these proteins have been reported before, and this study presents for the first time novel vaccine candidates consisting of immunodominant regions of PspA and PhtD-C (a fusion construct of the two proteins and two individual constructs). Finally, the immunogenicity and protective effects of the constructs were compared individually, in combination and fusion form in mouse model.

On the basis of the immunoinformatics data of the study, the high-scoring and overlapping B and Th cell epitopes shared on multiple servers were taken into account to select the final peptides for PspA (region A, region B for two families 1 and 2, and region C)

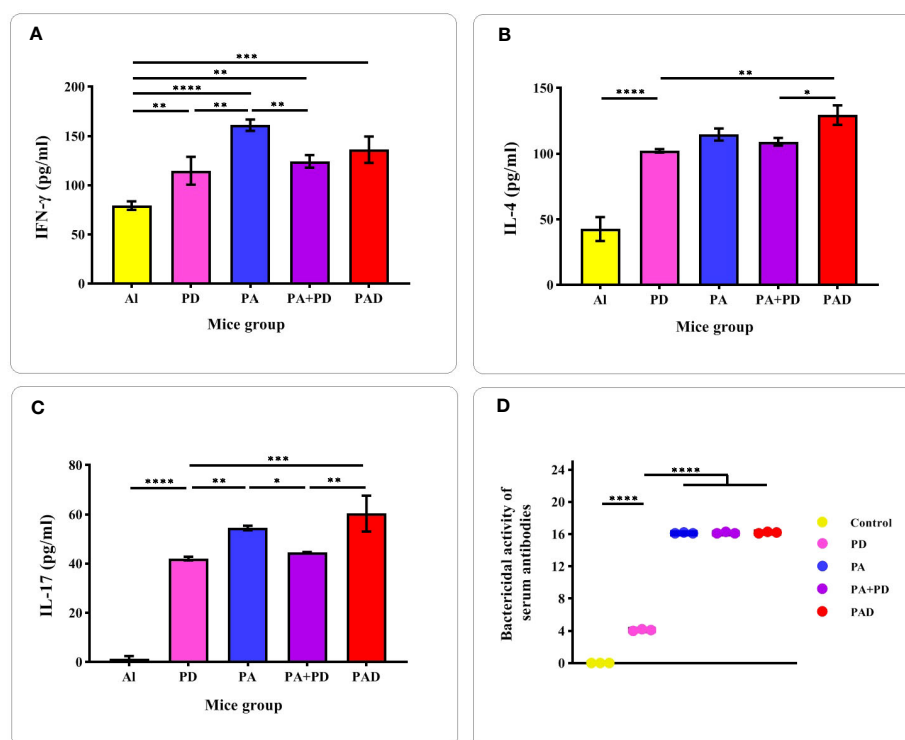


FIGURE 10

Evaluation of the levels of cytokines and the bactericidal activity of antibodies. (A–C) Measurement of the cytokines IFN- $\gamma$ , IL-4, and IL-17 in test and control mice ( $n = 5$  per group) was performed 2 weeks after the 3th injection. (D) The complement-mediated bactericidal activity of anti-recombinant proteins antibodies was evaluated 2 weeks after the 4th injection ( $n = 3$ ). The Y-axis is the reverse of the dilution of serum in which more than 50% of the bacteria are killed compared to the control. The activity of antibodies in the sera of PA, PAD and PA+PD groups was higher than that in the serum of PD group. There was no significant difference in the serum activity of PA, PAD and PA+PD groups. \* $p < 0.05$ , \*\* $p < 0.01$ , \*\*\* $p < 0.001$  and \*\*\*\* $p < 0.0001$ .

and PhtD-C (Table 1). An epitope-rich peptide of 64 amino acids was selected for the A region of PspA protein. After analyzing the protein sequence of the B region in different PspAs, it was found that clades 1 and 4 have the most overlap with other clades, and hence only consensus epitope sequences of region B corresponding to clades 1 and 4 were considered in the final construct: Cons-Clade 1 + 2 (29 residues covering clades 1 and 2), Cons-Clade 1 (26 amino acids covering clade 1), Cons-Clade 3 + 4 (32 residues covering clades 3 and 4) and Cons-Clade 4 + 5 (28 residues covering clades 4 and 5). Thus, it can be said that all 5 clades can be targeted by selecting these consensus sequences. To select the epitope in the C region of PspA, the 15-amino acid peptide PPAKPEQPAPAPK was chosen, which had the highest overlap in the epitopes experimentally identified in recent studies. Approximately 46% of pneumococcal strains were found to express a copy of the repeat PKPEQP capable of eliciting protective Abs in animal models (Daniels et al., 2010), so this important motif was taken into account in this study. The epitope-rich regions of PhtD-C that were selected in this study included two peptides from amino acids 648 to 700 and amino acids 782 to 826 (53 and 45 residues in length, respectively).

In the next step of this research, the final selected peptides were connected to each other by glycine-rich flexible linkers (GGGS and GGSSGG) capable of improving solubility and enabling the

neighboring domains to act freely (Kavoosi et al., 2007; Kar et al., 2020). A histidine tag was added by a glycine to the C-terminal of the developed constructs to aid protein purification. Finally, two individual protein constructs (PA: composed of PspA epitopes and PD: composed of PhtD-C epitopes) and one fusion construct (PAD: composed of PspA and PhtD-C epitopes) were designed with the aim of comparing them in the form of individual, combination and fusion proteins (Figure 3).

The physicochemical and immunological characteristics of the designed constructs were evaluated using different web servers (Table 2). The molecular weights of constructs were less than 110 kDa, showing them acceptable for vaccine development because proteins with MWs below 110 kDa are easier to purify (Sanami et al., 2020). The theoretical pI of the constructs indicated that the constructs are acidic in nature which may be useful for protein purification (Zhao et al., 2019). The instability index of the PAD or PD was less than 40, thus they were classified as stable constructs. While the instability index of the PA was above 40, so the construct stability should be confirmed in experimental tests. The predicted aliphatic indexes suggested that the constructs were thermostable (Ikai, 1980). The GRAVY indexes of the constructs were negative values which showed the hydrophilic nature of proteins and their strong interaction with water molecules and therefore their high solubility (Kyte and Doolittle, 1982). Further predictions revealed

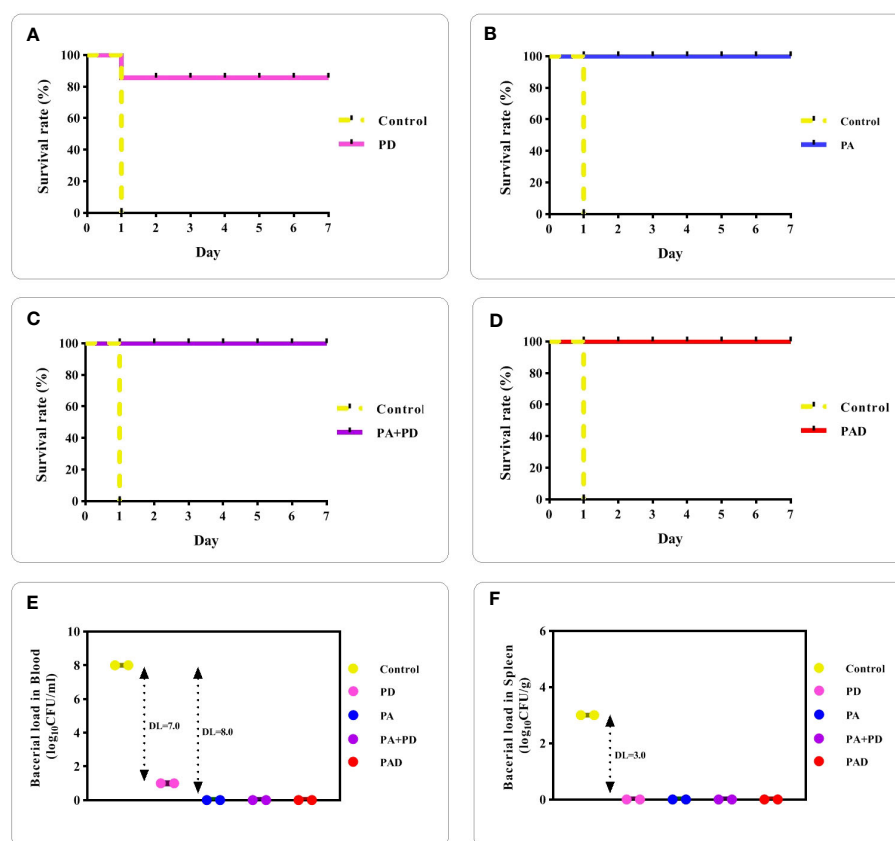


FIGURE 11

Assessment of mice survival rates and bacterial loads after pneumococcal challenge. (A–D) mice in the control group died one day after the challenge. The survival rate of mice up to 7 days after challenge in the PD group was 80% and in the PA, PA+PD or PAD groups was 100% ( $n = 3$  per group). (E, F) Bacterial loads present in blood and spleen tissue of control and immunized mice ( $n = 2$ ) were counted one day after the challenge. DLs in the blood were 7.0 Log<sub>10</sub> (CFU/ml) for mice immunized with PD and 8.0 Log<sub>10</sub> (CFU/ml) for the other three groups. DLs in the spleen of mice immunized with PD, PA, PA+PD and PAD were 3.0 Log<sub>10</sub> (CFU/g).

that the designed vaccine candidates have a high solubility percentage upon overexpressed in *E. coli*, as well as they are antigenic, non-allergenic and non-toxic.

The primary 3D structures of the vaccine candidates were modeled using Robetta Server and then refined by GalaxyRefine software resulting in higher quality 3D models. The quality assessment of the initial and refined models was conducted using Ramachandran diagrams, ProSA Z-scores and ERRAT scores. The obtained results showed that the refined structures possessed better quality than the initial 3D structures (Table 3). The prediction of B cell structural epitopes in the final constructs was done using the ElliPro server after confirming the 3D structures. The server predicted five and three potential non-linear B-cell epitopes in the PAD/PA and PD constructs, respectively (Supplementary Table S20). The results confirm that the vaccine candidates are able to induce the humoral immune response, which is necessary for protection against pneumococci. The proposed immunogenic regions should interact effectively with the HLA molecules for inducing efficiently immune responses. The potential interaction between the selected peptides and HLA-DRB1\_01:01 was evaluated by molecular docking analysis. The results confirmed that the peptides possessed affinity for the HLA receptor (Supplementary

Table S21). The elicitation of memory B and T cell responses is considered one of the criteria for effective vaccine candidates (Bahadori et al., 2022). The immune simulation results showed that memory cells were increased with each dose of vaccines, showing the suitability of the constructs. Moreover, it was found that the IFN- $\gamma$  production was increased following the repeated the injections. The results showed that the constructs have the potential to induce humoral and cellular responses providing a basis for immunity against pneumococcal infections.

In the next step, to ensure high-level expression in *E. coli* K12, the reverse translation and codon optimization of the designed constructs were conducted using the Jcat server. For the optimized sequence of PAD, PA or PD, the GC content and the CAI value were favorable for high protein expression in the bacteria. Finally, for the purpose of *in silico* cloning, the gene sequences of vaccine candidates were successfully inserted into the pET28a(+) expression vectors. Overall, the *in silico* data showed that the vaccine candidates may be highly effective against pneumococcal infections, but in order to confirm these *in silico* results, further experimental studies were performed *in vitro* and *in vivo*.

The experimental results of expression and purification of PAD, PA and PD recombinant proteins showed that all three proteins are

stable. The computational results were confirmed by expressing PAD, PA and PD recombinant proteins in *E. coli* BL21 after induction by IPTG. The computational prediction of the solubility of PAD, PA and PD proteins was confirmed by their *in vitro* purification under native conditions on Ni-NTA column. In the SDS-PAGE technique, the presence of bands corresponding to PAD, PA and PD recombinant proteins demonstrated acceptable expression and codon optimization. The band near 11, 35, or 48 kDa of the protein ladder corresponds to the PD, PA, or PAD construct, respectively. The predicted MW of PA and PAD are lower than the apparent MW on SDS-PAGE gel, indicating the slow movement of these proteins. In a study by Shirai et al., it was shown that the differences between estimated and apparent MWs could be due to the GRAVY score (Shirai et al., 2008). Due to the preferential binding of SDS to hydrophobic parts of the proteins, those that are more hydrophilic and have a lower GRAVY tend to bind less SDS, resulting in lower electrophoretic mobility and appearing to have a higher MW. This research group also demonstrated that the isoelectric point of a protein could influence the electrophoretic mobility (Shirai et al., 2008). This confirms what Guan and colleagues hypothesize, namely that a protein with many charges is likely to result in repulsion of the SDS charge and subsequently abnormal mobility on the gel (Guan et al., 2015). Moreover, the proline content in a protein also should be taken into account as another cause of greater apparent MW (Scheller et al., 2021). Since the ring structure of the proline molecule inhibits rotation of the C-N bond, the presence of proline in a protein can cause a kink in the secondary structure, leading to the polypeptide being unable to be fully stretched following reduction and SDS-binding.

In the next step, to check the immunogenic and protective effect of vaccine candidates, the purified recombinant proteins along with Alum adjuvant were injected into female BALB/c mice. The Alum adjuvant mainly induces Th2 responses, leading to increased production of antigen-specific antibodies (Leroux-Roels, 2010; Younis et al., 2019). Since pneumococcus is an extracellular pathogen and a strong Th2 response could be effective against the infection (Mizrachi-Nebenzahl et al., 2003), Alum was chosen as an adjuvant in this study. The BALB/c mice produce a stronger humoral response than other inbred strains, and it has also been shown that female BALB/c mice can induce regulatory T cells better than male mice (Elderman et al., 2018). Immunization was done subcutaneously in the mice groups PD, PA, PA+PD, PAD and Al (adjuvant control) on days 0, 14, 28 and 42. Drug injection is a preferred way for drug delivery to achieve the desired effect quickly and directly. Among the various methods of drug injection, subcutaneous injection is the one that is applied to the fat layer of the subcutaneous tissue just under the skin. Because the subcutaneous tissue possess few blood vessels, the injected drug is released very slowly with a constant rate of absorption. Therefore, it is very effective in the administration of drugs such as vaccines, which require sustained delivery at low doses (Kim et al., 2017). Two weeks after each immunization, mouse sera were collected and analyzed for active antibody production against pneumococci and cytokine production.

In confirmation of the computational predictions, the experimental results revealed that the PAD, PA and PD

constructs are non-allergenic and non-toxic, so that no increased body temperature, decreased weight, allergic reactions, hypersensitivity or restlessness was observed in the animal models following the injection of the proteins. In addition, the experimental data also verified the computational analysis of the antigenicity of the recombinant proteins. The PAD, PA and PD proteins were able to increase the levels of IgG antibodies in the test mice groups compared to the control group, at different injection times (Figure 9). The anti-PA IgG responses showed an upward trend after the first injection, and this increase continued after the 2nd injection, but the responses remained approximately in the same range two weeks after the 3rd or 4th injections. On the 14th day, a significant difference in anti-PA IgG responses was observed among the test groups, with the superiority of the PAD group. The analysis of anti-PD IgG levels showed that the responses were increased after the 2nd injection and this increase continued after the subsequent injections. On the 28th day, a significant difference was observed among the test groups in terms of anti-PD IgG response, with the superiority of the PAD group. The anti-PA IgG1/IgG2a serum ratio in PA, PA+PD and PAD groups is close to one, indicating the balance between Th1 and Th2 responses. The anti-PD IgG1/IgG2a serum ratio in the PD, PA+PD and PAD groups is greater than one, showing that the Th2 response is dominant (Supplementary Table S23). A possible reason for this Th2 polarization could be the use of Alum adjuvant, which promotes Th2 immune response effective against extracellular pathogens such as pneumococcus. However, this polarization might be associated with the nature of antigens or the immunological pathway. This result is consistent with recent literature which reported that the PspA or PhtD antigens could stimulate dominant Th2 responses (Kothari et al., 2015; Malekan et al., 2019; Afshari et al., 2023b).

In the experimental phase, the levels of cytokines IFN- $\gamma$ , IL-4 and IL-17A in the immunized mice groups was investigated (Figure 10) and the results of computational immune simulation were confirmed. The findings showed that the designed vaccine candidates were able to induce a combination of Th1, Th2 and Th17 immune responses. Cytokine IFN- $\gamma$  showed a significant difference in the immunized groups of PA, PD, PA+PD and PAD compared to the control group. The highest level of IFN- $\gamma$  was induced in the PA group, although it was not significantly different from the PAD group. These results show that Th1 cell responses are significantly activated by subcutaneous immunization with PA, PD (individually as well as in combination) and PAD proteins. Similarly, IL-4 and IL-17A cytokines were significantly increased in all immunized groups compared to the control group. Among the immunized groups, a significant difference was observed between the PA+PD and PAD groups, with the superiority of the fusion protein group in terms of the production of IL-4 and IL-17 cytokines. These results indicate that Th2 and Th17 responses are activated through subcutaneous immunization with PA, PD (individually and in combination) and PAD proteins, and meanwhile the PAD protein fusion activates these responses more strongly.

Serum bactericidal assay was used to evaluate *in vitro* the potential protective effects of vaccine candidates against pneumococcal strain. In this test, the complement-mediated killing activity of anti-recombinant proteins antibodies was



analyzed after the last injection. The activity of Abs in destroying almost 50% of bacteria compared to the control was considered at a dilution of 1:16 for the PA, PA+PD or PAD group, and at a dilution of 1:4 for the PD group (Figure 10D). The results show that these antibodies could be able to clear the bacteria with the help of complement.

In this study, the protective effect of epitope-based vaccine candidates against *Streptococcus pneumoniae* strain ATCC 6303 was investigated after the final injection. The results of the challenge showed that the PA construct is more effective than the PD construct in the survival of mice. The survival rate of mice in the PA, PA+PD and PAD groups was 100% and complete clearing of bacteria in blood/spleen was observed one day after the challenge. While in the PD group, the survival rate was 80%, and the bacterial loads in the blood was reduced to  $10^1$  CFU (DL=7.0), while complete clearing of bacteria was observed in the spleen.

As seen in the present study, in comparison between individual constructs, although the PD construct is a suitable vaccine target, it is not as effective as the PA construct alone as an immunogen and is not sufficient to provide complete protection against pneumococcal infections. The different immunoreactivity results of the two individual formulations PD and PA may be attributed to several factors, e.g. protein molecular weight, chemical/physical properties, composition and degradability (Schellekens, 2005). However, the PD construct played an important role by stimulating the production of cytokines. It has been found that IL-17 plays a key role in protecting against pneumococcus by decreasing bacterial density and colonization in the nasopharynx (Lu et al., 2015). In general, based on the findings, it can be concluded that the most effective formulation against pneumococcus is the one containing both constructs in order to produce broader immune responses. In the comparison between the combination of constructs and the fusion construct, it can be said that both formulations were able to elicit relatively similar protective effects, although the fusion peptide enhanced Th2 and Th17 responses more favorably. This shows that in the fusion construct, the addition of peptides to each other has not changed their structure, and the immunogenic epitopes have been made available and the antigenic properties of the peptides have been preserved. Another advantage of the fusion construct was that it could simplify the process of production/purification of antigens and facilitate product quality control. Overall, the existing data confirm that in the vaccine development, a protein fusion could be more effective than a protein alone or a combination of proteins.

These results are consistent with those of Nguyen et al., who found that immunization of mice with FlaB–PspA fusion protein, compared to immunization with PspA alone or a mixture of PspA and FlaB, is able to induce more effective mucosal immunity against pneumococcal infection (Nguyen et al., 2011). The FlaB–PspA fusion protein had longer half-life, potentiated IgG and IgA antibody responses, and provided the best protection against challenge with *S. pneumoniae*. FlaB–PspA fusion protein stimulated IL-4 and IFN- $\gamma$  production and significantly enhanced IL-4 production and Th2 responses, being consistent with the IgG

subtype responses. Also, our results agree with the results of Lu et al. that showed PsaA–PspA fusion protein could stimulate production of high-titered antibodies against *S. pneumoniae* strains comparable to each antigen alone (Lu et al., 2015). The PsaA–PspA significantly reduced bacterial levels in blood/organs and provided a high survival rate of up to 100% for some strains after intraperitoneal challenge. The PsaA–PspA fusion protein could induce a much higher level of IL-17A than the other formulations. Furthermore, our results are consistent with those of Converso et al., who reported rPspA–PotD fusion protein could induce an increased antibody production when compared with the individual proteins (Converso et al., 2017a). The rPspA–PotD fusion group presented the highest secretion of IL-17 which was associated with a reduced pneumococcal colonization. The rPspA–PotD was able to enhance phagocytosis, reduce bacterial loads in the nasopharynx and elicit wide protection against infection.

Moreover, the results of this study reveal the success of computational tools in designing epitope-based vaccine candidates, which are consistent with various studies proving the reliability of immunoinformatics approaches (Ahmadi et al., 2019; Hasanzadeh et al., 2020; Cheng et al., 2023). In this context, Zhang et al. designed and evaluated a multi-epitope subunit vaccine against group B *Streptococcus* (GBS) infection, and experimental results consistent with *in silico* data showed that the proposed construct is capable of inducing strong immune responses and is an ideal vaccine candidate against GBS (Zhang et al., 2022).

## 5 Conclusion

In the present study, the epitope-based vaccine candidate in the form of a fusion of PspA and PhtD epitopes was compared with the individual and combination formulations. The obtained findings confirmed that the fusion formulation was relatively more efficient and effective than the other formulations, although this issue requires further studies. The fusion construct was able to produce a high specific IgG titer and was able to induce a combination of Th1, Th2 and Th17 immune responses. Also, antisera raised against the fusion construct had a favorable effect on the mediation of complement-dependent bacterial killing and provided 100% survival in immunized mice after bacterial challenge. The experimental validation results of the designed vaccine candidate also confirmed the immunoinformatics studies. Overall, it can be concluded that the fusion construct can be considered as a promising vaccine candidate against pneumococcal infection with significant prospects. The next plans for optimizing the vaccine candidate will be to change the adjuvant, concentration of immunogen, and injection route/timing, as well as the assessment of mucosal immunity and the use of different pneumococcus strains expressing other clades of PspA for investigating the cross-reactive antibodies responses. Further studies in the future can focus on other epitope-based fusion constructs consisting of promising immunogenic antigen candidates for achieving more robust immune response and protection.

## Data availability statement

The datasets presented in this study can be found in online repositories. The names of the repository/repository and accession number(s) can be found in the article/[Supplementary Material](#).

## Ethics statement

The animal study was approved by Animal Ethical Committee of Semnan University of Medical Sciences, Semnan, Iran (Approved Number: IR.SEMUMS.REC.1399.128). The study was conducted in accordance with the local legislation and institutional requirements.

## Author contributions

MS: Conceptualization, Data curation, Formal analysis, Investigation, Methodology, Validation, Writing - review & editing, Writing original draft. ZB: Conceptualization, Data curation, Formal analysis, Investigation, Methodology, Validation, Writing-original draft. SB: Methodology. EA: Methodology. HM: Validation. SM: Project administration, Supervision. AS: Project administration, Supervision.

## Funding

The author(s) declare financial support was received for the research, authorship, and/or publication of this article. This study (PhD thesis) was supported by a grant number of 1790 from the Semnan University of Medical Sciences, Semnan, Iran.

## References

- Afshari, E., Ahangari Cohan, R., Shams Nosrati, M. S., and Mousavi, S. F. (2023a). Development of a bivalent protein-based vaccine against invasive pneumococcal diseases based on novel pneumococcal surface protein A in combination with pneumococcal histidine triad protein D. *Front. Immunol.* 14, 1187773. doi: 10.3389/fimmu.2023.1187773
- Afshari, E., Cohan, R. A., Sotoodehnejadnematalahi, F., and Mousavi, S. F. (2023b). In-silico design and evaluation of an epitope-based serotype-independent promising vaccine candidate for highly cross-reactive regions of pneumococcal surface protein A. *J. Trans. Med.* 21 (1), 13. doi: 10.1186/s12967-022-03864-z
- Ahmadi, K., Pouladfar, G., Kalani, M., Faezi, S., Pourmand, M. R., Hasanazadeh, S., et al. (2019). Epitope-based immunoinformatics study of a novel Hla-MntC-SACOL0723 fusion protein from *Staphylococcus aureus*: Induction of multi-pattern immune responses. *Mol. Immunol.* 114, 88–99. doi: 10.1016/j.molimm.2019.05.016
- Akbari, E., Negahdari, B., Faraji, F., Behdani, M., Kazemi-Lomedasht, F., and Habibi-Anboui, M. (2019). Protective responses of an engineered PspA recombinant antigen against *Streptococcus pneumoniae*. *Biotechnol. Rep.* 24, e00385. doi: 10.1016/j.btre.2019.e00385
- Bahadori, Z., Shabani, A. A., and Minuchehr, Z. (2021). Rational design of hyperglycosylated human follicle-stimulating hormone analogs (a bioinformatics approach). *J. Biomol. Struct. Dyn.* 40 (19), 9114–9125. doi: 10.1080/07391102.2021.1924268
- Bahadori, Z., Shafaghi, M., Madanchi, H., Ranjbar, M. M., Shabani, A. A., and Mousavi, S. F. (2022). In silico designing of a novel epitope-based candidate vaccine against *Streptococcus pneumoniae* with introduction of a new domain of PepO as adjuvant. *J. Trans. Med.* 20 (1), 389. doi: 10.1186/s12967-022-03590-6
- Cheng, P., Jiang, F., Wang, G., Wang, J., Xue, Y., Wang, L., et al. (2023). Bioinformatics analysis and consistency verification of a novel tuberculosis vaccine candidate HP13138PB. *Front. Immunol.* 14, 1102578. doi: 10.3389/fimmu.2023.1102578
- Cheng, P., Xue, Y., Wang, J., Jia, Z., Wang, L., and Gong, W. (2022). Evaluation of the consistence between the results of immunoinformatics predictions and real-world animal experiments of a new tuberculosis vaccine MP3RT. *Front. Cell. Infect. Microbiol.* 12, 1047306. doi: 10.3389/fcimb.2022.1047306
- Colovos, C., and Yeates, T. O. (1993). Verification of protein structures: patterns of nonbonded atomic interactions. *Protein Sci.* 2 (9), 1511–1519. doi: 10.1002/pro.5560020916
- Converso, T., Assoni, L., André, G., Darrieux, M., and Leite, L. C. d. C. (2020). The long search for a serotype independent pneumococcal vaccine. *Expert Rev. Vaccines* 19 (1), 57–70. doi: 10.1080/14760584.2020.1711055
- Converso, T. R., Goulart, C., Darrieux, M., and Leite, L. C. d. C. (2017a). A protein chimera including PspA in fusion with PotD is protective against invasive pneumococcal infection and reduces nasopharyngeal colonization in mice. *Vaccine* 35 (38), 5140–5147. doi: 10.1016/j.vaccine.2017.08.010
- Converso, T. R., Goulart, C., Rodriguez, D., Darrieux, M., and Leite, L. (2017b). Rational selection of broadly cross-reactive family 2 PspA molecules for inclusion in chimeric pneumococcal vaccines. *Microb. Pathogen.* 109, 233–238. doi: 10.1016/j.micpath.2017.06.004
- Daniels, C. C., Coan, P., King, J., Hale, J., Benton, K. A., Briles, D. E., et al. (2010). The proline-rich region of pneumococcal surface proteins A and C contains surface-accessible epitopes common to all pneumococci and elicits antibody-mediated protection against sepsis. *Infect. Immun.* 78 (5), 2163–2172. doi: 10.1128/IAI.01199-09
- Darrieux, M., Moreno, A. T., Ferreira, D. M., Pimenta, F. C., de Andrade, A. L. S., Lopes, A. P., et al. (2008). Recognition of pneumococcal isolates by antisera raised against PspA fragments from different clades. *J. Med. Microbiol.* 57 (3), 273–278. doi: 10.1099/jmm.0.47661-0

## Acknowledgments

We are thankful to Dr. Mohammad Mehdi Ranjbar, Professor of immunology, Razi Vaccine and Serum Research Institute, Karaj, Iran, and Dr. Mohammad Reza Pourshafie, Professor of Microbiology, Pasteur Institute of Iran, for their invaluable helps in completing this study.

## Conflict of interest

The authors declare that the research was conducted in the absence of any commercial or financial relationships that could be construed as a potential conflict of interest.

## Publisher's note

All claims expressed in this article are solely those of the authors and do not necessarily represent those of their affiliated organizations, or those of the publisher, the editors and the reviewers. Any product that may be evaluated in this article, or claim that may be made by its manufacturer, is not guaranteed or endorsed by the publisher.

## Supplementary material

The Supplementary Material for this article can be found online at: <https://www.frontiersin.org/articles/10.3389/fcimb.2023.1271143/full#supplementary-material>

- Dimitrov, I., Bangov, I., Flower, D. R., and Doytchinova, I. (2014). AllerTOP v. 2—a server for in silico prediction of allergens. *J. Mol. Model.* 20 (6), 1–6. doi: 10.1007/s00894-014-2278-5
- Doytchinova, I. A., and Flower, D. R. (2007). VaxiJen: a server for prediction of protective antigens, tumour antigens and subunit vaccines. *BMC Bioinf.* 8 (1), 1–7. doi: 10.1186/1471-2105-8-4
- Elderman, M., Hugenholtz, F., Belzer, C., Boekschoten, M., van Beek, A., de Haan, B., et al. (2018). Sex and strain dependent differences in mucosal immunology and microbiota composition in mice. *Biol. Sex Dif.* 9 (1), 1–18. doi: 10.1186/s13293-018-0186-6
- Emini, E. A., Hughes, J. V., Perlow, D., and Boger, J. (1985). Induction of hepatitis A virus-neutralizing antibody by a virus-specific synthetic peptide. *J. Virol.* 55 (3), 836–839. doi: 10.1128/jvi.55.3.836-839.1985
- Fereshteh, S., Ajdary, S., Sepehr, A., Bolourchi, N., Barzi, S. M., Jouriani, F. H., et al. (2023). Immunization with recombinant DcaP-like protein and AbOmpA revealed protections against sepsis infection of multi-drug resistant *Acinetobacter baumannii* ST2Pas in a C57BL/6 mouse model. *Microb. Pathogen.* 174, 105882. doi: 10.1016/j.micpath.2022.105882
- Fereshteh, S., Goodarzi, N. N., Sepehr, A., Shafiei, M., Ajdary, S., and Badmasti, F. (2022). In silico analyses of extracellular proteins of *acinetobacter baumannii* as immunogenic candidates. *Iranian J. Pharm. Res.* 21 (1), e126559. doi: 10.5812/ijpr-126559
- Gasteiger, E., Hoogland, C., Gattiker, A., Wilkins, M. R., Appel, R. D., and Bairoch, A. (2005). Protein identification and analysis tools on the ExPASy server. *Proteomics Protoc. Handb.*, 571–607. doi: 10.1385/1-59259-890-0:571
- Goulart, C., Darrieux, M., Rodriguez, D., Pimenta, F. C., Brandileone, M. C. C., de Andrade, A. L. S., et al. (2011). Selection of family 1 PspA molecules capable of inducing broad-ranging cross-reactivity by complement deposition and opsonophagocytosis by murine peritoneal cells. *Vaccine* 29 (8), 1634–1642. doi: 10.1016/j.vaccine.2010.12.074
- Goulart, C., d. Silva, T. R., Rodriguez, D., Politano, W. R., Leite, L. C., and Darrieux, M. (2013). Characterization of protective immune responses induced by pneumococcal surface protein A in fusion with pneumolysin derivatives. *PLoS One* 8 (3), e59605. doi: 10.1371/journal.pone.0059605
- Goulart, C., Rodriguez, D., Kanno, A. I., Lu, Y.-J., Malley, R., and Leite, L. C. (2017). Recombinant BCG expressing a PspA-PdT fusion protein protects mice against pneumococcal lethal challenge in a prime-boost strategy. *Vaccine* 35 (13), 1683–1691. doi: 10.1016/j.vaccine.2017.02.029
- Grote, A., Hiller, K., Scheer, M., Münch, R., Nörtemann, B., Hempel, D. C., et al. (2005). JCat: a novel tool to adapt codon usage of a target gene to its potential expression host. *Nucleic Acids Res.* 33 (suppl\_2), W526–W531. doi: 10.1093/nar/gki376
- Guan, Y., Zhu, Q., Huang, D., Zhao, S., Jan Lo, L., and Peng, J. (2015). An equation to estimate the difference between theoretically predicted and SDS PAGE-displayed molecular weights for an acidic peptide. *Sci. Rep.* 5 (1), 1–11. doi: 10.1038/srep13370
- Gupta, S., Kapoor, P., Chaudhary, K., Gautam, A., Kumar, R., Consortium, O. S. D. D., et al. (2013). In silico approach for predicting toxicity of peptides and proteins. *PLoS One* 8 (9), e73957. doi: 10.1371/journal.pone.0073957
- Guyot, P., Ades, A., Ouwens, M. J., and Welton, N. J. (2012). Enhanced secondary analysis of survival data: reconstructing the data from published Kaplan-Meier survival curves. *BMC Med. Res. Method.* 12, 1–13. doi: 10.1186/1471-2288-12-9
- Hasanzadeh, S., Habibi, M., Shokrgozar, M. A., Cohan, R. A., Ahmadi, K., Karam, M. R. A., et al. (2020). In silico analysis and in vivo assessment of a novel epitope-based vaccine candidate against uropathogenic *Escherichia coli*. *Sci. Rep.* 10 (1), 1–16. doi: 10.1038/s41598-020-73179-w
- Hollingshead, S. K., Becker, R., and Briles, D. E. (2000). Diversity of PspA: mosaic genes and evidence for past recombination in *Streptococcus pneumoniae*. *Infect. Immun.* 68 (10), 5889–5900. doi: 10.1128/IAI.68.10.5889-5900.2000
- Ikai, A. (1980). Thermostability and aliphatic index of globular proteins. *J. Biochem.* 88 (6), 1895–1898. doi: 10.1093/oxfordjournals.jbchem.a133168
- Jensen, K. K., Andreatta, M., Marcatili, P., Buus, S., Greenbaum, J. A., Yan, Z., et al. (2018). Improved methods for predicting peptide binding affinity to MHC class II molecules. *Immunology* 154 (3), 394–406. doi: 10.1111/imm.12889
- Jones, B. J., Kan, C. N. E., Luo, C., and Kazlauskas, R. J. (2020). Consensus Finder web tool to predict stabilizing substitutions in proteins. *Methods Enzymol.* 643, 129–148. doi: 10.1016/bs.mie.2020.07.010
- Kar, T., Narsaria, U., Basak, S., Deb, D., Castiglione, F., Mueller, D. M., et al. (2020). A candidate multi-epitope vaccine against SARS-CoV-2. *Sci. Rep.* 10 (1), 1–24. doi: 10.1038/s41598-020-67749-1
- Kavoosi, M., Creagh, A. L., Kilburn, D. G., and Haynes, C. A. (2007). Strategy for selecting and characterizing linker peptides for CBM9-tagged fusion proteins expressed in *Escherichia coli*. *Biotechnol. Bioeng.* 98 (3), 599–610. doi: 10.1002/bit.21396
- Kim, D. E., Chivian, D., and Baker, D. (2004). Protein structure prediction and analysis using the Robetta server. *Nucleic Acids Res.* 32 (suppl\_2), W526–W531. doi: 10.1093/nar/gkh468
- Kim, H., Park, H., and Lee, S. J. (2017). Effective method for drug injection into subcutaneous tissue. *Sci. Rep.* 7 (1), 1–11. doi: 10.1038/s41598-017-10110-w
- Kothari, N., Kothari, S., Choi, Y. J., Dey, A., Briles, D. E., Rhee, D. K., et al. (2015). A bivalent conjugate vaccine containing PspA families 1 and 2 has the potential to protect against a wide range of *Streptococcus pneumoniae* strains and *Salmonella Typhi*. *Vaccine* 33 (6), 783–788. doi: 10.1016/j.vaccine.2014.12.032
- Kozakov, D., Hall, D. R., Xia, B., Porter, K. A., Padhorny, D., Yueh, C., et al. (2017). The ClusPro web server for protein–protein docking. *Nat. Protoc.* 12 (2), 255–278. doi: 10.1038/nprot.2016.169
- Kringelum, J. V., Lundegaard, C., Lund, O., and Nielsen, M. (2012). Reliable B cell epitope predictions: impacts of method development and improved benchmarking. *PLoS Comput. Biol.* 8 (12), e1002829. doi: 10.1371/journal.pcbi.1002829
- Kristian, S. A., Ota, T., Bubeck, S. S., Cho, R., Groff, B. C., Kubota, T., et al. (2016). Generation and improvement of effector function of a novel broadly reactive and protective monoclonal antibody against pneumococcal surface protein A of *Streptococcus pneumoniae*. *PLoS One* 11 (5), e0154616. doi: 10.1371/journal.pone.0154616
- Krogh, A., Larsson, B., Von Heijne, G., and Sonnhammer, E. L. (2001). Predicting transmembrane protein topology with a hidden Markov model: application to complete genomes. *J. Mol. Biol.* 305 (3), 567–580. doi: 10.1006/jmbi.2000.4315
- Kyte, J., and Doolittle, R. F. (1982). A simple method for displaying the hydropathic character of a protein. *J. Mol. Biol.* 157 (1), 105–132. doi: 10.1016/0022-2836(82)90515-0
- Lagousi, T., Basdeki, P., Routsias, J., and Spoulou, V. (2019). Novel protein-based pneumococcal vaccines: assessing the use of distinct protein fragments instead of full-length proteins as vaccine antigens. *Vaccines* 7 (1), 9. doi: 10.3390/vaccines7010009
- Laskowski, R. A., Jabłońska, J., Pravda, L., Vařeková, R. S., and Thornton, J. M. (2018). PDBsum: Structural summaries of PDB entries. *Protein Sci.* 27 (1), 129–134. doi: 10.1002/pro.3289
- Laskowski, R. A., MacArthur, M. W., Moss, D. S., and Thornton, J. M. (1993). PROCHECK: a program to check the stereochemical quality of protein structures. *J. Appl. Crystallogr.* 26 (2), 283–291. doi: 10.1107/S0021889892009944
- Leroux-Roels, G. (2010). Unmet needs in modern vaccinology: adjuvants to improve the immune response. *Vaccine* 28, C25–C36. doi: 10.1016/j.vaccine.2010.07.021
- Lu, J., Sun, T., Wang, D., Dong, Y., Xu, M., Hou, H., et al. (2015). Protective immune responses elicited by fusion protein containing PsaA and PspA fragments. *Immunol. Invest.* 44 (5), 482–496. doi: 10.3109/08820139.2015.1037956
- Magnan, C. N., Randall, A., and Baldi, P. (2009). SOLpro: accurate sequence-based prediction of protein solubility. *Bioinformatics* 25 (17), 2200–2207. doi: 10.1093/bioinformatics/btp386
- Magnan, C. N., Zeller, M., Kayala, M. A., Vigil, A., Randall, A., Felgner, P. L., et al. (2010). High-throughput prediction of protein antigenicity using protein microarray data. *Bioinformatics* 26 (23), 2936–2943. doi: 10.1093/bioinformatics/btq551
- Malekan, M., Siadat, S. D., Aghasadeh, M., Shahrokhi, N., Eybpoosh, S., and Afshari, E. (2019). Assessment of PhtD C-terminal immunogenicity by opsonophagocytosis assay (OPA) with OMVs as adjuvants. *Vaccine Res.* 6 (2), 37–41. doi: 10.29252/vacres.6.2.37
- Marriam, S., Afghan, M. S., Nadeem, M., Sajid, M., Ahsan, M., Basit, A., et al. (2023). Elucidation of novel compounds and epitope-based peptide vaccine design against C30 endopeptidase regions of SARS-CoV-2 using immunoinformatics approaches. *Front. Cell. Infect. Microbiol.* 13, 568. doi: 10.3389/fcimb.2023.1134802
- Masomian, M., Ahmad, Z., Ti Gew, L., and Poh, C. L. (2020). Development of next generation *Streptococcus pneumoniae* vaccines conferring broad protection. *Vaccines* 8 (1), 132. doi: 10.3390/vaccines8010132
- McDaniel, L. S., Ralph, B. A., McDaniel, D. O., and Briles, D. E. (1994). Localization of protection-eliciting epitopes on PspA of *Streptococcus pneumoniae* between amino acid residues 192 and 260. *Microb. Pathogen.* 17 (5), 323–337. doi: 10.1006/mpat.1994.1078
- Miyaji, E. N., Ferreira, D. M., Lopes, A. P., Brandileone, M. C. C., Dias, W. O., and Leite, L. C. (2002). Analysis of serum cross-reactivity and cross-protection elicited by immunization with DNA vaccines against *Streptococcus pneumoniae* expressing PspA fragments from different clades. *Infect. Immun.* 70 (9), 5086–5090. doi: 10.1128/IAI.70.9.5086-5090.2002
- Mizrachi-Nebenahl, Y., Lifshitz, S., Teitelbaum, R., Novick, S., Levi, A., Benharroch, D., et al. (2003). Differential activation of the immune system by virulent *Streptococcus pneumoniae* strains determines recovery or death of the host. *Clin. Exp. Immunol.* 134 (1), 23–31. doi: 10.1046/j.1365-2249.2003.02261.x
- Mukerji, R., Hendrickson, C., Genschmer, K. R., Park, S.-S., Bouchet, V., Goldstein, R., et al. (2018). The diversity of the proline-rich domain of pneumococcal surface protein A (PspA): Potential relevance to a broad-spectrum vaccine. *Vaccine* 36 (45), 6834–6843. doi: 10.1016/j.vaccine.2018.08.045
- Mukerji, R., Mirza, S., Roche, A. M., Widener, R. W., Crony, C. M., Rhee, D.-K., et al. (2012). Pneumococcal surface protein A inhibits complement deposition on the pneumococcal surface by competing with the binding of C-reactive protein to cell-surface phosphocholine. *J. Immunol.* 189 (11), 5327–5335. doi: 10.4049/jimmunol.1201967
- Nabizadeh, Z., Minuchehr, Z., and Shabani, A. A. (2020). Rational design of hyperglycosylated human chorionic gonadotropin analogs (a bioinformatics approach). *Lett Drug Des Discov.* 17 (8), 1001–1014. doi: 10.2174/1570180817666200225101938
- Nachbagauer, R., and Palese, P. (2020). Is a universal influenza virus vaccine possible? *Annu. Rev. Med.* 71, 315–327. doi: 10.1146/annurev-med-120617-041310
- Naz, A., Shahid, F., Butt, T. T., Awan, F. M., Ali, A., and Malik, A. (2020). Designing multi-epitope vaccines to combat emerging coronavirus disease 2019 (COVID-19) by



- employing immuno-informatics approach. *Front. Immunol.* 11, 1663. doi: 10.3389/fimmu.2020.01663
- Nguyen, C. T., Kim, S. Y., Kim, M. S., Lee, S. E., and Rhee, J. H. (2011). Intranasal immunization with recombinant PspA fused with a flagellin enhances cross-protective immunity against *Streptococcus pneumoniae* infection in mice. *Vaccine* 29 (34), 5731–5739. doi: 10.1016/j.vaccine.2011.05.095
- Nielsen, H. (2017). Predicting secretory proteins with SignalP. *Protein Function Prediction: Methods Mol. Biol.* 1611, 59–73. doi: 10.1007/978-1-4939-7015-5\_6
- Norollahi, F., Siadat, S. D., Malekan, M., Mousavi, S. H., Janani, A., and Mousavi, S. F. (2020). Relationship between prevalence of pneumococcal serotypes and their neuraminidases in carriers, predictive facts? *Arch. Pediatr. Infect. Dis.* 8 (1), e14100. doi: 10.5812/pedinf.14100
- Oli, A. N., Obialor, W. O., Ifeanyichukwu, M. O., Odimegwu, D. C., Okoyeh, J. N., Emechebe, G. O., et al. (2020). Immunoinformatics and vaccine development: an overview. *ImmunoTargets Ther.* 9, 13. doi: 10.2147/ITT.S241064
- Petersen, E. F., Goddard, T. D., Huang, C. C., Couch, G. S., Greenblatt, D. M., Meng, E. C., et al. (2004). UCSF Chimera—a visualization system for exploratory research and analysis. *J. Comput. Chem.* 25 (13), 1605–1612. doi: 10.1002/jcc.20084
- Plumtree, C. D., Ogunniyi, A. D., and Paton, J. C. (2012). Polyhistidine triad proteins of pathogenic streptococci. *Trends Microbiol.* 20 (10), 485–493. doi: 10.1016/j.tim.2012.06.004
- Plumtree, C. D., Ogunniyi, A. D., and Paton, J. C. (2013a). Surface association of Pht proteins of *Streptococcus pneumoniae*. *Infect. Immun.* 81 (10), 3644–3651. doi: 10.1128/IAI.00562-13
- Plumtree, C. D., Ogunniyi, A. D., and Paton, J. C. (2013b). Vaccination against *Streptococcus pneumoniae* using truncated derivatives of polyhistidine triad protein D. *PLoS One* 8 (10), e78916. doi: 10.1371/journal.pone.0078916
- Ponomarenko, J., Bui, H.-H., Li, W., Fusseder, N., Bourne, P. E., Sette, A., et al. (2008). ElliPro: a new structure-based tool for the prediction of antibody epitopes. *BMC Bioinf.* 9 (1), 1–8. doi: 10.1186/1471-2105-9-514
- Rapin, N., Lund, O., Bernaschi, M., and Castiglione, F. (2010). Computational immunology meets bioinformatics: the use of prediction tools for molecular binding in the simulation of the immune system. *PLoS One* 5 (4), e9862. doi: 10.1371/journal.pone.0009862
- Roche, H., Håkansson, A., Hollingshead, S. K., and Briles, D. E. (2003). Regions of PspA/EF3296 best able to elicit protection against *Streptococcus pneumoniae* in a murine infection model. *Infect. Immun.* 71 (3), 1033–1041. doi: 10.1128/IAI.71.3.1033-1041.2003
- Saha, S., and Raghava, G. P. S. (2006). Prediction of continuous B-cell epitopes in an antigen using recurrent neural network. *Proteins: Struct. Funct. Bioinf.* 65 (1), 40–48. doi: 10.1002/prot.21078
- Saha, S., and Raghava, G. (2007). AlgPred: prediction of allergenic proteins and mapping of IgE epitopes. *Nucleic Acids Res.* 34 (suppl\_2), W202–W209. doi: 10.1093/nar/gkl343
- Saha, S., Vashishtha, S., Kundu, B., and Ghosh, M. (2022). In-silico design of an immunoinformatics based multi-epitope vaccine against *Leishmania donovani*. *BMC Bioinf.* 23 (1), 1–28. doi: 10.1186/s12859-022-04816-6
- Saitou, N., and Nei, M. (1987). The neighbor-joining method: a new method for reconstructing phylogenetic trees. *Mol. Biol. Evol.* 4 (4), 406–425. doi: 10.1093/oxfordjournals.molbev.a040454
- Sanami, S., Zandi, M., Pourhossein, B., Mobini, G.-R., Safaei, M., Abed, A., et al. (2020). Design of a multi-epitope vaccine against SARS-CoV-2 using immunoinformatics approach. *Int. J. Biol. Macromol.* 164, 871–883. doi: 10.1016/j.jbiomac.2020.07.117
- Schellekens, H. (2005). Factors influencing the immunogenicity of therapeutic proteins. *Nephrol. Dialysis Transplant.* 20 (suppl\_6), vi3–vi9. doi: 10.1093/ndt/gfh1092
- Scheller, C., Krebs, F., Wiesner, R., Wätzig, H., and Oltmann-Norden, I. (2021). A comparative study of CE-SDS, SDS-PAGE, and Simple Western—Precision, repeatability, and apparent molecular mass shifts by glycosylation. *Electrophoresis* 42 (14–15), 1521–1531. doi: 10.1002/elps.202100068
- Shafaghi, M., Bahadori, Z., Madanchi, H., Ranjbar, M. M., Shabani, A. A., and Mousavi, S. F. (2023). Immunoinformatics-aided design of a new multi-epitope vaccine adjuvanted with domain 4 of pneumolysin against *Streptococcus pneumoniae* strains. *BMC Bioinf.* 24 (1), 1–27. doi: 10.1186/s12859-023-05175-6
- Shafaghi, M., Shabani, A. A., and Minuchehr, Z. (2019). Rational design of hyperglycosylated human luteinizing hormone analogs (a bioinformatics approach). *Comput. Biol. Chem.* 79, 16–23. doi: 10.1016/j.compbiolchem.2019.01.002
- Shaper, M., Hollingshead, S. K., Benjamin, W. H. Jr., and Briles, D. E. (2004). PspA protects *Streptococcus pneumoniae* from killing by apolactoferrin, and antibody to PspA enhances killing of pneumococci by apolactoferrin. *Infect. Immun.* 72 (9), 5031–5040. doi: 10.1128/IAI.72.9.5031-5040.2004
- Shin, W.-H., Lee, G. R., Heo, L., Lee, H., and Seok, C. (2014). Prediction of protein structure and interaction by GALAXY protein modeling programs. *Bio Design* 2 (1), 1–11.
- Shirai, A., Matsuyama, A., Yashiroda, Y., Hashimoto, A., Kawamura, Y., Arai, R., et al. (2008). Global analysis of gel mobility of proteins and its use in target identification. *J. Biol. Chem.* 283 (16), 10745–10752. doi: 10.1074/jbc.M709211200
- Sievers, F., Wilm, A., Dineen, D., Gibson, T. J., Karplus, K., Li, W., et al. (2011). Fast, scalable generation of high-quality protein multiple sequence alignments using Clustal Omega. *Mol. Syst. Biol.* 7 (1), 539. doi: 10.1038/msb.2011.75
- Singh, H., Ansari, H. R., and Raghava, G. P. (2013). Improved method for linear B-cell epitope prediction using antigen's primary sequence. *PLoS One* 8 (5), e62216. doi: 10.1371/journal.pone.0062216
- Singh, R., Singh, S., Sharma, P. K., Singh, U. P., Briles, D. E., Hollingshead, S. K., et al. (2010). Helper T cell epitope-mapping reveals MHC-peptide binding affinities that correlate with T helper cell responses to pneumococcal surface protein A. *PLoS One* 5 (2), e9432. doi: 10.1371/journal.pone.0009432
- Tamborini, M., Geib, N., Marrero-Nodarse, A., Jud, M., Hauser, J., Aho, C., et al. (2015). A synthetic virus-like particle streptococcal vaccine candidate using B-cell epitopes from the proline-rich region of pneumococcal surface protein A. *Vaccines* 3 (4), 850–874. doi: 10.3390/vaccines3040850
- Tapia, D., Ross, B. N., Kalita, A., Kalita, M., Hatcher, C. L., Muruato, L. A., et al. (2016). From in silico protein epitope density prediction to testing *Escherichia coli* O157: H7 vaccine candidates in a murine model of colonization. *Front. Cell. Infect. Microbiol.* 6, 94. doi: 10.3389/fcimb.2016.00094
- Tian, H., Hou, X., and Liu, X. (2013). Real-time SPR characterization of the interactions between multi-epitope proteins and antibodies against classical swine fever virus. *Biochem. Biophys. Res. Commun.* 431 (2), 315–320. doi: 10.1016/j.bbrc.2012.12.104
- Vadesilho, C. F., Ferreira, D. M., Gordon, S. B., Briles, D. E., Moreno, A. T., Oliveira, M. L. S., et al. (2014). Mapping of epitopes recognized by antibodies induced by immunization of mice with PspA and PspC. *Clin. Vaccine Immunol.* 21 (7), 940–948. doi: 10.1128/CI.00239-14
- Wang, P., Sidney, J., Dow, C., Mothé, B., Sette, A., and Peters, B. (2008). A systematic assessment of MHC class II peptide binding predictions and evaluation of a consensus approach. *PLoS Comput. Biol.* 4 (4), e1000048. doi: 10.1371/journal.pcbi.1000048
- Waterhouse, A., Bertoni, M., Bienert, S., Studer, G., Tauriello, G., Gumienny, R., et al. (2018). SWISS-MODEL: homology modelling of protein structures and complexes. *Nucleic Acids Res.* 46 (W1), W296–W303. doi: 10.1093/nar/gky427
- Wiederstein, M., and Sippl, M. J. (2007). ProSA-web: interactive web service for the recognition of errors in three-dimensional structures of proteins. *Nucleic Acids Res.* 35 (suppl\_2), W407–W410. doi: 10.1093/nar/gkm290
- Xu, D., and Zhang, Y. (2011). Improving the physical realism and structural accuracy of protein models by a two-step atomic-level energy minimization. *Biophys. J.* 101 (10), 2525–2534. doi: 10.1016/j.bpj.2011.10.024
- Yang, J., Yan, R., Roy, A., Xu, D., Poisson, J., and Zhang, Y. (2015). The I-TASSER Suite: protein structure and function prediction. *Nat. Methods* 12 (1), 7–8. doi: 10.1038/nmeth.3213
- Younis, S., Faber, B. W., Kocken, C. H., and Remarque, E. J. (2019). Identification of adjuvants for clinical trials performed with *Plasmodium falciparum* AMA1 in rabbits. *BMC Immunol.* 20, 1–12. doi: 10.1186/s12865-019-0307-y
- Zhang, S., Jin, S., and Xue, B. (2013). Accurate prediction of protein dihedral angles through conditional random field. *Front. Biol.* 8, 353–361. doi: 10.1007/s11515-013-1261-3
- Zhang, Y., Liang, S., Zhang, S., Zhang, S., Yu, Y., Yao, H., et al. (2022). Development and evaluation of a multi-epitope subunit vaccine against group B *Streptococcus* infection. *Emerg. Microbes Infect.* 11 (1), 2371–2382. doi: 10.1080/22221751.2022.2122585
- Zhao, X., Zhang, F., Li, Z., Wang, H., An, M., Li, Y., et al. (2019). Bioinformatics analysis of EgA31 and EgG1Y162 proteins for designing a multi-epitope vaccine against *Echinococcus granulosus*. *Infect. Genet. Evol.* 73, 98–108. doi: 10.1016/j.jmeegid.2019.04.017



## OPEN ACCESS

## EDITED BY

Simone Brogi,  
University of Pisa, Italy

## REVIEWED BY

Chengliang Deng,  
Affiliated Hospital of Zunyi Medical  
University, China  
Saad Alghamdi,  
Umm al-Qura University, Saudi Arabia

## \*CORRESPONDENCE

YunJun Liao  
✉ yunjun1000@sina.com

<sup>†</sup>These authors have contributed  
equally to this work and share  
first authorship

RECEIVED 24 July 2023

ACCEPTED 17 November 2023

PUBLISHED 08 December 2023

## CITATION

You X, Yao Y, Gao J and Liao Y (2023)  
*Corynebacterium bovis* infection after  
autologous fat grafting in breast  
augmentation: a case report.  
*Front. Cell. Infect. Microbiol.* 13:1265872.  
doi: 10.3389/fcimb.2023.1265872

## COPYRIGHT

© 2023 You, Yao, Gao and Liao. This is an  
open-access article distributed under the  
terms of the [Creative Commons Attribution  
License \(CC BY\)](#). The use, distribution or  
reproduction in other forums is permitted,  
provided the original author(s) and the  
copyright owner(s) are credited and that  
the original publication in this journal is  
cited, in accordance with accepted  
academic practice. No use, distribution or  
reproduction is permitted which does not  
comply with these terms.

# *Corynebacterium bovis* infection after autologous fat grafting in breast augmentation: a case report

Xin You<sup>†</sup>, Yao Yao<sup>†</sup>, JianHua Gao and YunJun Liao\*

Department of Plastic and Cosmetic Surgery, Nanfang Hospital, Southern Medical University, Guang  
Zhou, Guang Dong, China

In this report, we present a case study of a rare human bacterium, *Corynebacterium bovis*, which caused an infection in a patient who had undergone autologous fat-based breast augmentation using cryopreserved fat. This infection occurred during a secondary fat grafting procedure. To identify the bacteria causing the infection, we used high-throughput DNA sequencing technology since this bacterium is seldomly reported in human infections. The patient was successfully treated with intravenous imipenem. We also discuss potential factors that may have contributed to this unusual bacterial infection and propose that DNA sequencing can be a useful tool in cases where standard culture techniques fail to identify the causative agent. Additionally, we highlight the importance of further research on the cryopreservation of fat. In summary, this case highlights the possibility of rare bacterial infections occurring after fat grafting procedures and emphasizes the importance of identifying the causative agent through advanced techniques such as DNA sequencing. Further research is needed to improve our understanding of the risks associated with cryopreservation of fat and to identify ways to prevent these types of infections in the future.

## KEYWORDS

fat graft, breast augmentation, *Corynebacterium bovis*, high-throughput DNA sequencing, bacterial infection

## Introduction

Breast augmentation through autologous fat-only grafting is a common procedure in the fields of plastic and aesthetic surgery. However, postoperative infections can occur and may lead to unsatisfactory results, including implant loss, breast deformation, and in rare cases, systemic infections (Groen et al., 2016; Ørholt et al., 2020). *Corynebacterium bovis*, a bacterium typically associated with bovine mastitis (Ajitkumar et al., 2012), has only been reported to cause rare infections in humans, with only 14 documented cases to date. These cases encompass a range of conditions, such as line-related sepsis, ventriculi jugular shunt nephritis, meningitis, leg ulcer, chronic otitis media, epidural abscess, keratitis, chronic



conjunctivitis, shoulder prosthetic joint infection, and infectious endocarditis (Bolton et al., 1975; Vale and Scott, 1977; Dalal et al., 2008; Ajitkumar et al., 2012; Chow et al., 2015; Elsheikh et al., 2021).

Here, we present that a case of a patient who developed a *C. bovis* infection after autologous fat-only breast augmentation and describes the treatment process, as well as a discussion of possible causes of the infection. The infection was noted following a secondary fat grafting with cryopreserved fat from the initial operation, highlighting the potential risk of cryopreservation in the transmission of bacteria. To our knowledge, this marks the first reported case of *C. bovis* infection in the context of human fat breast augmentation.

In this paper, we delineate the treatment process for this uncommon infection and delve into potential sources of the infection, encompassing aspects like cryopreservation and the utilization of contaminated instruments during the surgical procedure. Furthermore, we propose the potential use of DNA sequencing to identify the causative organism in culture-negative infections. Our findings highlight the importance of considering rare bacterial species as potential pathogens in postoperative infections and suggest the need for further investigation into the safety of cryopreservation in fat grafting procedures.

## Case report

In May 2022, a 46-year-old female patient underwent thigh liposuction and subsequently fat breast augmentation. The liposuction procedure utilized a 3-mm multiport cannula, which incorporated several 1 mm sharp side holes and operated at a suction pressure of -0.75 atm. The duration of the procedure was

approximately one hour, and the extracted fat was subsequently subjected to centrifugation at 1200 g for 3 minutes to produce Coleman fat. A total volume of 800ml of Coleman fat was prepared, with 300ml of Coleman fat being administered to each breast for augmentation purposes. The remaining fat was cryopreserved at -18°C without the inclusion of a cryoprotectant solution. The patient did not exhibit any discernible symptoms of fever or infection following the initial liposuction and lipofilling operations.

One month after post-breast augmentation surgery, the patient underwent a second procedure using residual fat due to dissatisfaction with the initial outcome. The total filling volume was 175ml, with 75ml in the left breast and 100ml in the right breast.

Following the second procedure, the patient experienced localized redness and swelling at both filling ports, along with breast pain and swelling. Despite treatment with prednisone and antibiotics, the symptoms persisted and worsened over time, leading to referral to our hospital. Despite the absence of indications of systemic inflammation, notable symptoms of localized inflammation were observed, including swelling and pain in both breasts, along with local erythema and the discharge of purulent exudate from the injection port (Figure 1). Breast ultrasound detected the presence of multiple areas with no echo in both mammary glands, with the largest measuring 2.2 x 1.9 cm. Further MRI results revealed the existence of numerous adipose nodules at varying levels. Additionally, circular anomalous signal shadows, measuring approximately 2.0 x 2.0 x 1.4 cm, were visible in the lower quadrant of the right breast, indicative of infection and abscess formation (Figure 2).

To determine the causative agents, we employed high-throughput DNA sequencing technology. High-throughput DNA

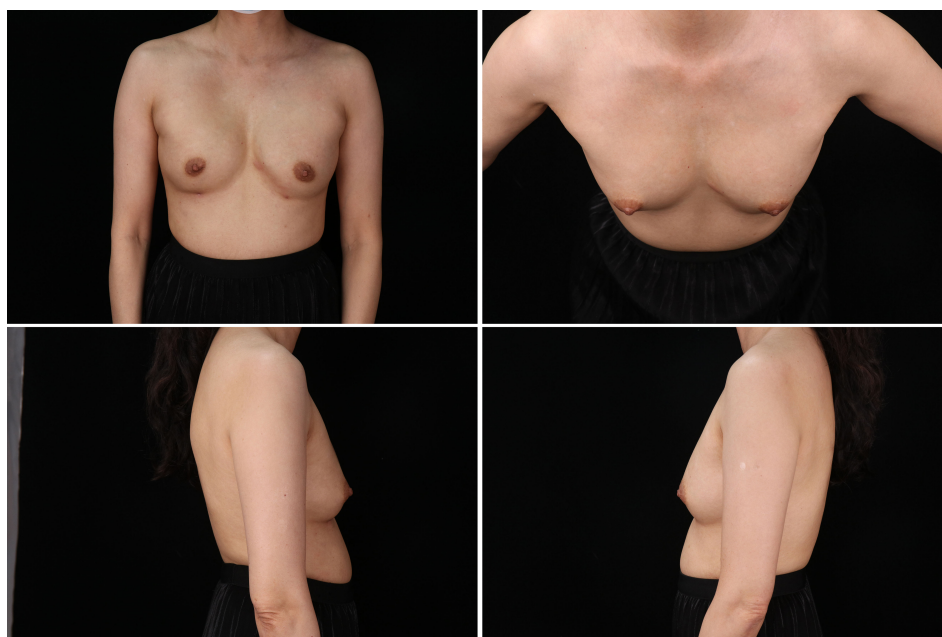


FIGURE 1

The preoperative photo of the breast, exhibited the existence of edema and indications of localized inflammation at the injection port.

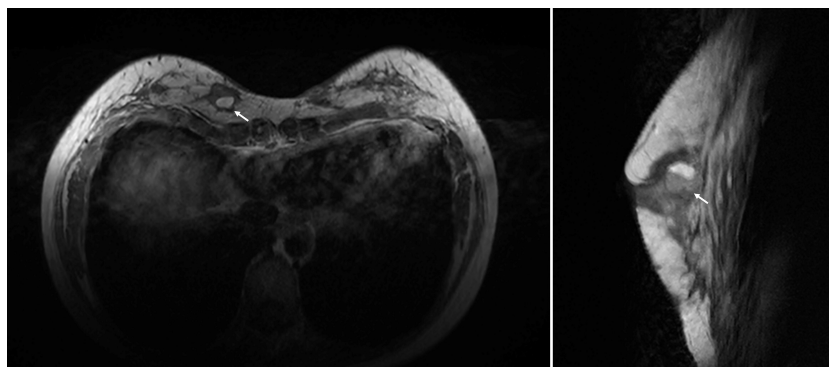


FIGURE 2

The preoperative photos of MRI images, revealed the presence of a circular abnormality measuring 2.0 x 2.0 x 1.4 cm in the right breast (white arrow).

sequencing is a non-culture-based technique that enables direct nucleic acid sequencing of clinical samples, enabling the identification, tracing, detection, and typing of infectious pathogens through database comparison. Sample was extracted from the purulent exudate of the injection port and sent for sequencing. The sequencing analysis yielded a total of twelve bacterial sequences, while no evidence of fungi, viruses, parasites, or other pathogens was detected. Upon comparison with the database, all the bacterial sequences were confirmed as *C. bovis*. Due to the absence of residual fat, pathogenic testing was not possible.

To address the source of infection, we investigated the sterilization process and storage container that the residual fat was stored in. The sterilization process was performed in accordance with standard clinical procedures, and the storage container was a sterile polypropylene container. However, the fat

was cryopreserved at  $-18^{\circ}\text{C}$  without the inclusion of a cryoprotectant solution. Cryopreservation has been shown to cause damage to cell membranes and could result in bacterial contamination due to the formation of ice crystals, which could facilitate bacterial entry into the cells.

In line with previous literature (Elsheikh et al., 2021), after undergoing debridement surgery, the patient was administered intravenous imipenem for a duration of one week in order to alleviate the breast infection. The turnaround time for the DNA sequencing test was five days. During the test, the patient was administered ceftriaxone and cefuroxime. Upon confirmation of the *C. bovis* infection, the patient was switched to imipenem. After the eight-week follow-up, no discernible clinical or laboratory indications of infection were detected, and the previously present local redness and swelling in the left breast had resolved (Figure 3). The MRI findings at 3 months after the operation indicated a

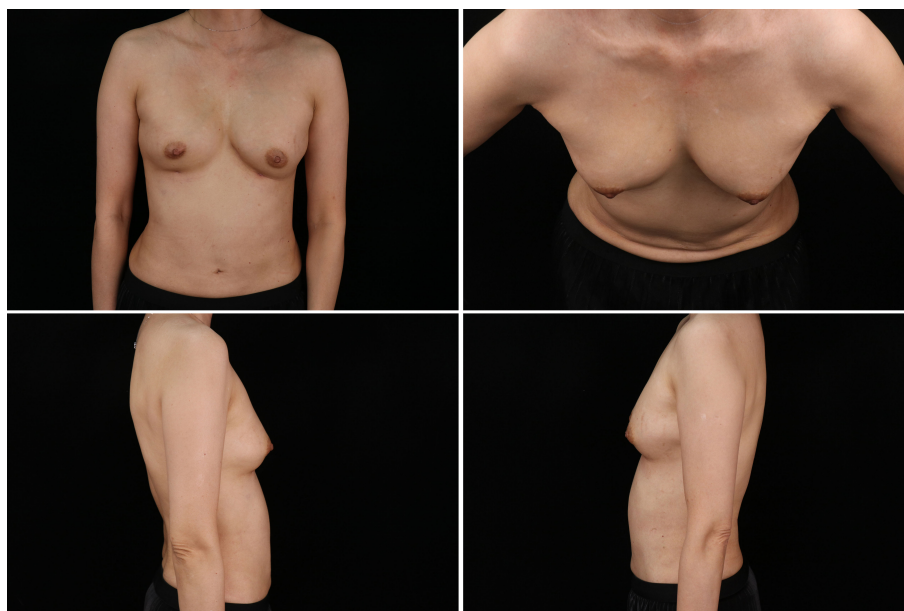


FIGURE 3

The photo of final clinical outcome, signs of local redness and swelling resolved.

notable decrease in the size of the infection site as compared to the earlier one (Figure 4).

## Discussion

Autologous fat grafting for breast augmentation is a common procedure in cosmetic surgery, but it can lead to various complications such as pain, hematoma formation, oil cyst development. Another challenge is that fat grafting has a high absorption rate and unstable volume retention rate. This can lead to unsatisfactory results, necessitating additional injections. To avoid multiple procedures, adipose tissue can be cryopreserved for future injections. However, there is no universally accepted technique for cryopreserving fat, although evidence suggests that an effective and appropriate cryopreservation method can maintain cellular activity and function (Gal and Pu, 2020).

Unfortunately, the patient in this case developed a *C. bovis* infection after the second injection of cryopreserved fat, which was suspected to be the source of infection. The infection's likely cause was the use of cryopreserved fat harvested during the initial procedure and stored for four weeks before reinjection. The cryopreservation process involved slowly cooling the adipose tissue to  $-30^{\circ}\text{C}$  before storing it in a refrigerator at the same temperature without any protective agent added to the fat. This creates an environment that may promote bacterial growth, as cryopreservation typically involves slowing down metabolic processes but does not completely eliminate the presence of microorganisms. Cryoprotective agents can be added to protect cells from the damaging effects of ice crystal formation during freezing. However, the subsequent removal of the protective agent can be challenging, requiring repeated cleaning, and increasing the risk of contamination and infection. To mitigate this risk, it's crucial to implement proper protocols for cryopreservation, ensuring that the storage temperature and conditions are not conducive to microbial proliferation. Moreover, the use of sterile, well-sealed containers can reduce the risk of contamination during storage.

Moreover, there is also a possibility of infection during the supplemental injection process. Anytime a needle is inserted into the skin, there is a risk of introducing bacteria or other harmful

pathogens into the body. Proper sterilization and disinfection of all equipment and the surgical field are vital to minimize this risk. The surgical team should adhere to stringent aseptic techniques and ensure that all equipment, including needles, syringes, and other instruments, are sterile. Although not analyzed in this particular case, the storage container and the sterilization process for residual fat should not be overlooked. The choice of storage containers can impact the integrity of the adipose tissue and the risk of contamination. Sterilization methods for equipment used during fat processing and storage should be thoroughly validated to ensure their effectiveness in eliminating microbial contaminants. Evaluating the container materials and sterilization procedures as potential sources of infection should be a part of comprehensive quality control measures in fat grafting procedures.

Regarding the DNA testing, the authors used fluid from the pocket for analysis. The absence of residual fat in the patient prevented pathogenic testing. The authors utilized high-throughput sequencing technology, which presents a unique advantage as it enables direct nucleic acid detection in clinical samples and subsequent comparison with an established database. For instance, Achermann et al. (2009) identified *C. bovis* as the pathogen by sequencing the 16S rRNA gene and comparing it with the gene database. The turnaround time for this DNA testing was five days. The turnaround time for the DNA sequencing test was five days. During the test, the patient was administered ceftriaxone and cefuroxime. Upon confirmation of the *C. bovis* infection, the patient was switched to imipenem.

*C. bovis* is a Gram-positive, facultatively anaerobic bacterium that is known to cause infrequent infections in humans. The etiology of *C. bovis* infection is often associated with traumatic injury or the introduction of exogenous medical devices. For example, Vale et al (Vale and Scott, 1977). found that out of a case series of six patients with *C. bovis* infections, two were associated with traumatic injury and two with the implantation of heart valves. In addition, Dalal et al. (2008) reported on an 84-year-old female who acquired a *C. bovis* infection through a peripherally inserted central catheter (PICC) following a cerebrovascular accident. Contact with contaminated cows or their products has also been identified as a possible source of *C. bovis* infection. For instance, Elsheikh et al. (2021) documented a case of persistent

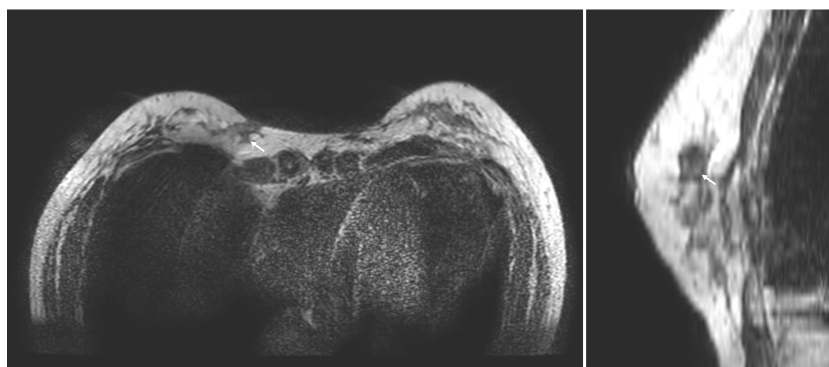


FIGURE 4

The photos of MRI images at 3 months after surgery, revealed the lesion is significantly smaller than before (white arrow).

bacterial keratitis, where the patient had recent cattle contact, suggesting that hand-to-eye contact with infected cattle was the likely mode of transmission. Similarly, Achermann et al. (2009) described a case of shoulder prosthetic joint infection, where the author postulated that the infection may have been due to contaminated milk or the patient's own skin flora.

This study reports the initial occurrence of *C. bovis* infection in a fat breast augmentation case. The etiology of the infection remains undetermined. The patient denied any exposure to livestock or contaminated cattle products and had no history of breast trauma. The preoperative evaluation revealed no signs of HIV infection or other forms of immunosuppression. Overall, our findings highlight the importance of considering unusual pathogens and performing comprehensive diagnostic workups when facing culture-negative infections. While traditional culture techniques remain the standard of care for identifying bacterial pathogens, the use of high-throughput sequencing technology can provide valuable information in cases of suspected unusual infections, enabling more targeted antibiotic treatment and potentially preventing future infections. High-throughput DNA sequencing, despite its numerous benefits in microbiology and infectious disease diagnosis, comes with several notable limitations. Firstly, its cost remains relatively high compared to traditional culture methods, limiting its adoption in resource-limited settings. The technique is also complex and requires specialized expertise in molecular biology and bioinformatics, which may hinder its widespread use. Turnaround time can be an issue, as it can still take hours to days to obtain results. Furthermore, the technology's sensitivity can lead to false positives, and data interpretation is challenging due to the vast amount of information generated. Sample quality and preparation are crucial, and not all healthcare facilities have access to this technology. Ethical and legal concerns, particularly regarding patient privacy and data security, can also arise. Despite these limitations, ongoing advancements may address some of these issues, and high-throughput sequencing continues to hold promise for the future of infectious disease diagnosis.

## Conclusion

In conclusion, autologous fat grafting remains a popular cosmetic procedure despite the associated risks of complications. Our case report highlights the potential risks of using cryopreserved fat-derived products, which may increase the risk of infection and adipocyte necrosis. Furthermore, it underscores the importance of thorough preoperative evaluation and postoperative monitoring for early identification and treatment of complications. Finally, the use of high-throughput sequencing technology can be a valuable tool in diagnosing culture-negative infections and guiding antibiotic treatment. Further studies are needed to investigate the safety and efficacy of cryopreservation techniques for autologous fat grafting

and to identify additional measures to prevent infections in cosmetic procedures.

## Data availability statement

The original contributions presented in the study are included in the article/supplementary material. Further inquiries can be directed to the corresponding author.

## Ethics statement

The studies involving humans were approved by Ethics Committee, Nanfang Hospital, Southern Medical University. The studies were conducted in accordance with the local legislation and institutional requirements. The participants provided their written informed consent to participate in this study. Written informed consent was obtained from the individual(s) for the publication of any potentially identifiable images or data included in this article. Written informed consent was obtained from the participant/patient(s) for the publication of this case report.

## Author contributions

XY: Writing – original draft. YY: Writing – original draft. JG: Writing – review & editing. YL: Writing – review & editing.

## Funding

The author(s) declare financial support was received for the research, authorship, and/or publication of this article. This work was supported by Guangdong Basic and Applied Basic Research Foundation (2023A1515030103).

## Conflict of interest

The authors declare that the research was conducted in the absence of any commercial or financial relationships that could be construed as a potential conflict of interest.

## Publisher's note

All claims expressed in this article are solely those of the authors and do not necessarily represent those of their affiliated organizations, or those of the publisher, the editors and the reviewers. Any product that may be evaluated in this article, or claim that may be made by its manufacturer, is not guaranteed or endorsed by the publisher.

## References

- Achermann, Y., Trampuz, A., Moro, F., Wüst, J., and Vogt, M. (2009). *Corynebacterium bovis* shoulder prosthetic joint infection: the first reported case. *Diagn. Microbiol. Infect. Dis.* 64 (2), 213–215. doi: 10.1016/j.diagmicrobio.2009.02.003
- Ajitkumar, P., Barkema, H. W., and De Buck, J. (2012). Rapid identification of bovine mastitis pathogens by high-resolution melt analysis of 16S rDNA sequences. *Vet. Microbiol.* 155 (2–4), 332–340. doi: 10.1016/j.vetmic.2011.08.033
- Bolton, W. K., Sande, M. A., Normansell, D. E., Sturgill, B. C., and Westervelt, F. B. Jr. (1975). Ventriculojugular shunt nephritis with *Corynebacterium bovis*. *Successful Ther. antibiotics. Am. J. Med.* 59 (3), 417–423. doi: 10.1016/0002-9343(75)90401-5
- Chow, S. K., Bui, U., and Clarridge, J. E. (2015). *Corynebacterium bovis* eye infections, washington, USA, 2013. *Emerg. Infect. Dis.* 21 (9), 1687–1689. doi: 10.3201/eid2109.150520
- Dalal, A., Urban, C., Ahluwalia, M., and Rubin, D. (2008). *Corynebacterium bovis* line related septicemia: a case report and review of the literature. *Scand. J. Infect. Dis.* 40 (6–7), 575–577. doi: 10.1080/00365540701772448
- Elsheikh, M., Elsayed, A., Bennett, N., and Connor, M. (2021). *Corynebacterium bovis*: A rare case of persistent bacterial keratitis and corneal perforation. *Cureus* 13 (8), e16913. doi: 10.7759/cureus.16913
- Gal, S., and Pu, L. L. Q. (2020). An update on cryopreservation of adipose tissue. *Plast. Reconstr Surg.* 145 (4), 1089–1097. doi: 10.1097/PRS.0000000000006699
- Groen, J. W., Negenborn, V. L., Twisk, J. W., Ket, J. C., Mullender, M. G., and Smit, J. M. (2016). Autologous fat grafting in cosmetic breast augmentation: A systematic review on radiological safety, complications, volume retention, and patient/surgeon satisfaction. *Aesthet Surg. J.* 36 (9), 993–1007. doi: 10.1093/asj/sjw105
- Ørholt, M., Larsen, A., Hemmingsen, M. N., Mirian, C., Zocchi, M. L., Vester-Glowinski, P. V., et al. (2020). Complications after breast augmentation with fat grafting: A systematic review. *Plast. Reconstr. Surg.* 145 (3), 530e–537e. doi: 10.1097/PRS.0000000000006569
- Vale, J. A., and Scott, G. W. (1977). *Corynebacterium bovis* as a cause of human disease. *Lancet* 2 (8040), 682–684. doi: 10.1016/s0140-6736(77)90495-0



# Frontiers in Cellular and Infection Microbiology

Investigates how microorganisms interact with their hosts

Explores bacteria, fungi, parasites, viruses, endosymbionts, prions and all microbial pathogens as well as the microbiota and its effect on health and disease in various hosts.

## Discover the latest Research Topics

[See more →](#)

### Frontiers

Avenue du Tribunal-Fédéral 34  
1005 Lausanne, Switzerland  
[frontiersin.org](https://frontiersin.org)

### Contact us

+41 (0)21 510 17 00  
[frontiersin.org/about/contact](https://frontiersin.org/about/contact)

